



Raymond and Beverly Sackler Faculty of Exact Sciences
Blavatnik School of Computer Science

Understanding Deep Learning via Notions of Rank

Author:
Noam Razin

Supervisor:
Dr. Nadav Cohen

*A dissertation submitted for the degree of
Doctor of Philosophy in Computer Science*

August 2024

Acknowledgements

It is hard to imagine how my PhD would have looked like without the support and guidance of the people around me.

I had the privilege of being the first graduate student of my advisor, Nadav Cohen. This meant a unique opportunity to learn from him the ins and outs of being an academic: from acquiring research taste to technical and presentation skills. Though I see myself as somewhat of a perfectionist, when working with Nadav you quickly learn that you can always strive for better. His guidance has undoubtedly left a strong imprint on me. Above all, I greatly appreciate Nadav for consistently pushing me forward while having my professional and personal benefits in mind. I could not have wished for a better advisor.

I want to thank my collaborators, friends, and mentors from Tel Aviv University and Apple, for making this experience such an enjoyable and productive one, including: Asaf Maman, Tom Verbin, Yotam Alexander, Nimrod De La Vega, Yoni Slutzky, Yuval Milo, Raja Giryes, Amir Globerson, Hattie Zhou, Arwen Bradley, Omid Saremi, Vimal Thilak, Preetum Nakkiran, Joshua Susskind, and Etai Littwin.

I am deeply grateful to my family for their unconditional love and everything that they have done to support me. In particular, my parents have always been models of excellence for me. While they never pushed me towards any specific direction, I believe that they have successfully instilled in me a drive to fully pursue my interests, to which I owe much of the ability to complete my PhD. I also want to thank Prof. Rivka Dresner-Pollak for her close care, for which I will forever be indebted.

Lastly, during my studies I was fortunate to meet the love of my life, Eshbal. Besides making my life more complete, she is largely responsible for any especially well-designed figure, slide, or poster that I have presented (you might be able to guess when we met by the style of figures in this thesis). Even if it was just for meeting Eshbal, doing a PhD was well worth it.

Abstract

Despite the extreme popularity of deep learning in science and industry, its formal understanding is limited. Common practices are based primarily on trial-and-error and intuition, often leading to suboptimal results. As a result, there is significant interest in developing a formal theory of deep learning, with the hopes that it will shed light on empirical findings, and lead to principled methods for improving the efficiency, reliability, and performance of neural networks.

This thesis puts forth notions of *rank* as key for developing a theory of deep learning. Specifically, building on a connection between certain neural network architectures and tensor factorizations, we employ notions of rank for studying the fundamental aspects of *generalization* and *expressiveness*.

With regards to generalization, the mysterious ability of neural networks to generalize is widely believed to stem from an *implicit regularization* — a tendency of gradient-based training towards predictors of low complexity, for some yet unknown measure of complexity. Through dynamical analyses, we establish an implicit regularization towards low rank in several types of neural network architectures (for corresponding notions of rank). Notably, this implicit rank minimization differs from any type of norm minimization, in contrast to prior beliefs. Implications of this finding for explaining generalization over natural data (*e.g.*, audio, images, and text), as well as practical applications (novel regularization schemes), are presented.

With regards to expressiveness, we theoretically characterize the ability of graph neural networks to model interactions via *separation rank* — a measure commonly used for quantifying entanglement in quantum physics. As a practical application of our theory, we design an edge sparsification algorithm that preserves the ability of graph neural networks to model interactions. Empirical evaluations demonstrate that it markedly outperform alternative methods.

Contents

Acknowledgements	i
Abstract	ii
I Introduction	1
II Generalization via Implicit Rank Minimization	5
1 Implicit Regularization in Deep Learning May Not Be Explainable by Norms	6
1.1 Background and Overview	6
1.2 Deep Matrix Factorization	8
1.3 Implicit Regularization Can Drive All Norms to Infinity	9
1.4 Experiments	15
2 Implicit Regularization in Tensor Factorization	19
2.1 Background and Overview	19
2.2 Tensor Factorization	20
2.3 Dynamical Characterization	22
2.4 Implicit Tensor Rank Minimization	24
2.5 Experiments	27
3 Implicit Regularization in Hierarchical Tensor Factorization and Deep Convolutional Neural Networks	30
3.1 Background and Overview	30
3.2 Preliminaries: Matrix and Tensor Factorizations	31
3.3 Hierarchical Tensor Factorization	35
3.4 Incremental Hierarchical Tensor Rank Learning	39
3.5 Low Hierarchical Tensor Rank Implies Locality	45
3.6 Countering Locality of Convolutional Networks via Regularization	46
4 Related Work	49
III Expressiveness of Graph Neural Networks via Separation Rank	51
5 On the Ability of Graph Neural Networks to Model Interactions Between Vertices	52
5.1 Background and Overview	52
5.2 Preliminaries	54
5.3 Graph Neural Networks	55

5.4	Theoretical Analysis: The Effect of Input Graph Structure and Neural Network Architecture on Modeled Interactions	57
5.5	Practical Application: Expressivity Preserving Edge Sparsification	62
6	Related Work	66
IV	Conclusion	68
A	Implicit Regularization in Deep Learning May Not Be Explainable by Norms	85
A.1	Extension to Different Matrix Dimensions	85
A.2	Further Experiments and Implementation Details	86
A.3	Deferred Proofs	89
B	Implicit Regularization in Tensor Factorization	113
B.1	Extension to Tensor Sensing	113
B.2	Further Experiments and Implementation Details	114
B.3	Deferred Proofs	117
C	Implicit Regularization in Hierarchical Tensor Factorization and Deep Convolutional Neural Networks	136
C.1	Hierarchical Tensor Factorization as Deep Non-Linear Convolutional Network	136
C.2	Evolution of Local Component Norms Under Arbitrary Initialization	138
C.3	Hierarchical Tensor Rank as Measure of Long-Range Dependencies	138
C.4	Further Experiments and Implementation Details	139
C.5	Deferred Proofs	145
D	On the Ability of Graph Neural Networks to Model Interactions Between Vertices	167
D.1	Tightness of Upper Bounds for Separation Rank	167
D.2	Extension of Analysis to Directed Graphs With Multiple Edge Types	168
D.3	Representing Graph Neural Networks With Product Aggregation as Tensor Networks	170
D.4	General Walk Index Sparsification	176
D.5	Efficient Implementation of 1-Walk Index Sparsification	176
D.6	Further Experiments and Implementation Details	177
D.7	Deferred Proofs	181

Part I

Introduction

In the past decade, *deep learning* has been experiencing unprecedented success, and is largely responsible for the technological breakthroughs referred to in the public as “artificial intelligence” (see, *e.g.*, [128, 153, 195, 77, 31, 2]). However, despite the extreme popularity of deep learning in science and industry, its formal understanding is limited. Common practices are based primarily on trial-and-error and intuition, often leading to suboptimal results, as well as compromise in important aspects including safety and robustness [201, 144]. As a result, there is significant interest in developing a formal theory of deep learning, with the hopes that it will shed light on empirical phenomena, and lead to principled methods for improving the efficiency, reliability, and performance of neural networks.

From the perspective of learning theory, understanding deep learning requires addressing the fundamental questions of *optimization*, *generalization*, and *expressiveness*. Optimization concerns the effectiveness of gradient-based methods in minimizing neural network training objectives that are non-convex. Generalization treats the performance of a neural network beyond its training data. Lastly, expressiveness refers to the ability of practically sized neural networks to represent rich classes of functions.

This thesis focuses on two of the fundamental questions — generalization and expressiveness. It puts forth notions of rank as key for developing a theory of deep learning. Our approach adopts tools from dynamical systems theory and tensor analysis, building on a recent connection between certain neural network architectures and *tensor factorizations* [51, 48, 52, 132, 118, 119].¹ The main theoretical contributions and their practical implications are summarized below.

Generalization via Implicit Rank Minimization (Part II)

One of the central mysteries in deep learning is the ability of neural networks to generalize over natural data (*e.g.*, audio, images, and text) when trained via gradient-based methods, despite having far more learnable parameters than training examples. This generalization takes place even in the absence of any explicit regularization [226]. Thus, conventional wisdom is that gradient-based training induces an *implicit regularization* — a tendency to fit training examples with predictors of minimal complexity, for some measure of complexity [166, 165]. The fact that natural data gives rise to generalization is accordingly understood to result from an agreement between the complexity measure implicitly minimized during training and the complexity of the data. More specifically, from the amenability of natural data to be fit with predictors of low complexity.

Mathematically formalizing the above intuition is regarded as a major open problem in the theory of deep learning. A significant challenge towards doing so is that we lack definitions for predictor complexity that are both implicitly minimized during training of neural networks and capture the essence of natural data (in the sense of natural data being fittable with low complexity). One widespread hope, initially articulated in [166], is that a characterization based on minimization of norms may apply. Namely, it is known that for linear regression gradient-based methods converge to the solution with minimal Euclidean norm (see, *e.g.*, Section 5 in [226]), and the hope is that this result can carry over to neural networks if we

¹For the sake of this thesis, *tensors* can be thought of as N -dimensional arrays, with $N \in \mathbb{N}$ arbitrary. For example, matrices correspond to the special case $N = 2$ and vectors to $N = 1$.

allow replacing the Euclidean norm with a different (possibly architecture-dependent) norm [81, 197, 83, 82, 140, 109, 217, 216].

A standard testbed for studying this prospect is *matrix factorization* — a model equivalent to *linear neural networks*, *i.e.* fully-connected neural networks with no non-linearity [188]. In Chapter 1 (based on [177]) we prove that, in contrast to prior belief [81], the implicit regularization in matrix factorization cannot be captured by norms. Specifically, we show that there exist settings in which it drives *all* norms towards *infinity* in favor of minimizing *rank*. This indicates that, rather than perceiving the implicit regularization via norms, a potentially more useful interpretation is minimization of rank.

Capitalizing on this interpretation, in Chapters 2 and 3 (based on [178] and [179], respectively), we establish that the tendency towards low rank extends from linear neural networks to more practical *non-linear neural networks* (with polynomial non-linearity), which are equivalent to *tensor factorizations*. By characterizing the dynamics that gradient-based methods induce on such networks, we show that these result in a bias towards low rank, for architecture-dependent notions of rank defined over tensors. To the best of my knowledge, our results constituted the first evidence for implicit regularization minimizing a notion of rank in non-linear neural networks. Subsequent works have demonstrated that an analogous phenomenon occurs in other types of neural networks as well [106, 213, 204, 65].

Motivated by the fact that notions of rank capture implicit regularization in certain non-linear neural networks, we empirically explore their potential as measures of complexity for explaining generalization over natural data. We find that it is possible to fit standard image recognition datasets with predictors of extremely low rank. This leads us to believe that notions of rank may pave way to explaining both implicit regularization in deep learning and properties of natural data translating it to generalization.

In terms of practical impact, based on our theory we develop an explicit regularization scheme for improving the performance of convolutional neural networks over tasks involving non-local interactions. Other research groups have also built upon our analyses of implicit rank minimization for designing practical deep learning systems [112, 102].

Expressiveness of Graph Neural Networks via Separation Rank (Part III)

In Chapter 5 (based on [180]), we extend the aforementioned connection between neural networks and tensor factorizations for studying the expressiveness of graph neural networks (GNNs) [89]. GNNs are widely used for modeling complex interactions between entities represented as vertices of a graph [58, 122, 73, 222, 218]. Yet, a formal characterization of their ability to model interactions is lacking. We address this gap by formalizing strength of interactions via *separation rank* [24, 49] — a measure widely used for quantifying entanglement in quantum physics. Through this notion of rank, we characterize the ability of certain GNNs to model interaction between a given subset of vertices and its complement, *i.e.* between the sides of a given partition of input vertices.

Our analysis reveals that the ability of a GNN to model interaction is primarily determined by the partition's *walk index* — a graph-theoretical characteristic defined by the number of walks originating from the boundary of the partition. This formalizes

conventional wisdom by which GNNs can model stronger interaction between regions of the input graph that are more interconnected. Experiments corroborate the result by demonstrating that GNNs perform better on tasks requiring interactions across partitions with a higher walk index.

As a practical application of our theory, we design an *edge sparsification* algorithm. Edge sparsification concerns removal of edges from a graph for reducing computational and/or memory costs, while attempting to maintain selected properties of the graph (cf. [21, 198, 87, 36, 186, 211, 138, 39]). In the context of GNNs, our interest lies in maintaining the prediction accuracy as the number of edges removed increases.

We propose an algorithm for removing edges, called *Walk Index Sparsification (WIS)*, which preserves the ability of a GNN to model interactions. WIS is simple, computationally efficient, and in our experiments has markedly outperformed alternative methods in terms of attainable prediction accuracies across edge sparsity levels. More broadly, it showcases the potential of improving GNNs by theoretically analyzing the interactions they can model via separation rank.

Included Work

To recap, this thesis is based on the contents of the following papers.

1. Chapter 1 is based on [177] (published at NeurIPS 2020).
2. Chapter 2 is based on [178] (published at ICML 2021).
3. Chapter 3 is based on [179] (published at ICML 2022).
4. Chapter 5 is based on [180] (published at NeurIPS 2023).

Excluded Work

Aside from the research included in the thesis, during my doctoral studies I led or contributed to several other works, listed below.

1. [3] (published at NeurIPS 2023) uses tools from quantum physics to characterize which properties of a data distribution make it suitable for locally connected neural networks.
2. [228] (published at ICLR 2024) studies the length generalization ability of Transformer neural networks.
3. [182] (published at ICLR 2024) identifies a fundamental vanishing gradients problem that occurs when finetuning language models via reinforcement learning.
4. [181] (published at ICML 2024) characterizes how the implicit regularization of policy gradient affects extrapolation to unseen initial states, focusing on linear quadratic control.

Part II

Generalization via Implicit Rank Minimization

Chapter 1

Implicit Regularization in Deep Learning May Not Be Explainable by Norms

This chapter covers the results of [177].

1.1 Background and Overview

As discussed in Part I, the ability of neural networks to generalize is widely believed to stem from an implicit regularization of gradient-based training towards predictors of low complexity. A prominent test-bed for studying implicit regularization in deep learning is *matrix completion* (cf. [81, 9]): given a randomly chosen subset of entries from an unknown matrix \mathbf{W}^* , the task is to recover the unseen entries. This may be viewed as a prediction problem, where each entry in \mathbf{W}^* stands for a data point: observed entries constitute the training set, and the average reconstruction error over the unobserved entries is the test error, quantifying generalization.

Fitting the observed entries in matrix completion is obviously an underdetermined problem with multiple solutions. However, an extensive body of work (see [55] for a survey) has shown that if \mathbf{W}^* is low-rank, certain technical assumptions (e.g. “incoherence”) are satisfied and sufficiently many entries are observed, then various algorithms can achieve approximate or even exact recovery. Of these, a well-known method based upon convex optimization finds the minimal nuclear norm¹ matrix among those fitting observations (see [34]).

One may try to solve matrix completion using shallow neural networks. A natural approach, *matrix factorization*, boils down to parameterizing the solution as a product of two matrices — $\mathbf{W} = \mathbf{W}_2\mathbf{W}_1$ — and optimizing the resulting (non-convex) objective for fitting observations. Formally, this can be viewed as training a depth two linear neural network. It is possible to explicitly constrain the rank of the produced solution by limiting the shared dimension of \mathbf{W}_1 and \mathbf{W}_2 . However, [81] showed that in practice, even when the rank is unconstrained, running gradient descent with small learning rate (step size) and initialization close to the origin (zero) tends to produce low-rank solutions, and thus allows accurate recovery if \mathbf{W}^* is low-rank. Accordingly, they conjectured that the implicit regularization in matrix factorization boils down to minimization of nuclear norm:

¹The *nuclear norm* of a matrix is the sum of its singular values.

Conjecture 1 (from [81], informally stated). *With small enough learning rate and initialization close enough to the origin, gradient descent on a full-dimensional matrix factorization converges to a minimal nuclear norm solution.*

In a subsequent work, [9] considered *deep matrix factorization*, obtained by adding depth to the setting studied in [81]. Namely, they considered solving matrix completion by training a depth L linear neural network, *i.e.* by running gradient descent on the parameterization $\mathbf{W} = \mathbf{W}_L \cdots \mathbf{W}_1$, with $L \in \mathbb{N}$ arbitrary (and the dimensions of $\{\mathbf{W}_l\}_{l=1}^L$ set such that rank is unconstrained). It was empirically shown that deeper matrix factorizations (larger L) yield more accurate recovery when \mathbf{W}^* is low-rank. Moreover, it was conjectured that the implicit regularization, for any depth $L \geq 2$, can *not* be described as minimization of a mathematical norm (or quasi-norm²).

Conjecture 2 (based on [9], informally stated). *Given a (shallow or deep) matrix factorization, for any norm (or quasi-norm) $\|\cdot\|$, there exists a set of observed entries with which small learning rate and initialization close to the origin can not ensure convergence of gradient descent to a minimal (in terms of $\|\cdot\|$) solution.*

Conjectures 1 and 2 contrast each other, and more broadly, represent opposing perspectives on the question of whether norms may be able to explain implicit regularization in deep learning. In this chapter, we resolve the tension between the two conjectures by affirming the latter. In particular, we prove that there exist natural matrix completion problems where fitting observations via gradient descent on a depth $L \geq 2$ matrix factorization leads — with probability 0.5 or more over (arbitrarily small) random initialization — *all* norms (and quasi-norms) to *grow towards infinity*, while the rank essentially decreases towards its minimum. This result is in fact stronger than the one suggested by Conjecture 2, in the sense that: (i) not only is each norm (or quasi-norm) disqualified by some setting, but there are actually settings that jointly disqualify all norms (and quasi-norms); and (ii) not only are norms (and quasi-norms) not necessarily minimized, but they can grow towards infinity. We corroborate the analysis with empirical demonstrations.

Our findings imply that, rather than viewing implicit regularization in (shallow or deep) matrix factorization as minimizing a norm, a potentially more useful interpretation is *minimization of rank*. As a step towards assessing the generality of this interpretation, we empirically explore an extension of matrix factorization to *tensor factorization*. Our experiments show that in analogy with matrix factorization, gradient descent on a tensor factorization tends to produce solutions with low rank, where rank is defined in the context of tensors (we will theoretically establish this tendency towards low rank in Chapter 2).

Similarly to how matrix factorization corresponds to a linear neural network whose input-output mapping is represented by a matrix, it is known (see [51]) that tensor factorization corresponds to a certain *non-linear convolutional* neural network whose input-output mapping is represented by a tensor. We thus obtain a second exemplar of a neural network architecture whose implicit regularization strives to lower a notion of rank for its input-output mapping. This indicates that the phenomenon may be general, and formalizing notions of rank for input-output mappings of contemporary models may be key to explaining generalization in deep learning. In Chapters 2 and 3

²A *quasi-norm* $\|\cdot\|$ on a vector space \mathcal{V} is a function from \mathcal{V} to $\mathbb{R}_{\geq 0}$ that satisfies the same axioms as a norm, except for the triangle inequality, which is replaced by the weaker requirement: there exists $c \geq 1$ such that for all $\mathbf{v}_1, \mathbf{v}_2 \in \mathcal{V}$ it holds that $\|\mathbf{v}_1 + \mathbf{v}_2\| \leq c \cdot (\|\mathbf{v}_1\| + \|\mathbf{v}_2\|)$.

we theoretically support this hypothesis by employing the equivalence between tensor factorizations and certain neural networks.

The remainder of the chapter is organized as follows. Section 1.2 presents the deep matrix factorization model. Section 1.3 delivers our analysis, showing that its implicit regularization can drive all norms to infinity. Lastly, experiments with both the analyzed setting and tensor factorization are given in Section 1.4.

1.2 Deep Matrix Factorization

Suppose we would like to complete a D -by- D' matrix based on a set of observations $\{y_{i,j} \in \mathbb{R}\}_{(i,j) \in \Omega}$, where $\Omega \subset \{1, 2, \dots, D\} \times \{1, 2, \dots, D'\}$. A standard (underdetermined) loss function for the task is:

$$\mathcal{L}_M : \mathbb{R}^{D \times D'} \rightarrow \mathbb{R}_{\geq 0} \quad , \quad \mathcal{L}_M(\mathbf{W}) = \frac{1}{2} \sum_{(i,j) \in \Omega} ((\mathbf{W})_{i,j} - y_{i,j})^2. \quad (1.1)$$

Employing a depth L matrix factorization, with hidden dimensions $D_1, \dots, D_{L-1} \in \mathbb{N}$, amounts to optimizing the *overparameterized objective*:

$$\phi_M(\mathbf{W}_1, \dots, \mathbf{W}_L) := \mathcal{L}_M(\mathbf{W}_M) = \frac{1}{2} \sum_{(i,j) \in \Omega} ((\mathbf{W}_M)_{i,j} - y_{i,j})^2, \quad (1.2)$$

where $\mathbf{W}_l \in \mathbb{R}^{D_l \times D_{l-1}}$, $l = 1, \dots, L$, with $D_L := D, D_0 := D'$, and:

$$\mathbf{W}_M := \mathbf{W}_L \cdots \mathbf{W}_1, \quad (1.3)$$

referred to as the *end matrix* of the factorization. Our interest lies on the implicit regularization of gradient descent, *i.e.* on the type of end matrices (Equation (1.3)) it will find when applied to the overparameterized objective (Equation (1.2)). Accordingly, and in line with prior work (*cf.* [81, 9]), we focus on the case in which the search space is unconstrained, meaning $\min\{D_l\}_{l=0}^L = \min\{D_0, D_L\}$ (rank is not limited by the parameterization).

As a theoretical surrogate for gradient descent with small learning rate and near-zero initialization, similarly to [81] and [9] (as well as other works analyzing linear neural networks, *e.g.* [188, 7, 129, 8]), we study *gradient flow* (gradient descent with infinitesimally small learning rate):³

$$\dot{\mathbf{W}}_l(t) := \frac{d}{dt} \mathbf{W}_l(t) = -\frac{\partial}{\partial \mathbf{W}_l} \phi(\mathbf{W}_1(t), \dots, \mathbf{W}_L(t)) \quad , \quad t \geq 0, \quad l = 1, \dots, L, \quad (1.4)$$

and assume *balancedness* at initialization, *i.e.*:

$$\mathbf{W}_{l+1}(0)^\top \mathbf{W}_{l+1}(0) = \mathbf{W}_l(0) \mathbf{W}_l(0)^\top \quad , \quad l = 1, \dots, L-1. \quad (1.5)$$

In particular, when considering random initialization, we assume that $\{\mathbf{W}_l(0)\}_{l=1}^L$ are drawn from a joint probability distribution by which Equation (1.5) holds almost surely. This is an idealization of standard random near-zero initializations, *e.g.* Xavier [75] and He [93], by which Equation (1.5) holds approximately with high

³A technical subtlety of optimization in continuous time is that in principle, it is possible to asymptote (diverge to infinity) after finite time. In such a case, the asymptote is regarded as the end of optimization, and time tending to infinity ($t \rightarrow \infty$) is to be interpreted as tending towards that point.

probability. The condition of balanced initialization (Equation (1.5)) played an important role in the analysis of [7], facilitating derivation of a differential equation governing the end matrix of a linear neural network (see Lemma 4 in Appendix A.3.2.1). It was shown in [7] empirically (and will be demonstrated again in Section 1.4) that there is an excellent match between the theoretical predictions of gradient flow with balanced initialization, and its practical realization via gradient descent with small learning rate and near-zero initialization. Other works (*e.g.*, [8, 109]) have supported this match theoretically, and we provided additional support in Appendix A of [177] by extending our theory to the case of unbalanced initialization (Equation (1.5) holding approximately).

Formally stated, Conjecture 1 from [81] treats the case $L = 2$, where the end matrix \mathbf{W}_M (Equation (1.3)) holds $\alpha \cdot \mathbf{W}_{init}$ at initialization, \mathbf{W}_{init} being a fixed arbitrary full-rank matrix, and α a varying positive scalar.⁴ Taking time to infinity ($t \rightarrow \infty$) and then initialization size to zero ($\alpha \rightarrow 0^+$), the conjecture postulates that if the limit end matrix $\overline{\mathbf{W}}_M := \lim_{\alpha \rightarrow 0^+} \lim_{t \rightarrow \infty} \mathbf{W}_M$ exists and is a global optimum for the loss $\mathcal{L}_M(\cdot)$ (Equation (1.1)), *i.e.* $\mathcal{L}_M(\overline{\mathbf{W}}_M) = 0$, then it will be a global optimum with minimal nuclear norm, meaning $\overline{\mathbf{W}}_M \in \operatorname{argmin}_{\mathbf{W}: \mathcal{L}_M(\mathbf{W})=0} \|\mathbf{W}\|_{nuclear}$.

In contrast to Conjecture 1, Conjecture 2 from [9] can be interpreted as saying that for any depth $L \geq 2$ and any norm or quasi-norm $\|\cdot\|$, there exist observations $\{y_{i,j}\}_{(i,j) \in \Omega}$ for which global optimization of loss ($\lim_{\alpha \rightarrow 0^+} \lim_{t \rightarrow \infty} \mathcal{L}_M(\mathbf{W}_M) = 0$) does not imply minimization of $\|\cdot\|$ (*i.e.* we may have $\lim_{\alpha \rightarrow 0^+} \lim_{t \rightarrow \infty} \|\mathbf{W}_M\| \neq \min_{\mathbf{W}: \mathcal{L}_M(\mathbf{W})=0} \|\mathbf{W}\|$). Due to technical subtleties (for example the requirement of Conjecture 1 that a double limit of the end matrix with respect to time and initialization size exists), Conjectures 1 and 2 are not necessarily contradictory. However, they are in direct opposition in terms of the stances they represent — one supports the prospect of norms being able to explain implicit regularization in matrix factorization, and the other does not. The current chapter seeks a resolution.

1.3 Implicit Regularization Can Drive All Norms to Infinity

In this section we prove that for matrix factorization of depth $L \geq 2$, there exist observations $\{y_{i,j}\}_{(i,j) \in \Omega}$ with which optimizing the overparameterized objective (Equation (1.2)) via gradient flow (Equations (1.4) and (1.5)) leads — with probability 0.5 or more over random (“symmetric”) initialization — *all* norms and quasi-norms of the end matrix (Equation (1.3)) to *grow towards infinity*, while its rank essentially decreases towards minimum. By this we not only affirm Conjecture 2, but in fact go beyond it in the following sense: (i) the conjecture allows chosen observations to depend on the norm or quasi-norm under consideration, while we show that the same set of observations can apply jointly to all norms and quasi-norms; and (ii) the conjecture requires norms and quasi-norms to be larger than minimal, while we establish growth towards infinity.

For simplicity of presentation, the current section delivers our construction and analysis in the setting $D = D' = 2$ (*i.e.* 2-by-2 matrix completion) — extension to different dimensions is straightforward (see Appendix A.1). We begin (Section 1.3.1)

⁴The formal statement in [81] applies to symmetric matrix factorization and positive definite \mathbf{W}_{init} , but it is claimed thereafter that affirming the conjecture would imply the same for the asymmetric setting considered here. We also note that the conjecture is stated in the context of matrix sensing, thus in particular applies to matrix completion (a special case).

by introducing our chosen observations $\{y_{i,j}\}_{(i,j)\in\Omega}$ and discussing their properties. Subsequently (Section 1.3.2), we show that with these observations, decreasing loss often increases all norms and quasi-norms while lowering rank. Minimization of loss is treated thereafter (Section 1.3.3). Finally (Section 1.3.4), robustness of our construction to perturbations is established.

1.3.1 A Simple Matrix Completion Problem

Consider the problem of completing a 2-by-2 matrix based on the following observations:

$$\Omega = \{(1,2), (2,1), (2,2)\} \quad , \quad y_{1,2} = 1, \quad y_{2,1} = 1, \quad y_{2,2} = 0. \quad (1.6)$$

The solution set for this problem (*i.e.* the set of matrices obtaining zero loss) is:

$$\mathcal{S} = \{\mathbf{W} \in \mathbb{R}^{2 \times 2} : (\mathbf{W})_{1,2} = 1, (\mathbf{W})_{2,1} = 1, (\mathbf{W})_{2,2} = 0\}. \quad (1.7)$$

Proposition 1 below states that minimizing a norm or quasi-norm along $\mathbf{W} \in \mathcal{S}$ requires confining $(\mathbf{W})_{1,1}$ to a bounded interval, which for Schatten- p (quasi-)norms (in particular for nuclear, Frobenius, and spectral norms)⁵ is simply the singleton $\{0\}$.

Proposition 1. *For any norm or quasi-norm over matrices $\|\cdot\|$ and any $\epsilon > 0$, there exists a bounded interval $I_{\|\cdot\|,\epsilon} \subset \mathbb{R}$ such that if $\mathbf{W} \in \mathcal{S}$ is an ϵ -minimizer of $\|\cdot\|$ (*i.e.* $\|\mathbf{W}\| \leq \inf_{\mathbf{W}' \in \mathcal{S}} \|\mathbf{W}'\| + \epsilon$) then necessarily $(\mathbf{W})_{1,1} \in I_{\|\cdot\|,\epsilon}$. If $\|\cdot\|$ is a Schatten- p (quasi-)norm, then in addition $\mathbf{W} \in \mathcal{S}$ minimizes $\|\cdot\|$ (*i.e.* $\|\mathbf{W}\| = \inf_{\mathbf{W}' \in \mathcal{S}} \|\mathbf{W}'\|$) if and only if $(\mathbf{W})_{1,1} = 0$.*

Proof sketch (proof in Appendix A.3.3). The (weakened) triangle inequality allows lower bounding $\|\cdot\|$ by $|(\mathbf{W})_{1,1}|$ (up to multiplicative and additive constants). Thus, the set of $(\mathbf{W})_{1,1}$ values corresponding to ϵ -minimizers must be bounded. If $\|\cdot\|$ is a Schatten- p (quasi-)norm, a straightforward analysis shows it is monotonically increasing with respect to $|(\mathbf{W})_{1,1}|$, implying it is minimized if and only if $(\mathbf{W})_{1,1} = 0$. \square

In addition to norms and quasi-norms, we are also interested in the evolution of rank throughout optimization of a deep matrix factorization. More specifically, we are interested in the prospect of rank being implicitly minimized, as demonstrated empirically in [81, 9]. The discrete nature of rank renders its direct analysis unfavorable from a dynamical perspective (the rank of a matrix implies little about its proximity to low-rank), thus we consider the following surrogate measures: (i) *effective rank* (Definition 1 below; from [185]) — a continuous extension of rank used for numerical analyses; and (ii) *distance from infimal rank* (Definition 2 below) — (Frobenius) distance from the minimal rank that a given set of matrices may approach.

According to Proposition 2 below, these measures independently imply that, although all solutions to our matrix completion problem — *i.e.* all $\mathbf{W} \in \mathcal{S}$ (see Equation (1.7)) — have rank 2, it is possible to essentially minimize the rank to 1 by taking $|(\mathbf{W})_{1,1}| \rightarrow \infty$. Recalling Proposition 1, we conclude that in our setting, there is a direct contradiction between minimizing norms or quasi-norms and minimizing rank — the former requires confinement to some bounded interval, whereas the latter demands divergence towards infinity. This is the critical feature of our construction, allowing us to deem

⁵For $p \in (0, \infty]$, the Schatten- p (quasi-)norm of a matrix $\mathbf{W} \in \mathbb{R}^{D \times D'}$ with singular values $\{\sigma_r(\mathbf{W})\}_{r=1}^{\min\{D,D'\}}$ is defined as $(\sum_{r=1}^{\min\{D,D'\}} \sigma_r^p(\mathbf{W}))^{1/p}$ if $p < \infty$ and as $\max\{\sigma_r(\mathbf{W})\}_{r=1}^{\min\{D,D'\}}$ if $p = \infty$. It is a norm if $p \geq 1$ and a quasi-norm if $p < 1$. Notable special cases are nuclear (trace), Frobenius and spectral norms, corresponding to $p = 1, 2$, and ∞ , respectively.

whether the implicit regularization in deep matrix factorization favors norms (or quasi-norms) over rank or vice versa.

Definition 1 (from [185]). The *effective rank* of a matrix $0 \neq \mathbf{W} \in \mathbb{R}^{D \times D'}$ with singular values $\{\sigma_r(\mathbf{W})\}_{r=1}^{\min\{D, D'\}}$ is defined to be:

$$\text{erank}(\mathbf{W}) := \exp\left(H\left(\rho_1(\mathbf{W}), \dots, \rho_{\min\{D, D'\}}(\mathbf{W})\right)\right),$$

where $\{\rho_r(\mathbf{W}) := \sigma_r(\mathbf{W}) / \sum_{r'=1}^{\min\{D, D'\}} \sigma_{r'}(\mathbf{W})\}_{r=1}^{\min\{D, D'\}}$ is a distribution induced by the singular values, and $H(\rho_1(\mathbf{W}), \dots, \rho_{\min\{D, D'\}}(\mathbf{W})) := -\sum_{r=1}^{\min\{D, D'\}} \rho_r(\mathbf{W}) \cdot \ln \rho_r(\mathbf{W})$ is its Shannon entropy (by convention $0 \cdot \ln 0 = 0$).

Definition 2. We denote by $\mathcal{D}_{\text{Fro}}(\mathcal{S}, \mathcal{S}') := \inf\{\|\mathbf{W} - \mathbf{W}'\|_{\text{Fro}} : \mathbf{W} \in \mathcal{S}, \mathbf{W}' \in \mathcal{S}'\}$ the (Frobenius) distance between $\mathcal{S}, \mathcal{S}' \subset \mathbb{R}^{D \times D'}$, by $\mathcal{D}_{\text{Fro}}(\mathbf{W}, \mathcal{S}') := \inf\{\|\mathbf{W} - \mathbf{W}'\|_{\text{Fro}} : \mathbf{W}' \in \mathcal{S}'\}$ the distance between $\mathbf{W} \in \mathbb{R}^{D \times D'}$ and \mathcal{S}' , and by $\mathcal{M}_R := \{\mathbf{W} \in \mathbb{R}^{D \times D'} : \text{rank}(\mathbf{W}) \leq R\}$, for $R = 0, \dots, \min\{D, D'\}$, the set of matrices with rank R or less. The *infimal rank* of the set \mathcal{S} , denoted $\text{irank}(\mathcal{S})$, is defined to be the minimal R such that $\mathcal{D}_{\text{Fro}}(\mathcal{S}, \mathcal{M}_R) = 0$. The *distance of a matrix $\mathbf{W} \in \mathbb{R}^{D \times D'}$ from the infimal rank of \mathcal{S}* is defined to be $\mathcal{D}_{\text{Fro}}(\mathbf{W}, \mathcal{M}_{\text{irank}(\mathcal{S})})$.

Proposition 2. The *effective rank* (Definition 1) takes the values $(1, 2]$ along \mathcal{S} (Equation (1.7)). For $\mathbf{W} \in \mathcal{S}$, it is maximized when $(\mathbf{W})_{1,1} = 0$, and monotonically decreases to 1 as $|(\mathbf{W})_{1,1}|$ grows. Correspondingly, the *infimal rank* (Definition 2) of \mathcal{S} is 1, and the *distance of $\mathbf{W} \in \mathcal{S}$ from this infimal rank* is maximized when $(\mathbf{W})_{1,1} = 0$, monotonically decreasing to 0 as $|(\mathbf{W})_{1,1}|$ grows.

Proof sketch (proof in Appendix A.3.4). Analyzing the singular values of $\mathbf{W} \in \mathcal{S}$ — $\sigma_1(\mathbf{W}) \geq \sigma_2(\mathbf{W}) \geq 0$ — reveals that: (i) $\sigma_1(\mathbf{W})$ attains a minimal value of 1 when $(\mathbf{W})_{1,1} = 0$, monotonically increasing to ∞ as $|(\mathbf{W})_{1,1}|$ grows; and (ii) $\sigma_2(\mathbf{W})$ attains a maximal value of 1 when $(\mathbf{W})_{1,1} = 0$, monotonically decreasing to 0 as $|(\mathbf{W})_{1,1}|$ grows. The results for effective rank, infimal rank and distance from infimal rank readily follow from this characterization. \square

1.3.2 Decreasing Loss Increases Norms

Consider the process of solving our matrix completion problem (Section 1.3.1) with gradient flow over a depth $L \geq 2$ matrix factorization (Section 1.2). Theorem 1 below states that if the end matrix (Equation (1.3)) has positive determinant at initialization, lowering the loss leads norms and quasi-norms to increase, while the rank essentially decreases.

Theorem 1. Suppose we complete the observations in Equation (1.6) by employing a depth $L \geq 2$ matrix factorization, i.e. by minimizing the overparameterized objective (Equation (1.2)) via gradient flow (Equations (1.4) and (1.5)). Denote by $\mathbf{W}_M(t)$ the end matrix (Equation (1.3)) at time $t \geq 0$ of optimization, and by $\mathcal{L}_M(t) := \mathcal{L}_M(\mathbf{W}_M(t))$ the corresponding loss (Equation (1.1)). Assume that $\det(\mathbf{W}_M(0)) > 0$. Then, for any norm or quasi-norm over matrices $\|\cdot\|$:

$$\|\mathbf{W}_M(t)\| \geq a_{\|\cdot\|} \cdot \frac{1}{\sqrt{\mathcal{L}_M(t)}} - b_{\|\cdot\|} \quad , \quad t \geq 0, \quad (1.8)$$

where $b_{\|\cdot\|} := \max\{\sqrt{2}a_{\|\cdot\|}, 8c_{\|\cdot\|}^2 \max_{i,j \in \{1,2\}} \|\mathbf{e}_i \mathbf{e}_j^\top\|\}$, $a_{\|\cdot\|} := \|\mathbf{e}_1 \mathbf{e}_1^\top\| / (\sqrt{2}c_{\|\cdot\|})$, the vectors $\mathbf{e}_1, \mathbf{e}_2 \in \mathbb{R}^2$ form the standard basis, and $c_{\|\cdot\|} \geq 1$ is a constant with which $\|\cdot\|$

satisfies the weakened triangle inequality (see Footnote 2). On the other hand:

$$\text{erank}(\mathbf{W}_M(t)) \leq \inf_{\mathbf{W}' \in \mathcal{S}} \text{erank}(\mathbf{W}') + \frac{2\sqrt{12}}{\ln(2)} \cdot \sqrt{\mathcal{L}_M(t)} \quad , \quad t \geq 0, \quad (1.9)$$

$$\mathcal{D}_{\text{Fro}}(\mathbf{W}_M(t), \mathcal{M}_{\text{irank}(\mathcal{S})}) \leq 3\sqrt{2} \cdot \sqrt{\mathcal{L}_M(t)} \quad , \quad t \geq 0, \quad (1.10)$$

where $\text{erank}(\cdot)$ stands for effective rank (Definition 1), and $D(\cdot, \mathcal{M}_{\text{irank}(\mathcal{S})})$ represents distance from the infimal rank (Definition 2) of the solution set \mathcal{S} (Equation (1.7)).

Proof sketch (proof in Appendix A.3.5). Using a dynamical characterization for the singular values of the end matrix, developed in [9] (restated in Appendix A.3.2.1 as Lemma 5), we show that the latter's determinant does not change sign, *i.e.* it remains positive. This allows us to lower bound $|(\mathbf{W}_M)_{1,1}(t)|$ by $1/\sqrt{\mathcal{L}_M(t)}$ (up to multiplicative and additive constants). Relating $|(\mathbf{W}_M)_{1,1}(t)|$ to (quasi-)norms, effective rank and distance from infimal rank then leads to the desired bounds. \square

An immediate consequence of Theorem 1 is that, if the end matrix (Equation (1.3)) has positive determinant at initialization, convergence to zero loss leads *all* norms and quasi-norms to *grow to infinity*, while the rank is essentially minimized. This is formalized in Corollary 1 below.

Corollary 1. *Under the conditions of Theorem 1, if the loss is globally optimized, *i.e.* if $\lim_{t \rightarrow \infty} \mathcal{L}_M(t) = 0$, then for any norm or quasi-norm over matrices $\|\cdot\|$:*

$$\lim_{t \rightarrow \infty} \|\mathbf{W}_M(t)\| = \infty,$$

where $\mathbf{W}_M(t)$ is the end matrix of the deep factorization (Equation (1.3)) at time t of optimization. On the other hand:

$$\lim_{t \rightarrow \infty} \text{erank}(\mathbf{W}_M(t)) = \inf_{\mathbf{W}' \in \mathcal{S}} \text{erank}(\mathbf{W}') \quad , \quad \lim_{t \rightarrow \infty} \mathcal{D}_{\text{Fro}}(\mathbf{W}_M(t), \mathcal{M}_{\text{irank}(\mathcal{S})}) = 0,$$

where $\text{erank}(\cdot)$ stands for effective rank (Definition 1), and $D(\cdot, \mathcal{M}_{\text{irank}(\mathcal{S})})$ represents distance from the infimal rank (Definition 2) of the solution set \mathcal{S} (Equation (1.7)).

Proof. Taking the limit $\mathcal{L}_M(t) \rightarrow 0$ in the bounds given by Theorem 1 establishes the results. \square

Theorem 1 and Corollary 1 imply that in our setting (Section 1.3.1), where minimizing norms (or quasi-norms) and minimizing rank contradict each other, the implicit regularization of deep matrix factorization is willing to completely give up on the former in favor of the latter, at least on the condition that the end matrix (Equation (1.3)) has positive determinant at initialization. How probable is this condition? By Proposition 3 below, it holds with probability 0.5 if the end matrix is initialized by any one of a wide array of common distributions, including matrix Gaussian distribution with zero mean and independent entries, and a product of such. We note that rescaling (multiplying by $\alpha > 0$) initialization does not change the sign of end matrix's determinant, therefore as postulated by Conjecture 2, initialization close to the origin does *not* ensure convergence to solution with minimal norm or quasi-norm.

Proposition 3. *If $\mathbf{W} \in \mathbb{R}^{D \times D}$ is a random matrix whose entries are drawn independently from continuous distributions, each symmetric about the origin, then $\Pr(\det(\mathbf{W}) > 0) = \Pr(\det(\mathbf{W}) < 0) = 0.5$. Furthermore, for $L \in \mathbb{N}$, if $\mathbf{W}_1, \dots, \mathbf{W}_L \in \mathbb{R}^{D \times D}$ are random matrices drawn independently from continuous distributions, and there exists $l \in \{1, \dots, L\}$*

with $\Pr(\det(\mathbf{W}_l) > 0) = 0.5$, then $\Pr(\det(\mathbf{W}_L \cdots \mathbf{W}_1) > 0) = \Pr(\det(\mathbf{W}_L \cdots \mathbf{W}_1) < 0) = 0.5$.

Proof sketch (proof in Appendix A.3.6). Multiplying a row of \mathbf{W} by -1 keeps its distribution intact while flipping the sign of its determinant. This implies $\Pr(\det(\mathbf{W}) > 0) = \Pr(\det(\mathbf{W}) < 0)$. The first result then follows from the fact that a matrix drawn from a continuous distribution is almost surely non-singular. The second result is an outcome of the same fact, as well as the multiplicativity of determinant and the law of total probability. \square

1.3.3 Convergence to Zero Loss

It is customary in the theory of deep learning (*cf.* [81, 83, 9]) to distinguish between implicit regularization — which concerns the type of solutions found in training — and the complementary question of whether training loss is globally optimized. We supplement our implicit regularization analysis (Section 1.3.2) by addressing this complementary question in two ways: (i) in Section 1.4 we empirically demonstrate that on the matrix completion problem we analyze (Section 1.3.1), gradient descent over deep matrix factorizations (Section 1.2) indeed drives training loss towards global optimum, *i.e.* towards zero; and (ii) in Proposition 4 below we theoretically establish convergence to zero loss for the special case of depth 2 and scaled identity initialization (treatment of additional depths and initialization schemes is left for future work). We note that when combined with Corollary 1, Proposition 4 affirms that in the latter special case, all norms and quasi-norms indeed grow to infinity while rank is essentially minimized.⁶

Proposition 4. *Consider the setting of Theorem 1 in the special case of depth $L = 2$ and initial end matrix (Equation (1.3)) $\mathbf{W}_M(0) = \alpha \cdot \mathbf{I}$, where \mathbf{I} stands for the identity matrix and $\alpha \in (0, 1]$. Under these conditions $\lim_{t \rightarrow \infty} \mathcal{L}_M(t) = 0$, *i.e.* the training loss is globally optimized.*

Proof sketch (proof in Appendix A.3.7). We first establish that the end matrix is positive definite for all t . This simplifies a dynamical characterization from [7] (restated as Lemma 4 in Appendix A.3.2), yielding lucid differential equations governing the entries of the end matrix. Careful analysis of these equations then completes the proof. \square

1.3.4 Robustness to Perturbations

Our analysis (Section 1.3.2) has shown that when applying a deep matrix factorization (Section 1.2) to the matrix completion problem defined in Section 1.3.1, if the end matrix (Equation (1.3)) has positive determinant at initialization — a condition that holds with probability 0.5 under the wide variety of random distributions specified by Proposition 3 — then the implicit regularization drives *all* norms and quasi-norms *towards infinity*, while rank is essentially driven towards its minimum. A natural question is how common this phenomenon is, and in particular, to what extent does it persist if the observed entries we defined (Equation (1.6)) are perturbed.

⁶Notice that under (positively) scaled identity initialization the determinant of the end matrix (Equation (1.3)) is positive, as required by Corollary 1.

Theorem 2 below generalizes Theorem 1 (from Section 1.3.2) to the case of arbitrary non-zero values for the off-diagonal observations $y_{1,2}, y_{2,1}$, and an arbitrary value for the diagonal observation $y_{2,2}$. In this generalization, the assumption (from Theorem 1) of the end matrix's determinant at initialization being positive is modified to an assumption of it having the same sign as $y_{1,2} \cdot y_{2,1}$ (the probability of which is also 0.5 under the random distributions covered by Proposition 3). Conditioned on the modified assumption, the smaller $|y_{2,2}|$ is compared to $|y_{1,2} \cdot y_{2,1}|$, the higher the implicit regularization is guaranteed to drive norms and quasi-norms, and the lower it is guaranteed to essentially drive the rank. Two immediate implications of Theorem 2 are: (i) if the diagonal observation is unperturbed ($y_{2,2} = 0$), the off-diagonal ones ($y_{1,2}, y_{2,1}$) can take on *any* non-zero values, and the phenomenon of implicit regularization driving norms and quasi-norms towards infinity (while essentially driving rank towards its minimum) will persist; and (ii) this phenomenon gracefully recedes as the diagonal observation is perturbed away from zero. We note that Theorem 2 applies even if the unobserved entry is repositioned, thus our construction is robust not only to perturbations in observed values, but also to an arbitrary change in the observed locations. See Appendix A.2.1 for empirical demonstrations.

Theorem 2. Consider the setting of Theorem 1 subject to the following changes: (i) the observations from Equation (1.6) are generalized to:

$$\Omega = \{(1,2), (2,1), (2,2)\} \quad , \quad y_{1,2} = z \in \mathbb{R} \setminus \{0\} \quad , \quad y_{2,1} = z' \in \mathbb{R} \setminus \{0\} \quad , \quad y_{2,2} = \epsilon \in \mathbb{R} \quad , \quad (1.11)$$

leading to the following solution set in place of that from Equation (1.7):

$$\tilde{\mathcal{S}} = \{\mathbf{W} \in \mathbb{R}^{2,2} : (\mathbf{W})_{1,2} = z, (\mathbf{W})_{2,1} = z', (\mathbf{W})_{2,2} = \epsilon\} ; \quad (1.12)$$

and (ii) the assumption $\det(\mathbf{W}_M(0)) > 0$ is generalized to $\text{sign}(\det(\mathbf{W}_M(0))) = \text{sign}(z \cdot z')$, where $\mathbf{W}_M(t)$ denotes the end matrix (Equation (1.3)) at time $t \geq 0$ of optimization. Under these conditions, for any norm or quasi-norm over matrices $\|\cdot\|$:

$$\|\mathbf{W}_M(t)\| \geq a_{\|\cdot\|} \cdot \frac{|z| \cdot |z'|}{|\epsilon| + \sqrt{2\mathcal{L}_M(t)}} - b_{\|\cdot\|} \quad , \quad t \geq 0, \quad (1.13)$$

where $b_{\|\cdot\|} := \max\{a_{\|\cdot\|} \cdot |z| \cdot |z'| / (|\epsilon| + \min\{|z|, |z'|\})\}$, $8c_{\|\cdot\|}^2 \max\{|z|, |z'|, |\epsilon|\} \max_{i,j \in \{1,2\}} \|\mathbf{e}_i \mathbf{e}_j^\top\|$, $a_{\|\cdot\|} := \|\mathbf{e}_1 \mathbf{e}_1^\top\| / c_{\|\cdot\|}$, the vectors $\mathbf{e}_1, \mathbf{e}_2 \in \mathbb{R}^2$ form the standard basis, and $c_{\|\cdot\|} \geq 1$ is a constant with which $\|\cdot\|$ satisfies the weakened triangle inequality (see Footnote 2). On the other hand:

$$\text{erank}(\mathbf{W}_M(t)) \leq \inf_{\mathbf{W}' \in \tilde{\mathcal{S}}} \text{erank}(\mathbf{W}') + \frac{16}{\min\{|z|, |z'|\}} \left(|\epsilon| + \sqrt{2\mathcal{L}_M(t)} \right) \quad , \quad t \geq 0, \quad (1.14)$$

$$\mathcal{D}_{\text{Fro}}(\mathbf{W}_M(t), \mathcal{M}_{\text{irank}(\tilde{\mathcal{S}})}) \leq 4|\epsilon| + \left(4 + \frac{\sqrt{|z| \cdot |z'|}}{\min\{|z|, |z'|\}} \right) \sqrt{2\mathcal{L}_M(t)} \quad , \quad t \geq 0, \quad (1.15)$$

where $\text{erank}(\cdot)$ stands for effective rank (Definition 1), and $D(\cdot, \mathcal{M}_{\text{irank}(\tilde{\mathcal{S}})})$ represents distance from the infimal rank (Definition 2) of the solution set $\tilde{\mathcal{S}}$. Moreover, Equations (1.13), (1.14) and (1.15) hold even if the above setting is further generalized as follows: (i) the unobserved entry resides in location $(i, j) \in \{1, 2\} \times \{1, 2\}$, with $z, z' \in \mathbb{R} \setminus \{0\}$ observed in the adjacent locations and $\epsilon \in \mathbb{R}$ in the diagonally-opposite one; and (ii) the sign of $\det(\mathbf{W}_M(0))$ is equal to that of $z \cdot z'$ if $i = j$, and opposite to it otherwise.

Proof sketch (proof in Appendix A.3.8). The proof follows a line similar to that of Theorem 1, with slightly more involved derivations. \square

Disqualifying implicit minimization of norms in finite settings. Theorem 1 (in Section 1.3.2), which applies to our original (unperturbed) matrix completion problem (Section 1.3.1), has shown that the implicit regularization of deep matrix factorization does not minimize norms or quasi-norms, by establishing lower bounds (Equation (1.8) with $\|\cdot\|$ ranging over all possible norms and quasi-norms) that tend to infinity as the training loss $\mathcal{L}_M(t)$ converges to zero. The more general Theorem 2 allows disqualifying implicit minimization of norms or quasi-norms without requiring divergence to infinity. To see this, consider the lower bounds it establishes (Equation (1.13) with $\|\cdot\|$ ranging over all norms and quasi-norms), and in particular their limits as $\mathcal{L}_M(t) \rightarrow 0$. If the observed value ϵ is different from zero, these limits are all finite. Moreover, given a particular norm or quasi-norm $\|\cdot\|$, we may choose ϵ different from zero, yet small enough such that the lower bound for $\|\cdot\|$ has limit arbitrarily larger than the infimum of $\|\cdot\|$ over the solution set.

1.4 Experiments

This section presents our empirical evaluations. We begin in Section 1.4.1 with deep matrix factorization (Section 1.2) applied to the settings we analyzed (Section 1.3). Then, we turn to Section 1.4.2 and experiment with an extension to tensor (multi-dimensional array) factorization. For brevity, many details behind our implementation, as well as some experiments, are deferred to Appendix A.2.

1.4.1 Analyzed Settings

In [81], Gunasekar *et al.* experimented with matrix factorization, arriving at Conjecture 1. In the following work [9], Arora *et al.* empirically evaluated additional settings, ultimately arguing against Conjecture 1, and raising Conjecture 2. Our analysis (Section 1.3) affirmed Conjecture 2, by providing a setting in which gradient descent (with infinitesimally small learning rate and initialization arbitrarily close to the origin) over (shallow or deep) matrix factorization provably drives *all* norms (and quasi-norms) *towards infinity*. Specifically, we established that running gradient descent on the overparameterized matrix completion objective in Equation (1.2), where the observed entries are those defined in Equation (1.6), leads the unobserved entry to diverge to infinity as loss converges to zero. Figure 1.1 demonstrates this phenomenon empirically. Figures A.1 and A.2 in Appendix A.2.1 extend the experiment by considering, respectively: different matrix dimensions (see Appendix A.1); and perturbations and repositionings applied to observations (*cf.* Section 1.3.4). The figures confirm that the inability of norms (and quasi-norms) to explain implicit regularization in matrix factorization translates from theory to practice.

1.4.2 From Matrix to Tensor Factorization

At the heart of our analysis (Section 1.3) lies a matrix completion problem whose solution set (Equation (1.7)) entails a direct contradiction between minimizing norms (or quasi-norms) and minimizing rank. We have shown that on this problem, gradient descent over (shallow or deep) matrix factorization is willing to completely give up on the former in favor of the latter. This suggests that, rather than viewing implicit regularization in matrix factorization through the lens of norms (or quasi-norms), a

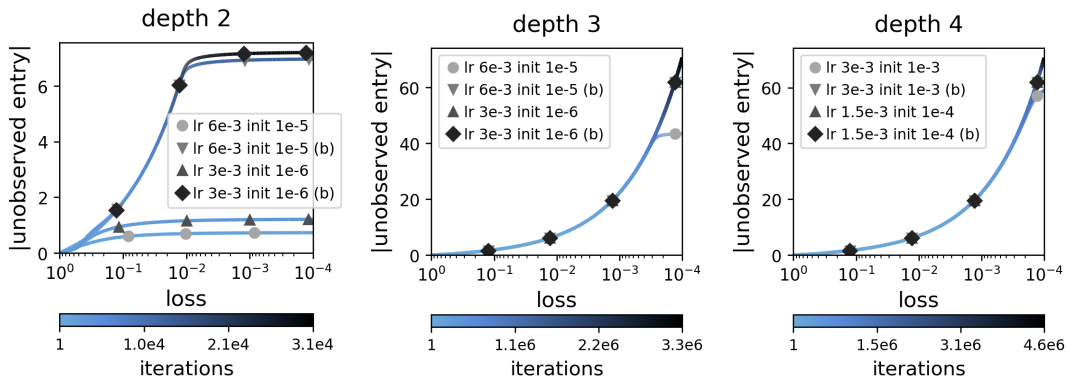


Figure 1.1: Implicit regularization in matrix factorization can drive *all* norms (and quasi-norms) *towards infinity*. For the matrix completion problem defined in Section 1.3.1, our analysis (Section 1.3.2) implies that with small learning rate and initialization close to the origin, when the product matrix (Equation (1.3)) is initialized to have positive determinant, gradient descent on a matrix factorization leads absolute value of unobserved entry to increase (which in turn means norms and quasi-norms increase) as loss decreases, *i.e.* as observations are fit. This is demonstrated in the plots above, which for representative runs, show absolute value of unobserved entry as a function of the loss (Equation 1.1), with iteration number encoded by color. Each plot corresponds to a different depth for the matrix factorization, and presents runs with varying configurations of learning rate and initialization (abbreviated as “lr” and “init”, respectively). Both balanced (Equation 1.5) and unbalanced (layer-wise independent) random initializations were evaluated (former is marked by “(b)”). Independently for each depth, runs were iteratively carried out, with both learning rate and standard deviation for initialization decreased after each run, until the point where further reduction did not yield a noticeable change (presented runs are those from the last iterations of this process). Notice that depth, balancedness, and small learning rate and initialization, all contribute to the examined effect (absolute value of unobserved entry increasing as loss decreases), with the transition from depth 2 to 3 or more being most significant. Notice also that all runs initially follow the same curve, differing from one another in the point at which they divert (enter a phase where examined effect is lesser). A complete investigation of these phenomena is left for future work. For further implementation details, and similar experiments with different matrix dimensions, as well as perturbed and repositioned observations, see Appendix A.2.

potentially more useful interpretation is *minimization of rank*. Indeed, while global minimization of rank is in the worst case computationally hard (*cf.* [184]), it has been shown in [9] (theoretically as well as empirically) that the dynamics of gradient descent over matrix factorization promote sparsity of singular values, and thus they may be interpreted as searching for low rank locally. As a step towards assessing the generality of this interpretation, we empirically explore an extension of matrix factorization to *tensor factorization*.⁷

In the context of matrix completion, (depth 2) matrix factorization amounts to optimizing the loss in Equation (1.1) by applying gradient descent to the parameterization $\mathbf{W} = \sum_{r=1}^R \mathbf{w}_r \otimes \mathbf{w}'_r$, where $R \in \mathbb{N}$ is a predetermined constant, \otimes stands for tensor product (*i.e.* outer product), and $\{\mathbf{w}_r \in \mathbb{R}^D\}_{r=1}^R, \{\mathbf{w}'_r \in \mathbb{R}^{D'}\}_{r=1}^R$ are the optimized parameters.⁸ The minimal R required for this parameterization to be able to express a given $\bar{\mathbf{W}} \in \mathbb{R}^{D \times D'}$ is precisely the latter’s rank. Implicit regularization towards low rank means that even when R is large enough for expressing any matrix (*i.e.* $R \geq \min\{D, D'\}$), solutions expressible (or approximable) with small R tend to be learned.

⁷There exist many types of tensor factorizations (*cf.* [124, 85]). We treat here the classic and most basic one, known as *CANDECOMP/PARAFAC (CP)*.

⁸To see that this parameterization is equivalent to the usual form $\mathbf{W} = \mathbf{W}_2 \mathbf{W}_1$, simply view R as the dimension shared between \mathbf{W}_1 and \mathbf{W}_2 , $\{\mathbf{w}_r\}_{r=1}^R$ as the columns of \mathbf{W}_2 , and $\{\mathbf{w}'_r\}_{r=1}^R$ as the rows of \mathbf{W}_1 .

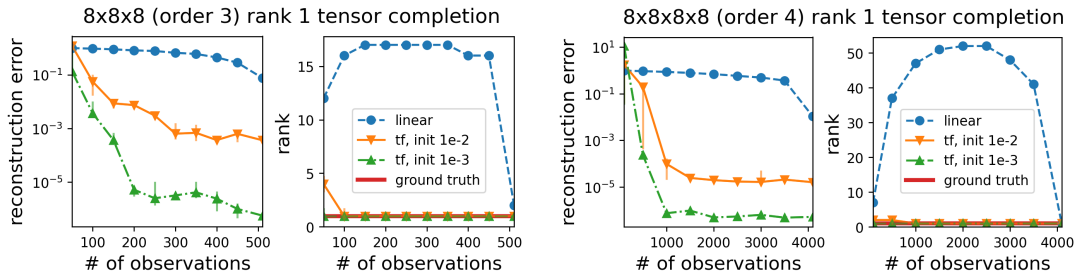


Figure 1.2: Gradient descent over tensor factorization exhibits an implicit regularization towards low tensor rank. Plots above report results of tensor completion experiments, comparing: (i) minimization of loss (Equation (1.16)) via gradient descent over tensor factorization (Equation (1.17)) with R large enough for expressing any tensor) starting from (small) random initialization (method is abbreviated as “tf”); against (ii) trivial baseline that matches observations while holding zeros in unobserved locations — equivalent to minimizing loss via gradient descent over linear parameterization (*i.e.* directly over \mathcal{W}) starting from zero initialization (hence this method is referred to as “linear”). Each pair of plots corresponds to a randomly drawn low-rank ground truth tensor, from which multiple sets of observations varying in size were randomly chosen. The ground truth tensors corresponding to left and right pairs both have rank 1 (for results obtained with additional ground truth ranks see Figure A.3 in Appendix A.2.1), with sizes 8-by-8-by-8 (order 3) and 8-by-8-by-8-by-8 (order 4) respectively. The plots in each pair show reconstruction errors (Frobenius distance from ground truth) and ranks (numerically estimated) of final solutions as a function of the number of observations in the task, with error bars spanning interquartile range (25th to 75th percentiles) over multiple trials (differing in random seed for initialization), and markers showing median. For gradient descent over tensor factorization, we employed an adaptive learning rate scheme to reduce run times (see Appendix A.2.2 for details), and iteratively ran with decreasing standard deviation for initialization, until the point at which further reduction did not yield a noticeable change (presented results are those from the last iterations of this process, with the corresponding standard deviations annotated by “init”). Notice that gradient descent over tensor factorization indeed exhibits an implicit tendency towards low rank (leading to accurate reconstruction of low-rank ground truth tensors), and that this tendency is stronger with smaller initialization. For further details and experiments see Appendix A.2.

A generalization of the above is obtained by switching from matrices (tensors of order 2) to tensors of arbitrary order $N \in \mathbb{N}$. This gives rise to a *tensor completion* problem, with corresponding loss:

$$\mathcal{L}_T : \mathbb{R}^{D_1 \times \dots \times D_N} \rightarrow \mathbb{R}_{\geq 0} \quad , \quad \mathcal{L}_T(\mathcal{W}) = \frac{1}{2} \sum_{(i_1, \dots, i_N) \in \Omega} ((\mathcal{W})_{i_1, \dots, i_N} - y_{i_1, \dots, i_N})^2, \quad (1.16)$$

where $\{y_{i_1, \dots, i_N} \in \mathbb{R}\}_{(i_1, \dots, i_N) \in \Omega}$, $\Omega \subset \{1, \dots, D_1\} \times \dots \times \{1, 2, \dots, D_N\}$, stands for the set of observed entries. One may employ a tensor factorization by minimizing the loss in Equation (1.16) via gradient descent over the parameterization:

$$\mathcal{W} = \sum_{r=1}^R \mathbf{w}_r^1 \otimes \dots \otimes \mathbf{w}_r^N \quad , \quad \mathbf{w}_r^n \in \mathbb{R}^{D_n} \quad , \quad r = 1, \dots, R \quad , \quad n = 1, \dots, N, \quad (1.17)$$

where again, $R \in \mathbb{N}$ is a predetermined constant, \otimes stands for tensor product (*i.e.* outer product), and $\{\mathbf{w}_r^n\}_{r=1, n=1}^{R, N}$ are the optimized parameters. In analogy with the matrix case, the minimal R required for this parameterization to be able to express a given $\overline{\mathcal{W}} \in \mathbb{R}^{D_1 \times \dots \times D_N}$ is defined to be the latter’s *tensor rank*.⁹ An implicit regularization towards low rank here would mean that even when R is large enough for expressing any tensor, solutions expressible (or approximable) with small R tend to be learned.

⁹When referring to tensor rank, we mean the classic *CP-rank* (see [124]).

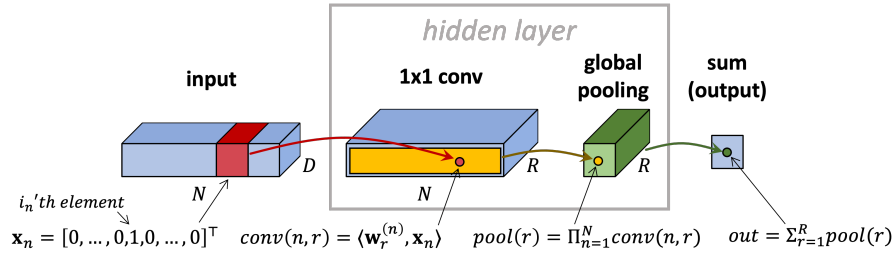


Figure 1.3: Tensor factorization corresponds to a *non-linear* convolutional neural network (with polynomial non-linearity), analogously to how matrix factorization corresponds to a linear neural network. The input to the network is a tuple $(i_1, \dots, i_N) \in \{1, \dots, D_1\} \times \dots \times \{1, \dots, D_N\}$, represented via one-hot vectors $(\mathbf{x}_1, \dots, \mathbf{x}_N) \in \mathbb{R}^{D_1} \times \dots \times \mathbb{R}^{D_N}$ (illustration assumes $D_1 = \dots = D_N = D$ to avoid clutter). These vectors are processed by a hidden layer comprising: (i) locally connected linear operator with R channels, the r 'th one computing inner products against filters $(\mathbf{w}_r^1, \dots, \mathbf{w}_r^N) \in \mathbb{R}^{D_1} \times \dots \times \mathbb{R}^{D_N}$ (this operator is referred to as “ 1×1 conv”, appealing to the case of weight sharing, i.e. $\mathbf{w}_r^1 = \dots = \mathbf{w}_r^N$); followed by (ii) global pooling computing products of all activations in each channel (which induces polynomial non-linearity). The result of the hidden layer is then reduced through summation to a scalar — output of the network. Overall, given input tuple (i_1, \dots, i_N) , the network outputs $(\mathcal{W})_{i_1, \dots, i_N}$, where $\mathcal{W} \in \mathbb{R}^{D_1 \times \dots \times D_N}$ is given by the tensor factorization in Equation (1.17). Notice that the number of terms (R) and the tunable parameters $(\{\mathbf{w}_r^n\}_{r,n})$ in the factorization respectively correspond to the width and the learnable filters of the network. Our tensor factorization (Equation (1.17)) was derived as an extension of a shallow (depth 2) matrix factorization, and accordingly, the convolutional neural network it corresponds to is shallow (has a single hidden layer). Endowing the factorization with hierarchical structures would render it equivalent to a *deep* convolutional neural network (see [51] for details). We will investigate the implicit regularization of these models in Chapter 3.

Figure 1.2 displays results of tensor completion experiments, in which tensor factorization (optimization of loss in Equation (1.16) via gradient descent over parameterization in Equation (1.17)) is applied to observations drawn from a low-rank ground truth tensor. As can be seen in terms of both reconstruction error (distance from ground truth tensor) and tensor rank of the produced solutions, tensor factorizations indeed exhibit an implicit regularization towards low rank. The phenomenon thus goes beyond the special case of matrix (order 2 tensor) factorization. In Chapter 2 we will theoretically support this finding.

As discussed in Section 1.1, matrix completion can be seen as a prediction problem, and matrix factorization as its solution with a *linear neural network*. In a similar vein, tensor completion may be viewed as a prediction problem, and tensor factorization as its solution with a certain (depth 2) *non-linear* convolutional neural network — see Figure 1.3. The non-linearity of this neural network is polynomial and stems from product pooling layers. Analogously to how the input-output mapping of a linear neural network is naturally represented by a matrix, that of the neural network equivalent to tensor factorization admits a natural representation as a tensor. Our experiments (Figure 1.2 and Figure A.3 in Appendix A.2.1) show that when learned via gradient descent, this tensor tends to have low tensor rank. We thus obtain a second exemplar of a neural network architecture whose implicit regularization strives to lower a notion of rank for its input-output mapping. This indicates that the phenomenon may be general, and formalizing notions of rank for input-output mappings of contemporary models may be key to explaining generalization in deep learning. In Chapters 2 and 3 we theoretically support this hypothesis by employing the equivalence between tensor factorizations and certain neural networks.

Chapter 2

Implicit Regularization in Tensor Factorization

The contents of this chapter are based on [178].

2.1 Background and Overview

Chapter 1 considered the implicit regularization in matrix factorization, under the context of matrix completion problems. Recall that in matrix completion, we are given a randomly chosen subset of entries from an unknown matrix $\mathbf{W}^* \in \mathbb{R}^{D \times D'}$, and our goal is to recover unseen entries. This can be viewed as a prediction problem, where the set of possible inputs is $\mathcal{X} = \{1, \dots, D\} \times \{1, \dots, D'\}$, the possible labels are $\mathcal{Y} = \mathbb{R}$, and the label of $(i, j) \in \mathcal{X}$ is $(\mathbf{W}^*)_{i,j}$. Under this viewpoint, observed entries constitute the training set, and the average reconstruction error over unobserved entries is the test error, quantifying generalization. A predictor, *i.e.* a function from \mathcal{X} to \mathcal{Y} , can then be seen as a matrix.

Although it was initially conjectured that the implicit regularization in matrix factorization minimizes some norm [81], as we showed in Chapter 1, there exist cases in which no norm is being minimized. Specifically, there exist matrix completion problems in which fitting the observed entries leads *all norms to grow towards infinity* in favor of *minimizing rank*. Recent studies [9, 141] further suggest that gradient descent with small learning rate and near-zero initialization induces an incremental rank learning process, which results in low rank solutions.

A central question that arises is to what extent is the study of implicit regularization in matrix factorization relevant to more practical settings. The experiments in Section 1.4.2 have shown that the tendency towards low rank extends from matrices (two-dimensional arrays) to *tensors* (multi-dimensional arrays). Namely, in the task of *N-dimensional tensor completion*, which (analogously to matrix completion) can be viewed as a prediction problem over *N* input variables, training a *tensor factorization*¹ via gradient descent with small learning rate and near-zero initialization tends to produce tensors (predictors) with low *tensor rank*. Analogously to how matrix factorization may be viewed as a linear neural network, tensor factorization can be seen as a certain *non-linear* convolutional neural network (two-layer network with polynomial non-linearity, *cf.* [51]), and so it represents a setting much closer to practical deep learning.

¹Recall that by “tensor factorization” we refer throughout to the classic CP factorization [124].

In this chapter we theoretically analyze the implicit regularization in tensor factorization. We circumvent the notorious difficulty of tensor problems [95] by adopting a dynamical systems perspective. Characterizing the evolution that gradient descent with small learning rate and near-zero initialization induces on the components of a factorization, we show that their norms are subject to a momentum-like effect, in the sense that they move slower when small and faster when large. This implies a form of greedy low tensor rank search, generalizing phenomena known for the case of matrices. We employ the finding to prove that, with the classic Huber loss from robust statistics [101], arbitrarily small initialization leads tensor factorization to follow a trajectory of rank one tensors for an arbitrary amount of time or distance. Experiments validate our analysis, demonstrating implicit regularization towards low tensor rank in a wide array of configurations.

Recall that, as discussed in Part I, a major challenge towards understanding generalization in deep learning is that we lack definitions for predictor complexity that are both implicitly minimized during training of neural networks and capture the essence of natural data, in the sense of it being fittable with low complexity. Motivated by the fact that tensor rank captures the implicit regularization of a non-linear neural network, we empirically explore its potential to serve as a measure of complexity for multivariable predictors. We find that it is possible to fit standard image recognition datasets — MNIST [130] and Fashion-MNIST [220] — with predictors of extremely low tensor rank, far beneath what is required for fitting random data. This leads us to believe that tensor rank (or more advanced notions such as hierarchical tensor ranks) may pave way to explaining both implicit regularization of contemporary deep neural networks, and the properties of natural data translating this implicit regularization to generalization.

The remainder of the chapter is organized as follows. Section 2.2 presents the tensor factorization model, as well as its interpretation as a neural network. Section 2.3 characterizes its dynamics, followed by Section 2.4 which employs the characterization to establish (under certain conditions) implicit tensor rank minimization. Lastly, experiments demonstrating both the dynamics of learning and the ability of tensor rank to capture the essence of standard datasets are given in Section 2.5. Extension of our results to tensor sensing (more general setting than tensor completion) is discussed in Appendix B.1.

2.2 Tensor Factorization

Consider the task of completing an N -dimensional tensor ($N \geq 3$) with axis lengths $D_1, \dots, D_N \in \mathbb{N}$, or, in standard tensor analysis terminology, an *order* N tensor with *modes of dimensions* D_1, \dots, D_N . Given a set of observations $\{y_{i_1, \dots, i_N} \in \mathbb{R}\}_{(i_1, \dots, i_N) \in \Omega}$, where Ω is a subset of all possible index tuples, a standard (undetermined) loss function for the task is:

$$\mathcal{L}_T : \mathbb{R}^{D_1 \times \dots \times D_N} \rightarrow \mathbb{R}_{\geq 0} \quad , \quad \mathcal{L}_T(\mathcal{W}) = \frac{1}{|\Omega|} \sum_{(i_1, \dots, i_N) \in \Omega} \ell((\mathcal{W})_{i_1, \dots, i_N} - y_{i_1, \dots, i_N}) \quad , \quad (2.1)$$

where $\ell : \mathbb{R} \rightarrow \mathbb{R}_{\geq 0}$ is differentiable and locally smooth. A typical choice for $\ell(\cdot)$ is $\ell(z) = \frac{1}{2}z^2$, corresponding to ℓ_2 loss. Other options are also common, for example the Huber loss from robust statistics [101] — a differentiable surrogate for ℓ_1 loss.

Performing tensor completion with an R -component tensor factorization amounts to optimizing the following (non-convex) objective:

$$\phi_{\mathcal{T}}(\{\mathbf{w}_r^n\}_{r=1n=1}^{R N}) := \mathcal{L}_{\mathcal{T}}(\mathcal{W}_{\mathcal{T}}), \quad (2.2)$$

defined over *weight vectors* $\{\mathbf{w}_r^n \in \mathbb{R}^{D_n}\}_{r=1n=1}^{R N}$, where:

$$\mathcal{W}_{\mathcal{T}} := \sum_{r=1}^R \mathbf{w}_r^1 \otimes \dots \otimes \mathbf{w}_r^N \quad (2.3)$$

is referred to as the *end tensor* of the factorization, with \otimes representing tensor product (*i.e.* outer product). The minimal number of components R required in order for $\mathcal{W}_{\mathcal{T}}$ to be able to express a given tensor $\mathcal{W} \in \mathbb{R}^{D_1 \times \dots \times D_N}$, is defined to be the *tensor rank* of \mathcal{W} . One may explicitly restrict the tensor rank of solutions produced by the tensor factorization via limiting R . However, since our interest lies in the implicit regularization induced by gradient descent, *i.e.* in the type of end tensors (Equation (2.3)) it will find when applied to the objective $\phi_{\mathcal{T}}(\cdot)$ (Equation (2.2)) with no explicit constraints, we treat the case where R can be arbitrarily large.

In line with analyses of matrix factorization (*e.g.* [81, 7, 9, 59, 141]), we model small learning rate for gradient descent through the infinitesimal limit, *i.e.* through *gradient flow*:

$$\frac{d}{dt} \mathbf{w}_r^n(t) := - \frac{\partial}{\partial \mathbf{w}_r^n} \phi_{\mathcal{T}}(\{\mathbf{w}_{r'}^{n'}(t)\}_{r'=1n'=1}^{R N}), \quad t \geq 0, \quad r = 1, \dots, R, \quad n = 1, \dots, N, \quad (2.4)$$

where $\{\mathbf{w}_r^n(t)\}_{r=1n=1}^{R N}$ denote the weight vectors at time t of optimization.

Our aim is to theoretically investigate the prospect of implicit regularization towards low tensor rank, *i.e.* of gradient flow with near-zero initialization learning a solution that can be represented with a small number of components.

2.2.1 Interpretation as Neural Network

Tensor completion can be viewed as a prediction problem, where each mode corresponds to a discrete input variable. For an unknown tensor $\mathcal{W}^* \in \mathbb{R}^{D_1 \times \dots \times D_N}$, inputs are index tuples of the form (i_1, \dots, i_N) , and the label associated with such an input is $(\mathcal{W}^*)_{i_1, \dots, i_N}$. Under this perspective, the training set consists of the observed entries, and the average reconstruction error over unseen entries measures test error. The standard case, in which observations are drawn uniformly across the tensor and reconstruction error weighs all entries equally, corresponds to a data distribution that is uniform, but other distributions are also viable.

Consider for example the task of predicting a continuous label for a 100-by-100 binary image. This can be formulated as an order 10000 tensor completion problem, where all modes are of dimension 2. Each input image corresponds to a location (entry) in the tensor \mathcal{W}^* , holding its continuous label. As image pixels are (typically) not distributed independently and uniformly, locations in the tensor are not drawn uniformly when observations are generated, and are not weighted equally when reconstruction error is computed. See Figure 2.1 for further illustration of how a general prediction task (with discrete inputs and scalar output) can be formulated as a tensor completion problem.

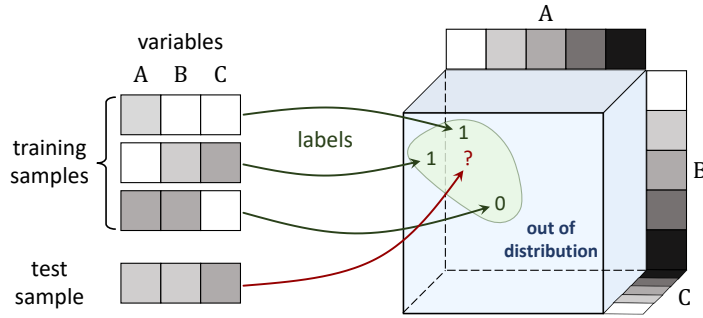


Figure 2.1: Prediction tasks over discrete variables can be viewed as tensor completion problems. Consider the task of learning a predictor from domain $\mathcal{X} = \{1, \dots, D_1\} \times \dots \times \{1, \dots, D_N\}$ to range $\mathcal{Y} = \mathbb{R}$ (figure assumes $N = 3$ and $D_1 = \dots = D_N = 5$ for the sake of illustration). Each input sample is associated with a location in an order N tensor with mode (axis) dimensions D_1, \dots, D_N , where the value of a variable (depicted as a shade of gray) determines the index of the corresponding mode (marked by “A”, “B” or “C”). The associated location stores the label of the sample. Under this viewpoint, training samples are observed entries, drawn according to an unknown distribution from a ground truth tensor. Learning a predictor amounts to completing the unobserved entries, with test error measured by (weighted) average reconstruction error. In many standard prediction tasks (*e.g.* image recognition), only a small subset of the input domain has non-negligible probability. From the tensor completion perspective this means that observed entries reside in a restricted part of the tensor, and reconstruction error is weighted accordingly (entries outside the support of the distribution are neglected).

As discussed in Section 1.4.2 of Chapter 1, under the above formulation, tensor factorization can be viewed as a two-layer convolutional neural network with polynomial non-linearity, where the non-linearity stems from product pooling layers. Given an input, *i.e.* a location in the tensor, the network produces an output equal to the value that the factorization holds at the given location. This equivalence between tensor factorization and a non-linear convolutional neural network was illustrated in Figure 1.3 of Chapter 1. A major drawback of matrix factorization as a theoretical surrogate for modern deep learning is that it misses the critical aspect of non-linearity. Tensor factorization goes beyond the realm of linear predictors — a significant step towards practical neural networks.

2.3 Dynamical Characterization

In this section we derive a dynamical characterization for the norms of individual components in the tensor factorization. The characterization implies that with small learning rate and near-zero initialization, components tend to be learned incrementally, giving rise to a bias towards low tensor rank solutions. This finding is used in Section 2.4 to prove (under certain conditions) implicit tensor rank minimization, and is demonstrated empirically in Section 2.5.²

For the rest of the chapter, unless specified otherwise, when referring to a norm we mean the standard Frobenius (Euclidean) norm, denoted by $\|\cdot\|$.

The following lemma establishes an invariant of the dynamics, showing that the differences between squared norms of vectors in the same component are constant

²We note that all results in this section apply even if the tensor completion loss $\mathcal{L}_T(\cdot)$ (Equation (2.1)) is replaced by any differentiable and locally smooth function. The proofs in Appendix B.3 already account for this more general setting.

through time.

Lemma 1. For all $r \in \{1, \dots, R\}$ and $n, \bar{n} \in \{1, \dots, N\}$:

$$\|\mathbf{w}_r^n(t)\|^2 - \|\mathbf{w}_r^{\bar{n}}(t)\|^2 = \|\mathbf{w}_r^n(0)\|^2 - \|\mathbf{w}_r^{\bar{n}}(0)\|^2, \quad t \geq 0.$$

Proof sketch (for proof see Lemma 29 in Appendix B.3.2.2). The claim readily follows by showing that under gradient flow $\frac{d}{dt}\|\mathbf{w}_r^n(t)\|^2 = \frac{d}{dt}\|\mathbf{w}_r^{\bar{n}}(t)\|^2$ for all $t \geq 0$. \square

Lemma 1 naturally leads to the definition below.

Definition 3. The *unbalancedness magnitude* of the weight vectors $\{\mathbf{w}_r^n \in \mathbb{R}^{D_n}\}_{r=1, n=1}^{R, N}$ is defined to be:

$$\max_{r \in \{1, \dots, R\}, n, \bar{n} \in \{1, \dots, N\}} \left| \|\mathbf{w}_r^n\|^2 - \|\mathbf{w}_r^{\bar{n}}\|^2 \right|.$$

By Lemma 1, the unbalancedness magnitude is constant during optimization, and thus, is determined at initialization. When weight vectors are initialized near the origin — regime of interest — the unbalancedness magnitude is small, approaching zero as initialization scale decreases.

Theorem 3 below provides a dynamical characterization for norms of individual components in the tensor factorization.

Theorem 3. Assume unbalancedness magnitude $\epsilon \geq 0$ at initialization, and denote by $\mathcal{W}_T(t)$ the end tensor (Equation (2.3)) at time $t \geq 0$ of optimization. Then, for any $r \in \{1, \dots, R\}$ and time $t \geq 0$ at which $\|\otimes_{n=1}^N \mathbf{w}_r^n(t)\| > 0$:³

- If $\gamma_r(t) := \langle -\nabla \mathcal{L}_T(\mathcal{W}_T(t)), \otimes_{n=1}^N \widehat{\mathbf{w}}_r^n(t) \rangle \geq 0$, then:

$$\begin{aligned} \frac{d}{dt} \|\otimes_{n=1}^N \mathbf{w}_r^n(t)\| &\leq N\gamma_r(t) (\|\otimes_{n=1}^N \mathbf{w}_r^n(t)\|^{\frac{2}{N}} + \epsilon)^{N-1}, \\ \frac{d}{dt} \|\otimes_{n=1}^N \mathbf{w}_r^n(t)\| &\geq N\gamma_r(t) \cdot \frac{\|\otimes_{n=1}^N \mathbf{w}_r^n(t)\|^2}{\|\otimes_{n=1}^N \mathbf{w}_r^n(t)\|^{\frac{2}{N}} + \epsilon}, \end{aligned} \quad (2.5)$$

- otherwise, if $\gamma_r(t) < 0$, then:

$$\begin{aligned} \frac{d}{dt} \|\otimes_{n=1}^N \mathbf{w}_r^n(t)\| &\geq N\gamma_r(t) (\|\otimes_{n=1}^N \mathbf{w}_r^n(t)\|^{\frac{2}{N}} + \epsilon)^{N-1}, \\ \frac{d}{dt} \|\otimes_{n=1}^N \mathbf{w}_r^n(t)\| &\leq N\gamma_r(t) \cdot \frac{\|\otimes_{n=1}^N \mathbf{w}_r^n(t)\|^2}{\|\otimes_{n=1}^N \mathbf{w}_r^n(t)\|^{\frac{2}{N}} + \epsilon}, \end{aligned} \quad (2.6)$$

where $\widehat{\mathbf{w}}_r^n(t) := \mathbf{w}_r^n(t) / \|\mathbf{w}_r^n(t)\|$ for $n = 1, \dots, N$.

Proof sketch (proof in Appendix B.3.3). Differentiating a component's norm with respect to time, we obtain $\frac{d}{dt} \|\otimes_{n=1}^N \mathbf{w}_r^n(t)\| = \gamma_r(t) \cdot \sum_{n=1}^N \prod_{n' \neq n} \|\mathbf{w}_r^{n'}(t)\|^2$. The desired bounds then follow from using conservation of unbalancedness magnitude (as implied by Lemma 1), and showing that $\|\mathbf{w}_r^{n'}(t)\|^2 \leq \|\otimes_{n=1}^N \mathbf{w}_r^n(t)\|^{2/N} + \epsilon$ for all $t \geq 0$ and $n' \in \{1, \dots, N\}$. \square

Theorem 3 shows that when unbalancedness magnitude at initialization (denoted ϵ) is small, the evolution rates of component norms are roughly proportional to their

³When $\|\otimes_{n=1}^N \mathbf{w}_r^n(t)\|$ is zero it may not be differentiable.

size exponentiated by $2 - 2/N$, where N is the order of the tensor factorization. Consequently, component norms are subject to a momentum-like effect, by which they move slower when small and faster when large. This suggests that when initialized near zero, components tend to remain close to the origin, and then, upon reaching a critical threshold, quickly grow until convergence, creating an incremental learning effect that yields implicit regularization towards low tensor rank. This phenomenon is used in Section 2.4 to formally prove (under certain conditions) implicit tensor rank minimization, and is demonstrated empirically in Section 2.5.

When the unbalancedness magnitude at initialization is exactly zero, our dynamical characterization takes on a particularly lucid form.

Corollary 2. *Assume unbalancedness magnitude zero at initialization. Then, with notations of Theorem 3, for any $r \in \{1, \dots, R\}$, the norm of the r 'th component evolves by:*

$$\frac{d}{dt} \|\otimes_{n=1}^N \mathbf{w}_r^n(t)\| = N\gamma_r(t) \cdot \|\otimes_{n=1}^N \mathbf{w}_r^n(t)\|^{2-\frac{2}{N}}, \quad (2.7)$$

where by convention $\widehat{\mathbf{w}}_r^n(t) = 0$ if $\mathbf{w}_r^n(t) = 0$.

Proof sketch (proof in Appendix B.3.4). If the time t is such that $\|\otimes_{n=1}^N \mathbf{w}_r^n(t)\| > 0$, Equation (2.7) readily follows from applying Theorem 3 with $\epsilon = 0$. For the case where $\|\otimes_{n=1}^N \mathbf{w}_r^n(t)\| = 0$, we show that the component $\otimes_{n=1}^N \mathbf{w}_r^n(t)$ must be identically zero throughout, hence both sides of Equation (2.7) are equal to zero. \square

It is worthwhile highlighting the relation to matrix factorization. There, an implicit bias towards low rank emerges from incremental learning dynamics similar to above, with singular values standing in place of component norms. In fact, the dynamical characterization given in Corollary 2 is structurally identical to the one provided by Theorem 3 in [9] for singular values of a matrix factorization. We thus obtained a generalization from matrices to tensors, notwithstanding the notorious difficulty often associated with the latter (cf. [95]).

2.4 Implicit Tensor Rank Minimization

In this section we employ the dynamical characterization derived in Section 2.3 to theoretically establish implicit regularization towards low tensor rank. Specifically, we prove that under certain technical conditions, arbitrarily small initialization leads tensor factorization to follow a trajectory of rank one tensors for an arbitrary amount of time or distance. As a corollary, we obtain that if the tensor completion problem admits a rank one solution, and all rank one trajectories uniformly converge to it, tensor factorization with infinitesimal initialization will converge to it as well. Our analysis generalizes to tensor factorization recent results developed in [141] for matrix factorization. As typical in transitioning from matrices to tensors, this generalization entails significant challenges necessitating use of fundamentally different techniques.

For technical reasons, our focus in this section lies on the Huber loss from robust statistics [101], given by:

$$\ell_h : \mathbb{R} \rightarrow \mathbb{R}_{\geq 0} \quad , \quad \ell_h(z) := \begin{cases} \frac{1}{2}z^2 & , |z| < \delta_h \\ \delta_h(|z| - \frac{1}{2}\delta_h) & , \text{otherwise} \end{cases} \quad (2.8)$$

where $\delta_h > 0$, referred to as the transition point of the loss, is predetermined. Huber loss is often used as a differentiable surrogate for ℓ_1 loss, in which case δ_h is chosen to be small. We will assume it is smaller than observed tensor entries:⁴

Assumption 1. $\delta_h < |y_{i_1, \dots, i_N}|, \forall (i_1, \dots, i_N) \in \Omega$.

We will consider an initialization $\{\mathbf{a}_r^n \in \mathbb{R}^{D_n}\}_{r=1, n=1}^{R, N}$ for the weight vectors of the tensor factorization, and will scale this initialization towards zero. In line with infinitesimal initializations being captured by unbalancedness magnitude zero (cf. Section 2.3), we assume that this is the case:

Assumption 2. The initialization $\{\mathbf{a}_r^n\}_{r=1, n=1}^{R, N}$ has unbalancedness magnitude zero.

We further assume that within $\{\mathbf{a}_r^n\}_{r, n}$ there exists a leading component (subset $\{\mathbf{a}_{\bar{r}}^n\}_n$), in the sense that it is larger than others, while having positive projection on the attracting force at the origin, i.e. on minus the gradient of the loss $\mathcal{L}_T(\cdot)$ (Equation (2.1)) at zero:

Assumption 3. There exists $\bar{r} \in \{1, \dots, R\}$ such that:

$$\begin{aligned} & \left\langle -\nabla \mathcal{L}_T(0), \otimes_{n=1}^N \widehat{\mathbf{a}}_{\bar{r}}^n \right\rangle > 0, \\ & \|\mathbf{a}_{\bar{r}}^n\| > \|\mathbf{a}_r^n\| \cdot \left(\frac{\|\nabla \mathcal{L}_T(0)\|}{\left\langle -\nabla \mathcal{L}_T(0), \otimes_{n=1}^N \widehat{\mathbf{a}}_{\bar{r}}^n \right\rangle} \right)^{1/(N-2)}, \quad \forall r \neq \bar{r}, \end{aligned} \quad (2.9)$$

where $\widehat{\mathbf{a}}_{\bar{r}}^n := \mathbf{a}_{\bar{r}}^n / \|\mathbf{a}_{\bar{r}}^n\|$ for $n = 1, \dots, N$.

Let $\alpha > 0$, and suppose we run gradient flow on the tensor factorization (see Section 2.2) starting from the initialization $\{\mathbf{a}_r^n\}_{r, n}$ scaled by α . That is, we set:

$$\mathbf{w}_r^n(0) = \alpha \cdot \mathbf{a}_r^n, \quad r = 1, \dots, R, n = 1, \dots, N,$$

and let $\{\mathbf{w}_r^n(t)\}_{r, n}$ evolve per Equation (2.4). Denote by $\mathcal{W}_T(t)$, $t \geq 0$, the trajectory induced on the end tensor (Equation (2.3)). We will study the evolution of this trajectory through time. A hurdle that immediately arises is that, by the dynamical characterization of Section 2.3, when the initialization scale α tends to zero (regime of interest), the time it takes $\mathcal{W}_T(t)$ to escape the origin grows to infinity.⁵ We overcome this hurdle by considering a *reference sphere* — a sphere around the origin with sufficiently small radius:

$$\mathcal{S} := \{\mathcal{W} \in \mathbb{R}^{d_1, \dots, d_N} : \|\mathcal{W}\| = \rho\}, \quad (2.10)$$

where $\rho \in (0, \min_{(i_1, \dots, i_N) \in \Omega} |y_{i_1, \dots, i_N}| - \delta_h)$ can be chosen arbitrarily. With the reference sphere \mathcal{S} at hand, we define a time-shifted version of the trajectory $\mathcal{W}_T(t)$, aligning $t = 0$ with the moment at which \mathcal{S} is reached:

$$\overline{\mathcal{W}}_T(t) := \mathcal{W}_T(t + \inf\{t' \geq 0 : \mathcal{W}_T(t') \in \mathcal{S}\}), \quad (2.11)$$

where by definition $\inf\{t' \geq 0 : \mathcal{W}_T(t') \in \mathcal{S}\} = 0$ if $\mathcal{W}_T(t)$ does not reach \mathcal{S} . Unlike the original trajectory $\mathcal{W}_T(t)$, the shifted one $\overline{\mathcal{W}}_T(t)$ disregards the process of escaping

⁴Note that this entails assumption of non-zero observations.

⁵To see this, divide both sides of Equation (2.7) from Corollary 2 by $\|\otimes_{n=1}^N \mathbf{w}_r^n(t)\|^{2-2/N}$, and integrate with respect to t . It follows that the norm of a component at any fixed time tends to zero as initialization scale α decreases. This implies that for any $D > 0$, when taking $\alpha \rightarrow 0$, the time required for a component to reach norm D grows to infinity.

the origin, and thus admits a concrete meaning to the time elapsing from optimization commencement.

We will establish proximity of $\overline{\mathcal{W}}_T(t)$ to trajectories of rank one tensors. We say that $\mathcal{W}_1(t) \in \mathbb{R}^{D_1 \times \dots \times D_N}$, $t \geq 0$, is a *rank one trajectory*, if it coincides with some trajectory of an end tensor in a one-component factorization, *i.e.* if there exists an initialization for gradient flow over a tensor factorization with $R = 1$ components, leading the induced end tensor to evolve by $\mathcal{W}_1(t)$. If the latter initialization has unbalancedness magnitude zero (*cf.* Definition 3), we further say that $\mathcal{W}_1(t)$ is a *balanced rank one trajectory*.⁶

We are now in a position to state our main result, by which arbitrarily small initialization leads tensor factorization to follow a (balanced) rank one trajectory for an arbitrary amount of time or distance.

Theorem 4. *Under Assumptions 1, 2 and 3, for any distance from origin $B > 0$, time duration $T > 0$, and degree of approximation $\epsilon \in (0, 1)$, if initialization scale α is sufficiently small,⁷ then: (i) $\mathcal{W}_T(t)$ reaches the reference sphere \mathcal{S} ; and (ii) there exists a balanced rank one trajectory $\mathcal{W}_1(t)$ emanating from \mathcal{S} , such that $\|\overline{\mathcal{W}}_T(t) - \mathcal{W}_1(t)\| \leq \epsilon$ at least until $t \geq T$ or $\|\overline{\mathcal{W}}_T(t)\| \geq B$.*

Proof sketch (proof in Appendix B.3.5). Using the dynamical characterization from Section 2.3 (Lemma 1 and Corollary 2), and the fact that $\nabla \mathcal{L}_T(\cdot)$ is locally constant around the origin, we establish that (i) $\mathcal{W}_T(t)$ reaches the reference sphere \mathcal{S} ; and (ii) at that time, the norm of the \bar{r} 'th component is of constant scale (independent of α), while the norms of all other components are $\mathcal{O}(\alpha^N)$. Thus, taking α towards zero leads $\mathcal{W}_T(t)$ to arrive at \mathcal{S} while being arbitrarily close to the initialization of a balanced rank one trajectory — $\mathcal{W}_1(t)$. Since the objective is locally smooth, this ensures $\overline{\mathcal{W}}_T(t)$ is within distance ϵ from $\mathcal{W}_1(t)$ for an arbitrary amount of time or distance. That is, if α is sufficiently small, $\|\overline{\mathcal{W}}_T(t) - \mathcal{W}_1(t)\| \leq \epsilon$ at least until $t \geq T$ or $\|\overline{\mathcal{W}}_T(t)\| \geq B$. \square

As an immediate corollary of Theorem 4, we obtain that if all balanced rank one trajectories uniformly converge to a global minimum, tensor factorization with infinitesimal initialization will do so too. In particular, its implicit regularization will direct it towards a solution with tensor rank one.

Corollary 3. *Assume the conditions of Theorem 4 (Assumptions 1, 2 and 3), and in addition, that all balanced rank one trajectories emanating from \mathcal{S} converge to a tensor $\mathcal{W}^* \in \mathbb{R}^{D_1 \times \dots \times D_N}$ uniformly, in the sense that they are all confined to some bounded domain, and for any $\epsilon > 0$, there exists a time T after which they are all within distance ϵ from \mathcal{W}^* . Then, for any $\epsilon > 0$, if initialization scale α is sufficiently small, there exists a time T for which $\|\mathcal{W}_T(T) - \mathcal{W}^*\| \leq \epsilon$.*

Proof sketch (proof in Appendix B.3.6). Let $T' > 0$ be a time at which all balanced rank one trajectories that emanated from \mathcal{S} are within distance $\epsilon/2$ from \mathcal{W}^* . By Theorem 4, if α is sufficiently small, $\overline{\mathcal{W}}_T(t)$ is guaranteed to be within distance $\epsilon/2$ from a balanced rank one trajectory that emanated from \mathcal{S} , at least until time T' . Recalling that $\overline{\mathcal{W}}_T(t)$ is a time-shifted version of $\mathcal{W}_T(t)$, the desired result follows from the triangle inequality. \square

⁶Note that the definitions of rank one trajectory and balanced rank one trajectory allow for $\mathcal{W}_1(t)$ to have rank zero (*i.e.* to be equal to zero) at some or all times $t \geq 0$.

⁷Hiding problem-dependent constants, an initialization scale of $\epsilon B^{-1} \exp(-\mathcal{O}(B^2 T))$ suffices. Exact constants are specified at the beginning of the proof in Appendix B.3.5.

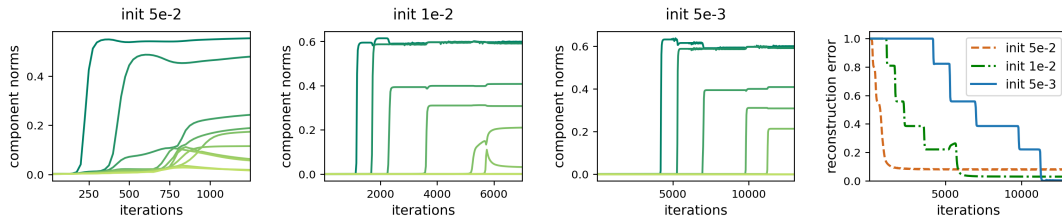


Figure 2.2: Dynamics of gradient descent over tensor factorization — incremental learning of components yields low tensor rank solutions. Presented plots correspond to the task of completing a (tensor) rank 5 ground truth tensor of size 10-by-10-by-10-by-10 (order 4) based on 2000 observed entries chosen uniformly at random without repetition (smaller sample sizes led to solutions with tensor rank lower than that of the ground truth tensor). In each experiment, the ℓ_2 loss (more precisely, Equation (2.1) with $\ell(z) := z^2$) was minimized via gradient descent over a tensor factorization with $R = 1000$ components (large enough to express any tensor), starting from (small) random initialization. First (left) three plots show (Frobenius) norms of the ten largest components under three standard deviations for initialization — 0.05, 0.01, and 0.005. Further reduction of initialization scale yielded no noticeable change. The rightmost plot compares reconstruction errors (Frobenius distance from ground truth) from the three runs. To facilitate more efficient experimentation, we employed an adaptive learning rate scheme (see Appendix B.2.2 for details). Notice that, in accordance with the theoretical analysis of Section 2.3, component norms move slower when small and faster when large, creating an incremental process in which components are learned one after the other. This effect is enhanced as initialization scale is decreased, producing low tensor rank solutions that accurately reconstruct the low (tensor) rank ground truth tensor. In particular, even though the factorization consists of 1000 components, when initialization is sufficiently small, only five (tensor rank of the ground truth tensor) substantially depart from zero. Appendix B.2 provides further implementation details, as well as similar experiments with: (i) Huber loss (see Equation (2.8)) instead of ℓ_2 loss; (ii) ground truth tensors of different orders and (tensor) ranks; and (iii) tensor sensing (see Appendix B.1).

2.5 Experiments

In this section we present our experiments. Section 2.5.1 corroborates our theoretical analyses (Sections 2.3 and 2.4), evaluating tensor factorization (Section 2.2) on synthetic low (tensor) rank tensor completion problems. Section 2.5.2 explores tensor rank as a measure of complexity, examining its ability to capture the essence of standard datasets. For brevity, we defer a description of implementation details, as well as some experiments, to Appendix B.2.

2.5.1 Dynamics of Learning

In Section 1.4.2 of Chapter 1 we empirically showed that, with small learning rate and near-zero initialization, gradient descent over tensor factorization exhibits an implicit regularization towards low tensor rank. The theory in Sections 2.3 and 2.4 explains this implicit regularization through a dynamical analysis — we prove that the movement of component norms is attenuated when small and enhanced when large, thus creating an incremental learning effect which becomes more potent as initialization scale decreases. Figure 2.2 demonstrates this phenomenon empirically on synthetic low (tensor) rank tensor completion problems. Figures B.1, B.2 and B.3 in Appendix B.2.1 extend the experiment, corroborating our analyses in a wide array of settings.

2.5.2 Tensor Rank as Measure of Complexity

Implicit regularization in deep learning is typically viewed as a tendency of gradient-based optimization to fit training examples with predictors whose “complexity” is as low as possible. The fact that “natural” data gives rise to generalization while other types of data (*e.g.* random) do not, is understood to result from the former being amenable to fitting by predictors of lower complexity. A major challenge in formalizing this intuition is that we lack definitions for predictor complexity that are both quantitative (*i.e.* admit quantitative generalization bounds) and capture the essence of natural data (types of data on which neural networks generalize in practice), in the sense of it being fittable with low complexity.

As discussed in Section 2.2.1, learning a predictor with multiple discrete input variables and a continuous output can be viewed as a tensor completion problem. Specifically, with $N \in \mathbb{N}$, $D_1, \dots, D_N \in \mathbb{N}$, learning a predictor from domain $\mathcal{X} = \{1, \dots, D_1\} \times \dots \times \{1, \dots, D_N\}$ to range $\mathcal{Y} = \mathbb{R}$ corresponds to completion of an order N tensor with mode (axis) dimensions D_1, \dots, D_N . Under this correspondence, any predictor can simply be thought of as a tensor, and vice versa. We have shown that solving tensor completion via tensor factorization amounts to learning a predictor through a certain neural network (Section 2.2.1), whose implicit regularization favors solutions with low tensor rank (Sections 2.3 and 2.4). Motivated by these connections, the current subsection empirically explores tensor rank as a measure of complexity for predictors, by evaluating the extent to which it captures natural data, *i.e.* allows the latter to be fit with low complexity predictors.

As representatives of natural data, we chose the classic MNIST dataset [130] — perhaps the most common benchmark for demonstrating ideas in deep learning — and its more modern counterpart Fashion-MNIST [220]. A hurdle posed by these datasets is that they involve classification into multiple categories, whereas the equivalence to tensors applies to predictors whose output is a scalar. It is possible to extend the equivalence by equating a multi-output predictor with multiple tensors, in which case the predictor is associated with multiple tensor ranks. However, to facilitate a simple presentation, we avoid this extension and simply map each dataset into multiple one-vs-all binary classification problems. For each problem, we associate the label 1 with the active category and 0 with all the rest, and then attempt to fit training examples with predictors of low tensor rank, reporting the resulting mean squared error, *i.e.* the residual of the fit. This is compared against residuals obtained when fitting two types of random data: one generated via shuffling labels, and the other by replacing inputs with noise.

Both MNIST and Fashion-MNIST comprise 28-by-28 grayscale images, with each pixel taking one of 256 possible values. Tensors associated with predictors are thus of order 784, with dimension 256 in each mode (axis).⁸ A general rank one tensor can then be expressed as a tensor product (*i.e.* outer product) between 784 vectors of dimension 256 each, and accordingly has roughly $784 \cdot 256$ degrees of freedom. This significantly exceeds the number of training examples in the datasets (60000), hence it is no surprise that we could easily fit them, as well as their random variants,

⁸In practice, when associating predictors with tensors, it is often beneficial to modify the representation of the input (*cf.* [51]). For example, in the context under discussion, rather than having the discrete input variables hold pixel intensities, they may correspond to small image patches, where each patch is represented by the index of a centroid it is closest to, with centroids determined via clustering applied to all patches across all images in the dataset. For simplicity, we did not transform representations in our experiments, and simply operated over raw image pixels.



Figure 2.3: Evaluation of tensor rank as measure of complexity — standard datasets can be fit accurately with predictors of extremely low tensor rank (far beneath what is required by random datasets), suggesting it may capture the essence of natural data. Left and right plots show results of fitting MNIST and Fashion-MNIST datasets, respectively, with predictors of increasing tensor rank. Original datasets are compared against two random variants: one generated by replacing images with noise (“rand image”), and the other via shuffling labels (“rand label”). As described in the text (Section 2.5.2), for simplicity of presentation, each dataset was mapped into multiple (ten) one-vs-all prediction tasks (label 1 for active category, 0 for the rest), with fit measured via mean squared error. Separately for each one-vs-all prediction task and each value $k \in \{1, \dots, 15\}$ for the tensor rank, we applied an approximate numerical method (see Appendix B.2.2.2 for details) to find the predictor of tensor rank k (or less) with which the mean squared error over training examples is minimal. We report this mean squared error, as well as that obtained by the predictor on the test set (to mitigate impact of outliers, large squared errors over test samples were clipped — see Appendix B.2.2.2 for details). Plots show, for each value of k , mean (as marker) and standard deviation (as error bar) of these errors taken over the different one-vs-all prediction tasks. Notice that the original datasets are fit accurately (low train error) by predictors of tensor rank as low as one, whereas random datasets are not (with tensor rank one, residuals of their fit are close to trivial, *i.e.* to the variance of the label). This suggests that tensor rank as a measure of complexity for predictors has potential to capture the essence of natural data. Notice also that, as expected, accurate fit with low tensor rank coincides with accurate prediction on test set, *i.e.* with generalization. For further details, as well as an experiment showing that linear predictors are incapable of accurately fitting the datasets, see Appendix B.2.

with a predictor whose tensor rank is one. To account for the comparatively small training sets, and render their fit more challenging, we quantized pixels to hold one of two values, *i.e.* we reduced images from grayscale to black and white. Following the quantization, tensors associated with predictors have dimension two in each mode, and the number of degrees of freedom in a general rank one tensor is roughly $784 \cdot 2$ — well below the number of training examples. We may thus expect to see a difference between the tensor ranks needed for fitting original datasets and those required by the random ones. This is confirmed by Figure 2.3, displaying the results of the experiment.

Figure 2.3 shows that with predictors of low tensor rank, MNIST and Fashion-MNIST can be fit much more accurately than the random datasets. Moreover, as one would presume, accurate fit with low tensor rank coincides with accurate prediction on unseen data (test set), *i.e.* with generalization. Combined with the rest of our results, we interpret this finding as an indication that tensor rank may shed light on both implicit regularization of neural networks, and the properties of natural data translating this implicit regularization to generalization.

Chapter 3

Implicit Regularization in Hierarchical Tensor Factorization and Deep Convolutional Neural Networks

The contents of this chapter are based on [179].

3.1 Background and Overview

Chapters 1 and 2 focused on the implicit regularization in matrix and tensor factorization. Matrix factorization refers to minimizing a given loss (over matrices) by parameterizing the solution as a product of matrices, and optimizing the resulting objective via gradient descent. Tensor factorization is a generalization of this procedure to multi-dimensional arrays. There, a tensor is learned through gradient descent over a sum-of-outer-products parameterization (see Section 2.2). By adopting a dynamical viewpoint, in Chapter 2 we established that gradient descent (with small learning rate and near-zero initialization) over tensor factorization induces a momentum-like effect on the components of the factorization, leading them to move slowly when small and quickly when large. This implies a form of incremental learning that results in low tensor rank solutions, analogous to the incremental rank learning phenomenon identified by [9] for matrix factorization.

From a deep learning perspective, matrix factorization can be seen as a linear neural network, and, in a similar vein, tensor factorization corresponds to a certain shallow (depth two) non-linear convolutional neural network (see Section 2.2.1). As theoretical surrogates for deep learning, the practical relevance of these models is limited. The former lacks non-linearity, while the latter misses depth — both crucial features of modern neural networks. A natural extension of matrix and tensor factorizations that accounts for both non-linearity and depth is *hierarchical tensor factorization*,¹ which corresponds to a class of *deep non-linear* convolutional neural networks [51] (with polynomial non-linearity) that have demonstrated promising performance in practice [47, 50, 193, 200, 78, 63], and have been key to the study of expressiveness in deep learning [51, 48, 49, 52, 53, 192, 132, 133, 16, 118, 119, 134].

¹The term “hierarchical tensor factorization” refers throughout to a variant of the Hierarchical Tucker factorization [86], presented in Section 3.3.

In this chapter, we provide the first analysis of implicit regularization in hierarchical tensor factorization. As opposed to tensor factorization, which is a simple construct dating back to at least the early 20'th century [96], hierarchical tensor factorization was formally introduced only recently [86], and is much more elaborate. We circumvent the challenges brought forth by the added hierarchy through identification of *local components*, and characterization of their evolution under gradient descent (with small learning rate and near-zero initialization). The characterization reveals that they are subject to a momentum-like effect, identical to that in matrix and tensor factorizations. Accordingly, local components are learned incrementally, leading to solutions with low *hierarchical tensor rank* — a central concept in tensor analysis [79, 80]. Theoretical and empirical demonstrations validate our analysis.

For the deep convolutional networks corresponding to hierarchical tensor factorization, hierarchical tensor rank is known to measure the strength of dependencies modeled between spatially distant input regions (patches of pixels in the context of image classification) — see [49, 132, 133]. The established tendency towards low hierarchical tensor rank therefore implies a bias towards local (short-range) dependencies, in accordance with the fact that convolutional networks often struggle or completely fail to learn tasks entailing long-range dependencies (see, *e.g.*, [212, 143, 155, 97, 120]). However, while this failure is typically attributed solely to a limitation in expressive capability (*i.e.* to an inability of convolutional networks to represent functions modeling long-range dependencies — see [49, 143, 120]), our analysis reveals that it also originates from implicit regularization. This suggests that the difficulty in learning long-range dependencies may be countered via *explicit* regularization, in contrast to conventional wisdom by which architectural modifications are needed. Through a series of controlled experiments we confirm this prospect, demonstrating that explicit regularization designed to promote high hierarchical tensor rank can significantly improve the performance of modern convolutional networks (*e.g.* ResNet18 and ResNet34 from [94]) on tasks involving long-range dependencies.

Our results bring forth the possibility that deep learning architectures considered sub-optimal for certain tasks (*e.g.* convolutional networks for natural language processing tasks) may be greatly improved through a right choice of explicit regularization. Theoretical understanding of implicit regularization may be key to discovering such regularizers.

The remainder of the chapter is organized as follows. For completeness, in Section 3.2 we outline relevant dynamical characterizations of implicit regularization in matrix and tensor factorizations (from [9] and Chapter 2, respectively). Section 3.3 presents the hierarchical tensor factorization model, as well as its interpretation as a deep non-linear convolutional network. In Section 3.4 we characterize the dynamics of gradient descent over hierarchical tensor factorization, establishing that they lead to low hierarchical tensor rank. Section 3.5 explains why low hierarchical tensor rank means locality for the corresponding convolutional network. Lastly, Section 3.6 demonstrates that the locality of modern convolutional networks can be countered using dedicated explicit regularization.

3.2 Preliminaries: Matrix and Tensor Factorizations

The dynamical analysis delivered in the current chapter for hierarchical tensor factorization is analogous to prior dynamical analyses for matrix and tensor factorization,

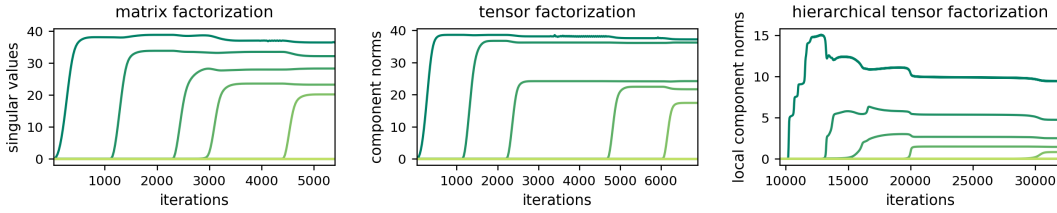


Figure 3.1: Dynamics of gradient descent over matrix, tensor, and hierarchical tensor factorizations — incremental learning leads to low matrix, tensor, and hierarchical tensor ranks, respectively. **Left:** top 10 singular values of the end matrix in a depth 3 matrix factorization when minimizing the mean squared error over observed entries from a matrix rank 5 ground truth (matrix completion loss). **Middle:** top 10 component norms of an order 3 tensor factorization when minimizing the mean squared error over observed entries from a tensor rank 5 ground truth (tensor completion loss). **Right:** top 10 local component norms at node $\{1, 2, 3, 4\}$ of an order 4 hierarchical tensor factorization induced by a perfect binary mode tree (Definition 4), when minimizing the mean squared error over observed entries from a hierarchical tensor rank $(5, 5, 5, 5, 5)$ (Definition 7) ground truth (tensor completion loss). **All:** initial factorization weights were sampled independently from a zero-mean Gaussian distribution. Notice that, in accordance with existing analyses for matrix and tensor factorizations (Section 3.2) and our analysis for hierarchical tensor factorization (Section 3.4), the singular values, component norms, and local component norms move slowly when small and quickly when large, creating an incremental learning process that results in effectively low matrix, tensor, and hierarchical tensor rank solutions, respectively. In all factorizations this implicit regularization led to accurate reconstruction of the low rank ground truth (reconstruction errors were 0.001, 0.001, and 0.005, respectively). For further details such as loss definitions and factorization dimensions, as well as additional experiments for hierarchical tensor factorization, see Appendix C.4.

carried out in [9] and Chapter 2, respectively. For completeness, this section overviews these analyses under a unified notation.

Throughout the chapter, when referring to a norm we mean the standard Frobenius (Euclidean) norm, denoted $\|\cdot\|$. For $N \in \mathbb{N}$, we let $[N] := \{1, \dots, N\}$. For vectors, matrices, or tensors, parenthesized superscripts denote elements in a collection, e.g. $(\mathbf{w}^{(n)} \in \mathbb{R}^D)_{n=1}^N$, while subscripts refer to entries, e.g. $\mathbf{W}_{i,j} \in \mathbb{R}$ is the (i, j) 'th entry of $\mathbf{W} \in \mathbb{R}^{D \times D'}$. A colon indicates all entries in an axis, e.g. $\mathbf{W}_{i,:} \in \mathbb{R}^{D'}$ is the i 'th row and $\mathbf{W}_{:,j} \in \mathbb{R}^D$ is the j 'th column of \mathbf{W} .

3.2.1 Matrix Factorization: Incremental Matrix Rank Learning

Consider the task of minimizing a differentiable and locally smooth² loss $\mathcal{L}_M : \mathbb{R}^{D \times D'} \rightarrow \mathbb{R}_{\geq 0}$ ($D, D' \in \mathbb{N}$). For example, \mathcal{L}_M can be a matrix completion loss — mean squared error over observed entries from a ground truth matrix. Matrix factorization with hidden dimensions $D_2, \dots, D_L \in \mathbb{N}$ refers to parameterizing the solution $\mathbf{W}_M \in \mathbb{R}^{D \times D'}$ as a product of L matrices, i.e. as $\mathbf{W}_M = \mathbf{W}^{(L)} \cdots \mathbf{W}^{(1)}$, where $\mathbf{W}^{(l)} \in \mathbb{R}^{D_l \times D_{l-1}}$ for $l = 1, \dots, L$, $D_0 := D'$, and $D_L := D$, and minimizing the resulting objective $\phi_M(\mathbf{W}^{(1)}, \dots, \mathbf{W}^{(L)}) := \mathcal{L}_M(\mathbf{W}_M)$ using gradient descent. We call \mathbf{W}_M the *end matrix* of the factorization. It is possible to explicitly constrain the values that \mathbf{W}_M can take by limiting the hidden dimensions D_2, \dots, D_L . However, from an implicit regularization perspective, the case of interest is where the

²A differentiable function $g : \mathbb{R}^D \rightarrow \mathbb{R}$ is *locally smooth* if for any compact subset $\mathcal{B} \subset \mathbb{R}^D$ there exists $\beta \in \mathbb{R}_{\geq 0}$ such that $\|\nabla g(\mathbf{x}) - \nabla g(\mathbf{y})\| \leq \beta \cdot \|\mathbf{x} - \mathbf{y}\|$ for all $\mathbf{x}, \mathbf{y} \in \mathcal{B}$.

search space is unconstrained, thus we consider $D_2, \dots, D_L \geq \min\{D, D'\}$. Matrix factorization can be viewed as applying a linear neural network for minimizing \mathcal{L}_M , and as such, serves a prominent theoretical model in deep learning (see e.g. [81, 57, 140, 9, 71, 159, 26, 74, 177, 44, 224, 141]).

Several characterizations of implicit regularization in matrix factorization have suggested that gradient descent, with small learning rate and near-zero initialization, induces a form of incremental matrix rank learning [71, 74, 44, 141]. Below we follow the presentation of [9], which in line with other analyses, modeled small learning rate through the infinitesimal limit, i.e. via *gradient flow*:

$$\frac{d}{dt} \mathbf{W}^{(l)}(t) = -\frac{\partial}{\partial \mathbf{W}^{(l)}} \phi_M(\mathbf{W}^{(1)}(t), \dots, \mathbf{W}^{(L)}(t))$$

for all $t \geq 0$ and $l \in [L]$. Under gradient flow, the difference $\mathbf{W}^{(l)}(t) \mathbf{W}^{(l)}(t)^\top - \mathbf{W}^{(l+1)}(t) \mathbf{W}^{(l+1)}(t)^\top$ remains constant through time for any $l \in [L-1]$ (see [7]). This implies that the *unbalancedness magnitude*, defined as $\max_l \|\mathbf{W}^{(l)}(t) \mathbf{W}^{(l)}(t)^\top - \mathbf{W}^{(l+1)}(t) \mathbf{W}^{(l+1)}(t)^\top\|$, does not change through time, thus becomes relatively small as optimization moves away from the origin, more so the closer initialization is to zero. Accordingly, it is common practice to treat the case of unbalancedness magnitude zero as an idealization of standard near-zero initializations (see, e.g., [188, 7, 20, 129, 9, 61, 13]).

With unbalancedness magnitude zero, the r 'th singular value of the end matrix $\mathbf{W}_M(t) = \mathbf{W}^{(L)}(t) \cdots \mathbf{W}^{(1)}(t)$ ($r \in [\min\{D, D'\}]$), denoted $\sigma_M^{(r)}(t) \in \mathbb{R}$, evolves by (cf. [9]):³

$$\frac{d}{dt} \sigma_M^{(r)}(t) = \sigma_M^{(r)}(t)^{2-\frac{2}{L}} L \langle -\nabla \mathcal{L}_M(\mathbf{W}_M(t)), \mathcal{C}_M^{(r)}(t) \rangle, \quad (3.1)$$

where $\mathcal{C}_M^{(r)}(t) := \mathbf{u}^{(r)}(t) \mathbf{v}^{(r)}(t)^\top \in \mathbb{R}^{D \times D'}$ is the r 'th singular component of $\mathbf{W}_M(t)$, meaning $\mathbf{u}^{(r)}(t) \in \mathbb{R}^D$ and $\mathbf{v}^{(r)}(t) \in \mathbb{R}^{D'}$ are, respectively, left and right singular vectors of $\mathbf{W}_M(t)$ corresponding to $\sigma_M^{(r)}(t)$. As evident from Equation (3.1), two factors govern the evolution rate of a singular value $\sigma_M^{(r)}(t)$. The first factor, $\langle -\nabla \mathcal{L}_M(\mathbf{W}_M(t)), \mathcal{C}_M^{(r)}(t) \rangle$, is a projection of the singular component $\mathcal{C}_M^{(r)}(t)$ onto $-\nabla \mathcal{L}_M(\mathbf{W}_M(t))$, the direction of steepest descent with respect to the end matrix. The more the singular component is aligned with $-\nabla \mathcal{L}_M(\mathbf{W}_M(t))$, the faster the singular value grows. The second, more critical factor, is $\sigma_M^{(r)}(t)^{2-\frac{2}{L}} L$, which implies that the rate of change of the singular value is proportional to its size exponentiated by $2 - 2/L$ (recall that L is the depth of the matrix factorization). This brings rise to a momentum-like effect, which attenuates the movement of small singular values and accelerates the movement of large ones. We may thus expect that if the matrix factorization is initialized near the origin, singular values progress slowly at first, and then, one after the other they reach a critical threshold and quickly rise, until convergence is attained. Such incremental learning phenomenon leads to low matrix rank solutions. It is demonstrated empirically in Figure 3.1 (left), which reproduces an experiment from [9]. We note that under certain technical conditions, the incremental matrix rank learning phenomenon can be used to prove exact matrix rank minimization [141].

³The dynamical characterization of singular values in Equation (3.1) requires \mathcal{L}_M to be analytic, a property met by standard loss functions such as the square and cross-entropy losses.

3.2.2 Tensor Factorization: Incremental Tensor Rank Learning

A depth two matrix factorization boils down to parameterizing a sought-after solution as a sum of tensor (outer) products between column vectors of $\mathbf{W}^{(2)}$ and row vectors of $\mathbf{W}^{(1)}$. Namely, since $\mathbf{W}_M = \mathbf{W}^{(2)}\mathbf{W}^{(1)}$ we may write $\mathbf{W}_M = \sum_{r=1}^R \mathbf{W}_{:,r}^{(2)} \otimes \mathbf{W}_{r,:}^{(1)}$, where R is the dimension shared between $\mathbf{W}^{(1)}$ and $\mathbf{W}^{(2)}$, and \otimes stands for the tensor product. Note that the minimal number of summands R required for \mathbf{W}_M to express a given matrix \mathbf{W} is precisely the latter's matrix rank.

By allowing each summand to be a tensor product of more than two vectors, we may transition from a factorization for matrices to a factorization for tensors. In tensor factorization, a sought-after solution $\mathcal{W}_T \in \mathbb{R}^{D_1 \times \dots \times D_N}$ — an *order* $N \geq 3$ tensor with *modes* (axes) of *dimensions* $D_1, \dots, D_N \in \mathbb{N}$ — is parameterized as $\mathcal{W}_T = \sum_{r=1}^R \mathbf{W}_{:,r}^{(1)} \otimes \dots \otimes \mathbf{W}_{:,r}^{(N)}$, where $\mathbf{W}^{(n)} \in \mathbb{R}^{D_n \times R}$ for $n \in [N]$. Each term $\mathbf{W}_{:,r}^{(1)} \otimes \dots \otimes \mathbf{W}_{:,r}^{(N)}$ in this sum is called a *component*, and \mathcal{W}_T is referred to as the *end tensor* of the factorization. Given a differentiable and locally smooth loss $\mathcal{L}_T : \mathbb{R}^{D_1 \times \dots \times D_N} \rightarrow \mathbb{R}_{\geq 0}$, e.g. mean squared error over observed entries from a ground truth tensor (i.e. a tensor completion loss), the goal is to minimize the objective $\phi_T(\mathbf{W}^{(1)}, \dots, \mathbf{W}^{(N)}) := \mathcal{L}_T(\mathcal{W}_T)$. In analogy with matrix factorization, the minimal number of components R required for \mathcal{W}_T to express a given tensor $\mathcal{W} \in \mathbb{R}^{D_1 \times \dots \times D_N}$ is defined to be the latter's *tensor rank*, and the case of interest is when R is sufficiently large to not restrict tensor rank (i.e. to admit an unconstrained search space).

Similarly to how matrix factorization corresponds to a linear neural network, tensor factorization is known (see Section 2.2.1) to be equivalent to a certain shallow (depth two) non-linear convolutional network (with polynomial non-linearity). By virtue of this equivalence, illustrated in Figure 3.2 (top), tensor factorization is considered closer to practical deep learning than matrix factorization.

As in matrix factorization, gradient flow over tensor factorization induces invariants of optimization. In particular, the differences between squared norms of vectors in the same component, i.e. $\|\mathbf{W}_{:,r}^{(n)}(t)\|^2 - \|\mathbf{W}_{:,r}^{(n')}(t)\|^2$ for $n, n' \in [N]$ and $r \in [R]$, are constant through time (cf. Lemma 1 in Section 2.3). This leads to the following definition of unbalancedness magnitude: $\max_{n,n',r} \|\|\mathbf{W}_{:,r}^{(n)}(t)\|^2 - \|\mathbf{W}_{:,r}^{(n')}(t)\|^2\|$, which does not change during optimization, therefore remains small throughout if initialization is close to the origin. Under the idealized assumption of unbalancedness magnitude zero (corresponding to infinitesimally small initialization), the norm of the r 'th component in the factorization ($r \in [R]$), i.e. $\sigma_T^{(r)}(t) := \|\otimes_{n=1}^N \mathbf{W}_{:,r}^{(n)}(t)\|$, evolves by (cf. Corollary 2 in Section 2.3):

$$\frac{d}{dt} \sigma_T^{(r)}(t) = \sigma_T^{(r)}(t)^{2-\frac{2}{N}} N \langle -\nabla \mathcal{L}_T(\mathcal{W}_T(t)), \mathcal{C}_T^{(r)}(t) \rangle, \quad (3.2)$$

where $\mathcal{C}_T^{(r)}(t) := \otimes_{n=1}^N \bar{\mathbf{W}}_{:,r}^{(n)}(t)$, with $\bar{\mathbf{W}}_{:,r}^{(n)}(t)$ defined as $\mathbf{W}_{:,r}^{(n)}(t) / \|\mathbf{W}_{:,r}^{(n)}(t)\|$ for all $n \in [N]$ (by convention, if $\mathbf{W}_{:,r}^{(n)}(t) = 0$ then $\bar{\mathbf{W}}_{:,r}^{(n)}(t) = 0$), denotes the r 'th normalized component. Comparing Equation (3.2) to Equation (3.1) reveals that the evolution rate of a component norm in tensor factorization is *structurally identical* to that of a singular value in matrix factorization. Specifically, it is determined by two factors, analogous to those in Equation (3.1): (i) a projection of the normalized component $\mathcal{C}_T^{(r)}(t)$ onto $-\nabla \mathcal{L}_T(\mathcal{W}_T(t))$, which encourages growth of components that are aligned with the direction of steepest descent with respect to the end tensor; and (ii) $\sigma_T^{(r)}(t)^{2-\frac{2}{N}} N$, which induces a momentum-like effect, leading component norms

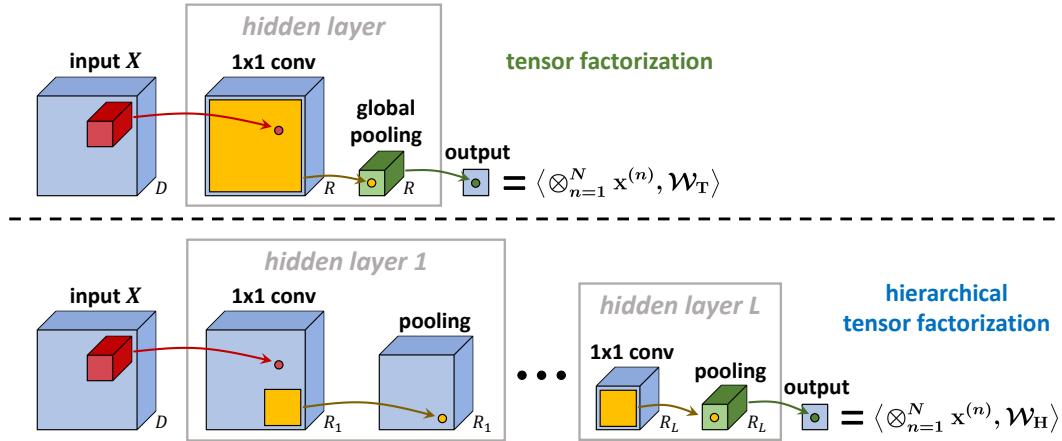


Figure 3.2: Tensor factorization corresponds to a class of shallow (depth two) non-linear convolutional networks, while hierarchical tensor factorization corresponds to a class of *deep* non-linear convolutional networks (with polynomial non-linearity). **Top:** illustration of the shallow network equivalent to tensor factorization processes. The illustration is analogous to Figure 1.3 from Chapter 1, and is repeated for ease of comparison with the deep non-linear convolutional network corresponding to hierarchical tensor factorization. Given an input $(\mathbf{x}^{(1)}, \dots, \mathbf{x}^{(N)}) \in \mathbb{R}^{D_1} \times \dots \times \mathbb{R}^{D_N}$ (illustration assumes $D_1 = \dots = D_N = D$ to avoid clutter), the network processes it using a single hidden layer, which consists of: (i) locally connected linear operator with R channels, computing $(\mathbf{W}^{(1)})^\top \mathbf{x}^{(1)}, \dots, (\mathbf{W}^{(N)})^\top \mathbf{x}^{(N)}$ with learnable weights $\mathbf{W}^{(1)}, \dots, \mathbf{W}^{(N)}$ (this operator is referred to as “ 1×1 conv” in appeal to the common case of weight sharing, *i.e.* $\mathbf{W}^{(1)} = \dots = \mathbf{W}^{(N)}$); and (ii) channel-wise global product pooling (which induces polynomial non-linearity). Summing over the resulting activations then yields the scalar output $\langle \otimes_{n=1}^N \mathbf{x}^{(n)}, \sum_{r=1}^R \otimes_{n=1}^N \mathbf{W}_{:,r}^{(n)} \rangle = \langle \otimes_{n=1}^N \mathbf{x}^{(n)}, \mathcal{W}_T \rangle$. Hence, functions realized by this class of networks are naturally represented via tensor factorization, where the number of components R and the weight matrices $\mathbf{W}^{(1)}, \dots, \mathbf{W}^{(N)}$ of the factorization correspond to the width and learnable weights of the network, respectively. **Bottom:** for a hierarchical tensor factorization induced by a perfect P -ary mode tree (Definition 4), the equivalent network is a deep variant of that associated with tensor factorization. It has $L = \log_P N$ hidden layers instead of just one, with channel-wise product pooling operating over windows of size P as opposed to globally. After passing an input $(\mathbf{x}^{(1)}, \dots, \mathbf{x}^{(N)}) \in \mathbb{R}^{D_1} \times \dots \times \mathbb{R}^{D_N}$ through all hidden layers, a final linear layer produces the network’s scalar output $\langle \otimes_{n=1}^N \mathbf{x}^{(n)}, \mathcal{W}_H \rangle$, where \mathcal{W}_H is the end tensor of the hierarchical tensor factorization (Equation (3.3)), whose weight matrices are equal to the network’s learnable weights. Thus, functions realized by this class of networks are naturally represented via hierarchical tensor factorization. We note that, as shown in [48], by considering *generalized hierarchical tensor factorizations* it is possible to account for various non-linearities beyond polynomial, *i.e.* for product pooling being converted to a different pooling operator (*e.g.* max or average), optionally preceded by a non-linear activation (*e.g.* rectified linear unit).

to move slower when small and faster when large. This suggests that, in analogy with matrix factorization, components tend to be learned incrementally, yielding a bias towards low tensor rank. For completeness, Figure 3.1 (middle) demonstrates the phenomenon empirically, reproducing the experiment from Section 2.5.1. Recall that, similarly to the case of matrix factorization, under certain technical conditions we used in Section 2.4 the incremental tensor rank learning phenomenon to prove exact tensor rank minimization.

3.3 Hierarchical Tensor Factorization

In this section we present the hierarchical tensor factorization model. We begin by informally introducing the core concepts (Section 3.3.1), after which we delve into the formal definitions (Section 3.3.2).

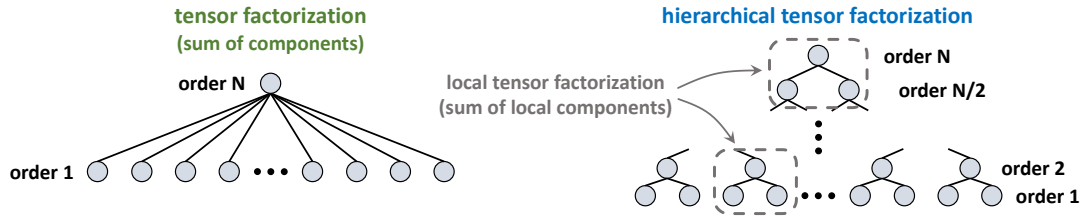


Figure 3.3: Hierarchical tensor factorization consists of multiple local tensor factorizations. **Left:** tensor factorization represents an order N tensor as a sum of components, each combining N vectors through the tensor product operator. Accordingly, it is represented by a shallow tree where all leaves are directly connected to the root. **Right:** hierarchical tensor factorization adheres to an arbitrary tree structure (figure depicts a perfect binary tree), producing an order N tensor by iteratively combining multiple local tensor factorizations. The components of the local tensor factorizations constituting the hierarchical tensor factorization are defined to be its local components. For a formal description of hierarchical tensor factorization see Section 3.3.2.

3.3.1 Informal Overview and Interpretation as Deep Non-Linear Convolutional Network

As discussed in Section 3.2.2, tensor factorization produces an order N end tensor through a sum of components, each combining N vectors using the tensor product operator. It is customary to represent this computation through a shallow tree structure with N leaves, corresponding to the weight matrices $\mathbf{W}^{(1)}, \dots, \mathbf{W}^{(N)}$, that are directly connected to the root, which computes the end tensor $\mathcal{W}_T = \sum_{r=1}^R \mathbf{W}_{:,r}^{(1)} \otimes \dots \otimes \mathbf{W}_{:,r}^{(N)}$.

Generalizing this scheme to an arbitrary tree gives rise to hierarchical tensor factorization. Given a tree, or formally, a *mode tree* of the hierarchical tensor factorization (Definition 4), the scheme progresses from leaves to root. Each internal node combines tensors produced by its children to form higher-order tensors, until finally the root outputs an order N end tensor. Different mode trees bring about different hierarchical tensor factorizations, which are essentially a composition of many local tensor factorizations, each corresponding to a different location in the mode tree. We refer to the components of these local tensor factorizations as the *local components* (Definition 5) of the hierarchical factorization — see Figure 3.3 for an illustration.

A mode tree of a hierarchical tensor factorization induces a notion of rank called *hierarchical tensor rank* (Definition 7). The hierarchical tensor rank is a tuple whose entries correspond to locations in the mode tree. The value held by an entry is characterized by the number of local components at the corresponding location, similarly to how tensor rank is characterized by the number of components in a tensor factorization (see Section 3.2.2). Motivated by matrix and tensor ranks being implicitly minimized in matrix and tensor factorizations, respectively (Section 3.2), in Section 3.4 we explore the possibility of hierarchical tensor rank being implicitly minimized in hierarchical tensor factorization. That is, we investigate the prospect of gradient descent (with small learning rate and near-zero initialization) over hierarchical tensor factorization learning solutions that can be represented with few local components at all locations of the mode tree.

Equivalence to a class of deep non-linear convolutional networks. As discussed in Section 3.2, matrix factorization can be seen as a linear neural network, and, in a similar vein, tensor factorization corresponds to a certain shallow (depth two) non-linear convolutional network (with polynomial non-linearity). A drawback of

these models as theoretical surrogates for deep learning is that the former lacks non-linearity, while the latter misses depth. Hierarchical tensor factorization accounts for both of these limitations: for appropriate mode trees, it is known (see [51]) to be equivalent to a class of deep non-linear convolutional networks (with polynomial non-linearity). These networks have demonstrated promising performance in practice [47, 50, 193, 200, 78, 63], and their equivalence to hierarchical tensor factorization has been key to the study of expressiveness in deep learning [51, 48, 49, 52, 53, 192, 132, 133, 16, 118, 119, 134]. The equivalence is illustrated in Figure 3.2 (bottom) and rigorously proven in Appendix C.1.

3.3.2 Formal Presentation

The structure of a hierarchical tensor factorization is determined by a mode tree.

Definition 4. Let $N \in \mathbb{N}$. A *mode tree* \mathcal{T} over $[N]$ is a rooted tree in which:

- every node is labeled by a subset of $[N]$;
- there are exactly N leaves, labeled $\{1\}, \dots, \{N\}$; and
- the label of an interior (non-leaf) node is the union of the labels of its children.

We identify nodes with their labels, *i.e.* with the corresponding subsets of $[N]$, and accordingly treat \mathcal{T} as a subset of $2^{[N]}$. Furthermore, we denote the set of all interior nodes by $\text{int}(\mathcal{T}) \subset \mathcal{T}$, the parent of a non-root node $v \in \mathcal{T} \setminus \{[N]\}$ by $Pa(v) \in \mathcal{T}$, and the children of $v \in \text{int}(\mathcal{T})$ by $C(v) \subset \mathcal{T}$. When enumerating over children of a node, *i.e.* over $C(v)$ for $v \in \text{int}(\mathcal{T})$, an arbitrary fixed ordering is assumed.

One may consider various mode trees, each leading to a different hierarchical tensor factorization. Notable choices include: (i) a shallow tree (comprising only leaves and root), which reduces the hierarchical tensor factorization to a tensor factorization (Section 3.2.2); and (ii) a perfect binary tree (applicable if N is a power of 2) whose corresponding hierarchical tensor factorization is perhaps the most extensively studied. Figure 3.4(a) illustrates these two choices.

Along with a mode tree \mathcal{T} , what defines a hierarchical tensor factorization are the number of local components at each interior node, denoted $(R_v \in \mathbb{N})_{v \in \text{int}(\mathcal{T})}$. The induced hierarchical tensor factorization is parameterized by weight matrices $(\mathbf{W}^{(v)} \in \mathbb{R}^{R_v \times R_{Pa(v)}})_{v \in \mathcal{T}}$, where $R_{Pa([N])} := 1$ and $R_{\{1\}} := D_1, \dots, R_{\{N\}} := D_N$. It creates the *end tensor* $\mathcal{W}_H \in \mathbb{R}^{D_1 \times \dots \times D_N}$ by constructing intermediate tensors of increasing order while traversing \mathcal{T} from leaves to root as follows:

for all $v \in \{\{1\}, \dots, \{N\}\}$ and $r \in [R_{Pa(v)}]$:

$$\underbrace{\mathcal{W}^{(v,r)}}_{\text{order } 1} := \mathbf{W}_{:,r}^{(v)},$$

for all $v \in \text{int}(\mathcal{T}) \setminus \{[N]\}$ and $r \in [R_{Pa(v)}]$ (traverse interior nodes of \mathcal{T} from leaves to root, non-inclusive):

$$\underbrace{\mathcal{W}^{(v,r)}}_{\text{order } |v|} := \pi_v \left(\sum_{r'=1}^{R_v} \mathbf{W}_{r',r}^{(v)} \left[\otimes_{v_c \in C(v)} \mathcal{W}^{(v_c,r')} \right] \right),$$

$$\underbrace{\mathcal{W}_H}_{\text{order } N} := \pi_{[N]} \left(\sum_{r'=1}^{R_{[N]}} \mathbf{W}_{r',1}^{([N])} \left[\otimes_{v_c \in C([N])} \mathcal{W}^{(v_c,r')} \right] \right),$$

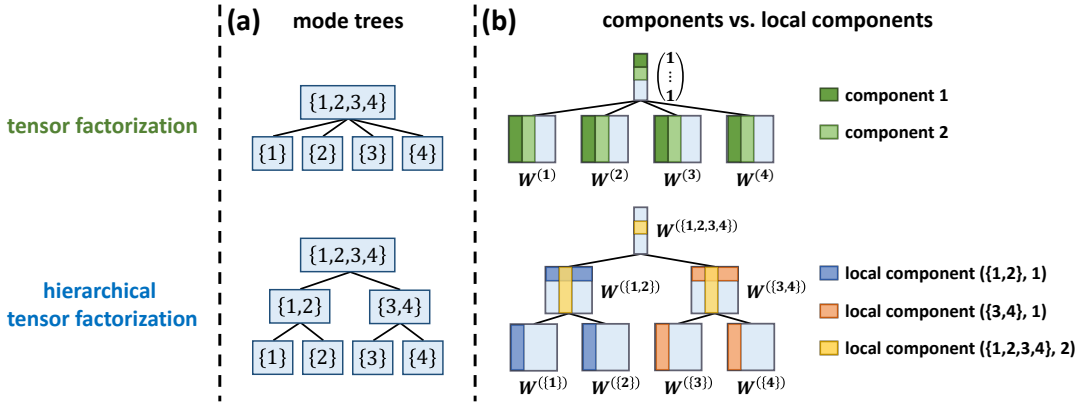


Figure 3.4: (a) Exemplar mode trees (Definition 4) for order $N = 4$ hierarchical tensor factorization. Top corresponds to the degenerate case of tensor factorization, while bottom represents the most common choice (perfect binary tree). (b) Components of a tensor factorization (top) vs. local components (Definition 5) of a hierarchical tensor factorization (bottom). The r 'th component of a tensor factorization can be seen as the tensor product between a linear coefficient, which is set to 1, and the r 'th columns of $\mathbf{W}^{(1)}, \dots, \mathbf{W}^{(N)}$. The local components of a hierarchical tensor factorization are the components of the local tensor factorizations forming it. For example, the r 'th local component at node $\{1, 2\}$ in the hierarchical tensor factorization illustrated above is the tensor product between the r 'th row of $\mathbf{W}^{(\{1,2\})}$ and the r 'th columns of its children's weight matrices $\mathbf{W}^{(\{1\})}$ and $\mathbf{W}^{(\{2\})}$.

where π_ν , for $\nu \in \mathcal{T}$, is a *mode permutation* operator which arranges the modes (axes) of its input such that they comply with an ascending order of ν .⁴

Hierarchical tensor factorization can be viewed as a composition of multiple local tensor factorizations, one for each interior node in the mode tree. The local tensor factorization for $\nu \in \text{int}(\mathcal{T})$ comprises R_ν components, referred to as the local components at node ν of the hierarchical tensor factorization — see Figure 3.4(b) for an illustration, and Definition 5 below.

Definition 5. For $\nu \in \text{int}(\mathcal{T})$ and $r \in [R_\nu]$, the (ν, r) 'th *local component* of the hierarchical tensor factorization is $\mathbf{W}_{r,:}^{(\nu)} \otimes (\otimes_{\nu_c \in \mathcal{C}(\nu)} \mathbf{W}_{:,r}^{(\nu_c)})$. We use $\text{LC}(\nu, r)$ to denote the set comprising $\mathbf{W}_{r,:}^{(\nu)}$ and $(\mathbf{W}_{:,r}^{(\nu_c)})_{\nu_c \in \mathcal{C}(\nu)}$, and $\sigma_{\text{H}}^{(\nu,r)} := \|\otimes_{\mathbf{w} \in \text{LC}(\nu,r)} \mathbf{w}\|$ to denote the norm of the (ν, r) 'th local component.

Mode trees of hierarchical tensor factorizations give rise to the notion of hierarchical tensor rank (cf. [80]), which is based on matrix ranks of specific *matricizations* of a tensor (cf. Section 3.4 in [125]).

Definition 6. The *matricization* of $\mathcal{W} \in \mathbb{R}^{D_1 \times \dots \times D_N}$ with respect to $I \subset [N]$, denoted $\llbracket \mathcal{W}; I \rrbracket \in \mathbb{R}^{\prod_{i \in I} D_i \times \prod_{j \in [N] \setminus I} D_j}$, is its arrangement as a matrix where rows correspond to modes indexed by I and columns correspond to the remaining modes.⁵

Definition 7. The *hierarchical tensor rank* of $\mathcal{W} \in \mathbb{R}^{D_1 \times \dots \times D_N}$ with respect to mode tree \mathcal{T} is the tuple comprising the matrix ranks of \mathcal{W} 's matricizations according to all

⁴For $\nu \in \text{int}(\mathcal{T})$, denote its $K := |\mathcal{C}(\nu)|$ children by ν_1, \dots, ν_K , and the elements of ν_k by $j_1^k < \dots < j_{|\nu_k|}^k$ for $k \in [K]$. Let $h: [|\nu|] \rightarrow [|\nu|]$ be the permutation sorting $(j_1^1, \dots, j_{|\nu_1|}^1, \dots, j_1^K, \dots, j_{|\nu_K|}^K)$ in ascending order. Then, the mode permutation operator for ν is defined by: $\pi_\nu(\mathcal{W})_{d_1, \dots, d_{|\nu|}} = \mathcal{W}_{d_{h(1)}, \dots, d_{h(|\nu|)}}$, where \mathcal{W} is an order $|\nu|$ tensor.

⁵Denoting the elements in I by $i_1 < \dots < i_{|I|}$ and those in $[N] \setminus I$ by $j_1 < \dots < j_{N-|I|}$, the matricization $\llbracket \mathcal{W}; I \rrbracket$ holds the entries of \mathcal{W} such that $\mathcal{W}_{d_1, \dots, d_N}$ is placed in row index $1 + \sum_{l=1}^{|I|} (d_{i_l} - 1) \prod_{l'=1}^{l-1} D_{i_{l'}}$ and column index $1 + \sum_{l=1}^{N-|I|} (d_{j_l} - 1) \prod_{l'=1}^{l-1} D_{j_{l'}}$.

nodes in \mathcal{T} except for the root, *i.e.* $(\text{rank}[\mathcal{W}; v])_{v \in \mathcal{T} \setminus \{[N]\}}$. The order of entries in the tuple does not matter as long as it is consistent.

Unless stated otherwise, when referring to the hierarchical tensor rank of a hierarchical tensor factorization's end tensor, the rank is with respect to the mode tree of the factorization. Hierarchical tensor rank differs markedly from tensor rank. Specifically, even when the hierarchical tensor rank is low, *i.e.* the matrix ranks of matricizations according to all nodes in the mode tree are low, the tensor rank is typically extremely high (exponential in the order of the tensor — see [50]).

Lemma 2 below states that the number of local components in a hierarchical tensor factorization controls the hierarchical tensor rank of its end tensor. More precisely, R_v — the number of local components at $v \in \text{int}(\mathcal{T})$ — upper bounds the matrix rank of matricizations according to the children of v .

Lemma 2 (adaptation of Theorem 7 in [53]). *For any interior node $v \in \text{int}(\mathcal{T})$ and child $v_c \in C(v)$, it holds that $\text{rank}[\mathcal{W}_H; v_c] \leq R_v$.*

Proof. Deferred to Appendix C.5.3. □

We may explicitly restrict the hierarchical tensor rank of end tensors \mathcal{W}_H (Equation (3.3)) by limiting $(R_v)_{v \in \text{int}(\mathcal{T})}$. However, since our interest lies in the implicit regularization of gradient descent, *i.e.* in the types of end tensors it will find without explicit constraints, we treat the case where $(R_v)_{v \in \text{int}(\mathcal{T})}$ can be arbitrarily large.

Given a differentiable and locally smooth loss $\mathcal{L}_H : \mathbb{R}^{D_1 \times \dots \times D_N} \rightarrow \mathbb{R}_{\geq 0}$, we consider parameterizing the solution as a hierarchical tensor factorization (Equation (3.3)), and optimizing the resulting (non-convex) objective:

$$\phi_H((\mathbf{W}^{(v)})_{v \in \mathcal{T}}) := \mathcal{L}_H(\mathcal{W}_H). \quad (3.4)$$

In line with analyses of implicit regularization in matrix and tensor factorizations (see Section 3.2), we model small learning rate for gradient descent via gradient flow:

$$\frac{d}{dt} \mathbf{W}^{(v)}(t) = - \frac{\partial}{\partial \mathbf{W}^{(v)}} \phi_H((\mathbf{W}^{(v')}(t))_{v' \in \mathcal{T}}) \quad (3.5)$$

for all $t \geq 0$ and $v \in \mathcal{T}$, where $(\mathbf{W}^{(v)}(t))_{v \in \mathcal{T}}$ denote the weight matrices at time t of optimization.

Over matrix and tensor factorizations, gradient flow initialized near zero is known to minimize matrix and tensor ranks, respectively (Section 3.2). In particular, it leads to solutions that can be represented using few components. A natural question that arises is whether a similar phenomenon takes place in hierarchical tensor factorization: does gradient flow with small initialization learn solutions that can be represented with few local components at all locations of the mode tree? That is, does it learn solutions of low hierarchical tensor rank? In Section 3.4 we answer this question affirmatively.

3.4 Incremental Hierarchical Tensor Rank Learning

In this section we theoretically analyze the implicit regularization in hierarchical tensor factorization. Our analysis extends known results for matrix and tensor factorizations outlined in Section 3.2. In particular, we show that the implicit regularization

in hierarchical tensor factorization induces an incremental learning process that results in low hierarchical tensor rank, similarly to how matrix and tensor factorizations incrementally learn solutions with low matrix and tensor ranks, respectively. To facilitate this extension, while overcoming the challenges arising from the complexity of the hierarchical tensor factorization model, we characterize the evolution of the local components introduced in Section 3.3. Our analysis is delivered in Sections 3.4.2, 3.4.3, and 3.4.4. For the convenience of the reader, Section 3.4.1 provides an informal overview.

3.4.1 Informal Overview

As discussed in Section 3.2, for both matrix and tensor factorizations, there exists an invariant of optimization whose deviation from zero is referred to as unbalancedness magnitude, and it is common to treat the case of unbalancedness magnitude zero as an idealization of standard near-zero initializations. With unbalancedness magnitude zero, singular values in a matrix factorization evolve by Equation (3.1), and component norms in a tensor factorization move per Equation (3.2). Equations (3.1) and (3.2) are structurally identical, and are interpreted as implying incremental learning of singular values and component norms, respectively, *i.e.* of matrix and tensor ranks, respectively. This interpretation was initially supported by experiments (such as those reported in Figure 3.1 (left and middle)), and later via proofs of exact matrix and tensor rank minimization under certain technical conditions.

In Section 3.4.2 we show that in analogy with matrix and tensor factorizations, hierarchical tensor factorization entails an invariant of optimization (Lemma 3), which leads to a corresponding notion of unbalancedness magnitude (Definition 8). For the canonical case of unbalancedness magnitude zero (corresponding to standard near-zero initializations), we prove that the norm of the r 'th local component associated with node ν in the mode tree, denoted $\sigma_{\text{H}}^{(\nu,r)}(t)$, evolves by (Theorem 5):

$$\frac{d}{dt}\sigma_{\text{H}}^{(\nu,r)}(t) = \sigma_{\text{H}}^{(\nu,r)}(t)^{2-\frac{2}{L_\nu}} L_\nu \langle -\nabla \mathcal{L}_{\text{H}}(\mathcal{W}_{\text{H}}(t)), \mathcal{C}_{\text{H}}^{(\nu,r)}(t) \rangle, \quad (3.6)$$

where L_ν is the number of weight vectors in the local component and $\mathcal{C}_{\text{H}}^{(\nu,r)}(t)$ is the direction it imposes on the end tensor $\mathcal{W}_{\text{H}}(t)$. Appendix C.2 generalizes the above theorem by relieving the assumption of unbalancedness magnitude zero. Namely, it establishes that Equation (3.6) holds approximately when unbalancedness magnitude at initialization is small. Equation (3.6) is structurally identical to Equations (3.1) and (3.2), therefore the evolution rate of a local component norm in hierarchical tensor factorization mirrors the evolution rates of a singular value in matrix factorization and a component norm in tensor factorization. One is thus led to interpret Equation (3.6) as implying incremental learning of local component norms, *i.e.* of hierarchical tensor rank (see Section 3.3). We support this interpretation through experiments analogous to those typically conducted for supporting the interpretation of Equations (3.1) and (3.2) as implying incremental learning of matrix and tensor ranks, respectively — see Figure 3.1 (right) as well as Appendix C.4. Moreover, we consider technical conditions similar to those assumed for proving exact matrix and tensor rank minimization by matrix and tensor factorizations, respectively, and establish theoretical results aimed at facilitating a proof of exact hierarchical tensor

rank minimization — see Section 3.4.3. Completing the missing steps for deriving such a proof is regarded as a promising direction for future work.

Lastly, we discuss the fact that hierarchical tensor rank does not adhere to a natural total ordering, and the potential of partially ordered complexity measures to further our understanding of implicit regularization in deep learning. See Section 3.4.4 for details.

3.4.2 Evolution of Local Component Norms

Lemma 3 below establishes an invariant of optimization: the differences between squared norms of weight vectors in the same local component are constant through time.

Lemma 3. *For all $v \in \text{int}(\mathcal{T})$, $r \in [R_v]$, and $\mathbf{w}, \mathbf{w}' \in \text{LC}(v, r)$:*

$$\|\mathbf{w}(t)\|^2 - \|\mathbf{w}'(t)\|^2 = \|\mathbf{w}(0)\|^2 - \|\mathbf{w}'(0)\|^2, \quad t \geq 0.$$

Proof sketch (proof in Appendix C.5.4). We show that $\frac{d}{dt}\|\mathbf{w}(t)\|^2 = \frac{d}{dt}\|\mathbf{w}'(t)\|^2$ for all $t \geq 0$. Then, integrating both sides with respect to time completes the proof. \square

The above invariant leads to the following definition of unbalancedness magnitude.

Definition 8. The *unbalancedness magnitude* of a hierarchical tensor factorization (Equation (3.3)) is:

$$\max_{v \in \text{int}(\mathcal{T}), r \in [R_v], \mathbf{w}, \mathbf{w}' \in \text{LC}(v, r)} \left| \|\mathbf{w}\|^2 - \|\mathbf{w}'\|^2 \right|.$$

Lemma 3 implies that the unbalancedness magnitude remains constant throughout optimization. In the common regime of near-zero initialization, it will start off small, and stay small throughout. The closer initialization is to zero, the smaller the unbalancedness magnitude is. In accordance with analyses for matrix and tensor factorizations (see Section 3.2), we treat the case of unbalancedness magnitude zero as an idealization of standard near-zero initializations. Theorem 5 analyzes this case, characterizing the dynamics for norms of local components.

Theorem 5. *Assume unbalancedness magnitude zero at initialization. Let $\mathcal{W}_H(t)$ denote the end tensor (Equation (3.3)) and $(\sigma_H^{(v,r)}(t))_{v \in \text{int}(\mathcal{T}), r \in [R_v]}$ denote the norms of local components (Definition 5) at time $t \geq 0$ of optimization. Then, for any $v \in \text{int}(\mathcal{T})$ and $r \in [R_v]$:*

$$\frac{d}{dt}\sigma_H^{(v,r)}(t) = \sigma_H^{(v,r)}(t)^{2-\frac{2}{L_v}} L_v \langle -\nabla \mathcal{L}_H(\mathcal{W}_H(t)), \mathcal{C}_H^{(v,r)}(t) \rangle, \quad (3.7)$$

where $L_v := |\mathcal{C}(v)| + 1$ is the number of weight vectors in a local component at node v , and $\mathcal{C}_H^{(v,r)}(t) \in \mathbb{R}^{D_1 \dots D_N}$ is the end tensor obtained by normalizing the r 'th local component at node v and setting all other local components at node v to zero, i.e. by replacing in Equation (3.3) $\mathcal{W}^{(v,r')}$ with $\pi_v((\sigma_H^{(v,r)})^{-1} \mathbf{W}_{r,r'}^{(v)} [\otimes_{v_c \in \mathcal{C}(v)} \mathcal{W}^{(v_c,r')}])$ for all $r' \in [R_{Pa(v)}]$. By convention, $\mathcal{C}_H^{(v,r)}(t) = 0$ if $\sigma_H^{(v,r)}(t) = 0$.

Proof sketch (proof in Appendix C.5.5). If $\sigma_H^{(v,r)}(t)$ is zero at some $t \geq 0$, then we show that it must be identically zero through time, leading both sides of Equation (3.7) to be equal to zero. Otherwise, differentiating the local component's norm with respect

to time, we obtain:

$$\frac{d}{dt}\sigma_{\text{H}}^{(v,r)}(t) = \langle -\nabla\mathcal{L}_{\text{H}}(\mathcal{W}_{\text{H}}(t)), \mathcal{C}_{\text{H}}^{(v,r)}(t) \rangle \cdot \sum_{\mathbf{w} \in \text{LC}(v,r)} \prod_{\mathbf{w}' \in \text{LC}(v,r) \setminus \{\mathbf{w}\}} \|\mathbf{w}'(t)\|^2.$$

Since the unbalancedness magnitude is zero at initialization, Lemma 3 implies that $\|\mathbf{w}(t)\|^2 = \|\mathbf{w}'(t)\|^2 = \sigma_{\text{H}}^{(v,r)}(t)^{2/L_v}$ for all $\mathbf{w}, \mathbf{w}' \in \text{LC}(v,r)$, which together with the expression above for $\frac{d}{dt}\sigma_{\text{H}}^{(v,r)}(t)$ establishes Equation (3.7). \square

As can be seen from Equation (3.7), the evolution of local component norms in a hierarchical tensor factorization is structurally identical to the evolution of singular values in matrix factorization (Equation (3.1)) and component norms in tensor factorization (Equation (3.2)). Specifically, it is dictated by two factors: a projection term, $\langle -\nabla\mathcal{L}_{\text{H}}(\mathcal{W}_{\text{H}}(t)), \mathcal{C}_{\text{H}}^{(v,r)}(t) \rangle$, and a self-dependence term, $\sigma_{\text{H}}^{(v,r)}(t)^{2-\frac{2}{L_v}L_v}$. Analogous to a singular component $\mathcal{C}_{\text{M}}^{(r)}(t)$ in matrix factorization and a normalized component $\mathcal{C}_{\text{T}}^{(r)}(t)$ in tensor factorization, $\mathcal{C}_{\text{H}}^{(v,r)}(t)$ is the direction that the (v,r) 'th local component imposes on $\mathcal{W}_{\text{H}}(t)$.⁶ The projection of $\mathcal{C}_{\text{H}}^{(v,r)}(t)$ onto $-\nabla\mathcal{L}_{\text{H}}(\mathcal{W}_{\text{H}}(t))$ therefore promotes growth of local components that align $\mathcal{W}_{\text{H}}(t)$ with $-\nabla\mathcal{L}_{\text{H}}(\mathcal{W}_{\text{H}}(t))$, the direction of steepest descent. More critical is the self-dependence term, $\sigma_{\text{H}}^{(v,r)}(t)^{2-\frac{2}{L_v}L_v}$, which induces a momentum-like effect that attenuates the movement of small local components and accelerates the movement of large ones. It suggests that, in analogy with matrix and tensor factorizations, local components tend to be learned incrementally, yielding a bias towards low hierarchical tensor rank. This prospect is affirmed empirically in Figure 3.1 (right) as well as Appendix C.4, and is supported theoretically in Section 3.4.3.

Evolution of local component norms under arbitrary initialization. Theorem 5 can be extended to account for arbitrary initialization, *i.e.* for initialization with unbalancedness magnitude different from zero. For conciseness we defer this extension to Appendix C.2, while noting that if initialization has small unbalancedness magnitude — as is the case with any near-zero initialization — then local component norms approximately evolve per Equation (3.7), *i.e.* the result of Theorem 5 approximately holds.

3.4.3 Implicit Hierarchical Tensor Rank Minimization

As discussed in Section 3.2, under certain technical conditions, the incremental matrix and tensor rank learning phenomena, induced by the implicit regularization in matrix and tensor factorizations, can be used to prove exact matrix and tensor rank minimization, respectively. Below we consider similar technical conditions, and provide theoretical results aimed at facilitating an analogous proof for hierarchical tensor factorization, *i.e.* a proof that its implicit regularization leads to exact hierarchical tensor rank minimization. We begin by illustrating how, under said conditions, the incremental hierarchical tensor rank learning phenomenon established in Theorem 5 leads to solutions with many small local components (Section 3.4.3.1). We then show that this implies proximity to low hierarchical tensor rank (Section 3.4.3.2). Throughout the above, the main step missing in order to derive a complete proof of

⁶Indeed, just as in matrix factorization $\mathbf{W}_{\text{M}} = \sum_r \sigma_{\text{M}}^{(r)} \cdot \mathcal{C}_{\text{M}}^{(r)}$, and in tensor factorization $\mathcal{W}_{\text{T}} = \sum_r \sigma_{\text{T}}^{(r)} \cdot \mathcal{C}_{\text{T}}^{(r)}$, the end tensor of a hierarchical tensor factorization decomposes as $\mathcal{W}_{\text{H}} = \sum_{r=1}^{R_v} \sigma_{\text{H}}^{(v,r)} \cdot \mathcal{C}_{\text{H}}^{(v,r)}$ (implied by Lemmas 39 and 46 in Appendix C.5).

exact hierarchical tensor rank minimization, is confirmation that a certain alignment inequality (Equation (3.8)) holds throughout optimization. We regard this as an important direction for future work.

3.4.3.1 Illustrative Demonstration of Small Local Components

Below we qualitatively demonstrate how the dynamical characterization derived in Section 3.4.2 implies that the implicit regularization in hierarchical tensor factorization can lead to solutions with small local components. Under the setting and notation of Theorem 5, consider an initialization $(\mathbf{U}^{(v)} \in \mathbb{R}^{R_v \times R_{Pa(v)}})_{v \in \mathcal{T}}$ for the weight matrices of the hierarchical tensor factorization, scaled by $\alpha \in \mathbb{R}_{>0}$. That is, $\mathbf{W}^{(v)}(0) = \alpha \cdot \mathbf{U}^{(v)}$ for all $v \in \mathcal{T}$. Focusing on some interior node $v \in \text{int}(\mathcal{T})$, let $r, \bar{r} \in [R_v]$, and assume for simplicity that v is not degenerate, in the sense that it has more than one child. Suppose also that at initialization the norm of the (v, r) 'th local component is greater than the norm of the (v, \bar{r}) 'th local component, i.e. $\sigma_{\mathbf{H}}^{(v,r)}(0) > \sigma_{\mathbf{H}}^{(v,\bar{r})}(0)$, and that $\mathcal{C}_{\mathbf{H}}^{(v,r)}(t)$ is at least as aligned as $\mathcal{C}_{\mathbf{H}}^{(v,\bar{r})}(t)$ with the direction of steepest descent up to a time $T > 0$, i.e. for all $t \in [0, T]$:

$$\langle -\nabla \mathcal{L}_{\mathbf{H}}(\mathcal{W}_{\mathbf{H}}(t)), \mathcal{C}_{\mathbf{H}}^{(v,r)}(t) \rangle \geq \langle -\nabla \mathcal{L}_{\mathbf{H}}(\mathcal{W}_{\mathbf{H}}(t)), \mathcal{C}_{\mathbf{H}}^{(v,\bar{r})}(t) \rangle. \quad (3.8)$$

Then, by Theorem 5 for all $t \in [0, T]$:⁷

$$\sigma_{\mathbf{H}}^{(v,\bar{r})}(t)^{-2+\frac{2}{L_v}} \frac{d}{dt} \sigma_{\mathbf{H}}^{(v,\bar{r})}(t) \leq \sigma_{\mathbf{H}}^{(v,r)}(t)^{-2+\frac{2}{L_v}} \frac{d}{dt} \sigma_{\mathbf{H}}^{(v,r)}(t).$$

Integrating both sides with respect to time, we may upper bound $\sigma_{\mathbf{H}}^{(v,\bar{r})}(t)$ with a function of $\sigma_{\mathbf{H}}^{(v,r)}(t)$:

$$\sigma_{\mathbf{H}}^{(v,\bar{r})}(t) \leq \left[\sigma_{\mathbf{H}}^{(v,r)}(t)^{-\frac{L_v-2}{L_v}} + \alpha^{-(L_v-2)} \cdot \text{const} \right]^{-\frac{L_v}{L_v-2}}, \quad (3.9)$$

where *const* stands for a positive value that does not depend on t and α . Equation (3.9) reveals a gap between $\sigma_{\mathbf{H}}^{(v,r)}(t)$ and $\sigma_{\mathbf{H}}^{(v,\bar{r})}(t)$ that is more significant the smaller the initialization scale α is. In particular, regardless of how large $\sigma_{\mathbf{H}}^{(v,r)}(t)$ is, $\sigma_{\mathbf{H}}^{(v,\bar{r})}(t)$ is upper bounded by a value that approaches zero as $\alpha \rightarrow 0$. Hence, initializing near zero produces solutions with small local components.

3.4.3.2 Small Local Components Imply Proximity to Low Hierarchical Tensor Rank

The following proposition establishes that small local components in a hierarchical tensor factorization imply that its end tensor can be well approximated with low hierarchical tensor rank.

Proposition 5. *Consider an assignment for the weight matrices $(\mathbf{W}^{(v)} \in \mathbb{R}^{R_v \times R_{Pa(v)}})_{v \in \mathcal{T}}$ of a hierarchical tensor factorization, and let $B := \max_{v \in \mathcal{T}} \|\mathbf{W}^{(v)}\|$. Assume without loss of generality that at each $v \in \text{int}(\mathcal{T})$, local components are ordered by their norms, i.e. $\sigma_{\mathbf{H}}^{(v,1)} \geq \dots \geq \sigma_{\mathbf{H}}^{(v,R_v)}$. Then, for any $\epsilon \geq 0$ and $(R'_v \in \mathbb{N})_{v \in \text{int}(\mathcal{T})}$, if $\sum_{r=R'_v+1}^{R_v} \sigma_{\mathbf{H}}^{(v,r)} \leq$*

⁷A local component cannot reach the origin unless it was initialized there (implied by Lemma 48 in Appendix C.5). Accordingly, we disregard the trivial case where $\sigma_{\mathbf{H}}^{(v,\bar{r})}(t) = 0$ for some $t \in [0, T]$.

$\epsilon \cdot (|\mathcal{T}| - N)^{-1} B^{|\mathcal{C}(v)|+1-|\mathcal{T}|}$ for all $v \in \text{int}(\mathcal{T})$, it holds that:

$$\inf_{\substack{\mathcal{W} \in \mathbb{R}^{D_1 \times \dots \times D_N} \text{ s.t.} \\ \forall v \in \mathcal{T} \setminus \{[N]\}: \text{rank}[\mathcal{W}; v] \leq R'_{Pa(v)}}} \|\mathcal{W}_H - \mathcal{W}\| \leq \epsilon,$$

i.e. \mathcal{W}_H is within ϵ -distance from the set of tensors whose hierarchical tensor rank is no greater (element-wise) than $(R'_{Pa(v)})_{v \in \mathcal{T} \setminus \{[N]\}}$.

Proof sketch (proof in Appendix C.5.6). Let $\overline{\mathcal{W}}_H^S$ be the end tensor obtained after pruning all local components indexed by $\mathcal{S} := \{(v, r) : v \in \text{int}(\mathcal{T}), r \in \{R'_v + 1, \dots, R_v\}\}$, i.e. after setting to zero the r 'th row of $\mathbf{W}^{(v)}$ and the r 'th column of $\mathbf{W}^{(v_c)}$ for all $(v, r) \in \mathcal{S}$ and $v_c \in \mathcal{C}(v)$. The desired result follows by showing that $\text{rank}[\overline{\mathcal{W}}_H^S; v] \leq R'_{Pa(v)}$ for all $v \in \mathcal{T} \setminus \{[N]\}$, and upper bounding $\|\mathcal{W}_H - \overline{\mathcal{W}}_H^S\|$ by ϵ . \square

3.4.4 Partially Ordered Complexity Measure

Existing attempts to explain implicit regularization in deep learning typically argue for reduction of some complexity measure that is *totally ordered* (meaning that within any two values for this measure, there must be one smaller than or equal to the other), for example a norm [81, 197, 140, 216, 149]. Recent evidence suggests that obtaining a complete explanation through such complexity measures may not be possible [177, 207]. Hierarchical tensor rank (which we have shown to be implicitly reduced by a class of deep non-linear convolutional networks) represents a new type of complexity measure, in the sense that it is *partially ordered*. Specifically, while it entails a standard (product) partial order — $(r_1, \dots, r_K) \leq (r'_1, \dots, r'_K)$ if and only if $r_i \leq r'_i$ for all $i \in [K]$ — it does not admit a natural total order. Indeed, Proposition 6 below shows that there exist simple learning problems in which, among the data-fitting solutions, there are multiple minimal hierarchical tensor ranks, none smaller than or equal to the other. We believe the notion of a partially ordered complexity measure may pave the way to furthering our understanding of implicit regularization in deep learning.

Proposition 6. *For every order $N \in \mathbb{N}_{\geq 3}$ and mode dimensions $D_1, \dots, D_N \in \mathbb{N}_{\geq 2}$, there exists a tensor completion problem (i.e. a loss $\mathcal{L}(\mathcal{W}) = \frac{1}{|\Omega|} \sum_{(d_1, \dots, d_N) \in \Omega} (\mathcal{W}_{d_1, \dots, d_N} - \mathcal{W}_{d_1, \dots, d_N}^*)^2$ with ground truth $\mathcal{W}^* \in \mathbb{R}^{D_1 \times \dots \times D_N}$ and set of observed entries $\Omega \subset [D_1] \times \dots \times [D_N]$) in which, for every mode tree \mathcal{T} over $[N]$ (Definition 4), the set of hierarchical tensor ranks for tensors fitting the observations includes multiple minimal elements (under the standard product partial order), none smaller than or equal to the other. That is, the set $\mathcal{R}_{\mathcal{T}} := \left\{ (\text{rank}[\mathcal{W}; v])_{v \in \mathcal{T} \setminus \{[N]\}} : \mathcal{W} \in \mathbb{R}^{D_1 \times \dots \times D_N}, \mathcal{L}(\mathcal{W}) = 0 \right\}$ includes elements $(R_v)_{v \in \mathcal{T} \setminus \{[N]\}}$ and $(R'_v)_{v \in \mathcal{T} \setminus \{[N]\}}$ for which the following hold: (i) there exists no $(R''_v)_{v \in \mathcal{T} \setminus \{[N]\}} \in \mathcal{R}_{\mathcal{T}} \setminus \{(R_v)_{v \in \mathcal{T} \setminus \{[N]\}}, (R'_v)_{v \in \mathcal{T} \setminus \{[N]\}}\}$ satisfying $(R''_v)_v \leq (R_v)_v$ or $(R''_v)_v \leq (R'_v)_v$; and (ii) neither $(R_v)_v \leq (R'_v)_v$ nor $(R'_v)_v \leq (R_v)_v$.*

Proof sketch (proof in Appendix C.5.7). We construct a tensor completion problem and two solutions \mathcal{W} and \mathcal{W}' (tensors fitting observed entries) such that, for every mode tree \mathcal{T} , the hierarchical tensor ranks with respect to \mathcal{T} of \mathcal{W} and \mathcal{W}' are two different minimal elements of $\mathcal{R}_{\mathcal{T}}$. \square

3.5 Low Hierarchical Tensor Rank Implies Locality

In Section 3.4 we established that the implicit regularization in hierarchical tensor factorization favors solutions with low hierarchical tensor rank. A natural question that arises is what are the implications of this tendency for the class of deep convolutional networks equivalent to hierarchical tensor factorization (illustrated in Figure 3.2 (bottom)). It is known [49, 132, 133] that for this class of networks, hierarchical tensor rank measures the strength of dependencies modeled between spatially distant input regions (patches of pixels in the context of image classification) — see brief explanation in Section 3.5.1 below, and formal derivation in Appendix C.3. An implicit regularization towards low hierarchical tensor rank thus implies a bias towards local (short-range) dependencies. While seemingly benign, this observation is shown in Section 3.6 to bring forth a practical method for improving performance of contemporary convolutional networks (*e.g.* ResNet18 and ResNet34 from [94]) on tasks with long-range dependencies.

3.5.1 Locality via Separation Rank

Given a multivariate function f with scalar output, a popular measure of dependencies between a set of input variables and its complement is known as *separation rank*. The separation rank, formally presented in Definition 9 below, was originally introduced in [23], and has since been employed for various applications [91, 84, 24], as well as analyses of expressiveness in deep learning [49, 52, 132, 133, 135, 215, 136]. It is also prevalent in quantum physics, where it serves as a measure of entanglement [133].

Consider the convolutional network equivalent to a hierarchical tensor factorization with mode tree \mathcal{T} . It turns out (see formal derivation in Appendix C.3) that for functions realized by this network, separation ranks measuring dependencies between distinct regions of the input are precisely equal to entries of the hierarchical tensor rank with respect to \mathcal{T} (recall that, as discussed in Section 3.3, the hierarchical tensor rank is a tuple). Thus, low hierarchical tensor rank implies that the separation ranks are low, which in turn means that dependencies modeled between distinct input regions are weak, *i.e.* that only local dependencies are prominent.

Definition 9. The *separation rank* of $f : \times_{n=1}^N \mathbb{R}^{D_n} \rightarrow \mathbb{R}$ with respect to $I \subset [N]$, denoted $\text{sep}(f; I)$, is the minimal $R \in \mathbb{N} \cup \{0\}$ for which there exist $g_1, \dots, g_R : \times_{i \in I} \mathbb{R}^{D_i} \rightarrow \mathbb{R}$ and $\bar{g}_1, \dots, \bar{g}_R : \times_{j \in [N] \setminus I} \mathbb{R}^{D_j} \rightarrow \mathbb{R}$ such that:

$$f(\mathbf{x}^{(1)}, \dots, \mathbf{x}^{(N)}) = \sum_{r=1}^R g_r((\mathbf{x}^{(i)})_{i \in I}) \cdot \bar{g}_r((\mathbf{x}^{(j)})_{j \in [N] \setminus I}).$$

Interpretation. The separation rank of f with respect to I is the minimal number of summands required to express f , where each summand is a product of two functions — one that operates over variables indexed by I , and another that operates over the remaining variables. If $\text{sep}(f; I) = 1$, the function is separable, meaning it does not model any interaction between the sets of variables. In a statistical setting, where f is a probability density function, this would mean that $(\mathbf{x}^{(i)})_{i \in I}$ and $(\mathbf{x}^{(j)})_{j \in [N] \setminus I}$ are statistically independent. The higher $\text{sep}(f; I)$ is, the farther f is from separability, *i.e.* the stronger the dependencies it models between $(\mathbf{x}^{(i)})_{i \in I}$ and $(\mathbf{x}^{(j)})_{j \in [N] \setminus I}$.

3.6 Countering Locality of Convolutional Networks via Regularization

Convolutional networks often struggle or completely fail to learn tasks that entail strong dependence between spatially distant regions of the input (patches of pixels in image classification or tokens in natural language processing tasks) — see, *e.g.*, [212, 143, 155, 97, 120]. Conventional wisdom attributes this failure to the local nature of the architecture, *i.e.* to its inability to express long-range dependencies (see, *e.g.*, [49, 143, 120]). This suggests that addressing the problem requires modifying the architecture. Our theory reveals that there is also an implicit regularization at play, giving rise to the possibility of countering the locality of convolutional networks via *explicit* regularization, without modifying their architecture. In the current section we affirm this possibility, demonstrating that carefully designed regularization can greatly improve the performance of contemporary convolutional networks on tasks involving long-range dependencies. For brevity, we defer some implementation details and experiments to Appendix C.4.

We conducted a series of experiments, using the ubiquitous ResNet18 and ResNet34 convolutional networks [94], over two types of image classification datasets in which the distance between salient regions can be controlled. The first type, referred to as "IsSameClass," comprises datasets we constructed, where the goal is to predict whether two randomly sampled CIFAR10 [127] images are of the same class. Each input sample is a 32×224 image filled with zeros, in which the CIFAR10 images are placed (symmetrically around the center) at a predetermined distance from each other (to comply with ResNets, inputs were padded to have size 224×224). By increasing the predetermined distance between CIFAR10 images, we produce datasets requiring stronger modeling of long-range dependencies. The second type of datasets is taken from the Pathfinder challenge [143, 120, 202] — a standard benchmark for modeling long-range dependencies. In Pathfinder, each image contains two white circles and multiple dashed paths (curves) over a black background, and the goal is to predict whether the circles are connected by a path. The length of connecting paths is predetermined, allowing control over the (spatial) range of dependencies necessary to model. Representative examples from IsSameClass and Pathfinder datasets are displayed in Figure 3.5.

Figure 3.6 shows that when fitting IsSameClass and Pathfinder datasets, increasing the strength of long-range dependencies (*i.e.* the distance between images in IsSameClass, and the connecting path length in Pathfinder) leads to significant degradation in test accuracy, oftentimes resulting in performance no better than random guessing. This phenomenon complies with existing evidence from [143, 120] showing failure of convolutional networks in learning tasks with long-range dependencies. However, while [143, 120] address the problem by modifying the architecture, we tackle it through explicit regularization (described in Section 3.6.1 below) designed to promote high separation ranks (Definition 9), *i.e.* long-range dependencies between image regions. As evident in Figure 3.6, our regularization significantly improves test accuracy. This implies that the tendency towards locality of modern convolutional networks may in large part be due to implicit regularization, and not an inherent limitation of expressive power as often believed. Our findings showcase that deep learning architectures considered suboptimal for certain tasks may be greatly improved through a right choice of explicit regularization. Theoretical understanding of implicit regularization may be key to discovering such regularizers.

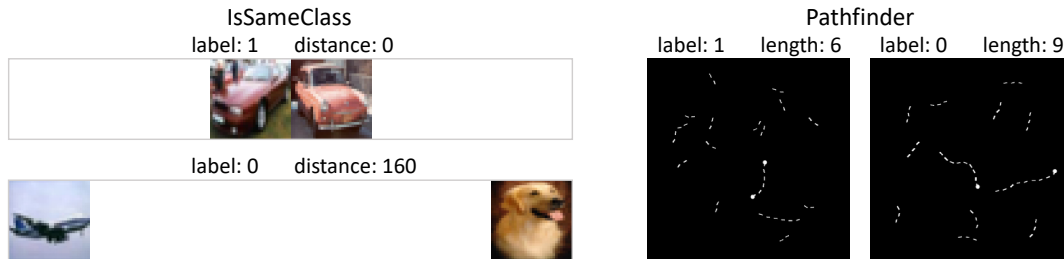


Figure 3.5: Samples from IsSameClass and Pathfinder datasets. For further details on their creation process see Appendix C.4.2.2. **Left:** positive and negative samples from IsSameClass datasets with 0 and 160 pixels between images, respectively. The label is 1 if the two CIFAR10 images are of the same class, and 0 otherwise. For the sake of illustration, background is displayed as white instead of black, and padding is not shown (*i.e.* only the raw 32×224 input is presented). **Right:** positive and negative samples from Pathfinder challenge [143] datasets with connecting path lengths 6 and 9, respectively. A connecting path is one that joins the two circles, and if present, its length is measured in the number of dashes. The label of a sample is 1 if it includes a connecting path (*i.e.* if the two circles are connected), and 0 otherwise.

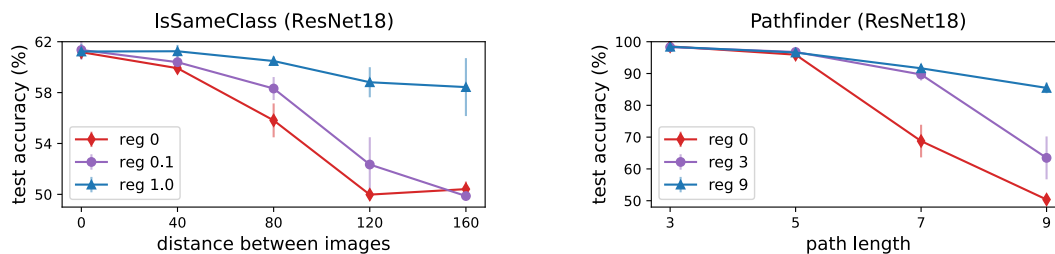


Figure 3.6: Dedicated explicit regularization can counter the locality of convolutional networks, significantly improving performance on tasks with long-range dependencies. Plots present test accuracies achieved by a randomly initialized ResNet18 over IsSameClass (left) and Pathfinder (right) datasets, with varying spatial distances between salient regions of the input (CIFAR10 images in IsSameClass and connected circles in Pathfinder — see Figure 3.5). For each dataset, the network was trained via stochastic gradient descent to minimize a regularized objective, consisting of the binary cross-entropy loss and the dedicated regularization described in Section 3.6.1. The legend specifies the regularization coefficients used. Markers and error bars report means and standard deviations, respectively, taken over five different runs for the corresponding combination of dataset and regularization coefficient. As expected, when increasing the (spatial) range of dependencies required to be modeled, the test accuracy obtained by an unregularized network (regularization coefficient zero) substantially deteriorates, reaching the vicinity of the trivial value 50%. Conventional wisdom attributes this failure to a limitation in the expressive capability of convolutional networks (*i.e.* to their inability to represent functions modeling long-range dependencies). However, as can be seen, applying the dedicated regularization significantly improved performance, without any architectural modification. Appendix C.4 provides further implementation details, as well as additional experiments: (i) using ResNet34; and (ii) showing similar improvements when the baseline network (“reg 0”) is already regularized via standard techniques (weight decay or dropout).

3.6.1 Explicit Regularization Promoting Long-Range Dependencies

We describe below the explicit regularization applied in our experiments to counter the locality of convolutional networks. We emphasize that this regularization is based on our theory, and merely serves as an example to how the performance of convolutional networks on tasks involving long-range dependencies can be improved without modifying their architecture. Further evaluation and improvement of our regularization are regarded as promising directions for future work.

Denote by $f_{\Theta}(\mathbf{X})$ the output of a neural network, where Θ stands for its learnable weights, and $\mathbf{X} := (\mathbf{x}^{(1)}, \dots, \mathbf{x}^{(N)})$ represents an input image, with each $\mathbf{x}^{(n)}$ standing for a pixel. Suppose we are given a subset of indices $I \subset [N]$, with complement $J := [N] \setminus I$, and we would like to encourage the network to learn a function f_{Θ} that models strong dependence between $\mathbf{X}_I := (\mathbf{x}^{(i)})_{i \in I}$ (pixels indexed by I) and $\mathbf{X}_J := (\mathbf{x}^{(j)})_{j \in J}$ (those indexed by J). As discussed in Section 3.5.1, a standard measure of such dependence is the separation rank, provided in Definition 9. If the separation rank of f_{Θ} with respect to I is one, meaning no dependence between \mathbf{X}_I and \mathbf{X}_J is modeled, then we may write $f_{\Theta}(\mathbf{X}) = g(\mathbf{X}_I) \cdot \bar{g}(\mathbf{X}_J)$ for some functions g and \bar{g} . This implies that $\nabla_{\mathbf{X}_I} f_{\Theta}(\mathbf{X}) = \bar{g}(\mathbf{X}_J) \cdot \nabla g(\mathbf{X}_I)$, meaning that a change in \mathbf{X}_J (with \mathbf{X}_I held fixed) does not affect the direction of $\nabla_{\mathbf{X}_I} f_{\Theta}(\mathbf{X})$, only its magnitude (and possibly its sign). This observation suggests that, in order to learn a function f_{Θ} modeling strong dependence between \mathbf{X}_I and \mathbf{X}_J , one may add a regularization term that promotes a change in the direction of $\nabla_{\mathbf{X}_I} f_{\Theta}(\mathbf{X})$ whenever \mathbf{X}_J is altered (with \mathbf{X}_I held fixed).

The regularization applied in our experiments is of the type outlined above, with I and J chosen to promote long-range dependencies. Namely, at each iteration of stochastic gradient descent we randomly choose disjoint subsets of indices I and J corresponding to contiguous (distinct) image regions. Then, for each image \mathbf{X} in the iteration's batch, we let \mathbf{X}' be the result of replacing the pixels in \mathbf{X} indexed by J with alternative values taken from a different image in the training set. Finally, we compute $|\langle \nabla_{\mathbf{X}_I} f_{\Theta}(\mathbf{X}), \nabla_{\mathbf{X}_I} f_{\Theta}(\mathbf{X}') \rangle| \cdot \|\nabla_{\mathbf{X}_I} f_{\Theta}(\mathbf{X})\|^{-1} \|\nabla_{\mathbf{X}_I} f_{\Theta}(\mathbf{X}')\|^{-1}$ — (absolute value of) cosine of the angle between $\nabla_{\mathbf{X}_I} f_{\Theta}(\mathbf{X})$ and $\nabla_{\mathbf{X}_I} f_{\Theta}(\mathbf{X}')$ — average it across the batch, multiply the average by a constant coefficient, and add the result to the minimized objective.⁸ For further details see Appendix C.4.2.2.

⁸Each artificially generated image \mathbf{X}' is used only to compute the regularization term, not as an additional training instance incurring its own loss. Our proposed regularization is therefore fundamentally different from data augmentation.

Chapter 4

Related Work

Implicit regularization. A large and growing body of literature has theoretically investigated the implicit regularization brought forth by gradient-based optimization. Works along this line have treated various models, including: linear predictors [197, 83, 162, 110, 191]; polynomially parameterized linear models with a single output [109, 216, 156, 11, 90, 175, 142, 45]; shallow non-linear neural networks [98, 207, 187, 160, 149]; homogeneous networks [148, 208]; and ultra-wide networks [170, 43]. Arguably the most widely analyzed model is matrix factorization [81, 57, 140, 9, 71, 159, 26, 74, 177, 44, 60, 224, 154, 141], whose study we extended to tensor and hierarchical tensor factorizations in Chapters 2 and 3. Among other contributions, our results generalize existing dynamical characterizations for matrix factorization (see Section 3.2) to tensor and hierarchical tensor factorizations — considerably richer and more complex models.

With regards to convolutional networks, theoretical investigations of their implicit regularization are scarce. Existing works in this category treat linear [83, 107, 123] and homogeneous [161, 148, 111] models.¹ None of these works have pointed out an implicit regularization towards local dependencies, as our theory does (Sections 3.4 and 3.5). Although the locality of convolutional networks is widely accepted, it is typically ascribed to expressive properties determined by their architecture (see, e.g., [49, 143, 120]). Our work is the first to indicate that it also originates from implicit regularization. As we demonstrate in Section 3.6, this observation can have far reaching implications to the performance of convolutional networks in practice.

Matrix factorization. The literature on matrix factorization for low-rank matrix recovery is far too broad to cover here — we refer to [42] for a recent survey, while mentioning that the technique is often attributed to [32]. Notable works proving successful recovery of a low-rank matrix via matrix factorization trained by gradient descent with no explicit regularization are [206, 150, 140]. Of these, [140] can be viewed as affirming Conjecture 1 (from [81]) for a certain special case. [22] has affirmed Conjecture 1 under different assumptions, but nonetheless argued empirically that it does not hold true in general, resonating with Conjecture 2 (from [9]). To the best of our knowledge, no theoretical support for the latter was provided prior to its proof in [177], on which Chapter 1 is based.

Tensor factorizations. Recovery of low rank tensors from incomplete observations via tensor factorizations is a setting of growing interest (cf. [1, 164, 6, 108, 223, 115, 219, 229, 33] and the survey [196]). In particular, hierarchical tensor factorization was recently introduced in [86], and used for recovery of low hierarchical tensor rank

¹There have also been works studying implicit effects of explicit regularizers for convolutional networks [62], but these are outside the scope of our paper.

tensors [54, 199, 176, 113, 114]. By virtue of its equivalence to different types of non-linear neural networks (with polynomial non-linearity), it has also been paramount to the study of expressiveness in deep learning [51, 193, 48, 49, 52, 192, 53, 132, 133, 16, 118, 119, 134]. To the best of our knowledge, [178, 179], on which Chapters 2 and 3 are based, provided the first analysis of the implicit regularization induced by gradient-based optimization for tensor and hierarchical tensor factorizations.

Part III

Expressiveness of Graph Neural Networks via Separation Rank

Chapter 5

On the Ability of Graph Neural Networks to Model Interactions Between Vertices

In Part II we employed a connection between neural networks (with polynomial non-linearity) and tensor factorizations for studying implicit regularization. In this chapter, which is based on [180], we extend this connection to analyze the expressive power of certain *graph neural networks (GNNs)*. Specifically, we show that message-passing GNNs [89] with product aggregation can be formulated via *tensor networks* — a graphical language for expressing tensor factorizations.¹ The formulation of GNNs as tensor networks then allows analyzing their ability to model interactions in an input graph.

5.1 Background and Overview

GNNs are a family of deep learning architectures, designed to model complex interactions between entities represented as vertices of a graph. In recent years, GNNs have been successfully applied across a wide range of domains, including social networks, biochemistry, and recommender systems (see, *e.g.*, [58, 122, 73, 88, 209, 222, 218, 30]). Consequently, significant interest in developing a mathematical theory behind GNNs has arisen.

One of the fundamental questions a theory of GNNs should address is *expressiveness*, which concerns the class of functions a given architecture can realize. Existing studies of expressiveness largely fall into three categories. First, and most prominent, are characterizations of ability to distinguish non-isomorphic graphs [221, 157, 151, 146, 15, 27, 19, 29, 70, 69, 171], as measured by equivalence to classical Weisfeiler-Leman graph isomorphism tests [214]. Second, are proofs for universal approximation of continuous permutation invariant or equivariant functions, possibly up to limitations in distinguishing some classes of graphs [152, 117, 40, 145, 10, 69]. Last, are works examining specific properties of GNNs such as frequency response [167, 14] or computability of certain graph attributes, *e.g.* moments, shortest paths, and substructure multiplicity [56, 18, 41, 66, 145, 38, 29, 225].

A major drawback of many existing approaches — in particular proofs of equivalence to Weisfeiler-Leman tests and those of universality — is that they operate in

¹Tensor networks are widely used for constructing compact representations of quantum states in areas of physics (see, *e.g.*, [210, 169]).

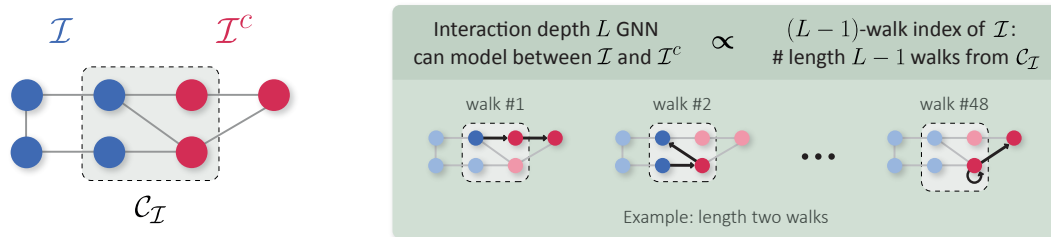


Figure 5.1: Illustration of our main theoretical contribution: quantifying the ability of GNNs to model interactions between vertices of an input graph. Consider a partition of vertices $(\mathcal{I}, \mathcal{I}^c)$, illustrated on the left, and a depth L GNN with product aggregation (Section 5.3). For graph prediction, as illustrated on the right, the strength of interaction the GNN can model between \mathcal{I} and \mathcal{I}^c , measured via separation rank (Section 5.2.2), is primarily determined by the partition’s $(L - 1)$ -walk index — the number of length $L - 1$ walks emanating from $\mathcal{C}_{\mathcal{I}}$, which is the set of vertices with an edge crossing the partition. The same holds for vertex prediction, except that there walk index is defined while only considering walks ending at the target vertex.

asymptotic regimes of unbounded network width or depth. Moreover, to the best of our knowledge, none of the existing approaches formally characterize the strength of interactions GNNs can model between vertices, and how that depends on the structure of the input graph and the architecture of the neural network.

The current chapter addresses the foregoing gaps. Namely, it theoretically quantifies the ability of fixed-size GNNs to model interactions between vertices, delineating the impact of the input graph structure and the neural network architecture (width and depth). Strength of modeled interactions is formalized via *separation rank* [23] — a commonly used measure for the interaction a function models between a subset of input variables and its complement (the rest of the input variables).² Given a function and a partition of its input variables, the higher the separation rank, the more interaction the function models between the sides of the partition. Separation rank is prevalent in quantum physics, where it can be viewed as a measure of entanglement [133]. It was previously used for analyzing variants of convolutional, recurrent, and self-attention neural networks, yielding both theoretical insights and practical tools [49, 52, 132, 133, 135, 215, 136]. We employ it for studying GNNs.

We treat both graph prediction, where a single output is produced for an entire input graph, and vertex prediction, in which the network produces an output for every vertex. For graph prediction, we prove that the separation rank of a depth L GNN with respect to a partition of vertices is primarily determined by the partition’s $(L - 1)$ -walk index — a graph-theoretical characteristic defined to be the number of length $L - 1$ walks originating from vertices with an edge crossing the partition. The same holds for vertex prediction, except that there walk index is defined while only considering walks ending at the target vertex. Our result, illustrated in Figure 5.1, implies that for a given input graph, the ability of GNNs to model interaction between a subset of vertices \mathcal{I} and its complement \mathcal{I}^c , predominantly depends on the number of walks originating from the boundary between \mathcal{I} and \mathcal{I}^c . We corroborate this proposition through experiments with standard GNN architectures, such as Graph Convolutional Network (GCN) [122] and Graph Isomorphism Network (GIN) [221].

Our theory formalizes conventional wisdom by which GNNs can model stronger

²Recall that, in Sections 3.5 and 3.6, we employed separation rank for designing an explicit regularization scheme that improves the performance convolutional neural networks over tasks involving long-range interactions.

interaction between regions of the input graph that are more interconnected. More importantly, we show that it facilitates an *edge sparsification* algorithm that preserves the expressive power of GNNs (in terms of ability to model interactions). Edge sparsification concerns removal of edges from a graph for reducing computational and/or memory costs, while attempting to maintain selected properties of the graph (cf. [21, 198, 87, 36, 186, 211, 138, 39]). In the context of GNNs, our interest lies in maintaining prediction accuracy as the number of edges removed from the input graph increases.

We propose an algorithm for removing edges, guided by our separation rank characterization. The algorithm, named *Walk Index Sparsification (WIS)*, is demonstrated to yield high predictive performance for GNNs (e.g. GCN and GIN) over standard benchmarks of various scales, even when removing a significant portion of edges. WIS is simple, computationally efficient, and in our experiments has markedly outperformed alternative methods in terms of induced prediction accuracies across edge sparsity levels. More broadly, WIS showcases the potential of improving GNNs by theoretically analyzing the interactions they can model, and we believe its further empirical investigation is a promising direction for future research.

The remainder of the chapter is organized as follows. Section 5.2 introduces notation and, for completeness, reintroduces the concept of separation rank (which was previously introduced in Section 3.5). Section 5.3 presents the theoretically analyzed GNN architecture. Section 5.4 theoretically quantifies (via separation rank) its ability to model interactions between vertices of an input graph. Finally, Section 5.5 proposes and evaluates WIS — an edge sparsification algorithm for arbitrary GNNs, born from our theory.

5.2 Preliminaries

5.2.1 Notation

For $N \in \mathbb{N}$, let $[N] := \{1, \dots, N\}$. We consider an undirected input graph $\mathcal{G} = (\mathcal{V}, \mathcal{E})$ with vertices $\mathcal{V} = [|\mathcal{V}|]$ and edges $\mathcal{E} \subseteq \{\{i, j\} : i, j \in \mathcal{V}\}$. Vertices are equipped with features $\mathbf{X} := (\mathbf{x}^{(1)}, \dots, \mathbf{x}^{(|\mathcal{V}|)}) \in \mathbb{R}^{D_x \times |\mathcal{V}|}$ — one D_x -dimensional feature vector per vertex ($D_x \in \mathbb{N}$). For $i \in \mathcal{V}$, we use $\mathcal{N}(i) := \{j \in \mathcal{V} : \{i, j\} \in \mathcal{E}\}$ to denote its set of neighbors, and, as customary in the context of GNNs, assume the existence of all self-loops, i.e. $i \in \mathcal{N}(i)$ for all $i \in \mathcal{V}$ (cf. [122, 89]). Furthermore, for $\mathcal{I} \subseteq \mathcal{V}$ we let $\mathcal{N}(\mathcal{I}) := \cup_{i \in \mathcal{I}} \mathcal{N}(i)$ be the neighbors of vertices in \mathcal{I} , and $\mathcal{I}^c := \mathcal{V} \setminus \mathcal{I}$ be the complement of \mathcal{I} . We use $\mathcal{C}_{\mathcal{I}}$ to denote the boundary of the partition $(\mathcal{I}, \mathcal{I}^c)$, i.e. the set of vertices with an edge crossing the partition, defined by $\mathcal{C}_{\mathcal{I}} := \{i \in \mathcal{I} : \mathcal{N}(i) \cap \mathcal{I}^c \neq \emptyset\} \cup \{j \in \mathcal{I}^c : \mathcal{N}(j) \cap \mathcal{I} \neq \emptyset\}$.³ Lastly, we denote the number of length $l \in \mathbb{N}_{\geq 0}$ walks from any vertex in $\mathcal{I} \subseteq \mathcal{V}$ to any vertex in $\mathcal{J} \subseteq \mathcal{V}$ by $\rho_l(\mathcal{I}, \mathcal{J})$.⁴ In particular, $\rho_l(\mathcal{I}, \mathcal{J}) = \sum_{i \in \mathcal{I}, j \in \mathcal{J}} \rho_l(\{i\}, \{j\})$.

Note that we focus on undirected graphs for simplicity of presentation. As discussed in Section 5.4, our results are extended to directed graphs in Appendix D.2.

³Due to the existence of self-loops, $\mathcal{C}_{\mathcal{I}}$ is exactly the shared neighbors of \mathcal{I} and \mathcal{I}^c , i.e. $\mathcal{C}_{\mathcal{I}} = \mathcal{N}(\mathcal{I}) \cap \mathcal{N}(\mathcal{I}^c)$.

⁴For $l \in \mathbb{N}_{\geq 0}$, a sequence of vertices $i_0, \dots, i_l \in \mathcal{V}$ is a length l walk if $\{i_{l'-1}, i_{l'}\} \in \mathcal{E}$ for all $l' \in [l]$.

5.2.2 Separation Rank: A Measure of Modeled Interaction

Separation rank is a prominent measure quantifying the interaction a multivariate function models between a subset of input variables and its complement (*i.e.* all other variables). It was introduced in Section 3.5, but for completeness we introduce it here once more.

The separation rank was originally defined in [23], and has since been employed for various applications [91, 84, 24]. It is also a common measure of *entanglement*, a profound concept in quantum physics quantifying interaction between particles [133]. In the context of deep learning, it enabled analyses of expressiveness and generalization in certain convolutional, recurrent, and self-attention neural networks, resulting in theoretical insights and practical methods (guidelines for neural architecture design, pretraining schemes, and regularizers — see [49, 52, 132, 133, 135, 215, 136] and Chapter 3).

Given a multivariate function $f : (\mathbb{R}^{D_x})^N \rightarrow \mathbb{R}$, its separation rank with respect to a subset of input variables $\mathcal{I} \subseteq [N]$ is the minimal number of summands required to express it, where each summand is a product of two functions — one that operates over variables indexed by \mathcal{I} , and another that operates over the remaining variables. Formally:

Definition 10. The *separation rank* of $f : (\mathbb{R}^{D_x})^N \rightarrow \mathbb{R}$ with respect to $\mathcal{I} \subseteq [N]$ is the minimal $R \in \mathbb{N} \cup \{0\}$ for which there exist $g^{(1)}, \dots, g^{(R)} : (\mathbb{R}^{D_x})^{|\mathcal{I}|} \rightarrow \mathbb{R}$ and $\bar{g}^{(1)}, \dots, \bar{g}^{(R)} : (\mathbb{R}^{D_x})^{|\mathcal{I}^c|} \rightarrow \mathbb{R}$ such that:

$$f(\mathbf{X}) = \sum_{r=1}^R g^{(r)}(\mathbf{X}_{\mathcal{I}}) \cdot \bar{g}^{(r)}(\mathbf{X}_{\mathcal{I}^c}), \quad (5.1)$$

where $\mathbf{X} := (\mathbf{x}^{(1)}, \dots, \mathbf{x}^{(N)})$, $\mathbf{X}_{\mathcal{I}} := (\mathbf{x}^{(i)})_{i \in \mathcal{I}}$, and $\mathbf{X}_{\mathcal{I}^c} := (\mathbf{x}^{(j)})_{j \in \mathcal{I}^c}$. By convention, if f is identically zero then $\text{sep}(f; \mathcal{I}) = 0$, and if the set on the right hand side of Equation (5.1) is empty then $\text{sep}(f; \mathcal{I}) = \infty$.

Interpretation. If $\text{sep}(f; \mathcal{I}) = 1$, the function is separable, meaning it does not model any interaction between $\mathbf{X}_{\mathcal{I}}$ and $\mathbf{X}_{\mathcal{I}^c}$, *i.e.* between the sides of the partition $(\mathcal{I}, \mathcal{I}^c)$. Specifically, it can be represented as $f(\mathbf{X}) = g(\mathbf{X}_{\mathcal{I}}) \cdot \bar{g}(\mathbf{X}_{\mathcal{I}^c})$ for some functions g and \bar{g} . In a statistical setting, where f is a probability density function, this would mean that $\mathbf{X}_{\mathcal{I}}$ and $\mathbf{X}_{\mathcal{I}^c}$ are statistically independent. The higher $\text{sep}(f; \mathcal{I})$ is, the farther f is from separability, implying stronger modeling of interaction between $\mathbf{X}_{\mathcal{I}}$ and $\mathbf{X}_{\mathcal{I}^c}$.

5.3 Graph Neural Networks

GNNs architectures predominantly follow the message-passing paradigm [73, 89], whereby each vertex is associated with a hidden embedding that is updated according to its neighbors. The initial embedding of $i \in \mathcal{V}$ is taken to be its input features: $\mathbf{h}^{(0,i)} := \mathbf{x}^{(i)} \in \mathbb{R}^{D_x}$. Then, in a depth L message-passing GNN, a common update scheme for the hidden embedding of $i \in \mathcal{V}$ at layer $l \in [L]$ is:

$$\mathbf{h}^{(l,i)} = \text{AGGREGATE}\left(\left\{\left\{\mathbf{W}^{(l)}\mathbf{h}^{(l-1,j)} : j \in \mathcal{N}(i)\right\}\right\}\right), \quad (5.2)$$

where $\{\cdot\}$ denotes a multiset, $\mathbf{W}^{(1)} \in \mathbb{R}^{D_h \times D_x}$, $\mathbf{W}^{(2)} \in \mathbb{R}^{D_h \times D_h}$, \dots , $\mathbf{W}^{(L)} \in \mathbb{R}^{D_h \times D_h}$ are learnable weight matrices, with $D_h \in \mathbb{N}$ being the network's width (*i.e.* hidden

dimension), and AGGREGATE is a function combining multiple input vectors into a single vector. A notable special case is GCN [122], in which AGGREGATE performs a weighted average followed by a non-linear activation function (*e.g.* ReLU).⁵ Other aggregation operators are also viable, *e.g.* element-wise sum, max, or product (*cf.* [88, 100]). We note that distinguishing self-loops from other edges, and more generally, treating multiple edge types, is possible through the use of different weight matrices for different edge types [88, 189]. For conciseness, we hereinafter focus on the case of a single edge type, and treat multiple edge types in Appendix D.2.

After L layers, the GNN generates hidden embeddings $\mathbf{h}^{(L,1)}, \dots, \mathbf{h}^{(L,|\mathcal{V}|)} \in \mathbb{R}^{D_h}$. For graph prediction, where a single output is produced for the whole graph, the hidden embeddings are usually combined into a single vector through the AGGREGATE function. A final linear layer with weights $\mathbf{W}^{(o)} \in \mathbb{R}^{1 \times D_h}$ is then applied to the resulting vector.⁶ Overall, the function realized by a depth L graph prediction GNN receives an input graph \mathcal{G} with vertex features $\mathbf{X} := (\mathbf{x}^{(1)}, \dots, \mathbf{x}^{(|\mathcal{V}|)}) \in \mathbb{R}^{D_x \times |\mathcal{V}|}$, and returns:

$$\text{(graph prediction)} \quad f^{(\theta, \mathcal{G})}(\mathbf{X}) := \mathbf{W}^{(o)} \text{AGGREGATE}(\{\{\mathbf{h}^{(L,i)} : i \in \mathcal{V}\}\}), \quad (5.3)$$

with $\theta := (\mathbf{W}^{(1)}, \dots, \mathbf{W}^{(L)}, \mathbf{W}^{(o)})$ denoting the network’s learnable weights. For vertex prediction tasks, where the network produces an output for every $t \in \mathcal{V}$, the final linear layer is applied to each $\mathbf{h}^{(L,t)}$ separately. That is, for a target vertex $t \in \mathcal{V}$, the function realized by a depth L vertex prediction GNN is given by:

$$\text{(vertex prediction)} \quad f^{(\theta, \mathcal{G}, t)}(\mathbf{X}) := \mathbf{W}^{(o)} \mathbf{h}^{(L,t)}. \quad (5.4)$$

Our aim is to investigate the ability of GNNs to model interactions between vertices. Prior studies of interactions modeled by different deep learning architectures have focused on neural networks with polynomial non-linearity, building on their representation as tensor networks [51, 49, 53, 192, 132, 133, 16, 118, 134, 135, 215, 136]. Although neural networks with polynomial non-linearity are less common in practice, they have demonstrated competitive performance [47, 50, 193, 200, 46, 63, 100], and hold promise due to their compatibility with quantum computation [78, 25] and fully homomorphic encryption [72]. More importantly, their analyses brought forth numerous insights that were demonstrated empirically and led to development of practical tools for widespread deep learning models (with non-linearities such as ReLU).

Following the above, in our theoretical analysis (Section 5.4) we consider GNNs with (element-wise) product aggregation, which are polynomial functions of their inputs. Namely, the AGGREGATE operator from Equations (5.2) and (5.3) is taken to be:

$$\text{AGGREGATE}(\mathcal{X}) := \odot_{\mathbf{x} \in \mathcal{X}} \mathbf{x}, \quad (5.5)$$

where \odot stands for the Hadamard product and \mathcal{X} is a multiset of vectors. The resulting architecture can be viewed as a variant of the GNN proposed in [100], where it was shown to achieve competitive performance in practice. Central to our proofs are tensor network representations of GNNs with product aggregation

⁵In GCN, AGGREGATE also has access to the degrees of vertices, which are used for computing the averaging weights. We omit the dependence on vertex degrees in our notation for conciseness.

⁶We treat the case of output dimension one merely for the sake of presentation. Extension of our theory (delivered in Section 5.4) to arbitrary output dimension is straightforward — the results hold as stated for each of the functions computing an output entry.

(formally established in Appendix D.3), analogous to those used for analyzing other types of neural networks. We empirically demonstrate our theoretical findings on popular GNNs (Section 5.4.3), such as GCN and GIN with ReLU non-linearity, and use them to derive a practical edge sparsification algorithm (Section 5.5).

We note that some of the aforementioned analyses of neural networks with polynomial non-linearity were extended to account for additional non-linearities, including ReLU, through constructs known as *generalized tensor networks* [48]. We thus believe our theory may be similarly extended, and regard this as an interesting direction for future work.

5.4 Theoretical Analysis: The Effect of Input Graph Structure and Neural Network Architecture on Modeled Interactions

In this section, we employ separation rank (Definition 10) to theoretically quantify how the input graph structure and network architecture (width and depth) affect the ability of a GNN with product aggregation to model interactions between input vertices. We begin with an overview of the main results and their implications (Section 5.4.1), after which we delve into the formal analysis (Section 5.4.2). Experiments demonstrate our theory’s implications on common GNNs, such as GCN and GIN with ReLU non-linearity (Section 5.4.3).

5.4.1 Overview and Implications

Consider a depth L GNN with width D_h and product aggregation (Section 5.3). Given a graph \mathcal{G} , any assignment to the weights of the network θ induces a multivariate function — $f^{(\theta, \mathcal{G})}$ for graph prediction (Equation (5.3)) and $f^{(\theta, \mathcal{G}, t)}$ for prediction over a given vertex $t \in \mathcal{V}$ (Equation (5.4)) — whose variables correspond to feature vectors of input vertices. The separation rank of this function with respect to $\mathcal{I} \subseteq \mathcal{V}$ thus measures the interaction modeled across the partition $(\mathcal{I}, \mathcal{I}^c)$, *i.e.* between the vertices in \mathcal{I} and those in \mathcal{I}^c . The higher the separation rank is, the stronger the modeled interaction.

Key to our analysis are the following notions of *walk index*, defined by the number of walks emanating from the boundary of the partition $(\mathcal{I}, \mathcal{I}^c)$, *i.e.* from vertices with an edge crossing the partition induced by \mathcal{I} (see Figure 5.1 for an illustration).

Definition 11. Let $\mathcal{I} \subseteq \mathcal{V}$. Denote by $\mathcal{C}_{\mathcal{I}}$ the set of vertices with an edge crossing the partition $(\mathcal{I}, \mathcal{I}^c)$, *i.e.* $\mathcal{C}_{\mathcal{I}} := \{i \in \mathcal{I} : \mathcal{N}(i) \cap \mathcal{I}^c \neq \emptyset\} \cup \{j \in \mathcal{I}^c : \mathcal{N}(j) \cap \mathcal{I} \neq \emptyset\}$, and recall that $\rho_l(\mathcal{C}_{\mathcal{I}}, \mathcal{J})$ denotes the number of length $l \in \mathbb{N}_{\geq 0}$ walks from any vertex in $\mathcal{C}_{\mathcal{I}}$ to any vertex in $\mathcal{J} \subseteq \mathcal{V}$. For $L \in \mathbb{N}$:

- (graph prediction) we define the $(L - 1)$ -walk index of \mathcal{I} , denoted $\text{WI}_{L-1}(\mathcal{I})$, to be the number of length $L - 1$ walks originating from $\mathcal{C}_{\mathcal{I}}$, *i.e.* $\text{WI}_{L-1}(\mathcal{I}) := \rho_{L-1}(\mathcal{C}_{\mathcal{I}}, \mathcal{V})$; and
- (vertex prediction) for $t \in \mathcal{V}$ we define the $(L - 1, t)$ -walk index of \mathcal{I} , denoted $\text{WI}_{L-1, t}(\mathcal{I})$, to be the number of length $L - 1$ walks from $\mathcal{C}_{\mathcal{I}}$ that end at t , *i.e.* $\text{WI}_{L-1, t}(\mathcal{I}) := \rho_{L-1}(\mathcal{C}_{\mathcal{I}}, \{t\})$.

As our main theoretical contribution, we prove:

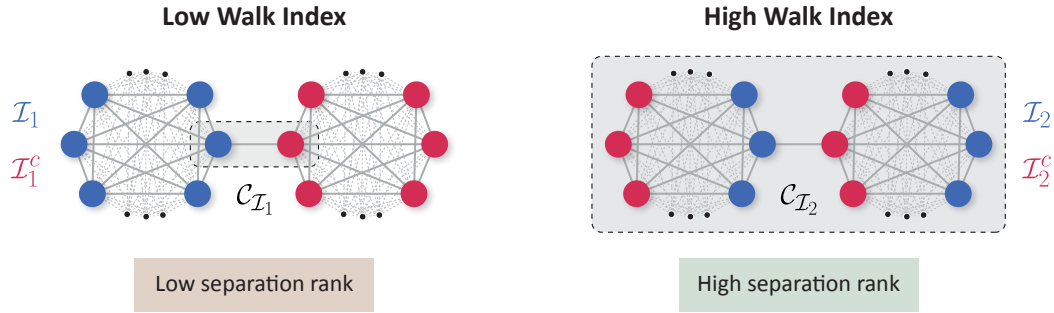


Figure 5.2: Depth L GNNs can model stronger interactions between sides of partitions that have a higher walk index (Definition 11). The partition $(\mathcal{I}_1, \mathcal{I}_1^c)$ (left) divides the vertices into two separate cliques, connected by a single edge. Only two vertices reside in $\mathcal{C}_{\mathcal{I}_1}$ — the set of vertices with an edge crossing the partition. Taking for example depth $L = 3$, the 2-walk index of \mathcal{I}_1 is $\Theta(|\mathcal{V}|^2)$ and its $(2, t)$ -walk index is $\Theta(|\mathcal{V}|)$, for $t \in \mathcal{V}$. In contrast, the partition $(\mathcal{I}_2, \mathcal{I}_2^c)$ (right) equally divides the vertices in each clique to different sides. All vertices reside in $\mathcal{C}_{\mathcal{I}_2}$, meaning the 2-walk index of \mathcal{I}_2 is $\Theta(|\mathcal{V}|^3)$ and its $(2, t)$ -walk index is $\Theta(|\mathcal{V}|^2)$, for $t \in \mathcal{V}$. Hence, in both graph and vertex prediction scenarios, the walk index of \mathcal{I}_1 is relatively low compared to that of \mathcal{I}_2 . Our analysis (Sections 5.4.1 and 5.4.2) states that a higher separation rank can be attained with respect to \mathcal{I}_2 , meaning stronger interaction can be modeled across $(\mathcal{I}_2, \mathcal{I}_2^c)$ than across $(\mathcal{I}_1, \mathcal{I}_1^c)$. We empirically confirm this prospect in Section 5.4.3.

Theorem 6 (informally stated). *For all weight assignments θ and $t \in \mathcal{V}$:*

$$(\text{graph prediction}) \quad \log(\text{sep}(f^{(\theta, \mathcal{G})}; \mathcal{I})) = \mathcal{O}(\log(D_h) \cdot \text{WI}_{L-1}(\mathcal{I})),$$

$$(\text{vertex prediction}) \quad \log(\text{sep}(f^{(\theta, \mathcal{G}, t)}; \mathcal{I})) = \mathcal{O}(\log(D_h) \cdot \text{WI}_{L-1, t}(\mathcal{I})).$$

Moreover, nearly matching lower bounds hold for almost all weight assignments.⁷

The upper and lower bounds are formally established by Theorems 7 and 8 in Section 5.4.2, respectively, and are generalized to input graphs with directed edges and multiple edge types in Appendix D.2. Theorem 6 implies that, the $(L - 1)$ -walk index of \mathcal{I} in graph prediction and its $(L - 1, t)$ -walk index in vertex prediction control the separation rank with respect to \mathcal{I} , and are thus paramount for modeling interaction between \mathcal{I} and \mathcal{I}^c — see Figure 5.2 for an illustration. It thereby formalizes the conventional wisdom by which GNNs can model stronger interaction between areas of the input graph that are more interconnected. We support this finding empirically with common GNN architectures (e.g. GCN and GIN with ReLU non-linearity) in Section 5.4.3.

One may interpret Theorem 6 as encouraging addition of edges to an input graph. Indeed, the theorem states that such addition can enhance the GNN’s ability to model interactions between input vertices. This accords with existing evidence by which increasing connectivity can improve the performance of GNNs in practice (see, e.g., [67, 4]). However, special care needs to be taken when adding edges: it may distort the semantic meaning of the input graph, and may lead to plights known as over-smoothing and over-squashing [139, 168, 37, 4, 17]. Rather than employing Theorem 6 for adding edges, we use it to select which edges to preserve in a setting where some must be removed. That is, we employ it for designing an edge sparsification algorithm. The algorithm, named *Walk Index Sparsification (WIS)*, is simple, computationally efficient, and in our experiments has markedly outperformed

⁷Almost all in the sense that the lower bounds hold for all weight assignments but a set of Lebesgue measure zero.

alternative methods in terms of induced prediction accuracy. We present and evaluate it in Section 5.5.

5.4.2 Formal Presentation

We begin by upper bounding the separation ranks a GNN can achieve.

Theorem 7. *For an undirected graph \mathcal{G} and $t \in \mathcal{V}$, let $f^{(\theta, \mathcal{G})}$ and $f^{(\theta, \mathcal{G}, t)}$ be the functions realized by depth L graph and vertex prediction GNNs, respectively, with width D_h , learnable weights θ , and product aggregation (Equations (5.2) to (5.5)). Then, for any $\mathcal{I} \subseteq \mathcal{V}$ and assignment of weights θ it holds that:*

$$\text{(graph prediction)} \quad \log(\text{sep}(f^{(\theta, \mathcal{G})}; \mathcal{I})) \leq \log(D_h) \cdot \underbrace{4 \rho_{L-1}(\mathcal{C}_{\mathcal{I}}, \mathcal{V}) + 1}_{\text{WI}_{L-1}(\mathcal{I})}, \quad (5.6)$$

$$\text{(vertex prediction)} \quad \log(\text{sep}(f^{(\theta, \mathcal{G}, t)}; \mathcal{I})) \leq \log(D_h) \cdot \underbrace{4 \rho_{L-1}(\mathcal{C}_{\mathcal{I}}, \{t\})}_{\text{WI}_{L-1, t}(\mathcal{I})}. \quad (5.7)$$

Proof sketch (proof in Appendix D.7.2). In Appendix D.3, we show that the computations performed by a GNN with product aggregation can be represented as a *tensor network*. In brief, a tensor network is a weighted graph that describes a sequence of arithmetic operations known as tensor contractions (see Appendices D.3.1 and D.3.2 for a self-contained introduction to tensor networks). The tensor network corresponding to a GNN with product aggregation adheres to a tree structure — its leaves are associated with input vertex features and interior nodes embody the operations performed by the GNN. Importing machinery from tensor analysis literature, we prove that $\text{sep}(f^{(\theta, \mathcal{G})}; \mathcal{I})$ is upper bounded by a minimal cut weight in the corresponding tensor network, among cuts separating leaves associated with input vertices in \mathcal{I} from leaves associated with input vertices in \mathcal{I}^c . Equation (5.6) then follows by finding such a cut in the tensor network with sufficiently low weight. Equation (5.7) is established analogously. \square

A natural question is whether the upper bounds in Theorem 7 are tight, *i.e.* whether separation ranks close to them can be attained. We show that nearly matching lower bounds hold for almost all assignments of weights θ . To this end, we define *admissible subsets* of $\mathcal{C}_{\mathcal{I}}$, based on a notion of vertex subsets with *no repeating shared neighbors*.

Definition 12. We say that $\mathcal{I}, \mathcal{J} \subseteq \mathcal{V}$ have *no repeating shared neighbors* if every $k \in \mathcal{N}(\mathcal{I}) \cap \mathcal{N}(\mathcal{J})$ has only a single neighbor in each of \mathcal{I} and \mathcal{J} , *i.e.* $|\mathcal{N}(k) \cap \mathcal{I}| = |\mathcal{N}(k) \cap \mathcal{J}| = 1$.

Definition 13. For $\mathcal{I} \subseteq \mathcal{V}$, we refer to $\mathcal{C} \subseteq \mathcal{C}_{\mathcal{I}}$ as an *admissible subset* of $\mathcal{C}_{\mathcal{I}}$ if there exist $\mathcal{I}' \subseteq \mathcal{I}, \mathcal{J}' \subseteq \mathcal{I}^c$ with no repeating shared neighbors such that $\mathcal{C} = \mathcal{N}(\mathcal{I}') \cap \mathcal{N}(\mathcal{J}')$. We use $\mathcal{S}(\mathcal{I})$ to denote the set comprising all admissible subsets of $\mathcal{C}_{\mathcal{I}}$:

$$\mathcal{S}(\mathcal{I}) := \{\mathcal{C} \subseteq \mathcal{C}_{\mathcal{I}} : \mathcal{C} \text{ is an admissible subset of } \mathcal{C}_{\mathcal{I}}\}.$$

Theorem 8 below establishes that almost all possible values for the network's weights lead the upper bounds in Theorem 7 to be tight, up to logarithmic terms and to the number of walks from $\mathcal{C}_{\mathcal{I}}$ being replaced with the number of walks from any single $\mathcal{C} \in \mathcal{S}(\mathcal{I})$. The extent to which $\mathcal{C}_{\mathcal{I}}$ can be covered by an admissible subset thus determines how tight the upper bounds are. Trivially, at least the shared neighbors

of any $i \in \mathcal{I}, j \in \mathcal{I}^c$ can be covered, since $\mathcal{N}(i) \cap \mathcal{N}(j) \in \mathcal{S}(\mathcal{I})$. Appendix D.1 shows that for various canonical graphs all of $\mathcal{C}_{\mathcal{I}}$, or a large part of it, can be covered by an admissible subset.

Theorem 8. *Consider the setting and notation of Theorem 7. Given $\mathcal{I} \subseteq \mathcal{V}$, for almost all assignments of weights θ , i.e. for all but a set of Lebesgue measure zero, it holds that:*

$$\text{(graph prediction)} \quad \log(\text{sep}(f^{(\theta, \mathcal{G})}; \mathcal{I})) \geq \max_{\mathcal{C} \in \mathcal{S}(\mathcal{I})} \log(\alpha_{\mathcal{C}}) \cdot \rho_{L-1}(\mathcal{C}, \mathcal{V}), \quad (5.8)$$

$$\text{(vertex prediction)} \quad \log(\text{sep}(f^{(\theta, \mathcal{G}, t)}; \mathcal{I})) \geq \max_{\mathcal{C} \in \mathcal{S}(\mathcal{I})} \log(\alpha_{\mathcal{C}, t}) \cdot \rho_{L-1}(\mathcal{C}, \{t\}), \quad (5.9)$$

where:

$$\alpha_{\mathcal{C}} := \begin{cases} D^{1/\rho_0(\mathcal{C}, \mathcal{V})} & , \text{if } L = 1 \\ (D - 1) \cdot \rho_{L-1}(\mathcal{C}, \mathcal{V})^{-1} + 1 & , \text{if } L \geq 2 \end{cases} \\ \alpha_{\mathcal{C}, t} := \begin{cases} D & , \text{if } L = 1 \\ (D - 1) \cdot \rho_{L-1}(\mathcal{C}, \{t\})^{-1} + 1 & , \text{if } L \geq 2 \end{cases}$$

with $D := \min\{D_x, D_h\}$. If $\rho_{L-1}(\mathcal{C}, \mathcal{V}) = 0$ or $\rho_{L-1}(\mathcal{C}, \{t\}) = 0$, the respective lower bound (right hand side of Equation (5.8) or Equation (5.9)) is zero by convention.

Proof sketch (proof in Appendix D.7.3). Our proof follows a line similar to that used in [135, 215, 136] for lower bounding the separation rank of self-attention neural networks. The separation rank of any $f : (\mathbb{R}^{D_x})^{|\mathcal{V}|} \rightarrow \mathbb{R}$ can be lower bounded by examining its outputs over a grid of inputs. Specifically, for $M \in \mathbb{N}$ template vectors $\mathbf{v}^{(1)}, \dots, \mathbf{v}^{(M)} \in \mathbb{R}^{D_x}$, we can create a grid tensor for f by evaluating it over each point in $\{(\mathbf{v}^{(d_1)}, \dots, \mathbf{v}^{(d_{|\mathcal{V}|})})\}_{d_1, \dots, d_{|\mathcal{V}|}=1}^M$ and storing the outcomes in a tensor with $|\mathcal{V}|$ axes of dimension M each. Arranging the grid tensor as a matrix $\mathbf{B}(f)$ where rows correspond to axes indexed by \mathcal{I} and columns correspond to the remaining axes, we show that $\text{rank}(\mathbf{B}(f)) \leq \text{sep}(f; \mathcal{I})$. The proof proceeds by establishing that for almost every assignment of θ , there exist template vectors with which $\log(\text{rank}(\mathbf{B}(f^{(\theta, \mathcal{G})})))$ and $\log(\text{rank}(\mathbf{B}(f^{(\theta, \mathcal{G}, t)})))$ are greater than (or equal to) the right hand sides of Equations (5.8) and (5.9), respectively. \square

Directed edges and multiple edge types. Appendix D.2 generalizes Theorems 7 and 8 to the case of graphs with directed edges and an arbitrary number of edge types.

5.4.3 Empirical Demonstration

Our theoretical analysis establishes that, the strength of interaction GNNs can model across a partition of input vertices is primarily determined by the partition’s walk index — a graph-theoretical characteristic defined by the number of walks originating from the boundary of the partition (see Definition 11). The analysis formally applies to GNNs with product aggregation (see Section 5.3), yet we empirically demonstrate that its conclusions carry over to various other message-passing GNN architectures, namely GCN [122], GAT [209], and GIN [221] (with ReLU non-linearity). Specifically, through controlled experiments, we show that such models perform better on tasks in which the partitions that require strong interaction are ones with higher walk index, given that all other aspects of the tasks are the same. A description

Table 5.1: In accordance with our theory (Sections 5.4.1 and 5.4.2), GNNs can better fit datasets in which the partitions (of input vertices) that require strong interaction are ones with higher walk index (Definition 11). Table reports means and standard deviations, taken over five runs, of train and test accuracies obtained by GNNs of depth 3 and width 16 on two datasets: one in which the essential partition — *i.e.* the main partition requiring strong interaction — has low walk index, and another in which it has high walk index (see Section 5.4.3 for a detailed description of the datasets). For all GNNs, the train accuracy attained over the second dataset is considerably higher than that attained over the first dataset. Moreover, the better train accuracy translates to better test accuracy. See Appendix D.6.2 for further implementation details.

		Essential Partition Walk Index	
		Low	High
GCN	Train Acc. (%)	70.4 ± 1.7	81.4 ± 2.0
	Test Acc. (%)	52.7 ± 1.9	66.2 ± 1.1
GAT	Train Acc. (%)	82.8 ± 2.6	88.5 ± 1.1
	Test Acc. (%)	69.6 ± 0.6	72.1 ± 1.2
GIN	Train Acc. (%)	83.2 ± 0.8	94.2 ± 0.8
	Test Acc. (%)	53.7 ± 1.8	64.8 ± 1.4

of these experiments follows. For brevity, we defer some implementation details to Appendix D.6.2.

We constructed two graph prediction datasets, in which the vertex features of each input graph are patches of pixels from two randomly sampled Fashion-MNIST [220] images, and the goal is to predict whether the two images are of the same class.⁸ In both datasets, all input graphs have the same structure: two separate cliques with 16 vertices each, connected by a single edge. The datasets differ in how the image patches are distributed among the vertices: in the first dataset each clique holds all the patches of a single image, whereas in the second dataset each clique holds half of the patches from the first image and half of the patches from the second image. Figure 5.2 illustrates how image patches are distributed in the first (left hand side of the figure) and second (right hand side of the figure) datasets, with blue and red marking assignment of vertices to images.

Each dataset requires modeling strong interaction across the partition separating the two images, referred to as the *essential partition* of the dataset. In the first dataset the essential partition separates the two cliques, thus it has low walk index. In the second dataset each side of the essential partition contains half of the vertices from the first clique and half of the vertices from the second clique, thus the partition has high walk index. For an example illustrating the gap between these walk indices see Figure 5.2.

Table 5.1 reports the train and test accuracies achieved by GCN, GAT, and GIN (with ReLU non-linearity) over both datasets. In compliance with our theory, the GNNs fit the dataset whose essential partition has high walk index significantly better than they fit the dataset whose essential partition has low walk index. Furthermore, the improved train accuracy translates to improvements in test accuracy.

⁸Images are sampled such that the amount of positive and negative examples are roughly balanced.

5.5 Practical Application: Expressivity Preserving Edge Sparsification

Section 5.4 theoretically characterizes the ability of a GNN to model interactions between input vertices. It reveals that this ability is controlled by a graph-theoretical property we call walk index (Definition 11). The current section derives a practical application of our theory, specifically, an *edge sparsification* algorithm named *Walk Index Sparsification (WIS)*, which preserves the ability of a GNN to model interactions when input edges are removed. We present WIS, and show that it yields high predictive performance for GNNs over standard vertex prediction benchmarks of various scales, even when removing a significant portion of edges. In particular, we evaluate WIS using GCN [122], GIN [221], and ResGCN [137] over multiple datasets, including: Cora [190], which contains thousands of edges, DBLP [28], which contains tens of thousands of edges, and OGBN-Arxiv [99], which contains more than a million edges. WIS is simple, computationally efficient, and in our experiments has markedly outperformed alternative methods in terms of induced prediction accuracy across edge sparsity levels. We believe its further empirical investigation is a promising direction for future research.

5.5.1 Walk Index Sparsification (WIS)

Running GNNs over large-scale graphs can be prohibitively expensive in terms of runtime and memory. A natural way to tackle this problem is edge sparsification — removing edges from an input graph while attempting to maintain prediction accuracy (cf. [138, 39]).^{9,10}

Our theory (Section 5.4) establishes that, the strength of interaction a depth L GNN can model across a partition of input vertices is determined by the partition’s walk index, a quantity defined by the number of length $L - 1$ walks originating from the partition’s boundary. This brings forth a recipe for pruning edges. First, choose partitions across which the ability to model interactions is to be preserved. Then, for every input edge (excluding self-loops), compute a tuple holding what the walk indices of the chosen partitions will be if the edge is to be removed. Lastly, remove the edge whose tuple is maximal according to a preselected order over tuples (e.g. an order based on the sum, min, or max of a tuple’s entries). This process repeats until the desired number of edges are removed. The idea behind the above-described recipe, which we call *General Walk Index Sparsification*, is that each iteration greedily prunes the edge whose removal takes the smallest toll in terms of ability to model interactions across chosen partitions — see Algorithm 3 in Appendix D.4 for a formal outline. Below we describe a specific instantiation of the recipe for vertex prediction tasks, which are particularly relevant with large-scale graphs, yielding our proposed algorithm — Walk Index Sparsification (WIS).

In vertex prediction tasks, the interaction between an input vertex and the remainder of the input graph is of central importance. Thus, it is natural to choose the partitions induced by singletons (i.e. the partitions $(\{t\}, \mathcal{V} \setminus \{t\})$, where $t \in \mathcal{V}$) as those across which the ability to model interactions is to be preserved. We would like to remove

⁹As opposed to *edge rewiring* methods that add or remove only a few edges with the goal of improving prediction accuracy (e.g., [227, 147, 205, 17]).

¹⁰An alternative approach is to remove vertices from an input graph (see, e.g., [131]). However, this approach is unsuitable for vertex prediction tasks, so we limit our attention to edge sparsification.

Algorithm 1 $(L - 1)$ -Walk Index Sparsification (WIS) (instance of a general scheme described in Appendix D.4)

Input: \mathcal{G} — graph, $L \in \mathbb{N}$ — GNN depth, $N \in \mathbb{N}$ — number of edges to remove

Result: Sparsified graph obtained by removing N edges from \mathcal{G}

```

for  $n = 1, \dots, N$  do
  # for every edge, compute walk indices of partitions induced by  $\{t\}$ , for  $t \in \mathcal{V}$ ,
  # after the edge's removal
  for  $e \in \mathcal{E}$  (excluding self-loops) do
    initialize  $\mathbf{s}^{(e)} = (0, \dots, 0) \in \mathbb{R}^{|\mathcal{V}|}$ 
    remove  $e$  from  $\mathcal{G}$  (temporarily)
    for every  $t \in \mathcal{V}$ , set  $\mathbf{s}_t^{(e)} = \text{WI}_{L-1,t}(\{t\})$ 
    add  $e$  back to  $\mathcal{G}$ 
  end for
  # prune edge whose removal harms walk indices the least according to an order
  # over  $(\mathbf{s}^{(e)})_{e \in \mathcal{E}}$ 
  for  $e \in \mathcal{E}$ , sort the entries of  $\mathbf{s}^{(e)}$  in ascending order
  let  $e' \in \text{argmax}_{e \in \mathcal{E}} \mathbf{s}^{(e)}$  according to lexicographic order over tuples
  remove  $e'$  from  $\mathcal{G}$  (permanently)
end for

```

edges while avoiding a significant deterioration in the ability to model interaction under any of the chosen partitions. To that end, we compare walk index tuples according to their minimal entries, breaking ties using the second smallest entries, and so forth. This is equivalent to sorting (in ascending order) the entries of each tuple separately, and then ordering the tuples lexicographically.

Algorithm 1 provides a self-contained description of the method attained by the foregoing choices. We refer to this method as $(L - 1)$ -Walk Index Sparsification (WIS), where the “ $(L - 1)$ ” indicates that only walks of length $L - 1$ take part in the walk indices. Since $(L - 1)$ -walk indices can be computed by taking the $(L - 1)$ 'th power of the graph's adjacency matrix, $(L - 1)$ -WIS runs in $\mathcal{O}(N|\mathcal{E}||\mathcal{V}|^3 \log(L))$ time and requires $\mathcal{O}(|\mathcal{E}||\mathcal{V}| + |\mathcal{V}|^2)$ memory, where N is the number of edges to be removed. For large graphs a runtime cubic in the number of vertices can be restrictive. Fortunately, 1-WIS, which can be viewed as an approximation for $(L - 1)$ -WIS with $L > 2$, facilitates a particularly simple and efficient implementation based solely on vertex degrees, requiring only linear time and memory — see Algorithm 2 (whose equivalence to 1-WIS is explained in Appendix D.5). Specifically, 1-WIS runs in $\mathcal{O}(N|\mathcal{E}| + |\mathcal{V}|)$ time and requires $\mathcal{O}(|\mathcal{E}| + |\mathcal{V}|)$ memory.

5.5.2 Empirical Evaluation

Below is an empirical evaluation of WIS. For brevity, we defer to Appendix D.6 some implementation details, as well as experiments with additional GNN architectures (GIN and ResGCN) and datasets (Chameleon [174], Squirrel [174], and Amazon Computers [194]). Overall, our evaluation includes six standard vertex prediction datasets in which we observed the graph structure to be crucial for accurate prediction, as measured by the difference between the test accuracy of a GCN trained and

Algorithm 2 1-Walk Index Sparsification (WIS) (efficient implementation of Algorithm 1 for $L = 2$)

Input: \mathcal{G} — graph, $N \in \mathbb{N}$ — number of edges to remove

Result: Sparsified graph obtained by removing N edges from \mathcal{G}

```

compute vertex degrees, i.e.  $\text{deg}(i) = |\mathcal{N}(i)|$  for  $i \in \mathcal{V}$ 
for  $n = 1, \dots, N$  do
  for  $\{i, j\} \in \mathcal{E}$  (excluding self-loops) do
    let  $\text{deg}_{\min}(i, j) := \min\{\text{deg}(i), \text{deg}(j)\}$ 
    let  $\text{deg}_{\max}(i, j) := \max\{\text{deg}(i), \text{deg}(j)\}$ 
  end for
  # prune  $\{i, j\} \in \mathcal{E}$  with maximal  $\text{deg}_{\min}(i, j)$ , breaking ties using  $\text{deg}_{\max}(i, j)$ 
  let  $e' \in \text{argmax}_{\{i, j\} \in \mathcal{E}}(\text{deg}_{\min}(i, j), \text{deg}_{\max}(i, j))$  according to lexicographic order
  over pairs
  remove  $e'$  from  $\mathcal{G}$ 
  decrease by one the degree of vertices connected by  $e'$ 
end for

```

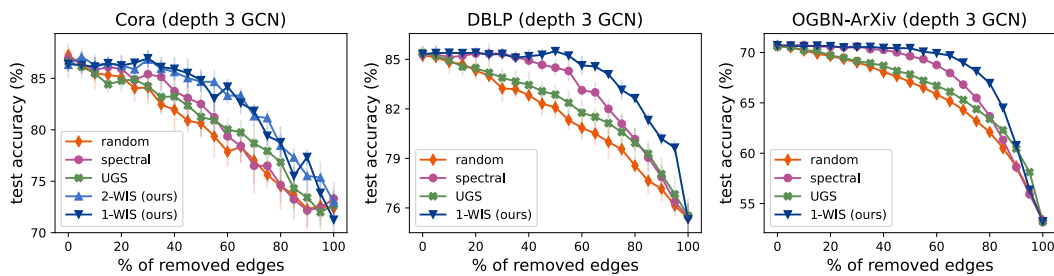


Figure 5.3: Comparison of GNN accuracies following sparsification of input edges — WIS, the edge sparsification algorithm brought forth by our theory (Algorithm 1), markedly outperforms alternative methods. Plots present test accuracies achieved by a depth $L = 3$ GCN of width 64 over the Cora (left), DBLP (middle), and OGBN-ArXiv (right) vertex prediction datasets, with increasing percentage of removed edges (for each combination of dataset, edge sparsification algorithm, and percentage of removed edges, a separate GCN was trained and evaluated). WIS, designed to maintain the ability of a GNN to model interactions between input vertices, is compared against: (i) removing edges uniformly at random; (ii) a spectral sparsification method [198]; and (iii) an adaptation of UGS [39]. For Cora, we run both 2-WIS, which is compatible with the GNN’s depth, and 1-WIS, which can be viewed as an approximation that admits a particularly efficient implementation (Algorithm 2). For DBLP and OGBN-ArXiv, due to their larger scale only 1-WIS is evaluated. Markers and error bars report means and standard deviations, respectively, taken over ten runs per configuration. Note that 1-WIS achieves results similar to 2-WIS, suggesting that the efficiency it brings does not come at a significant cost in performance. Appendix D.6 provides further implementation details and experiments with additional GNN architectures (GIN and ResGCN) and datasets (Chameleon, Squirrel, and Amazon Computers). Code for reproducing the experiment is available at https://github.com/noamrazin/gnn_interactions.

evaluated over the original graph and its test accuracy when trained and evaluated over the graph after all of the graph’s edges were removed. We also considered, but excluded, the following datasets in which the accuracy difference was insignificant (less than five percentage points): Citeseer [190], PubMed [163], Coauthor CS and Physics [194], and Amazon Photo [194].

Using depth $L = 3$ GNNs (with ReLU non-linearity), we evaluate over the Cora

dataset both 2-WIS, which is compatible with the GNNs' depth, and 1-WIS, which can be viewed as an efficient approximation. Over the DBLP and OGBN-Arxiv datasets, due to their larger scale only 1-WIS is evaluated. Figure 5.3 (and Figure D.5 in Appendix D.6) shows that WIS significantly outperforms the following alternative methods in terms of induced prediction accuracy: (i) a baseline in which edges are removed uniformly at random; (ii) a well-known spectral algorithm [198] designed to preserve the spectrum of the sparsified graph's Laplacian; and (iii) an adaptation of UGS [39] — a recent supervised approach for learning to prune edges.¹¹ Both 2-WIS and 1-WIS lead to higher test accuracies, while (as opposed to UGS) avoiding the need for labels, and for training a GNN over the original (non-sparsified) graph — a procedure which in some settings is prohibitively expensive in terms of runtime and memory. Interestingly, 1-WIS performs similarly to 2-WIS, indicating that the efficiency it brings does not come at a sizable cost in performance.

¹¹UGS [39] jointly prunes input graph edges and GNN weights. For fair comparison, we adapt it to only remove edges.

Chapter 6

Related Work

Expressiveness of GNNs. The expressiveness of GNNs has been predominantly evaluated through ability to distinguish non-isomorphic graphs, as measured by correspondence to Weisfeiler-Leman (WL) graph isomorphism tests (see [158] for a recent survey). [221, 157] instigated this thread of research, establishing that message-passing GNNs are at most as powerful as the WL algorithm, and can match it under certain technical conditions. Subsequently, architectures surpassing WL were proposed, with expressiveness measured via higher-order WL variants (see, *e.g.*, [157, 151, 40, 68, 15, 27, 19, 69, 29, 171]). Another line of inquiry regards universality among continuous permutation invariant or equivariant functions [152, 117, 145, 10, 69]. [40] showed that distinguishing non-isomorphic graphs and universality are, in some sense, equivalent. Lastly, there exist analyses of expressiveness focused on the frequency response of GNNs [167, 14] and their capacity to compute specific graph functions, *e.g.* moments, shortest paths, and substructure counting [56, 18, 66, 145, 41, 38, 29].

Although a primary purpose of GNNs is to model interactions between vertices, none of the past works formally characterize their ability to do so, as our theory does. Chapter 5 thus provides a novel perspective on the expressive power of GNNs. Furthermore, a major limitation of existing approaches — in particular, proofs of equivalence to WL tests and universality — is that they often operate in asymptotic regimes of unbounded network width or depth. Consequently, they fall short of addressing which type of functions can be realized by GNNs of practical size. In contrast, we characterize how the modeled interactions depend on both the input graph structure and the neural network architecture (width and depth). As shown in Section 5.5, this facilitates designing an efficient and effective edge sparsification algorithm.

Measuring modeled interactions via separation rank. Separation rank (Section 5.2.2) has been paramount to the study of interactions modeled by certain convolutional, recurrent, and self-attention neural networks. It enabled theoretically analyzing how different architectural parameters impact expressiveness [51, 48, 49, 53, 16, 192, 133, 132, 118, 119, 135, 215, 136] and implicit regularization (Chapter 3).¹ On the practical side, insights brought forth by separation rank led to tools for improving

¹We note that, over a two-dimensional grid graph, a message-passing GNN can be viewed as a convolutional neural network with overlapping convolutional windows. Similarly, over a chain graph, it can be viewed as a bidirectional recurrent neural network. Thus, for these special cases, our separation rank bounds (delivered in Section 5.4) extend those of [49, 132, 133, 118], which consider convolutional neural networks with non-overlapping convolutional windows and unidirectional recurrent neural networks.

performance, including: guidelines for architecture design [49, 133, 135, 215], pretraining schemes [136], and regularizers for countering locality in convolutional neural networks (Chapter 3). We employ separation rank for studying the interactions GNNs model between vertices, and similarly provide both theoretical insights and a practical application — edge sparsification algorithm (Section 5.5).

Edge sparsification. Computations over large-scale graphs can be prohibitively expensive in terms of runtime and memory. As a result, various methods were proposed for sparsifying graphs by removing edges while attempting to maintain structural properties, such as distances between vertices [21, 87], graph Laplacian spectrum [198, 186], and vertex degree distribution [211], or outcomes of graph analysis and clustering algorithms [36]. Most relevant to our work are recent edge sparsification methods aiming to preserve the prediction accuracy of GNNs as the number of removed edges increases [138, 39]. These methods require training a GNN over the original (non-sparsified) graph, hence only inference costs are reduced. Guided by our theory, in Section 5.5 we propose *Walk Index Sparsification (WIS)* — an edge sparsification algorithm that preserves expressive power in terms of ability to model interactions. WIS improves efficiency for both training and inference. Moreover, comparisons with the spectral algorithm of [198] and a recent method from [39] demonstrate that WIS brings about higher prediction accuracies across edge sparsity levels.

Part IV

Conclusion

Two pillars on which the theory of deep learning rests are generalization and expressiveness. Strengthening the formal understanding of these pillars can facilitate principled methods for improving the efficiency, reliability, and performance of neural networks. A major challenge towards doing so is finding suitable complexity measures. That is, measures with which it is possible to characterize the ability of neural networks to generalize over natural data (*e.g.*, images, audio, and text) and express rich classes of functions. This thesis puts forth notions of rank as promising measures of complexity for developing a theory of deep learning.

In Part II, we focused on the mystery of generalization in deep learning: why do neural networks generalize despite having far more learnable parameters than training examples? Conventional wisdom suggests that this generalization stems from an implicit regularization induced by gradient-based training, *i.e.* its tendency to fit training examples with predictors of minimal complexity [165]. A widespread hope was that this tendency can be characterized as minimization of some norm [166, 81]. Contradicting prior belief [81], we proved that implicit regularization cannot be captured by norms in the context of matrix factorization — a model equivalent to linear neural networks. Instead, we showed that it is more faithfully described as an implicit minimization of rank. Then, capitalizing on this interpretation, we established that the tendency towards low rank extends from linear neural networks to more practical non-linear neural networks (with polynomial non-linearity), which are equivalent to tensor factorizations.

In Part III, we employed the connection between neural networks and tensor factorizations to study the expressiveness of graph neural networks (GNNs). Our analysis characterized the ability of certain GNNs to model interactions between vertices via an established measure known as separation rank [24, 49]. In particular, it formalized intuition by which GNNs can model stronger interactions between areas of the graph that are more interconnected.

In terms of practical impact, based on the presented theory we developed: (i) a regularization scheme for improving the performance of convolutional neural networks over tasks involving non-local interactions; and (ii) a state of the art edge sparsification algorithm, called Walk Index Sparsification (WIS), that preserves the ability of GNNs to model interactions. Moreover, other research groups have also built upon our analyses of implicit rank minimization for designing practical deep learning systems [112, 102].

Overall, our work highlights that notions of rank may be key for explaining the remarkable performance of neural networks over natural data.

Future Work

Our theoretical analysis considered neural networks with polynomial non-linearity, by employing their connection with tensor factorizations. Such neural networks have demonstrated competitive performance in practice [47, 193, 200, 46], and we empirically demonstrated (in Sections 3.6 and 5.4.3) that conclusions from their analysis apply to neural networks with more popular non-linearities, such as ReLU. Nonetheless, we view extending our theory to account for additional non-linearities as a promising direction for future research. A possible approach is to build on the connection between *generalized tensor factorizations* [48] and neural networks with non-polynomial non-linearities.

Our work also raises several interesting directions concerning WIS — the edge sparsification algorithm introduced in Section 5.5. A naive implementation of $(L - 1)$ -WIS has runtime cubic in the number of vertices (*cf.* Section 5.5.1). Since this can be restrictive for large-scale graphs, the evaluation in Section 5.5.2 mostly focused on 1-WIS, which can be viewed as an efficient approximation of $(L - 1)$ -WIS (its runtime and memory requirements are linear — see Section 5.5.1). Future work can develop efficient exact implementations of $(L - 1)$ -WIS (*e.g.* using parallelization) and investigate regimes where it outperforms 1-WIS in terms of induced prediction accuracy. Additionally, $(L - 1)$ -WIS is a specific instantiation of the general WIS scheme (given in Appendix D.4), tailored for preserving the ability to model interactions across certain partitions. Exploring other instantiations, as well as methods for automatically choosing the partitions across which the ability to model interactions is preserved, are valuable directions for further research.

Bibliography

- [1] Evrim Acar, Daniel M Dunlavy, Tamara G Kolda, and Morten Mørup. Scalable tensor factorizations for incomplete data. *Chemometrics and Intelligent Laboratory Systems*, 106(1):41–56, 2011.
- [2] Josh Achiam, Steven Adler, Sandhini Agarwal, Lama Ahmad, Ilge Akkaya, Florencia Leoni Aleman, Diogo Almeida, Janko Alvenschmidt, Sam Altman, Shyamal Anadkat, et al. Gpt-4 technical report. *arXiv preprint arXiv:2303.08774*, 2023.
- [3] Yotam Alexander, Nimrod De La Vega, Noam Razin, and Nadav Cohen. What makes data suitable for a locally connected neural network? a necessary and sufficient condition based on quantum entanglement. In *Advances in Neural Information Processing Systems*, 2023.
- [4] Uri Alon and Eran Yahav. On the bottleneck of graph neural networks and its practical implications. *International Conference on Learning Representations (ICLR)*, 2021.
- [5] Arash Amini, Amin Karbasi, and Farokh Marvasti. Low-rank matrix approximation using point-wise operators. *IEEE transactions on information theory*, 58(1):302–310, 2011.
- [6] Animashree Anandkumar, Rong Ge, Daniel Hsu, Sham M Kakade, and Matus Telgarsky. Tensor decompositions for learning latent variable models. *Journal of Machine Learning Research*, 15:2773–2832, 2014.
- [7] Sanjeev Arora, Nadav Cohen, and Elad Hazan. On the optimization of deep networks: Implicit acceleration by overparameterization. In *International Conference on Machine Learning*, 2018.
- [8] Sanjeev Arora, Nadav Cohen, Noah Golowich, and Wei Hu. A convergence analysis of gradient descent for deep linear neural networks. *International Conference on Learning Representations*, 2019.
- [9] Sanjeev Arora, Nadav Cohen, Wei Hu, and Yuping Luo. Implicit regularization in deep matrix factorization. *Advances in Neural Information Processing Systems*, 2019.
- [10] Waiss Azizian and Marc Lelarge. Expressive power of invariant and equivariant graph neural networks. *International Conference on Learning Representations (ICLR)*, 2021.
- [11] Shahar Azulay, Edward Moroshko, Mor Shpigel Nacson, Blake Woodworth, Nathan Srebro, Amir Globerson, and Daniel Soudry. On the implicit bias of initialization shape: Beyond infinitesimal mirror descent. *International Conference on Machine Learning (ICML)*, 2021.
- [12] Jimmy Lei Ba, Jamie Ryan Kiros, and Geoffrey E Hinton. Layer normalization. *arXiv preprint arXiv:1607.06450*, 2016.
- [13] Bubacarr Bah, Holger Rauhut, Ulrich Terstiege, and Michael Westdickenberg. Learning deep linear neural networks: Riemannian gradient flows and convergence to global minimizers. *Information and Inference: A Journal of the IMA*, 11(1):307–353, 2022.
- [14] Muhammet Balçilar, Renton Guillaume, Pierre Héroux, Benoit Gaüzère, Sébastien Adam, and Paul Honeine. Analyzing the expressive power of graph neural networks in a spectral perspective. *International Conference on Learning Representations (ICLR)*, 2021.

- [15] Muhammet Balcilar, Pierre Hérroux, Benoit Gauzere, Pascal Vasseur, Sébastien Adam, and Paul Honeine. Breaking the limits of message passing graph neural networks. In *International Conference on Machine Learning (ICML)*, 2021.
- [16] Emilio Rafael Balda, Arash Behboodi, and Rudolf Mathar. A tensor analysis on dense connectivity via convolutional arithmetic circuits. 2018.
- [17] Pradeep Kr Banerjee, Kedar Karhadkar, Yu Guang Wang, Uri Alon, and Guido Montúfar. Oversquashing in gnns through the lens of information contraction and graph expansion. In *2022 58th Annual Allerton Conference on Communication, Control, and Computing (Allerton)*, pages 1–8. IEEE, 2022.
- [18] Pablo Barceló, Egor Kostylev, Mikael Monet, Jorge Pérez, Juan Reutter, and Juan-Pablo Silva. The logical expressiveness of graph neural networks. *International Conference on Learning Representations (ICLR)*, 2020.
- [19] Pablo Barceló, Floris Geerts, Juan Reutter, and Maksimilian Ryschkov. Graph neural networks with local graph parameters. In *Advances in Neural Information Processing Systems (NeurIPS)*, 2021.
- [20] Peter Bartlett, Dave Helmbold, and Phil Long. Gradient descent with identity initialization efficiently learns positive definite linear transformations. In *International Conference on Machine Learning*, 2018.
- [21] Surender Baswana and Sandeep Sen. A simple and linear time randomized algorithm for computing sparse spanners in weighted graphs. *Random Structures & Algorithms*, 30(4):532–563, 2007.
- [22] Mohamed Ali Belabbas. On implicit regularization: Morse functions and applications to matrix factorization. *arXiv preprint arXiv:2001.04264*, 2020.
- [23] Gregory Beylkin and Martin J Mohlenkamp. Numerical operator calculus in higher dimensions. *Proceedings of the National Academy of Sciences*, 99(16):10246–10251, 2002.
- [24] Gregory Beylkin, Jochen Garcke, and Martin J Mohlenkamp. Multivariate regression and machine learning with sums of separable functions. *SIAM Journal on Scientific Computing*, 31(3):1840–1857, 2009.
- [25] Amandeep Singh Bhatia, Mandeep Kaur Saggi, Ajay Kumar, and Sushma Jain. Matrix product state-based quantum classifier. *Neural computation*, 31(7):1499–1517, 2019.
- [26] Guy Blanc, Neha Gupta, Gregory Valiant, and Paul Valiant. Implicit regularization for deep neural networks driven by an ornstein-uhlenbeck like process. In *Conference on Learning Theory*, 2020.
- [27] Cristian Bodnar, Fabrizio Frasca, Nina Otter, Yuguang Wang, Pietro Lio, Guido F Montufar, and Michael Bronstein. Weisfeiler and lehman go cellular: Cw networks. In *Advances in Neural Information Processing Systems (NeurIPS)*, 2021.
- [28] Aleksandar Bojchevski and Stephan Günnemann. Deep gaussian embedding of graphs: Unsupervised inductive learning via ranking. *International Conference on Learning Representations (ICLR)*, 2018.
- [29] Giorgos Bouritsas, Fabrizio Frasca, Stefanos P Zafeiriou, and Michael Bronstein. Improving graph neural network expressivity via subgraph isomorphism counting. *IEEE Transactions on Pattern Analysis and Machine Intelligence*, 2022.
- [30] Michael M Bronstein, Joan Bruna, Taco Cohen, and Petar Veličković. Geometric deep learning: Grids, groups, graphs, geodesics, and gauges. *arXiv preprint arXiv:2104.13478*, 2021.

- [31] Tom Brown, Benjamin Mann, Nick Ryder, Melanie Subbiah, Jared D Kaplan, Prafulla Dhariwal, Arvind Neelakantan, Pranav Shyam, Girish Sastry, Amanda Askell, et al. Language models are few-shot learners. *Advances in neural information processing systems*, 2020.
- [32] Samuel Burer and Renato DC Monteiro. A nonlinear programming algorithm for solving semidefinite programs via low-rank factorization. *Mathematical Programming*, 95(2):329–357, 2003.
- [33] Changxiao Cai, Gen Li, H Vincent Poor, and Yuxin Chen. Nonconvex low-rank tensor completion from noisy data. In *Advances in Neural Information Processing Systems (NeurIPS)*, pages 1863–1874, 2019.
- [34] Emmanuel J Candès and Benjamin Recht. Exact matrix completion via convex optimization. *Foundations of Computational mathematics*, 9(6):717, 2009.
- [35] Richard Caron and Tim Traynor. The zero set of a polynomial. *WSMR Report*, pages 05–02, 2005.
- [36] Alireza Chakeri, Hamidreza Farhidzadeh, and Lawrence O Hall. Spectral sparsification in spectral clustering. In *2016 23rd international conference on pattern recognition (icpr)*, pages 2301–2306. IEEE, 2016.
- [37] Deli Chen, Yankai Lin, Wei Li, Peng Li, Jie Zhou, and Xu Sun. Measuring and relieving the over-smoothing problem for graph neural networks from the topological view. In *Proceedings of the AAAI Conference on Artificial Intelligence (AAAI)*, 2020.
- [38] Lei Chen, Zhengdao Chen, and Joan Bruna. On graph neural networks versus graph-augmented mlps. *International Conference on Learning Representations (ICLR)*, 2021.
- [39] Tianlong Chen, Yongduo Sui, Xuxi Chen, Aston Zhang, and Zhangyang Wang. A unified lottery ticket hypothesis for graph neural networks. In *International Conference on Machine Learning (ICML)*, 2021.
- [40] Zhengdao Chen, Soledad Villar, Lei Chen, and Joan Bruna. On the equivalence between graph isomorphism testing and function approximation with gnns. In *Advances in Neural Information Processing Systems (NeurIPS)*, 2019.
- [41] Zhengdao Chen, Lei Chen, Soledad Villar, and Joan Bruna. Can graph neural networks count substructures? In *Advances in Neural Information Processing Systems (NeurIPS)*, 2020.
- [42] Yuejie Chi, Yue M Lu, and Yuxin Chen. Nonconvex optimization meets low-rank matrix factorization: An overview. *IEEE Transactions on Signal Processing*, 67(20):5239–5269, 2019.
- [43] Lenaic Chizat and Francis Bach. Implicit bias of gradient descent for wide two-layer neural networks trained with the logistic loss. In *Conference on Learning Theory (COLT)*, pages 1305–1338, 2020.
- [44] Hung-Hsu Chou, Carsten Gieshoff, Johannes Maly, and Holger Rauhut. Gradient descent for deep matrix factorization: Dynamics and implicit bias towards low rank. *arXiv preprint arXiv:2011.13772*, 2020.
- [45] Hung-Hsu Chou, Johannes Maly, and Holger Rauhut. More is less: Inducing sparsity via overparameterization. *arXiv preprint arXiv:2112.11027*, 2021.
- [46] Grigorios G Chrysos, Stylianos Moschoglou, Giorgos Bouritsas, Yannis Panagakis, Jiankang Deng, and Stefanos Zafeiriou. P-nets: Deep polynomial neural networks. In *Proceedings of the IEEE/CVF Conference on Computer Vision and Pattern Recognition (CVPR)*, pages 7325–7335, 2020.

- [47] Nadav Cohen and Amnon Shashua. Simnets: A generalization of convolutional networks. *Advances in Neural Information Processing Systems, Deep Learning Workshop*, 2014.
- [48] Nadav Cohen and Amnon Shashua. Convolutional rectifier networks as generalized tensor decompositions. *International Conference on Machine Learning*, 2016.
- [49] Nadav Cohen and Amnon Shashua. Inductive bias of deep convolutional networks through pooling geometry. *International Conference on Learning Representations*, 2017.
- [50] Nadav Cohen, Or Sharir, and Amnon Shashua. Deep simnets. *IEEE Conference on Computer Vision and Pattern Recognition*, 2016.
- [51] Nadav Cohen, Or Sharir, and Amnon Shashua. On the expressive power of deep learning: A tensor analysis. *Conference On Learning Theory*, 2016.
- [52] Nadav Cohen, Or Sharir, Yoav Levine, Ronen Tamari, David Yakira, and Amnon Shashua. Analysis and design of convolutional networks via hierarchical tensor decompositions. *Intel Collaborative Research Institute for Computational Intelligence (ICRI-CI) Special Issue on Deep Learning Theory*, 2017.
- [53] Nadav Cohen, Ronen Tamari, and Amnon Shashua. Boosting dilated convolutional networks with mixed tensor decompositions. *International Conference on Learning Representations*, 2018.
- [54] Curt Da Silva and Felix J Herrmann. Optimization on the hierarchical tucker manifold—applications to tensor completion. *Linear Algebra and its Applications*, 481:131–173, 2015.
- [55] Mark A Davenport and Justin Romberg. An overview of low-rank matrix recovery from incomplete observations. *IEEE Journal of Selected Topics in Signal Processing*, 10(4): 608–622, 2016.
- [56] Nima Dehmamy, Albert-László Barabási, and Rose Yu. Understanding the representation power of graph neural networks in learning graph topology. In *Advances in Neural Information Processing Systems (NeurIPS)*, 2019.
- [57] Simon S Du, Wei Hu, and Jason D Lee. Algorithmic regularization in learning deep homogeneous models: Layers are automatically balanced. In *Advances in Neural Information Processing Systems*, 2018.
- [58] David K Duvenaud, Dougal Maclaurin, Jorge Iparraguirre, Rafael Bombarell, Timothy Hirzel, Alán Aspuru-Guzik, and Ryan P Adams. Convolutional networks on graphs for learning molecular fingerprints. *Advances in neural information processing systems*, 2015.
- [59] Armin Eftekhari and Konstantinos Zygalakis. Implicit regularization in matrix sensing: A geometric view leads to stronger results. *arXiv preprint arXiv:2008.12091*, 2020.
- [60] Armin Eftekhari and Konstantinos Zygalakis. Limitations of implicit bias in matrix sensing: Initialization rank matters. *arXiv preprint arXiv:2008.12091*, 2021.
- [61] Omer Elkabetz and Nadav Cohen. Continuous vs. discrete optimization of deep neural networks. In *Advances in Neural Information Processing Systems*, 2021.
- [62] Tolga Ergen and Mert Pilanci. Implicit convex regularizers of cnn architectures: Convex optimization of two-and three-layer networks in polynomial time. *International Conference on Learning Representations (ICLR)*, 2021.
- [63] Timo Felser, Marco Trenti, Lorenzo Sestini, Alessio Gianelle, Davide Zuliani, Donatella Lucchesi, and Simone Montangero. Quantum-inspired machine learning on high-energy physics data. *npj Quantum Information*, 7(1):1–8, 2021.

- [64] Matthias Fey and Jan Eric Lenssen. Fast graph representation learning with pytorch geometric. *arXiv preprint arXiv:1903.02428*, 2019.
- [65] Spencer Frei, Gal Vardi, Peter L Bartlett, Nathan Srebro, and Wei Hu. Implicit bias in leaky relu networks trained on high-dimensional data. *International Conference on Learning Representations*, 2023.
- [66] Vikas Garg, Stefanie Jegelka, and Tommi Jaakkola. Generalization and representational limits of graph neural networks. In *International Conference on Machine Learning (ICML)*, 2020.
- [67] Johannes Gasteiger, Stefan Weißenberger, and Stephan Günnemann. Diffusion improves graph learning. In *Advances in Neural Information Processing Systems (NeurIPS)*, 2019.
- [68] Floris Geerts. The expressive power of kth-order invariant graph networks. *arXiv preprint arXiv:2007.12035*, 2020.
- [69] Floris Geerts and Juan L Reutter. Expressiveness and approximation properties of graph neural networks. *International Conference on Learning Representations (ICLR)*, 2022.
- [70] Floris Geerts, Filip Mazowiecki, and Guillermo Perez. Let’s agree to degree: Comparing graph convolutional networks in the message-passing framework. In *International Conference on Machine Learning (ICML)*, 2021.
- [71] Gauthier Gidel, Francis Bach, and Simon Lacoste-Julien. Implicit regularization of discrete gradient dynamics in linear neural networks. In *Advances in Neural Information Processing Systems*, 2019.
- [72] Ran Gilad-Bachrach, Nathan Dowlın, Kim Laine, Kristin Lauter, Michael Naehrig, and John Wernsing. Cryptonets: Applying neural networks to encrypted data with high throughput and accuracy. In *International Conference on Machine Learning (ICML)*, 2016.
- [73] Justin Gilmer, Samuel S Schoenholz, Patrick F Riley, Oriol Vinyals, and George E Dahl. Neural message passing for quantum chemistry. In *International Conference on Machine Learning (ICML)*, 2017.
- [74] Daniel Gissin, Shai Shalev-Shwartz, and Amit Daniely. The implicit bias of depth: How incremental learning drives generalization. *International Conference on Learning Representations*, 2020.
- [75] Xavier Glorot and Yoshua Bengio. Understanding the difficulty of training deep feedforward neural networks. In *Proceedings of the thirteenth international conference on artificial intelligence and statistics*, 2010.
- [76] Gene H Golub and Charles F Van Loan. *Matrix computations*, volume 3. JHU press, 2012.
- [77] Ian Goodfellow, Yoshua Bengio, and Aaron Courville. *Deep learning*. MIT press, 2016.
- [78] Edward Grant, Marcello Benedetti, Shuxiang Cao, Andrew Hallam, Joshua Lockhart, Vid Stojevic, Andrew G Green, and Simone Severini. Hierarchical quantum classifiers. *npj Quantum Information*, 4(1):1–8, 2018.
- [79] Lars Grasedyck. Hierarchical singular value decomposition of tensors. *SIAM Journal on Matrix Analysis and Applications*, 31(4):2029–2054, 2010.
- [80] Lars Grasedyck, Daniel Kressner, and Christine Tobler. A literature survey of low-rank tensor approximation techniques. *GAMM-Mitteilungen*, 36(1):53–78, 2013.
- [81] Suriya Gunasekar, Blake E Woodworth, Srinadh Bhojanapalli, Behnam Neyshabur, and Nati Srebro. Implicit regularization in matrix factorization. In *Advances in Neural Information Processing Systems*, 2017.

- [82] Suriya Gunasekar, Jason Lee, Daniel Soudry, and Nathan Srebro. Characterizing implicit bias in terms of optimization geometry. In *International Conference on Machine Learning*, 2018.
- [83] Suriya Gunasekar, Jason D Lee, Daniel Soudry, and Nati Srebro. Implicit bias of gradient descent on linear convolutional networks. *Advances in neural information processing systems*, 2018.
- [84] Wolfgang Hackbusch. On the efficient evaluation of coalescence integrals in population balance models. *Computing*, 78(2):145–159, 2006.
- [85] Wolfgang Hackbusch. *Tensor spaces and numerical tensor calculus*, volume 42. Springer, 2012.
- [86] Wolfgang Hackbusch and Stefan Kühn. A new scheme for the tensor representation. *Journal of Fourier analysis and applications*, 15(5):706–722, 2009.
- [87] Michael Hamann, Gerd Lindner, Henning Meyerhenke, Christian L Staudt, and Dorothea Wagner. Structure-preserving sparsification methods for social networks. *Social Network Analysis and Mining*, 6(1):1–22, 2016.
- [88] Will Hamilton, Zhitao Ying, and Jure Leskovec. Inductive representation learning on large graphs. In *Advances in Neural Information Processing Systems (NeurIPS)*, 2017.
- [89] William L Hamilton. *Graph representation learning*. Morgan & Claypool Publishers, 2020.
- [90] Jeff Z HaoChen, Colin Wei, Jason Lee, and Tengyu Ma. Shape matters: Understanding the implicit bias of the noise covariance. In *Conference on Learning Theory (COLT)*, 2021.
- [91] Robert J Harrison, George I Fann, Takeshi Yanai, and Gregory Beylkin. Multiresolution quantum chemistry in multiwavelet bases. In *International Conference on Computational Science*, pages 103–110. Springer, 2003.
- [92] Johan Håstad. Tensor rank is np-complete. *Journal of algorithms (Print)*, 11(4):644–654, 1990.
- [93] Kaiming He, Xiangyu Zhang, Shaoqing Ren, and Jian Sun. Delving deep into rectifiers: Surpassing human-level performance on imagenet classification. In *Proceedings of the IEEE international conference on computer vision*, 2015.
- [94] Kaiming He, Xiangyu Zhang, Shaoqing Ren, and Jian Sun. Deep residual learning for image recognition. In *Proceedings of the IEEE conference on computer vision and pattern recognition (CVPR)*, 2016.
- [95] Christopher J Hillar and Lek-Heng Lim. Most tensor problems are np-hard. *Journal of the ACM (JACM)*, 60(6):1–39, 2013.
- [96] Frank L Hitchcock. The expression of a tensor or a polyadic as a sum of products. *Journal of Mathematics and Physics*, 6(1-4):164–189, 1927.
- [97] Danfeng Hong, Lianru Gao, Jing Yao, Bing Zhang, Antonio Plaza, and Jocelyn Chanussot. Graph convolutional networks for hyperspectral image classification. *IEEE Transactions on Geoscience and Remote Sensing*, 2020.
- [98] Wei Hu, Lechao Xiao, Ben Adlam, and Jeffrey Pennington. The surprising simplicity of the early-time learning dynamics of neural networks. In *Advances in Neural Information Processing Systems (NeurIPS)*, 2020.
- [99] Weihua Hu, Matthias Fey, Marinka Zitnik, Yuxiao Dong, Hongyu Ren, Bowen Liu, Michele Catasta, and Jure Leskovec. Open graph benchmark: Datasets for machine learning on graphs. In *Advances in Neural Information Processing Systems (NeurIPS)*, 2020.

- [100] Chenqing Hua, Guillaume Rabusseau, and Jian Tang. High-order pooling for graph neural networks with tensor decomposition. In *Advances in Neural Information Processing Systems (NeurIPS)*, 2022.
- [101] Peter J Huber. Robust estimation of a location parameter. *Annals of Mathematical Statistics*, 35:73–101, 1964.
- [102] Minyoung Huh, Hossein Mobahi, Richard Zhang, Brian Cheung, Pulkit Agrawal, and Phillip Isola. The low-rank simplicity bias in deep networks. *arXiv preprint arXiv:2103.10427*, 2021.
- [103] Shahana Ibrahim, Xiao Fu, and Xingguo Li. On recoverability of randomly compressed tensors with low cp rank. *IEEE Signal Processing Letters*, 27:1125–1129, 2020.
- [104] Yulij Ilyashenko and Sergei Yakovenko. *Lectures on analytic differential equations*, volume 86. American Mathematical Soc., 2008.
- [105] Sergey Ioffe and Christian Szegedy. Batch normalization: Accelerating deep network training by reducing internal covariate shift. In *International Conference on Machine Learning (ICML)*, 2015.
- [106] Arthur Jacot. Implicit bias of large depth networks: a notion of rank for nonlinear functions. In *International Conference on Learning Representations*, 2022.
- [107] Meena Jagadeesan, Ilya Razenshteyn, and Suriya Gunasekar. Inductive bias of multi-channel linear convolutional networks with bounded weight norm. *arXiv preprint arXiv:2102.12238*, 2021.
- [108] Prateek Jain and Sewoong Oh. Provable tensor factorization with missing data. In *Advances in Neural Information Processing Systems (NeurIPS)*, pages 1431–1439, 2014.
- [109] Ziwei Ji and Matus Telgarsky. Gradient descent aligns the layers of deep linear networks. *International Conference on Learning Representations*, 2019.
- [110] Ziwei Ji and Matus Telgarsky. The implicit bias of gradient descent on nonseparable data. In *Conference on Learning Theory (COLT)*, pages 1772–1798, 2019.
- [111] Ziwei Ji and Matus Telgarsky. Directional convergence and alignment in deep learning. In *Advances in Neural Information Processing Systems (NeurIPS)*, 2020.
- [112] Li Jing, Jure Zbontar, et al. Implicit rank-minimizing autoencoder. *Advances in Neural Information Processing Systems*, 2020.
- [113] Nikos Kargas and Nicholas D Sidiropoulos. Nonlinear system identification via tensor completion. In *Proceedings of the AAAI Conference on Artificial Intelligence*, 2020.
- [114] Nikos Kargas and Nicholas D Sidiropoulos. Supervised learning and canonical decomposition of multivariate functions. *IEEE Transactions on Signal Processing*, 69:1097–1107, 2021.
- [115] Lars Karlsson, Daniel Kressner, and André Uschmajew. Parallel algorithms for tensor completion in the cp format. *Parallel Computing*, 57:222–234, 2016.
- [116] Tosio Kato. *Perturbation theory for linear operators*, volume 132. Springer Science & Business Media, 2013.
- [117] Nicolas Keriven and Gabriel Peyré. Universal invariant and equivariant graph neural networks. In *Advances in Neural Information Processing Systems (NeurIPS)*, 2019.
- [118] Valentin Khruikov, Alexander Novikov, and Ivan Oseledets. Expressive power of recurrent neural networks. *International Conference on Learning Representations*, 2018.

- [119] Valentin Khrulkov, Oleksii Hrinchuk, and Ivan Oseledets. Generalized tensor models for recurrent neural networks. *International Conference on Learning Representations*, 2019.
- [120] Junkyung Kim, Drew Linsley, Kalpit Thakkar, and Thomas Serre. Disentangling neural mechanisms for perceptual grouping. *International Conference on Learning Representations*, 2020.
- [121] Diederik P Kingma and Jimmy Ba. Adam: A method for stochastic optimization. In *International Conference on Learning Representations*, 2015.
- [122] Thomas N Kipf and Max Welling. Semi-supervised classification with graph convolutional networks. *International Conference on Learning Representations*, 2017.
- [123] Kathlén Kohn, Thomas Merkh, Guido Montúfar, and Matthew Trager. Geometry of linear convolutional networks. *arXiv preprint arXiv:2108.01538*, 2021.
- [124] Tamara G Kolda and Brett W Bader. Tensor decompositions and applications. *SIAM review*, 51(3):455–500, 2009.
- [125] Tamara Gibson Kolda. Multilinear operators for higher-order decompositions. Technical report, 2006.
- [126] Steven G Krantz and Harold R Parks. *A primer of real analytic functions*. Springer Science & Business Media, 2002.
- [127] Alex Krizhevsky. Learning multiple layers of features from tiny images. Technical report, 2009.
- [128] Alex Krizhevsky, Ilya Sutskever, and Geoffrey E Hinton. Imagenet classification with deep convolutional neural networks. *Advances in neural information processing systems*, 2012.
- [129] Andrew K Lampinen and Surya Ganguli. An analytic theory of generalization dynamics and transfer learning in deep linear networks. *International Conference on Learning Representations*, 2019.
- [130] Yann LeCun. The mnist database of handwritten digits. <http://yann.lecun.com/exdb/mnist/>, 1998.
- [131] Jure Leskovec and Christos Faloutsos. Sampling from large graphs. In *Proceedings of the 12th ACM SIGKDD international conference on Knowledge discovery and data mining*, pages 631–636, 2006.
- [132] Yoav Levine, Or Sharir, and Amnon Shashua. Benefits of depth for long-term memory of recurrent networks. *International Conference on Learning Representations Workshop*, 2018.
- [133] Yoav Levine, David Yakira, Nadav Cohen, and Amnon Shashua. Deep learning and quantum entanglement: Fundamental connections with implications to network design. *International Conference on Learning Representations*, 2018.
- [134] Yoav Levine, Or Sharir, Nadav Cohen, and Amnon Shashua. Quantum entanglement in deep learning architectures. *Physical review letters*, 122(6):065301, 2019.
- [135] Yoav Levine, Noam Wies, Or Sharir, Hofit Bata, and Amnon Shashua. Limits to depth efficiencies of self-attention. In *Advances in Neural Information Processing Systems*, 2020.
- [136] Yoav Levine, Noam Wies, Daniel Jannai, Dan Navon, Yedid Hoshen, and Amnon Shashua. The inductive bias of in-context learning: Rethinking pretraining example design. *International Conference on Learning Representations*, 2022.
- [137] Guohao Li, Chenxin Xiong, Ali Thabet, and Bernard Ghanem. Deepergcn: All you need to train deeper gcns. *arXiv preprint arXiv:2006.07739*, 2020.

- [138] Jiayu Li, Tianyun Zhang, Hao Tian, Shengmin Jin, Makan Fardad, and Reza Zafarani. Sgcn: A graph sparsifier based on graph convolutional networks. In *Pacific-Asia Conference on Knowledge Discovery and Data Mining*, pages 275–287. Springer, 2020.
- [139] Qimai Li, Zhichao Han, and Xiao-Ming Wu. Deeper insights into graph convolutional networks for semi-supervised learning. In *Thirty-Second AAAI conference on artificial intelligence (AAAI)*, 2018.
- [140] Yuanzhi Li, Tengyu Ma, and Hongyang Zhang. Algorithmic regularization in over-parameterized matrix sensing and neural networks with quadratic activations. In *Conference On Learning Theory*, 2018.
- [141] Zhiyuan Li, Yuping Luo, and Kaifeng Lyu. Towards resolving the implicit bias of gradient descent for matrix factorization: Greedy low-rank learning. *International Conference on Learning Representations*, 2021.
- [142] Zhiyuan Li, Tianhao Wang, and Sanjeev Arora. What happens after sgd reaches zero loss?—a mathematical framework. *arXiv preprint arXiv:2110.06914*, 2021.
- [143] Drew Linsley, Junkyung Kim, Vijay Veerabadran, Charlie Windolf, and Thomas Serre. Learning long-range spatial dependencies with horizontal gated recurrent units. In *Advances in Neural Information Processing Systems*, 2018.
- [144] Ximeng Liu, Lehui Xie, Yaopeng Wang, Jian Zou, Jinbo Xiong, Zuobin Ying, and Athanasios V Vasilakos. Privacy and security issues in deep learning: A survey. *IEEE Access*, 9:4566–4593, 2020.
- [145] Andreas Loukas. What graph neural networks cannot learn: depth vs width. *International Conference on Learning Representations (ICLR)*, 2020.
- [146] Andreas Loukas. How hard is to distinguish graphs with graph neural networks? In *Advances in Neural Information Processing Systems (NeurIPS)*, 2020.
- [147] Dongsheng Luo, Wei Cheng, Wenchao Yu, Bo Zong, Jingchao Ni, Haifeng Chen, and Xiang Zhang. Learning to drop: Robust graph neural network via topological denoising. In *Proceedings of the 14th ACM international conference on web search and data mining*, pages 779–787, 2021.
- [148] Kaifeng Lyu and Jian Li. Gradient descent maximizes the margin of homogeneous neural networks. *International Conference on Learning Representations (ICLR)*, 2020.
- [149] Kaifeng Lyu, Zhiyuan Li, Runzhe Wang, and Sanjeev Arora. Gradient descent on two-layer nets: Margin maximization and simplicity bias. In *Advances in Neural Information Processing Systems*, 2021.
- [150] Cong Ma, Kaizheng Wang, Yuejie Chi, and Yuxin Chen. Implicit regularization in nonconvex statistical estimation: Gradient descent converges linearly for phase retrieval and matrix completion. In *International Conference on Machine Learning (ICML)*, pages 3351–3360, 2018.
- [151] Haggai Maron, Heli Ben-Hamu, Hadar Serviansky, and Yaron Lipman. Provably powerful graph networks. In *Advances in Neural Information Processing Systems (NeurIPS)*, 2019.
- [152] Haggai Maron, Ethan Fetaya, Nimrod Segol, and Yaron Lipman. On the universality of invariant networks. In *International Conference on Machine Learning (ICML)*, 2019.
- [153] Tomas Mikolov, Ilya Sutskever, Kai Chen, Greg S Corrado, and Jeff Dean. Distributed representations of words and phrases and their compositionality. *Advances in neural information processing systems*, 26, 2013.

- [154] Hancheng Min, Salma Tarmoun, Rene Vidal, and Enrique Mallada. On the explicit role of initialization on the convergence and implicit bias of overparametrized linear networks. *International Conference on Machine Learning (ICML)*, 2021.
- [155] Pawel Mlynarski, Hervé Delingette, Antonio Criminisi, and Nicholas Ayache. 3d convolutional neural networks for tumor segmentation using long-range 2d context. *Computerized Medical Imaging and Graphics*, 73:60–72, 2019.
- [156] Edward Moroshko, Suriya Gunasekar, Blake Woodworth, Jason D Lee, Nathan Srebro, and Daniel Soudry. Implicit bias in deep linear classification: Initialization scale vs training accuracy. In *Advances in Neural Information Processing Systems (NeurIPS)*, 2020.
- [157] Christopher Morris, Martin Ritzert, Matthias Fey, William L Hamilton, Jan Eric Lenssen, Gaurav Rattan, and Martin Grohe. Weisfeiler and leman go neural: Higher-order graph neural networks. In *Proceedings of the AAAI Conference on Artificial Intelligence*, volume 33, pages 4602–4609, 2019.
- [158] Christopher Morris, Yaron Lipman, Haggai Maron, Bastian Rieck, Nils M Kriege, Martin Grohe, Matthias Fey, and Karsten Borgwardt. Weisfeiler and leman go machine learning: The story so far. *arXiv preprint arXiv:2112.09992*, 2021.
- [159] Rotem Mulayoff and Tomer Michaeli. Unique properties of wide minima in deep networks. In *International Conference on Machine Learning*, 2020.
- [160] Rotem Mulayoff, Tomer Michaeli, and Daniel Soudry. The implicit bias of minima stability: A view from function space. In *Advances in Neural Information Processing Systems (NeurIPS)*, 2021.
- [161] Mor Shpigel Nacson, Suriya Gunasekar, Jason Lee, Nathan Srebro, and Daniel Soudry. Lexicographic and depth-sensitive margins in homogeneous and non-homogeneous deep models. In *International Conference on Machine Learning (ICML)*, 2019.
- [162] Mor Shpigel Nacson, Jason Lee, Suriya Gunasekar, Pedro Henrique Pamplona Savarese, Nathan Srebro, and Daniel Soudry. Convergence of gradient descent on separable data. In *Proceedings of the Twenty-Second International Conference on Artificial Intelligence and Statistics*, 2019.
- [163] Galileo Namata, Ben London, Lise Getoor, Bert Huang, and U Edu. Query-driven active surveying for collective classification. In *10th international workshop on mining and learning with graphs*, volume 8, page 1, 2012.
- [164] Atsuhiko Narita, Kohei Hayashi, Ryota Tomioka, and Hisashi Kashima. Tensor factorization using auxiliary information. *Data Mining and Knowledge Discovery*, 25(2): 298–324, 2012.
- [165] Behnam Neyshabur. Implicit regularization in deep learning. *arXiv preprint arXiv:1709.01953*, 2017.
- [166] Behnam Neyshabur, Ryota Tomioka, and Nathan Srebro. In search of the real inductive bias: On the role of implicit regularization in deep learning. In *International Conference on Learning Representations*, 2015.
- [167] Hoang NT and Takanori Maehara. Revisiting graph neural networks: All we have is low-pass filters. *arXiv preprint arXiv:1905.09550*, 2019.
- [168] Kenta Oono and Taiji Suzuki. Graph neural networks exponentially lose expressive power for node classification. *International Conference on Learning Representations (ICLR)*, 2020.
- [169] Román Orús. A practical introduction to tensor networks: Matrix product states and projected entangled pair states. *Annals of physics*, 349:117–158, 2014.

- [170] Samet Oymak and Mahdi Soltanolkotabi. Overparameterized nonlinear learning: Gradient descent takes the shortest path? In *International Conference on Machine Learning (ICML)*, pages 4951–4960, 2019.
- [171] Pál András Papp and Roger Wattenhofer. A theoretical comparison of graph neural network extensions. In *International Conference on Machine Learning (ICML)*, 2022.
- [172] Adam Paszke, Sam Gross, Francisco Massa, Adam Lerer, James Bradbury, Gregory Chanan, Trevor Killeen, Zeming Lin, Natalia Gimelshein, Luca Antiga, et al. Pytorch: An imperative style, high-performance deep learning library. *Advances in neural information processing systems*, 2019.
- [173] F. Pedregosa, G. Varoquaux, A. Gramfort, V. Michel, B. Thirion, O. Grisel, M. Blondel, P. Prettenhofer, R. Weiss, V. Dubourg, J. Vanderplas, A. Passos, D. Cournapeau, M. Brucher, M. Perrot, and E. Duchesnay. Scikit-learn: Machine learning in Python. *Journal of Machine Learning Research*, 12:2825–2830, 2011.
- [174] Hongbin Pei, Bingzhe Wei, Kevin Chen-Chuan Chang, Yu Lei, and Bo Yang. Geom-gcn: Geometric graph convolutional networks. *International Conference on Learning Representations (ICLR)*, 2020.
- [175] Scott Pesme, Loucas Pillaud-Vivien, and Nicolas Flammarion. Implicit bias of sgd for diagonal linear networks: a provable benefit of stochasticity. In *Advances in Neural Information Processing Systems (NeurIPS)*, 2021.
- [176] Holger Rauhut, Reinhold Schneider, and Željka Stojanac. Low rank tensor recovery via iterative hard thresholding. *Linear Algebra and its Applications*, 523:220–262, 2017.
- [177] Noam Razin and Nadav Cohen. Implicit regularization in deep learning may not be explainable by norms. In *Advances in Neural Information Processing Systems*, 2020.
- [178] Noam Razin, Asaf Maman, and Nadav Cohen. Implicit regularization in tensor factorization. In *International Conference on Machine Learning*, 2021.
- [179] Noam Razin, Asaf Maman, and Nadav Cohen. Implicit regularization in hierarchical tensor factorization and deep convolutional neural networks. In *International Conference on Machine Learning*, 2022.
- [180] Noam Razin, Tom Verbin, and Nadav Cohen. On the ability of graph neural networks to model interactions between vertices. In *Advances in Neural Information Processing Systems*, 2023.
- [181] Noam Razin, Yotam Alexander, Edo Cohen-Karlik, Raja Giryes, Amir Globerson, and Nadav Cohen. Implicit bias of policy gradient in linear quadratic control: Extrapolation to unseen initial states. *arXiv preprint arXiv:2402.07875*, 2024.
- [182] Noam Razin, Hattie Zhou, Omid Saremi, Vimal Thilak, Arwen Bradley, Preetum Nakkiran, Joshua Susskind, and Etai Littwin. Vanishing gradients in reinforcement finetuning of language models. In *International Conference on Learning Representations*, 2024.
- [183] Benjamin Recht, Maryam Fazel, and Pablo A Parrilo. Guaranteed minimum-rank solutions of linear matrix equations via nuclear norm minimization. *SIAM review*, 52(3):471–501, 2010.
- [184] Benjamin Recht, Weiyu Xu, and Babak Hassibi. Null space conditions and thresholds for rank minimization. *Mathematical programming*, 127(1):175–202, 2011.
- [185] Olivier Roy and Martin Vetterli. The effective rank: A measure of effective dimensionality. In *2007 15th European Signal Processing Conference*, pages 606–610. IEEE, 2007.

- [186] Veeru Sadhanala, Yu-Xiang Wang, and Ryan Tibshirani. Graph sparsification approaches for laplacian smoothing. In *Artificial Intelligence and Statistics*, pages 1250–1259. PMLR, 2016.
- [187] Roei Sarussi, Alon Brutzkus, and Amir Globerson. Towards understanding learning in neural networks with linear teachers. In *Advances in Neural Information Processing Systems (NeurIPS)*, 2021.
- [188] Andrew M Saxe, James L McClelland, and Surya Ganguli. Exact solutions to the nonlinear dynamics of learning in deep linear neural networks. *International Conference on Learning Representations*, 2014.
- [189] Michael Schlichtkrull, Thomas N Kipf, Peter Bloem, Rianne van den Berg, Ivan Titov, and Max Welling. Modeling relational data with graph convolutional networks. In *European semantic web conference*, pages 593–607. Springer, 2018.
- [190] Prithviraj Sen, Galileo Namata, Mustafa Bilgic, Lise Getoor, Brian Galligher, and Tina Eliassi-Rad. Collective classification in network data. *AI magazine*, 29(3):93–93, 2008.
- [191] Gal Shachaf, Alon Brutzkus, and Amir Globerson. A theoretical analysis of fine-tuning with linear teachers. In *Advances in Neural Information Processing Systems (NeurIPS)*, 2021.
- [192] Or Sharir and Amnon Shashua. On the expressive power of overlapping architectures of deep learning. *International Conference on Learning Representations*, 2018.
- [193] Or Sharir, Ronen Tamari, Nadav Cohen, and Amnon Shashua. Tensorial mixture models. *arXiv preprint*, 2016.
- [194] Oleksandr Shchur, Maximilian Mumme, Aleksandar Bojchevski, and Stephan Günnemann. Pitfalls of graph neural network evaluation. *arXiv preprint arXiv:1811.05868*, 2018.
- [195] David Silver, Aja Huang, Chris J Maddison, Arthur Guez, Laurent Sifre, George Van Den Driessche, Julian Schrittwieser, Ioannis Antonoglou, Veda Panneershelvam, Marc Lanctot, et al. Mastering the game of go with deep neural networks and tree search. *nature*, 529(7587):484–489, 2016.
- [196] Qingquan Song, Hancheng Ge, James Caverlee, and Xia Hu. Tensor completion algorithms in big data analytics. *ACM Transactions on Knowledge Discovery from Data (TKDD)*, 13(1):1–48, 2019.
- [197] Daniel Soudry, Elad Hoffer, Mor Shpigel Nacson, Suriya Gunasekar, and Nathan Srebro. The implicit bias of gradient descent on separable data. *Journal of Machine Learning Research*, 19(70):1–57, 2018.
- [198] Daniel A Spielman and Nikhil Srivastava. Graph sparsification by effective resistances. *SIAM Journal on Computing*, 40(6):1913–1926, 2011.
- [199] Michael Steinlechner. Riemannian optimization for high-dimensional tensor completion. *SIAM Journal on Scientific Computing*, 38(5):S461–S484, 2016.
- [200] E Miles Stoudenmire. Learning relevant features of data with multi-scale tensor networks. *Quantum Science and Technology*, 3(3):034003, 2018.
- [201] Christian Szegedy, Wojciech Zaremba, Ilya Sutskever, Joan Bruna, Dumitru Erhan, Ian Goodfellow, and Rob Fergus. Intriguing properties of neural networks. In *International Conference on Learning Representations*, 2014.
- [202] Yi Tay, Mostafa Dehghani, Samira Abnar, Yikang Shen, Dara Bahri, Philip Pham, Jinfeng Rao, Liu Yang, Sebastian Ruder, and Donald Metzler. Long range arena: A benchmark for efficient transformers. *International Conference on Learning Representations*, 2021.

- [203] Gerald Teschl. *Ordinary differential equations and dynamical systems*, volume 140. American Mathematical Soc., 2012.
- [204] Nadav Timor, Gal Vardi, and Ohad Shamir. Implicit regularization towards rank minimization in relu networks. In *International Conference on Algorithmic Learning Theory*, 2023.
- [205] Jake Topping, Francesco Di Giovanni, Benjamin Paul Chamberlain, Xiaowen Dong, and Michael M Bronstein. Understanding over-squashing and bottlenecks on graphs via curvature. *International Conference on Learning Representations (ICLR)*, 2022.
- [206] Stephen Tu, Ross Boczar, Max Simchowitz, Mahdi Soltanolkotabi, and Ben Recht. Low-rank solutions of linear matrix equations via procrustes flow. In *International Conference on Machine Learning (ICML)*, pages 964–973, 2016.
- [207] Gal Vardi and Ohad Shamir. Implicit regularization in relu networks with the square loss. In *Conference on Learning Theory (COLT)*, 2021.
- [208] Gal Vardi, Ohad Shamir, and Nathan Srebro. On margin maximization in linear and relu networks. *arXiv preprint arXiv:2110.02732*, 2021.
- [209] Petar Veličković, Guillem Cucurull, Arantxa Casanova, Adriana Romero, Pietro Lio, and Yoshua Bengio. Graph attention networks. *International Conference on Learning Representations (ICLR)*, 2018.
- [210] Guifré Vidal. Class of quantum many-body states that can be efficiently simulated. *Physical review letters*, 101(11):110501, 2008.
- [211] Elli Voudigari, Nikos Salamanos, Theodore Papageorgiou, and Emmanuel J Yannakoudakis. Rank degree: An efficient algorithm for graph sampling. In *2016 IEEE/ACM International Conference on Advances in Social Networks Analysis and Mining (ASONAM)*, pages 120–129. IEEE, 2016.
- [212] Limin Wang, Yuanjun Xiong, Zhe Wang, Yu Qiao, Dahua Lin, Xiaoou Tang, and Luc Van Gool. Temporal segment networks: Towards good practices for deep action recognition. In *European conference on computer vision*, pages 20–36. Springer, 2016.
- [213] Zihan Wang and Arthur Jacot. Implicit bias of sgd in l_2 -regularized linear dnns: One-way jumps from high to low rank. *arXiv preprint arXiv:2305.16038*, 2023.
- [214] Boris Weisfeiler and Andrei Leman. The reduction of a graph to canonical form and the algebra which appears therein. *NTI, Series*, 2(9):12–16, 1968.
- [215] Noam Wies, Yoav Levine, Daniel Jannai, and Amnon Shashua. Which transformer architecture fits my data? a vocabulary bottleneck in self-attention. *International Conference on Machine Learning*, 2021.
- [216] Blake Woodworth, Suriya Gunasekar, Jason D Lee, Edward Moroshko, Pedro Savarese, Itay Golan, Daniel Soudry, and Nathan Srebro. Kernel and rich regimes in over-parametrized models. In *Conference on Learning Theory*, 2020.
- [217] Xiaoxia Wu, Edgar Dobriban, Tongzheng Ren, Shanshan Wu, Zhiyuan Li, Suriya Gunasekar, Rachel Ward, and Qiang Liu. Implicit regularization and convergence for weight normalization. *Advances in Neural Information Processing Systems*, 2020.
- [218] Zonghan Wu, Shirui Pan, Fengwen Chen, Guodong Long, Chengqi Zhang, and S Yu Philip. A comprehensive survey on graph neural networks. *IEEE transactions on neural networks and learning systems*, 32(1):4–24, 2020.
- [219] Dong Xia and Ming Yuan. On polynomial time methods for exact low rank tensor completion. *arXiv preprint arXiv:1702.06980*, 2017.

- [220] Han Xiao, Kashif Rasul, and Roland Vollgraf. Fashion-mnist: a novel image dataset for benchmarking machine learning algorithms. *arXiv preprint arXiv:1708.07747*, 2017.
- [221] Keyulu Xu, Weihua Hu, Jure Leskovec, and Stefanie Jegelka. How powerful are graph neural networks? *International Conference on Learning Representations (ICLR)*, 2019.
- [222] Rex Ying, Ruining He, Kaifeng Chen, Pong Eksombatchai, William L Hamilton, and Jure Leskovec. Graph convolutional neural networks for web-scale recommender systems. In *Proceedings of the 24th ACM SIGKDD international conference on knowledge discovery & data mining*, 2018.
- [223] Tatsuya Yokota, Qibin Zhao, and Andrzej Cichocki. Smooth parafac decomposition for tensor completion. *IEEE Transactions on Signal Processing*, 64(20):5423–5436, 2016.
- [224] Chulhee Yun, Shankar Krishnan, and Hossein Mobahi. A unifying view on implicit bias in training linear neural networks. *International Conference on Learning Representations*, 2021.
- [225] Bohang Zhang, Shengjie Luo, Liwei Wang, and Di He. Rethinking the expressive power of gnns via graph biconnectivity. *International Conference on Learning Representations (ICLR)*, 2023.
- [226] Chiyuan Zhang, Samy Bengio, Moritz Hardt, Benjamin Recht, and Oriol Vinyals. Understanding deep learning (still) requires rethinking generalization. *Communications of the ACM*, 64(3):107–115, 2021.
- [227] Cheng Zheng, Bo Zong, Wei Cheng, Dongjin Song, Jingchao Ni, Wenchao Yu, Haifeng Chen, and Wei Wang. Robust graph representation learning via neural sparsification. In *International Conference on Machine Learning (ICML)*, 2020.
- [228] Hattie Zhou, Arwen Bradley, , Etai Littwin, Noam Razin, Omid Saremi, Joshua Susskind, Samy Bengio, and Preetum Nakkiran. What algorithms can transformers learn? a study in length generalization. In *International Conference on Learning Representations*, 2024.
- [229] Pan Zhou, Canyi Lu, Zhouchen Lin, and Chao Zhang. Tensor factorization for low-rank tensor completion. *IEEE Transactions on Image Processing*, 27(3):1152–1163, 2017.

Appendix A

Implicit Regularization in Deep Learning May Not Be Explainable by Norms

A.1 Extension to Different Matrix Dimensions

In this appendix we outline an extension of the construction and analysis given in Sections 1.3.1 and 1.3.2, respectively, to completion of matrices with dimensions beyond 2-by-2. The extension presented here is not unique, but rather one simple option out of many. It is demonstrated empirically in Figure A.1.

Beginning with square matrices, for $2 \leq D \in \mathbb{N}$, consider completion of a D -by- D matrix based on the following observations:

$$\begin{aligned} \Omega &= \{1, \dots, D\} \times \{1, \dots, D\} \setminus \{(1, 1)\}, \\ y_{i,j} &= \begin{cases} 1 & , \text{if } i = j \geq 3 \text{ or } (i, j) \in \{(1, 2), (2, 1)\} \\ 0 & , \text{otherwise} \end{cases} \text{ , for } (i, j) \in \Omega, \end{aligned} \quad (\text{A.1})$$

where, as in Section 1.2, Ω represents the set of observed locations, and $\{y_{i,j} \in \mathbb{R}\}_{(i,j) \in \Omega}$ the corresponding set of observed values. The solution set for this problem (*i.e.* the set of matrices zeroing the loss in Equation (1.1)) is:

$$\mathcal{S}_D := \left\{ \begin{pmatrix} w_{1,1} & 1 & 0 & 0 & \cdots & 0 \\ 1 & 0 & 0 & 0 & \cdots & 0 \\ 0 & 0 & 1 & 0 & \cdots & 0 \\ 0 & 0 & 0 & 1 & & 0 \\ \vdots & \vdots & \vdots & & \ddots & \\ 0 & 0 & 0 & 0 & & 1 \end{pmatrix} \in \mathbb{R}^{D \times D} : w_{1,1} \in \mathbb{R} \right\}. \quad (\text{A.2})$$

Observing \mathcal{S}_D , while comparing to the solution set \mathcal{S} in our original construction (Equation (1.7)), we see that the former has a 2-by-2 block diagonal structure, with the top-left block holding the latter, and the bottom-right block set to identity. This implies that $D - 2$ of the singular values along \mathcal{S}_D are fixed to one, and the remaining two are identical to the singular values along \mathcal{S} . Results analogous to Propositions 1 and 2 can therefore easily be proven. Since the determinant along \mathcal{S}_D is bounded below and away from zero (it is equal to -1), approaching \mathcal{S}_D while having positive determinant necessarily means that absolute value of unobserved entry (*i.e.* of the entry in location $(1, 1)$) grows towards infinity. Combining this with the fact that

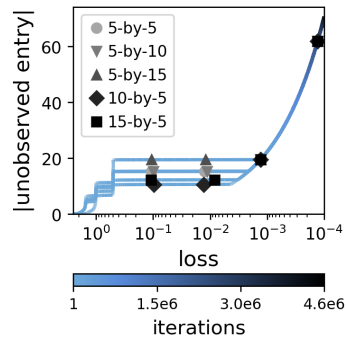


Figure A.1: Phenomenon of implicit regularization in matrix factorization driving *all* norms (and quasi-norms) *towards infinity* extends to arbitrary matrix dimensions. Appendix A.1 outlines an extension of the construction and analysis given in Sections 1.3.1 and 1.3.2, respectively, to completion of matrices with arbitrary dimensions. The extension implies that for any $2 \leq D, D' \in \mathbb{N}$, when applying matrix factorization to the specified D -by- D' matrix completion problem, decreasing loss, *i.e.* fitting observations, can lead absolute value of unobserved entry to increase (which in turn means norms and quasi-norms increase). This is demonstrated in the plot above, which for representative runs corresponding to different choices of D and D' , shows absolute value of unobserved entry as a function of the loss (Equation 1.1), with iteration number encoded by color. Runs were obtained with a depth 3 matrix factorization initialized randomly by an unbalanced (layer-wise independent) distribution, with the latter’s standard deviation and the learning rate for gradient descent set to the smallest values used for depth 3 in Figure 1.1 (other settings we evaluated produced similar results). For further implementation details see Appendix A.2.2.1.

the end matrix (Equation (1.3)) of a depth $L \geq 2$ matrix factorization maintains the sign of its determinant (see Lemma 6 in Appendix A.3.2.1), results analogous to Theorem 1 and Corollary 1 may readily be established. That is, one may show that, with probability 0.5 or more over random near-zero initialization, gradient descent with small learning rate drives *all* norms (and quasi-norms) *towards infinity*, while essentially driving rank towards its minimum.

Moving on to the rectangular case, for $2 \leq D, D' \in \mathbb{N}$, consider completion of a D -by- D' matrix based on the same observations as in Equation (A.1), but with additional zero observations such that only the entry in location $(1, 1)$ is unobserved. The singular values along the solution set for this problem are the same as those along \mathcal{S}_D (Equation (A.2)). Moreover, assuming without loss of generality that $D \leq D'$, if a matrix factorization applied to this problem is initialized such that its end matrix holds zeros in columns $D + 1$ to D' , then a dynamical characterization from [7] (restated as Lemma 4 in Appendix A.3.2.1), along with the structure of the loss (Equation (1.1)), ensure the leftmost D -by- D submatrix of the end matrix evolves precisely as in the square case discussed above, while the remaining columns ($D + 1$ to D') stay at zero. Results thus carry over from the square to the rectangular case.

A.2 Further Experiments and Implementation Details

A.2.1 Further Experiments

Figures A.1 and A.2 supplement Figure 1.1 from Section 1.4.1, by demonstrating empirically that the phenomenon of implicit regularization in matrix factorization driving all norms (and quasi-norms) towards infinity is, respectively: (i) applicable

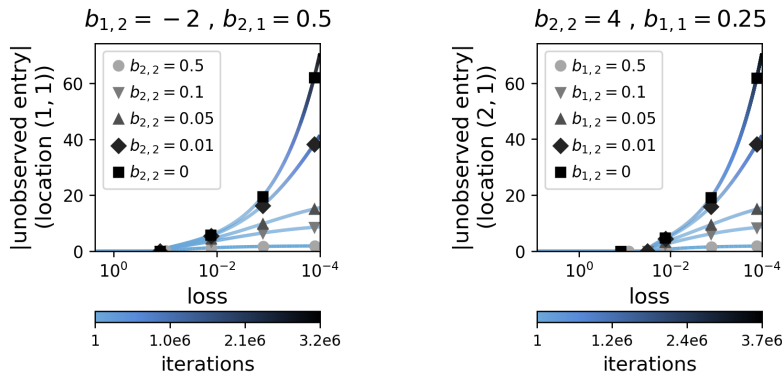


Figure A.2: Phenomenon of implicit regularization in matrix factorization driving *all* norms (and quasi-norms) *towards infinity* is robust to perturbations. Our analysis (Section 1.3.4) implies that, when applying matrix factorization to the matrix completion problem defined in Section 1.3.1, even if observations are perturbed and repositioned, decreasing loss, *i.e.* fitting them, leads absolute value of unobserved entry to increase (which in turn means norms and quasi-norms increase). Specifically, with $(i, j) \in \{1, 2\} \times \{1, 2\}$ representing the unobserved location and $\bar{i} := 3 - i, \bar{j} := 3 - j$, Theorem 2 implies that: (i) if the diagonally-opposite observation $y_{\bar{i}, \bar{j}}$ is unperturbed (stays at zero), the adjacent ones $y_{i, \bar{j}}, y_{\bar{i}, j}$ can take on *any* non-zero values, and as long as at initialization the sign of the end matrix’s (Equation 1.3) determinant accords with that of $y_{i, \bar{j}} \cdot y_{\bar{i}, j}$, the absolute value of unobserved entry will grow to infinity; and (ii) the extent to which absolute value of unobserved entry grows gracefully recedes as $y_{\bar{i}, \bar{j}}$ is perturbed away from zero. This is demonstrated in the plots above, which for representative runs, show absolute value of unobserved entry as a function of the loss (Equation 1.1), with iteration number encoded by color. Each plot corresponds to a different choice of (i, j) and a different assignment for $y_{i, \bar{j}}, y_{\bar{i}, j}$, presenting runs with varying values for $y_{\bar{i}, \bar{j}}$. Runs were obtained with a depth 3 matrix factorization initialized randomly by an unbalanced (layer-wise independent) distribution, with the latter’s standard deviation and the learning rate for gradient descent set to the smallest values used for depth 3 in Figure 1.1 (other settings we evaluated produced similar results). For further implementation details see Appendix A.2.2.1.

to arbitrary matrix dimensions, as outlined in Appendix A.1; and (ii) robust to perturbations, as proven in Section 1.3.4. Figure A.3 supplements Figure 1.2 from Section 1.4.2, further demonstrating that gradient descent over tensor factorization exhibits an implicit regularization towards low tensor rank.

A.2.2 Implementation Details

Below we provide implementation details omitted from the experimental reports in Section 1.4 and Appendix A.2.1. Source code for reproducing our results and figures, based on the PyTorch framework [172], can be found at https://github.com/noamrazin/imp_reg_dl_not_norms.

A.2.2.1 Deep Matrix Factorization (Figures 1.1, A.1, and A.2)

In all experiments with deep matrix factorization, hidden dimensions were set to the minimal value ensuring unconstrained search space, *i.e.* to the minimum between the number of rows and the number of columns in the matrix to complete. Gradient descent was run with fixed learning rate until loss (Equation (1.1)) reached a value lower than 10^{-4} or $5 \cdot 10^6$ iterations elapsed. Both balanced (Equation (1.5)) and unbalanced (layer-wise independent) random initializations were calibrated according to a desired standard deviation $\alpha > 0$ for the entries of the initial end

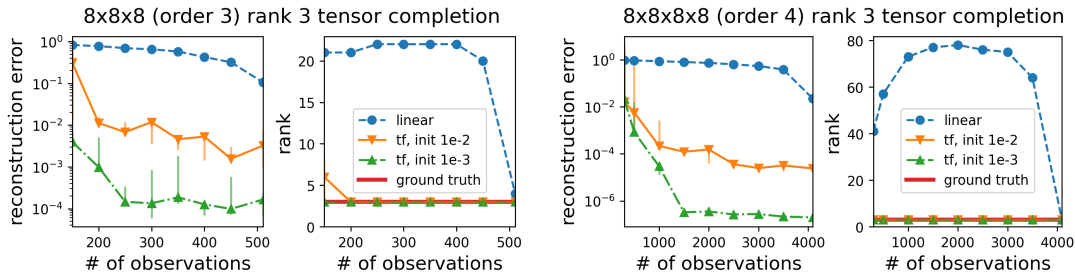


Figure A.3: Gradient descent over tensor factorization exhibits an implicit regularization towards low tensor rank. This figure is identical to Figure 1.2, except that the experiments it portrays had ground truth tensors of rank 3 (instead of 1). For further details see caption of Figure 1.2, as well as Appendix A.2.2.2.

matrix (Equation (1.3)). Namely: (i) under unbalanced initialization, entries of all weight matrices were sampled independently from a Gaussian distribution with zero mean and standard deviation $(\alpha^2/\bar{D}^{L-1})^{1/2L}$, where L stands for the depth of the factorization, and \bar{D} for the size of its hidden dimensions; and (ii) under balanced initialization, we used Procedure 1 from [8], based on a Gaussian distribution with independent entries, zero mean and standard deviation α .

In accordance with the description in Appendix A.1, if the matrix to complete was rectangular, we ensured that excess rows or columns of the initial end matrix held zeros, by clearing (setting to zero) corresponding rows or columns of the initial leftmost or rightmost (respectively) matrix in the factorization.¹ Random initializations were repeated until the determinant of the initial end matrix (or of its top-left $\min\{D, D'\}$ -by- $\min\{D, D'\}$ submatrix if its size was D -by- D' with $D \neq D'$) was of the necessary sign,² taking two attempts on average. In the experiment reported by Figure 1.1, runs with matrix factorization depths 2 and 3 were carried out with learning rates $\{6 \cdot 10^{-2}, 3 \cdot 10^{-2}, 9 \cdot 10^{-3}, 6 \cdot 10^{-3}, 3 \cdot 10^{-3}, 9 \cdot 10^{-4}\}$ and corresponding standard deviations for initialization $\{10^{-2}, 10^{-3}, 10^{-4}, 10^{-5}, 10^{-6}, 10^{-7}\}$. Factorizations of depth 4 were slightly more sensitive to changes in learning rate, thus we refined attempted values to $\{6 \cdot 10^{-3}, 4.5 \cdot 10^{-3}, 3 \cdot 10^{-3}, 1.5 \cdot 10^{-3}, 10^{-3}\}$, with corresponding standard deviations for initialization $\{10^{-1}, 10^{-2}, 10^{-3}, 10^{-4}, 10^{-5}\}$.

A.2.2.2 Tensor Factorization (Figures 1.2 and A.3)

In all experiments with tensor factorization (Equation (1.17)), the number of terms R was set to ensure an unconstrained search space, *i.e.* it was set to 8^2 and 8^3 for tensor sizes 8-by-8-by-8 and 8-by-8-by-8-by-8 respectively.³ Horizontal axes in all plots begin from the smallest number of observations producing stable results, and end when all entries but one are observed. Specifically: (i) in the experiments with rank 1 ground truth tensors (Figure 1.2), the number of observations ranged over $\{50, 100, 150, \dots, 400, 450, 511\}$ and $\{100, 500, 1000, 1500, \dots, 3000, 3500, 4095\}$ for orders 3 and 4 respectively; and (ii) for experiments with rank 3 ground truth tensors

¹That is, if the matrix to complete had size D -by- D' with $D \neq D'$, we cleared rows $D' + 1$ to D of $\mathbf{W}_L(0)$ if $D > D'$, and columns $D + 1$ to D' of $\mathbf{W}_1(0)$ if $D' > D$.

²Positive for the experiments reported by Figures 1.1 and A.1, and negative for those reported by Figure A.2.

³As shown in [85], for any $D_1, \dots, D_N \in \mathbb{N}$, using $R = (\prod_{n=1}^N D_n) / \max\{D_n\}_{n=1}^N$ suffices for expressing all tensors in $\mathbb{R}^{D_1 \times \dots \times D_N}$.

(Figure A.3), the minimal number of observations was increased threefold (*i.e.* ranges of $\{150, 200, 250, \dots, 400, 450, 511\}$ and $\{300, 500, 1000, 1500, \dots, 3000, 3500, 4095\}$ were used for orders 3 and 4 respectively).

Gradient descent was run until the mean squared error over observations reached a value lower than 10^{-6} or 10^6 iterations elapsed. For initialization, weights were sampled independently from a Gaussian distribution with zero mean and varying standard deviation. In particular, five trials (differing in random seed) were conducted for each standard deviation in the range $\{10^{-1}, 10^{-2}, 10^{-3}, 10^{-4}\}$. To facilitate more efficient experimentation, we employed an adaptive learning rate scheme, where at each iteration a base learning rate of 10^{-2} was divided by the square root of an exponential moving average of squared gradient norms. That is, with base learning rate $\eta = 10^{-2}$ and weighted average coefficient $\beta = 0.99$, at iteration t the learning rate was set to $\eta_t = \eta / (\sqrt{\gamma_t / (1 - \beta^t)} + 10^{-6})$, where $\gamma_t = \beta \cdot \gamma_{t-1} + (1 - \beta) \cdot \sum_{r=1}^R \sum_{n=1}^N \|\partial / \partial \mathbf{w}_r^n \ell(\{\mathbf{w}_r^n(t)\}_{r,n})\|_{Fro}^2$, with $\gamma_0 = 0$ and $\ell(\cdot)$ standing for the mean squared error over observations. We emphasize that only the learning rate (step size) is affected by this scheme, not the direction of movement. Comparisons between the scheme and a fixed (small) learning rate schedule have shown no noticeable impact on the end result, with significant difference in terms of run time.

While exact inference of tensor rank is in the worst case computationally hard (*cf.* [92]), in practice, a standard way to estimate it is by the minimal number of terms (R in Equation (1.17)) for which the Alternating Least Squares (ALS) algorithm achieves reconstruction (mean squared) error below a certain threshold (see [124] for further details). We follow this method with a threshold of 10^{-6} . Generating a ground truth rank R^* tensor $\mathcal{W}^* \in \mathbb{R}^{D_1 \times \dots \times D_N}$ was done by computing:

$$\mathcal{W}^* = \sum_{r=1}^{R^*} \mathbf{v}_r^1 \otimes \dots \otimes \mathbf{v}_r^N, \quad \mathbf{v}_r^n \in \mathbb{R}^{D_n}, \quad r = 1, \dots, R^*, \quad n = 1, \dots, N,$$

with $\{\mathbf{v}_r^n\}_{r=1}^{R^*} \sum_{n=1}^N$ drawn independently from the standard normal distribution. After every such generation, we estimated the rank of the obtained tensor (its construction only ensures a rank of *at most* R^*), and repeated the process if it was smaller than R^* . For convenience, we subsequently normalized the ground truth tensor to be of unit Frobenius norm.

A.3 Deferred Proofs

A.3.1 Notation

We define a few notational conventions that will be used throughout our proofs. For $N \in \mathbb{N}$, let $[N]$ denote the set $\{1, \dots, N\}$. Let $\{\mathbf{e}_i\}_{i=1}^D \subset \mathbb{R}^D$ be the standard basis vectors, *i.e.* \mathbf{e}_i holds 1 in its i 'th coordinate and 0 elsewhere. The singular values of a matrix $\mathbf{W} \in \mathbb{R}^{D \times D'}$ are denoted by $\sigma_1(\mathbf{W}) \geq \dots \geq \sigma_{\min\{D, D'\}}(\mathbf{W}) \geq 0$, where by convention $\sigma_i(\mathbf{W}) := 0$ for $i > \min\{D, D'\}$. Similarly, the eigenvalues of a symmetric matrix $\mathbf{W} \in \mathbb{R}^{D \times D}$ are denoted by $\lambda_1(\mathbf{W}) \geq \dots \geq \lambda_D(\mathbf{W})$. We let $\|\mathbf{W}\|_{S_p}$, with $p \in (0, \infty]$, stand for the Schatten- p (quasi-)norm of a matrix $\mathbf{W} \in \mathbb{R}^{D \times D'}$, and denote by $\|\mathbf{W}\|_{Fro}$ the special case $p = 2$, *i.e.* the Frobenius norm. The Euclidean norm of a vector $\mathbf{w} \in \mathbb{R}^D$ is denoted by $\|\mathbf{w}\|_2$. Since norms are a special case of quasi-norms, when providing results applicable to both, only the latter is explicitly treated. To

admit a compact representation of matrix products, given $1 \leq a \leq b \leq L$ and matrices $\mathbf{W}_1, \dots, \mathbf{W}_L$ for which the product $\mathbf{W}_L \cdots \mathbf{W}_1$ is defined, we denote:

$$\begin{aligned} \prod_a^{r=b} \mathbf{W}_r &:= \mathbf{W}_b \cdots \mathbf{W}_a, \\ \prod_{r=a}^b \mathbf{W}_r^\top &:= \mathbf{W}_a^\top \cdots \mathbf{W}_b^\top. \end{aligned}$$

By definition, if $a > b$, then both $\prod_a^{r=b} \mathbf{W}_r$ and $\prod_{r=a}^b \mathbf{W}_r^\top$ are identity matrices, with size to be inferred by context. The k 'th derivative of a function (from \mathbb{R} to \mathbb{R}) $f(t)$ is denoted by $f^{(k)}(t)$, with $f^{(0)}(t) := f(t)$ by convention. For consistency with differential equations literature, when the variable t is regarded as a time index, we also denote the first order derivative by $\dot{f}(t)$. Lastly, when clear from context, a time index t will often be omitted.

A.3.2 Useful Lemmas

A.3.2.1 Deep Matrix Factorization

For completeness, we include the following result from [7], which characterizes the evolution of the end matrix under gradient flow on a deep matrix factorization:

Lemma 4 (adaptation of Theorem 1 in [7]). *Let $\mathcal{L}_M : \mathbb{R}^{D \times D'} \rightarrow \mathbb{R}_{\geq 0}$ be an analytic⁴ loss, overparameterized by a depth L matrix factorization:*

$$\phi_M(\mathbf{W}_1, \dots, \mathbf{W}_L) = \mathcal{L}_M(\mathbf{W}_L \cdots \mathbf{W}_1).$$

Suppose we run gradient flow over the factorization:

$$\dot{\mathbf{W}}_l(t) := \frac{d}{dt} \mathbf{W}_l(t) = -\frac{\partial}{\partial \mathbf{W}_l} \phi_M(\mathbf{W}_1(t), \dots, \mathbf{W}_L(t)) \quad , \quad t \geq 0, \quad l = 1, \dots, L,$$

with a balanced initialization, i.e.:

$$\mathbf{W}_{l+1}(0)^\top \mathbf{W}_{l+1}(0) = \mathbf{W}_l(0) \mathbf{W}_l(0)^\top \quad , \quad l = 1, \dots, L-1.$$

Then, the end matrix $\mathbf{W}_M(t) = \mathbf{W}_L(t) \cdots \mathbf{W}_1(t)$ obeys the following dynamics:

$$\dot{\mathbf{W}}_M(t) = -\sum_{l=1}^L \left[\mathbf{W}_M(t) \mathbf{W}_M(t)^\top \right]^{\frac{l-1}{L}} \cdot \nabla \mathcal{L}_M(\mathbf{W}_M(t)) \cdot \left[\mathbf{W}_M(t)^\top \mathbf{W}_M(t) \right]^{\frac{l-1}{L}},$$

where $[\cdot]^\beta$, $\beta \in \mathbb{R}_{\geq 0}$, stands for a power operator defined over positive semidefinite matrices (with $\beta = 0$ yielding identity by definition).

Additionally, recall from [9] the following characterization for the singular values of $\mathbf{W}_M(t)$:

Lemma 5 (adaptation of Lemma 1 and Theorem 3 in [9]). *Consider the setting of Lemma 4 for depth $2 \leq L \in \mathbb{N}$. Then, there exist analytical functions $\{\sigma_r : [0, \infty) \rightarrow \mathbb{R}_{\geq 0}\}_{r=1}^{\min\{D, D'\}}$, $\{\mathbf{u}_r : [0, \infty) \rightarrow \mathbb{R}^D\}_{r=1}^{\min\{D, D'\}}$ and $\{\mathbf{v}_r : [0, \infty) \rightarrow \mathbb{R}^{D'}\}_{r=1}^{\min\{D, D'\}}$ such*

⁴An infinitely differentiable function $f : \mathcal{D} \rightarrow \mathbb{R}$ is *analytic* if at every $\mathbf{x} \in \mathcal{D}$ its Taylor series converges to it on some neighborhood of \mathbf{x} (see [126] for further details). Specifically, the matrix completion loss considered (Equation (1.1)) is analytic.

that:

$$\mathbf{u}_r(t)^\top \mathbf{u}_{r'}(t) = \mathbf{v}_r(t)^\top \mathbf{v}_{r'}(t) = \begin{cases} 1 & , r = r' \\ 0 & , r \neq r' \end{cases} \quad , t \geq 0, r, r' \in [\min\{D, D'\}] ,$$

$$\mathbf{W}_M(t) = \sum_{r=1}^{\min\{D, D'\}} \sigma_r(t) \mathbf{u}_r(t) \mathbf{v}_r(t)^\top ,$$

i.e. $\sigma_r(t) \geq 0$ are the singular values of $\mathbf{W}_M(t)$, and $\mathbf{u}_r(t), \mathbf{v}_r(t)$ are corresponding left and right (respectively) singular vectors. Furthermore, the singular values $\sigma_r(t)$ evolve by:

$$\dot{\sigma}_r(t) = -L \cdot (\sigma_r^2(t))^{1-1/L} \cdot \left\langle \nabla \mathcal{L}_M(\mathbf{W}_M(t)), \mathbf{u}_r(t) \mathbf{v}_r(t)^\top \right\rangle \quad , r = 1, \dots, \min\{D, D'\} . \quad (\text{A.3})$$

We rely on this result to establish that for square end matrices the sign of $\det(\mathbf{W}_M(t))$ does not change throughout time.

Lemma 6. Consider the setting of Lemma 4 with depth $2 \leq L \in \mathbb{N}$ and $D = D'$. Then, the determinant of $\mathbf{W}_M(t)$ has the same sign as its initial value $\det(\mathbf{W}_M(0))$. That is, $\det(\mathbf{W}_M(t))$ is identically zero if $\det(\mathbf{W}_M(0)) = 0$, is positive if $\det(\mathbf{W}_M(0)) > 0$, and is negative if $\det(\mathbf{W}_M(0)) < 0$.

Proof. We prove an analogous claim for the singular values of $\mathbf{W}_M(t)$, from which the lemma readily follows. That is, for $r \in [D]$, the singular value $\sigma_r(t)$ is identically zero if $\sigma_r(0) = 0$, and is positive if $\sigma_r(0) > 0$.

For conciseness, define $g(t) := -L \cdot \left\langle \nabla \mathcal{L}_M(\mathbf{W}_M(t)), \mathbf{u}_r(t) \mathbf{v}_r(t)^\top \right\rangle$. Invoking Lemma 5, let us solve the differential equation for $\sigma_r(t)$. If $L = 2$, the solution to Equation (A.3) is $\sigma_r(t) = \sigma_r(0) \cdot \exp\left(\int_{t'=0}^t g(t') dt'\right)$. Clearly, $\sigma_r(t)$ is either identically zero or positive according to its initial value. If $L > 2$, Equation (A.3) is solved by:

$$\sigma_r(t) = \begin{cases} \left(\sigma_r(0)^{\frac{2}{L}-1} + \left(\frac{2}{L} - 1\right) \int_{t'=0}^t g(t') dt' \right)^{\frac{1}{\frac{2}{L}-1}} & , \sigma_r(0) > 0 \\ 0 & , \sigma_r(0) = 0 \end{cases} .$$

As before, if $\sigma_r(0) = 0$, then $\sigma_r(t) = 0$ for all $t \geq 0$. If $\sigma_r(0) > 0$, divergence in finite time of $\sigma_r(t)$ is possible, however, its positivity is preserved until that occurs nonetheless.

Turning our attention to the determinant of $\mathbf{W}_M(t)$, suppose $\det(\mathbf{W}_M(0)) = 0$. Then, $\mathbf{W}_M(0)$ has a singular value which is 0, and for all t that singular value and the determinant remain 0. If $\det(\mathbf{W}_M(0)) \neq 0$, the end matrix remains full rank for all t . The proof then immediately follows from the continuity of $\det(\mathbf{W}_M(t))$. \square

We will also make use of the following lemmas:

Lemma 7 (adapted from [9]). Under the setting of Lemma 4, $\mathbf{W}_1(t), \dots, \mathbf{W}_L(t), \mathbf{W}_M(t)$ and $\nabla \mathcal{L}_M(\mathbf{W}_M(t))$ are analytic functions of t .

Proof. Analytic functions are closed under summation, multiplication, and composition. The analyticity of $\mathcal{L}_M(\cdot)$ therefore implies that $\phi_M(\cdot)$ (Equation (1.2)) is analytic as well. From Theorem 1.1 in [104], it then follows that under gradient flow (Equation (1.4)) $\mathbf{W}_1(t), \dots, \mathbf{W}_L(t)$ are analytic functions of t . Lastly, the aforementioned closure properties imply that $\mathbf{W}_M(t)$ and $\nabla \mathcal{L}_M(\mathbf{W}_M(t))$ are also analytic in t . \square

A.3.2.2 Technical

Included below are a few technical lemmas used in our analyses.

Lemma 8. Let $h : [0, 1] \rightarrow \mathbb{R}$ be the binary entropy function $h(p) := -p \cdot \ln(p) - (1-p) \ln(1-p)$, where by convention $0 \cdot \ln(0) = 0$. Then, for all $p \in [0, 1]$:

$$h(p) \leq 2\sqrt{p}.$$

Proof. We present a tighter inequality, $h(p) \leq 2\sqrt{p(1-p)}$, from which the proof immediately follows since $2\sqrt{p(1-p)} \leq 2\sqrt{p}$ for $p \in [0, 1]$.

Define the function $f(p) := \frac{h(p)^2}{p(1-p)}$ over the open interval $(0, 1)$. Differentiating it with respect to p we have:

$$\frac{d}{dp}f(p) = \frac{(-p \cdot \ln(p))^2 - (-(1-p) \cdot \ln(1-p))^2}{p^2(1-p)^2}.$$

Introducing $g(p) := -p \cdot \ln(p)$, we show that $g(p)^2 > g(1-p)^2$ for all $p \in (0, \frac{1}{2})$. It is easily verified that $g(p) - g(1-p)$ is concave on the interval $(0, \frac{1}{2})$ (second derivative is negative). Since for $p = 0$ and $p = 1/2$ we have exactly $g(p) - g(1-p) = 0$, it holds that $g(p) - g(1-p) \geq 0$ and $g(p)^2 \geq g(1-p)^2$ for all $p \in (0, \frac{1}{2})$. Noticing $\frac{d}{dp}f(p) = (g(p)^2 - g(1-p)^2) / p^2(1-p)^2$, it follows that $f(\cdot)$ is monotonically non-decreasing on $(0, \frac{1}{2})$. Due to the fact that $f(p) = f(1-p)$, it is non-increasing on $(\frac{1}{2}, 1)$, and attains its maximal value over $(0, 1)$ at $p = \frac{1}{2}$. Putting it all together, for $p \in (0, 1)$ we have:

$$h(p) \leq \sqrt{p(1-p)} \cdot \sqrt{f(1/2)} = 2\ln(2) \cdot \sqrt{p(1-p)} \leq 2\sqrt{p(1-p)},$$

and for $p = 0, 1$ there is exact equality, completing the proof. \square

Lemma 9. Let $f, g : [0, \infty) \rightarrow \mathbb{R}$ be real analytic functions (see Footnote 4) such that $f^{(k)}(0) = g^{(k)}(0)$ for all $k \in \mathbb{N} \cup \{0\}$. Then, $f(t) = g(t)$ for all $t \geq 0$.

Proof. Define the function $h(t) := f(t) - g(t)$. Since analytic functions are closed under subtraction, $h(\cdot)$ is analytic as well. An analytic function with all zero derivatives at a point is constant on the corresponding connected component. Noticing that $h^{(k)}(0) = 0$ for all $k \in \mathbb{N} \cup \{0\}$, we may conclude that $h(t) = 0$ and $f(t) = g(t)$ for all $t \geq 0$. \square

Lemma 10. Let $\mathbf{A}, \mathbf{B} \in \mathbb{R}^{D \times D}$, and suppose \mathbf{B} is positive semidefinite. Then,

$$\text{Tr}(\mathbf{A}^\top \mathbf{B} \mathbf{A}) \geq \lambda_1(\mathbf{B}) \cdot \sigma_D(\mathbf{A})^2.$$

Proof. The matrix $\mathbf{A}^\top \mathbf{B} \mathbf{A}$ is positive semidefinite since for all $\mathbf{y} \in \mathbb{R}^D$ we have:

$$\mathbf{y}^\top \mathbf{A}^\top \mathbf{B} \mathbf{A} \mathbf{y} = (\mathbf{A} \mathbf{y})^\top \mathbf{B} (\mathbf{A} \mathbf{y}) \geq 0.$$

Therefore, $\text{Tr}(\mathbf{A}^\top \mathbf{B} \mathbf{A}) \geq \lambda_1(\mathbf{A}^\top \mathbf{B} \mathbf{A})$. Let $\mathbf{B} = \mathbf{O} \mathbf{D} \mathbf{O}^\top$ be an orthogonal eigenvalue decomposition of \mathbf{B} , i.e. $\mathbf{O} \in \mathbb{R}^{D \times D}$ is an orthogonal matrix with columns $\{\mathbf{o}_i\}_{i=1}^D$ and $\mathbf{D} \in \mathbb{R}^{D \times D}$ is diagonal holding the non-negative eigenvalues of \mathbf{B} . Additionally, let $\mathbf{A} = \mathbf{U} \mathbf{\Sigma} \mathbf{V}^\top$ be a singular value decomposition of \mathbf{A} , where $\mathbf{U}, \mathbf{V} \in \mathbb{R}^{D \times D}$ are

orthogonal matrices, and $\Sigma \in \mathbb{R}_{\geq 0}^{D \times D}$ is diagonal holding the singular values of \mathbf{A} . For any unit vector (with respect to the Euclidean norm) $\mathbf{y} \in \mathbb{R}^D$ it holds that:

$$\mathbf{y}^\top \mathbf{A}^\top \mathbf{B} \mathbf{A} \mathbf{y} = \sum_{i=1}^D \lambda_i(\mathbf{B}) (\mathbf{o}_i^\top \mathbf{A} \mathbf{y})^2 \geq \lambda_1(\mathbf{B}) (\mathbf{o}_1^\top \mathbf{A} \mathbf{y})^2.$$

Replacing \mathbf{A} with its singular value decomposition and choosing $\mathbf{y} = \mathbf{V} \mathbf{U}^\top \mathbf{o}_1$:

$$\lambda_1(\mathbf{B}) (\mathbf{o}_1^\top \mathbf{A} \mathbf{y})^2 = \lambda_1(\mathbf{B}) (\mathbf{o}_1^\top \mathbf{U} \Sigma \mathbf{U}^\top \mathbf{o}_1)^2.$$

Recalling that for any unit vector the quadratic form of a symmetric matrix is bounded by the maximal and minimal eigenvalues completes the proof:

$$\text{Tr}(\mathbf{A}^\top \mathbf{B} \mathbf{A}) \geq \lambda_1(\mathbf{A}^\top \mathbf{B} \mathbf{A}) \geq \lambda_1(\mathbf{B}) (\mathbf{o}_1^\top \mathbf{U} \Sigma \mathbf{U}^\top \mathbf{o}_1)^2 \geq \lambda_1(\mathbf{B}) \cdot \sigma_d(\mathbf{A})^2.$$

□

Lemma 11. *Let $g : [0, \infty) \rightarrow \mathbb{R}$ be a continuously differentiable function, and fix some $t > 0$. If $g(t) < g(0)$, then for any $a \in (g(t), g(0))$ there exists $t_a \in [0, t)$ such that $g(t_a) = a$ and $\dot{g}(t_a) \leq 0$. Similarly, if $g(t) > g(0)$, then for any $a \in [g(0), g(t))$ there exists $t_a \in [0, t)$ such that $g(t_a) = a$ and $\dot{g}(t_a) \geq 0$.*

Proof. Let $t > 0$ be such that $g(t) < g(0)$, and fix some $a \in (g(t), g(0))$. Define $t_a := \max\{t' : t' \leq t \text{ and } g(t') = a\}$. Continuity of $g(\cdot)$, along with the intermediate value theorem, imply that t_a is well defined (maximum of a closed non-empty set bounded from above). Assume by contradiction that $\dot{g}(t_a) > 0$. Then, $g(\cdot)$ is monotonically increasing on some neighborhood of t_a . Thus, by the intermediate value theorem, there exists $t' \in (t_a, t)$ such that $g(t') = a$, in contradiction to the definition of t_a . An identical argument establishes the analogous result for the case $g(t) > g(0)$. □

Lemma 12. *Let $g : [0, \infty) \rightarrow \mathbb{R}$ be a non-negative differentiable function. Assume there exist constants $a, b > 0$ such that $\int_{t'=0}^t g(t') dt' \leq a$ and $\dot{g}(t) \leq b$ for all $t \geq 0$. Then, $\lim_{t \rightarrow \infty} g(t) = 0$.*

Proof. By way of contradiction let us assume that $g(t)$ does not converge to 0. Let $\epsilon > 0$ be such that for all $M > 0$ there exists $t > M$ with $g(t) > \epsilon$.

We claim that for all $M, \epsilon' > 0$ there exists $t > M$ such that $g(t) < \epsilon'$. Otherwise, we have a contradiction to the bound on the integral of $g(\cdot)$. Combined with our assumption, this means that for all $M > 0$ we can find an interval $[t_1, t_2]$, with $t_1 > M$, where $g(t)$ transitions from $\frac{\epsilon}{2}$ to ϵ . We now examine one such interval. Formally, for t_0 with $g(t_0) < \frac{\epsilon}{2}$, we define:

$$t_2 := \min \{t | t \geq t_0 \text{ and } g(t) = \epsilon\} \quad , \quad t_1 := \max \{t | t \leq t_2 \text{ and } g(t) = \epsilon/2\}.$$

Due to the fact that $g(\cdot)$ is continuous, t_2 and t_1 are well defined as they are the minimum and maximum, respectively, of closed non-empty sets bounded from below and above, respectively. Furthermore, notice that $t_0 < t_1 < t_2$. From the mean value theorem and the bound on the derivative of $g(\cdot)$ we have $t_2 - t_1 \geq \epsilon/2b$. Since $g(t) \geq \epsilon/2$ over the interval $[t_1, t_2]$, this gives us $\int_{t'=t_1}^{t_2} g(t') dt' \geq \epsilon^2/4b$. Recall there are infinitely many such occurrences, implying that $\int_{t'=0}^{\infty} g(t') dt' = \infty$, in contradiction to the bound on the integral. □

A.3.3 Proof of Proposition 1

For a quasi-norm $\|\cdot\|$, the weakened triangle inequality (see Footnote 2) implies that there exists a constant $c_{\|\cdot\|} \geq 1$ for which

$$\begin{aligned} \|W\| &\geq \frac{1}{c_{\|\cdot\|}} \|(\mathbf{W})_{1,1} \mathbf{e}_1 \mathbf{e}_1^\top\| - \|W - (\mathbf{W})_{1,1} \mathbf{e}_1 \mathbf{e}_1^\top\| \\ &= |(\mathbf{W})_{1,1}| \frac{\|\mathbf{e}_1 \mathbf{e}_1^\top\|}{c_{\|\cdot\|}} - \|\mathbf{e}_2 \mathbf{e}_1^\top + \mathbf{e}_1 \mathbf{e}_3^\top\|, \end{aligned} \quad (\text{A.4})$$

for any $\mathbf{W} \in \mathcal{S}$. Fix some $\epsilon > 0$ and define $M_{\|\cdot\|, \epsilon} := \{(\mathbf{W})_{1,1} \in \mathbb{R} : \|\mathbf{W}\| \leq \inf_{\mathbf{W}' \in \mathcal{S}} \|\mathbf{W}'\| + \epsilon, \mathbf{W} \in \mathcal{S}\}$, the set of $(\mathbf{W})_{1,1}$ values corresponding to ϵ -minimizers of $\|\cdot\|$. The first part of the proposition thus boils down to showing $M_{\|\cdot\|, \epsilon}$ is bounded. By Equation (A.4), there exist a $C > 0$ such that $|(\mathbf{W})_{1,1}| > C$ means $\|\mathbf{W}\| > \inf_{\mathbf{W}' \in \mathcal{S}} \|\mathbf{W}'\| + \epsilon$. Hence, $M_{\|\cdot\|, \epsilon} \subset I_{\|\cdot\|, \epsilon} := [-C, C]$.

If in addition $\|\cdot\|$ is a Schatten- p quasi-norm for $p \in (0, \infty]$, we now show that W is its minimizer over \mathcal{S} if and only if $(\mathbf{W})_{1,1} = 0$. Let $\mathbf{W}_x \in \mathcal{S}$ denote the solution matrix with $(\mathbf{W}_x)_{1,1} = x$ for $x \in \mathbb{R}$. The singular values of an arbitrary such \mathbf{W}_x are:

$$\{\sigma_1(\mathbf{W}_x), \sigma_2(\mathbf{W}_x)\} = \left\{ \left| (x + \sqrt{x^2 + 4}) / 2 \right|, \left| (x - \sqrt{x^2 + 4}) / 2 \right| \right\}. \quad (\text{A.5})$$

Starting with $p = \infty$, the corresponding norm is the spectral norm $\|\mathbf{W}_x\|_{S_\infty} := \sigma_1(\mathbf{W}_x)$. When $x = 0$, we have that $\sigma_1(\mathbf{W}_0) = 1$. If $x > 0$, then $\sigma_1(\mathbf{W}_x) = (x + \sqrt{x^2 + 4}) / 2 > 1$. Similarly, if $x < 0$, then $\sigma_1(\mathbf{W}_x) = (-x + \sqrt{x^2 + 4}) / 2 > 1$. Therefore, $\|\mathbf{W}_x\|_{S_\infty}$ attains its minimal value of 1 if and only if $x = 0$.

Moving to the case of $p \in (0, \infty)$, the corresponding quasi-norm is $\|\mathbf{W}_x\|_{S_p} := (\sigma_1(\mathbf{W}_x)^p + \sigma_2(\mathbf{W}_x)^p)^{\frac{1}{p}}$. We now examine $\|\mathbf{W}_x\|_{S_p}^p$ for $x > 0$:

$$\|\mathbf{W}_x\|_{S_p}^p = \left(\frac{x + \sqrt{x^2 + 4}}{2} \right)^p + \left(\frac{-x + \sqrt{x^2 + 4}}{2} \right)^p.$$

Differentiating with respect to x , we arrive at:

$$\begin{aligned} &\frac{p}{2^p} \left(\left(x + \sqrt{x^2 + 4} \right)^{p-1} \left(1 + \frac{x}{\sqrt{x^2 + 4}} \right) + \left(-x + \sqrt{x^2 + 4} \right)^{p-1} \left(-1 + \frac{x}{\sqrt{x^2 + 4}} \right) \right) \\ &> \frac{p}{2^p} \left(\left(x + \sqrt{x^2 + 4} \right)^{p-1} - \left(-x + \sqrt{x^2 + 4} \right)^{p-1} \right) \\ &> 0, \end{aligned}$$

where in the first transition we used the fact that both $(x + \sqrt{x^2 + 4})^{p-1} > 0$ and $(-x + \sqrt{x^2 + 4})^{p-1} > 0$ (as well as $x > 0$). It then directly follows that $\|\mathbf{W}_x\|_{S_p}^p$ and thus $\|\mathbf{W}_x\|_{S_p}$ are monotonically increasing with respect to x on $(0, \infty)$.

Similar arguments show that when $x < 0$ the Schatten- p quasi-norm of \mathbf{W}_x is monotonically decreasing with respect to x , implying that $\|\mathbf{W}_x\|_{S_p}$ is minimized if and only if $x = 0$.⁵ \square

⁵The claim relies on the fact that the Schatten- p quasi-norm of \mathbf{W}_x is continuous with respect to x for all $p \in (0, \infty)$. We note, however, that quasi-norms in general may be discontinuous.

A.3.4 Proof of Proposition 2

As in the proof of Proposition 1 (Appendix A.3.3), we denote by $\mathbf{W}_x \in \mathcal{S}$ the solution matrix with $(\mathbf{W}_x)_{1,1} = x$. We begin by analyzing the behavior of $\sigma_1(\mathbf{W}_x)$ and $\sigma_2(\mathbf{W}_x)$ with respect to x . When $x = 0$ the singular values are simply $\sigma_1(\mathbf{W}_0) = \sigma_2(\mathbf{W}_0) = 1$. When x is positive, the singular values may be written as:

$$\sigma_1(\mathbf{W}_x) = \frac{x + \sqrt{x^2 + 4}}{2}, \quad \sigma_2(\mathbf{W}_x) = \frac{-x + \sqrt{x^2 + 4}}{2}.$$

Taking the derivative with respect to x , we arrive at:

$$\frac{d}{dx}\sigma_1(\mathbf{W}_x) = \frac{1}{2} + \frac{x}{2\sqrt{x^2 + 4}}, \quad \frac{d}{dx}\sigma_2(\mathbf{W}_x) = -\frac{1}{2} + \frac{x}{2\sqrt{x^2 + 4}}.$$

Since $x > 0$, we have that $d/dx \sigma_1(\mathbf{W}_x) > 0$ and $d/dx \sigma_2(\mathbf{W}_x) < 0$. In other words, $\sigma_1(\mathbf{W}_x)$ is monotonically increasing, while $\sigma_2(\mathbf{W}_x)$ is monotonically decreasing, when $x > 0$. It can easily be verified that $\sigma_1(\mathbf{W}_x)$ and $\sigma_2(\mathbf{W}_x)$ are even functions of x , i.e. $\sigma_1(\mathbf{W}_x) = \sigma_1(\mathbf{W}_{-x})$ and $\sigma_2(\mathbf{W}_x) = \sigma_2(\mathbf{W}_{-x})$. It then follows that $\sigma_1(\mathbf{W}_x)$ is monotonically decreasing (conversely $\sigma_2(\mathbf{W}_x)$ is monotonically increasing) when $x < 0$. Noticing that $\lim_{x \rightarrow \infty} \sigma_1(\mathbf{W}_x) = \infty$ and $\lim_{x \rightarrow \infty} \sigma_2(\mathbf{W}_x) = 0$ (accordingly $\lim_{x \rightarrow -\infty} \sigma_1(\mathbf{W}_x) = \infty$ and $\lim_{x \rightarrow -\infty} \sigma_2(\mathbf{W}_x) = 0$), we have a characterization of the behavior of $\sigma_1(\mathbf{W}_x)$ and $\sigma_2(\mathbf{W}_x)$.

We are now in a position to obtain the desired results for effective and infimal ranks. The effective rank (Definition 1) of \mathbf{W}_x can be written as

$$\text{erank}(\mathbf{W}_x) = \exp \left(H \left(\frac{\sigma_1(\mathbf{W}_x)}{\sigma_1(\mathbf{W}_x) + \sigma_2(\mathbf{W}_x)}, \frac{\sigma_2(\mathbf{W}_x)}{\sigma_1(\mathbf{W}_x) + \sigma_2(\mathbf{W}_x)} \right) \right).$$

The binary entropy function is bounded by $\ln(2)$, hence, the effective rank over \mathcal{S} is bounded by 2. This upper bound is attained at $x = 0$. According to the singular values analysis, when $|x| \rightarrow \infty$ we have that $\rho_1(\mathbf{W}_x)$ monotonically increases towards 1, starting from the value $\rho_1(\mathbf{W}_0) = \frac{1}{2}$. Noticing that this implies the entropy function and effective rank monotonically decrease towards 0 and 1, respectively, completes the effective rank analysis.

Next, we analyze the infimal rank of \mathcal{S} and the distance of \mathbf{W}_x from that infimal rank. The distance of \mathbf{W}_x from \mathcal{M}_1 is $\mathcal{D}_{\text{Fro}}(\mathbf{W}_x, \mathcal{M}_1) = \sigma_2(\mathbf{W}_x)$. Since $\lim_{x \rightarrow \infty} \sigma_2(\mathbf{W}_x) = 0$, we have $\mathcal{D}_{\text{Fro}}(\mathcal{S}, \mathcal{M}_1) = 0$. Clearly $\mathcal{D}_{\text{Fro}}(\mathcal{S}, \mathcal{M}_0) > 0$, leading to the conclusion that the infimal rank of \mathcal{S} is 1. Finally, the analysis of $\sigma_2(\mathbf{W}_x)$ directly implies that the distance of \mathbf{W}_x from the infimal rank of \mathcal{S} is maximized when $x = 0$, monotonically tending to 0 as $|x| \rightarrow \infty$. \square

A.3.5 Proof of Theorem 1

In the following, as stated in Appendix A.3.1, for results that hold for all $t \geq 0$ or when clear from the context, we omit the time index t . Furthermore, we denote the entries of the end matrix \mathbf{W}_M by $\{w_{i,j}\}_{i,j \in [2]}$.

We begin by deriving loss-dependent bounds for $|w_{1,1}|$, $\sigma_1(\mathbf{W}_M)$, and $\sigma_2(\mathbf{W}_M)$. Writing the loss explicitly:

$$\mathcal{L}_M(\mathbf{W}_M) = \frac{1}{2} [(w_{1,2} - 1)^2 + (w_{2,1} - 1)^2 + w_{2,2}^2],$$

we can upper bound each of the non-negative terms separately. Multiplying by 2 and taking the square root of both sides yields:

$$|w_{2,2}| \leq \sqrt{2\mathcal{L}_M(\mathbf{W}_M)} \quad , \quad |w_{1,2} - 1| \leq \sqrt{2\mathcal{L}_M(\mathbf{W}_M)} \quad , \quad |w_{2,1} - 1| \leq \sqrt{2\mathcal{L}_M(\mathbf{W}_M)}. \quad (\text{A.6})$$

The following lemma characterizes the relation between $|w_{1,1}|$ and the loss.

Lemma 13. *Suppose $\mathcal{L}_M(\mathbf{W}_M) < \frac{1}{2}$. Then:*

$$|w_{1,1}| > \frac{(1 - \sqrt{2\mathcal{L}_M(\mathbf{W}_M)})^2}{\sqrt{2\mathcal{L}_M(\mathbf{W}_M)}} = \frac{1}{\sqrt{2\mathcal{L}_M(\mathbf{W}_M)}} - 2 + \sqrt{2\mathcal{L}_M(\mathbf{W}_M)}.$$

Proof. From Lemma 6, the determinant of \mathbf{W}_M does not change signs and remains positive, i.e.:

$$\det(\mathbf{W}_M) = w_{1,1}w_{2,2} - w_{1,2}w_{2,1} > 0. \quad (\text{A.7})$$

Under the assumption that $\mathcal{L}_M(\mathbf{W}_M) < \frac{1}{2}$, both $w_{1,2}$ and $w_{2,1}$ are positive and lie inside the open interval $(0, 2)$. Since the determinant is positive, $w_{2,2} \neq 0$ and $w_{1,1}w_{2,2} > 0$ must hold. Rearranging Equation (A.7), we may therefore write $|w_{1,1}w_{2,2}| > w_{1,2}w_{2,1}$. Dividing both sides by $|w_{2,2}|$ and applying the bounds from Equation (A.6) completes the proof:

$$|w_{1,1}| > \frac{(1 - \sqrt{2\mathcal{L}_M(\mathbf{W}_M)})^2}{\sqrt{2\mathcal{L}_M(\mathbf{W}_M)}} = \frac{1}{\sqrt{2\mathcal{L}_M(\mathbf{W}_M)}} - 2 + \sqrt{2\mathcal{L}_M(\mathbf{W}_M)}. \quad \square$$

An immediate consequence of the lemma above is that decreasing the loss towards zero drives $|w_{1,1}|$ towards infinity.

With this bound in hand, Lemma 14 below establishes bounds on the singular values of \mathbf{W}_M . In turn, they will allow us to obtain the necessary results for effective rank (Definition 1) and distance from infimal rank of \mathcal{S} (Definition 2).

Lemma 14. *The singular values of \mathbf{W}_M fulfill:*

$$\sigma_1(\mathbf{W}_M) \geq |w_{1,1}| - \sqrt{2\mathcal{L}_M(\mathbf{W}_M)} \quad , \quad \sigma_2(\mathbf{W}_M) \leq 3\sqrt{2\mathcal{L}_M(\mathbf{W}_M)}. \quad (\text{A.8})$$

Furthermore, if $\mathcal{L}_M(\mathbf{W}_M) < \frac{1}{2}$, then:

$$\sigma_1(\mathbf{W}_M) \geq \frac{1}{\sqrt{2\mathcal{L}_M(\mathbf{W}_M)}} - 2. \quad (\text{A.9})$$

Proof. Define $\mathbf{W}_\mathcal{S} := \begin{pmatrix} w_{1,1} & 1 \\ 1 & 0 \end{pmatrix}$, the orthogonal projection of \mathbf{W}_M onto the solution set \mathcal{S} . By Corollary 8.6.2 in [76] we have that:

$$|\sigma_i(\mathbf{W}_M) - \sigma_i(\mathbf{W}_\mathcal{S})| \leq \|\mathbf{W}_M - \mathbf{W}_\mathcal{S}\|_{Fro} = \sqrt{2\mathcal{L}_M(\mathbf{W}_M)} \quad , \quad i = 1, 2. \quad (\text{A.10})$$

One can easily verify that \mathbf{W}_S is a symmetric indefinite matrix with eigenvalues

$$\{\lambda_1(\mathbf{W}_S), \lambda_2(\mathbf{W}_S)\} = \left\{ \left(w_{1,1} + \sqrt{w_{1,1}^2 + 4} \right) / 2, \left(w_{1,1} - \sqrt{w_{1,1}^2 + 4} \right) / 2 \right\}.$$

Suppose that $w_{1,1} \geq 0$. We thus have:

$$\sigma_1(\mathbf{W}_S) = \max_{i=1,2} |\lambda_i(\mathbf{W}_S)| = \frac{w_{1,1} + \sqrt{w_{1,1}^2 + 4}}{2} \geq |w_{1,1}|,$$

and

$$\begin{aligned} \sigma_2(\mathbf{W}_S) &= \min_{i=1,2} |\lambda_i(\mathbf{W}_S)| \\ &= \frac{\sqrt{w_{1,1}^2 + 4} - w_{1,1}}{2} \\ &= \frac{2}{\sqrt{w_{1,1}^2 + 4} + w_{1,1}} \\ &\leq \frac{2}{2 + w_{1,1}}, \end{aligned}$$

where in the third transition we made use of the identity $a - b = \frac{a^2 - b^2}{a + b}$ for $a, b \in \mathbb{R}$ such that $a + b \neq 0$. If $\mathcal{L}_M(\mathbf{W}_M) \geq \frac{1}{2}$, it holds that $\sigma_2(\mathbf{W}_S) \leq 2/(2 + w_{1,1}) \leq 1 \leq 2\sqrt{2\mathcal{L}_M(\mathbf{W}_M)}$. Otherwise, we may apply the lower bound on $w_{1,1}$ (Lemma 13) and conclude that $\sigma_2(\mathbf{W}_S) \leq 2\sqrt{2\mathcal{L}_M(\mathbf{W}_M)}$ for any loss value. Having established that $\sigma_1(\mathbf{W}_S) \geq |w_{1,1}|$ and $\sigma_2(\mathbf{W}_S) \leq 2\sqrt{2\mathcal{L}_M(\mathbf{W}_M)}$, Equation (A.10) completes the proof of Equation (A.8). It remains to see that if $\mathcal{L}_M(\mathbf{W}_M) < \frac{1}{2}$, from the lower bound on $w_{1,1}$ (Lemma 13), Equation (A.9) immediately follows.

By similar arguments, Equations (A.8) and (A.9) hold for $w_{1,1} < 0$ as well. \square

A.3.5.1 Proof of Equation (1.8) (Lower Bound for Quasi-Norm)

We turn to lower bound the quasi-norm of the end matrix. It holds that:

$$\|\mathbf{W}_M\| \geq \frac{1}{c_{\|\cdot\|}} \|w_{1,1} \mathbf{e}_1 \mathbf{e}_1^\top\| - \|\mathbf{W}_M - w_{1,1} \mathbf{e}_1 \mathbf{e}_1^\top\|, \quad (\text{A.11})$$

where $c_{\|\cdot\|} \geq 1$ is a constant for which $\|\cdot\|$ satisfies the weakened triangle inequality (see Footnote 2). We now assume that $\mathcal{L}_M(\mathbf{W}_M) < \frac{1}{2}$. Later this assumption will be lifted, providing a bound that holds for all loss values. Subsequent applications of the weakened triangle inequality, together with homogeneity of $\|\cdot\|$ and the bounds

on the entries of \mathbf{W}_M (Equation (A.6)), give:

$$\begin{aligned}
\|\mathbf{W}_M - w_{1,1}\mathbf{e}_1\mathbf{e}_1^\top\| &\leq c_{\|\cdot\|}|w_{2,2}|\|\mathbf{e}_2\mathbf{e}_2^\top\| + c_{\|\cdot\|}^2 \left(|w_{2,1}|\|\mathbf{e}_2\mathbf{e}_1^\top\| + |w_{1,2}|\|\mathbf{e}_1\mathbf{e}_2^\top\| \right) \\
&\leq c_{\|\cdot\|}\sqrt{2\mathcal{L}_M(\mathbf{W}_M)}\|\mathbf{e}_2\mathbf{e}_2^\top\| \\
&\quad + c_{\|\cdot\|}^2 \left(1 + \sqrt{2\mathcal{L}_M(\mathbf{W}_M)} \right) \left(\|\mathbf{e}_2\mathbf{e}_1^\top\| + \|\mathbf{e}_1\mathbf{e}_2^\top\| \right) \\
&\leq c_{\|\cdot\|}\|\mathbf{e}_2\mathbf{e}_2^\top\| + 2c_{\|\cdot\|}^2 \left(\|\mathbf{e}_2\mathbf{e}_1^\top\| + \|\mathbf{e}_1\mathbf{e}_2^\top\| \right) \\
&\leq 2c_{\|\cdot\|}^2 \left(\|\mathbf{e}_2\mathbf{e}_2^\top\| + \|\mathbf{e}_2\mathbf{e}_1^\top\| + \|\mathbf{e}_1\mathbf{e}_2^\top\| \right).
\end{aligned}$$

Plugging the inequality above and the lower bound on $|w_{1,1}|$ (Lemma 13) into Equation (A.11), we have:

$$\begin{aligned}
\|\mathbf{W}_M\| &\geq \frac{\|\mathbf{e}_1\mathbf{e}_1^\top\|}{c_{\|\cdot\|}} \frac{1}{\sqrt{2\mathcal{L}_M(\mathbf{W}_M)}} - 2 \frac{\|\mathbf{e}_1\mathbf{e}_1^\top\|}{c_{\|\cdot\|}} - 2c_{\|\cdot\|}^2 \left(\|\mathbf{e}_2\mathbf{e}_2^\top\| + \|\mathbf{e}_2\mathbf{e}_1^\top\| + \|\mathbf{e}_1\mathbf{e}_2^\top\| \right) \\
&\geq \frac{\|\mathbf{e}_1\mathbf{e}_1^\top\|}{c_{\|\cdot\|}} \frac{1}{\sqrt{2\mathcal{L}_M(\mathbf{W}_M)}} - 2c_{\|\cdot\|}^2 \left(\|\mathbf{e}_1\mathbf{e}_1^\top\| + \|\mathbf{e}_2\mathbf{e}_2^\top\| + \|\mathbf{e}_2\mathbf{e}_1^\top\| + \|\mathbf{e}_1\mathbf{e}_2^\top\| \right).
\end{aligned}$$

Since $\|\mathbf{W}_M\|$ is trivially lower bounded by zero, defining the constants

$$a_{\|\cdot\|} := \frac{\|\mathbf{e}_1\mathbf{e}_1^\top\|}{\sqrt{2}c_{\|\cdot\|}}, \quad b_{\|\cdot\|} := \max \left\{ \sqrt{2}a_{\|\cdot\|}, 8c_{\|\cdot\|}^2 \max_{i,j \in \{1,2\}} \|\mathbf{e}_i\mathbf{e}_j^\top\| \right\},$$

allows us, on the one hand, to arrive at a bound of the form:

$$\|\mathbf{W}_M\| \geq a_{\|\cdot\|} \cdot \frac{1}{\sqrt{\mathcal{L}_M(\mathbf{W}_M)}} - b_{\|\cdot\|},$$

and on the other hand, to lift our previous assumption on the loss: when $\mathcal{L}_M(\mathbf{W}_M) \geq \frac{1}{2}$ the bound is vacuous, *i.e.* non-positive and trivially holds. Noticing this is exactly Equation (1.8) (recall we omitted the time index t), concludes the first part of the proof.

A.3.5.2 Proof of Equation (1.9) (Upper Bound for Effective Rank)

During the following effective rank (Definition 1) analysis we operate under the assumption of $\mathcal{L}_M(\mathbf{W}_M) < \frac{1}{32}$. We later remove this assumption, delivering a bound that holds for all loss values. Making use of the obtained bounds on $\sigma_1(\mathbf{W}_M)$ and

$\sigma_2(\mathbf{W}_M)$ (Lemma 14) we arrive at:

$$\begin{aligned}
\rho_1(\mathbf{W}_M) &= \frac{\sigma_1(\mathbf{W}_M)}{\sigma_1(\mathbf{W}_M) + \sigma_2(\mathbf{W}_M)} \\
&\geq \frac{\sigma_1(\mathbf{W}_M)}{\sigma_1(\mathbf{W}_M) + 3\sqrt{2\mathcal{L}_M(\mathbf{W}_M)}} \\
&= 1 - \frac{3\sqrt{2\mathcal{L}_M(\mathbf{W}_M)}}{\sigma_1(\mathbf{W}_M) + 3\sqrt{2\mathcal{L}_M(\mathbf{W}_M)}} \\
&\geq 1 - \frac{3\sqrt{2\mathcal{L}_M(\mathbf{W}_M)}}{\frac{1}{\sqrt{2\mathcal{L}_M(\mathbf{W}_M)}} - 2 + 3\sqrt{2\mathcal{L}_M(\mathbf{W}_M)}} \\
&= 1 - \frac{6\mathcal{L}_M(\mathbf{W}_M)}{6\mathcal{L}_M(\mathbf{W}_M) - 2\sqrt{2\mathcal{L}_M(\mathbf{W}_M)} + 1}.
\end{aligned}$$

Given our assumption on the loss, we have $1 - 2\sqrt{2\mathcal{L}_M(\mathbf{W}_M)} \geq \frac{1}{2}$ and thus

$$\rho_2(\mathbf{W}_M) = 1 - \rho_1(\mathbf{W}_M) \leq \frac{6\mathcal{L}_M(\mathbf{W}_M)}{6\mathcal{L}_M(\mathbf{W}_M) + \frac{1}{2}} \leq 12\mathcal{L}_M(\mathbf{W}_M). \quad (\text{A.12})$$

Let $h(\rho_2(\mathbf{W}_M)) := -\rho_2(\mathbf{W}_M) \cdot \ln(\rho_2(\mathbf{W}_M)) - (1 - \rho_2(\mathbf{W}_M)) \cdot \ln(1 - \rho_2(\mathbf{W}_M))$ denote the binary entropy function, and recall that the effective rank of \mathbf{W}_M is defined to be $\text{erank}(\mathbf{W}_M) := \exp\{h(\rho_2(\mathbf{W}_M))\}$. The exponent function is convex and therefore upper bounded on the interval $[0, \ln(2)]$ by the linear function that intersects it at these points. Formally, for $x \in [0, \ln(2)]$ it holds that $\exp(x) \leq 1 + \frac{1}{\ln(2)}x$, yielding the following bound:

$$\text{erank}(\mathbf{W}_M) \leq 1 + \frac{1}{\ln(2)} \cdot h(\rho_2(\mathbf{W}_M)).$$

By Lemma 8 we have that $h(\rho_2(\mathbf{W}_M)) \leq 2\sqrt{\rho_2(\mathbf{W}_M)}$. Combined with Equation (A.12), since $\inf_{\mathbf{W}' \in \mathcal{S}} \text{erank}(\mathbf{W}') = 1$ (Proposition 2), this leads to:

$$\text{erank}(\mathbf{W}_M) \leq \inf_{\mathbf{W}' \in \mathcal{S}} \text{erank}(\mathbf{W}') + \frac{2\sqrt{12}}{\ln(2)} \cdot \sqrt{\mathcal{L}_M(\mathbf{W}_M)}.$$

Recall that the time index t is omitted, and the result holds for all $t \geq 0$, *i.e.* this is exactly Equation (1.9). To remove our assumption on the loss, notice that when $\mathcal{L}_M(\mathbf{W}_M) \geq \frac{1}{32}$ the bound is trivial, as the right-hand side is greater than 2, which is the maximal effective rank (for a 2-by-2 matrix).

A.3.5.3 Proof of Equation (1.10) (Upper Bound for Distance from Infimal Rank)

According to Proposition 2, the infimal rank of \mathcal{S} is 1. The quantity we seek to upper bound is therefore $\mathcal{D}_{\text{Fro}}(\mathbf{W}_M(t), \mathcal{M}_1) = \sigma_2(\mathbf{W}_M(t))$. By Equation (A.8) in Lemma 14, for all $t \geq 0$ we have

$$\mathcal{D}_{\text{Fro}}(\mathbf{W}_M(t), \mathcal{M}_1) \leq 3\sqrt{2} \cdot \sqrt{\mathcal{L}_M(t)},$$

completing the proof. \square

A.3.6 Proof of Proposition 3

Define \mathbf{W}_{-1} to be the matrix obtained from \mathbf{W} by multiplying its first row by -1 . On the one hand, symmetry around the origin implies that \mathbf{W}_{-1} and \mathbf{W} follow the same distribution. On the other hand, $\det(\mathbf{W}_{-1}) = -\det(\mathbf{W})$. Due to the fact that the set of matrices with zero determinant has probability 0 under continuous distributions (see, e.g., Remark 2.5 in [85]), we may conclude $\Pr(\det(\mathbf{W}) > 0) = \Pr(\det(\mathbf{W}) < 0) = 0.5$.

For $\mathbf{W}_1, \dots, \mathbf{W}_L$ random matrices drawn independently, let $l \in [L]$ be the index such that $\Pr(\det(\mathbf{W}_l) > 0) = 0.5$. Since $\Pr(\det(\mathbf{W}_{l'}) = 0) = 0$ for any $l' \in [L]$, the proof readily follows from determinant multiplicativity and the law of total probability:

$$\begin{aligned} \Pr(\det(\mathbf{W}_L \cdots \mathbf{W}_1) > 0) &= \Pr(\det(\mathbf{W}_l) > 0) \cdot \Pr(\prod_{i \neq l} \det(\mathbf{W}_i) > 0) \\ &\quad + \Pr(\det(\mathbf{W}_l) < 0) \cdot \Pr(\prod_{i \neq l} \det(\mathbf{W}_i) < 0) \\ &= \frac{1}{2} [\Pr(\prod_{i \neq l} \det(\mathbf{W}_i) > 0) + \Pr(\prod_{i \neq l} \det(\mathbf{W}_i) < 0)] \\ &= 0.5. \end{aligned}$$

An identical computation yields $\Pr(\det(\mathbf{W}_L \cdots \mathbf{W}_1) < 0) = 0.5$. \square

A.3.7 Proof of Proposition 4

The proof makes use of the following lemma, proven in Appendix A.3.7.1.

Lemma 15. *Consider the setting of Theorem 1 (arbitrary depth $L \in \mathbb{N}$) in the special case of an initial end matrix $\mathbf{W}_M(0) = \alpha \cdot \mathbf{I}$, where \mathbf{I} stands for identity matrix and $\alpha \in (0, 1]$. Then, $\mathbf{W}_M(t)$ is positive definite for all $t \geq 0$.*

With Lemma 15 in place, we may derive the exact differential equations governing the end matrix in our setting of depth $L = 2$. Then, a detailed analysis of the dynamics will yield convergence of the loss to global minimum, i.e. $\lim_{t \rightarrow \infty} \mathcal{L}_M(t) = 0$. As usual, we omit the time index t when stating results for all t or when clear from the context.

According to Lemma 15, the end matrix \mathbf{W}_M is symmetric and positive definite. Thus, we may write the loss and its gradient with respect to \mathbf{W}_M as:

$$\mathcal{L}_M(\mathbf{W}_M) = \frac{1}{2} [w_{2,2}^2 + 2(w_{1,2} - 1)^2] \quad , \quad \nabla \mathcal{L}_M(\mathbf{W}_M) = \begin{pmatrix} 0 & w_{1,2} - 1 \\ w_{1,2} - 1 & w_{2,2} \end{pmatrix}, \quad (\text{A.13})$$

where $\{w_{i,j}\}_{i,j \in [2]}$ are the entries of \mathbf{W}_M . Since the factors \mathbf{W}_1 and \mathbf{W}_2 are balanced at initialization (Equation (1.5)), the differential equation governing the end matrix (Lemma 4) for depth $L = 2$ gives:

$$\begin{aligned} \dot{\mathbf{W}}_M &= - \left[\mathbf{W}_M \mathbf{W}_M^\top \right]^{\frac{1}{2}} \cdot \nabla \mathcal{L}_M(\mathbf{W}_M) - \nabla \mathcal{L}_M(\mathbf{W}_M) \cdot \left[\mathbf{W}_M^\top \mathbf{W}_M \right]^{\frac{1}{2}} \\ &= -\mathbf{W}_M \nabla \mathcal{L}_M(\mathbf{W}_M) - \nabla \mathcal{L}_M(\mathbf{W}_M) \mathbf{W}_M, \end{aligned} \quad (\text{A.14})$$

where the transition is by positive definiteness of \mathbf{W}_M . Writing the differential equation of each entry separately, we have:

$$\begin{aligned}\dot{w}_{1,1} &= 2w_{1,2}(1 - w_{1,2}), \\ \dot{w}_{2,2} &= 2w_{1,2}(1 - w_{1,2}) - 2w_{2,2}^2, \\ \dot{w}_{1,2} &= w_{2,2}(1 - 2w_{1,2}) + w_{1,1}(1 - w_{1,2}).\end{aligned}\tag{A.15}$$

Let us characterize the behavior of these entries throughout time.

Lemma 16. *The following holds for all $t \geq 0$:*

1. $w_{1,1} > 0$ and is monotonically non-decreasing.
2. $0 \leq w_{1,2} \leq 1$.
3. $0 < w_{2,2} \leq 1$.

Proof. Since \mathbf{W}_M is positive definite, it follows that $w_{1,1}$ and $w_{2,2}$ are positive. Examining the behavior of $w_{1,2}$ (Equation (A.15)): on the one hand, when $w_{1,2} = 0$ then $\dot{w}_{1,2} = w_{2,2} + w_{1,1} > 0$, and on the other hand, when $w_{1,2} = 1$ then $\dot{w}_{1,2} = -w_{2,2} < 0$. Because $w_{1,2}$ is initialized at 0, it stays in the interval $[0, 1]$. Otherwise, by Lemma 11, we have a contradiction to the positivity of $\dot{w}_{1,2}$ when $w_{1,2} = 0$ or its negativity when $w_{1,2} = 1$. Similarly, if $w_{2,2} > \frac{1}{2}$ we have $\dot{w}_{2,2} < 2w_{1,2}(1 - w_{1,2}) - \frac{1}{2} \leq 0$. Since at initialization $w_{2,2}(0) = \alpha \leq 1$, by Lemma 11, it will not go above 1. Lastly, since $w_{1,2}$ is in the interval $[0, 1]$, it holds that $\dot{w}_{1,1} \geq 0$, i.e. $w_{1,1}$ is monotonically non-decreasing. \square

We turn our focus to the derivative of the loss with respect to t :

$$\frac{d}{dt}\mathcal{L}_M(\mathbf{W}_M) = \langle \nabla \mathcal{L}_M(\mathbf{W}_M), \dot{\mathbf{W}}_M \rangle.$$

Plugging in Equation (A.14) and recalling the fact that $\langle \mathbf{A}, \mathbf{B} \rangle = \text{Tr}(\mathbf{A}^\top \mathbf{B})$ for matrices \mathbf{A}, \mathbf{B} of the same size:

$$\frac{d}{dt}\mathcal{L}_M(\mathbf{W}_M) = -\text{Tr}(\nabla \mathcal{L}_M(\mathbf{W}_M)^\top \mathbf{W}_M \nabla \mathcal{L}_M(\mathbf{W}_M)) - \text{Tr}(\nabla \mathcal{L}_M(\mathbf{W}_M)^\top \nabla \mathcal{L}_M(\mathbf{W}_M) \mathbf{W}_M).$$

From the cyclic property of the trace operator and symmetry of $\nabla \mathcal{L}_M(\mathbf{W}_M)$ (Equation (A.13)), we arrive at the following expression:

$$\frac{d}{dt}\mathcal{L}_M(\mathbf{W}_M) = -2 \text{Tr}(\nabla \mathcal{L}_M(\mathbf{W}_M) \mathbf{W}_M \nabla \mathcal{L}_M(\mathbf{W}_M)).$$

Notice that since $\nabla \mathcal{L}_M(\mathbf{W}_M) \mathbf{W}_M \nabla \mathcal{L}_M(\mathbf{W}_M)$ is positive semidefinite the trace is non-negative and $\frac{d}{dt}\mathcal{L}_M(\mathbf{W}_M) \leq 0$. That is, the loss is monotonically non-increasing throughout time. Invoking Lemma 10, we can upper bound the derivative by:

$$\frac{d}{dt}\mathcal{L}_M(\mathbf{W}_M) \leq -2\lambda_1(\mathbf{W}_M) \cdot \sigma_2(\nabla \mathcal{L}_M(\mathbf{W}_M))^2,\tag{A.16}$$

where $\lambda_1(\mathbf{W}_M)$ is the maximal eigenvalue of \mathbf{W}_M and $\sigma_2(\nabla \mathcal{L}_M(\mathbf{W}_M))$ is the minimal singular value of $\nabla \mathcal{L}_M(\mathbf{W}_M)$. The maximal eigenvalue of a symmetric matrix is greater than its diagonal entries. Therefore, $\lambda_1(\mathbf{W}_M) \geq w_{1,1}$. Since $w_{1,1}$ is initialized at $\alpha > 0$, and by Lemma 16 is monotonically non-decreasing, we have $\lambda_1(\mathbf{W}_M) \geq \alpha$.

Writing the eigenvalues of $\nabla \mathcal{L}_M(\mathbf{W}_M)$ explicitly:

$$\begin{aligned}\lambda_1(\nabla \mathcal{L}_M(\mathbf{W}_M)) &= \frac{w_{2,2} + \sqrt{w_{2,2}^2 + 4(1 - w_{1,2})^2}}{2}, \\ \lambda_2(\nabla \mathcal{L}_M(\mathbf{W}_M)) &= \frac{w_{2,2} - \sqrt{w_{2,2}^2 + 4(1 - w_{1,2})^2}}{2},\end{aligned}$$

we can see that, since $w_{2,2}$ is positive (Lemma 16):

$$\sigma_2(\nabla \mathcal{L}_M(\mathbf{W}_M)) = \min_{i=1,2} |\lambda_i(\nabla \mathcal{L}_M(\mathbf{W}_M))| = \frac{\sqrt{w_{2,2}^2 + 4(1 - w_{1,2})^2} - w_{2,2}}{2}.$$

Applying the identity $a - b = \frac{a^2 - b^2}{a + b}$ for $a, b \in \mathbb{R}$ such that $a + b \neq 0$, and the bounds on $w_{2,2}$ and $w_{1,2}$ (Lemma 16):

$$\begin{aligned}\sigma_2(\nabla \mathcal{L}_M(\mathbf{W}_M)) &= \frac{2(1 - w_{1,2})^2}{\sqrt{w_{2,2}^2 + 4(1 - w_{1,2})^2} + w_{2,2}} \\ &\geq \frac{2(1 - w_{1,2})^2}{\sqrt{1 + 4(1 - w_{1,2})^2} + 1} \\ &\geq \frac{2(1 - w_{1,2})^2}{2|(1 - w_{1,2})| + 2} \\ &\geq \frac{1}{2}(1 - w_{1,2})^2,\end{aligned}$$

where in the penultimate transition we bounded the square root of a sum by the sum of square roots. Returning to Equation (A.16) we have:

$$\frac{d}{dt} \mathcal{L}_M(\mathbf{W}_M) \leq -b(1 - w_{1,2})^4,$$

for $b = \frac{1}{2}\alpha$. We are now in a position to prove that $w_{1,2} \rightarrow 1$ as t tends to infinity. Integrating both sides with respect to time:

$$\mathcal{L}_M(\mathbf{W}_M(t)) - \mathcal{L}_M(\mathbf{W}_M(0)) \leq -b \int_{t'=0}^t (1 - w_{1,2}(t'))^4 dt'.$$

Since $\mathcal{L}_M(\mathbf{W}_M(t)) \geq 0$, by rearranging the inequality we may write:

$$\int_{t'=0}^t (1 - w_{1,2}(t'))^4 dt' \leq \frac{\mathcal{L}_M(\mathbf{W}_M(0))}{b}.$$

Going back to the differential equation of $w_{1,2}$ (Equation (A.15)), by applying the bounds on $w_{1,2}$ and $w_{2,2}$ (Lemma 16) we have that $\dot{w}_{1,2} \geq -1$. Defining $g(t) := (1 - w_{1,2}(t))^4$, it then holds that $\dot{g}(t) \leq 4$. Since $g(\cdot)$ is non-negative and has an upper bounded integral and derivative, from Lemma 12, we can conclude that $\lim_{t \rightarrow \infty} g(t) = 0$ and $\lim_{t \rightarrow \infty} w_{1,2}(t) = 1$.

Because $\mathcal{L}_M(\mathbf{W}_M(t))$ is monotonically non-increasing, we need only show that for each $\epsilon > 0$ there exists a $t_\epsilon > 0$ such that $\mathcal{L}_M(\mathbf{W}_M(t_\epsilon)) < \epsilon$. Having already established that $w_{1,2}(t)$ converges to 1, this amounts to finding a large enough t_ϵ for which $w_{2,2}(t_\epsilon)$ is sufficiently close to 0. Fix some $\epsilon > 0$ and let $\hat{t} > 0$ be such that for

all $t \geq \hat{t}$ the following holds:

$$2(1 - w_{1,2}(t))^2 < \epsilon \quad , \quad 2w_{1,2}(t)(1 - w_{1,2}(t)) < \epsilon . \quad (\text{A.17})$$

Such \hat{t} exists since all terms above converge to 0. Returning to the differential equation of $w_{2,2}$ (Equation (A.15)):

$$\dot{w}_{2,2}(t) < \epsilon - 2w_{2,2}(t)^2 . \quad (\text{A.18})$$

Recalling that $w_{2,2}(t) > 0$ (Lemma 16), it follows that there exists $t_\epsilon \geq \hat{t}$ with $w_{2,2}(t_\epsilon) > -\epsilon$ (otherwise $w_{2,2}(t)$ goes to $-\infty$ as $t \rightarrow \infty$, in contradiction to the positivity of $w_{2,2}(t)$). For the above t_ϵ , by rearranging the terms in Equation (A.18) we achieve $w_{2,2}(t_\epsilon) < \sqrt{\epsilon}$. Finally, combined with Equation (A.17), the result readily follows:

$$\mathcal{L}_M(\mathbf{W}_M(t_\epsilon)) = \frac{1}{2} [w_{2,2}(t_\epsilon)^2 + 2(w_{1,2}(t_\epsilon) - 1)^2] < \epsilon ,$$

concluding the proof. \square

A.3.7.1 Proof of Lemma 15

The proof proceeds as follows. We initially consider initializations where the matrices $\mathbf{W}_1(0), \dots, \mathbf{W}_L(0)$ form a *symmetric factorization* of $\mathbf{W}_M(0)$ (Definition 14), and show that this ensures the end matrix stays symmetric. Then, we establish that for every balanced initial factors (Equation (1.5)) with a positive definite end matrix there exist alternative balanced factors such that: (i) the initial end matrix is the same; and (ii) the factors form a symmetric factorization of the end matrix. Since the end matrices for the original and the constructed initializations obey the exact same dynamics (Lemma 4), the proof concludes.

Definition 14. We say that the matrices $\mathbf{W}_1, \dots, \mathbf{W}_L \in \mathbb{R}^{D \times D}$ form a *symmetric factorization* of $\mathbf{W} \in \mathbb{R}^{D \times D}$ if $\mathbf{W} = \mathbf{W}_L \cdots \mathbf{W}_1$ and

$$\mathbf{W}_l = \mathbf{W}_{L-l+1}^\top \quad , l \in \{1, \dots, \lfloor L/2 \rfloor + 1\} .$$

A straightforward result is that matrices with a symmetric factorization are symmetric themselves.

Lemma 17. *If a matrix $\mathbf{W} \in \mathbb{R}^{D \times D}$ has a symmetric factorization, then it is symmetric.*

Proof. Let $\mathbf{W}_1, \dots, \mathbf{W}_L \in \mathbb{R}^{D \times D}$ form a symmetric factorization of \mathbf{W} . It directly follows that

$$\mathbf{W} = \mathbf{W}_L \cdots \mathbf{W}_1 = \mathbf{W}_1^\top \cdots \mathbf{W}_L^\top = \mathbf{W}^\top .$$

\square

By Lemma 7, $\mathbf{W}_1(t), \dots, \mathbf{W}_L(t), \mathbf{W}_M(t)$ and $\nabla \mathcal{L}_M(\mathbf{W}_M(t))$ are analytic, and hence infinitely differentiable, with respect to t . Lemmas 18 and 19 below thus establish that if $\mathbf{W}_1(0), \dots, \mathbf{W}_L(0)$ form a symmetric factorization of $\mathbf{W}_M(0)$, then the end matrix stays symmetric for all t .

Lemma 18. *Under the setting of Lemma 15, assume that the matrices $\mathbf{W}_1(0), \dots, \mathbf{W}_L(0)$ form a symmetric factorization of $\mathbf{W}_M(0)$ (Definition 14). Then, for all $k \in \mathbb{N} \cup \{0\}$:*

$$\mathbf{W}_M^{(k)}(0) = \mathbf{W}_M^{(k)}(0)^\top , \quad (\text{A.19})$$

and

$$\mathbf{W}_l^{(k)}(0) = \mathbf{W}_{L-l+1}^{(k)}(0)^\top, \quad l \in \{1, \dots, \lfloor L/2 \rfloor + 1\}. \quad (\text{A.20})$$

Proof. The proof is by induction over k . For $k = 0$, the claim holds directly from the initialization assumption and Lemma 17. For $k \in \mathbb{N}$, suppose the claim is true for all $m \in \mathbb{N} \cup \{0\}$ with $m < k$. We begin by showing Equation (A.20) holds for k . In turn, this will lead to Equation (A.19) holding as well. For $l \in [L]$, the dynamics of $\mathbf{W}_l(t)$ under gradient flow are

$$\dot{\mathbf{W}}_l^{(1)}(t) = -\frac{\partial}{\partial \mathbf{W}_l} \phi_{\mathbf{M}}(\mathbf{W}_1(t), \dots, \mathbf{W}_L(t)) = -\prod_{r=l+1}^L \mathbf{W}_r(t)^\top \cdot \mathbf{G}(t) \cdot \prod_{r=1}^{l-1} \mathbf{W}_r(t)^\top,$$

where $\mathbf{G}(t) := \nabla \mathcal{L}_{\mathbf{M}}(\mathbf{W}_{\mathbf{M}}(t))$ denotes the loss gradient with respect to $\mathbf{W}_{\mathbf{M}}$ at time t . We can explicitly write the k 'th ($k \geq 1$) derivative with respect to t of each $\mathbf{W}_l(t)$ using the product rule for higher order derivatives:

$$\mathbf{W}_l^{(k)}(t) = -\sum_{i_1, \dots, i_L} \binom{k-1}{i_1, \dots, i_L} \prod_{r=l+1}^L \mathbf{W}_r^{(i_r)}(t)^\top \cdot \mathbf{G}^{(i)}(t) \cdot \prod_{r=1}^{l-1} \mathbf{W}_r^{(i_r)}(t)^\top,$$

where $\sum_{l=1}^L i_l = k-1$ and $\binom{k-1}{i_1, \dots, i_L} = (k-1)! / (i_1! \cdots i_L!)$ for $i_1, \dots, i_L \in \{0, \dots, k-1\}$. Taking the transpose of both sides we have:

$$\mathbf{W}_l^{(k)}(t)^\top = -\sum_{i_1, \dots, i_L} \binom{k-1}{i_1, \dots, i_L} \prod_{r=1}^{l-1} \mathbf{W}_r^{(i_r)}(t) \cdot \mathbf{G}^{(i)}(t)^\top \cdot \prod_{r=l+1}^L \mathbf{W}_r^{(i_r)}(t). \quad (\text{A.21})$$

Turning our attention to $\mathbf{G}(t)$, we may write it explicitly as:

$$\mathbf{G}(t) = \nabla \mathcal{L}_{\mathbf{M}}(\mathbf{W}_{\mathbf{M}}(t)) = \begin{pmatrix} 0 & w_{1,2}(t) - 1 \\ w_{2,1}(t) - 1 & w_{2,2}(t) \end{pmatrix},$$

where $\{w_{i,j}(t)\}_{i,j \in [2]}$ are the entries of $\mathbf{W}_{\mathbf{M}}(t)$. For $m < k$, note that when $\mathbf{W}_{\mathbf{M}}^{(m)}(t)$ is symmetric so is $\mathbf{G}^{(m)}(t)$. With this in hand, the inductive assumption (Equation (A.19)) implies that $\mathbf{G}^{(m)}(0)$ is symmetric (for all $m < k$). Combined with Equation (A.20) (for $m < k$, from the inductive assumption), we may write Equation (A.21) for $t = 0$ as:

$$\mathbf{W}_l^{(k)}(0)^\top = -\sum_{i_1, \dots, i_L} \binom{k-1}{i_1, \dots, i_L} \prod_{r=L-l+2}^L \mathbf{W}_r^{(i_{L-r+1})}(0)^\top \cdot \mathbf{G}^{(i)}(0) \cdot \prod_{r=1}^{L-l} \mathbf{W}_r^{(i_{L-r+1})}(0)^\top.$$

Reordering the sum according to $h_r := i_{L-r+1}$ and noticing that $\binom{k-1}{h_1, \dots, h_L} = \binom{k-1}{i_1, \dots, i_L}$, we conclude:

$$\mathbf{W}_l^{(k)}(0)^\top = -\sum_{h_1, \dots, h_L} \binom{k-1}{h_1, \dots, h_L} \prod_{r=L-l+2}^L \mathbf{W}_r^{(h_r)}(0)^\top \cdot \mathbf{G}^{(h_{L-l+1})}(0) \cdot \prod_{r=1}^{L-l} \mathbf{W}_r^{(h_r)}(0)^\top.$$

That is,

$$\mathbf{W}_l^{(k)}(0)^\top = \mathbf{W}_{L-l+1}^{(k)}(0),$$

proving Equation (A.20).

It remains to show that $\mathbf{W}_M^{(k)}(0)$ is symmetric. Similarly to before, we take the k 'th derivative of $\mathbf{W}_M(t) := \mathbf{W}_L(t) \cdots \mathbf{W}_1(t)$ using the product rule:

$$\mathbf{W}_M^{(k)}(t) = \sum_{i_1, \dots, i_L} \binom{k}{i_1, \dots, i_L} \prod_{l=1}^{l=L} \mathbf{W}_l^{(i_l)}(t),$$

where $\sum_{l=1}^L i_l = k$ and $\binom{k}{i_1, \dots, i_L} = k! / (i_1! \cdots i_L!)$ for $i_1, \dots, i_L \in \{0, \dots, k\}$. For convenience, we denote $\mathbf{B}_{i_1, \dots, i_L}(t) := \binom{k}{i_1, \dots, i_L} \prod_{l=1}^{l=L} \mathbf{W}_l^{(i_l)}(t)$. Pairing up elements in the sum with indices (i_1, \dots, i_L) that are a reverse order of each other, i.e. (i_1, \dots, i_L) is paired with (i_L, \dots, i_1) :

$$\mathbf{W}_M^{(k)}(t) = \sum_{i_1, \dots, i_L} \frac{1}{2} [\mathbf{B}_{i_1, \dots, i_L}(t) + \mathbf{B}_{i_L, \dots, i_1}(t)]. \quad (\text{A.22})$$

With Equation (A.22) in place, we can conclude the proof by showing $\mathbf{W}_M^{(k)}(0)$ is a sum of symmetric matrices. By the inductive assumption for Equation (A.20), which was established in the first part of the proof for k as well, we have:

$$\mathbf{B}_{i_1, \dots, i_L}(0) = \mathbf{B}_{i_L, \dots, i_1}(0)^\top, \quad (\text{A.23})$$

for each (i_1, \dots, i_L) . Therefore, the matrix $\mathbf{B}_{i_1, \dots, i_L}(0) + \mathbf{B}_{i_L, \dots, i_1}(0)$ is symmetric. Plugging Equation (A.23) into Equation (A.22) with $t = 0$, we arrive at a representation of $\mathbf{W}_M^{(k)}(0)$ as a sum of symmetric matrices. Thus, $\mathbf{W}_M^{(k)}(0)$ is symmetric, completing the proof. \square

Lemma 19. *Under the setting of Lemma 15, assume that the matrices $\mathbf{W}_1(0), \dots, \mathbf{W}_L(0)$ form a symmetric factorization of $\mathbf{W}_M(0)$ (Definition 14). Then, $\mathbf{W}_M(t)$ is symmetric for all $t \geq 0$.*

Proof. By Lemmas 18 and 9, we may conclude that for all $t \geq 0$:

$$\mathbf{W}_l(t) = \mathbf{W}_{L-l+1}(t)^\top, \quad l \in \{1, \dots, \lfloor L/2 \rfloor + 1\}.$$

In words, $\mathbf{W}_1(t), \dots, \mathbf{W}_L(t)$ form a symmetric factorization of $\mathbf{W}_M(t)$, and therefore $\mathbf{W}_M(t)$ is symmetric (Lemma 17). \square

Going back to the setting of Lemma 15 — initialization is balanced (Equation (1.5)), but does not necessarily comprise a symmetric factorization — we show that here too the end matrix remains symmetric throughout optimization. To do so, we first construct a factorization of $\mathbf{W}_M(0)$ that is both balanced and symmetric, for which Lemma 19 ensures the end matrix stays symmetric throughout optimization. We then prove that the trajectories of the end matrix for the original and the modified initializations coincide.

Recall that $\mathbf{W}_M(0) = \alpha \cdot \mathbf{I}$ and define $\bar{\mathbf{W}}_l(0) := \alpha^{\frac{1}{l}} \cdot \mathbf{I}$ for $l \in [L]$. It is easily verified that:

- $\mathbf{W}_M(0) = \bar{\mathbf{W}}_L(0) \cdots \bar{\mathbf{W}}_1(0)$.
- $\bar{\mathbf{W}}_l(0) = \bar{\mathbf{W}}_{L-l+1}(0)^\top$ for $l \in [L]$.
- $\bar{\mathbf{W}}_{l+1}(0)^\top \bar{\mathbf{W}}_{l+1}(0) = \bar{\mathbf{W}}_l(0) \bar{\mathbf{W}}_l(0)^\top$ for $l \in [L-1]$.

Meaning, $\bar{\mathbf{W}}_1(0), \dots, \bar{\mathbf{W}}_L(0)$ are balanced, and form a symmetric factorization of $\mathbf{W}_M(0)$. Suppose the factors $\bar{\mathbf{W}}_1(t), \dots, \bar{\mathbf{W}}_L(t)$ follow the gradient flow dynamics, with initial values $\bar{\mathbf{W}}_1(0), \dots, \bar{\mathbf{W}}_L(0)$, and let $\bar{\mathbf{W}}_M(t) := \bar{\mathbf{W}}_L(t) \cdots \bar{\mathbf{W}}_1(t)$ be the induced end matrix. From Lemma 19, it follows that $\bar{\mathbf{W}}_M(t)$ is symmetric for all $t \geq 0$.

As characterized in [7] (restated as Lemma 4), if the initial factors are balanced, the end matrix trajectory depends only on its initial value $\mathbf{W}_M(0)$. Since both the original and modified initializations are balanced and have the same end matrix, they lead to the exact same trajectory. Thus, $\mathbf{W}_M(t) = \bar{\mathbf{W}}_M(t)$ for all $t \geq 0$, and specifically, $\mathbf{W}_M(t)$ is symmetric.

The last step is to see that $\mathbf{W}_M(t)$ is not only symmetric, but positive definite as well. Since its initial value $\mathbf{W}_M(0)$ is positive definite, it suffices to show that its eigenvalues do not change sign. By Lemma 6, the determinant of $\mathbf{W}_M(t)$ is positive for all t . Specifically, the end matrix does not have zero eigenvalues. Recalling that $\mathbf{W}_M(t)$ is an analytic function of t (Lemma 7), Theorem 6.1 in [116] implies that its eigenvalues are continuous in t . Therefore, they can not change sign, as that would require them to pass through zero, concluding the proof. \square

A.3.8 Proof of Theorem 2

The proof follows a similar line to that of Theorem 1 (Appendix A.3.5), where the differences mostly stem from the fact that the solution set $\tilde{\mathcal{S}}$ (Equation (1.12)) is not confined to symmetric matrices, as opposed to the original \mathcal{S} (Equation (1.7)), slightly complicating the computation of singular values. For the sake of the proof, as mentioned in Appendix A.3.1, we omit the time index t when stating results for all $t \geq 0$ or when clear from context. We also let $\{w_{i,j}\}_{i,j \in [2]}$ denote the entries of the end matrix \mathbf{W}_M .

We begin by deriving loss-dependent bounds for $|w_{1,1}|, \sigma_1(\mathbf{W}_M)$ and $\sigma_2(\mathbf{W}_M)$. The entries of \mathbf{W}_M can be trivially bounded by the loss as follows:

$$|w_{2,2} - \epsilon| \leq \sqrt{2\mathcal{L}_M(\mathbf{W}_M)}, \quad |w_{1,2} - z| \leq \sqrt{2\mathcal{L}_M(\mathbf{W}_M)}, \quad |w_{2,1} - z'| \leq \sqrt{2\mathcal{L}_M(\mathbf{W}_M)}. \quad (\text{A.24})$$

Lemma 20 below, analogous to Lemma 13 from the proof of Theorem 1, characterizes the relation between $|w_{1,1}|$ and the loss.

Lemma 20. *Suppose $\mathcal{L}_M(\mathbf{W}_M) < \min\{z^2/2, z'^2/2\}$. Then:*

$$|w_{1,1}| > \frac{(|z| - \sqrt{2\mathcal{L}_M(\mathbf{W}_M)})(|z'| - \sqrt{2\mathcal{L}_M(\mathbf{W}_M)})}{|\epsilon| + \sqrt{2\mathcal{L}_M(\mathbf{W}_M)}} \geq \frac{|z| \cdot |z'|}{|\epsilon| + \sqrt{2\mathcal{L}_M(\mathbf{W}_M)}} - (|z| + |z'|).$$

Proof. According to Lemma 6, the determinant of \mathbf{W}_M does not change sign, i.e. it remains equal to $\text{sign}(z \cdot z')$ (the initial sign assumed). Under the assumption that $\mathcal{L}_M(\mathbf{W}_M) < \min\{z^2/2, z'^2/2\}$, both $w_{1,2}$ and $w_{2,1}$ have the same signs as z and z' , respectively, implying that $w_{2,2} \neq 0$ (otherwise we have a contradiction to the sign of the end matrix determinant). If $z \cdot z' > 0$, the determinant is positive as well, and it holds that $w_{1,1}w_{2,2} > w_{1,2}w_{2,1} > 0$. Otherwise, if $z \cdot z' < 0$ we have $w_{1,1}w_{2,2} < w_{1,2}w_{2,1} < 0$. Putting it together we may write $|w_{1,1}w_{2,2}| > |w_{1,2}w_{2,1}|$. Dividing by $|w_{2,2}|$ and applying the bounds from Equation (A.24) then completes the proof:

$$|w_{1,1}| > \frac{(|z| - \sqrt{2\mathcal{L}_M(\mathbf{W}_M)})(|z'| - \sqrt{2\mathcal{L}_M(\mathbf{W}_M)})}{|\epsilon| + \sqrt{2\mathcal{L}_M(\mathbf{W}_M)}} \geq \frac{|z| \cdot |z'|}{|\epsilon| + \sqrt{2\mathcal{L}_M(\mathbf{W}_M)}} - (|z| + |z'|).$$

□

We are now able to see that, indeed, the smaller $|\epsilon|$ is compared to $|z \cdot z'|$, the higher $|w_{1,1}|$ will be driven when the loss is minimized. With Lemma 20 in place, we are now able to bound the singular values of \mathbf{W}_M .

Lemma 21. *The singular values of \mathbf{W}_M fulfill:*

$$\begin{aligned}\sigma_1(\mathbf{W}_M) &\geq \frac{1}{\sqrt{2}} \cdot |w_{1,1}| - \sqrt{2\mathcal{L}_M(\mathbf{W}_M)}, \\ \sigma_2(\mathbf{W}_M) &\leq 4|\epsilon| + \left(4 + \frac{\sqrt{|z| \cdot |z'|}}{\min\{|z|, |z'|\}}\right) \sqrt{2\mathcal{L}_M(\mathbf{W}_M)}.\end{aligned}\tag{A.25}$$

Furthermore, if $\mathcal{L}_M(\mathbf{W}_M) < \min\{z^2/2, z'^2/2\}$, the bound on $\sigma_2(\mathbf{W}_M)$ may be simplified:

$$\sigma_2(\mathbf{W}_M) \leq 4|\epsilon| + 4\sqrt{2\mathcal{L}_M(\mathbf{W}_M)}.\tag{A.26}$$

Proof. Define $\mathbf{W}_{\tilde{\mathcal{S}}} := \begin{pmatrix} w_{1,1} & z' \\ z & \epsilon \end{pmatrix}$, the orthogonal projection of \mathbf{W}_M onto the solution set $\tilde{\mathcal{S}}$. From Corollary 8.6.2 in [76] we know that:

$$|\sigma_i(\mathbf{W}_M) - \sigma_i(\mathbf{W}_{\tilde{\mathcal{S}}})| \leq \|\mathbf{W}_M - \mathbf{W}_{\tilde{\mathcal{S}}}\|_{Fro} = \sqrt{2\mathcal{L}_M(\mathbf{W}_M)}, \quad i = 1, 2.\tag{A.27}$$

This means that any bound on the singular values of $\mathbf{W}_{\tilde{\mathcal{S}}}$ can be transferred to those of \mathbf{W}_M (up to an additive loss-dependent term). It is straightforwardly verified that the squared singular values of $\mathbf{W}_{\tilde{\mathcal{S}}}$ are

$$\begin{aligned}\sigma_1^2(\mathbf{W}_{\tilde{\mathcal{S}}}) &= \frac{1}{2} \left(w_{1,1}^2 + z^2 + z'^2 + \epsilon^2 + \sqrt{\left(w_{1,1}^2 + z^2 + z'^2 + \epsilon^2 \right)^2 - 4(w_{1,1}\epsilon - zz')^2} \right), \\ \sigma_2^2(\mathbf{W}_{\tilde{\mathcal{S}}}) &= \frac{1}{2} \left(w_{1,1}^2 + z^2 + z'^2 + \epsilon^2 - \sqrt{\left(w_{1,1}^2 + z^2 + z'^2 + \epsilon^2 \right)^2 - 4(w_{1,1}\epsilon - zz')^2} \right).\end{aligned}\tag{A.28}$$

Note that the term inside the square roots is non-negative for all $w_{1,1}, z, z', \epsilon$. Since all elements in the expression for $\sigma_1^2(\mathbf{W}_{\tilde{\mathcal{S}}})$ are non-negative, we have $\sigma_1(\mathbf{W}_{\tilde{\mathcal{S}}}) \geq (1/\sqrt{2}) \cdot |w_{1,1}|$. Combining this with Equation (A.27) completes the lower bound for $\sigma_1(\mathbf{W}_M)$.

Next, let $\mathbf{W}_{\tilde{\mathcal{S}}_0} := \begin{pmatrix} w_{1,1} & z' \\ z & 0 \end{pmatrix}$ be the matrix obtained by replacing the bottom-right entry of $\mathbf{W}_{\tilde{\mathcal{S}}}$ by 0. Replacing ϵ with 0 in Equation (A.28), and applying the identity $a - b = \frac{a^2 - b^2}{a + b}$ for $a, b \in \mathbb{R}$ such that $a + b \neq 0$, we get:

$$\begin{aligned}\sigma_2^2(\mathbf{W}_{\tilde{\mathcal{S}}_0}) &= \frac{2z^2z'^2}{w_{1,1}^2 + z^2 + z'^2 + \sqrt{\left(w_{1,1}^2 + z^2 + z'^2 \right)^2 - 4z^2z'^2}} \\ &\leq \frac{2z^2z'^2}{w_{1,1}^2 + z^2 + z'^2}.\end{aligned}\tag{A.29}$$

We initially prove Equation (A.26) in the case where $\mathcal{L}_M(\mathbf{W}_M) < \min \{z^2/2, z'^2/2\}$. By lifting said assumption we then show that the bound on $\sigma_2(\mathbf{W}_M)$ in Equation (A.25) holds for any loss value. Under the assumption that $\mathcal{L}_M(\mathbf{W}_M) < \min \{z^2/2, z'^2/2\}$, taking the square root of both sides in Equation (A.29), we arrive at the following bound:

$$\begin{aligned} \sigma_2(\mathbf{W}_{\tilde{\mathcal{S}}_0}) &\leq \sqrt{2} \cdot \frac{|z| \cdot |z'|}{\sqrt{w_{1,1}^2 + z^2 + z'^2}} \\ &\leq \sqrt{6} \cdot \frac{|z| \cdot |z'|}{|w_{1,1}| + |z| + |z'|} \\ &\leq \sqrt{6} \cdot \frac{|z| \cdot |z'|}{\frac{|z| \cdot |z'|}{|\epsilon| + \sqrt{2\mathcal{L}_M(\mathbf{W}_M)}}} \\ &\leq 3 \left(|\epsilon| + \sqrt{2\mathcal{L}_M(\mathbf{W}_M)} \right), \end{aligned}$$

where in the second transition we applied the inequality $\sqrt{w_{1,1}^2 + z^2 + z'^2} \geq (|w_{1,1}| + |z| + |z'|) / \sqrt{3}$, and in the third made use of the bound on $|w_{1,1}|$ (Lemma 20). Applying Corollary 8.6.2 from [76] twice, once for the matrices \mathbf{W}_M and $\mathbf{W}_{\tilde{\mathcal{S}}}$, and another for $\mathbf{W}_{\tilde{\mathcal{S}}}$ and $\mathbf{W}_{\tilde{\mathcal{S}}_0}$, we have:

$$\sigma_2(\mathbf{W}_M) \leq 3 \left(|\epsilon| + \sqrt{2\mathcal{L}_M(\mathbf{W}_M)} \right) + |\epsilon| + \sqrt{2\mathcal{L}_M(\mathbf{W}_M)} = 4 \left(|\epsilon| + \sqrt{2\mathcal{L}_M(\mathbf{W}_M)} \right),$$

achieving the desired result from Equation (A.26). It remains to see that the bound on $\sigma_2(\mathbf{W}_M)$ in Equation (A.25) holds regardless of the loss value. When $\mathcal{L}_M(\mathbf{W}_M) < \min \{z^2/2, z'^2/2\}$ it obviously holds since it is only looser than the bound already obtained under this assumption. Otherwise, going back to Equation (A.29), it can be seen that

$$\sigma_2^2(\mathbf{W}_{\tilde{\mathcal{S}}_0}) \leq \frac{2z^2z'^2}{(z - z')^2 + 2|z| \cdot |z'|} \leq |z| \cdot |z'|.$$

Thus, $\sigma_2(\mathbf{W}_{\tilde{\mathcal{S}}_0}) \leq \sqrt{|z| \cdot |z'|}$. Following the same procedure as before (applying Corollary 8.6.2 from [76]), combined with the fact that $\mathcal{L}_M(\mathbf{W}_M) \geq \min \{z^2/2, z'^2/2\}$ concludes the proof:

$$\begin{aligned} \sigma_2(\mathbf{W}_M) &\leq \sqrt{|z| \cdot |z'|} + |\epsilon| + \sqrt{2\mathcal{L}_M(\mathbf{W}_M)} \\ &\leq \frac{\sqrt{|z| \cdot |z'|}}{\min\{|z|, |z'|\}} \cdot \sqrt{2\mathcal{L}_M(\mathbf{W}_M)} + |\epsilon| + \sqrt{2\mathcal{L}_M(\mathbf{W}_M)} \\ &\leq 4|\epsilon| + \left(4 + \frac{\sqrt{|z| \cdot |z'|}}{\min\{|z|, |z'|\}} \right) \sqrt{2\mathcal{L}_M(\mathbf{W}_M)}. \end{aligned}$$

□

A.3.8.1 Proof of Equation (1.13) (Lower Bound for Quasi-Norm)

Turning our attention to $\|\mathbf{W}_M\|$, following the same steps as in the proof of Theorem 1 (Appendix A.3.5.1) will lead to a generalized bound. By the triangle inequality:

$$\|\mathbf{W}_M\| \geq \frac{1}{c_{\|\cdot\|}} \|w_{1,1} \mathbf{e}_1 \mathbf{e}_1^\top\| - \|\mathbf{W}_M - w_{1,1} \mathbf{e}_1 \mathbf{e}_1^\top\|, \quad (\text{A.30})$$

where $c_{\|\cdot\|} \geq 1$ is a constant with which $\|\cdot\|$ satisfies the weakened triangle inequality (see Footnote 2). Let us initially assume that $\mathcal{L}_M(\mathbf{W}_M) < \min\{z^2/2, z'^2/2\}$. We later lift this assumption, delivering a bound that holds for all loss values. Invoking Equation (A.24) we may bound the negative term in Equation (A.30) as follows:

$$\begin{aligned} \|\mathbf{W}_M - w_{1,1} \mathbf{e}_1 \mathbf{e}_1^\top\| &\leq c_{\|\cdot\|} |w_{2,2}| \|\mathbf{e}_2 \mathbf{e}_2^\top\| + c_{\|\cdot\|}^2 \left(|w_{2,1}| \|\mathbf{e}_2 \mathbf{e}_1^\top\| + |w_{1,2}| \|\mathbf{e}_1 \mathbf{e}_2^\top\| \right) \\ &\leq 3c_{\|\cdot\|}^2 \left(\max\{|z|, |z'|, |\epsilon|\} + \sqrt{2\mathcal{L}_M(\mathbf{W}_M)} \right) \max_{\substack{i,j \in \{1,2\} \\ (i,j) \neq (1,1)}} \|\mathbf{e}_i \mathbf{e}_j^\top\| \\ &\leq 6c_{\|\cdot\|}^2 \max\{|z|, |z'|, |\epsilon|\} \cdot \max_{\substack{i,j \in \{1,2\} \\ (i,j) \neq (1,1)}} \|\mathbf{e}_i \mathbf{e}_j^\top\|, \end{aligned}$$

Returning to Equation (A.30), applying the inequality above and the bound on $|w_{1,1}|$ (Lemma 20) we have:

$$\begin{aligned} \|\mathbf{W}_M\| &\geq \frac{\|\mathbf{e}_1 \mathbf{e}_1^\top\|}{c_{\|\cdot\|}} \left(\frac{|z| \cdot |z'|}{|\epsilon| + \sqrt{2\mathcal{L}_M(\mathbf{W}_M)}} - |z| - |z'| \right) \\ &\quad - 6c_{\|\cdot\|}^2 \max\{|z|, |z'|, |\epsilon|\} \max_{\substack{i,j \in \{1,2\} \\ (i,j) \neq (1,1)}} \|\mathbf{e}_i \mathbf{e}_j^\top\| \\ &\geq \frac{\|\mathbf{e}_1 \mathbf{e}_1^\top\|}{c_{\|\cdot\|}} \cdot \frac{|z| \cdot |z'|}{|\epsilon| + \sqrt{2\mathcal{L}_M(\mathbf{W}_M)}} - 8c_{\|\cdot\|}^2 \max\{|z|, |z'|, |\epsilon|\} \cdot \max_{i,j \in \{1,2\}} \|\mathbf{e}_i \mathbf{e}_j^\top\|. \end{aligned}$$

Since $\|\mathbf{W}_M\|$ is trivially lower bounded by zero, defining the constants

$$\begin{aligned} a_{\|\cdot\|} &:= \frac{\|\mathbf{e}_1 \mathbf{e}_1^\top\|}{c_{\|\cdot\|}}, \\ b_{\|\cdot\|} &:= \max \left\{ \frac{a_{\|\cdot\|} \cdot |z| \cdot |z'|}{|\epsilon| + \min\{|z|, |z'|\}}, 8c_{\|\cdot\|}^2 \max\{|z|, |z'|, |\epsilon|\} \max_{i,j \in \{1,2\}} \|\mathbf{e}_i \mathbf{e}_j^\top\| \right\}, \end{aligned}$$

allows us, on the one hand, to arrive at a bound of the form:

$$\|\mathbf{W}_M\| \geq a_{\|\cdot\|} \cdot \frac{|z| \cdot |z'|}{|\epsilon| + \sqrt{2\mathcal{L}_M(\mathbf{W}_M)}} - b_{\|\cdot\|},$$

and on the other hand, to remove the previous assumption on the loss: in the case where $\mathcal{L}_M(\mathbf{W}_M) \geq \min\{z^2/2, z'^2/2\}$, the bound is non-positive and trivially holds. Noticing this is exactly Equation (1.13) (recall we omitted the time index t), concludes this part of the proof.

A.3.8.2 Proof of Equation (1.14) (Upper Bound for Effective Rank)

Derivation of the upper bound for effective rank (Definition 1) is initially done under the assumption that $\mathcal{L}_M(\mathbf{W}_M) < \min\{z^2/8, z'^2/8\}$. We then remove this assumption, establishing a bound that holds for all loss values.

The bounds on $\sigma_1(\mathbf{W}_M)$ and $\sigma_2(\mathbf{W}_M)$ in Lemma 21 give:

$$\begin{aligned}
\rho_1(\mathbf{W}_M) &= \frac{\sigma_1(\mathbf{W}_M)}{\sigma_1(\mathbf{W}_M) + \sigma_2(\mathbf{W}_M)} \\
&\geq \frac{\sigma_1(\mathbf{W}_M)}{\sigma_1(\mathbf{W}_M) + 4\left(|\epsilon| + \sqrt{2\mathcal{L}_M(\mathbf{W}_M)}\right)} \\
&= 1 - \frac{4\left(|\epsilon| + \sqrt{2\mathcal{L}_M(\mathbf{W}_M)}\right)}{\sigma_1(\mathbf{W}_M) + 4\left(|\epsilon| + \sqrt{2\mathcal{L}_M(\mathbf{W}_M)}\right)} \\
&\geq 1 - \frac{4\left(|\epsilon| + \sqrt{2\mathcal{L}_M(\mathbf{W}_M)}\right)}{\frac{1}{\sqrt{2}} \cdot |w_{1,1}| + 4|\epsilon| + 3\sqrt{2\mathcal{L}_M(\mathbf{W}_M)}} \\
&\geq 1 - \frac{4\sqrt{2}\left(|\epsilon| + \sqrt{2\mathcal{L}_M(\mathbf{W}_M)}\right)}{|w_{1,1}|}.
\end{aligned}$$

Additionally, under our assumption that $\mathcal{L}_M(\mathbf{W}_M) < \min\{z^2/8, z'^2/8\}$, the bound on $|w_{1,1}|$ in Lemma 20 can be simplified to:

$$|w_{1,1}| \geq \frac{(|z| - \sqrt{2\mathcal{L}_M(\mathbf{W}_M)})(|z'| - \sqrt{2\mathcal{L}_M(\mathbf{W}_M)})}{|\epsilon| + \sqrt{2\mathcal{L}_M(\mathbf{W}_M)}} \geq \frac{\min\{|z|, |z'|\}^2}{4\left(|\epsilon| + \sqrt{2\mathcal{L}_M(\mathbf{W}_M)}\right)}.$$

Combining the last two inequalities we have:

$$\rho_2(\mathbf{W}_M) = 1 - \rho_1(\mathbf{W}_M) \leq \frac{16\sqrt{2}\left(|\epsilon| + \sqrt{2\mathcal{L}_M(\mathbf{W}_M)}\right)^2}{\min\{|z|, |z'|\}^2}.$$

It is now possible to see that, in accordance with Section 1.3.4, the smaller $|\epsilon|$ is compared to $\min\{|z|, |z'|\}$, the closer to zero $\rho_2(\mathbf{W}_M)$ becomes as the loss is minimized. Let $h(\rho_2(\mathbf{W}_M)) := -\rho_2(\mathbf{W}_M) \cdot \ln(\rho_2(\mathbf{W}_M)) - (1 - \rho_2(\mathbf{W}_M)) \cdot \ln(1 - \rho_2(\mathbf{W}_M))$ denote the binary entropy function, and recall that the effective rank of the end matrix defined to be $\text{erank}(\mathbf{W}_M) := \exp\{h(\rho_2(\mathbf{W}_M))\}$. As in the proof of Theorem 1 (Appendix A.3.5.2), we may bound the exponent on the interval $[0, \ln(2)]$ by the linear function intersecting it at these points. That is,

$$\text{erank}(\mathbf{W}_M) \leq 1 + \frac{1}{\ln(2)} \cdot h(\rho_2(\mathbf{W}_M)).$$

From Lemma 8 it holds that $h(\rho_2(\mathbf{W}_M)) \leq 2\sqrt{\rho_2(\mathbf{W}_M)}$. Plugging this into the inequality above leads to:

$$\begin{aligned} \text{erank}(\mathbf{W}_M) &\leq 1 + \frac{8 \cdot 2^{\frac{1}{4}}}{\ln(2) \cdot \min\{|z|, |z'|\}} \cdot \left(|\epsilon| + \sqrt{2\mathcal{L}_M(\mathbf{W}_M)} \right) \\ &\leq 1 + \frac{16}{\min\{|z|, |z'|\}} \cdot \left(|\epsilon| + \sqrt{2\mathcal{L}_M(\mathbf{W}_M)} \right), \end{aligned}$$

where the second transition is a slight simplification of the constants ($2^{1/4}/\ln(2) < 2$). As will be shown below, $\inf_{\mathbf{W}' \in \tilde{\mathcal{S}}} \text{erank}(\mathbf{W}') = 1$. We may thus conclude:

$$\text{erank}(\mathbf{W}_M) \leq \inf_{\mathbf{W}' \in \tilde{\mathcal{S}}} \text{erank}(\mathbf{W}') + \frac{16}{\min\{|z|, |z'|\}} \cdot \left(|\epsilon| + \sqrt{2\mathcal{L}_M(\mathbf{W}_M)} \right).$$

Notice that when $\mathcal{L}_M(\mathbf{W}_M) \geq \min\{z^2/8, z'^2/8\}$ the inequality trivially holds since the right-hand side is greater than 2 (the maximal effective rank for a 2×2 matrix). This establishes Equation (1.14) (time index is omitted).

It remains to prove that $\inf_{\mathbf{W}' \in \tilde{\mathcal{S}}} \text{erank}(\mathbf{W}') = 1$. If $\epsilon \neq 0$, it is trivial since there exists $\mathbf{W}' \in \tilde{\mathcal{S}}$ with $\text{rank}(\mathbf{W}') = 1$, meaning $\sigma_2(\mathbf{W}') = 0$ and $\text{erank}(\mathbf{W}') = 1$. If $\epsilon = 0$, examining the squared singular values of $\mathbf{W}' \in \tilde{\mathcal{S}}$ (Equation (A.28) with $(\mathbf{W}')_{1,1}$ in place of $w_{1,1}$) reveals that $\lim_{(\mathbf{W}')_{1,1} \rightarrow \infty} \sigma_2(\mathbf{W}') = 0$, while $\lim_{(\mathbf{W}')_{1,1} \rightarrow \infty} \sigma_1(\mathbf{W}') = \infty$. Thus, there exists a matrix in $\tilde{\mathcal{S}}$ with effective rank arbitrarily close to 1. Since the effective rank of any matrix is at least 1, this implies that $\inf_{\mathbf{W}' \in \tilde{\mathcal{S}}} \text{erank}(\mathbf{W}') = 1$.

A.3.8.3 Proof of Equation (1.15) (Upper Bound for Distance From Infimal Rank)

We claim that the infimal rank (Definition 2) of $\tilde{\mathcal{S}}$ is 1. Since $z, z' \neq 0$, it cannot be 0. If $\epsilon \neq 0$, our claim is trivial since there exists $\mathbf{W}' \in \tilde{\mathcal{S}}$ with $\text{rank}(\mathbf{W}') = 1$. Otherwise, inspecting the squared singular values of a matrix $\mathbf{W}' \in \tilde{\mathcal{S}}$ (Equation (A.28) with $(\mathbf{W}')_{1,1}$ in place of $w_{1,1}$), we can see that, when $\epsilon = 0$, taking $(\mathbf{W}')_{1,1}$ to infinity drives the minimal singular value towards zero ($\lim_{(\mathbf{W}')_{1,1} \rightarrow \infty} \sigma_2(\mathbf{W}') = 0$). Hence, the distance of $\tilde{\mathcal{S}}$ from the set of matrices with rank 1 or less is 0 in this case as well.

The distance of the end matrix from the infimal rank of $\tilde{\mathcal{S}}$ is therefore given by $\mathcal{D}_{\text{Fro}}(\mathbf{W}_M(t), \mathcal{M}_1) = \sigma_2(\mathbf{W}_M(t))$. From Lemma 21 we have

$$\mathcal{D}_{\text{Fro}}(\mathbf{W}_M(t), \mathcal{M}_1) \leq 4|\epsilon| + \left(4 + \frac{\sqrt{|z| \cdot |z'|}}{\min\{|z|, |z'|\}} \right) \sqrt{2\mathcal{L}_M(t)},$$

for all $t \geq 0$.

A.3.8.4 Robustness to Change in Observed Locations

Lastly, we prove that the established bounds (Equations (1.13), (1.14) and (1.15)) are robust to a change in observed locations. Let $(i, j) \in [2] \times [2]$ be the unobserved entry's location. Following proof steps analogous to those in Lemmas 20 and 21 — while recalling our assumption of $\det(\mathbf{W}_M(0))$ having same sign as $z \cdot z'$ if $i = j$ and opposite sign otherwise — yields identical bounds on the unobserved entry and singular

values of \mathbf{W}_M . Since the derivations of Equations (1.13), (1.14), and (1.15) in Appendices A.3.8.1, A.3.8.2, and A.3.8.3, respectively, rely solely on the aforementioned bounds, the proof concludes. \square

Appendix B

Implicit Regularization in Tensor Factorization

B.1 Extension to Tensor Sensing

Our theoretical analyses (Sections 2.3 and 2.4) are presented in the context of tensor completion, but readily extend to the more general task of *tensor sensing* — reconstruction of an unknown tensor from linear measurements (projections). In this appendix we outline the extension. Empirical demonstrations for tensor sensing are given in Appendix B.2.1 (Figure B.3).

For measurement tensors $\{\mathcal{A}_i \in \mathbb{R}^{D_1 \times \dots \times D_N}\}_{i=1}^M$ and a ground truth tensor $\mathcal{W}^* \in \mathbb{R}^{D_1 \times \dots \times D_N}$, the goal in tensor sensing is to reconstruct \mathcal{W}^* based on $\{\langle \mathcal{A}_i, \mathcal{W}^* \rangle \in \mathbb{R}\}_{i=1}^M$, where $\langle \cdot, \cdot \rangle$ represents the standard inner product. Similarly to tensor completion (cf. Equation (2.1)), a standard loss function for the task is:

$$\mathcal{L}_s(\mathcal{W}) = \frac{1}{M} \sum_{i=1}^M \ell(\langle \mathcal{A}_i, \mathcal{W} \rangle - \langle \mathcal{A}_i, \mathcal{W}^* \rangle),$$

where $\mathcal{L}_s : \mathbb{R}^{D_1 \times \dots \times D_N} \rightarrow \mathbb{R}_{\geq 0}$, and $\ell : \mathbb{R} \rightarrow \mathbb{R}_{\geq 0}$ is differentiable and locally smooth. Note that tensor completion is a special case, in which the measurement tensors hold 1 at a single entry and 0 elsewhere.

Beginning with Section 2.3, its results (in particular Lemma 1, Theorem 3 and Corollary 2) hold (and are proven in Appendix B.3) for any differentiable and locally smooth $\mathcal{L}_T(\cdot)$, thus they apply as is to tensor sensing. Turning to Section 2.4, the extension of Theorem 4 and Corollary 3 to tensor sensing (with Huber loss) is straightforward. Proofs rely on the specifics of tensor completion only in the preliminary Lemmas 32, 33 and 34 (Appendix B.3.5.1), for which analogous lemmas may readily be established. Thus, up to slight changes in constants if $\max_{i=1, \dots, M} \|\mathcal{A}_i\| > 1$, the results carry over.

B.1.1 Stronger Results Under Restricted Isometry Property

In the classic setting of *matrix sensing* (tensor sensing with order $N = 2$), a commonly studied condition on the measurement matrices is the *restricted isometry property*. This condition allows for efficient recovery when the ground truth matrix has low rank, and holds with high probability when the entries of the measurement matrices are drawn independently from a zero-mean sub-Gaussian distribution (cf. [183]). The notion of restricted isometry property extends from matrix to tensor sensing (i.e. from

order $N = 2$ to arbitrary $N \in \mathbb{N}_{\geq 2}$ — see [176, 103]. When it applies, the tensor sensing analogues of Theorem 4 and Corollary 3 can be strengthened as described below.

In the context of tensor sensing, the restricted isometry property is defined as follows.

Definition 15. We say that the measurement tensors $\{\mathcal{A}_i \in \mathbb{R}^{D_1 \times \dots \times D_N}\}_{i=1}^M$ satisfy *r-restricted isometry property (r-RIP)* with parameter $\delta \in [0, 1)$ if:

$$(1 - \delta)\|\mathcal{W}\|^2 \leq \sum_{i=1}^M \langle \mathcal{A}_i, \mathcal{W} \rangle^2 \leq (1 + \delta)\|\mathcal{W}\|^2,$$

for all $\mathcal{W} \in \mathbb{R}^{D_1 \times \dots \times D_N}$ of tensor rank r or less.

By [103], given $m \in \mathcal{O}(\log(N) \cdot \sum_{n=1}^N D_n)$ measurement tensors with entries drawn independently from a zero-mean sub-Gaussian distribution, 1-RIP holds with high probability. In this case, we may strengthen the tensor sensing analogue of Theorem 4, such that it ensures that arbitrarily small initialization leads tensor factorization to follow a rank one trajectory for an arbitrary amount of time, regardless of the distance traveled. That is, with the notations of Theorem 4, for any time duration $T > 0$ and degree of approximation $\epsilon \in (0, 1)$, if initialization is sufficiently small, $\overline{\mathcal{W}}_T(t)$ is within ϵ distance from a balanced rank one trajectory emanating from \mathcal{S} at least until time $t \geq T$. To see it is so, notice that since the loss function during gradient flow is monotonically non-increasing, $\sum_{i=1}^M \langle \mathcal{A}_i, \mathcal{W}_1(t) \rangle^2$ is bounded through time for any rank one trajectory $\mathcal{W}_1(t)$. In turn, since the measurement tensors satisfy 1-RIP, all such trajectories emanating from \mathcal{S} are confined to a ball of radius $B > 0$ about the origin, for some $B > 0$. By the tensor sensing analogue of Theorem 4, sufficiently small initialization ensures that there exists $\mathcal{W}_1(t)$ — a balanced rank one trajectory emanating from \mathcal{S} — such that $\overline{\mathcal{W}}_T(t)$ is within ϵ distance from it at least until $t \geq T$ or $\|\overline{\mathcal{W}}_T(t)\| \geq B + 1$. However, we know that $\|\mathcal{W}_1(t)\| \leq B$, and so $\overline{\mathcal{W}}_T(t)$ cannot reach norm of $B + 1$ before time T , as that would entail a contradiction — $\|\mathcal{W}_1(t)\| > B$. As a consequence of the above, in the tensor sensing analogue of Corollary 3, when 1-RIP is satisfied we need not assume all balanced rank one trajectories emanating from \mathcal{S} are jointly bounded.

B.2 Further Experiments and Implementation Details

B.2.1 Further Experiments

Figures B.1, B.2, and B.3 supplement Figure 2.2 from Section 2.5.1 by including, respectively: (i) Huber loss (Equation (2.8)) instead of ℓ_2 loss; (ii) ground truth tensors of different orders and (tensor) ranks; and (iii) tensor sensing (see Appendix B.1). Table B.1 supplements Figure 2.3, reporting mean squared errors of linear predictors fitted to the different datasets.

B.2.2 Implementation Details

Below are implementation details omitted from our experimental reports (Section 2.5 and Appendix B.2.1). Source code for reproducing our results and figures can be found at https://github.com/noamrazin/imp_reg_in_tf (based on the PyTorch framework [172]).

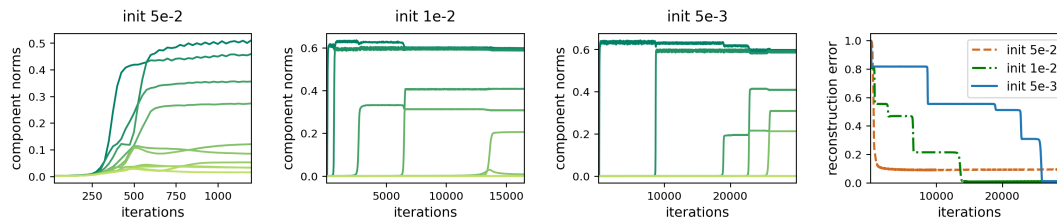


Figure B.1: Dynamics of gradient descent over tensor factorization (with Huber loss) — incremental learning of components yields low tensor rank solutions. This figure is identical to Figure 2.2, except that the minimized objective (Equation (2.1)) is based on Huber loss ($\ell_h(\cdot)$ from Equation (2.8)) instead of ℓ_2 loss. In accordance with Assumption 1, the transition point δ_h was set to $5 \cdot 10^{-7}$ — smaller than the absolute value of observed entries (though larger δ_h led to similar results). For further details see caption of Figure 2.2, as well as Appendix B.2.2.1.

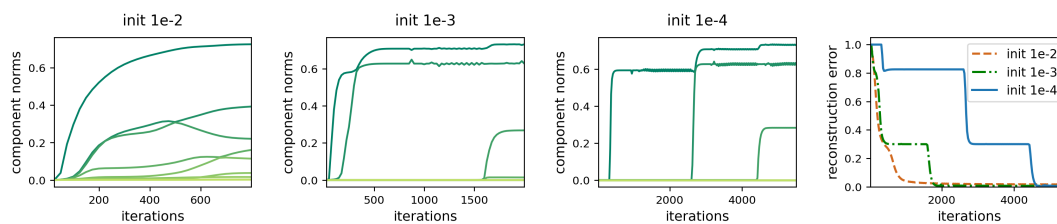


Figure B.2: Dynamics of gradient descent over (order 3) tensor factorization — incremental learning of components yields low tensor rank solutions. This figure is identical to Figure 2.2, except that: (i) the ground truth tensor is of (tensor) rank 3 with size 10-by-10-by-10 (order 3), completed based on 300 observed entries (smaller sample sizes led to solutions with tensor rank lower than that of the ground truth tensor); and (ii) the employed tensor factorization consists of $R = 100$ components (large enough to express any tensor). For further details see caption of Figure 2.2, as well as Appendix B.2.2.1.

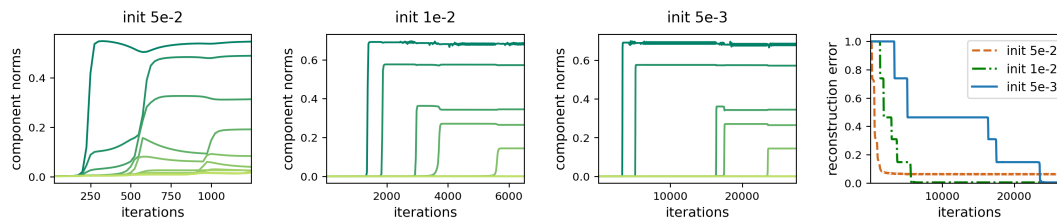


Figure B.3: Dynamics of gradient descent over tensor factorization (on tensor sensing task) — incremental learning of components yields low tensor rank solutions. This figure is identical to Figure 2.2, except that reconstruction of the ground truth tensor is based on 2000 linear measurements (instead of 2000 randomly chosen entries), *i.e.* on $\{\langle \mathcal{A}_i, \mathcal{W}^* \rangle\}_{i=1}^{2000}$, where $\mathcal{W}^* \in \mathbb{R}^{D_1 \times \dots \times D_N}$ is the ground truth tensor and $\mathcal{A}_1, \dots, \mathcal{A}_{2000} \in \mathbb{R}^{D_1 \times \dots \times D_N}$ are measurement tensors sampled independently from a zero-mean Gaussian distribution (see Appendix B.1 for a description of the tensor sensing task). For further details see caption of Figure 2.2, as well as Appendix B.2.2.1.

B.2.2.1 Dynamics of Learning (Figures 2.2, B.1, B.2, and B.3)

The number of components R was set to ensure an unconstrained search space, *i.e.* to 10^2 and 10^3 for tensor sizes 10-by-10-by-10 and 10-by-10-by-10-by-10 respectively.¹ Gradient descent was initialized randomly by sampling each weight independently from a zero-mean Gaussian distribution, and was run until the loss

¹For any $D_1, \dots, D_N \in \mathbb{N}$, setting $R = (\prod_{n=1}^N D_n) / \max\{D_n\}_{n=1}^N$ suffices for expressing all tensors in $\mathbb{R}^{D_1 \times \dots \times D_N}$ (*cf.* [85]).

Table B.1: Linear predictors are incapable of accurately fitting the datasets in the experiment reported by Figure 2.3. Table presents mean squared errors (over train and test sets) attained by fitting linear predictors to the one-vs-all prediction tasks induced by MNIST and Fashion-MNIST datasets, as well as their random variants (in compliance with Figure 2.3, to mitigate impact of outliers, large squared errors over test samples were clipped — see Appendix B.2.2.2 for details). For each dataset, mean and standard deviation of train and test errors, taken over the different one-vs-all prediction tasks, are reported. Notice that all errors are not far from 0.09 — the variance of the label — which is trivial to achieve. For further details see caption of Figure 2.3, as well as Appendix B.2.2.2.

	MNIST		Fashion-MNIST	
	Train	Test	Train	Test
Original	$3.90 \cdot 10^{-2} \pm 8.37 \cdot 10^{-3}$	$3.92 \cdot 10^{-2} \pm 8.04 \cdot 10^{-2}$	$4.09 \cdot 10^{-2} \pm 1.50 \cdot 10^{-2}$	$4.24 \cdot 10^{-2} \pm 1.58 \cdot 10^{-2}$
Rand Image	$8.88 \cdot 10^{-2} \pm 4.24 \cdot 10^{-3}$	$9.11 \cdot 10^{-2} \pm 4.80 \cdot 10^{-3}$	$8.88 \cdot 10^{-2} \pm 3.11 \cdot 10^{-5}$	$9.12 \cdot 10^{-2} \pm 2.07 \cdot 10^{-4}$
Rand Label	$8.89 \cdot 10^{-2} \pm 4.22 \cdot 10^{-3}$	$9.09 \cdot 10^{-2} \pm 4.77 \cdot 10^{-3}$	$8.88 \cdot 10^{-2} \pm 7.46 \cdot 10^{-5}$	$9.11 \cdot 10^{-2} \pm 2.23 \cdot 10^{-4}$

reached a value lower than 10^{-8} or 10^6 iterations elapsed. For each figure, experiments were carried out with standard deviation of initialization varying over $\{0.05, 0.01, 0.005, 0.001, 0.0005, 0.0001, 0.00005\}$. Reported are representative runs illustrating the different types of dynamics encountered. To facilitate more efficient experimentation, we employed the adaptive learning scheme described in Appendix A.2.2.2.

Generating a ground truth rank R^* tensor $\mathcal{W}^* \in \mathbb{R}^{D_1 \times \dots \times D_N}$ was done as in the experiments of Section 1.4.2, *i.e.* by computing $\mathcal{W}^* = \sum_{r=1}^{R^*} \mathbf{v}_r^1 \otimes \dots \otimes \mathbf{v}_r^N$, with $\{\mathbf{v}_r^n \in \mathbb{R}^{D_n}\}_{r=1}^{R^*} \}_{n=1}^N$ drawn independently from the standard normal distribution. For convenience, the ground truth tensor was normalized to be of unit Frobenius norm. In tensor completion experiments (Figures 2.2, B.1, and B.2), the subset of observed entries was chosen uniformly at random. For tensor sensing (Figure B.3), we sampled the entries of all measurement tensors independently from a zero-mean Gaussian distribution with standard deviation 10^{-2} (ensures measurement tensors have expected square Frobenius norm of 1).

B.2.2.2 Tensor Rank as Measure of Complexity (Figure 2.3 and Table B.1)

For both MNIST and Fashion-MNIST datasets, we quantized pixels to hold either 0 or 1 by rounding grayscale values to the nearest integer. Random input datasets were created by replacing all pixels in all images with random values (0 or 1) drawn independently from the uniform distribution. Random label datasets were generated by shuffling labels according to a random permutation, separately for train and test sets.

Given a prediction task, fitting the corresponding tensor completion problem with a predictor of tensor rank k (or less) was done by minimizing the mean squared error over a k -component tensor factorization. Stochastic gradient descent, using the Adam optimizer [121] with learning rate $5 \cdot 10^{-4}$, default β_1, β_2 coefficients, and a batch size of 5000, was run until the loss reached a value lower than 10^{-8} or 10^4 iterations elapsed. For numerical stability, factorization weights were initialized near one. Namely, their initial values were sampled independently from a Gaussian distribution with mean one and standard deviation 10^{-3} . To accelerate convergence, label values (0 or 1) were scaled up by two during optimization (thereby ensuring symmetry about initialization), with predictions of resulting models scaled down by the same factor during evaluation. Results reported in Table B.1 were obtained

using the ridge regression implementation of scikit-learn [173] with $\alpha = 0.5$ (setting $\alpha = 0$, *i.e.* using unregularized linear regression, led to numerical issues due to bad conditioning of the data). Lastly, to mitigate impact of outliers, in both Figure 2.3 and Table B.1 squared errors over test samples were clipped at one, *i.e.* taken to be the minimum between one and the calculated error.

B.3 Deferred Proofs

B.3.1 Notation

For $N \in \mathbb{N}$, let $[N] := \{1, \dots, N\}$. We use $\langle \cdot, \cdot \rangle$ to denote the standard Euclidean (Frobenius) inner product between two vectors, matrices, or tensors, and $\|\cdot\|$ to denote the norm induced by it. Furthermore, we denote the outer and Kronecker products by \otimes and \circ , respectively. For a tensor $\mathcal{W} \in \mathbb{R}^{D_1 \times \dots \times D_N}$ and $n \in [N]$, we let $\llbracket \mathcal{W} \rrbracket_n$ be the mode- n matricization of \mathcal{W} , *i.e.* its arrangement as a matrix where the rows correspond to the n 'th mode and the columns correspond to all other modes (see Section 2.4 in [124]).

B.3.2 Useful Lemmas

B.3.2.1 Technical

Following are several technical lemmas, which are used throughout the proofs.

Lemma 22. For any $\mathcal{W} \in \mathbb{R}^{D_1 \times \dots \times D_N}$ and $\{\mathbf{w}^n \in \mathbb{R}^{D_n}\}_{n=1}^N$, where $D_1, \dots, D_N \in \mathbb{N}$, it holds that:

$$\left\langle \mathcal{W}, \otimes_{n'=1}^N \mathbf{w}^{n'} \right\rangle = \left\langle \llbracket \mathcal{W} \rrbracket_n \cdot \circ_{n' \neq n} \mathbf{w}^{n'}, \mathbf{w}^n \right\rangle, \quad n = 1, \dots, N.$$

Proof. To simplify presentation, we prove the equality for $n = 1$. For $n = 2, \dots, N$, an analogous computation yields the desired result. By opening up the inner product and applying straightforward computations, we conclude:

$$\begin{aligned} \left\langle \mathcal{W}, \otimes_{n'=1}^N \mathbf{w}^{n'} \right\rangle &= \sum_{i_1=1}^{D_1} \dots \sum_{i_N=1}^{D_N} (\mathcal{W})_{i_1, \dots, i_N} \cdot \prod_{n'=1}^N (\mathbf{w}^{n'})_{i_{n'}} \\ &= \sum_{i_1=1}^{D_1} (\mathbf{w}^1)_{i_1} \sum_{i_2=1}^{D_2} \dots \sum_{i_N=1}^{D_N} (\mathcal{W})_{i_1, \dots, i_N} \cdot \prod_{n'=2}^N (\mathbf{w}^{n'})_{i_{n'}} \\ &= \left\langle \llbracket \mathcal{W} \rrbracket_1 \cdot \circ_{n'=2}^N \mathbf{w}^{n'}, \mathbf{w}^1 \right\rangle. \end{aligned}$$

□

Lemma 23. For any $\{\mathbf{a}^n \in \mathbb{R}^{D_n}\}_{n=1}^N, \{\mathbf{b}^n \in \mathbb{R}^{D_n}\}_{n=1}^N$, where $D_1, \dots, D_N \in \mathbb{N}$, it holds that:

$$\left\| \otimes_{n=1}^N \mathbf{a}^n - \otimes_{n=1}^N \mathbf{b}^n \right\| \leq \sum_{n=1}^N \|\mathbf{a}^n - \mathbf{b}^n\| \cdot \prod_{n' \neq n} \max \left\{ \|\mathbf{a}^{n'}\|, \|\mathbf{b}^{n'}\| \right\}.$$

Proof. The proof is by induction over $N \in \mathbb{N}$. For $N = 1$, the claim is trivial. Assuming it holds for $N - 1 \geq 1$, we show that it holds for N as well:

$$\begin{aligned} \left\| \otimes_{n=1}^N \mathbf{a}^n - \otimes_{n=1}^N \mathbf{b}^n \right\| &= \left\| \otimes_{n=1}^N \mathbf{a}^n - \left(\otimes_{n=1}^{N-1} \mathbf{a}^n \right) \otimes \mathbf{b}^N + \left(\otimes_{n=1}^{N-1} \mathbf{a}^n \right) \otimes \mathbf{b}^N - \otimes_{n=1}^N \mathbf{b}^n \right\| \\ &\leq \left\| \mathbf{a}^N - \mathbf{b}^N \right\| \cdot \left\| \otimes_{n=1}^{N-1} \mathbf{a}^n \right\| + \left\| \otimes_{n=1}^{N-1} \mathbf{a}^n - \otimes_{n=1}^{N-1} \mathbf{b}^n \right\| \cdot \left\| \mathbf{b}^N \right\| \\ &\leq \left\| \mathbf{a}^N - \mathbf{b}^N \right\| \cdot \prod_{n=1}^{N-1} \max \{ \|\mathbf{a}^n\|, \|\mathbf{b}^n\| \} \\ &\quad + \left\| \otimes_{n=1}^{N-1} \mathbf{a}^n - \otimes_{n=1}^{N-1} \mathbf{b}^n \right\| \cdot \max \{ \|\mathbf{a}^N\|, \|\mathbf{b}^N\| \}. \end{aligned}$$

The proof concludes by the inductive assumption for $N - 1$. \square

Lemma 24. Let $B_{\|\cdot\|}, B_{dist} > 0$ and $\{\mathbf{a}_r^n \in \mathbb{R}^{D_n}\}_{r=1, n=1}^R, \{\mathbf{b}_r^n \in \mathbb{R}^{D_n}\}_{r=1, n=1}^R$, where $D_1, \dots, D_N \in \mathbb{N}$, such that $\max\{\|\mathbf{a}_r^n\|, \|\mathbf{b}_r^n\|\}_{r=1, n=1}^R \leq B_{\|\cdot\|}$ and $(\sum_{r=1}^R \sum_{n=1}^N \|\mathbf{a}_r^n - \mathbf{b}_r^n\|^2)^{1/2} \leq B_{dist}$. Then:

$$\left\| \sum_{r=1}^R \otimes_{n=1}^N \mathbf{a}_r^n - \sum_{r=1}^R \otimes_{n=1}^N \mathbf{b}_r^n \right\| \leq \sqrt{RN} B_{\|\cdot\|}^{N-1} B_{dist}.$$

Proof. Applying the triangle inequality and Lemma 23, we have that:

$$\begin{aligned} \left\| \sum_{r=1}^R \otimes_{n=1}^N \mathbf{a}_r^n - \sum_{r=1}^R \otimes_{n=1}^N \mathbf{b}_r^n \right\| &\leq \sum_{r=1}^R \left\| \otimes_{n=1}^N \mathbf{a}_r^n - \otimes_{n=1}^N \mathbf{b}_r^n \right\| \\ &\leq \sum_{r=1}^R \sum_{n=1}^N \|\mathbf{a}_r^n - \mathbf{b}_r^n\| \cdot \prod_{n' \neq n} \max \{ \|\mathbf{a}_r^{n'}\|, \|\mathbf{b}_r^{n'}\| \} \\ &\leq B_{\|\cdot\|}^{N-1} \sum_{r=1}^R \sum_{n=1}^N \|\mathbf{a}_r^n - \mathbf{b}_r^n\|. \end{aligned}$$

The desired result readily follows from the fact that $\|\mathbf{x}\|_1 \leq \sqrt{D} \cdot \|\mathbf{x}\|$ for any $\mathbf{x} \in \mathbb{R}^D$:

$$\begin{aligned} \left\| \sum_{r=1}^R \otimes_{n=1}^N \mathbf{a}_r^n - \sum_{r=1}^R \otimes_{n=1}^N \mathbf{b}_r^n \right\| &\leq B_{\|\cdot\|}^{N-1} \sum_{r=1}^R \sum_{n=1}^N \|\mathbf{a}_r^n - \mathbf{b}_r^n\| \\ &\leq B_{\|\cdot\|}^{N-1} \sqrt{RN} \left(\sum_{r=1}^R \sum_{n=1}^N \|\mathbf{a}_r^n - \mathbf{b}_r^n\|^2 \right)^{1/2} \\ &\leq \sqrt{RN} B_{\|\cdot\|}^{N-1} B_{dist}. \end{aligned}$$

\square

Lemma 25. Let $f : [0, T_2) \rightarrow \mathbb{R}$ and $g : [0, T_1) \rightarrow \mathbb{R}$ be continuous functions, where $T_1 < T_2$. Suppose that $g(t)$ is bounded, $f(0) > 0$, and:

$$\frac{d}{dt} f(t) = f(t)^p \cdot g(t) \quad , \quad t \in [0, T_1), \quad (\text{B.1})$$

for $1 < p \in \mathbb{R}$. Then, $f(t) > 0$ for all $t \in [0, T_1]$.

Proof. Consider the initial value problem induced by Equation (B.1) over the interval $[0, T_1)$, with an initial value of $f(0)$. One can verify by differentiation that it is solved

by:

$$h(t) = \left(f(0)^{1-p} - (p-1) \int_{t'=0}^t g(t') dt' \right)^{-\frac{1}{p-1}}.$$

Since the problem has a unique solution (see, e.g., Theorem 2.2 in [203]), it follows that for any $t \in [0, T_1]$:²

$$\begin{aligned} f(t) &= h(t) \\ &= \left(f(0)^{1-p} - (p-1) \int_{t'=0}^t g(t') dt' \right)^{-\frac{1}{p-1}} \\ &\geq \left(f(0)^{1-p} + (p-1) \int_{t'=0}^t |g(t')| dt' \right)^{-\frac{1}{p-1}}. \end{aligned}$$

Recall that $g(t)$ is bounded. Hence, from the inequality above and continuity of $f(\cdot)$ we conclude:

$$f(t) \geq \left(f(0)^{1-p} + (p-1) \cdot \sup_{t' \in [0, T_1]} |g(t')| \cdot T_1 \right)^{-\frac{1}{p-1}} > 0, \quad t \in [0, T_1].$$

□

Lemma 26. Let $\theta, \theta' : [0, T] \rightarrow \mathbb{R}^D$, where $T > 0$, be two curves born from gradient flow over a continuously differentiable function $f : \mathbb{R}^D \rightarrow \mathbb{R}$:

$$\begin{aligned} \theta(0) &= \theta_0 \in \mathbb{R}^D, & \frac{d}{dt} \theta(t) &= -\nabla f(\theta(t)), \quad t \in [0, T], \\ \theta'(0) &= \theta'_0 \in \mathbb{R}^D, & \frac{d}{dt} \theta'(t) &= -\nabla f(\theta'(t)), \quad t \in [0, T]. \end{aligned}$$

Let $B > 0$, and suppose that $f(\cdot)$ is β -smooth over \mathcal{D}_{B+1} for some $\beta \geq 0$,³ where $\mathcal{D}_{B+1} := \{\theta \in \mathbb{R}^d : \|\theta\| \leq B+1\}$. Then, if $\|\theta(0) - \theta'(0)\| < \exp(-\beta \cdot T)$, it holds that:

$$\|\theta(t) - \theta'(t)\| \leq \|\theta(0) - \theta'(0)\| \cdot \exp(\beta \cdot t) \quad (\text{B.2})$$

at least until $t \geq T$ or $\|\theta'(t)\| \geq B$. That is, Equation (B.2) holds for all $t \in [0, \min\{T, T_B\}]$, where $T_B := \inf\{t \geq 0 : \|\theta'(t)\| \geq B\}$.

Proof. If $\|\theta'(0)\| \geq B$, the claim trivially holds. Suppose $\|\theta'(0)\| < B$, and notice that in this case $\|\theta(0)\| < \|\theta'(0)\| + \exp(-\beta \cdot T) < B+1$. We examine the initial time at which $\|\theta'(t)\| \geq B$ or $\|\theta(t)\| \geq B+1$. That is, let:

$$\bar{T}_B := \inf \{t \in [0, T] : \|\theta'(t)\| \geq B \text{ or } \|\theta(t)\| \geq B+1\},$$

where we take $\bar{T}_B := T$ if the set is empty. Since both $\|\theta'(t)\|$ and $\|\theta(t)\|$ are continuous in t , it must be that $\bar{T}_B > 0$. Furthermore, $\|\theta'(t)\| \leq B$ and $\|\theta(t)\| \leq B+1$ for all $t \in [0, \bar{T}_B]$.

²A technical subtlety is that, in principle, $h(\cdot)$ may asymptote at some $\bar{T}_1 \in [0, T_1)$. However, since the initial value problem has a unique solution, $f(t) = h(t)$ until that time. This means $h(\cdot)$ cannot asymptote before T_1 as that would contradict continuity of $f(\cdot)$ over $[0, T_2)$.

³That is, for any $\theta_1, \theta_2 \in \mathcal{D}_{B+1}$ it holds that $\|\nabla f(\theta_1) - \nabla f(\theta_2)\| \leq \beta \cdot \|\theta_1 - \theta_2\|$.

Now, define the function $g : [0, T] \rightarrow \mathbb{R}_{\geq 0}$ by $g(t) := \|\theta(t) - \theta'(t)\|^2$. For any $t \in [0, \bar{T}_B]$ it holds that:

$$\begin{aligned} \frac{d}{dt}g(t) &= 2 \left\langle \theta(t) - \theta'(t), \frac{d}{dt}\theta(t) - \frac{d}{dt}\theta'(t) \right\rangle \\ &= -2 \left\langle \theta(t) - \theta'(t), \nabla f(\theta(t)) - \nabla f(\theta'(t)) \right\rangle. \end{aligned}$$

By the Cauchy-Schwartz inequality and β -smoothness of $f(\cdot)$ over \mathcal{D}_{B+1} we have:

$$\frac{d}{dt}g(t) \leq 2\beta \cdot \|\theta(t) - \theta'(t)\|^2 = 2\beta \cdot g(t). \quad (\text{B.3})$$

Thus, Gronwall's inequality leads to $g(t) \leq g(0) \cdot \exp(2\beta \cdot t)$. Taking the square root of both sides then establishes Equation (B.2) for all $t \in [0, \bar{T}_B]$.

If $\bar{T}_B = T$, the proof concludes since Equation (B.2) holds over $[0, T]$. Otherwise, if $\bar{T}_B < T$, then either $\|\theta'(\bar{T}_B)\| = B$ or $\|\theta(\bar{T}_B)\| = B + 1$. It suffices to show that in both cases $T_B \leq \bar{T}_B$. In case $\|\theta'(\bar{T}_B)\| = B$, the definition of T_B implies $T_B = \bar{T}_B$. On the other hand, suppose $\|\theta(\bar{T}_B)\| = B + 1$. Since $\|\theta(0) - \theta'(0)\| < \exp(-\beta \cdot T)$, the fact that Equation (B.2) holds for \bar{T}_B gives $\|\theta(\bar{T}_B) - \theta'(\bar{T}_B)\| \leq 1$. Therefore, it must be that $\|\theta'(\bar{T}_B)\| \geq B$, and so $T_B \leq \bar{T}_B$, completing the proof. \square

B.3.2.2 Tensor Factorization

Suppose that we minimize the objective $\phi_T(\cdot)$ (Equations (2.2) and (2.3)) via gradient flow over an R -component tensor factorization (Equation (2.4)), where we allow the loss $\mathcal{L}_T(\cdot)$ in Equation (2.2) to be any differentiable and locally smooth function. Under this setting, the following lemmas establish several results which will be of use when proving the main theorems.

Lemma 27. For any $\{\mathbf{w}_r^n \in \mathbb{R}^{D_n}\}_{r=1, n=1}^{R, N}$:

$$\frac{\partial}{\partial \mathbf{w}_r^n} \phi_T \left(\{\mathbf{w}_{r'}^{n'}\}_{r'=1, n'=1}^{R, N} \right) = \llbracket \nabla \mathcal{L}_T(\mathcal{W}_T) \rrbracket_n \circ_{n' \neq n} \mathbf{w}_r^{n'} \quad , \quad r = 1, \dots, R, \quad n = 1, \dots, N,$$

where \mathcal{W}_T denotes the end tensor (Equation (2.3)) induced by $\{\mathbf{w}_r^n\}_{r=1, n=1}^{R, N}$.

Proof. For $r \in [R], n \in [N]$, we treat $\{\mathbf{w}_{r'}^{n'}\}_{(r', n') \neq (r, n)}$ as fixed, and with slight abuse of notation consider:

$$\phi_{r,n}(\mathbf{w}_r^n) := \phi_T \left(\{\mathbf{w}_{r'}^{n'}\}_{r'=1, n'=1}^{R, N} \right).$$

For $\Delta \in \mathbb{R}^{D_n}$, from the first order Taylor approximation of $\mathcal{L}_T(\cdot)$ we have that:

$$\begin{aligned} \phi_{r,n}(\mathbf{w}_r^n + \Delta) &= \mathcal{L}_T \left(\mathcal{W}_T + \left(\otimes_{n'=1}^{n-1} \mathbf{w}_r^{n'} \right) \otimes \Delta \otimes \left(\otimes_{n'=n+1}^N \mathbf{w}_r^{n'} \right) \right) \\ &= \mathcal{L}_T(\mathcal{W}_T) + \left\langle \nabla \mathcal{L}_T(\mathcal{W}_T), \left(\otimes_{n'=1}^{n-1} \mathbf{w}_r^{n'} \right) \otimes \Delta \otimes \left(\otimes_{n'=n+1}^N \mathbf{w}_r^{n'} \right) \right\rangle \\ &\quad + o(\|\Delta\|). \end{aligned}$$

Since $\mathcal{L}_T(\mathcal{W}_T) = \phi_{r,n}(\mathbf{w}_r^n)$, by applying Lemma 22 we arrive at:

$$\phi_{r,n}(\mathbf{w}_r^n + \Delta) = \phi_{r,n}(\mathbf{w}_r^n) + \left\langle \llbracket \nabla \mathcal{L}_T(\mathcal{W}_T) \rrbracket_n \circ_{n' \neq n} \mathbf{w}_r^{n'}, \Delta \right\rangle + o(\|\Delta\|).$$

Uniqueness of the linear approximation of $\phi_{r,n}(\cdot)$ at \mathbf{w}_r^n then implies:

$$\frac{\partial}{\partial \mathbf{w}_r^n} \phi_{\Gamma} \left(\{\mathbf{w}_{r'}^{n'}\}_{r'=1}^R \}_{n'=1}^N \right) = \frac{d}{d \mathbf{w}_r^n} \phi_{r,n}(\mathbf{w}_r^n) = \llbracket \nabla \mathcal{L}_{\Gamma}(\mathcal{W}_{\Gamma}) \rrbracket_n \cdot \circ_{n' \neq n} \mathbf{w}_r^{n'}.$$

□

Lemma 28. For any $r \in [R]$ and $n \in [N]$:

$$\frac{d}{dt} \|\mathbf{w}_r^n(t)\|^2 = -2 \left\langle \nabla \mathcal{L}_{\Gamma}(\mathcal{W}_{\Gamma}(t)), \otimes_{n'=1}^N \mathbf{w}_r^{n'}(t) \right\rangle.$$

Proof. Fix $r \in [R]$ and $n \in [N]$. Differentiating $\|\mathbf{w}_r^n(t)\|^2$ with respect to time, we have:

$$\frac{d}{dt} \|\mathbf{w}_r^n(t)\|^2 = 2 \left\langle \mathbf{w}_r^n(t), \frac{d}{dt} \mathbf{w}_r^n(t) \right\rangle = -2 \left\langle \mathbf{w}_r^n(t), \frac{\partial}{\partial \mathbf{w}_r^n} \phi_{\Gamma} \left(\{\mathbf{w}_{r'}^{n'}(t)\}_{r'=1}^R \}_{n'=1}^N \right) \right\rangle.$$

Applying Lemmas 27 and 22 completes the proof. □

Lemma 29 (Lemma 1 restated). For all $r \in [R]$ and $n, \bar{n} \in [N]$:

$$\|\mathbf{w}_r^n(t)\|^2 - \|\mathbf{w}_r^{\bar{n}}(t)\|^2 = \|\mathbf{w}_r^n(0)\|^2 - \|\mathbf{w}_r^{\bar{n}}(0)\|^2, \quad t \geq 0.$$

Proof of Lemma 29. For any $r \in [R]$ and $n, \bar{n} \in [N]$, by Lemma 28 it holds that:

$$\frac{d}{dt} \|\mathbf{w}_r^n(t)\|^2 = -2 \left\langle \nabla \mathcal{L}_{\Gamma}(\mathcal{W}_{\Gamma}(t)), \otimes_{n'=1}^N \mathbf{w}_r^{n'}(t) \right\rangle = \frac{d}{dt} \|\mathbf{w}_r^{\bar{n}}(t)\|^2.$$

Integrating both sides with respect to time gives:

$$\|\mathbf{w}_r^n(t)\|^2 - \|\mathbf{w}_r^n(0)\|^2 = \|\mathbf{w}_r^{\bar{n}}(t)\|^2 - \|\mathbf{w}_r^{\bar{n}}(0)\|^2.$$

Rearranging the equality above establishes the desired result. □

Lemma 30. Let $\tilde{R} > R$, and define:

$$\tilde{\mathbf{w}}_r^n(t) := \begin{cases} \mathbf{w}_r^n(t) & , r \in \{1, \dots, R\} \\ 0 \in \mathbb{R}^{D_n} & , r \in \{R+1, \dots, \tilde{R}\} \end{cases}, \quad t \geq 0, \quad n = 1, \dots, N. \quad (\text{B.4})$$

Then, $\{\tilde{\mathbf{w}}_r^n(t)\}_{r=1}^{\tilde{R}} \}_{n=1}^N$ follow a gradient flow path of an \tilde{R} -component factorization.

Proof. We verify that $\{\tilde{\mathbf{w}}_r^n(t)\}_{r=1}^{\tilde{R}} \}_{n=1}^N$ satisfy the differential equations governing gradient flow. Fix $n \in [N]$. For any $r \in [R]$ and $t \geq 0$ we have:

$$\frac{d}{dt} \tilde{\mathbf{w}}_r^n(t) = \frac{d}{dt} \mathbf{w}_r^n(t) = -\frac{\partial}{\partial \mathbf{w}_r^n} \phi_{\Gamma} \left(\{\mathbf{w}_{r'}^{n'}(t)\}_{r'=1}^R \}_{n'=1}^N \right).$$

Noticing that $\mathcal{W}_T(t) = \sum_{r'=1}^R \otimes_{n'=1}^N \mathbf{w}_{r'}^{n'}(t) = \sum_{r'=1}^{\tilde{R}} \otimes_{n'=1}^N \tilde{\mathbf{w}}_{r'}^{n'}(t) := \tilde{\mathcal{W}}_T(t)$, and invoking Lemma 27, we may write:

$$\begin{aligned} \frac{d}{dt} \tilde{\mathbf{w}}_r^n(t) &= - \left[\nabla \mathcal{L}_T(\mathcal{W}_T(t)) \right]_n \cdot \circ_{n' \neq n} \mathbf{w}_{r'}^{n'}(t) \\ &= - \left[\nabla \mathcal{L}_T(\tilde{\mathcal{W}}_T(t)) \right]_n \cdot \circ_{n' \neq n} \tilde{\mathbf{w}}_{r'}^{n'}(t) \\ &= - \frac{\partial}{\partial \tilde{\mathbf{w}}_r^n} \phi_T \left(\{ \tilde{\mathbf{w}}_{r'}^{n'}(t) \}_{r'=1, n'=1}^{\tilde{R}, N} \right). \end{aligned}$$

On the other hand, for any $r \in \{R+1, \dots, \tilde{R}\}$, recalling that $\tilde{\mathbf{w}}_r^n(t)$ is identically zero:

$$\frac{d}{dt} \tilde{\mathbf{w}}_r^n(t) = 0 = - \left[\nabla \mathcal{L}_T(\tilde{\mathcal{W}}_T(t)) \right]_n \cdot \circ_{n' \neq n} \tilde{\mathbf{w}}_{r'}^{n'}(t) = - \frac{\partial}{\partial \tilde{\mathbf{w}}_r^n} \phi_T \left(\{ \tilde{\mathbf{w}}_{r'}^{n'}(t) \}_{r'=1, n'=1}^{\tilde{R}, N} \right),$$

for all $t \geq 0$, completing the proof. \square

Lemma 31. For any $r \in [R]$:

- If $\|\mathbf{w}_r^1(0)\| = \dots = \|\mathbf{w}_r^N(0)\| = 0$, then:

$$\|\mathbf{w}_r^1(t)\| = \dots = \|\mathbf{w}_r^N(t)\| = 0 \quad , \quad t \geq 0. \quad (\text{B.5})$$

- On the other hand, if $\|\mathbf{w}_r^1(0)\| = \dots = \|\mathbf{w}_r^N(0)\| > 0$, then:

$$\|\mathbf{w}_r^1(t)\| = \dots = \|\mathbf{w}_r^N(t)\| > 0 \quad , \quad t \geq 0. \quad (\text{B.6})$$

Proof. The proof is divided into two separate parts, establishing Equations (B.5) and (B.6) under their respective conditions.

Proof of Equation (B.5) (if $\|\mathbf{w}_r^1(0)\| = \dots = \|\mathbf{w}_r^N(0)\| = 0$): To simplify presentation, we assume without loss of generality that $r = R$. Consider the following initial value problem induced by gradient flow over $\phi_T(\cdot)$:

$$\begin{aligned} \tilde{\mathbf{w}}_{\bar{r}}^n(0) &= \mathbf{w}_{\bar{r}}^n(0) \quad , \quad \bar{r} = 1, \dots, R, \quad n = 1, \dots, N, \\ \frac{d}{dt} \tilde{\mathbf{w}}_{\bar{r}}^n(t) &= - \frac{\partial}{\partial \tilde{\mathbf{w}}_{\bar{r}}^n} \phi_T \left(\{ \tilde{\mathbf{w}}_{r'}^{n'}(t) \}_{r'=1, n'=1}^R, N \right) \quad , \quad t \geq 0, \quad \bar{r} = 1, \dots, R, \quad n = 1, \dots, N. \end{aligned} \quad (\text{B.7})$$

By definition, $\{ \mathbf{w}_{\bar{r}}^n(t) \}_{\bar{r}=1, n=1}^R, N$ is a solution to the initial value problem above. Since it has a unique solution (see, e.g., Theorem 2.2 in [203]), we need only show that there exist $\{ \tilde{\mathbf{w}}_{\bar{r}}^n(t) \}_{\bar{r}=1, n=1}^R, N$ satisfying Equation (B.7) such that $\tilde{\mathbf{w}}_R^1(t) = \dots = \tilde{\mathbf{w}}_R^N(t) = 0$ for all $t \geq 0$.

If $R = 1$, i.e. the factorization consists of a single component, by Lemma 27:

$$- \frac{\partial}{\partial \tilde{\mathbf{w}}_1^n} \phi_T \left(\{ \tilde{\mathbf{w}}_1^{n'} \}_{n'=1}^N \right) = - \left[\nabla \mathcal{L}_T \left(\otimes_{n'=1}^N \tilde{\mathbf{w}}_1^{n'} \right) \right]_n \cdot \circ_{n' \neq n} \tilde{\mathbf{w}}_1^{n'} \quad , \quad n = 1, \dots, N,$$

for any $\tilde{\mathbf{w}}_1^1 \in \mathbb{R}^{D_1}, \dots, \tilde{\mathbf{w}}_1^N \in \mathbb{R}^{D_N}$. Hence, $\tilde{\mathbf{w}}_1^1(t) = \dots = \tilde{\mathbf{w}}_1^N(t) = 0$ for all $t \geq 0$ form a solution to the initial value problem in Equation (B.7). To see it is so, notice

that the initial conditions are met, and:

$$\frac{d}{dt} \tilde{\mathbf{w}}_1^n(t) = 0 = -\frac{\partial}{\partial \tilde{\mathbf{w}}_1^n} \phi_{\mathbb{T}} \left(\{ \tilde{\mathbf{w}}_1^{n'}(t) \}_{n'=1}^N \right) \quad , \quad t \geq 0, \quad n = 1, \dots, N.$$

If $R > 1$, with slight abuse of notation we let $\phi_{\mathbb{T}}(\{ \tilde{\mathbf{w}}_{\bar{r}}^n \}_{\bar{r}=1}^{R-1} \otimes_{n=1}^N \tilde{\mathbf{w}}_{\bar{r}}^n)$ be the objective over an $(R-1)$ -component tensor factorization. Let $\{ \tilde{\mathbf{w}}_{\bar{r}}^n(t) \}_{\bar{r}=1}^{R-1} \otimes_{n=1}^N$ be curves obtained by running gradient flow on this objective, initialized such that:

$$\tilde{\mathbf{w}}_{\bar{r}}^n(0) := \mathbf{w}_{\bar{r}}^n(0) \quad , \quad \bar{r} = 1, \dots, R-1, \quad n = 1, \dots, N.$$

Additionally, define $\tilde{\mathbf{w}}_R^1(t) = \dots = \tilde{\mathbf{w}}_R^N(t) = 0$ for all $t \geq 0$. According to Lemma 30, $\{ \tilde{\mathbf{w}}_{\bar{r}}^n(t) \}_{\bar{r}=1}^{R-1} \otimes_{n=1}^N$ form a valid solution to the original gradient flow over an R -component factorization, *i.e.* satisfy Equation (B.7). Thus, uniqueness of the solution implies $\mathbf{w}_R^1(t) = \dots = \mathbf{w}_R^N(t) = 0$ for all $t \geq 0$, completing the proof for Equation (B.5).

Proof of Equation (B.6) (if $\|\mathbf{w}_r^1(0)\| = \dots = \|\mathbf{w}_r^N(0)\| > 0$): From Lemma 1 it follows that $\|\mathbf{w}_r^1(t)\| = \dots = \|\mathbf{w}_r^N(t)\|$ for any $t \geq 0$. Hence, it suffices to show that $\|\mathbf{w}_r^1(t)\|$ stays positive. Assume by way of contradiction that there exists $\bar{t} > 0$ for which $\|\mathbf{w}_r^1(\bar{t})\| = 0$. Define:

$$t_0 := \inf \left\{ t \geq 0 : \|\mathbf{w}_r^1(t)\| = 0 \right\} ,$$

the initial time at which $\|\mathbf{w}_r^1(t)\|$ meets zero. Due to the fact that $\|\mathbf{w}_r^1(t)\|$ is continuous in t , $\|\mathbf{w}_r^1(t_0)\| = 0$ and $t_0 > 0$. Furthermore, $\|\mathbf{w}_r^1(t)\| > 0$ for all $t \in [0, t_0)$. We may therefore differentiate $\|\mathbf{w}_r^1(t)\|$ with respect to time over the interval $[0, t_0)$ as follows:

$$\begin{aligned} \frac{d}{dt} \|\mathbf{w}_r^1(t)\| &= \left(\frac{d}{dt} \|\mathbf{w}_r^1(t)\|^2 \right) \cdot 2^{-1} \|\mathbf{w}_r^1(t)\|^{-1} \\ &= \|\mathbf{w}_r^1(t)\|^{-1} \left\langle -\nabla \mathcal{L}_{\mathbb{T}}(\mathcal{W}_{\mathbb{T}}(t)), \otimes_{n=1}^N \mathbf{w}_r^n(t) \right\rangle \\ &= \|\mathbf{w}_r^1(t)\|^{N-1} \left\langle -\nabla \mathcal{L}_{\mathbb{T}}(\mathcal{W}_{\mathbb{T}}(t)), \otimes_{n=1}^N \widehat{\mathbf{w}}_r^n(t) \right\rangle , \end{aligned}$$

where the second transition is due to Lemma 28, and $\widehat{\mathbf{w}}_r^n(t) := \mathbf{w}_r^n(t) / \|\mathbf{w}_r^n(t)\|$ for $n = 1, \dots, N$. Define $g(t) := \left\langle -\nabla \mathcal{L}_{\mathbb{T}}(\mathcal{W}_{\mathbb{T}}(t)), \otimes_{n=1}^N \widehat{\mathbf{w}}_r^n(t) \right\rangle$. Since $\nabla \mathcal{L}_{\mathbb{T}}(\mathcal{W}_{\mathbb{T}}(t))$ is continuous with respect to time, $g(t)$ is bounded over $[0, t_0]$ and continuous over $[0, t_0)$. Thus, invoking Lemma 25 with $g(t)$, $T_1 := t_0$ and $f(t) := \|\mathbf{w}_r^1(t)\|$, we get that $\|\mathbf{w}_r^1(t)\| > 0$ for all $t \in [0, t_0]$, in contradiction to $\|\mathbf{w}_r^1(t_0)\| = 0$. This means that $\|\mathbf{w}_r^1(t)\| > 0$ for all $t \geq 0$, concluding the proof for Equation (B.6). \square

B.3.3 Proof of Theorem 3

Fix $r \in [R]$ and $t \geq 0$. Since $\|\otimes_{n=1}^N \mathbf{w}_r^n(t)\| = \prod_{n=1}^N \|\mathbf{w}_r^n(t)\|$, the product rule gives:

$$\frac{d}{dt} \|\otimes_{n=1}^N \mathbf{w}_r^n(t)\| = \sum_{n=1}^N \frac{d}{dt} \|\mathbf{w}_r^n(t)\| \cdot \prod_{n' \neq n} \|\mathbf{w}_r^{n'}(t)\| .$$

Notice that for any $n \in [N]$ we have $\|\mathbf{w}_r^n(t)\| > 0$, as otherwise $\|\otimes_{n'=1}^N \mathbf{w}_r^{n'}(t)\|$ must be zero. Thus, applying Lemma 28 we get $\frac{d}{dt} \|\mathbf{w}_r^n(t)\| = \frac{1}{2} \|\mathbf{w}_r^n(t)\|^{-1} \frac{d}{dt} \|\mathbf{w}_r^n(t)\|^2 = \|\mathbf{w}_r^n(t)\|^{-1} \langle -\nabla \mathcal{L}_T(\mathcal{W}_T(t)), \otimes_{n'=1}^N \mathbf{w}_r^{n'}(t) \rangle$. Combined with the equation above, we arrive at:

$$\begin{aligned} \frac{d}{dt} \|\otimes_{n=1}^N \mathbf{w}_r^n(t)\| &= \sum_{n=1}^N \|\mathbf{w}_r^n(t)\|^{-1} \left\langle -\nabla \mathcal{L}_T(\mathcal{W}_T(t)), \otimes_{n'=1}^N \mathbf{w}_r^{n'}(t) \right\rangle \cdot \prod_{n' \neq n} \|\mathbf{w}_r^{n'}(t)\| \\ &= \left\langle -\nabla \mathcal{L}_T(\mathcal{W}_T(t)), \otimes_{n'=1}^N \widehat{\mathbf{w}}_r^{n'}(t) \right\rangle \cdot \sum_{n=1}^N \prod_{n' \neq n} \|\mathbf{w}_r^{n'}(t)\|^2. \end{aligned} \quad (\text{B.8})$$

By Lemma 1, the differences between squared norms of vectors in the same component are constant through time. In particular, the unbalancedness magnitude (Definition 3) is conserved during gradient flow, implying that for any $n \in [N]$:

$$\|\mathbf{w}_r^n(t)\|^2 \leq \min_{n' \in [N]} \|\mathbf{w}_r^{n'}(t)\|^2 + \epsilon \leq \|\otimes_{n'=1}^N \mathbf{w}_r^{n'}(t)\|^{\frac{2}{N}} + \epsilon. \quad (\text{B.9})$$

Now, suppose that $\gamma_r(t) := \langle -\nabla \mathcal{L}_T(\mathcal{W}_T(t)), \otimes_{n=1}^N \widehat{\mathbf{w}}_r^n(t) \rangle \geq 0$. Going back to Equation (B.8), applying the inequality in Equation (B.9) for each $\|\mathbf{w}_r^{n'}(t)\|^2$ yields the desired upper bound from Equation (2.5). On the other hand, multiplying and dividing each summand in Equation (B.8) by the corresponding $\|\mathbf{w}_r^n(t)\|^2$, we may equivalently write:

$$\begin{aligned} \frac{d}{dt} \|\otimes_{n=1}^N \mathbf{w}_r^n(t)\| &= \left\langle -\nabla \mathcal{L}_T(\mathcal{W}_T(t)), \otimes_{n'=1}^N \widehat{\mathbf{w}}_r^{n'}(t) \right\rangle \cdot \sum_{n=1}^N \|\mathbf{w}_r^n(t)\|^{-2} \prod_{n'=1}^N \|\mathbf{w}_r^{n'}(t)\|^2 \\ &= \left\langle -\nabla \mathcal{L}_T(\mathcal{W}_T(t)), \otimes_{n'=1}^N \widehat{\mathbf{w}}_r^{n'}(t) \right\rangle \|\otimes_{n=1}^N \mathbf{w}_r^n(t)\|^2 \cdot \sum_{n=1}^N \|\mathbf{w}_r^n(t)\|^{-2}. \end{aligned}$$

Noticing that Equation (B.9) implies $\|\mathbf{w}_r^n(t)\|^{-2} \geq (\|\otimes_{n'=1}^N \mathbf{w}_r^{n'}(t)\|^{\frac{2}{N}} + \epsilon)^{-1}$, the lower bound from Equation (2.5) readily follows.

If $\gamma_r(t) < 0$, Equation (2.6) is established by following the same computations, up to differences in the direction of inequalities due to the negativity of $\gamma_r(t)$. \square

B.3.4 Proof of Corollary 2

Fix $r \in [R]$ and $t \geq 0$. The lower and upper bounds in Theorem 3 are equal to $N\gamma_r(t) \cdot \|\otimes_{n=1}^N \mathbf{w}_r^n(t)\|^{2-2/N}$ for unbalancedness magnitude $\epsilon = 0$. Therefore, if $\|\otimes_{n=1}^N \mathbf{w}_r^n(t)\| > 0$, Equation (2.7) immediately follows from Theorem 3.

If $\|\otimes_{n=1}^N \mathbf{w}_r^n(t)\| = 0$, we claim that necessarily $\|\otimes_{n=1}^N \mathbf{w}_r^n(t')\| = 0$ for all $t' \geq 0$, in which case both sides of Equation (2.7) are zero. Indeed, since the unbalancedness magnitude is zero at initialization and $\|\otimes_{n=1}^N \mathbf{w}_r^n(t)\| = \prod_{n=1}^N \|\mathbf{w}_r^n(t)\|$, by Lemma 31 we know that either $\|\otimes_{n=1}^N \mathbf{w}_r^n(t')\| = 0$ for all $t' \geq 0$, or $\|\otimes_{n=1}^N \mathbf{w}_r^n(t')\| > 0$ for all $t' \geq 0$. Hence, given that $\|\otimes_{n=1}^N \mathbf{w}_r^n(t)\| = 0$, the norm of the component must be identically zero through time. \square

B.3.5 Proof of Theorem 4

For conciseness, we consider the case where the number of components $R \geq 2$. For $R = 1$, existence of a time $T_0 > 0$ at which $\mathcal{W}_T(T_0) \in \mathcal{S}$ follows by analogous steps, disregarding parts pertaining to factorization components $2, \dots, R$. Furthermore, proximity to a balanced rank one trajectory becomes trivial as, by Assumption 2 and Lemma 1, $\mathcal{W}_T(t)$ is in itself such a trajectory.

Assume without loss of generality that Assumption 3 holds for $\bar{r} = 1$.

Before delving into the proof details, let us introduce some notation and specify the exact requirement on the initialization scale α . We let $\mathcal{L}_h : \mathbb{R}^{D_1 \times \dots \times D_N} \rightarrow \mathbb{R}_{\geq 0}$ be the tensor completion objective induced by the Huber loss (Equation (2.1) with $\ell_h(\cdot)$ in place of $\ell(\cdot)$), and $\phi_h(\cdot)$ be the corresponding tensor factorization objective (Equation (2.2) with $\mathcal{L}_h(\cdot)$ in place of $\mathcal{L}_T(\cdot)$). For reference sphere radius $\rho \in (0, \min_{(i_1, \dots, i_N) \in \Omega} |y_{i_1, \dots, i_N}| - \delta_h)$, distance from origin $B > 0$, time duration $T > 0$, and degree of approximation $\epsilon \in (0, 1)$, let:

$$\begin{aligned}
\|\mathbf{a}_r\| &:= \|\mathbf{a}_r^1\| = \dots = \|\mathbf{a}_r^N\| \quad , \quad r = 1, \dots, R, \\
A &:= \max_{r \in [R]} \|\mathbf{a}_r\|, \\
A_{-1} &:= \max_{r \in \{2, \dots, R\}} \|\mathbf{a}_r\|, \\
\tilde{B} &:= \sqrt{N} (\max\{B, \rho\} + 1)^{\frac{1}{N}}, \\
\beta &:= RN \left((\tilde{B} + 1)^{2(N-1)} + \delta_h (\tilde{B} + 1)^{N-2} \right), \\
\hat{\epsilon} &< \min \left\{ 2^{-\frac{N}{2}} R^{-N} N^{-N} (\tilde{B} + 1)^{N-N^2} \cdot \exp(-N\beta T) \cdot \epsilon^N, \rho(R-1)^{-1} \right\}, \\
\tilde{\epsilon} &:= \min \left\{ \hat{\epsilon}, (R-1)^{-1} \left(\rho - \left[\rho^{\frac{1}{N}} - (R-1)^{\frac{1}{N}} \cdot \hat{\epsilon}^{\frac{1}{N}} \right]^N \right) \right\}.
\end{aligned} \tag{B.10}$$

With the constants above in place, for the results of the theorem to hold it suffices to require that:

$$\alpha < \min \left\{ R^{-\frac{1}{N}} A^{-1} \rho^{\frac{1}{N}}, \left(A_{-1}^{2-N} - \|\mathbf{a}_1\|^{2-N} \frac{\|\nabla \mathcal{L}_T(0)\|}{\langle -\nabla \mathcal{L}_T(0), \otimes_{n=1}^N \hat{\mathbf{a}}_1^n \rangle} \right)^{\frac{1}{N-2}} \cdot \tilde{\epsilon}^{\frac{1}{N}} \right\}. \tag{B.11}$$

The proof is sectioned into three parts. We begin with several preliminary lemmas in Appendix B.3.5.1. Then, Appendix B.3.5.2 establishes the existence of a time $T_0 > 0$ at which $\mathcal{W}_T(t)$ initially reaches the reference sphere \mathcal{S} , *i.e.* $\|\mathcal{W}_T(T_0)\| = \rho$, while $\|\otimes_{n=1}^N \mathbf{w}_2^n(T_0)\|, \dots, \|\otimes_{n=1}^N \mathbf{w}_R^n(T_0)\|$ are still $\mathcal{O}(\alpha^N)$. Consequently, as shown in Appendix B.3.5.3, at that time the weight vectors of the R -component tensor factorization are close to weight vectors corresponding to a balanced rank one trajectory emanating from \mathcal{S} , denoted $\mathcal{W}_1(t)$. The proof concludes by showing that this implies the time-shifted trajectory $\mathcal{W}_T(t)$ is within ϵ distance from $\mathcal{W}_1(t)$ at least until $t \geq T$ or $\|\mathcal{W}_T(t)\| \geq B$.

B.3.5.1 Preliminary Lemmas

Lemma 32. Let $\mathcal{W} \in \mathbb{R}^{D_1 \times \dots \times D_N}$ be such that $\|\mathcal{W}\| \leq \rho$, where $\rho \in (0, \min_{(i_1, \dots, i_N) \in \Omega} |y_{i_1, \dots, i_N}| - \delta_h)$. Then:

$$\nabla \mathcal{L}_h(\mathcal{W}) = \frac{\delta_h}{|\Omega|} \sum_{(i_1, \dots, i_N) \in \Omega} \text{sign}(-y_{i_1, \dots, i_N}) \cdot \mathcal{E}_{i_1, \dots, i_N},$$

where $\mathcal{E}_{i_1, \dots, i_N} \in \mathbb{R}^{D_1 \times \dots \times D_N}$ holds 1 in its (i_1, \dots, i_N) 'th entry and 0 elsewhere.

Proof. Fix $I := (i_1, \dots, i_N) \in \Omega$, and let $\ell'_h(\cdot)$ denote the derivative of $\ell_h(\cdot)$. If $y_I > 0$, we have that $(\mathcal{W})_I - y_I \leq \|\mathcal{W}\| - y_I \leq \min_{(i_1, \dots, i_N) \in \Omega} |y_{i_1, \dots, i_N}| - \delta_h - y_I \leq -\delta_h$. Therefore, $\ell'_h((\mathcal{W})_I - y_I) = -\delta_h = \text{sign}(-y_I)\delta_h$. Similarly, if $y_I < 0$, we have that $(\mathcal{W})_I - y_I \geq \delta_h$ and $\ell'_h((\mathcal{W})_I - y_I) = \delta_h = \text{sign}(-y_I)\delta_h$. Note that y_I cannot be exactly zero as, by Assumption 1, $\min_{(i_1, \dots, i_N) \in \Omega} |y_{i_1, \dots, i_N}| > \delta_h > 0$. The proof concludes by the chain rule:

$$\begin{aligned} \nabla \mathcal{L}_h(\mathcal{W}) &= \frac{1}{|\Omega|} \sum_{I \in \Omega} \ell'_h((\mathcal{W})_I - y_I) \cdot \mathcal{E}_I \\ &= \frac{\delta_h}{|\Omega|} \sum_{I \in \Omega} \text{sign}(-y_I) \cdot \mathcal{E}_I. \end{aligned}$$

□

Lemma 33. The function $\mathcal{L}_h(\cdot)$ is 1-smooth, i.e. for any $\mathcal{W}_1, \mathcal{W}_2 \in \mathbb{R}^{D_1 \times \dots \times D_N}$:

$$\|\nabla \mathcal{L}_h(\mathcal{W}_1) - \nabla \mathcal{L}_h(\mathcal{W}_2)\| \leq \|\mathcal{W}_1 - \mathcal{W}_2\|.$$

Proof. Let $\mathcal{W}_1, \mathcal{W}_2 \in \mathbb{R}^{D_1 \times \dots \times D_N}$. Denote by $\ell'_h(\cdot)$ the derivative of $\ell_h(\cdot)$, i.e.:

$$\ell'_h(z) = \begin{cases} -\delta_h & , z < -\delta_h \\ z & , |z| \leq \delta_h \\ \delta_h & , z > \delta_h, \end{cases}$$

The result readily follows from the triangle inequality and the fact that $\ell'_h(\cdot)$ is 1-Lipschitz:

$$\begin{aligned} \|\nabla \mathcal{L}_h(\mathcal{W}_1) - \nabla \mathcal{L}_h(\mathcal{W}_2)\| &= \left\| \frac{1}{|\Omega|} \sum_{I \in \Omega} [\ell'_h((\mathcal{W}_1)_I - y_I) \cdot \mathcal{E}_I - \ell'_h((\mathcal{W}_2)_I - y_I) \cdot \mathcal{E}_I] \right\| \\ &\leq \frac{1}{|\Omega|} \sum_{I \in \Omega} |\ell'_h((\mathcal{W}_1)_I - y_I) - \ell'_h((\mathcal{W}_2)_I - y_I)| \\ &\leq \frac{1}{|\Omega|} \sum_{I \in \Omega} |(\mathcal{W}_1)_I - (\mathcal{W}_2)_I| \\ &\leq \|\mathcal{W}_1 - \mathcal{W}_2\|, \end{aligned}$$

where $\mathcal{E}_I \in \mathbb{R}^{D_1 \times \dots \times D_N}$ holds 1 in its I 'th entry and 0 elsewhere, for $I = (i_1, \dots, i_N) \in \Omega$. □

Lemma 34. Let $G \geq 0$, and denote $\mathcal{D}_G := \{ \{ \mathbf{w}_r^n \in \mathbb{R}^{D_n} \}_{r=1n=1}^R : (\sum_{r=1}^R \sum_{n=1}^N \|\mathbf{w}_r^n\|^2)^{1/2} \leq G \}$. Then, the objective $\phi_h(\cdot)$ is $RN(G^{2(N-1)} + \delta_h G^{N-2})$ -smooth over \mathcal{D}_G , i.e.:

$$\begin{aligned} & \left\| \nabla \phi_h(\{ \mathbf{w}_r^n \}_{r=1n=1}^R) - \nabla \phi_h(\{ \tilde{\mathbf{w}}_r^n \}_{r=1n=1}^R) \right\| \\ & \leq RN(G^{2(N-1)} + \delta_h G^{N-2}) \cdot \sqrt{\sum_{r=1}^R \sum_{n=1}^N \|\mathbf{w}_r^n - \tilde{\mathbf{w}}_r^n\|^2}, \end{aligned}$$

for any $\{ \mathbf{w}_r^n \}_{r=1n=1}^R, \{ \tilde{\mathbf{w}}_r^n \}_{r=1n=1}^R \in \mathcal{D}_G$.

Proof. Let $\{ \mathbf{w}_r^n \}_{r=1n=1}^R, \{ \tilde{\mathbf{w}}_r^n \}_{r=1n=1}^R \in \mathcal{D}_G$. By Lemma 27 we may write:

$$\begin{aligned} & \left\| \nabla \phi_h(\{ \mathbf{w}_r^n \}_{r=1n=1}^R) - \nabla \phi_h(\{ \tilde{\mathbf{w}}_r^n \}_{r=1n=1}^R) \right\|^2 \\ & = \sum_{r=1}^R \sum_{n=1}^N \left\| \left[\nabla \mathcal{L}_h(\mathcal{W}_T) \right]_n \cdot \circ_{n' \neq n} \mathbf{w}_r^{n'} - \left[\nabla \mathcal{L}_h(\tilde{\mathcal{W}}_T) \right]_n \cdot \circ_{n' \neq n} \tilde{\mathbf{w}}_r^{n'} \right\|^2, \end{aligned} \quad (\text{B.12})$$

where \mathcal{W}_T and $\tilde{\mathcal{W}}_T$ are the end tensors (Equation (2.3)) of $\{ \mathbf{w}_r^n \}_{r=1n=1}^R$ and $\{ \tilde{\mathbf{w}}_r^n \}_{r=1n=1}^R$, respectively. We turn to bound the square root of each term in the sum. Fix $r \in [R], n \in [N]$. By the triangle inequality and sub-multiplicativity of the Frobenius norm, we have that:

$$\begin{aligned} & \left\| \left[\nabla \mathcal{L}_h(\mathcal{W}_T) \right]_n \cdot \circ_{n' \neq n} \mathbf{w}_r^{n'} - \left[\nabla \mathcal{L}_h(\tilde{\mathcal{W}}_T) \right]_n \cdot \circ_{n' \neq n} \tilde{\mathbf{w}}_r^{n'} \right\| \\ & \leq \underbrace{\left\| \left[\nabla \mathcal{L}_h(\mathcal{W}_T) \right]_n - \left[\nabla \mathcal{L}_h(\tilde{\mathcal{W}}_T) \right]_n \right\|}_{(I)} \cdot \underbrace{\left\| \circ_{n' \neq n} \mathbf{w}_r^{n'} \right\|}_{(II)} \\ & \quad + \underbrace{\left\| \left[\nabla \mathcal{L}_h(\tilde{\mathcal{W}}_T) \right]_n \right\|}_{(III)} \cdot \underbrace{\left\| \circ_{n' \neq n} \mathbf{w}_r^{n'} - \circ_{n' \neq n} \tilde{\mathbf{w}}_r^{n'} \right\|}_{(IV)}. \end{aligned}$$

Below, we derive upper bounds for (I), (II), (III), and (IV) separately. Starting with (I), by Lemma 33, the triangle inequality and Lemma 23, it follows that:

$$\begin{aligned} (I) & = \left\| \nabla \mathcal{L}_h(\mathcal{W}_T) - \nabla \mathcal{L}_h(\tilde{\mathcal{W}}_T) \right\| \\ & \leq \left\| \mathcal{W}_T - \tilde{\mathcal{W}}_T \right\| \\ & \leq \sum_{r'=1}^R \left\| \otimes_{n'=1}^N \mathbf{w}_{r'}^{n'} - \otimes_{n'=1}^N \tilde{\mathbf{w}}_{r'}^{n'} \right\| \\ & \leq G^{N-1} \sum_{r'=1}^R \sum_{n'=1}^N \left\| \mathbf{w}_{r'}^{n'} - \tilde{\mathbf{w}}_{r'}^{n'} \right\|. \end{aligned}$$

Moving on to (II), we have that $\left\| \circ_{n' \neq n} \mathbf{w}_r^{n'} \right\| = \prod_{n' \neq n} \|\mathbf{w}_r^{n'}\| \leq G^{N-1}$. For (III), the triangle inequality and the fact that $\ell'_h(\cdot)$, the derivative of $\ell_h(\cdot)$, is bounded (in absolute value) by δ_h yield:

$$(III) = \left\| \frac{1}{|\Omega|} \sum_{I \in \Omega} \ell'_h \left((\tilde{\mathcal{W}}_T)_I - y_I \right) \cdot \mathcal{E}_I \right\| \leq \delta_h,$$

where $\mathcal{E}_I \in \mathbb{R}^{D_1 \times \dots \times D_N}$ holds 1 in its I 'th entry and 0 elsewhere, for $I = (i_1, \dots, i_N) \in \Omega$. Lastly, since $\left\| \circ_{n' \neq n} \mathbf{w}_r^{n'} - \circ_{n' \neq n} \tilde{\mathbf{w}}_r^{n'} \right\| = \left\| \otimes_{n' \neq n} \mathbf{w}_r^{n'} - \otimes_{n' \neq n} \tilde{\mathbf{w}}_r^{n'} \right\|$, by Lemma 23

we have that:

$$(IV) \leq G^{N-2} \sum_{n' \neq n} \left\| \mathbf{w}_r^{n'} - \tilde{\mathbf{w}}_r^{n'} \right\| \leq G^{N-2} \sum_{n'=1}^N \left\| \mathbf{w}_r^{n'} - \tilde{\mathbf{w}}_r^{n'} \right\|.$$

Putting it all together, we arrive at the following bound:

$$\begin{aligned} & \left\| \llbracket \nabla \mathcal{L}_h(\mathcal{W}_T) \rrbracket_n \cdot \circ_{n' \neq n} \mathbf{w}_r^{n'} - \llbracket \nabla \mathcal{L}_h(\tilde{\mathcal{W}}_T) \rrbracket_n \cdot \circ_{n' \neq n} \tilde{\mathbf{w}}_r^{n'} \right\| \\ & \leq G^{2(N-1)} \sum_{r'=1}^R \sum_{n'=1}^N \left\| \mathbf{w}_{r'}^{n'} - \tilde{\mathbf{w}}_{r'}^{n'} \right\| + \delta_h G^{N-2} \sum_{n'=1}^N \left\| \mathbf{w}_r^{n'} - \tilde{\mathbf{w}}_r^{n'} \right\| \\ & \leq (G^{2(N-1)} + \delta_h G^{N-2}) \sum_{r'=1}^R \sum_{n'=1}^N \left\| \mathbf{w}_{r'}^{n'} - \tilde{\mathbf{w}}_{r'}^{n'} \right\|. \end{aligned}$$

Applying the bound above to Equation (B.12), for all $r \in [R], n \in [N]$, leads to:

$$\begin{aligned} & \left\| \nabla \phi_h \left(\{\mathbf{w}_r^n\}_{r=1}^R \sum_{n=1}^N \right) - \nabla \phi_h \left(\{\tilde{\mathbf{w}}_r^n\}_{r=1}^R \sum_{n=1}^N \right) \right\|^2 \\ & \leq RN(G^{2(N-1)} + \delta_h G^{N-2})^2 \left(\sum_{r=1}^R \sum_{n=1}^N \left\| \mathbf{w}_r^n - \tilde{\mathbf{w}}_r^n \right\| \right)^2 \\ & \leq R^2 N^2 (G^{2(N-1)} + \delta_h G^{N-2})^2 \sum_{r=1}^R \sum_{n=1}^N \left\| \mathbf{w}_r^n - \tilde{\mathbf{w}}_r^n \right\|^2, \end{aligned}$$

where the last transition is by the fact that $\|\mathbf{x}\|_1 \leq \sqrt{D} \cdot \|\mathbf{x}\|$ for any $\mathbf{x} \in \mathbb{R}^D$. Taking the square root of both sides concludes the proof. \square

Lemma 35. Let $t' > 0$ and $r \in [R]$. Denote $\gamma_r(t) := \langle -\nabla \mathcal{L}_h(\mathcal{W}_T(t)), \otimes_{n=1}^N \hat{\mathbf{w}}_r^n(t) \rangle$, where $\hat{\mathbf{w}}_r^n(t) := \mathbf{w}_r^n(t) / \|\mathbf{w}_r^n(t)\|$ if $\mathbf{w}_r^n(t) \neq 0$, and $\hat{\mathbf{w}}_r^n(t) := 0$ otherwise, for $n = 1, \dots, N$. Suppose that $\nabla \mathcal{L}_h(\mathcal{W}_T(t)) = \nabla \mathcal{L}_h(0)$ for all $t \in [0, t']$. Then, $\gamma_r(t)$ is monotonically non-decreasing over the interval $[0, t']$.

Proof. In the following, unless explicitly stated otherwise, t is to be considered in the time interval $[0, t']$.

Recall that by Assumption 2 we have that $\|\mathbf{w}_r^1(0)\| = \dots = \|\mathbf{w}_r^N(0)\|$. If $\|\mathbf{w}_r^1(0)\| = \dots = \|\mathbf{w}_r^N(0)\| = 0$, then according to Lemma 31 $\|\mathbf{w}_r^1(t)\| = \dots = \|\mathbf{w}_r^N(t)\| = 0$ for all $t \geq 0$. In this case $\gamma_r(t) = 0$ over $[0, t']$, and is therefore non-decreasing.

Otherwise, if $\|\mathbf{w}_r^1(0)\| = \dots = \|\mathbf{w}_r^N(0)\| > 0$, from Lemma 31 we get that $\|\mathbf{w}_r^1(t)\| = \dots = \|\mathbf{w}_r^N(t)\| > 0$ for all $t \geq 0$. Thus:

$$\begin{aligned} \gamma_r(t) & = \left\| \otimes_{n=1}^N \mathbf{w}_r^n(t) \right\|^{-1} \langle -\nabla \mathcal{L}_h(\mathcal{W}_T(t)), \otimes_{n=1}^N \mathbf{w}_r^n(t) \rangle \\ & = \left\| \otimes_{n=1}^N \mathbf{w}_r^n(t) \right\|^{-1} \langle -\nabla \mathcal{L}_h(0), \otimes_{n=1}^N \mathbf{w}_r^n(t) \rangle, \end{aligned}$$

where the second transition is due to $\nabla \mathcal{L}_h(\mathcal{W}_T(t)) = \nabla \mathcal{L}_h(0)$. Differentiating with respect to time, we have that:

$$\begin{aligned} \frac{d}{dt} \gamma_r(t) & = - \underbrace{\frac{d}{dt} \left[\left\| \otimes_{n=1}^N \mathbf{w}_r^n(t) \right\| \right]}_{(I)} \cdot \underbrace{\left\| \otimes_{n=1}^N \mathbf{w}_r^n(t) \right\|^{-2} \langle -\nabla \mathcal{L}_h(0), \otimes_{n=1}^N \mathbf{w}_r^n(t) \rangle}_{(II)} \\ & \quad + \underbrace{\left\| \otimes_{n=1}^N \mathbf{w}_r^n(t) \right\|^{-1} \langle -\nabla \mathcal{L}_h(0), \frac{d}{dt} \otimes_{n=1}^N \mathbf{w}_r^n(t) \rangle}_{(II)}. \end{aligned} \tag{B.13}$$

We now treat (I) and (II) separately. Plugging the expression for $\frac{d}{dt} \|\otimes_{n=1}^N \mathbf{w}_r^n(t)\|$ from Corollary 2 into (I), and recalling that $\nabla \mathcal{L}_h(\mathcal{W}_T(t)) = \nabla \mathcal{L}_h(0)$, leads to:

$$(I) = N \|\otimes_{n=1}^N \mathbf{w}_r^n(t)\|^{-1-2/N} \left\langle -\nabla \mathcal{L}_h(0), \otimes_{n=1}^N \mathbf{w}_r^n(t) \right\rangle^2.$$

Due to the fact that $\|\otimes_{n=1}^N \mathbf{w}_r^n(t)\|^{-2/N} = \|\mathbf{w}_r^1(t)\|^{-2} = \dots = \|\mathbf{w}_r^N(t)\|^{-2}$, we may equivalently write:

$$(I) = \|\otimes_{n=1}^N \mathbf{w}_r^n(t)\|^{-1} \sum_{n=1}^N \|\mathbf{w}_r^n(t)\|^{-2} \left\langle -\nabla \mathcal{L}_h(0), \otimes_{n'=1}^N \mathbf{w}_r^{n'}(t) \right\rangle^2. \quad (\text{B.14})$$

For any $n \in [N]$, by Lemma 28 we know that $\frac{d}{dt} \|\mathbf{w}_r^n(t)\|^2 = -2 \langle \nabla \mathcal{L}_h(0), \otimes_{n'=1}^N \mathbf{w}_r^{n'}(t) \rangle$, which implies $\frac{d}{dt} \|\mathbf{w}_r^n(t)\| = \|\mathbf{w}_r^n(t)\|^{-1} \langle -\nabla \mathcal{L}_h(0), \otimes_{n'=1}^N \mathbf{w}_r^{n'}(t) \rangle$. Going back to Equation (B.14), we can see that:

$$(I) = \|\otimes_{n=1}^N \mathbf{w}_r^n(t)\|^{-1} \sum_{n=1}^N \left(\frac{d}{dt} \|\mathbf{w}_r^n(t)\| \right)^2.$$

Turning our attention to (II), by Lemmas 22 and 27 it follows that:

$$\begin{aligned} (II) &= \sum_{n=1}^N \left\langle -\nabla \mathcal{L}_h(0), \left(\otimes_{n'=1}^{n-1} \mathbf{w}_r^{n'}(t) \right) \otimes \frac{d}{dt} \mathbf{w}_r^n(t) \otimes \left(\otimes_{n'=n+1}^N \mathbf{w}_r^{n'}(t) \right) \right\rangle \\ &= \sum_{n=1}^N \left\langle \llbracket -\nabla \mathcal{L}_h(0) \rrbracket_n \cdot \circ_{n' \neq n} \mathbf{w}_r^{n'}(t), \frac{d}{dt} \mathbf{w}_r^n(t) \right\rangle \\ &= \sum_{n=1}^N \left\| \frac{d}{dt} \mathbf{w}_r^n(t) \right\|^2. \end{aligned}$$

Plugging the expressions we derived for (I) and (II) into Equation (B.13) yields:

$$\frac{d}{dt} \gamma_r(t) = \|\otimes_{n=1}^N \mathbf{w}_r^n(t)\|^{-1} \cdot \sum_{n=1}^N \left[\left\| \frac{d}{dt} \mathbf{w}_r^n(t) \right\|^2 - \left(\frac{d}{dt} \|\mathbf{w}_r^n(t)\| \right)^2 \right]. \quad (\text{B.15})$$

Notice that for any $n \in [N]$:

$$\begin{aligned} \left\| \frac{d}{dt} \mathbf{w}_r^n(t) \right\|^2 &\geq \|\Pi_{\mathbf{w}_r^n(t)} \left(\frac{d}{dt} \mathbf{w}_r^n(t) \right)\|^2 \\ &= \left\| \left\langle \frac{d}{dt} \mathbf{w}_r^n(t), \mathbf{w}_r^n(t) \right\rangle \frac{\mathbf{w}_r^n(t)}{\|\mathbf{w}_r^n(t)\|^2} \right\|^2 \\ &= \left(\|\mathbf{w}_r^n(t)\|^{-1} \left\langle \frac{d}{dt} \mathbf{w}_r^n(t), \mathbf{w}_r^n(t) \right\rangle \right)^2 \\ &= \left(\frac{d}{dt} \|\mathbf{w}_r^n(t)\| \right)^2, \end{aligned}$$

where $\Pi_{\mathbf{w}_r^n(t)}(\cdot)$ denotes the orthogonal projection onto the subspace spanned by $\mathbf{w}_r^n(t)$. The right hand side in Equation (B.15) is therefore non-negative, i.e. $\frac{d}{dt} \gamma_r(t) \geq 0$, concluding the proof. \square

B.3.5.2 Stage I: End Tensor Reaches Reference Sphere

Proposition 7. *The end tensor initially reaches reference sphere \mathcal{S} (Equation (2.10)) at some time $T_0 > 0$, and:*

$$\|\otimes_{n=1}^N \mathbf{w}_r^n(t)\| \leq \tilde{\epsilon} \quad , \quad t \in [0, T_0] \quad , \quad r = 2, \dots, R, \quad (\text{B.16})$$

$$\left| \|\otimes_{n=1}^N \mathbf{w}_1^n(T_0)\| - \rho \right| \leq (R-1) \cdot \tilde{\epsilon}, \quad (\text{B.17})$$

where $\tilde{\epsilon}$ is as defined in Equation (B.10).

Towards proving Proposition 7, we establish the following key lemma.

Lemma 36. *Let $t' \leq \frac{\alpha^{2-N} \|\mathbf{a}_1\|^{2-N} (N-2)^{-1}}{\langle -\nabla \mathcal{L}_h(0), \otimes_{n=1}^N \hat{\mathbf{a}}_1^n \rangle}$, and suppose that $\nabla \mathcal{L}_h(\mathcal{W}_T(t)) = \nabla \mathcal{L}_h(0)$ for all $t \in [0, t']$. Then:*

$$\|\otimes_{n=1}^N \mathbf{w}_1^n(t)\| \geq \left(\alpha^{2-N} \|\mathbf{a}_1\|^{2-N} - (N-2) \langle -\nabla \mathcal{L}_h(0), \otimes_{n=1}^N \hat{\mathbf{a}}_1^n \rangle \cdot t \right)^{-\frac{N}{N-2}}, \quad t \in [0, t'], \quad (\text{B.18})$$

$$\|\otimes_{n=1}^N \mathbf{w}_r^n(t)\| \leq \left(\alpha^{2-N} \|\mathbf{a}_r\|^{2-N} - (N-2) \|\nabla \mathcal{L}_h(0)\| \cdot t \right)^{-\frac{N}{N-2}}, \quad t \in [0, t'], \quad r = 2, \dots, R. \quad (\text{B.19})$$

In particular:

$$\|\otimes_{n=1}^N \mathbf{w}_r^n(t)\| \leq \alpha^N \left(\|\mathbf{a}_r\|^{2-N} - \|\mathbf{a}_1\|^{2-N} \frac{\|\nabla \mathcal{L}_h(0)\|}{\langle -\nabla \mathcal{L}_h(0), \otimes_{n=1}^N \hat{\mathbf{a}}_1^n \rangle} \right)^{-\frac{N}{N-2}}, \quad t \in [0, t'], \quad r = 2, \dots, R. \quad (\text{B.20})$$

Proof. For simplicity of notation we denote $\gamma_r(t) := \langle -\nabla \mathcal{L}_h(\mathcal{W}_T(t)), \otimes_{n=1}^N \hat{\mathbf{w}}_r^n(t) \rangle$, where $\hat{\mathbf{w}}_r^n(t) := \mathbf{w}_r^n(t) / \|\mathbf{w}_r^n(t)\|$ if $\mathbf{w}_r^n(t) \neq 0$, and $\hat{\mathbf{w}}_r^n(t) := 0$ otherwise, for $r = 1, \dots, R$, $n = 1, \dots, N$. In the following, unless explicitly stated otherwise, t is to be considered in the time interval $[0, t']$.

By Assumption 2, $\{\mathbf{a}_r^n\}_{r=1, n=1}^{R, N}$ have unbalancedness magnitude zero, thus, so do $\{\mathbf{w}_r^n(0)\}_{r=1, n=1}^{R, N}$ (recall $\mathbf{w}_r^n(0) = \alpha \cdot \mathbf{a}_r^n$ for $r = 1, \dots, R$, $n = 1, \dots, N$). According to Corollary 2 the evolution of a component's norm is given by:

$$\frac{d}{dt} \|\otimes_{n=1}^N \mathbf{w}_r^n(t)\| = N \gamma_r(t) \cdot \|\otimes_{n=1}^N \mathbf{w}_r^n(t)\|^{2-\frac{2}{N}} \quad , \quad r = 1, \dots, R. \quad (\text{B.21})$$

Proof of Equation (B.18) (lower bound for $\|\otimes_{n=1}^N \mathbf{w}_1^n(t)\|$): By Lemma 35, $\gamma_1(t)$ is monotonically non-decreasing. Thus, from Equation (B.21) we have:

$$\frac{d}{dt} \|\otimes_{n=1}^N \mathbf{w}_1^n(t)\| \geq N \gamma_1(0) \cdot \|\otimes_{n=1}^N \mathbf{w}_1^n(t)\|^{2-\frac{2}{N}}. \quad (\text{B.22})$$

Assumption 3 (second line in Equation (2.9)) necessarily means that $\mathbf{w}_1^n(0) = \alpha \cdot \mathbf{a}_1^n \neq 0$ for all $n \in [N]$. Recalling that the unbalancedness magnitude is zero at initialization, from Lemma 31 we get that $\|\mathbf{w}_1^1(t)\| = \dots = \|\mathbf{w}_1^N(t)\| > 0$, and so $\|\otimes_{n=1}^N \mathbf{w}_1^n(t)\|^{2-2/N} > 0$, for all $t \in [0, t']$. Therefore, we may divide both sides of Equation (B.22) by $\|\otimes_{n=1}^N \mathbf{w}_1^n(t)\|^{2-2/N}$. Doing so, and integrating with respect to

time, leads to:

$$\begin{aligned}
& \int_{\hat{t}=0}^t \left[\|\otimes_{n=1}^N \mathbf{w}_1^n(\hat{t})\|^{2/N-2} \frac{d}{d\hat{t}} \|\otimes_{n=1}^N \mathbf{w}_1^n(\hat{t})\| \right] d\hat{t} \geq N\gamma_1(0) \cdot t \\
\implies & \frac{N}{2-N} \left(\|\otimes_{n=1}^N \mathbf{w}_1^n(t)\|^{2/N-1} - \|\otimes_{n=1}^N \mathbf{w}_1^n(0)\|^{2/N-1} \right) \geq N\gamma_1(0) \cdot t \quad (\text{B.23}) \\
\implies & \|\otimes_{n=1}^N \mathbf{w}_1^n(t)\|^{2/N-1} \leq \|\otimes_{n=1}^N \mathbf{w}_1^n(0)\|^{2/N-1} - (N-2)\gamma_1(0) \cdot t.
\end{aligned}$$

Notice that $\gamma_1(0) = \langle -\nabla \mathcal{L}_h(\mathcal{W}_T(0)), \otimes_{n=1}^N \widehat{\mathbf{w}}_1^n(0) \rangle = \langle -\nabla \mathcal{L}_h(0), \otimes_{n=1}^N \widehat{\mathbf{a}}_1^n \rangle$. Since $\|\otimes_{n=1}^N \mathbf{w}_1^n(0)\| = \prod_{n=1}^N \|\mathbf{w}_1^n(0)\| = \alpha^N \|\mathbf{a}_1\|^N$ and $t < t' \leq \alpha^{2-N} \|\mathbf{a}_1\|^{2-N} (N-2)^{-1} \gamma_1(0)^{-1}$, we can see that:

$$\|\otimes_{n=1}^N \mathbf{w}_1^n(0)\|^{2/N-1} - (N-2)\gamma_1(0) \cdot t = \alpha^{2-N} \|\mathbf{a}_1\|^{2-N} - (N-2)\gamma_1(0) \cdot t > 0.$$

Therefore, Equation (B.18) readily follows by rearranging the last inequality in Equation (B.23):

$$\|\otimes_{n=1}^N \mathbf{w}_1^n(t)\| \geq \left(\alpha^{2-N} \|\mathbf{a}_1\|^{2-N} - (N-2)\gamma_1(0) \cdot t \right)^{-\frac{N}{N-2}}.$$

Proof of Equations (B.19) and (B.20) (upper bounds for $\|\otimes_{n=1}^N \mathbf{w}_r^n(t)\|$): Fix some $r \in \{2, \dots, R\}$. First, we deal with the case where $\|\mathbf{w}_r^1(0)\| = \dots = \|\mathbf{w}_r^N(0)\| = 0$. If it is so, by Lemma 31 we have that $\|\mathbf{w}_r^1(t)\| = \dots = \|\mathbf{w}_r^N(t)\| = 0$ for all $t \in [0, t']$. Hence, $\|\otimes_{n=1}^N \mathbf{w}_r^n(t)\| = 0$ for all $t \in [0, t']$, *i.e.* Equations (B.19) and (B.20) trivially hold.

Now we move to the case where $\|\mathbf{w}_r^1(0)\| = \dots = \|\mathbf{w}_r^N(0)\| > 0$. From Lemma 31 we know that $\|\mathbf{w}_r^1(t)\| = \dots = \|\mathbf{w}_r^N(t)\| > 0$ for all $t \in [0, t']$. Since $\nabla \mathcal{L}_h(\mathcal{W}_T(t)) = \nabla \mathcal{L}_h(0)$, by the Cauchy-Schwartz inequality we then have:

$$\gamma_r(t) = \left\langle -\nabla \mathcal{L}_h(0), \otimes_{n=1}^N \widehat{\mathbf{w}}_r^n(t) \right\rangle \leq \|\nabla \mathcal{L}_h(0)\| \|\otimes_{n=1}^N \widehat{\mathbf{w}}_r^n(t)\| = \|\nabla \mathcal{L}_h(0)\|.$$

Combined with Equation (B.21), we arrive at the following upper bound:

$$\frac{d}{dt} \|\otimes_{n=1}^N \mathbf{w}_r^n(t)\| \leq N \|\nabla \mathcal{L}_h(0)\| \cdot \|\otimes_{n=1}^N \mathbf{w}_r^n(t)\|^{2-\frac{2}{N}}.$$

Dividing both sides of the inequality by $\|\otimes_{n=1}^N \mathbf{w}_r^n(t)\|^{2-2/N}$ (is positive since $\|\mathbf{w}_r^1(t)\| = \dots = \|\mathbf{w}_r^N(t)\| > 0$), and integrating with respect to time, yields:

$$\begin{aligned}
& \int_{\hat{t}=0}^t \left[\|\otimes_{n=1}^N \mathbf{w}_r^n(\hat{t})\|^{2/N-2} \frac{d}{d\hat{t}} \|\otimes_{n=1}^N \mathbf{w}_r^n(\hat{t})\| \right] d\hat{t} \leq N \|\nabla \mathcal{L}_h(0)\| \cdot t \\
\implies & \frac{N}{2-N} \left(\|\otimes_{n=1}^N \mathbf{w}_r^n(t)\|^{2/N-1} - \|\otimes_{n=1}^N \mathbf{w}_r^n(0)\|^{2/N-1} \right) \leq N \|\nabla \mathcal{L}_h(0)\| \cdot t.
\end{aligned}$$

Rearranging the inequality above, and making use of the fact that $\|\otimes_{n=1}^N \mathbf{w}_r^n(0)\| = \prod_{n=1}^N \|\mathbf{w}_r^n(0)\| = \alpha^N \|\mathbf{a}_r\|^N$, we arrive at:

$$\begin{aligned}
\|\otimes_{n=1}^N \mathbf{w}_r^n(t)\|^{2/N-1} & \geq \|\otimes_{n=1}^N \mathbf{w}_r^n(0)\|^{2/N-1} - (N-2) \|\nabla \mathcal{L}_h(0)\| \cdot t \\
& = \alpha^{2-N} \|\mathbf{a}_r\|^{2-N} - (N-2) \|\nabla \mathcal{L}_h(0)\| \cdot t. \quad (\text{B.24})
\end{aligned}$$

Noticing $\gamma_1(0) = \langle -\nabla \mathcal{L}_h(\mathcal{W}_T(0)), \otimes_{n=1}^N \widehat{\mathbf{w}}_1^n(0) \rangle = \langle -\nabla \mathcal{L}_h(0), \otimes_{n=1}^N \widehat{\mathbf{a}}_1^n \rangle$, by Assumption 3 we have that $\|\mathbf{a}_1\| > \|\mathbf{a}_r\| \|\nabla \mathcal{L}_h(0)\|^{1/(N-2)} \cdot \gamma_1(0)^{-1/(N-2)}$. Therefore:

$$t' \leq \alpha^{2-N} \|\mathbf{a}_1\|^{2-N} (N-2)^{-1} \gamma_1(0)^{-1} < \alpha^{2-N} \|\mathbf{a}_r\|^{2-N} (N-2)^{-1} \|\nabla \mathcal{L}_h(0)\|^{-1}.$$

This implies that the right hand side in Equation (B.24) is positive for all $t \in [0, t']$. Thus, rearranging Equation (B.24) establishes Equation (B.19):

$$\|\otimes_{n=1}^N \mathbf{w}_r^n(t)\| \leq \left(\alpha^{2-N} \|\mathbf{a}_r\|^{2-N} - (N-2) \|\nabla \mathcal{L}_h(0)\| \cdot t \right)^{-\frac{N}{N-2}}.$$

Equation (B.20) then directly follows:

$$\begin{aligned} \|\otimes_{n=1}^N \mathbf{w}_r^n(t)\| &\leq \left(\alpha^{2-N} \|\mathbf{a}_r\|^{2-N} - (N-2) \|\nabla \mathcal{L}_h(0)\| \cdot t' \right)^{-\frac{N}{N-2}} \\ &\leq \left(\alpha^{2-N} \|\mathbf{a}_r\|^{2-N} - \alpha^{2-N} \|\mathbf{a}_1\|^{2-N} \|\nabla \mathcal{L}_h(0)\| \gamma_1(0)^{-1} \right)^{-\frac{N}{N-2}} \\ &= \alpha^N \left(\|\mathbf{a}_r\|^{2-N} - \|\mathbf{a}_1\|^{2-N} \|\nabla \mathcal{L}_h(0)\| \gamma_1(0)^{-1} \right)^{-\frac{N}{N-2}}. \end{aligned}$$

□

Proof of Proposition 7. Notice that at initialization $\|\mathcal{W}_T(0)\| \leq \sum_{r=1}^R \|\otimes_{n=1}^N \mathbf{w}_r^n(0)\| \leq R\alpha^N A^N < \rho$. We can therefore examine the trajectory up until the time at which $\|\mathcal{W}_T(t)\| = \rho$, *i.e.* until it reaches the reference sphere \mathcal{S} . Formally, define:

$$T_0 := \inf \{t \geq 0 : \mathcal{W}_T(t) \in \mathcal{S}\},$$

where by convention $T_0 := \infty$ if the set on the right hand side is empty. For all $t \in [0, T_0)$, clearly, $\|\mathcal{W}_T(t)\| < \rho$, and so by Lemma 32 $\nabla \mathcal{L}_h(\mathcal{W}_T(t)) = \nabla \mathcal{L}_h(0)$. We claim that T_0 is finite. Assume by way of contradiction that $T_0 = \infty$. For $t' := \alpha^{2-N} \|\mathbf{a}_1\|^{2-N} (N-2)^{-1} \langle -\nabla \mathcal{L}_h(0), \otimes_{n=1}^N \widehat{\mathbf{a}}_1^n \rangle^{-1}$, by Equation (B.18) from Lemma 36 we have that $\|\otimes_{n=1}^N \mathbf{w}_1^n(t)\|$ is lower bounded by a quantity that goes to ∞ as $t \rightarrow t'^-$. On the other hand, by Equation (B.20) from Lemma 36, $\|\otimes_{n=1}^N \mathbf{w}_2^n(t)\|, \dots, \|\otimes_{n=1}^N \mathbf{w}_R^n(t)\|$ are bounded over $[0, t']$. Taken together, there must exist $\hat{t} \in [0, t')$ at which:

$$\|\mathcal{W}_T(\hat{t})\| \geq \|\otimes_{n=1}^N \mathbf{w}_1^n(\hat{t})\| - \sum_{r=2}^R \|\otimes_{n=1}^N \mathbf{w}_r^n(\hat{t})\| \geq \rho.$$

Since $\|\mathcal{W}_T(t)\|$ is continuous in t , and $\|\mathcal{W}_T(0)\| < \rho$, this contradicts our assumption that $T_0 = \infty$. Hence, $T_0 < \infty$, and in particular $T_0 < t'$. Notice that continuity of $\|\mathcal{W}_T(t)\|$ further implies that $\|\mathcal{W}_T(T_0)\| = \rho$, *i.e.* T_0 is the initial time at which $\mathcal{W}_T(t)$ reaches the reference sphere \mathcal{S} . Applying our assumption on the size of α (Equation (B.11)) to Equation (B.20) from Lemma 36 establishes Equation (B.16). Equation (B.17) then readily follows by the triangle inequality:

$$\begin{aligned} \left| \|\otimes_{n=1}^N \mathbf{w}_1^n(T_0)\| - \rho \right| &= \left| \|\otimes_{n=1}^N \mathbf{w}_1^n(T_0)\| - \|\mathcal{W}_T(T_0)\| \right| \\ &\leq \|\otimes_{n=1}^N \mathbf{w}_1^n(T_0) - \mathcal{W}_T(T_0)\| \\ &= \left\| \sum_{r=2}^R \otimes_{n=1}^N \mathbf{w}_r^n(T_0) \right\| \\ &\leq (R-1) \cdot \tilde{\epsilon}. \end{aligned}$$

□

B.3.5.3 Stage II: End Tensor Follows Rank One Trajectory

As shown in Proposition 7 (Appendix B.3.5.2), the end tensor initially reaches reference sphere \mathcal{S} at some time $T_0 > 0$, for which Equations (B.16) and (B.17) hold. Therefore, the time-shifted trajectory is given by $\overline{\mathcal{W}}_T(t) = \mathcal{W}_T(t + T_0)$ for all $t \geq 0$. Denote the corresponding time-shifted factorization weight vectors by:

$$\overline{\mathbf{w}}_r^n(t) := \mathbf{w}_r^n(t + T_0) \quad , \quad t \geq 0, \quad r = 1, \dots, R, \quad n = 1, \dots, N.$$

We are now at a position to define the approximating rank one trajectory $\mathcal{W}_1(t)$ emanating from \mathcal{S} . Let $\{\tilde{\mathbf{w}}^n(t)\}_{n=1}^N$ be a curve born from gradient flow when minimizing $\phi_h(\cdot)$ with a one-component tensor factorization, initialized at:

$$\tilde{\mathbf{w}}^n(0) := \frac{\rho^{1/N}}{\|\overline{\mathbf{w}}_1^n(0)\|} \cdot \overline{\mathbf{w}}_1^n(0) \quad , \quad n = 1, \dots, N.$$

Notice that by definition $\|\tilde{\mathbf{w}}^1(0)\| = \dots = \|\tilde{\mathbf{w}}^N(0)\| = \rho^{1/N}$. Therefore, $\{\tilde{\mathbf{w}}^n(0)\}_{n=1}^N$ have unbalancedness magnitude zero (Definition 3). Denoting $\mathcal{W}_1(t) := \otimes_{n=1}^N \tilde{\mathbf{w}}^n(t)$, for $t \geq 0$, we can see that $\mathcal{W}_1(t)$ is a balanced rank one trajectory. Furthermore, $\|\mathcal{W}_1(0)\| = \|\otimes_{n=1}^N \tilde{\mathbf{w}}^n(0)\| = \prod_{n=1}^N \|\tilde{\mathbf{w}}^n(0)\| = \rho$, meaning $\mathcal{W}_1(0) \in \mathcal{S}$. It will be convenient to treat $\{\tilde{\mathbf{w}}^n(t)\}_{n=1}^N$ as an R -component factorization with components $2, \dots, R$ being zero. To this end, denote $\tilde{\mathbf{w}}_1^n(t) := \tilde{\mathbf{w}}^n(t)$, and define $\tilde{\mathbf{w}}_r^n(t) := 0$ for all $t \geq 0, r \in \{2, \dots, R\}$ and $n \in [N]$. Notice that, according to Lemma 30, $\{\tilde{\mathbf{w}}_r^n(t)\}_{r=1, n=1}^{R, N}$ indeed follow a gradient flow path of an R -component factorization.

Next, we turn to bound the distance between $\{\overline{\mathbf{w}}_r^n(0)\}_{r=1, n=1}^{R, N}$ and $\{\tilde{\mathbf{w}}_r^n(0)\}_{r=1, n=1}^{R, N}$. From Equation (B.16) in Proposition 7, recalling $\tilde{\epsilon} \leq \hat{\epsilon}$ (by their definition in Equation (B.10)), we obtain:

$$\|\overline{\mathbf{w}}_r^n(0)\| = \|\mathbf{w}_r^n(T_0)\| = \|\otimes_{n'=1}^N \mathbf{w}_r^{n'}(T_0)\|^{\frac{1}{N}} \leq \tilde{\epsilon}^{\frac{1}{N}} \leq \hat{\epsilon}^{\frac{1}{N}} \quad , \quad r = 2, \dots, R, \quad n = 1, \dots, N. \quad (\text{B.25})$$

As for the first component, for any $n \in [N]$, the fact that $\|\overline{\mathbf{w}}_1^n(0)\| = \|\mathbf{w}_1^n(T_0)\| = \|\otimes_{n'=1}^N \mathbf{w}_1^{n'}(T_0)\|^{1/N}$ and Equation (B.17) from Proposition 7 yield the following bound:

$$(\rho - (R-1) \cdot \tilde{\epsilon})^{\frac{1}{N}} \leq \|\overline{\mathbf{w}}_1^n(0)\| \leq (\rho + (R-1) \cdot \tilde{\epsilon})^{\frac{1}{N}}.$$

On the one hand, since the ℓ_1 norm is no greater than the ℓ_p norm for $p < 1$, we have that $(\rho + (R-1) \cdot \tilde{\epsilon})^{1/N} \leq \rho^{1/N} + (R-1)^{1/N} \cdot \tilde{\epsilon}^{1/N} \leq \rho^{1/N} + (R-1)^{1/N} \cdot \hat{\epsilon}^{1/N}$. On the other hand, since by definition $\tilde{\epsilon} \leq (R-1)^{-1}(\rho - [\rho^{1/N} - (R-1)^{1/N} \cdot \hat{\epsilon}^{1/N}]^N)$, it is straightforward to verify that $(\rho - (R-1) \cdot \tilde{\epsilon})^{1/N} \geq \rho^{1/N} - (R-1)^{1/N} \cdot \hat{\epsilon}^{1/N}$. Put together, while noticing that $\|\overline{\mathbf{w}}_1^n(0) - \tilde{\mathbf{w}}_1^n(0)\| = \left| \|\overline{\mathbf{w}}_1^n(0)\| - \rho^{1/N} \right|$, we arrive at:

$$\|\overline{\mathbf{w}}_1^n(0) - \tilde{\mathbf{w}}_1^n(0)\| = \left| \|\overline{\mathbf{w}}_1^n(0)\| - \rho^{1/N} \right| \leq (R-1)^{\frac{1}{N}} \cdot \hat{\epsilon}^{\frac{1}{N}} \quad , \quad n \in [N]. \quad (\text{B.26})$$

Equations (B.25) and (B.26) lead to the following bound on the distance between $\{\bar{\mathbf{w}}_r^n(0)\}_{r=1}^R \{\tilde{\mathbf{w}}_r^n(0)\}_{r=1}^R$ and $\{\tilde{\mathbf{w}}_r^n(0)\}_{r=1}^R \{\tilde{\mathbf{w}}_r^n(0)\}_{r=1}^R$:

$$\begin{aligned} \sum_{r=1}^R \sum_{n=1}^N \|\bar{\mathbf{w}}_r^n(0) - \tilde{\mathbf{w}}_r^n(0)\|^2 &= \sum_{n=1}^N \|\bar{\mathbf{w}}_1^n(0) - \tilde{\mathbf{w}}_1^n(0)\|^2 + \sum_{r=2}^R \sum_{n=1}^N \|\bar{\mathbf{w}}_r^n(0)\|^2 \\ &\leq (R-1)^{\frac{2}{N}} N \cdot \hat{\epsilon}^{\frac{2}{N}} + (R-1)N \cdot \hat{\epsilon}^{\frac{2}{N}} \\ &\leq 2(R-1)N \cdot \hat{\epsilon}^{\frac{2}{N}}, \end{aligned}$$

where the last transition is by $(R-1)^{2/N} \leq (R-1)$. Let $\tilde{B} := \sqrt{N} (\max\{B, \rho\} + 1)^{\frac{1}{N}}$ and $\beta := RN((\tilde{B} + 1)^{2(N-1)} + \delta_h(\tilde{B} + 1)^{N-2})$ (as defined in Equation (B.10)). According to Lemma 34, the objective $\phi_h(\cdot)$ is β -smooth over the closed ball of radius $\tilde{B} + 1$ around the origin. Furthermore, seeing that $2(R-1)N \cdot \hat{\epsilon}^{2/N} < \exp(-2\beta \cdot T)$ (by the definition of $\hat{\epsilon}$ in Equation (B.10)), we obtain:

$$\sum_{r=1}^R \sum_{n=1}^N \|\bar{\mathbf{w}}_r^n(0) - \tilde{\mathbf{w}}_r^n(0)\|^2 \leq 2(R-1)N \cdot \hat{\epsilon}^{\frac{2}{N}} < \exp(-2\beta \cdot T).$$

Thus, Lemma 26 implies that at least until $t \geq T$ or $(\sum_{r=1}^R \sum_{n=1}^N \|\tilde{\mathbf{w}}_r^n(t)\|^2)^{1/2} \geq \tilde{B}$ the following holds:

$$\begin{aligned} \sum_{r=1}^R \sum_{n=1}^N \|\bar{\mathbf{w}}_r^n(t) - \tilde{\mathbf{w}}_r^n(t)\|^2 &\leq \sum_{r=1}^R \sum_{n=1}^N \|\bar{\mathbf{w}}_r^n(0) - \tilde{\mathbf{w}}_r^n(0)\|^2 \cdot \exp(2\beta \cdot t) \\ &\leq 2(R-1)N \cdot \hat{\epsilon}^{\frac{2}{N}} \cdot \exp(2\beta \cdot t). \end{aligned} \quad (\text{B.27})$$

Suppose that $(\sum_{r=1}^R \sum_{n=1}^N \|\tilde{\mathbf{w}}_r^n(t)\|^2)^{1/2} < \tilde{B}$ for all $t \in [0, T]$. In this case, Equation (B.27) holds for all $t \in [0, T]$. Seeing that $2(R-1)N \cdot \hat{\epsilon}^{2/N} \cdot \exp(2\beta \cdot T) < 1$, Equation (B.27) gives $(\sum_{r=1}^R \sum_{n=1}^N \|\tilde{\mathbf{w}}_r^n(t)\|^2)^{1/2} < \tilde{B} + 1$. Then, Equation (B.27), the fact that $\mathcal{W}_1(t) = \otimes_{n=1}^N \tilde{\mathbf{w}}_1^n(t) = \sum_{r=1}^R \otimes_{n=1}^N \tilde{\mathbf{w}}_r^n(t)$, and Lemma 24 yield:

$$\|\bar{\mathcal{W}}_T(t) - \mathcal{W}_1(t)\| \leq \sqrt{2}RN(\tilde{B} + 1)^{N-1} \cdot \exp(\beta \cdot T) \cdot \hat{\epsilon}^{\frac{1}{N}}, \quad t \in [0, T].$$

Recalling that $\hat{\epsilon} \leq 2^{-\frac{N}{2}} R^{-N} N^{-N} (\tilde{B} + 1)^{N-N^2} \cdot \exp(-N\beta T) \cdot \epsilon^N$, we conclude:

$$\|\bar{\mathcal{W}}_T(t) - \mathcal{W}_1(t)\| \leq \epsilon, \quad (\text{B.28})$$

for all $t \in [0, T]$.

It remains to treat the case where $(\sum_{r=1}^R \sum_{n=1}^N \|\tilde{\mathbf{w}}_r^n(t)\|^2)^{1/2} \geq \tilde{B}$ for some $t \in [0, T]$. Let $t' \in [0, T]$ be the initial such time. The desired result readily follows by showing that: (i) Equation (B.28) holds for $t \in [0, t']$; and (ii) $\|\bar{\mathcal{W}}_T(t')\| \geq B$.

We start by proving that $\|\mathcal{W}_1(t')\| \geq \max\{B, \rho\} + 1$ and $t' > 0$. Recalling that $\tilde{\mathbf{w}}_r^1(t), \dots, \tilde{\mathbf{w}}_r^N(t)$ are identically zero for all $r \in \{2, \dots, R\}$, we have that:

$$\sum_{n=1}^N \|\tilde{\mathbf{w}}_1^n(t')\|^2 = \sum_{r=1}^R \sum_{n=1}^N \|\tilde{\mathbf{w}}_r^n(t')\|^2 \geq \tilde{B}^2.$$

Since $\|\tilde{\mathbf{w}}_1^1(0)\| = \dots = \|\tilde{\mathbf{w}}_1^N(0)\|$, Lemma 1 implies $\|\tilde{\mathbf{w}}_1^1(t')\| = \dots = \|\tilde{\mathbf{w}}_1^N(t')\|$. Thus, for any $n \in [N]$:

$$N\|\tilde{\mathbf{w}}_1^n(t')\|^2 = \sum_{n'=1}^N \|\tilde{\mathbf{w}}_1^{n'}(t')\|^2 \geq \tilde{B}^2,$$

which leads to $\|\tilde{\mathbf{w}}_1^n(t')\| \geq \tilde{B}N^{-1/2}$. In turn this yields $\|\mathcal{W}_1(t')\| = \|\otimes_{n=1}^N \tilde{\mathbf{w}}_1^n(t')\| = \prod_{n=1}^N \|\tilde{\mathbf{w}}_1^n(t')\| \geq \tilde{B}^N N^{-\frac{N}{2}}$. Plugging in $\tilde{B} := \sqrt{N}(\max\{B, \rho\} + 1)^{\frac{1}{N}}$, we conclude:

$$\|\mathcal{W}_1(t')\| \geq \max\{B, \rho\} + 1. \quad (\text{B.29})$$

Note that this necessarily means $t' > 0$ as $\mathcal{W}_1(0) \in \mathcal{S}$, *i.e.* $\|\mathcal{W}_1(0)\| = \rho < \max\{B, \rho\} + 1$.

Now, we focus on the time interval $[0, t']$, over which Equation (B.27) holds and $(\sum_{r=1}^R \sum_{n=1}^N \|\tilde{\mathbf{w}}_r^n(t)\|^2)^{1/2} < \tilde{B}$. By arguments analogous to those used in the case where $(\sum_{r=1}^R \sum_{n=1}^N \|\tilde{\mathbf{w}}_r^n(t)\|^2)^{1/2} < \tilde{B}$ for all $t \in [0, T]$, we obtain that Equation (B.28) holds for all $t \in [0, t']$. Continuity with respect to time then implies $\|\overline{\mathcal{W}}_T(t') - \mathcal{W}_1(t')\| \leq \epsilon < 1$. Lastly, together with Equation (B.29) this leads to $\|\overline{\mathcal{W}}_T(t')\| \geq \|\mathcal{W}_1(t')\| - 1 \geq B$.

Overall, we have shown that $\|\overline{\mathcal{W}}_T(t) - \mathcal{W}_1(t)\| \leq \epsilon$ at least until time T or time t' at which $\|\overline{\mathcal{W}}_T(t')\| \geq B$, establishing the desired result. \square

B.3.6 Proof of Corollary 3

For $\epsilon > 0$, there exists a time $T' > 0$ at which all balanced rank one trajectories emanating from \mathcal{S} are within distance $\epsilon/2$ from \mathcal{W}^* . Moreover, these trajectories are confined to a ball of radius B around the origin, for some $B > 0$. According to Theorem 4, if initialization scale α is sufficiently small, $\|\overline{\mathcal{W}}_T(t) - \mathcal{W}_1(t)\| \leq \min\{\epsilon/2, 1/2\}$ at least until $t \geq T'$ or $\|\overline{\mathcal{W}}_T(t)\| \geq B + 1$, where $\overline{\mathcal{W}}_T(t)$ is the time-shifted trajectory of $\mathcal{W}_T(t)$, and $\mathcal{W}_1(t)$ is a balanced rank one trajectory emanating from \mathcal{S} . We claim that the latter cannot hold, *i.e.* $\|\overline{\mathcal{W}}_T(t)\| < B + 1$ for all $t \in [0, T']$. To see it is so, assume by way of contradiction otherwise, and let $t' \in [0, T']$ be the initial time at which $\|\overline{\mathcal{W}}_T(t')\| \geq B + 1$. Since $\|\overline{\mathcal{W}}_T(t') - \mathcal{W}_1(t')\| < 1$, we have that $\|\mathcal{W}_1(t')\| > B$, in contradiction to $\mathcal{W}_1(t)$ being confined to a ball of radius B around the origin. Thus, $\|\overline{\mathcal{W}}_T(T') - \mathcal{W}_1(T')\| \leq \epsilon/2$. The proof concludes by the triangle inequality:

$$\|\overline{\mathcal{W}}_T(T') - \mathcal{W}^*\| \leq \|\overline{\mathcal{W}}_T(T') - \mathcal{W}_1(T')\| + \|\mathcal{W}_1(T') - \mathcal{W}^*\| \leq \epsilon.$$

\square

Appendix C

Implicit Regularization in Hierarchical Tensor Factorization and Deep Convolutional Neural Networks

C.1 Hierarchical Tensor Factorization as Deep Non-Linear Convolutional Network

In this appendix, we formally state and prove a known correspondence between hierarchical tensor factorization and certain deep non-linear convolutional networks (*cf.* [51]). For conciseness, we assume the tensor order N is a power of $P \in \mathbb{N}_{\geq 2}$ and the mode dimensions D_1, \dots, D_N are equal, and focus on the factorization induced by a perfect P -ary mode tree (Definition 4) that combines nodes with adjacent indices.

Let $L := \log_P N$ denote the height of the mode tree, and associate each of its nodes with a respective location (l, n) , where $l \in [L + 1]$ is the level in the tree (numbered from leaves to root in ascending order), and $n \in [N/P^{l-1}]$ is the index inside the level (see Figure C.1 for an illustration). Adapting Equation (3.3) to the current setting, the end tensor is computed as follows:

for all $n \in [N]$ and $r \in [R_1]$:

$$\underbrace{\mathcal{W}^{(1,n,r)}}_{\text{order 1}} := \mathbf{W}_{:,r}^{(1,n)},$$

for all $l \in \{2, \dots, L\}$, $n \in [N/P^{l-1}]$, and $r \in [R_l]$ (traverse interior nodes of \mathcal{T} from leaves to root, non-inclusive):

$$\underbrace{\mathcal{W}^{(l,n,r)}}_{\text{order } P^{l-1}} := \sum_{r'=1}^{R_{l-1}} \mathbf{W}_{r',r}^{(l,n)} \left[\otimes_{p=(n-1) \cdot P+1}^{n \cdot P} \mathcal{W}^{(l-1,p,r')} \right],$$

$$\underbrace{\mathcal{W}_H}_{\text{order } N} := \sum_{r'=1}^{R_L} \mathbf{W}_{r',1}^{(L+1,1)} \left[\otimes_{p=1}^P \mathcal{W}^{(L,p,r')} \right],$$

(C.1)

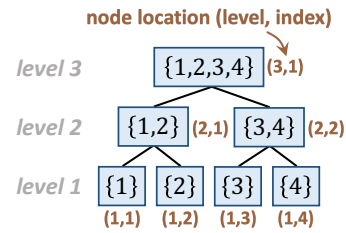


Figure C.1: Perfect P -ary mode tree that combines adjacent indices, for order $N = 4$ and $P = 2$.

where $(\mathbf{W}^{(l,n)} \in \mathbb{R}^{R_{l-1} \times R_l})_{l \in [L+1], n \in [N/P^{l-1}]}$ are the factorization's weight matrices, $R_{L+1} = 1$, and $R_0 := D_1 = \dots = D_N$.

The deep non-linear convolutional network corresponding to the above factorization (illustrated in Figure 3.2 (bottom)) has L hidden layers, the l 'th one comprising a locally connected linear operator with R_l channels followed by channel-wise product pooling with window size P (multiplicative non-linearity). Denoting by $(\mathbf{h}^{(l-1,1)}, \dots, \mathbf{h}^{(l-1, N/P^{l-1})}) \in \mathbb{R}^{R_{l-1}} \times \dots \times \mathbb{R}^{R_{l-1}}$ the output of the $l-1$ 'th hidden layer, where $(\mathbf{h}^{(0,1)}, \dots, \mathbf{h}^{(0,N)}) := (\mathbf{x}^{(1)}, \dots, \mathbf{x}^{(N)})$ is the network's input, the locally connected operator of the l 'th layer computes $(\mathbf{W}^{(l,n)})^\top \mathbf{h}^{(l-1,n)}$ for each index $n \in [N/P^{l-1}]$. We refer to this operator as "1 \times 1 conv" in appeal to the case of weight sharing, where $\mathbf{W}^{(l,1)} = \dots = \mathbf{W}^{(l, N/P^{l-1})}$. Following the locally connected operator, for each $n \in [N/P^l]$ and $r \in [R_l]$, the pooling operator computes $\prod_{p=(n-1) \cdot P+1}^{n \cdot P} [(\mathbf{W}^{(l,p)})^\top \mathbf{h}^{(l-1,p)}]_r$, thereby producing $(\mathbf{h}^{(l,1)}, \dots, \mathbf{h}^{(l, N/P^l)})$. After passing the input through all hidden layers, a final linear layer, whose weights are $\mathbf{W}^{(L+1,1)}$, yields the scalar output of the network $(\mathbf{W}^{(L+1,1)})^\top \mathbf{h}^{(L,1)}$. Notice that the weight matrices of the hierarchical tensor factorization are exactly the learnable weights of the network, and R_{l-1} — the number of local components (Definition 5) at nodes in level l of the factorization — is the width of the network's $l-1$ 'th hidden layer.

The above formulation of the network supports not only sequential inputs (e.g. audio and text), but also inputs arranged as multi-dimensional arrays (e.g. two-dimensional images). The choice of how to assign the indices $1, \dots, N$ to input elements determines the geometry of pooling windows throughout the network [49].

Proposition 8 below implies that we may view solution of a prediction task using the deep convolutional network described above as a hierarchical tensor factorization problem, and vice versa. For example, solving tensor completion and certain sensing problems using hierarchical tensor factorization amounts to applying the corresponding network to a regression task.

Proposition 8 (adapted from [51]). *Let $f_\Theta : \times_{n=1}^N \mathbb{R}^{D_n} \rightarrow \mathbb{R}$ be the function realized by the deep non-linear convolutional network described above, where Θ stands for the network's weights, i.e. $\Theta := (\mathbf{W}^{(l,n)})_{l \in [L+1], n \in [N/P^{l-1}]}$. Denote by \mathcal{W}_H the end tensor of the hierarchical tensor factorization specified in Equation (C.1). Then, for all $\mathbf{x}^{(1)} \in \mathbb{R}^{D_1}, \dots, \mathbf{x}^{(N)} \in \mathbb{R}^{D_N}$:*

$$f_\Theta(\mathbf{x}^{(1)}, \dots, \mathbf{x}^{(N)}) = \langle \otimes_{n=1}^N \mathbf{x}^{(n)}, \mathcal{W}_H \rangle.$$

Proof sketch (proof in Appendix C.5.8). By induction over the layers of the network, we show that the output of the l 'th convolutional layer (linear output layer for $l = L+1$) at index n and channel r is $\langle \otimes_{p=(n-1) \cdot P^{l-1}+1}^{n \cdot P^{l-1}} \mathbf{x}^{(p)}, \mathcal{W}^{(l,n,r)} \rangle$, where $\mathcal{W}^{(L+1,1,1)} := \mathcal{W}_H$, and all other $\mathcal{W}^{(l,n,r)}$ are the intermediate tensors formed when computing \mathcal{W}_H according to Equation (C.1). Since $f_\Theta(\mathbf{x}^{(1)}, \dots, \mathbf{x}^{(N)})$ is the output of the $L+1$ 'th layer at index 1 and channel 1, applying the inductive claim for $l = L+1, n = 1$, and $r = 1$ concludes the proof. \square

We conclude this appendix by noting that in the special case where $P = N$, if the weight matrix of the root node holds ones, the hierarchical tensor factorization reduces to a tensor factorization, and the corresponding convolutional network has a single hidden layer (with global product pooling) followed by a final summation layer. We

thus obtain the equivalence between tensor factorization and a shallow non-linear convolutional network as a corollary of Proposition 8.

C.2 Evolution of Local Component Norms Under Arbitrary Initialization

Theorem 5 in Section 3.4.2 characterizes the evolution of local component norms in a hierarchical tensor factorization, under the assumption of unbalancedness magnitude zero at initialization. Theorem 9 below extends the characterization to account for arbitrary initialization. It establishes that if the unbalancedness magnitude at initialization is small — as is the case under any near-zero initialization — local component norms approximately evolve per Theorem 5.

Theorem 9. *With the context and notations of Theorem 5, assume unbalancedness magnitude $\epsilon \geq 0$ at initialization. Then, for any $v \in \text{int}(\mathcal{T})$, $r \in [R_v]$, and time $t \geq 0$ at which $\sigma_H^{(v,r)}(t) > 0$:¹*

- If $\langle -\nabla \mathcal{L}_H(\mathcal{W}_H(t)), \mathcal{C}_H^{(v,r)}(t) \rangle \geq 0$, then:

$$\begin{aligned} \frac{d}{dt} \sigma_H^{(v,r)}(t) &\leq \left(\sigma_H^{(v,r)}(t)^{\frac{2}{L_v}} + \epsilon \right)^{L_v-1} \cdot L_v \langle -\nabla \mathcal{L}_H(\mathcal{W}_H(t)), \mathcal{C}_H^{(v,r)}(t) \rangle, \\ \frac{d}{dt} \sigma_H^{(v,r)}(t) &\geq \frac{\sigma_H^{(v,r)}(t)^2}{\sigma_H^{(v,r)}(t)^{\frac{2}{L_v}} + \epsilon} \cdot L_v \langle -\nabla \mathcal{L}_H(\mathcal{W}_H(t)), \mathcal{C}_H^{(v,r)}(t) \rangle; \end{aligned} \quad (\text{C.2})$$

- otherwise, if $\langle -\nabla \mathcal{L}_H(\mathcal{W}_H(t)), \mathcal{C}_H^{(v,r)}(t) \rangle < 0$, then:

$$\begin{aligned} \frac{d}{dt} \sigma_H^{(v,r)}(t) &\geq \left(\sigma_H^{(v,r)}(t)^{\frac{2}{L_v}} + \epsilon \right)^{L_v-1} \cdot L_v \langle -\nabla \mathcal{L}_H(\mathcal{W}_H(t)), \mathcal{C}_H^{(v,r)}(t) \rangle, \\ \frac{d}{dt} \sigma_H^{(v,r)}(t) &\leq \frac{\sigma_H^{(v,r)}(t)^2}{\sigma_H^{(v,r)}(t)^{\frac{2}{L_v}} + \epsilon} \cdot L_v \langle -\nabla \mathcal{L}_H(\mathcal{W}_H(t)), \mathcal{C}_H^{(v,r)}(t) \rangle. \end{aligned} \quad (\text{C.3})$$

Proof sketch (proof in Appendix C.5.9). The proof follows a line similar to that of Theorem 5, except that here conservation of unbalancedness magnitude leads to $\|\mathbf{w}(t)\|^2 \leq \sigma_H^{(v,r)}(t)^{\frac{2}{L_v}} + \epsilon$ for all $\mathbf{w} \in \text{LC}(v, r)$. Applying this inequality to:

$$\frac{d}{dt} \sigma_H^{(v,r)}(t) = \langle -\nabla \mathcal{L}_H(\mathcal{W}_H(t)), \mathcal{C}_H^{(v,r)}(t) \rangle \sum_{\mathbf{w} \in \text{LC}(v,r)} \prod_{\mathbf{w}' \in \text{LC}(v,r) \setminus \{\mathbf{w}\}} \|\mathbf{w}'(t)\|^2,$$

yields Equations (C.2) and (C.3). \square

C.3 Hierarchical Tensor Rank as Measure of Long-Range Dependencies

Section 3.5 discusses the known fact by which the hierarchical tensor rank (Definition 7) of a hierarchical tensor factorization measures the strength of long-range

¹Since norms are not differentiable at the origin, when $\sigma_H^{(v,r)}(t)$ is equal to zero it may not be differentiable with respect to time.

dependencies modeled by the equivalent convolutional network (see [49, 132, 133]). For the convenience of the reader, the current appendix formally explains this fact.

Consider a hierarchical tensor factorization with mode tree \mathcal{T} (Definition 4), weight matrices $\Theta := (\mathbf{W}^{(v)})_{v \in \mathcal{T}}$, and an equivalent convolutional network realizing a parametric input-output function f_Θ . As claimed in Section 3.3 (and formally justified in Appendix C.1), the function realized by the convolutional network takes the form $f_\Theta(\mathbf{x}^{(1)}, \dots, \mathbf{x}^{(N)}) = \langle \otimes_{n=1}^N \mathbf{x}^{(n)}, \mathcal{W}_H \rangle$, where \mathcal{W}_H stands for the end tensor of the factorization (Equation (3.3)). Proposition 9 below establishes that for any subset of indices $I \subset [N]$, the matrix rank of \mathcal{W}_H 's matricization according to I is equal to the separation rank (Definition 9) of f_Θ with respect to I , i.e. $\text{rank}[\mathcal{W}_H; I] = \text{sep}(f_\Theta; I)$. In particular, the hierarchical tensor rank of \mathcal{W}_H with respect to \mathcal{T} — $(\text{rank}[\mathcal{W}_H; \nu])_{\nu \in \mathcal{T} \setminus \{[N]\}}$ — amounts to $(\text{sep}(f_\Theta; \nu))_{\nu \in \mathcal{T} \setminus \{[N]\}}$. In the canonical case where nodes in \mathcal{T} hold adjacent indices, the separation ranks of f_Θ with respect to them measure the dependencies modeled between distinct areas of the input, i.e. the non-local (long-range) dependencies.

Proposition 9 (adaptation of Claim 1 in [49]). *Consider a hierarchical tensor factorization with mode tree \mathcal{T} (Definition 4) and weight matrices $\Theta := (\mathbf{W}^{(v)})_{v \in \mathcal{T}}$, and denote its end tensor by \mathcal{W}_H (Equation (3.3)). Let $f_\Theta : \times_{n=1}^N \mathbb{R}^{D_n} \rightarrow \mathbb{R}$ be defined by $f_\Theta(\mathbf{x}^{(1)}, \dots, \mathbf{x}^{(N)}) := \langle \otimes_{n=1}^N \mathbf{x}^{(n)}, \mathcal{W}_H \rangle$. Then, for all $I \subset [N]$:*

$$\text{rank}[\mathcal{W}_H; I] = \text{sep}(f_\Theta; I).$$

Proof sketch (proof in Appendix C.5.10). To prove that $\text{rank}[\mathcal{W}_H; I] \geq \text{sep}(f_\Theta; I)$, we derive a representation of f_Θ as a sum of $\text{rank}[\mathcal{W}_H; I]$ terms, each being a product between a function that operates over $(\mathbf{x}^{(i)})_{i \in I}$ and another that operates over the remaining input variables. For the converse, $\text{rank}[\mathcal{W}_H; I] \leq \text{sep}(f_\Theta; I)$, we prove that for any grid tensor \mathcal{W} of a function f , i.e. tensor holding the outputs of f over a grid of inputs, it holds that $\text{rank}[\mathcal{W}; I] \leq \text{sep}(f; I)$. We conclude by showing that \mathcal{W}_H is a grid tensor of f_Θ . \square

C.4 Further Experiments and Implementation Details

C.4.1 Further Experiments

Figures C.2, C.3, and C.4 supplement Figure 3.1 by including, respectively: (i) plots of additional local component norms and singular values during optimization in the experiment presented by Figure 3.1 (right); (ii) experiments with tensor sensing loss; and (iii) experiments with different hierarchical tensor factorization orders and mode trees, as well as different ground truth hierarchical tensor ranks. Figure C.5 portrays an experiment identical to that of Figure 3.6, but with ResNet34 in place of ResNet18. Figures C.6 and C.7 extend Figures 3.6 and C.5, respectively, by presenting results obtained with baseline networks that are already regularized using standard techniques (weight decay and dropout).

C.4.2 Implementation Details

In this subappendix we provide implementation details omitted from our experimental reports (Figure 3.1, Section 3.6, and Appendix C.4.1). Source code for reproducing

our results and figures, based on the PyTorch framework [172], can be found at https://github.com/asafmaman101/imp_reg_htf. All experiments were run on a single Nvidia RTX 2080 Ti GPU.

C.4.2.1 Incremental Hierarchical Tensor Rank Learning (Figures 3.1, C.2, C.3, and C.4)

Figure 3.1 (left): the minimized matrix completion loss was

$$\mathcal{L}_M(\mathbf{W}_M) = \frac{1}{|\Omega|} \sum_{(i,j) \in \Omega} ((\mathbf{W}_M)_{ij} - \mathbf{W}_{ij}^*)^2,$$

where Ω denotes a set of 2048 observed entries chosen uniformly at random (without repetition) from a matrix rank 5 ground truth $\mathbf{W}^* \in \mathbb{R}^{64 \times 64}$. We generated \mathbf{W}^* by computing $\mathbf{W}^{*(1)}\mathbf{W}^{*(2)}$, with each entry of $\mathbf{W}^{*(1)} \in \mathbb{R}^{64 \times 5}$ and $\mathbf{W}^{*(2)} \in \mathbb{R}^{5 \times 64}$ drawn independently from the standard normal distribution, and subsequently normalizing the result to be of Frobenius norm 64 (square root of its number of entries). Reconstruction error with respect to \mathbf{W}^* is based on normalized Frobenius distance, *i.e.* for a solution \mathbf{W}_M it is $\|\mathbf{W}_M - \mathbf{W}^*\| / \|\mathbf{W}^*\|$. The matrix factorization applied to the task was of depth 3 and had hidden dimensions 64 between its layers so that its rank was unconstrained. Standard deviation for initialization was set to 0.001.

Figure 3.1 (middle): the minimized tensor completion loss was:

$$\mathcal{L}_T(\mathcal{W}_T) = \frac{1}{|\Omega|} \sum_{(d_1, d_2, d_3) \in \Omega} ((\mathcal{W}_T)_{d_1, d_2, d_3} - \mathcal{W}_{d_1, d_2, d_3}^*)^2,$$

where Ω denotes a set of 2048 observed entries chosen uniformly at random (without repetition) from a tensor rank 5 ground truth $\mathcal{W}^* \in \mathbb{R}^{16, 16, 16}$. We generated \mathcal{W}^* by computing $\sum_{r=1}^5 \mathbf{W}_{:,r}^{*(1)} \otimes \mathbf{W}_{:,r}^{*(2)} \otimes \mathbf{W}_{:,r}^{*(3)}$, with each entry of $\mathbf{W}^{*(1)}$, $\mathbf{W}^{*(2)}$, and $\mathbf{W}^{*(3)} \in \mathbb{R}^{16 \times 5}$ drawn independently from the standard normal distribution, and subsequently normalizing the result to be of Frobenius norm 64 (square root of its number of entries). Reconstruction error with respect to \mathcal{W}^* is based on normalized Frobenius distance, *i.e.* for a solution \mathcal{W}_T it is $\|\mathcal{W}_T - \mathcal{W}^*\| / \|\mathcal{W}^*\|$. The tensor factorization applied to the task had $R = 256$ components so that its tensor rank was unconstrained.² Standard deviation for initialization was set to 0.001.

Figure 3.1 (right): the minimized tensor completion loss was:

$$\mathcal{L}_H(\mathcal{W}_H) = \frac{1}{|\Omega|} \sum_{(d_1, \dots, d_4) \in \Omega} ((\mathcal{W}_H)_{d_1, \dots, d_4} - \mathcal{W}_{d_1, \dots, d_4}^*)^2,$$

where Ω denotes a set of 2048 observed entries chosen uniformly at random (without repetition) from a hierarchical tensor rank $(5, 5, 5, 5, 5)$ ground truth $\mathcal{W}^* \in \mathbb{R}^{8 \times 8 \times 8 \times 8}$. We generated \mathcal{W}^* according to Equation (3.3) using a perfect binary mode tree \mathcal{T} over $[4]$ and weight matrices $(\mathbf{W}^{*(v)})_{v \in \mathcal{T}}$, where $\mathbf{W}^{*(v)} \in \mathbb{R}^{8 \times 5}$ for $v \in \{\{1\}, \dots, \{4\}\}$, $\mathbf{W}^{*(v)} \in \mathbb{R}^{5 \times 5}$ for $v \in \text{int}(\mathcal{T}) \setminus \{\{4\}\}$, and $\mathbf{W}^{*(\{4\})} \in \mathbb{R}^{5 \times 1}$. We sampled the entries of $(\mathbf{W}^{*(v)})_{v \in \mathcal{T}}$ independently from the standard normal distribution, and subsequently normalized the ground truth to be of Frobenius norm 64

²For any $D_1, \dots, D_N \in \mathbb{N}$, setting $R = (\prod_{n=1}^N D_n) / \max\{D_n\}_{n=1}^N$ suffices for expressing all tensors in $\mathbb{R}^{D_1 \times \dots \times D_N}$ (Lemma 3.41 in [85]).

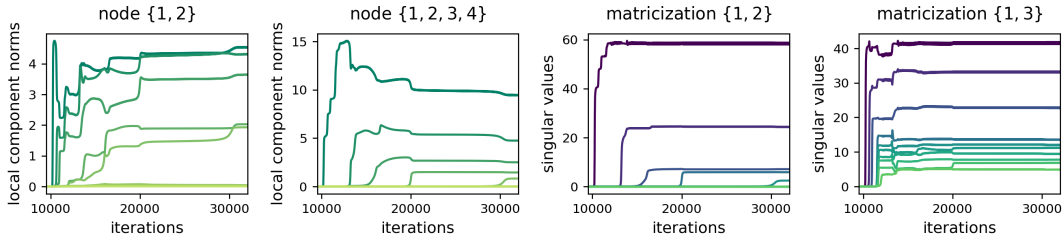


Figure C.2: Dynamics of gradient descent over order four hierarchical tensor factorization with a perfect binary mode tree (on tensor completion task) — incremental learning leads to low hierarchical tensor rank. For the hierarchical tensor factorization experiment in Figure 3.1 (right), plots present the evolution of additional quantities during optimization. **Left and second to left:** top 10 local component norms at nodes $\{1,2\}$ and $\{1,2,3,4\}$ (respectively) in the mode tree (the latter also appears in Figure 3.1 (right)). **Second to right and right:** top 10 singular values of the end tensor’s matricizations according to $\{1,2\}$ and $\{1,3\}$ (respectively). The former corresponds to a node in the mode tree, meaning its rank is part of the end tensor’s hierarchical tensor rank, whereas the latter does not. **All:** notice that, in line with our analysis (Section 3.4), local component norms move slower when small and faster when large, creating an incremental process that leads to low hierarchical tensor rank solutions. Moreover, the singular values of the end tensor’s matricizations according to nodes in the mode tree exhibit a similar behavior, whereas those of matricizations according to index sets outside the mode tree do not. The rank of a matricization lower bounds the (non-hierarchical) tensor rank (Remark 6.21 in [85]). Thus, while the hierarchical tensor rank of the obtained solution is low, its tensor rank is high. For further implementation details, such as loss definition and factorization size, see Appendix C.4.2.

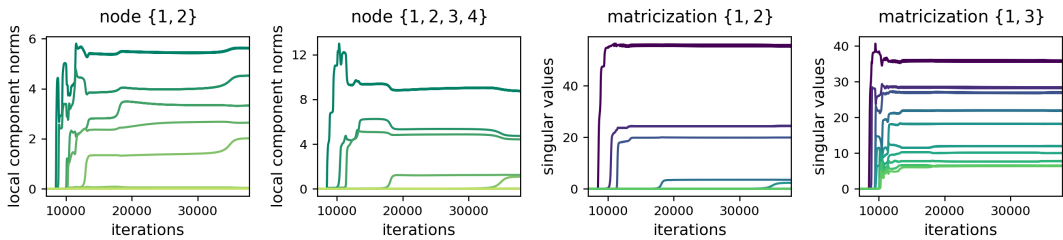


Figure C.3: Dynamics of gradient descent over order four hierarchical tensor factorization with a perfect binary mode tree (on tensor sensing task) — incremental learning leads to low hierarchical tensor rank. This figure is identical to Figure C.2, except that the minimized mean squared error was based on random linear measurements (instead of randomly chosen entries). For further implementation details, such as loss definition and factorization size, see Appendix C.4.2.

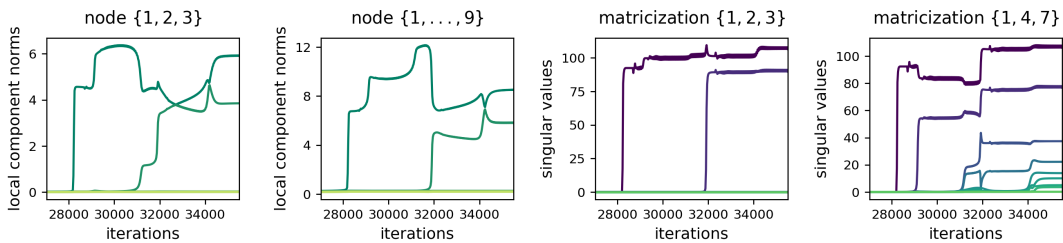


Figure C.4: Dynamics of gradient descent over order nine hierarchical tensor factorization with a perfect ternary mode tree — incremental learning leads to low hierarchical tensor rank. This figure is identical to Figure C.2, except that: (i) the hierarchical tensor factorization employed had order nine and complied with a perfect ternary mode tree; and (ii) the ground truth tensor was of hierarchical tensor rank $(2, \dots, 2)$ (Definition 7). For further implementation details, such as loss definition and factorization size, see Appendix C.4.2.

(square root of its number of entries). Reconstruction error with respect to \mathcal{W}^* is based on normalized Frobenius distance, *i.e.* for a solution \mathcal{W}_H it is $\|\mathcal{W}_H - \mathcal{W}^*\| / \|\mathcal{W}^*\|$. The hierarchical tensor factorization applied to the task had 512 local components at all interior nodes due to computational and memory considerations (increasing the number of local components had no substantial impact on the dynamics). Standard deviation for initialization was set to 0.01.

Figure C.2: plots correspond to the same experiment presented in Figure 3.1 (right).

Figure C.3: implementation details are identical to those of Figure 3.1 (right), except that the following tensor sensing loss was minimized:

$$\mathcal{L}_H(\mathcal{W}_H) = \sum_{i=1}^{2048} (\langle \otimes_{n=1}^4 \mathbf{x}^{(i,n)}, \mathcal{W}_H \rangle - \langle \otimes_{n=1}^4 \mathbf{x}^{(i,n)}, \mathcal{W}^* \rangle)^2,$$

where the entries of $(\mathbf{x}^{(i,1)}, \dots, \mathbf{x}^{(i,4)}) \in \mathbb{R}^8 \times \dots \times \mathbb{R}^8$ were sampled independently from a zero-mean Gaussian distribution with standard deviation $4096^{-1/8}$ (ensures each measurement tensor $\otimes_{n=1}^4 \mathbf{x}^{(i,n)}$ has expected square Frobenius norm 1).

Figure C.4: implementation details are identical to those of Figure 3.1 (right), except that: (i) the ground truth tensor was of order 9 with modes of dimension 3, Frobenius norm $\sqrt{19683}$ (square root of its number of entries), hierarchical tensor rank $(2, \dots, 2)$, and was generated according to a perfect ternary mode tree; (ii) reconstruction was based on 9840 entries chosen uniformly at random; (iii) the hierarchical tensor factorization applied to the task had 100 local components at all interior nodes; and (iv) standard deviation for initialization was set to 0.1.

All: using sample sizes smaller than those specified above led to similar results, up until a point where solutions found had fewer non-zero singular values, components, or local components (at all nodes) than the ground truths. Gradient descent was initialized randomly by sampling each weight in the factorization independently from a zero-mean Gaussian distribution, and was run until the loss remained under $5 \cdot 10^{-5}$ for 100 iterations in a row. For each figure, experiments were carried out with initialization standard deviations 0.1, 0.05, 0.01, 0.005, 0.001, and 0.0005. Reported are representative runs striking a balance between the potency of the incremental learning effect and run time. Reducing standard deviations further did not yield a significant change in the dynamics, yet resulted in longer optimization times due to vanishing gradients around the origin. To facilitate more efficient experimentation, we employed the adaptive learning scheme described in Appendix A.2.2.2.

C.4.2.2 Countering Locality of Convolutional Networks via Regularization (Figures 3.6, C.5, C.6, and C.7)

In all experiments, we randomly initialized the ResNet18 and ResNet34 networks according to the default PyTorch [172] implementation. The (regularized) binary cross-entropy loss was minimized via stochastic gradient descent with learning rate 0.01, momentum coefficient 0.9, and batch size 64 (for ResNet34 we used a batch size of 32 and accumulated gradients over two batches due to GPU memory considerations). Optimization proceeded until perfect training accuracy was attained for 20 consecutive epochs or 150 epochs elapsed (runs without regularization always reached perfect training accuracy). For each dataset and model combination, runs were carried out using the regularization described in Section 3.6.1 with coefficients 0, 0.1, 0.5, 1, 3, 6, 9, and 10. Values lower than those reported in Figures 3.6 and C.5 had

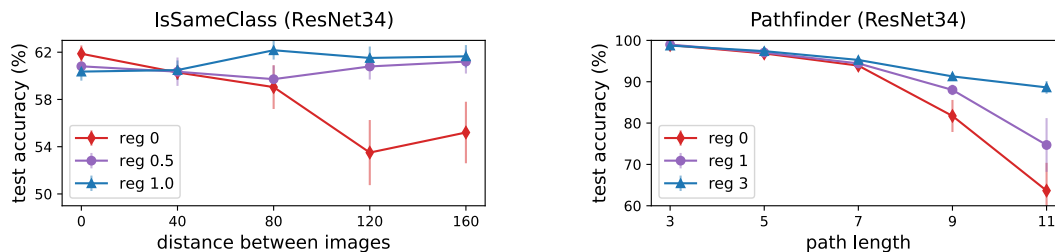


Figure C.5: Dedicated explicit regularization can counter the locality of convolutional networks, significantly improving performance on tasks with long-range dependencies. This figure is identical to Figure 3.6, except that: (i) experiments were carried out using a randomly initialized ResNet34 (as opposed to ResNet18); and (ii) it includes evaluation over a Pathfinder dataset with path length 11, since up until path length 9 an unregularized network still obtained non-trivial performance. For further details see Appendix C.4.2.2.

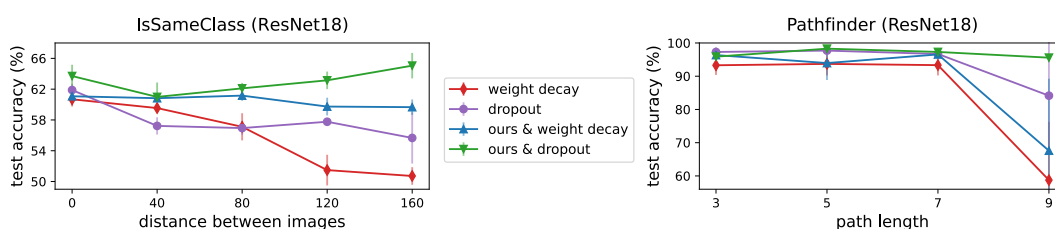


Figure C.6: Dedicated explicit regularization can counter the locality of convolutional networks (regularized via standard techniques), significantly improving performance on tasks with long-range dependencies. This figure is identical to Figure 3.6, except that instead of applying our regularizer (Section 3.6.1) to a baseline unregularized network, the baseline networks here were regularized using either weight decay or dropout, and are compared to the results obtained when applying our regularization in addition to them. Figure 3.6 shows that the test accuracy obtained by an unregularized network substantially deteriorates when increasing the (spatial) range of dependencies required to be modeled. From the plots above it is evident that, even when employing standard regularization techniques such as weight decay or dropout, a similar degradation in performance occurs. As was the case for unregularized networks, applying our dedicated regularization, in addition to these techniques, significantly improved performance. In particular, for the combination of our regularization and dropout, the test accuracy was high across all datasets. For further details such as regularization hyperparameters, see Appendix C.4.2.2.

no noticeable impact, whereas higher values typically did not allow fitting the training data. Table C.1 specifies the hyperparameters used for the different regularizations in the experiments of Figures C.6 and C.7. Dropout layers shared the same probability hyperparameter, and were inserted before blocks expanding the number of channels, *i.e.* before the first convolutional layers with 128, 256, and 512 output channels (the default ResNet18 and ResNet34 implementations do not include dropout).

At each stochastic gradient descent iteration, the subset of indices I and J used for computing the regularized objective were sampled as follows. For IsSameClass datasets, we set I to be the indices marking either the left or right CIFAR10 image uniformly at random, and then let J be the indices corresponding to the remaining CIFAR10 image. For Pathfinder datasets, I and J were set to non-overlapping 2×2 patches chosen uniformly across the input. In order to prevent additional computational overhead, alternative values for pixels indexed by J were taken from other images in the batch (as opposed to from the whole training set). Specifically, we used a permutation without fixed points to shuffle the pixel patches indexed by J across the batch.

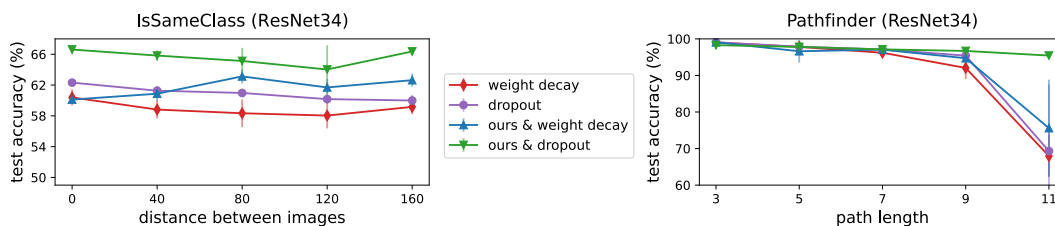


Figure C.7: Dedicated explicit regularization can counter the locality of convolutional networks (regularized via standard techniques), significantly improving performance on tasks with long-range dependencies. This figure is identical to Figure C.6, except that: (i) experiments were carried out using a randomly initialized ResNet34 (as opposed to ResNet18); and (ii) it includes evaluation over a Pathfinder dataset with path length 11, since up until path length 9 networks regularized using weight decay or dropout still obtained non-trivial performance. For further details such as regularization hyperparameters, see Appendix C.4.2.2.

Table C.1: Hyperparameters for the regularizations employed in the experiments of Figures C.6 and C.7. For every model and dataset type combination, table reports the weight decay coefficient and dropout probability used when applied individually, as well as when combined with our regularization (described in Section 3.6.1), whose coefficients are also specified. These hyperparameters were tuned on the datasets with largest spatial range between salient regions of the input. That is, for each model separately, their values on IsSameClass datasets were set to those achieving the best test accuracy over a dataset with 160 pixels between CIFAR10 images. Similarly, their values on Pathfinder datasets were set to those achieving the best test accuracy over a dataset with connecting path length 9 for ResNet18 and path length 11 for ResNet34. For further details see the captions of Figures C.6 and C.7, as well as Appendix C.4.2.2.

	ResNet18		ResNet34	
	IsSameClass	Pathfinder	IsSameClass	Pathfinder
Weight Decay	0.001	0.01	0.01	0.001
Dropout	0.6	0.5	0.3	0.2
Ours & Weight Decay	1 & 0.001	0.1 & 0.01	1 & 0.0001	0.1 & 0.001
Ours & Dropout	1 & 0.5	0.1 & 0.4	1 & 0.5	0.5 & 0.3

IsSameClass datasets consisted of 5000 training and 10000 test samples. Each sample was generated by first drawing uniformly at random a label from $\{0, 1\}$ and an image from CIFAR10. Then, depending on the chosen label, another image was sampled either from the same class (for label 1) or from all other classes (for label 0). Lastly, the CIFAR10 images were placed at a predetermined horizontal distance from each other around the center of a 224×224 image filled with zeros. For example, when the horizontal distance is 0, the CIFAR10 images are adjacent, and when it is 160, they reside in opposite borders of the 224×224 input. Pathfinder datasets consisted of 10000 training and 10000 test samples. Given a path length, the corresponding dataset was generated according to the protocol of [143], with hyperparameters: circle radius 3, paddle length 5, paddle thickness 2, inner paddle margin 3, and continuity 1.8. See [143] for additional information regarding the data generation process. As to be expected, when running a subset of all experiments using larger training set sizes (for both IsSameClass and Pathfinder datasets), we observed improved generalization across the board. Nevertheless, the addition of training samples did not alleviate the degradation in test accuracy observed for larger horizontal distances and path lengths, nor did it affect the beneficial impact of our regularization. That is, the trends observed in Figures 3.6, C.5, C.6, and C.7 remained intact up to a certain shift upwards.

C.5 Deferred Proofs

C.5.1 Additional Notation

Before delving into the proofs, we introduce the following notation.

General. A colon is used to indicate a range of entries in a mode, e.g. $\mathbf{W}_{i,:} \in \mathbb{R}^{D'}$ and $\mathbf{W}_{:,j} \in \mathbb{R}^D$ are the i 'th row and j 'th column of $\mathbf{W} \in \mathbb{R}^{D \times D'}$, respectively, and $\mathbf{W}_{:i,:j} \in \mathbb{R}^{i \times j}$ is the sub-matrix of \mathbf{W} consisting of its first i rows and j columns. For $\mathcal{W} \in \mathbb{R}^{D_1 \times \dots \times D_N}$, we let $\text{vec}(\mathcal{W}) \in \mathbb{R}^{\prod_{n=1}^N D_n}$ be its arrangement as a vector. The tensor and Kronecker products are denoted by \otimes and \circ , respectively.

Hierarchical tensor factorization. For a mode tree \mathcal{T} over $[N]$ (Definition 4), we denote the set of nodes in the sub-tree of \mathcal{T} whose root is $\nu \in \mathcal{T}$ by $\mathcal{T}(\nu) \subset \mathcal{T}$. The sets of left and right siblings of $\nu \in \mathcal{T}$ are denoted by $\overleftarrow{\mathcal{S}}(\nu)$ and $\overrightarrow{\mathcal{S}}(\nu)$, respectively. For $\nu \in \mathcal{T}$, we let $\mathcal{W}^{(\nu,:)}$ be the tensor obtained by stacking $(\mathcal{W}^{(\nu,r)})_{r=1}^{R_{pa(\nu)}}$ into a single tensor, i.e. $\mathcal{W}_{:, \dots, :, r}^{(\nu,:)} = \mathcal{W}^{(\nu,r)}$ for all $r \in [R_{pa(\nu)}]$. Given weight matrices $(\mathbf{W}^{(\nu)} \in \mathbb{R}^{R_\nu, R_{pa(\nu)}})_{\nu \in \mathcal{T}}$, the function mapping them to the end tensor they produce according to Equation (3.3) is denoted by $\mathcal{H}((\mathbf{W}^{(\nu)})_{\nu \in \mathcal{T}})$. For $\nu \in \mathcal{T}$, with slight abuse of notation we let $\mathcal{H}((\mathbf{W}^{(\nu')})_{\nu' \in \mathcal{T} \setminus \mathcal{T}(\nu)}, \mathcal{W}^{(\nu,:)})$ be the function mapping $(\mathcal{W}^{(\nu,r)})_{r=1}^{R_{pa(\nu)}}$ and weight matrices outside of $\mathcal{T}(\nu)$ to the end tensor they produce.

C.5.2 Useful Lemmas

C.5.2.1 Technical

Lemma 37. For any $\mathcal{U} \in \mathbb{R}^{D_1 \times \dots \times D_N}$, $\mathcal{V} \in \mathbb{R}^{H_1 \times \dots \times H_K}$, and $I \subset [N + K]$:

$$\llbracket \mathcal{U} \otimes \mathcal{V}; I \rrbracket = \llbracket \mathcal{U}; I \cap [N] \rrbracket \circ \llbracket \mathcal{V}; I - N \cap [K] \rrbracket,$$

where $I - N := \{i - N : i \in I\}$.

Proof. The identity follows directly from the definitions of the tensor and Kronecker products. \square

Lemma 38. For any $\mathbf{U} \in \mathbb{R}^{D_1 \times D_2}$, $\mathbf{V} \in \mathbb{R}^{D_2 \times D_3}$, and $\mathbf{w} \in \mathbb{R}^{D_4}$, the following holds:

$$(\mathbf{UV}) \circ \mathbf{w}^\top = \mathbf{U} (\mathbf{V} \circ \mathbf{w}^\top) \quad , \quad \mathbf{w}^\top \circ (\mathbf{UV}) = \mathbf{U} (\mathbf{w}^\top \circ \mathbf{V}) .$$

Proof. According to the mixed-product property of the Kronecker product, for any matrices $\mathbf{A}, \mathbf{A}', \mathbf{B}, \mathbf{B}'$ for which \mathbf{AA}' and \mathbf{BB}' are defined, it holds that $(\mathbf{AA}') \circ (\mathbf{BB}') = (\mathbf{A} \circ \mathbf{B})(\mathbf{A}' \circ \mathbf{B}')$. Thus:

$$(\mathbf{UV}) \circ \mathbf{w}^\top = (\mathbf{UV}) \circ (\mathbf{1} \cdot \mathbf{w}^\top) = (\mathbf{U} \circ \mathbf{1})(\mathbf{V} \circ \mathbf{w}^\top) = \mathbf{U}(\mathbf{V} \circ \mathbf{w}^\top),$$

where $\mathbf{1}$ is treated as the 1-by-1 identity matrix. Similarly:

$$\mathbf{w}^\top \circ (\mathbf{UV}) = (\mathbf{1} \cdot \mathbf{w}^\top) \circ (\mathbf{UV}) = (\mathbf{1} \circ \mathbf{U})(\mathbf{w}^\top \circ \mathbf{V}) = \mathbf{U}(\mathbf{w}^\top \circ \mathbf{V}).$$

\square

C.5.2.2 Hierarchical Tensor Factorization

Suppose that use a hierarchical tensor factorization with mode tree \mathcal{T} , weight matrices $(\mathbf{W}^{(v)} \in \mathbb{R}^{R_v \times R_{Pa(v)}})_{v \in \mathcal{T}}$, and end tensor $\mathcal{W}_H \in \mathbb{R}^{D_1 \times \dots \times D_N}$ (Equations (3.3)) to minimize ϕ_H (Equation (3.4)) via gradient flow (Equation (3.5)). Under this setting, we prove the following technical lemmas.

Lemma 39. *The functions $\mathcal{H}((\mathbf{W}^{(v)})_{v \in \mathcal{T}})$ and $\mathcal{H}((\mathbf{W}^{(v')})_{v' \in \mathcal{T} \setminus \mathcal{T}(v)}, \mathcal{W}^{(v,:)}),$ for $v \in \mathcal{T}$, defined in Appendix C.5.1, are multilinear.*

Proof. We begin by proving that $\mathcal{H}((\mathbf{W}^{(v)})_{v \in \mathcal{T}})$ is multilinear. Fix $v \in \mathcal{T}$, and let $\mathbf{W}^{(v)}, \mathbf{U}^{(v)} \in \mathbb{R}^{R_v, R_{Pa(v)}}$, and $\alpha > 0$.

Homogeneity. Denote by $(\mathcal{U}_\alpha^{(v',r)})_{v' \in \mathcal{T}, r \in [R_{Pa(v')}]}$ the intermediate tensors produced when computing the end tensor $\mathcal{H}((\mathbf{W}^{(v')})_{v' \in \mathcal{T} \setminus \{v\}}, \alpha \cdot \mathbf{W}^{(v)})$ according to Equation (3.3) (there denoted $(\mathcal{W}^{(v',r)})_{v',r}$). If v is a leaf node, then $\mathcal{U}_\alpha^{(v,r)} = \alpha \cdot \mathbf{W}_{:,r}^{(v)} = \alpha \cdot \mathcal{W}^{(v,r)}$ for all $r \in [R_{Pa(v)}]$. Otherwise, if v is an interior node, a straightforward computation leads to the same conclusion, *i.e.* for all $r \in [R_{Pa(v)}]$:

$$\begin{aligned} \mathcal{U}_\alpha^{(v,r)} &= \pi_v \left(\sum_{r'=1}^{R_v} \alpha \cdot \mathbf{W}_{r',r}^{(v)} \left[\otimes_{v_c \in \mathcal{C}(v)} \mathcal{W}^{(v_c, r')} \right] \right) \\ &= \alpha \cdot \pi_v \left(\sum_{r'=1}^{R_v} \mathbf{W}_{r',r}^{(v)} \left[\otimes_{v_c \in \mathcal{C}(v)} \mathcal{W}^{(v_c, r')} \right] \right) \\ &= \alpha \cdot \mathcal{W}^{(v,r)}, \end{aligned}$$

where the second equality is by the linearity of π_v (recall it is merely a reordering of the tensor entries). Moving on to the parent of v , multilinearity of the tensor product implies that for all $r \in [R_{Pa(Pa(v))}]$:

$$\begin{aligned} \mathcal{U}_\alpha^{(Pa(v),r)} &= \pi_{Pa(v)} \left(\sum_{r'=1}^{R_{Pa(v)}} \mathbf{W}_{r',r}^{(Pa(v))} \left[\left(\otimes_{v_c \in \overleftarrow{\mathcal{S}}(v)} \mathcal{W}^{(v_c, r')} \right) \otimes \mathcal{U}_\alpha^{(v,r')} \otimes \left(\otimes_{v_c \in \overrightarrow{\mathcal{S}}(v)} \mathcal{W}^{(v_c, r')} \right) \right] \right) \\ &= \pi_{Pa(v)} \left(\sum_{r'=1}^{R_{Pa(v)}} \mathbf{W}_{r',r}^{(Pa(v))} \left[\left(\otimes_{v_c \in \overleftarrow{\mathcal{S}}(v)} \mathcal{W}^{(v_c, r')} \right) \otimes (\alpha \cdot \mathcal{W}^{(v,r')}) \otimes \left(\otimes_{v_c \in \overrightarrow{\mathcal{S}}(v)} \mathcal{W}^{(v_c, r')} \right) \right] \right) \\ &= \alpha \cdot \pi_{Pa(v)} \left(\sum_{r'=1}^{R_{Pa(v)}} \mathbf{W}_{r',r}^{(Pa(v))} \left[\otimes_{v_c \in \mathcal{C}(Pa(v))} \mathcal{W}^{(v_c, r')} \right] \right) \\ &= \alpha \cdot \mathcal{W}^{(Pa(v),r)}. \end{aligned}$$

An inductive claim over the path from v to the root $[N]$ therefore yields:

$$\mathcal{H}((\mathbf{W}^{(v')})_{v' \in \mathcal{T} \setminus \{v\}}, \alpha \cdot \mathbf{W}^{(v)}) = \alpha \cdot \mathcal{H}((\mathbf{W}^{(v')})_{v' \in \mathcal{T}}). \quad (\text{C.4})$$

Additivity. We let $(\mathcal{U}^{(v',r)})_{v' \in \mathcal{T}, r \in [R_{Pa(v')}]}$ and $(\mathcal{U}_+^{(v',r)})_{v' \in \mathcal{T}, r \in [R_{Pa(v')}]}$ denote the intermediate tensors produced when computing

$$\mathcal{H}((\mathbf{W}^{(v')})_{v' \in \mathcal{T} \setminus \{v\}}, \mathbf{U}^{(v)})$$

and

$$\mathcal{H}((\mathbf{W}^{(v')})_{v' \in \mathcal{T} \setminus \{v\}}, \mathbf{W}^{(v)} + \mathbf{U}^{(v)})$$

according to Equation (3.3), respectively. If v is a leaf node, we have that $\mathcal{U}_+^{(v,r)} = \mathbf{W}_{:,r}^{(v)} + \mathbf{U}_{:,r}^{(v)} = \mathcal{W}^{(v,r)} + \mathcal{U}^{(v,r)}$ for all $r \in [R_{Pa(v)}]$. Otherwise, if v is an interior node,

we arrive at the same conclusion, *i.e.* for all $r \in [R_{Pa(v)}]$:

$$\begin{aligned}\mathcal{U}_+^{(v,r)} &= \pi_v \left(\sum_{r'=1}^{R_v} \left(\mathbf{W}_{r',r}^{(v)} + \mathbf{U}_{r',r}^{(v)} \right) \left[\otimes_{v_c \in C(v)} \mathcal{W}^{(v_c,r')} \right] \right) \\ &= \pi_v \left(\sum_{r'=1}^{R_v} \mathbf{W}_{r',r}^{(v)} \left[\otimes_{v_c \in C(v)} \mathcal{W}^{(v_c,r')} \right] \right) + \pi_v \left(\sum_{r'=1}^{R_v} \mathbf{U}_{r',r}^{(v)} \left[\otimes_{v_c \in C(v)} \mathcal{W}^{(v_c,r')} \right] \right) \\ &= \mathcal{W}^{(v,r)} + \mathcal{U}^{(v,r)},\end{aligned}$$

where the second equality is by the linearity of π_v . Then, for any $r \in [R_{Pa(Pa(v))}]$:

$$\begin{aligned}\mathcal{U}_+^{(Pa(v),r)} &= \pi_{Pa(v)} \left(\sum_{r'=1}^{R_{Pa(v)}} \mathbf{W}_{r',r}^{(Pa(v))} \left[\left(\otimes_{v_c \in \overleftarrow{S}(v)} \mathcal{W}^{(v_c,r')} \right) \otimes \mathcal{U}_+^{(v,r')} \otimes \left(\otimes_{v_c \in \overrightarrow{S}(v)} \mathcal{W}^{(v_c,r')} \right) \right] \right) \\ &= \pi_{Pa(v)} \left(\sum_{r'=1}^{R_{Pa(v)}} \mathbf{W}_{r',r}^{(Pa(v))} \left[\left(\otimes_{v_c \in \overleftarrow{S}(v)} \mathcal{W}^{(v_c,r')} \right) \otimes \left(\mathcal{W}^{(v,r')} + \mathcal{U}^{(v,r')} \right) \otimes \left(\otimes_{v_c \in \overrightarrow{S}(v)} \mathcal{W}^{(v_c,r')} \right) \right] \right) \\ &= \pi_{Pa(v)} \left(\sum_{r'=1}^{R_{Pa(v)}} \mathbf{W}_{r',r}^{(Pa(v))} \left[\otimes_{v_c \in C(Pa(v))} \mathcal{W}^{(v_c,r')} \right] \right) + \\ &\quad \pi_{Pa(v)} \left(\sum_{r'=1}^{R_{Pa(v)}} \mathbf{W}_{r',r}^{(Pa(v))} \left[\left(\otimes_{v_c \in \overleftarrow{S}(v)} \mathcal{W}^{(v_c,r')} \right) \otimes \mathcal{U}^{(v,r')} \otimes \left(\otimes_{v_c \in \overrightarrow{S}(v)} \mathcal{W}^{(v_c,r')} \right) \right] \right) \\ &= \mathcal{W}^{(Pa(v),r)} + \mathcal{U}^{(Pa(v),r)},\end{aligned}$$

where the penultimate equality is by multilinearity of the tensor product as well as linearity of $\pi_{Pa(v)}$. An induction over the path from v to the root thus leads to:

$$\mathcal{H}((\mathbf{W}^{(v')})_{v' \in \mathcal{T} \setminus \{v\}}, \mathbf{W}^{(v)} + \mathbf{U}^{(v)}) = \mathcal{H}((\mathbf{W}^{(v')})_{v' \in \mathcal{T}}) + \mathcal{H}((\mathbf{W}^{(v')})_{v' \in \mathcal{T} \setminus \{v\}}, \mathbf{U}^{(v)}). \quad (\text{C.5})$$

Equations (C.4) and (C.5) establish that $\mathcal{H}((\mathbf{W}^{(v)})_{v \in \mathcal{T}})$ is multilinear. The proof for $\mathcal{H}((\mathbf{W}^{(v')})_{v' \in \mathcal{T} \setminus \mathcal{T}(v)}, \mathcal{W}^{(v,:)})$ follows by analogous derivations. \square

Lemma 40. *Suppose there exists $v \in \mathcal{T}$ such that $\mathcal{W}^{(v,r)} = 0$ for all $r \in [R_{Pa(v)}]$, where $\mathcal{W}^{(v,r)}$ is as defined in Equation (3.3). Then, $\mathcal{W}_H = 0$.*

Proof. Since $\mathcal{W}^{(v,r)} = 0$ for all $r \in [R_{Pa(v)}]$, for any $r' \in [R_{Pa(Pa(v))}]$ we have that:

$$\begin{aligned}\mathcal{W}^{(Pa(v),r')} &= \pi_{Pa(v)} \left(\sum_{r=1}^{R_{Pa(v)}} \mathbf{W}_{r,r'}^{(Pa(v))} \left[\left(\otimes_{v_c \in \overleftarrow{S}(v)} \mathcal{W}^{(v_c,r)} \right) \otimes \mathcal{W}^{(v,r)} \otimes \left(\otimes_{v_c \in \overrightarrow{S}(v)} \mathcal{W}^{(v_c,r)} \right) \right] \right) \\ &= \pi_{Pa(v)} \left(\sum_{r=1}^{R_{Pa(v)}} \mathbf{W}_{r,r'}^{(Pa(v))} \left[\left(\otimes_{v_c \in \overleftarrow{S}(v)} \mathcal{W}^{(v_c,r)} \right) \otimes 0 \otimes \left(\otimes_{v_c \in \overrightarrow{S}(v)} \mathcal{W}^{(v_c,r)} \right) \right] \right) \\ &= 0.\end{aligned}$$

Thus, the claim readily follows by an induction up the path from v to the root $[N]$. \square

Lemma 41. *For any $v \in \text{int}(\mathcal{T})$ and $r \in [R_{Pa(v)}]$:*

$$\|\mathcal{W}^{(v,r)}\| \leq \|\mathbf{W}_{:,r}^{(v)}\| \cdot \prod_{v_c \in C(v)} \|\mathcal{W}^{(v_c,:)}\|,$$

where $\mathcal{W}^{(v_c,:)}$, for $v_c \in C(v)$, is the tensor obtained by stacking $(\mathcal{W}^{(v_c,r')})_{r'=1}^{R_v}$ into a single tensor, *i.e.* $\mathcal{W}_{:, \dots, :; r'}^{(v_c,:)} = \mathcal{W}^{(v_c,r')}$ for all $r' \in [R_v]$.

Proof. By the definition of $\mathcal{W}^{(v,r)}$ (Equation (3.3)) we have that:

$$\begin{aligned}\|\mathcal{W}^{(v,r)}\| &= \left\| \pi_v \left(\sum_{r'=1}^{R_v} \mathbf{W}_{r',r}^{(v)} \left[\otimes_{v_c \in C(v)} \mathcal{W}^{(v_c,r')} \right] \right) \right\| \\ &= \left\| \sum_{r'=1}^{R_v} \mathbf{W}_{r',r}^{(v)} \left[\otimes_{v_c \in C(v)} \mathcal{W}^{(v_c,r')} \right] \right\|,\end{aligned}$$

where the second equality is due to the fact that π_v merely reorders entries of a tensor, and therefore does not alter its Frobenius norm. Vectorizing each $\otimes_{v_c \in C(v)} \mathcal{W}^{(v_c, r')}$, we may write $\|\mathcal{W}^{(v, r)}\|$ as the Frobenius norm of a matrix-vector product:

$$\|\mathcal{W}^{(v, r)}\| = \left\| \left(\text{vec}(\otimes_{v_c \in C(v)} \mathcal{W}^{(v_c, 1)}), \dots, \text{vec}(\otimes_{v_c \in C(v)} \mathcal{W}^{(v_c, R_v)}) \right) \mathbf{W}_{:,r}^{(v)} \right\|.$$

Hence, sub-multiplicativity of the Frobenius norm gives:

$$\|\mathcal{W}^{(v, r)}\| \leq \|\mathbf{W}_{:,r}^{(v)}\| \cdot \left\| \left(\text{vec}(\otimes_{v_c \in C(v)} \mathcal{W}^{(v_c, 1)}), \dots, \text{vec}(\otimes_{v_c \in C(v)} \mathcal{W}^{(v_c, R_v)}) \right) \right\|. \quad (\text{C.6})$$

Notice that:

$$\begin{aligned} \left\| \left(\text{vec}(\otimes_{v_c \in C(v)} \mathcal{W}^{(v_c, 1)}), \dots, \text{vec}(\otimes_{v_c \in C(v)} \mathcal{W}^{(v_c, R_v)}) \right) \right\|^2 &= \sum_{r'=1}^{R_v} \|\otimes_{v_c \in C(v)} \mathcal{W}^{(v_c, r')}\|^2 \\ &= \sum_{r'=1}^{R_v} \prod_{v_c \in C(v)} \|\mathcal{W}^{(v_c, r')}\|^2 \\ &\leq \prod_{v_c \in C(v)} \left(\sum_{r'=1}^{R_v} \|\mathcal{W}^{(v_c, r')}\|^2 \right) \\ &= \prod_{v_c \in C(v)} \|\mathcal{W}^{(v_c, :)}\|^2, \end{aligned}$$

where the second transition is by the fact that the norm of a tensor product is equal to the product of the norms, and the inequality is due to $\prod_{v_c \in C(v)} \left(\sum_{r'=1}^{R_v} \|\mathcal{W}^{(v_c, r')}\|^2 \right)$ being a sum of non-negative elements which includes $\sum_{r'=1}^{R_v} \prod_{v_c \in C(v)} \|\mathcal{W}^{(v_c, r')}\|^2$. Taking the square root of both sides in the equation above and plugging it into Equation (C.6) completes the proof. \square

Lemma 42. For any $v \in \text{int}(\mathcal{T})$:

$$\|\mathcal{W}^{(v, :)}\| \leq \|\mathbf{W}^{(v)}\| \cdot \prod_{v_c \in C(v)} \|\mathcal{W}^{(v_c, :)}\|,$$

where $\mathcal{W}^{(v_c, :)}$, for $v_c \in C(v)$, is the tensor obtained by stacking $(\mathcal{W}^{(v_c, r)})_{r=1}^{R_v}$ into a single tensor, i.e. $\mathcal{W}_{:, \dots, :; r}^{(v_c, :)} = \mathcal{W}^{(v_c, r)}$ for all $r \in [R_v]$.

Proof. We may explicitly write $\|\mathcal{W}^{(v, :)}\|^2$ as follows:

$$\|\mathcal{W}^{(v, :)}\|^2 = \sum_{r=1}^{R_{Pa(v)}} \|\mathcal{W}^{(v, r)}\|^2. \quad (\text{C.7})$$

For each $r \in [R_{Pa(v)}]$, by Lemma 41 we know that:

$$\|\mathcal{W}^{(v, r)}\|^2 \leq \|\mathbf{W}_{:,r}^{(v)}\|^2 \cdot \prod_{v_c \in C(v)} \|\mathcal{W}^{(v_c, :)}\|^2.$$

Thus, going back to Equation (C.7) we arrive at:

$$\|\mathcal{W}^{(v, :)}\|^2 \leq \sum_{r=1}^{R_{Pa(v)}} \|\mathbf{W}_{:,r}^{(v)}\|^2 \cdot \prod_{v_c \in C(v)} \|\mathcal{W}^{(v_c, :)}\|^2 = \|\mathbf{W}^{(v)}\|^2 \cdot \prod_{v_c \in C(v)} \|\mathcal{W}^{(v_c, :)}\|^2.$$

Taking the square root of both sides concludes the proof. \square

Lemma 43. For any $v \in \mathcal{T}$ and $\Delta \in \mathbb{R}^{R_v \times R_{Pa(v)}}$:

$$\left\langle \frac{\partial}{\partial \mathbf{W}^{(v)}} \phi_H((\mathbf{W}^{(v')})_{v' \in \mathcal{T}}), \Delta \right\rangle = \left\langle \nabla \mathcal{L}_H(\mathcal{W}_H), \mathcal{H}((\mathbf{W}^{(v')})_{v' \in \mathcal{T} \setminus \{v\}}, \Delta) \right\rangle.$$

Proof. We treat $(\mathbf{W}^{(v')})_{v' \in \mathcal{T} \setminus \{v\}}$ as fixed, and with slight abuse of notation consider:

$$\phi_{\mathbf{H}}^{(v)}(\mathbf{W}^{(v)}) := \phi_{\mathbf{H}}((\mathbf{W}^{(v')})_{v' \in \mathcal{T}}).$$

For $\Delta \in \mathbb{R}^{R_v \times R_{Pa(v)}}$, by multilinearity of \mathcal{H} (Lemma 39) we have that:

$$\begin{aligned} \phi_{\mathbf{H}}^{(v)}(\mathbf{W}^{(v)} + \Delta) &= \mathcal{L}_{\mathbf{H}} \left(\mathcal{H} \left((\mathbf{W}^{(v')})_{v' \in \mathcal{T} \setminus \{v\}}, \mathbf{W}^{(v)} + \Delta \right) \right) \\ &= \mathcal{L}_{\mathbf{H}} \left(\mathcal{W}_{\mathbf{H}} + \mathcal{H} \left((\mathbf{W}^{(v')})_{v' \in \mathcal{T} \setminus \{v\}}, \Delta \right) \right). \end{aligned}$$

According to the first order Taylor approximation of $\mathcal{L}_{\mathbf{H}}$ we may write:

$$\begin{aligned} \phi_{\mathbf{H}}^{(v)}(\mathbf{W}^{(v)} + \Delta) &= \mathcal{L}_{\mathbf{H}}(\mathcal{W}_{\mathbf{H}}) + \left\langle \nabla \mathcal{L}_{\mathbf{H}}(\mathcal{W}_{\mathbf{H}}), \mathcal{H} \left((\mathbf{W}^{(v')})_{v' \in \mathcal{T} \setminus \{v\}}, \Delta \right) \right\rangle + o(\|\Delta\|) \\ &= \phi_{\mathbf{H}}^{(v)}(\mathbf{W}^{(v)}) + \left\langle \nabla \mathcal{L}_{\mathbf{H}}(\mathcal{W}_{\mathbf{H}}), \mathcal{H} \left((\mathbf{W}^{(v')})_{v' \in \mathcal{T} \setminus \{v\}}, \Delta \right) \right\rangle + o(\|\Delta\|). \end{aligned}$$

The term $\left\langle \nabla \mathcal{L}_{\mathbf{H}}(\mathcal{W}_{\mathbf{H}}), \mathcal{H} \left((\mathbf{W}^{(v')})_{v' \in \mathcal{T} \setminus \{v\}}, \Delta \right) \right\rangle$ is a linear function of Δ . Therefore, uniqueness of the linear approximation of $\phi_{\mathbf{H}}^{(v)}$ at $\mathbf{W}^{(v)}$ implies:

$$\left\langle \frac{d}{d\mathbf{W}^{(v)}} \phi_{\mathbf{H}}^{(v)}(\mathbf{W}^{(v)}), \Delta \right\rangle = \left\langle \nabla \mathcal{L}_{\mathbf{H}}(\mathcal{W}_{\mathbf{H}}), \mathcal{H} \left((\mathbf{W}^{(v')})_{v' \in \mathcal{T} \setminus \{v\}}, \Delta \right) \right\rangle.$$

Noticing that $\frac{\partial}{\partial \mathbf{W}^{(v)}} \phi_{\mathbf{H}}((\mathbf{W}^{(v')})_{v' \in \mathcal{T}}) = \frac{d}{d\mathbf{W}^{(v)}} \phi_{\mathbf{H}}^{(v)}(\mathbf{W}^{(v)})$ completes the proof. \square

Lemma 44. For any $v \in \text{int}(\mathcal{T})$, $r \in [R_v]$, and $\Delta \in \mathbb{R}^{R_{Pa(v)}}$:

$$\left\langle \frac{\partial}{\partial \mathbf{W}_{r,:}^{(v)}} \phi_{\mathbf{H}}((\mathbf{W}^{(v')})_{v' \in \mathcal{T}}), \Delta^{\top} \right\rangle = \left\langle \nabla \mathcal{L}_{\mathbf{H}}(\mathcal{W}_{\mathbf{H}}), \mathcal{H} \left((\mathbf{W}^{(v')})_{v' \in \mathcal{T} \setminus \{v\}}, \text{PadR}_r(\Delta^{\top}) \right) \right\rangle, \quad (\text{C.8})$$

where $\text{PadR}_r(\Delta^{\top}) \in \mathbb{R}^{R_v \times R_{Pa(v)}}$ is the matrix whose r 'th row is Δ^{\top} , and all the rest are zero. Furthermore, for any $v_c \in \mathcal{C}(v)$ and $\Delta \in \mathbb{R}^{R_{v_c}}$:

$$\left\langle \frac{\partial}{\partial \mathbf{W}_{:,r}^{(v_c)}} \phi_{\mathbf{H}}((\mathbf{W}^{(v')})_{v' \in \mathcal{T}}), \Delta \right\rangle = \left\langle \nabla \mathcal{L}_{\mathbf{H}}(\mathcal{W}_{\mathbf{H}}), \mathcal{H} \left((\mathbf{W}^{(v')})_{v' \in \mathcal{T} \setminus \{v_c\}}, \text{PadC}_r(\Delta) \right) \right\rangle, \quad (\text{C.9})$$

where $\text{PadC}_r(\Delta) \in \mathbb{R}^{R_{v_c} \times R_v}$ is the matrix whose r 'th column is Δ , and all the rest are zero.

Proof. Equations (C.8) and (C.9) are direct implications of Lemma 43 since:

$$\left\langle \frac{\partial}{\partial \mathbf{W}_{r,:}^{(v)}} \phi_{\mathbf{H}}((\mathbf{W}^{(v')})_{v' \in \mathcal{T}}), \Delta^{\top} \right\rangle = \left\langle \frac{\partial}{\partial \mathbf{W}^{(v)}} \phi_{\mathbf{H}}((\mathbf{W}^{(v')})_{v' \in \mathcal{T}}), \text{PadR}_r(\Delta^{\top}) \right\rangle,$$

and

$$\left\langle \frac{\partial}{\partial \mathbf{W}_{:,r}^{(v_c)}} \phi_{\mathbf{H}}((\mathbf{W}^{(v')})_{v' \in \mathcal{T}}), \Delta \right\rangle = \left\langle \frac{\partial}{\partial \mathbf{W}^{(v_c)}} \phi_{\mathbf{H}}((\mathbf{W}^{(v')})_{v' \in \mathcal{T}}), \text{PadC}_r(\Delta) \right\rangle.$$

\square

Lemma 45. *Let $v \in \text{int}(\mathcal{T})$, $v_c \in C(v)$, and $r \in [R_v]$. If both $\mathbf{W}_{r,:}^{(v)} = 0$ and $\mathbf{W}_{:,r}^{(v_c)} = 0$, then:*

$$\frac{\partial}{\partial \mathbf{W}_{r,:}^{(v)}} \phi_H((\mathbf{W}^{(v')})_{v' \in \mathcal{T}}) = 0, \quad (\text{C.10})$$

and

$$\frac{\partial}{\partial \mathbf{W}_{:,r}^{(v_c)}} \phi_H((\mathbf{W}^{(v')})_{v' \in \mathcal{T}}) = 0. \quad (\text{C.11})$$

Proof. We show that $\mathcal{H}((\mathbf{W}^{(v')})_{v' \in \mathcal{T} \setminus \{v\}}, \text{PadR}_r(\Delta^\top)) = 0$ for all $\Delta \in \mathbb{R}^{Pa(v)}$. Equation (C.10) then follows from Equation (C.8) in Lemma 44. Fix some $\Delta \in \mathbb{R}^{Pa(v)}$ and let $(\mathcal{U}^{(v',r')})_{v' \in \mathcal{T}, r' \in [R_{Pa(v)}]}$ be the intermediate tensors produced when computing

$$\mathcal{H}((\mathbf{W}^{(v')})_{v' \in \mathcal{T} \setminus \{v\}}, \text{PadR}_r(\Delta^\top))$$

according to Equation (3.3) (there denoted $(\mathcal{W}^{(v',r')})_{v',r'}$). For any $\bar{r} \in [R_{Pa(v)}]$ we have that:

$$\mathcal{U}^{(v,\bar{r})} = \pi_v \left(\sum_{r'=1}^{R_v} \text{PadR}_r(\Delta^\top)_{r',\bar{r}} \left[\otimes_{v' \in C(v)} \mathcal{W}^{(v',r')} \right] \right) = \pi_v \left(\Delta_{\bar{r}} \left[\otimes_{v' \in C(v)} \mathcal{W}^{(v',r')} \right] \right).$$

The fact that $\mathbf{W}_{:,r}^{(v_c)} = 0$ implies that $\mathcal{W}^{(v_c,r)} := \pi_{v_c} \left(\sum_{r'=1}^{R_{v_c}} \mathbf{W}_{r',r}^{(v_c)} \left[\otimes_{v' \in C(v)} \mathcal{W}^{(v',r')} \right] \right) = 0$, and so for every $r' \in [R_{Pa(v)}]$:

$$\mathcal{U}^{(v,\bar{r})} = \pi_v \left(\Delta_{\bar{r}} \left[\left(\otimes_{v' \in \overleftarrow{S}(v_c)} \mathcal{W}^{(v',r')} \right) \otimes 0 \otimes \left(\otimes_{v' \in \overrightarrow{S}(v_c)} \mathcal{W}^{(v',r')} \right) \right] \right) = 0.$$

Lemma 40 then gives $\mathcal{H}((\mathbf{W}^{(v')})_{v' \in \mathcal{T} \setminus \{v\}}, \text{PadR}_r(\Delta^\top)) = 0$, completing this part of the proof.

Next, we show that $\mathcal{H}((\mathbf{W}^{(v')})_{v' \in \mathcal{T} \setminus \{v_c\}}, \text{PadC}_r(\Delta)) = 0$ for all $\Delta \in \mathbb{R}^{v_c}$. Equation (C.9) in Lemma 44 then yields Equation (C.11). Fix some $\Delta \in \mathbb{R}^{v_c}$ and let $(\mathcal{V}^{(v',r')})_{v' \in \mathcal{T}, r' \in [R_{Pa(v)}]}$ be the intermediate tensors produced when computing

$$\mathcal{H}((\mathbf{W}^{(v')})_{v' \in \mathcal{T} \setminus \{v_c\}}, \text{PadC}_r(\Delta))$$

according to Equation (3.3). For any $\bar{r} \in [R_v] \setminus \{r\}$:

$$\begin{aligned} \mathcal{U}^{(v_c,\bar{r})} &= \pi_{v_c} \left(\sum_{r'=1}^{R_{v_c}} \text{PadC}_r(\Delta)_{r',\bar{r}} \left[\otimes_{v' \in C(v_c)} \mathcal{W}^{(v',r')} \right] \right) \\ &= \pi_{v_c} \left(\sum_{r'=1}^{R_{v_c}} 0 \cdot \left[\otimes_{v' \in C(v_c)} \mathcal{W}^{(v',r')} \right] \right) \\ &= 0. \end{aligned}$$

Thus, for any $\hat{r} \in [R_{Pa(v)}]$ we may write $\mathcal{U}^{(v,\hat{r})} = \pi_v(\mathbf{W}_{r,\hat{r}}^{(v)} \left[\otimes_{v' \in C(v)} \mathcal{U}^{(v',r')} \right])$. Since $\mathbf{W}_{r,:}^{(v)} = 0$, we get that $\mathcal{U}^{(v,\hat{r})} = 0$ for all $\hat{r} \in [R_{Pa(v)}]$, which by Lemma 40 leads to $\mathcal{H}((\mathbf{W}^{(v')})_{v' \in \mathcal{T} \setminus \{v_c\}}, \text{PadC}_r(\Delta)) = 0$. \square

Lemma 46. *For any $v \in \text{int}(\mathcal{T})$, $v_c \in C(v)$, and $r \in [R_v]$, the following hold:*

$$\mathcal{H}((\mathbf{W}^{(v')})_{v' \in \mathcal{T} \setminus \{v\}}, \text{PadR}_r(\mathbf{W}_{r,:}^{(v)})) = \sigma_H^{(v,r)} \cdot \mathcal{C}_H^{(v,r)}, \quad (\text{C.12})$$

and

$$\mathcal{H}\left(\left(\mathbf{W}^{(v')}\right)_{v' \in \mathcal{T} \setminus \{v_c\}}, \text{PadC}_r\left(\mathbf{W}_{:,r}^{(v_c)}\right)\right) = \sigma_H^{(v,r)} \cdot \mathcal{C}_H^{(v,r)}, \quad (\text{C.13})$$

where $\text{PadR}_r(\Delta^\top) \in \mathbb{R}^{R_v \times R_{Pa(v)}}$ is the matrix whose r 'th row is Δ^\top , and all the rest are zero, $\text{PadC}_r(\Delta) \in \mathbb{R}^{R_{v_c} \times R_v}$ is the matrix whose r 'th column is Δ , and all the rest are zero, and $\mathcal{C}_H^{(v,r)}$ is as defined in Theorem 5.

Proof. Starting with Equation (C.12), let $(\mathcal{U}^{(v',r')})_{v' \in \mathcal{T}, r' \in [R_{Pa(v')}]}$ be the intermediate tensors formed when computing $\mathcal{H}\left(\left(\mathbf{W}^{(v')}\right)_{v' \in \mathcal{T} \setminus \{v\}}, \text{PadR}_r\left(\mathbf{W}_{r,:}^{(v)}\right)\right)$ according to Equation (3.3) (there denoted $(\mathcal{W}^{(v',r')})_{v',r'}$). Clearly, for any $v' \in \mathcal{T}(v) \setminus \{v\}$ — a node in the subtree of v which is not v — it holds that $\mathcal{U}^{(v',r')} = \mathcal{W}^{(v',r')}$ for all $r' \in [R_{Pa(v')}]$. Thus, for all $r' \in [R_{Pa(v)}]$ we have that:

$$\mathcal{U}^{(v,r')} = \pi_v \left(\sum_{\bar{r}=1}^{R_v} \text{PadR}_r\left(\mathbf{W}_{r,:}^{(v)}\right)_{\bar{r},r'} \left[\otimes_{v' \in \mathcal{C}(v)} \mathcal{W}^{(v',\bar{r})} \right] \right) = \pi_v \left(\mathbf{W}_{r,r'}^{(v)} \left[\otimes_{v' \in \mathcal{C}(v)} \mathcal{W}^{(v',r')} \right] \right). \quad (\text{C.14})$$

If $\sigma_H^{(v,r)} = \|\mathbf{W}_{r,:}^{(v)} \otimes (\otimes_{v' \in \mathcal{C}(v)} \mathbf{W}_{:,r'}^{(v')})\| = \|\mathbf{W}_{r,:}^{(v)}\| \prod_{v' \in \mathcal{C}(v)} \|\mathbf{W}_{:,r'}^{(v')}\| = 0$, then either $\mathbf{W}_{r,:}^{(v)} = 0$ or $\mathbf{W}_{:,r'}^{(v')} = 0$ for some $v' \in \mathcal{C}(v)$. We claim that in both cases $\mathcal{U}^{(v,r')} = 0$ for all $r' \in [R_{Pa(v)}]$. Indeed, if $\mathbf{W}_{r,:}^{(v)} = 0$ this immediately follows from Equation (C.14). On the other hand, if $\mathbf{W}_{:,r'}^{(v')} = 0$ for some $v' \in \mathcal{C}(v)$, then $\mathcal{W}^{(v',r')} = 0$, which combined with Equation (C.14) also implies that $\mathcal{U}^{(v,r')} = 0$ for all $r' \in [R_{Pa(v)}]$. Hence, Lemma 40 establishes Equation (C.13) for the case of $\sigma_H^{(v,r)} = 0$:

$$\mathcal{H}\left(\left(\mathbf{W}^{(v')}\right)_{v' \in \mathcal{T} \setminus \{v\}}, \text{PadR}_r\left(\mathbf{W}_{r,:}^{(v)}\right)\right) = 0 = \sigma_H^{(v,r)} \cdot \mathcal{C}_H^{(v,r)}.$$

Now, suppose that $\sigma_H^{(v,r)} \neq 0$ and let $\mathcal{U}^{(v,:)}$ be the tensor obtained by stacking $(\mathcal{U}^{(v',r')})_{r'=1}^{R_{Pa(v)}}$ into a single tensor, i.e. $\mathcal{U}_{:, \dots, :, r'}^{(v,:)} = \mathcal{U}^{(v,r')}$ for all $r' \in [R_{Pa(v)}]$. Multilinearity of $\mathcal{H}\left(\left(\mathbf{W}^{(v')}\right)_{v' \in \mathcal{T} \setminus \mathcal{T}(v)}, \mathcal{U}^{(v,:)}\right)$ (Lemma 39) leads to:

$$\begin{aligned} \mathcal{H}\left(\left(\mathbf{W}^{(v')}\right)_{v' \in \mathcal{T} \setminus \{v\}}, \text{PadR}_r\left(\mathbf{W}_{r,:}^{(v)}\right)\right) &= \mathcal{H}\left(\left(\mathbf{W}^{(v')}\right)_{v' \in \mathcal{T} \setminus \mathcal{T}(v)}, \mathcal{U}^{(v,:)}\right) \\ &= \sigma_H^{(v,r)} \cdot \mathcal{H}\left(\left(\mathbf{W}^{(v')}\right)_{v' \in \mathcal{T} \setminus \mathcal{T}(v)}, (\sigma_H^{(v,r)})^{-1} \mathcal{U}^{(v,:)}\right). \end{aligned} \quad (\text{C.15})$$

From Equation (C.14) we know that $(\sigma_H^{(v,r)})^{-1} \mathcal{U}_{:, \dots, :, r'}^{(v,:)} = \pi_v \left((\sigma_H^{(v,r)})^{-1} \mathbf{W}_{r,r'}^{(v)} \left[\otimes_{v' \in \mathcal{C}(v)} \mathcal{W}^{(v',r')} \right] \right)$ for all $r' \in [R_{Pa(v)}]$. Thus, by the definition of $\mathcal{C}_H^{(v,r)}$ we may conclude that:

$$\mathcal{H}\left(\left(\mathbf{W}^{(v')}\right)_{v' \in \mathcal{T} \setminus \mathcal{T}(v)}, (\sigma_H^{(v,r)})^{-1} \mathcal{U}^{(v,:)}\right) = \mathcal{C}_H^{(v,r)}. \quad (\text{C.16})$$

Combining Equations (C.15) and (C.16) yields Equation (C.13), completing this part of the proof.

Turning our attention to Equation (C.13), let $(\mathcal{V}^{(v',r')})_{v' \in \mathcal{T}, r' \in [R_{Pa(v')}]}$ be the intermediate tensors produced when computing $\mathcal{H}\left(\left(\mathbf{W}^{(v')}\right)_{v' \in \mathcal{T} \setminus \{v_c\}}, \text{PadC}_r\left(\mathbf{W}_{:,r}^{(v_c)}\right)\right)$ according to Equation (3.3) (there denoted $(\mathcal{W}^{(v',r')})_{v',r'}$). Clearly, for any $v' \in \mathcal{T}(v) \setminus \{v, v_c\}$ — a node in the subtree of v which is not v nor v_c — it holds that $\mathcal{V}^{(v',r')} = \mathcal{W}^{(v',r')}$ for all

$r' \in [R_{Pa}(v')]$. Thus, $\mathcal{V}^{(v_c, r')} = \pi_{v_c} \left(\sum_{\bar{r}=1}^{R_{v_c}} \text{PadC}_r(\mathbf{W}_{:,r}^{(v_c)})_{\bar{r}, r'} \left[\otimes_{v' \in C(v_c)} \mathcal{W}^{(v', \bar{r})} \right] \right) = \mathcal{W}^{(v_c, r)}$, whereas for any $r' \in [R_v] \setminus \{r\}$:

$$\begin{aligned} \mathcal{V}^{(v_c, r')} &= \pi_{v_c} \left(\sum_{\bar{r}=1}^{R_{v_c}} \text{PadC}_r(\mathbf{W}_{:,r}^{(v_c)})_{\bar{r}, r'} \left[\otimes_{v' \in C(v_c)} \mathcal{W}^{(v', \bar{r})} \right] \right) \\ &= \pi_v \left(\sum_{\bar{r}=1}^{R_{v_c}} \mathbf{0} \cdot \left[\otimes_{v' \in C(v_c)} \mathcal{W}^{(v', \bar{r})} \right] \right) \\ &= \mathbf{0}. \end{aligned}$$

Putting it all together, for any $r' \in [R_{Pa}(v)]$ we may write:

$$\mathcal{V}^{(v, r')} = \pi_v \left(\sum_{\bar{r}=1}^{R_v} \mathbf{W}_{\bar{r}, r'}^{(v)} \left[\otimes_{v' \in C(v)} \mathcal{U}^{(v', \bar{r})} \right] \right) = \pi_v \left(\mathbf{W}_{r, r'}^{(v)} \left[\otimes_{v' \in C(v)} \mathcal{W}^{(v', r)} \right] \right).$$

From this point, following steps analogous to those used for proving Equation (C.12) based on Equation (C.14) yields Equation (C.13). \square

Lemma 47. For any $v \in \text{int}(\mathcal{T})$, $v_c \in C(v)$, and $r \in [R_v]$:

$$\frac{d}{dt} \|\mathbf{W}_{r,:}^{(v)}(t)\|^2 = 2\sigma_H^{(v, r)}(t) \left\langle -\nabla \mathcal{L}_H(\mathcal{W}_H(t)), \mathcal{C}_H^{(v, r)}(t) \right\rangle = \frac{d}{dt} \|\mathbf{W}_{:,r}^{(v_c)}(t)\|^2,$$

where $\mathcal{C}_H^{(v, r)}(t)$ is as defined in Theorem 5.

Proof. Differentiating $\|\mathbf{W}_{:,r}^{(v_c)}(t)\|^2$ with respect to time we get:

$$\begin{aligned} \frac{d}{dt} \|\mathbf{W}_{:,r}^{(v_c)}(t)\|^2 &= 2 \left\langle \mathbf{W}_{:,r}^{(v_c)}(t), \frac{d}{dt} \mathbf{W}_{:,r}^{(v_c)}(t) \right\rangle \\ &= -2 \left\langle \mathbf{W}_{:,r}^{(v_c)}(t), \frac{\partial}{\partial \mathbf{W}_{:,r}^{(v_c)}} \phi_H \left((\mathbf{W}^{(v')}(t))_{v' \in \mathcal{T}} \right) \right\rangle. \end{aligned}$$

By Equation (C.9) from Lemma 44 we have that:

$$\frac{d}{dt} \|\mathbf{W}_{:,r}^{(v_c)}(t)\|^2 = -2 \left\langle \nabla \mathcal{L}_H(\mathcal{W}_H(t)), \mathcal{H} \left((\mathbf{W}^{(v')}(t))_{v' \in \mathcal{T} \setminus \{v_c\}}, \text{PadC}_r(\mathbf{W}_{:,r}^{(v_c)}(t)) \right) \right\rangle.$$

Then, applying Equation (C.13) from Lemma 46 concludes:

$$\frac{d}{dt} \|\mathbf{W}_{:,r}^{(v_c)}(t)\|^2 = 2\sigma_H^{(v, r)}(t) \left\langle -\nabla \mathcal{L}_H(\mathcal{W}_H(t)), \mathcal{C}_H^{(v, r)}(t) \right\rangle.$$

A similar argument yields the desired result for $\|\mathbf{W}_{r,:}^{(v)}(t)\|^2$. Differentiating with respect to time we obtain:

$$\frac{d}{dt} \|\mathbf{W}_{r,:}^{(v)}(t)\|^2 = 2 \left\langle \mathbf{W}_{r,:}^{(v)}(t), \frac{d}{dt} \mathbf{W}_{r,:}^{(v)}(t) \right\rangle = -2 \left\langle \mathbf{W}_{r,:}^{(v)}(t), \frac{\partial}{\partial \mathbf{W}_{r,:}^{(v)}} \phi_H \left((\mathbf{W}^{(v')}(t))_{v' \in \mathcal{T}} \right) \right\rangle.$$

By Equation (C.8) from Lemma 44 we may write:

$$\frac{d}{dt} \|\mathbf{W}_{r,:}^{(v)}(t)\|^2 = -2 \left\langle \nabla \mathcal{L}_H(\mathcal{W}_H(t)), \mathcal{H} \left((\mathbf{W}^{(v')}(t))_{v' \in \mathcal{T} \setminus \{v\}}, \text{PadR}_r(\mathbf{W}_{r,:}^{(v)}(t)) \right) \right\rangle.$$

Lastly, applying Equation (C.12) from Lemma 46 completes the proof:

$$\frac{d}{dt} \|\mathbf{W}_{r,:}^{(v)}(t)\|^2 = 2\sigma_{\mathbf{H}}^{(v,r)}(t) \left\langle -\nabla \mathcal{L}_{\mathbf{H}}(\mathcal{W}_{\mathbf{H}}(t)), \mathcal{C}_{\mathbf{H}}^{(v,r)}(t) \right\rangle.$$

□

Lemma 48. *Let $v \in \text{int}(\mathcal{T})$ and $r \in [R_v]$. If there exists a time $t_0 \geq 0$ at which $\mathbf{w}(t_0) = 0$ for all $\mathbf{w} \in \text{LC}(v, r)$, then:*

$$\mathbf{w}(t) = 0 \quad , t \geq 0, \quad \mathbf{w} \in \text{LC}(v, r),$$

i.e. $\mathbf{w}(t)$ is identically zero for all $\mathbf{w} \in \text{LC}(v, r)$.

Proof. Standard existence and uniqueness theorems (e.g. Theorem 2.2 in [203]) imply that the system of differential equations governing gradient flow over $\phi_{\mathbf{H}}$ (Equation (3.5)) has a unique solution that passes through $(\mathbf{W}^{(v')}(t_0))_{v' \in \mathcal{T}}$ at time t_0 . It therefore suffices to show that there exist $(\bar{\mathbf{W}}^{(v')}(t))_{v' \in \mathcal{T}}$ satisfying Equation (3.5) such that $\bar{\mathbf{W}}^{(v')}(t_0) = \mathbf{W}^{(v')}(t_0)$ for all $v' \in \mathcal{T}$, for which $\bar{\mathbf{W}}_{r,:}^{(v)}(t)$ and $(\bar{\mathbf{W}}_{:,r}^{(v_c)}(t))_{v_c \in \mathcal{C}(v)}$ are zero for all $t \geq 0$ (recall that $\text{LC}(v, r)$ consists of $\mathbf{W}_{r,:}^{(v)}$ and $(\mathbf{W}_{:,r}^{(v_c)})_{v_c \in \mathcal{C}(v)}$).

We denote by $\Theta_{v,r}(t)$ all factorization weights at time $t \geq 0$, except for those in $\text{LC}(v, r)$, *i.e.*:

$$\Theta_{v,r}(t) := (\mathbf{W}^{(v')}(t))_{v' \in \mathcal{T} \setminus (\{v\} \cup \mathcal{C}(v))} \cup (\mathbf{W}_{:,r'}^{(v_c)}(t))_{v_c \in \mathcal{C}(v), r' \in [R_v] \setminus \{r\}} \cup (\mathbf{W}_{r'}^{(v)}(t))_{r' \in [R_v] \setminus \{r\}}.$$

We construct $(\bar{\mathbf{W}}^{(v')}(t))_{v' \in \mathcal{T}}$ as follows. First, let $\bar{\mathbf{W}}_{r,:}^{(v)}(t) := 0$ and $\bar{\mathbf{W}}_{:,r}^{(v_c)}(t) := 0$ for all $v_c \in \mathcal{C}(v)$ and $t \geq 0$. Then, considering $\mathbf{W}_{r,:}^{(v)}(t)$ and $(\mathbf{W}_{:,r}^{(v_c)}(t))_{v_c \in \mathcal{C}(v)}$ as fixed to zero, we denote by $\bar{\phi}_{\mathbf{H}}(\Theta_{v,r}(t))$ the induced objective over all other weights, and let

$$\bar{\Theta}_{v,r}(t) := (\bar{\mathbf{W}}^{(v')}(t))_{v' \in \mathcal{T} \setminus (\{v\} \cup \mathcal{C}(v))} \cup (\bar{\mathbf{W}}_{:,r'}^{(v_c)}(t))_{v_c \in \mathcal{C}(v), r' \in [R_v] \setminus \{r\}} \cup (\bar{\mathbf{W}}_{r'}^{(v)}(t))_{r' \in [R_v] \setminus \{r\}}$$

be a gradient flow path over $\bar{\phi}_{\mathbf{H}}$ satisfying $\bar{\Theta}_{v,r}(t_0) = \Theta_{v,r}(t_0)$. By definition, it holds that $\bar{\mathbf{W}}^{(v')}(t_0) = \mathbf{W}^{(v')}(t_0)$ for all $v' \in \mathcal{T}$. Thus, it remains to show that $(\bar{\mathbf{W}}^{(v')}(t))_{v' \in \mathcal{T}}$ obey the differential equations defining gradient flow over $\phi_{\mathbf{H}}$ (Equation (3.5)). To see it is so, notice that since $\bar{\mathbf{W}}_{r,:}^{(v)}(t)$ and $(\bar{\mathbf{W}}_{:,r}^{(v_c)}(t))_{v_c \in \mathcal{C}(v)}$ are identically zero, by the definition of $\bar{\phi}_{\mathbf{H}}$ we have that:

$$\frac{d}{dt} \bar{\Theta}_{v,r}(t) = -\frac{d}{d\Theta_{v,r}} \bar{\phi}_{\mathbf{H}}(\bar{\Theta}_{v,r}(t)) = -\frac{\partial}{\partial \Theta_{v,r}} \phi_{\mathbf{H}}((\bar{\mathbf{W}}^{(v')}(t))_{v' \in \mathcal{T}}). \quad (\text{C.17})$$

Furthermore, by Lemma 45 we obtain:

$$\frac{d}{dt} \bar{\mathbf{W}}_{r,:}^{(v)}(t) = 0 = -\frac{\partial}{\partial \mathbf{W}_{r,:}^{(v)}} \phi_{\mathbf{H}}((\bar{\mathbf{W}}^{(v')}(t))_{v' \in \mathcal{T}}), \quad (\text{C.18})$$

and for all $v_c \in \mathcal{C}(v)$:

$$\frac{d}{dt} \bar{\mathbf{W}}_{:,r}^{(v_c)}(t) = 0 = -\frac{\partial}{\partial \mathbf{W}_{:,r}^{(v_c)}} \phi_{\mathbf{H}}((\bar{\mathbf{W}}^{(v')}(t))_{v' \in \mathcal{T}}). \quad (\text{C.19})$$

Combining Equations (C.17), (C.18), and (C.19), completes the proof:

$$\frac{d}{dt} \overline{\mathbf{W}}^{(v')}(t) = -\frac{\partial}{\partial \mathbf{W}^{(v')}} \phi_{\mathbb{H}}(\overline{\mathbf{W}}^{(\bar{v})}(t))_{\bar{v} \in \mathcal{T}} \quad , v' \in \mathcal{T}.$$

□

C.5.3 Proof of Lemma 2

The proof follows a line similar to that of Theorem 7 in [53], extending from binary to arbitrary trees its upper bound on $(\text{rank}[\mathcal{W}_{\mathbb{H}}; \nu])_{\nu \in \mathcal{T}}$.

Towards deriving a matricized form of Equation (3.3), we define the notion of *index set reduction*. The reduction of $\nu \in \mathcal{T}$ onto $\nu' \in \mathcal{T}$, whose elements are denoted by $i_1 < \dots < i_{|\nu'|}$, is defined by:

$$\nu|_{\nu'} := \{n \in [|\nu'|] : i_n \in \nu \cap \nu'\}.$$

Now, fix $\nu \in \text{int}(\mathcal{T})$ and $\nu_c \in C(\nu)$. By Lemma 37 and the linearity of the matricization operator, we may write the computation of $[\mathcal{W}_{\mathbb{H}}; \nu_c]$ based on Equation (3.3) as follows:

For $\bar{\nu} \in \{\{1\}, \dots, \{N\}\}$ (traverses leaves of \mathcal{T}):

$$\mathcal{W}^{(\bar{\nu}, r)} := \mathbf{W}_{:,r}^{(\bar{\nu})} \quad , r \in [R_{Pa(\bar{\nu})}],$$

for $\bar{\nu} \in \text{int}(\mathcal{T}) \setminus \{[N]\}$ (traverses interior nodes of \mathcal{T} from leaves to root):

$$[\mathcal{W}^{(\bar{\nu}, r)}; \nu_c|_{\bar{\nu}}] := \mathbf{Q}^{(\bar{\nu})} \left(\sum_{r'=1}^{R_{\bar{\nu}}} \mathbf{W}_{r',r}^{(\bar{\nu})} \left[\circ_{\nu' \in C(\bar{\nu})} [\mathcal{W}^{(\nu', r')}; \nu_c|_{\nu'}] \right] \right) \bar{\mathbf{Q}}^{(\bar{\nu})} \quad , r \in [R_{Pa(\bar{\nu})}],$$

$$[\mathcal{W}_{\mathbb{H}}; \nu_c] = \mathbf{Q}^{([N])} \left(\sum_{r'=1}^{R_{[N]}} \mathbf{W}_{r',1}^{([N])} \left[\circ_{\nu' \in C([N])} [\mathcal{W}^{(\nu', r')}; \nu_c|_{\nu'}] \right] \right) \bar{\mathbf{Q}}^{([N])},$$

where $\mathbf{Q}^{(\bar{\nu})}$ and $\bar{\mathbf{Q}}^{(\bar{\nu})}$, for $\bar{\nu} \in \text{int}(\mathcal{T})$, are permutation matrices rearranging the rows and columns, respectively, to accord with an ascending order of $\bar{\nu}$, *i.e.* they fulfill the role of $\pi_{\bar{\nu}}$ in Equation (3.3). For $r \in [R_{Pa(\bar{\nu})}]$, let us focus on $[\mathcal{W}^{(\nu, r)}; \nu_c|_{\nu}]$. Since $\nu_c|_{\nu_c} = [|\nu_c|]$ and $\nu_c|_{\nu'} = \emptyset$ for all $\nu' \in C(\nu) \setminus \{\nu_c\}$, we have that:

$$\begin{aligned} & [\mathcal{W}^{(\nu, r)}; \nu_c|_{\nu}] \\ &= \mathbf{Q}^{(\nu)} \left(\sum_{r'=1}^{R_{\nu}} \mathbf{W}_{r',r}^{(\nu)} \left[\left(\circ_{\nu' \in \overleftarrow{\mathcal{S}}(\nu_c)} [\mathcal{W}^{(\nu', r')}; \emptyset] \right) \circ [\mathcal{W}^{(\nu_c, r')}; [|\nu_c|]] \circ \left(\circ_{\nu' \in \overrightarrow{\mathcal{S}}(\nu_c)} [\mathcal{W}^{(\nu', r')}; \emptyset] \right) \right] \right) \bar{\mathbf{Q}}^{(\nu)}. \end{aligned}$$

Notice that $[\mathcal{W}^{(\nu', r')}; \emptyset]$ is a row vector, whereas $[\mathcal{W}^{(\nu_c, r')}; [|\nu_c|]]$ is a column vector, for each $\nu' \in C(\nu) \setminus \{\nu_c\}$ and $r' \in [R_{\nu}]$. Commutativity of the Kronecker product between a row and column vectors therefore leads to:

$$\begin{aligned} [\mathcal{W}^{(\nu, r)}; \nu_c|_{\nu}] &= \mathbf{Q}^{(\nu)} \left(\sum_{r'=1}^{R_{\nu}} \mathbf{W}_{r',r}^{(\nu)} \left[\left[[\mathcal{W}^{(\nu_c, r')}; [|\nu_c|]] \right] \circ \left(\circ_{\nu' \in C(\nu) \setminus \{\nu_c\}} [\mathcal{W}^{(\nu', r')}; \emptyset] \right) \right] \right) \bar{\mathbf{Q}}^{(\nu)} \\ &= \mathbf{Q}^{(\nu)} \left(\sum_{r'=1}^{R_{\nu}} \mathbf{W}_{r',r}^{(\nu)} \left[\left[[\mathcal{W}^{(\nu_c, r')}; [|\nu_c|]] \right] \left(\circ_{\nu' \in C(\nu) \setminus \{\nu_c\}} [\mathcal{W}^{(\nu', r')}; \emptyset] \right) \right] \right) \bar{\mathbf{Q}}^{(\nu)}, \end{aligned}$$

where the second equality is by the fact that for any column vector \mathbf{u} and row vector \mathbf{v} it holds that $\mathbf{u} \circ \mathbf{v} = \mathbf{u}\mathbf{v}$. Defining $\mathbf{B}^{(\nu_c)}$ to be the matrix whose column vectors are $[\mathcal{W}^{(\nu_c, 1)}; [|\nu_c|]], \dots, [\mathcal{W}^{(\nu_c, R_{\nu})}; [|\nu_c|]]$, we can express the term between $\mathbf{Q}^{(\nu)}$ and $\bar{\mathbf{Q}}^{(\nu)}$ in the equation above as a $\mathbf{B}^{(\nu_c)} \mathbf{A}^{(\nu, r)}$, where $\mathbf{A}^{(\nu, r)}$ is defined to be the matrix whose

rows are $\mathbf{W}_{1,r}^{(v)}(\circ_{v' \in C(v) \setminus \{v_c\}} \llbracket \mathcal{W}^{(v',1)}; \emptyset \rrbracket), \dots, \mathbf{W}_{R_v,r}^{(v)}(\circ_{v' \in C(v) \setminus \{v_c\}} \llbracket \mathcal{W}^{(v',R_v)}; \emptyset \rrbracket)$. That is:

$$\llbracket \mathcal{W}^{(v,r)}; v_c | v \rrbracket = \mathbf{Q}^{(v)} \mathbf{B}^{(v_c)} \mathbf{A}^{(v,r)} \bar{\mathbf{Q}}^{(v)}. \quad (\text{C.20})$$

The proof proceeds by propagating $\mathbf{B}^{(v_c)}$ and the left permutation matrices up the tree, until reaching a representation of $\llbracket \mathcal{W}_H; v_c \rrbracket$ as a product of matrices that includes $\mathbf{B}^{(v_c)}$. Since $\mathbf{B}^{(v_c)}$ has R_v columns, this will imply that the rank of $\llbracket \mathcal{W}_H; v_c \rrbracket$ is at most R_v , as required.

We begin with the propagation step from v to $Pa(v)$. For $r \in [R_{Pa(Pa(v))}]$, we examine:

$$\begin{aligned} & (\mathbf{Q}^{(Pa(v))})^{-1} \llbracket \mathcal{W}^{(Pa(v),r)}; v_c | Pa(v) \rrbracket (\bar{\mathbf{Q}}^{(Pa(v))})^{-1} \\ &= \sum_{r'=1}^{R_{Pa(v)}} \mathbf{W}_{r',r}^{(Pa(v))} \left[\left(\circ_{v' \in \overleftarrow{S}(v)} \llbracket \mathcal{W}^{(v',r')}; v_c | v' \rrbracket \right) \circ \llbracket \mathcal{W}^{(v,r)}; v_c | v \rrbracket \circ \left(\circ_{v' \in \overrightarrow{S}(v)} \llbracket \mathcal{W}^{(v',r')}; v_c | v' \rrbracket \right) \right]. \end{aligned}$$

Plugging in Equation (C.20) while noticing that $v_c | v' = \emptyset$ for any v' which is not an ancestor of v_c , we arrive at:

$$\sum_{r'=1}^{R_{Pa(v)}} \mathbf{W}_{r',r}^{(Pa(v))} \left[\left(\circ_{v' \in \overleftarrow{S}(v)} \llbracket \mathcal{W}^{(v',r')}; \emptyset \rrbracket \right) \circ \left(\mathbf{Q}^{(v)} \mathbf{B}^{(v_c)} \mathbf{A}^{(v,r')} \bar{\mathbf{Q}}^{(v)} \right) \circ \left(\circ_{v' \in \overrightarrow{S}(v)} \llbracket \mathcal{W}^{(v',r')}; \emptyset \rrbracket \right) \right]. \quad (\text{C.21})$$

Let $r' \in [R_{Pa(v)}]$. Since $\llbracket \mathcal{W}^{(v',r')}; \emptyset \rrbracket$ is a row vector for any $v' \in C(Pa(v)) \setminus \{v\}$, so are $\circ_{v' \in \overleftarrow{S}(v)} \llbracket \mathcal{W}^{(v',r')}; \emptyset \rrbracket$ and $\circ_{v' \in \overrightarrow{S}(v)} \llbracket \mathcal{W}^{(v',r')}; \emptyset \rrbracket$. Applying Lemma 38 twice we therefore have that:

$$\begin{aligned} & \left(\circ_{v' \in \overleftarrow{S}(v)} \llbracket \mathcal{W}^{(v',r')}; \emptyset \rrbracket \right) \circ \left(\mathbf{Q}^{(v)} \mathbf{B}^{(v_c)} \mathbf{A}^{(v,r')} \bar{\mathbf{Q}}^{(v)} \right) \circ \left(\circ_{v' \in \overrightarrow{S}(v)} \llbracket \mathcal{W}^{(v',r')}; \emptyset \rrbracket \right) \\ &= \left(\mathbf{Q}^{(v)} \mathbf{B}^{(v_c)} \left[\left(\circ_{v' \in \overleftarrow{S}(v)} \llbracket \mathcal{W}^{(v',r')}; \emptyset \rrbracket \right) \circ \left(\mathbf{A}^{(v,r')} \bar{\mathbf{Q}}^{(v)} \right) \right] \right) \circ \left(\circ_{v' \in \overrightarrow{S}(v)} \llbracket \mathcal{W}^{(v',r')}; \emptyset \rrbracket \right) \\ &= \mathbf{Q}^{(v)} \mathbf{B}^{(v_c)} \left[\left(\circ_{v' \in \overleftarrow{S}(v)} \llbracket \mathcal{W}^{(v',r')}; \emptyset \rrbracket \right) \circ \left(\mathbf{A}^{(v,r')} \bar{\mathbf{Q}}^{(v)} \right) \circ \left(\circ_{v' \in \overrightarrow{S}(v)} \llbracket \mathcal{W}^{(v',r')}; \emptyset \rrbracket \right) \right]. \end{aligned}$$

Going back to Equation (C.21), we obtain:

$$\begin{aligned} & \sum_{r'=1}^{R_{Pa(v)}} \mathbf{W}_{r',r}^{(Pa(v))} \left[\left(\circ_{v' \in \overleftarrow{S}(v)} \llbracket \mathcal{W}^{(v',r')}; \emptyset \rrbracket \right) \circ \left(\mathbf{Q}^{(v)} \mathbf{B}^{(v_c)} \mathbf{A}^{(v,r')} \bar{\mathbf{Q}}^{(v)} \right) \circ \left(\circ_{v' \in \overrightarrow{S}(v)} \llbracket \mathcal{W}^{(v',r')}; \emptyset \rrbracket \right) \right] \\ &= \sum_{r'=1}^{R_{Pa(v)}} \mathbf{W}_{r',r}^{(Pa(v))} \left(\mathbf{Q}^{(v)} \mathbf{B}^{(v_c)} \left[\left(\circ_{v' \in \overleftarrow{S}(v)} \llbracket \mathcal{W}^{(v',r')}; \emptyset \rrbracket \right) \circ \left(\mathbf{A}^{(v,r')} \bar{\mathbf{Q}}^{(v)} \right) \circ \left(\circ_{v' \in \overrightarrow{S}(v)} \llbracket \mathcal{W}^{(v',r')}; \emptyset \rrbracket \right) \right] \right) \\ &= \mathbf{Q}^{(v)} \mathbf{B}^{(v_c)} \left(\sum_{r'=1}^{R_{Pa(v)}} \mathbf{W}_{r',r}^{(Pa(v))} \left[\left(\circ_{v' \in \overleftarrow{S}(v)} \llbracket \mathcal{W}^{(v',r')}; \emptyset \rrbracket \right) \circ \left(\mathbf{A}^{(v,r')} \bar{\mathbf{Q}}^{(v)} \right) \circ \left(\circ_{v' \in \overrightarrow{S}(v)} \llbracket \mathcal{W}^{(v',r')}; \emptyset \rrbracket \right) \right] \right). \quad (\text{C.22}) \end{aligned}$$

For brevity, we denote the matrix multiplying $\mathbf{Q}^{(v)} \mathbf{B}^{(v_c)}$ from the right in the equation above by $\mathbf{A}^{(Pa(v),r)}$, *i.e.*:

$$\mathbf{A}^{(Pa(v),r)} := \sum_{r'=1}^{R_{Pa(v)}} \mathbf{W}_{r',r}^{(Pa(v))} \left[\left(\circ_{v' \in \overleftarrow{S}(v)} \llbracket \mathcal{W}^{(v',r')}; \emptyset \rrbracket \right) \circ \left(\mathbf{A}^{(v,r')} \bar{\mathbf{Q}}^{(v)} \right) \circ \left(\circ_{v' \in \overrightarrow{S}(v)} \llbracket \mathcal{W}^{(v',r')}; \emptyset \rrbracket \right) \right].$$

Recalling that the expression in Equation (C.22) is of

$$\left(\mathbf{Q}^{(Pa(v))} \right)^{-1} \llbracket \mathcal{W}^{(Pa(v),r)}; v_c | Pa(v) \rrbracket \left(\bar{\mathbf{Q}}^{(Pa(v))} \right)^{-1}$$

completes the propagation step:

$$\llbracket \mathcal{W}^{(Pa(v),r)}; v_c | Pa(v) \rrbracket = \mathbf{Q}^{(Pa(v))} \mathbf{Q}^{(v)} \mathbf{B}^{(v_c)} \mathbf{A}^{(Pa(v),r)} \bar{\mathbf{Q}}^{(Pa(v))}.$$

Continuing this process, we propagate $\mathbf{B}^{(v_c)}$, along with the left permutation matrices, upwards in the tree until reaching the root. This brings forth the following representation of $\llbracket \mathcal{W}_H; v_c \rrbracket$:

$$\llbracket \mathcal{W}_H; v_c \rrbracket = \mathbf{Q}^{([N])} \mathbf{Q} \mathbf{B}^{(v_c)} \mathbf{A}^{([N])} \bar{\mathbf{Q}}^{([N])},$$

for appropriate \mathbf{Q} and $\mathbf{A}^{([N])}$ encompassing the propagated permutation matrices and the “remainder” of the decomposition, respectively. Since $\mathbf{B}^{(v_c)}$ has R_v columns, we may conclude:

$$\text{rank} \llbracket \mathcal{W}_H; v_c \rrbracket \leq \text{rank} \mathbf{B}^{(v_c)} \leq R_v.$$

□

C.5.4 Proof of Lemma 3

For any $v \in \text{int}(\mathcal{T})$, $r \in [R_v]$, and $\mathbf{w}, \mathbf{w}' \in \text{LC}(v, r)$, Lemma 47 implies that:

$$\frac{d}{dt} \|\mathbf{w}(t)\|^2 = 2\sigma_H^{(v,r)}(t) \left\langle -\nabla \mathcal{L}_H(\mathcal{W}_H(t)), \mathcal{C}_H^{(v,r)}(t) \right\rangle = \frac{d}{dt} \|\mathbf{w}'(t)\|^2,$$

where $\mathcal{C}_H^{(v,r)}(t)$ is as defined in Theorem 5. For $t \geq 0$, integrating both sides with respect to time leads to:

$$\|\mathbf{w}(t)\|^2 - \|\mathbf{w}(0)\|^2 = \|\mathbf{w}'(t)\|^2 - \|\mathbf{w}'(0)\|^2.$$

Rearranging the equality above yields the desired result. □

C.5.5 Proof of Theorem 5

Let $t \geq 0$.

First, suppose that $\sigma_H^{(v,r)}(t) = 0$. Since the unbalancedness magnitude at initialization is zero, from Lemma 3 we know that $\|\mathbf{w}(t)\| = \|\mathbf{w}'(t)\|$ for any $\mathbf{w}, \mathbf{w}' \in \text{LC}(v, r)$. Hence, the fact that $\sigma_H^{(v,r)}(t) = 0$ implies that $\|\mathbf{w}(t)\| = 0$ for all $\mathbf{w} \in \text{LC}(v, r)$. Lemma 48 then establishes that $\sigma_H^{(v,r)}(t')$ is identically zero through time, in which case both sides of Equation (3.7) are equal to zero.

We now move to the case where $\sigma_H^{(v,r)}(t) > 0$. Since $\sigma_H^{(v,r)}(t) = \|\otimes_{\mathbf{w} \in \text{LC}(v,r)} \mathbf{w}(t)\| = \prod_{\mathbf{w} \in \text{LC}(v,r)} \|\mathbf{w}(t)\|$ (the norm of a tensor product is equal to the product of the norms), by the product rule of differentiation we have that:

$$\frac{d}{dt} \sigma_H^{(v,r)}(t)^2 = \sum_{\mathbf{w} \in \text{LC}(v,r)} \frac{d}{dt} \|\mathbf{w}(t)\|^2 \cdot \prod_{\mathbf{w}' \in \text{LC}(v,r) \setminus \{\mathbf{w}\}} \|\mathbf{w}'(t)\|^2.$$

Applying Lemma 47 then leads to:

$$\begin{aligned} & \frac{d}{dt} \sigma_H^{(v,r)}(t)^2 \\ &= \sum_{\mathbf{w} \in \text{LC}(v,r)} 2\sigma_H^{(v,r)}(t) \left\langle -\nabla \mathcal{L}_H(\mathcal{W}_H(t)), \mathcal{C}_H^{(v,r)}(t) \right\rangle \cdot \prod_{\mathbf{w}' \in \text{LC}(v,r) \setminus \{\mathbf{w}\}} \|\mathbf{w}'(t)\|^2 \\ &= 2\sigma_H^{(v,r)}(t) \left\langle -\nabla \mathcal{L}_H(\mathcal{W}_H(t)), \mathcal{C}_H^{(v,r)}(t) \right\rangle \sum_{\mathbf{w} \in \text{LC}(v,r)} \prod_{\mathbf{w}' \in \text{LC}(v,r) \setminus \{\mathbf{w}\}} \|\mathbf{w}'(t)\|^2. \end{aligned}$$

From the chain rule we know that $\frac{d}{dt}\sigma_{\mathbf{H}}^{(v,r)}(t)^2 = 2\sigma_{\mathbf{H}}^{(v,r)}(t) \cdot \frac{d}{dt}\sigma_{\mathbf{H}}^{(v,r)}(t)$ (note that $\frac{d}{dt}\sigma_{\mathbf{H}}^{(v,r)}(t)$ surely exists because $\sigma_{\mathbf{H}}^{(v,r)}(t) > 0$). Thus:

$$\begin{aligned} \frac{d}{dt}\sigma_{\mathbf{H}}^{(v,r)}(t) &= \frac{1}{2}\sigma_{\mathbf{H}}^{(v,r)}(t)^{-1}\frac{d}{dt}\sigma_{\mathbf{H}}^{(v,r)}(t)^2 \\ &= \left\langle -\nabla\mathcal{L}_{\mathbf{H}}(\mathcal{W}_{\mathbf{H}}(t)), \mathcal{C}_{\mathbf{H}}^{(v,r)}(t) \right\rangle \sum_{\mathbf{w} \in \text{LC}(v,r)} \prod_{\mathbf{w}' \in \text{LC}(v,r) \setminus \{\mathbf{w}\}} \|\mathbf{w}'(t)\|^2. \end{aligned} \quad (\text{C.23})$$

According to Lemma 3, the unbalancedness magnitude remains zero through time, and so $\|\mathbf{w}(t)\| = \|\mathbf{w}'(t)\|$ for any $\mathbf{w}, \mathbf{w}' \in \text{LC}(v, r)$. Recalling that $L_v := C(v) + 1$ is the number of weight vectors in a local component at v , this implies that for each $\mathbf{w} \in \text{LC}(v, r)$:

$$\|\mathbf{w}(t)\|^2 = \|\mathbf{w}(t)\|^{L_v \cdot \frac{2}{L_v}} = \left(\prod_{\mathbf{w}' \in \text{LC}(v,r)} \|\mathbf{w}'(t)\| \right)^{\frac{2}{L_v}} = \sigma_{\mathbf{H}}^{(v,r)}(t)^{\frac{2}{L_v}}. \quad (\text{C.24})$$

Plugging Equation (C.24) into Equation (C.23) completes the proof. \square

C.5.6 Proof of Proposition 5

We begin by establishing the following key lemma, which upper bounds the distance between the end tensor $\mathcal{W}_{\mathbf{H}}$ and the one obtained after setting a local component to zero.

Lemma 49. *Let $v \in \text{int}(\mathcal{T})$ and $r \in [R_v]$. Denote by $\overline{\mathcal{W}}_{\mathbf{H}}^{(v,r)}$ the end tensor obtained by pruning the (v, r) 'th local component, i.e. by setting the r 'th row of $\mathbf{W}^{(v)}$ and the r 'th columns of $(\mathbf{W}^{(v_c)})_{v_c \in C(v)}$ to zero. Then:*

$$\|\mathcal{W}_{\mathbf{H}} - \overline{\mathcal{W}}_{\mathbf{H}}^{(v,r)}\| \leq \sigma_{\mathbf{H}}^{(v,r)} \cdot \prod_{v' \in \mathcal{T} \setminus (\{v\} \cup C(v))} \|\mathbf{W}^{(v')}\|.$$

Proof. Let $(\overline{\mathbf{W}}^{(v')})_{v' \in \mathcal{T}}$ be the weight matrices corresponding to $\overline{\mathcal{W}}_{\mathbf{H}}^{(v,r)}$, i.e. $\overline{\mathbf{W}}^{(v)}$ is the weight matrix obtained by setting the r 'th row of $\mathbf{W}^{(v)}$ to zero, $(\overline{\mathbf{W}}^{(v_c)})_{v_c \in C(v)}$ are the weight matrices obtained by setting the r 'th columns of $(\mathbf{W}^{(v_c)})_{v_c \in C(v)}$ to zero, and $\overline{\mathbf{W}}^{(v')} = \mathbf{W}^{(v')}$ for all $v' \in \mathcal{T} \setminus (\{v\} \cup C(v))$. Accordingly, we denote by $(\overline{\mathcal{W}}^{(v',r')})_{v' \in \mathcal{T}, r' \in [R_{p(v')}]}$ the intermediate tensors produced when computing $\overline{\mathcal{W}}_{\mathbf{H}}^{(v,r)}$ according to Equation (3.3) (there denoted $(\mathcal{W}^{(v',r')})_{v', r'}$).

By definition, $\mathcal{H}((\mathbf{W}^{(v')})_{v' \in \mathcal{T} \setminus \mathcal{T}(v)}, \mathcal{W}^{(v,:)}) = \mathcal{W}_{\mathbf{H}}$ and $\mathcal{H}((\overline{\mathbf{W}}^{(v')})_{v' \in \mathcal{T} \setminus \mathcal{T}(v)}, \overline{\mathcal{W}}^{(v,:)}) = \overline{\mathcal{W}}_{\mathbf{H}}^{(v,r)}$. Since \mathcal{H} is multilinear (Lemma 39) and $\overline{\mathbf{W}}^{(v')} = \mathbf{W}^{(v')}$ for all $v' \in \mathcal{T} \setminus \mathcal{T}(v)$, we have that:

$$\begin{aligned} \|\mathcal{W}_{\mathbf{H}} - \overline{\mathcal{W}}_{\mathbf{H}}^{(v,r)}\| &= \left\| \mathcal{H}((\mathbf{W}^{(v')})_{v' \in \mathcal{T} \setminus \mathcal{T}(v)}, \mathcal{W}^{(v,:)}) - \mathcal{H}((\overline{\mathbf{W}}^{(v')})_{v' \in \mathcal{T} \setminus \mathcal{T}(v)}, \overline{\mathcal{W}}^{(v,:)}) \right\| \\ &= \left\| \mathcal{H}((\mathbf{W}^{(v')})_{v' \in \mathcal{T} \setminus \mathcal{T}(v)}, \mathcal{W}^{(v,:)} - \overline{\mathcal{W}}^{(v,:)}) \right\|. \end{aligned}$$

Heading from the root downwards, subsequent applications of Lemma 42 over all nodes in the mode tree, except those belonging to the sub-tree whose root is v , then yield:

$$\|\mathcal{W}_{\mathbf{H}} - \overline{\mathcal{W}}_{\mathbf{H}}^{(v,r)}\| \leq \|\mathcal{W}^{(v,:)} - \overline{\mathcal{W}}^{(v,:)}\| \cdot \prod_{v' \in \mathcal{T} \setminus \mathcal{T}(v)} \|\mathbf{W}^{(v')}\|. \quad (\text{C.25})$$

Notice that for any $r' \in [R_{Pa(v)}]$:

$$\begin{aligned} (\mathcal{W}^{(v,:)} - \overline{\mathcal{W}}^{(v,:)})_{:, \dots, :, r'} &= \sum_{\bar{r} \in [R_v]} \mathbf{w}_{\bar{r}, r'}^{(v)} \otimes_{v_c \in C(v)} \mathcal{W}^{(v_c, \bar{r})} - \sum_{\bar{r} \in [R_v] \setminus \{r\}} \mathbf{w}_{\bar{r}, r'}^{(v)} \otimes_{v_c \in C(v)} \mathcal{W}^{(v_c, \bar{r})} \\ &= \mathbf{w}_{r, r'}^{(v)} \otimes_{v_c \in C(v)} \mathcal{W}^{(v_c, r)}. \end{aligned}$$

Thus, a straightforward computation shows:

$$\begin{aligned} \|\mathcal{W}^{(v,:)} - \overline{\mathcal{W}}^{(v,:)}\|^2 &= \sum_{r'=1}^{R_{Pa(v)}} \|\mathbf{w}_{r, r'}^{(v)} \otimes_{v_c \in C(v)} \mathcal{W}^{(v_c, r)}\|^2 \\ &= \sum_{r'=1}^{R_{Pa(v)}} \left(\mathbf{w}_{r, r'}^{(v)}\right)^2 \cdot \prod_{v_c \in C(v)} \|\mathcal{W}^{(v_c, r)}\|^2 \\ &= \|\mathbf{w}_{r, :}^{(v)}\|^2 \cdot \prod_{v_c \in C(v)} \|\mathcal{W}^{(v_c, r)}\|^2, \end{aligned}$$

where the second equality is by the fact that the norm of a tensor product is equal to the product of the norms. From Lemma 41 we get that $\|\mathcal{W}^{(v_c, r)}\| \leq \|\mathbf{w}_{:, r}^{(v_c)}\| \cdot \prod_{v' \in C(v_c)} \|\mathcal{W}^{(v', :)}\|$ for all $v_c \in C(v)$, which leads to:

$$\begin{aligned} \|\mathcal{W}^{(v,:)} - \overline{\mathcal{W}}^{(v,:)}\|^2 &\leq \|\mathbf{w}_{r, :}^{(v)}\|^2 \cdot \prod_{v_c \in C(v)} \left(\|\mathbf{w}_{:, r}^{(v_c)}\|^2 \cdot \prod_{v' \in C(v_c)} \|\mathcal{W}^{(v', :)}\|^2 \right) \\ &= \left(\sigma_{\mathbb{H}}^{(v, r)}\right)^2 \cdot \prod_{v_c \in C(v), v' \in C(v_c)} \|\mathcal{W}^{(v', :)}\|^2. \end{aligned}$$

Taking the square root of both sides and plugging the inequality above into Equation (C.25), we arrive at:

$$\|\mathcal{W}_{\mathbb{H}} - \overline{\mathcal{W}}_{\mathbb{H}}^{(v, r)}\| \leq \sigma_{\mathbb{H}}^{(v, r)} \cdot \prod_{v_c \in C(v), v' \in C(v_c)} \|\mathcal{W}^{(v', :)}\| \cdot \prod_{v' \in \mathcal{T} \setminus \mathcal{T}(v)} \|\mathbf{w}^{(v')}\|.$$

Applying Lemma 42 iteratively over the sub-trees whose roots are $C(v_c)$ gives:

$$\prod_{v_c \in C(v), v' \in C(v_c)} \|\mathcal{W}^{(v', :)}\| \leq \prod_{v' \in \mathcal{T}(v) \setminus (\{v\} \cup C(v))} \|\mathbf{w}^{(v')}\|,$$

concluding the proof. \square

With Lemma 49 in hand, we are now in a position to prove Proposition 5. Let

$$\mathcal{S} := \{(v, r) : v \in \text{int}(\mathcal{T}), r \in \{R'_v + 1, \dots, R_v\}\},$$

and denote by $\overline{\mathcal{W}}_{\mathbb{H}}^{\mathcal{S}}$ the end tensor obtained by pruning all local components in \mathcal{S} , i.e. by setting to zero the r' th row of $\mathbf{W}^{(v)}$ and the r' th column of $\mathbf{W}^{(v_c)}$ for all $(v, r) \in \mathcal{S}$ and $v_c \in C(v)$. As can be seen from Equation (3.3), we may equivalently discard these weight vectors instead of setting them to zero. Doing so, we arrive at a representation of $\overline{\mathcal{W}}_{\mathbb{H}}^{\mathcal{S}}$ as the end tensor of $(\overline{\mathbf{W}}^{(v)} \in \mathbb{R}^{R'_v \times R'_{Pa(v)}})_{v \in \mathcal{T}}$, where $R'_{Pa([N])} = 1$, $R'_{\{n\}} = D_n$ for $n \in [N]$, and $\overline{\mathbf{W}}^{(v)} = \mathbf{w}_{:, R'_v : R'_{Pa(v)}}^{(v)}$ for all $v \in \mathcal{T}$. Hence, Lemma 2 implies that for any $v \in \mathcal{T}$ the rank of $\llbracket \overline{\mathcal{W}}_{\mathbb{H}}^{\mathcal{S}}; v \rrbracket$ is at most $R'_{Pa(v)}$. This means that it suffices to show that:

$$\|\mathcal{W}_{\mathbb{H}} - \overline{\mathcal{W}}_{\mathbb{H}}^{\mathcal{S}}\| \leq \epsilon. \quad (\text{C.26})$$

For $i \in \llbracket |\mathcal{S}| \rrbracket$, let $\mathcal{S}_i \subset \mathcal{S}$ be the set comprising the first i local components in \mathcal{S} according to an arbitrary order. Adding and subtracting $\overline{\mathcal{W}}_{\mathbb{H}}^{\mathcal{S}_i}$ for all $i \in \llbracket |\mathcal{S}| - 1 \rrbracket$, and

applying the triangle inequality, we have:

$$\left\| \mathcal{W}_H - \overline{\mathcal{W}}_H^S \right\| \leq \sum_{i=0}^{|S|-1} \left\| \overline{\mathcal{W}}_H^{S_i} - \overline{\mathcal{W}}_H^{S_{i+1}} \right\|,$$

where $\overline{\mathcal{W}}_H^{S_0} := \mathcal{W}_H$. Upper bounding each term in the sum according to Lemma 49, while noticing that pruning a local component can only decrease the norms of weight matrices and other local components in the factorization, we obtain:

$$\begin{aligned} \left\| \mathcal{W}_H - \overline{\mathcal{W}}_H^S \right\| &\leq \sum_{\nu \in \text{int}(\mathcal{T})} \sum_{r=R'_\nu+1}^{R_\nu} \sigma_H^{(\nu,r)} \cdot \prod_{\nu' \in \mathcal{T} \setminus (\{\nu\} \cup C(\nu))} \left\| \mathbf{W}^{(\nu')} \right\| \\ &\leq \sum_{\nu \in \text{int}(\mathcal{T})} B^{|\mathcal{T}|-1-|C(\nu)|} \cdot \sum_{r=R'_\nu+1}^{R_\nu} \sigma_H^{(\nu,r)}, \end{aligned}$$

where the latter inequality is by recalling that $B = \max_{\nu \in \mathcal{T}} \left\| \mathbf{W}^{(\nu)} \right\|$. Since for all $\nu \in \text{int}(\mathcal{T})$ we have that $\sum_{r=R'_\nu+1}^{R_\nu} \sigma_H^{(\nu,r)} \leq \epsilon \cdot (|\mathcal{T}| - N)^{-1} B^{|C(\nu)|+1-|\mathcal{T}|}$, Equation (C.26) readily follows. \square

C.5.7 Proof of Proposition 6

Consider the tensor completion problem defined by the set of observed entries

$$\Omega = \{(1, \dots, 1, 1, 1, 1), (1, \dots, 1, 1, 1, 2), (1, \dots, 1, 2, 2, 1), (1, \dots, 1, 2, 2, 2)\}$$

and ground truth $\mathcal{W}^* \in \mathbb{R}^{D_1 \times \dots \times D_N}$, whose values at those locations are:

$$\mathcal{W}_{1,\dots,1,1,2,2}^* = \begin{bmatrix} 1 & 0 \\ ? & ? \end{bmatrix}, \quad \mathcal{W}_{1,\dots,1,2,2,2}^* = \begin{bmatrix} ? & ? \\ 0 & 1 \end{bmatrix}, \quad (\text{C.27})$$

where ? stands for an unobserved entry. We define two solutions for the tensor completion problem, \mathcal{W} and \mathcal{W}' in $\mathbb{R}^{D_1 \times \dots \times D_N}$, as follows:

$$\begin{aligned} \mathcal{W}_{1,\dots,1,1,2,2} &:= \begin{bmatrix} 1 & 0 \\ 1 & 0 \end{bmatrix}, \quad \mathcal{W}_{1,\dots,1,2,2,2} := \begin{bmatrix} 0 & 1 \\ 0 & 1 \end{bmatrix}, \\ \mathcal{W}'_{1,\dots,1,1,2,2} &:= \begin{bmatrix} 1 & 0 \\ 0 & 1 \end{bmatrix}, \quad \mathcal{W}'_{1,\dots,1,2,2,2} := \begin{bmatrix} 1 & 0 \\ 0 & 1 \end{bmatrix}, \end{aligned}$$

and the remaining entries of \mathcal{W} and \mathcal{W}' hold zero. Clearly, $\mathcal{L}(\mathcal{W}) = \mathcal{L}(\mathcal{W}') = 0$.

Fix a mode tree \mathcal{T} over $[N]$. Since \mathcal{W} and \mathcal{W}' fit the observed entries their hierarchical tensor ranks with respect to \mathcal{T} , $(\text{rank}[\mathcal{W}; \nu])_{\nu \in \mathcal{T} \setminus \{[N]\}}$ and $(\text{rank}[\mathcal{W}'; \nu])_{\nu \in \mathcal{T} \setminus \{[N]\}}$, are in $\mathcal{R}_{\mathcal{T}}$. We prove that neither $(\text{rank}[\mathcal{W}; \nu])_{\nu \in \mathcal{T} \setminus \{[N]\}} \leq (\text{rank}[\mathcal{W}'; \nu])_{\nu \in \mathcal{T} \setminus \{[N]\}}$ nor $(\text{rank}[\mathcal{W}'; \nu])_{\nu \in \mathcal{T} \setminus \{[N]\}} \leq (\text{rank}[\mathcal{W}; \nu])_{\nu \in \mathcal{T} \setminus \{[N]\}}$ (with respect to the standard product partial order), by examining the matrix ranks of the matricizations of \mathcal{W} and \mathcal{W}' according to $\{N-2\} \in \mathcal{T}$ and $\{N-1\} \in \mathcal{T}$ (recall that any mode tree has leaves $\{1\}, \dots, \{N\}$). For $\{N-2\}$, we have that $\text{rank}[\mathcal{W}; \{N-2\}] = 2$ whereas $\text{rank}[\mathcal{W}'; \{N-2\}] = 1$. To see it is so, notice that:

$$[\mathcal{W}; \{N-2\}]_{:,2,4} = \begin{bmatrix} 1 & 0 & 1 & 0 \\ 0 & 1 & 0 & 1 \end{bmatrix}, \quad [\mathcal{W}'; \{N-2\}]_{:,2,4} = \begin{bmatrix} 1 & 0 & 0 & 1 \\ 1 & 0 & 0 & 1 \end{bmatrix},$$

and all other entries of $[\mathcal{W}; \{N-2\}]$ and $[\mathcal{W}'; \{N-2\}]$ hold zero. This means that $(\text{rank}[\mathcal{W}; \nu])_{\nu \in \mathcal{T} \setminus \{[N]\}} \leq (\text{rank}[\mathcal{W}'; \nu])_{\nu \in \mathcal{T} \setminus \{[N]\}}$ does not hold. On the other hand, for $\{N-1\}$ we have that $\text{rank}[\mathcal{W}; \{N-1\}] = 1$ while $\text{rank}[\mathcal{W}'; \{N-1\}] = 2$,

because:

$$\llbracket \mathcal{W}; \{N-1\} \rrbracket_{:2;4} = \begin{bmatrix} 1 & 0 & 0 & 1 \\ 1 & 0 & 0 & 1 \end{bmatrix}, \quad \llbracket \mathcal{W}'; \{N-1\} \rrbracket_{:2;4} = \begin{bmatrix} 1 & 0 & 1 & 0 \\ 0 & 1 & 0 & 1 \end{bmatrix},$$

and the remaining entries of $\llbracket \mathcal{W}; \{N-1\} \rrbracket$ and $\llbracket \mathcal{W}'; \{N-1\} \rrbracket$ hold zero. This implies that $(\text{rank} \llbracket \mathcal{W}'; \nu \rrbracket)_{\nu \in \mathcal{T} \setminus \{[N]\}} \leq (\text{rank} \llbracket \mathcal{W}; \nu \rrbracket)_{\nu \in \mathcal{T} \setminus \{[N]\}}$ does not hold, and so the hierarchical tensor ranks of \mathcal{W} and \mathcal{W}' are incomparable, *i.e.* neither is smaller than or equal to the other.

It remains to show that there exists no

$$(R''_{\nu})_{\nu \in \mathcal{T} \setminus \{[N]\}} \in \mathcal{R}_{\mathcal{T}} \setminus \left\{ (\text{rank} \llbracket \mathcal{W}; \nu \rrbracket)_{\nu \in \mathcal{T} \setminus \{[N]\}}, (\text{rank} \llbracket \mathcal{W}'; \nu \rrbracket)_{\nu \in \mathcal{T} \setminus \{[N]\}} \right\}$$

satisfying

$$(R''_{\nu})_{\nu \in \mathcal{T} \setminus \{[N]\}} \leq (\text{rank} \llbracket \mathcal{W}; \nu \rrbracket)_{\nu \in \mathcal{T} \setminus \{[N]\}}$$

or

$$(R''_{\nu})_{\nu \in \mathcal{T} \setminus \{[N]\}} \leq (\text{rank} \llbracket \mathcal{W}'; \nu \rrbracket)_{\nu \in \mathcal{T} \setminus \{[N]\}}.$$

Assume by way of contradiction that there exists such $(R''_{\nu})_{\nu \in \mathcal{T} \setminus \{[N]\}}$, and let $\mathcal{W}'' \in \mathbb{R}^{D_1 \times \dots \times D_N}$ be a solution of this hierarchical tensor rank. We now prove that

$$(R''_{\nu})_{\nu \in \mathcal{T} \setminus \{[N]\}} \leq (\text{rank} \llbracket \mathcal{W}; \nu \rrbracket)_{\nu \in \mathcal{T} \setminus \{[N]\}}$$

entails a contradiction. Since $(R''_{\nu})_{\nu \in \mathcal{T} \setminus \{[N]\}}$ is not equal to the hierarchical tensor rank of \mathcal{W} , there exists $\nu \in \mathcal{T} \setminus \{[N]\}$ for which $\text{rank} \llbracket \mathcal{W}''; \nu \rrbracket = R''_{\nu} < \text{rank} \llbracket \mathcal{W}; \nu \rrbracket$. Let us examine the possible cases:

- If ν does not contain $N-2, N-1$, and N , then $\text{rank} \llbracket \mathcal{W}; \nu \rrbracket = 1$ as all rows but the first of this matricization are zero. In this case $\llbracket \mathcal{W}''; \nu \rrbracket = R''_{\nu} = 0$, implying that \mathcal{W}'' is the zero tensor, in contradiction to it fitting the (non-zero) observed entries from Equation (C.27).
- If ν contains N but not $N-2$ and $N-1$, then $\text{rank} \llbracket \mathcal{W}; \nu \rrbracket = 2$ since:

$$\llbracket \mathcal{W}; \nu \rrbracket_{:2;4} = \begin{bmatrix} 1 & 1 & 0 & 0 \\ 0 & 0 & 1 & 1 \end{bmatrix},$$

and all other entries of $\llbracket \mathcal{W}; \nu \rrbracket$ hold zero. In this case $\llbracket \mathcal{W}''; \nu \rrbracket = R''_{\nu} < 2$. However, the fact that \mathcal{W}'' fits the observed entries from Equation (C.27) leads to a contradiction, as $\llbracket \mathcal{W}''; \nu \rrbracket$ must contain at least two linearly independent columns. To see it is so, notice that:

$$\llbracket \mathcal{W}^*; \nu \rrbracket_{:2;4} = \begin{bmatrix} 1 & ? & ? & 0 \\ 0 & ? & ? & 1 \end{bmatrix},$$

where recall that ? stands for an unobserved entry.

- If ν contains $N-1$ but not $N-2$ and N , then $\text{rank} \llbracket \mathcal{W}; \nu \rrbracket = 1$ since:

$$\llbracket \mathcal{W}; \nu \rrbracket_{:2;4} = \begin{bmatrix} 1 & 0 & 0 & 1 \\ 1 & 0 & 0 & 1 \end{bmatrix},$$

and all other entries of $\llbracket \mathcal{W}; \nu \rrbracket$ hold zero. In this case $\llbracket \mathcal{W}''; \nu \rrbracket = R''_\nu = 0$, which means that \mathcal{W}'' is the zero tensor, in contradiction to it fitting the (non-zero) observed entries from Equation (C.27).

- If ν contains $N - 2$ but not $N - 1$ and N , then $\text{rank}\llbracket \mathcal{W}; \nu \rrbracket = 2$ since:

$$\llbracket \mathcal{W}; \nu \rrbracket_{:2,:4} = \begin{bmatrix} 1 & 0 & 1 & 0 \\ 0 & 1 & 0 & 1 \end{bmatrix},$$

and all other entries of $\llbracket \mathcal{W}; \nu \rrbracket$ hold zero. In this case $\llbracket \mathcal{W}''; \nu \rrbracket = R''_\nu < 2$. Noticing that $\llbracket \mathcal{W}''; \{N - 2\} \rrbracket_{:2,:4} = \llbracket \mathcal{W}''; \nu \rrbracket_{:2,:4}$, and that entries of $\llbracket \mathcal{W}''; \{N - 2\} \rrbracket$ outside its top 2-by-4 submatrix hold zero, we get that $\llbracket \mathcal{W}''; \{N - 2\} \rrbracket = \llbracket \mathcal{W}''; \nu \rrbracket < 2$. Furthermore, from the assumption that $(R''_\nu)_{\nu \in \mathcal{T} \setminus \{N\}} \leq (\text{rank}\llbracket \mathcal{W}; \nu \rrbracket)_{\nu \in \mathcal{T} \setminus \{N\}}$ and the previous three cases, we know that $R''_{\{n\}} = \llbracket \mathcal{W}; \{n\} \rrbracket = 1$ for all $n \in [N - 3]$, $R''_{\{N\}} = \llbracket \mathcal{W}; \{N\} \rrbracket = 2$, and $R''_{\{N-1\}} = \llbracket \mathcal{W}; \{N - 1\} \rrbracket = 1$. Any tensor $\mathcal{V} \in \mathbb{R}^{D_1 \times \dots \times D_N}$ that satisfies $\text{rank}\llbracket \mathcal{V}; \{n\} \rrbracket \leq R_{\{n\}} \in \mathbb{N}$ for all $n \in [N]$ can be represented as:

$$\mathcal{V} = \sum_{r_1=1}^{R_{\{1\}}} \dots \sum_{r_N=1}^{R_{\{N\}}} \mathcal{C}_{r_1, \dots, r_N} \otimes_{n=1}^N \mathbf{U}_{:,r_n}^{(n)},$$

where $\mathcal{C} \in \mathbb{R}^{R_{\{1\}} \times \dots \times R_{\{N\}}}$ and $(\mathbf{U}^{(n)} \in \mathbb{R}^{D_n \times R_{\{n\}}})_{n=1}^N$ (see, e.g., Section 4 in [124]). Thus, there exist $c_1, c_2 \in \mathbb{R}$, $(\mathbf{U}^{(n)} \in \mathbb{R}^{D_n \times 1})_{n=1}^{N-1}$, and $\mathbf{U}^{(N)} \in \mathbb{R}^{D_N \times 2}$ such that:

$$\mathcal{W}'' = c_1 \cdot (\otimes_{n=1}^{N-1} \mathbf{U}_{:,1}^{(n)}) \otimes \mathbf{U}_{:,1}^{(N)} + c_2 \cdot (\otimes_{n=1}^{N-1} \mathbf{U}_{:,1}^{(n)}) \otimes \mathbf{U}_{:,2}^{(N)}.$$

By multilinearity of the tensor product, we may write: $\mathcal{W}'' = (\otimes_{n=1}^{N-1} \mathbf{U}_{:,1}^{(n)}) \otimes (c_1 \cdot \mathbf{U}_{:,1}^{(N)} + c_2 \cdot \mathbf{U}_{:,2}^{(N)})$, and so \mathcal{W}'' has tensor rank one (it can be represented as a single non-zero tensor product between vectors). Since the tensor rank of a given tensor upper bounds the ranks of its matricizations (Remark 6.21 in [85]), $R''_{\{n\}} = \text{rank}\llbracket \mathcal{W}''; \{n\} \rrbracket = 1$ for all $n \in [N]$ (the matrix ranks of these matricizations cannot be zero as \mathcal{W}'' is not the zero tensor). Hence, we have arrived at a contradiction — $2 = R''_{\{N\}} \leq 1$.

- Contradictions in the remaining cases, where ν contains $N - 2, N - 1$, and N , or any two of them, readily follow from the previous cases due to the fact that $\llbracket \mathcal{V}; \nu \rrbracket = \llbracket \mathcal{V}; [N] \setminus \nu \rrbracket^\top$ for any tensor $\mathcal{V} \in \mathbb{R}^{D_1 \times \dots \times D_N}$, and that the matrix rank of a matrix is equal to the matrix rank of its transpose. In particular, for any such ν , it holds that $\text{rank}\llbracket \mathcal{W}''; \nu \rrbracket = \text{rank}\llbracket \mathcal{W}''; [N] \setminus \nu \rrbracket$ and $\text{rank}\llbracket \mathcal{W}; \nu \rrbracket = \text{rank}\llbracket \mathcal{W}; [N] \setminus \nu \rrbracket$. Therefore, if $\text{rank}\llbracket \mathcal{W}''; \nu \rrbracket = R''_\nu < \text{rank}\llbracket \mathcal{W}; \nu \rrbracket$, then $\text{rank}\llbracket \mathcal{W}''; [N] \setminus \nu \rrbracket < \text{rank}\llbracket \mathcal{W}; [N] \setminus \nu \rrbracket$. Since ν contains $N - 2, N - 1$, and N , or any two of them, its complement $[N] \setminus \nu$ contains none or just one of them. Each of these scenarios was already covered in previous cases, which imply that $\text{rank}\llbracket \mathcal{W}''; [N] \setminus \nu \rrbracket < \text{rank}\llbracket \mathcal{W}; [N] \setminus \nu \rrbracket$ entails a contradiction.

In all cases, we have established that the existence of $(R''_\nu)_{\nu \in \mathcal{T} \setminus \{N\}} \in \mathcal{R}_{\mathcal{T}}$, different from $(\text{rank}\llbracket \mathcal{W}; \nu \rrbracket)_{\nu \in \mathcal{T} \setminus \{N\}}$ and $(\text{rank}\llbracket \mathcal{W}'; \nu \rrbracket)_{\nu \in \mathcal{T} \setminus \{N\}}$, satisfying $(R''_\nu)_{\nu \in \mathcal{T} \setminus \{N\}} \leq (\text{rank}\llbracket \mathcal{W}; \nu \rrbracket)_{\nu \in \mathcal{T} \setminus \{N\}}$ leads to a contradiction. The claim for \mathcal{W}' , i.e. that there exists no such $(R''_\nu)_{\nu \in \mathcal{T} \setminus \{N\}}$ satisfying $(R''_\nu)_{\nu \in \mathcal{T} \setminus \{N\}} \leq (\text{rank}\llbracket \mathcal{W}'; \nu \rrbracket)_{\nu \in \mathcal{T} \setminus \{N\}}$, is proven analogously. Combined with the previous part of the proof, in which we established that neither $(\text{rank}\llbracket \mathcal{W}; \nu \rrbracket)_{\nu \in \mathcal{T} \setminus \{N\}}$ nor $(\text{rank}\llbracket \mathcal{W}'; \nu \rrbracket)_{\nu \in \mathcal{T} \setminus \{N\}}$ is smaller than or equal

to the other, we conclude that $(\text{rank}[\mathcal{W}; \nu])_{\nu \in \mathcal{T} \setminus \{[N]\}}$ and $(\text{rank}[\mathcal{W}'; \nu])_{\nu \in \mathcal{T} \setminus \{[N]\}}$ are two different minimal elements of $\mathcal{R}_{\mathcal{T}}$. \square

C.5.8 Proof of Proposition 8

For $l \in [L]$, the output of the l 'th convolutional layer at index $n \in [N/P^{l-1}]$ and channel $r \in [R_l]$ depends solely on inputs $\mathbf{x}^{((n-1) \cdot P^{l-1} + 1)}, \dots, \mathbf{x}^{(n \cdot P^{l-1})}$. Hence, we denote it by $\text{conv}_{l,n,r}(\mathbf{x}^{((n-1) \cdot P^{l-1} + 1)}, \dots, \mathbf{x}^{(n \cdot P^{l-1})})$. We may view the output linear layer as a 1×1 convolutional layer with a single output channel. Accordingly, let $\text{conv}_{L+1,1,1}(\mathbf{x}^{(1)}, \dots, \mathbf{x}^{(N)}) := f_{\theta}(\mathbf{x}^{(1)}, \dots, \mathbf{x}^{(N)})$ and $\mathcal{W}^{(L+1,1,1)} := \mathcal{W}_H$.

We show by induction over the layer $l \in [L+1]$ that for any $n \in [N/P^{l-1}]$ and $r \in [R_l]$:

$$\text{conv}_{l,n,r}(\mathbf{x}^{((n-1) \cdot P^{l-1} + 1)}, \dots, \mathbf{x}^{(n \cdot P^{l-1})}) = \left\langle \otimes_{p=(n-1) \cdot P^{l-1} + 1}^{n \cdot P^{l-1}} \mathbf{x}^{(p)}, \mathcal{W}^{(l,n,r)} \right\rangle. \quad (\text{C.28})$$

For $l = 1$, let $n \in [N]$ and $r \in [R_1]$. From the definition of $\mathcal{W}^{(1,n,r)}$ (Equation (C.1)) we can see that:

$$\text{conv}_{1,n,r}(\mathbf{x}^{(n)}) = \left\langle \mathbf{x}^{(n)}, \mathbf{W}_{:,r}^{(1,n)} \right\rangle = \left\langle \mathbf{x}^{(n)}, \mathcal{W}^{(1,n,r)} \right\rangle.$$

Now, assuming that the inductive claim holds for $l-1 \geq 1$, we prove that it holds for l . Fix some $n \in [N/P^{l-1}]$ and $r \in [R_l]$. The l 'th convolutional layer is applied to the output of the $l-1$ 'th hidden layer, denoted $(\mathbf{h}^{(l-1,1)}, \dots, \mathbf{h}^{(l-1,N/P^{l-1})}) \in \mathbb{R}^{R_{l-1}} \times \dots \times \mathbb{R}^{R_{l-1}}$. Each $\mathbf{h}^{(l-1,n)}$, for $n \in [N/P^{l-1}]$, is a result of the product pooling operation (with window size P) applied to the output of the $l-1$ 'th convolutional layer. Thus:

$$\begin{aligned} & \text{conv}_{l,n,r}(\mathbf{x}^{((n-1) \cdot P^{l-1} + 1)}, \dots, \mathbf{x}^{(n \cdot P^{l-1})}) \\ &= \sum_{r'=1}^{R_{l-1}} \mathbf{W}_{r',r}^{(l,n)} \cdot \mathbf{h}_{r'}^{(l-1,n)} \\ &= \sum_{r'=1}^{R_{l-1}} \mathbf{W}_{r',r}^{(l,n)} \cdot \prod_{p=(n-1) \cdot P + 1}^{n \cdot P} \text{conv}_{l-1,p,r'}(\mathbf{x}^{((p-1) \cdot P^{l-2} + 1)}, \dots, \mathbf{x}^{(p \cdot P^{l-2})}). \end{aligned}$$

The inductive assumption for $l-1$ then implies that:

$$\begin{aligned} & \text{conv}_{l,n,r}(\mathbf{x}^{((n-1) \cdot P^{l-1} + 1)}, \dots, \mathbf{x}^{(n \cdot P^{l-1})}) \\ &= \sum_{r'=1}^{R_{l-1}} \mathbf{W}_{r',r}^{(l,n)} \cdot \prod_{p=(n-1) \cdot P + 1}^{n \cdot P} \left\langle \otimes_{n'=(p-1) \cdot P^{l-2} + 1}^{p \cdot P^{l-2}} \mathbf{x}^{(n')}, \mathcal{W}^{(l-1,p,r')} \right\rangle. \end{aligned}$$

For any tensors $\mathcal{A}, \mathcal{A}', \mathcal{B}, \mathcal{B}'$ such that \mathcal{A} is of the same dimensions as \mathcal{A}' and \mathcal{B} is of the same dimensions as \mathcal{B}' , it holds that $\langle \mathcal{A} \otimes \mathcal{B}, \mathcal{A}' \otimes \mathcal{B}' \rangle = \langle \mathcal{A}, \mathcal{A}' \rangle \cdot \langle \mathcal{B}, \mathcal{B}' \rangle$. We

may therefore write:

$$\begin{aligned}
& \text{conv}_{l,n,r}(\mathbf{x}^{((n-1)\cdot P^{l-1}+1)}, \dots, \mathbf{x}^{(n\cdot P^{l-1})}) \\
&= \sum_{r'=1}^{R_{l-1}} \mathbf{W}_{r',r}^{(l,n)} \cdot \left\langle \otimes_{p=(n-1)\cdot P+1}^{n\cdot P} \left(\otimes_{n'=(p-1)\cdot P^{l-2}+1}^{p\cdot P^{l-2}} \mathbf{x}^{(n')} \right), \otimes_{p=(n-1)\cdot P+1}^{n\cdot P} \mathcal{W}^{(l-1,p,r')} \right\rangle \\
&= \sum_{r'=1}^{R_{l-1}} \mathbf{W}_{r',r}^{(l,n)} \cdot \left\langle \otimes_{p=(n-1)\cdot P^{l-1}+1}^{n\cdot P^{l-1}} \mathbf{x}^{(p)}, \otimes_{p=(n-1)\cdot P+1}^{n\cdot P} \mathcal{W}^{(l-1,p,r')} \right\rangle \\
&= \left\langle \otimes_{p=(n-1)\cdot P^{l-1}+1}^{n\cdot P^{l-1}} \mathbf{x}^{(p)}, \sum_{r'=1}^{R_{l-1}} \mathbf{W}_{r',r}^{(l,n)} \left[\otimes_{p=(n-1)\cdot P+1}^{n\cdot P} \mathcal{W}^{(l-1,p,r')} \right] \right\rangle.
\end{aligned}$$

Noticing that $\mathcal{W}^{(l,n,r)} = \sum_{r'=1}^{R_{l-1}} \mathbf{W}_{r',r}^{(l,n)} \left[\otimes_{p=(n-1)\cdot P+1}^{n\cdot P} \mathcal{W}^{(l-1,p,r')} \right]$ (Equation (C.1)) establishes Equation (C.28).

Applying the inductive claim for $l = L + 1, n = 1$, and $r = 1$, while recalling that $L = \log_p N$, yields:

$$\begin{aligned}
f_\theta(\mathbf{x}^{(1)}, \dots, \mathbf{x}^{(N)}) &= \text{conv}_{L+1,1,1}(\mathbf{x}^{(1)}, \dots, \mathbf{x}^{(N)}) \\
&= \left\langle \otimes_{n=1}^N \mathbf{x}^{(n)}, \mathcal{W}^{(L+1,1,1)} \right\rangle \\
&= \left\langle \otimes_{n=1}^N \mathbf{x}^{(n)}, \mathcal{W}_H \right\rangle.
\end{aligned}$$

□

C.5.9 Proof of Theorem 9

Let $t \geq 0$ be a time at which $\sigma_H^{(v,r)}(t) := \left\| \otimes_{\mathbf{w} \in \text{LC}(v,r)} \mathbf{w}(t) \right\| = \prod_{\mathbf{w} \in \text{LC}(v,r)} \|\mathbf{w}(t)\| > 0$. We differentiate $\sigma_H^{(v,r)}(t)^2$ with respect to time as done in the proof of Theorem 5 (Appendix C.5.5). From the product rule and Lemma 47 we get that:

$$\frac{d}{dt} \sigma_H^{(v,r)}(t)^2 = 2\sigma_H^{(v,r)}(t) \left\langle -\nabla \mathcal{L}_H(\mathcal{W}_H(t)), \mathcal{C}_H^{(v,r)}(t) \right\rangle \sum_{\mathbf{w} \in \text{LC}(v,r)} \prod_{\mathbf{w}' \in \text{LC}(v,r) \setminus \{\mathbf{w}\}} \|\mathbf{w}'(t)\|^2.$$

Since according to the chain rule $\frac{d}{dt} \sigma_H^{(v,r)}(t)^2 = 2\sigma_H^{(v,r)}(t) \cdot \frac{d}{dt} \sigma_H^{(v,r)}(t)$, the equation above leads to:

$$\frac{d}{dt} \sigma_H^{(v,r)}(t) = \left\langle -\nabla \mathcal{L}_H(\mathcal{W}_H(t)), \mathcal{C}_H^{(v,r)}(t) \right\rangle \sum_{\mathbf{w} \in \text{LC}(v,r)} \prod_{\mathbf{w}' \in \text{LC}(v,r) \setminus \{\mathbf{w}\}} \|\mathbf{w}'(t)\|^2. \tag{C.29}$$

By Lemma 3, the unbalancedness magnitude is constant through time, and so it remains equal to ϵ — its value at initialization. Hence, for any $\mathbf{w} \in \text{LC}(v,r)$:

$$\|\mathbf{w}(t)\|^2 \leq \min_{\mathbf{w}' \in \text{LC}(v,r)} \|\mathbf{w}'(t)\|^2 + \epsilon = \left(\min_{\mathbf{w}' \in \text{LC}(v,r)} \|\mathbf{w}'(t)\| \right)^{L_v \cdot \frac{2}{L_v}} + \epsilon \leq \sigma_H^{(v,r)}(t)^{\frac{2}{L_v}} + \epsilon. \tag{C.30}$$

If $\left\langle -\nabla \mathcal{L}_H(\mathcal{W}_H(t)), \mathcal{C}_H^{(v,r)}(t) \right\rangle \geq 0$, applying the inequality above to each $\|\mathbf{w}'(t)\|^2$ in Equation (C.29) yields the upper bound from Equation (C.2):

$$\begin{aligned}
\frac{d}{dt} \sigma_H^{(v,r)}(t) &\leq \left\langle -\nabla \mathcal{L}_H(\mathcal{W}_H(t)), \mathcal{C}_H^{(v,r)}(t) \right\rangle \sum_{\mathbf{w} \in \text{LC}(v,r)} \prod_{\mathbf{w}' \in \text{LC}(v,r) \setminus \{\mathbf{w}\}} \left(\sigma_H^{(v,r)}(t)^{\frac{2}{L_v}} + \epsilon \right) \\
&= \left(\sigma_H^{(v,r)}(t)^{\frac{2}{L_v}} + \epsilon \right)^{L_v-1} \cdot L_v \left\langle -\nabla \mathcal{L}_H(\mathcal{W}_H(t)), \mathcal{C}_H^{(v,r)}(t) \right\rangle.
\end{aligned}$$

To prove the lower bound from Equation (C.2), we multiply and divide each summand on the right hand side of Equation (C.29) by the corresponding $\|\mathbf{w}(t)\|^2$ (non-zero because $\sigma_{\mathbf{H}}^{(v,r)}(t) > 0$), *i.e.*:

$$\begin{aligned} \frac{d}{dt}\sigma_{\mathbf{H}}^{(v,r)}(t) &= \left\langle -\nabla\mathcal{L}_{\mathbf{H}}(\mathcal{W}_{\mathbf{H}}(t)), \mathcal{C}_{\mathbf{H}}^{(v,r)}(t) \right\rangle \sum_{\mathbf{w} \in \text{LC}(v,r)} \|\mathbf{w}(t)\|^{-2} \cdot \prod_{\mathbf{w}' \in \text{LC}(v,r)} \|\mathbf{w}'(t)\|^2 \\ &= \left\langle -\nabla\mathcal{L}_{\mathbf{H}}(\mathcal{W}_{\mathbf{H}}(t)), \mathcal{C}_{\mathbf{H}}^{(v,r)}(t) \right\rangle \sigma_{\mathbf{H}}^{(v,r)}(t) \cdot \sum_{\mathbf{w} \in \text{LC}(v,r)} \|\mathbf{w}(t)\|^{-2}. \end{aligned}$$

By Equation (C.30) we know that $\|\mathbf{w}(t)\|^{-2} \geq (\sigma_{\mathbf{H}}^{(v,r)}(t)^{\frac{2}{L_v}} + \epsilon)^{-1}$. Thus, applying this inequality to the equation above establishes the desired lower bound.

If $\left\langle -\nabla\mathcal{L}_{\mathbf{H}}(\mathcal{W}_{\mathbf{H}}(t)), \mathcal{C}_{\mathbf{H}}^{(v,r)}(t) \right\rangle < 0$, the upper and lower bounds in Equation (C.3) readily follow by similar derivations, where the difference in the direction of inequalities is due to the negativity of $\left\langle -\nabla\mathcal{L}_{\mathbf{H}}(\mathcal{W}_{\mathbf{H}}(t)), \mathcal{C}_{\mathbf{H}}^{(v,r)}(t) \right\rangle$. \square

C.5.10 Proof of Proposition 9

We partition the proof into two parts: the first shows that $\text{rank}[\mathcal{W}_{\mathbf{H}}; I] \geq \text{sep}(f_{\Theta}; I)$, and the second establishes the converse.

Proof of lower bound ($\text{rank}[\mathcal{W}_{\mathbf{H}}; I] \geq \text{sep}(f_{\Theta}; I)$). Denote $R := \text{rank}[\mathcal{W}_{\mathbf{H}}; I]$, and assume without loss of generality that $I = [|I|]$. Since $[\mathcal{W}_{\mathbf{H}}; I]$ is a rank R matrix, there exist $\mathbf{v}^{(1)}, \dots, \mathbf{v}^{(R)} \in \mathbb{R}^{\prod_{n=1}^{|I|} D_n}$ and $\bar{\mathbf{v}}^{(1)}, \dots, \bar{\mathbf{v}}^{(R)} \in \mathbb{R}^{\prod_{n=|I|+1}^N D_n}$ such that:

$$[\mathcal{W}_{\mathbf{H}}; I] = \sum_{r=1}^R \mathbf{v}^{(r)} (\bar{\mathbf{v}}^{(r)})^{\top}.$$

For each $r \in [R]$, let $\mathcal{V}^{(r)} \in \mathbb{R}^{D_1 \times \dots \times D_{|I|}}$ be the tensor whose arrangement as a column vector is equal to $\mathbf{v}^{(r)}$, *i.e.* $[\mathcal{V}^{(r)}; I] = \mathbf{v}^{(r)}$. Similarly, for every $r \in [R]$ let $\bar{\mathcal{V}}^{(r)} \in \mathbb{R}^{D_{|I|+1} \times \dots \times D_N}$ be the tensor whose arrangement as a row vector is equal to $(\bar{\mathbf{v}}^{(r)})^{\top}$, *i.e.* $[\bar{\mathcal{V}}^{(r)}; \emptyset] = (\bar{\mathbf{v}}^{(r)})^{\top}$. Then:

$$\begin{aligned} [\mathcal{W}_{\mathbf{H}}; I] &= \sum_{r=1}^R \mathbf{v}^{(r)} (\bar{\mathbf{v}}^{(r)})^{\top} \\ &= \sum_{r=1}^R \left[[\mathcal{V}^{(r)}; I] \circ [\bar{\mathcal{V}}^{(r)}; \emptyset] \right] \\ &= \sum_{r=1}^R \left[[\mathcal{V}^{(r)} \otimes \bar{\mathcal{V}}^{(r)}; I] \right] \\ &= \left[\sum_{r=1}^R \mathcal{V}^{(r)} \otimes \bar{\mathcal{V}}^{(r)}; I \right], \end{aligned}$$

where the third equality makes use of Lemma 37, and the last equality is by linearity of the matricization operator. Since matricizations merely reorder the entries of tensors, the equation above implies that $\mathcal{W}_{\mathbf{H}} = \sum_{r=1}^R \mathcal{V}^{(r)} \otimes \bar{\mathcal{V}}^{(r)}$. We therefore have that:

$$\begin{aligned} f_{\Theta}(\mathbf{x}^{(1)}, \dots, \mathbf{x}^{(N)}) &= \left\langle \otimes_{n=1}^N \mathbf{x}^{(n)}, \mathcal{W}_{\mathbf{H}} \right\rangle \\ &= \left\langle \otimes_{n=1}^N \mathbf{x}^{(n)}, \sum_{r=1}^R \mathcal{V}^{(r)} \otimes \bar{\mathcal{V}}^{(r)} \right\rangle \\ &= \sum_{r=1}^R \left\langle \otimes_{n=1}^N \mathbf{x}^{(n)}, \mathcal{V}^{(r)} \otimes \bar{\mathcal{V}}^{(r)} \right\rangle. \end{aligned}$$

For any $\mathcal{A}, \mathcal{A}' \in \mathbb{R}^{D_1 \times \dots \times D_{|I|}}$ and $\mathcal{B}, \mathcal{B}' \in \mathbb{R}^{D_{|I|+1} \times \dots \times D_N}$ it holds that $\langle \mathcal{A} \otimes \mathcal{B}, \mathcal{A}' \otimes \mathcal{B}' \rangle = \langle \mathcal{A}, \mathcal{A}' \rangle \cdot \langle \mathcal{B}, \mathcal{B}' \rangle$. Thus:

$$\begin{aligned} f_{\Theta}(\mathbf{x}^{(1)}, \dots, \mathbf{x}^{(N)}) &= \sum_{r=1}^R \left\langle \otimes_{n=1}^N \mathbf{x}^{(n)}, \mathcal{V}^{(r)} \otimes \bar{\mathcal{V}}^{(r)} \right\rangle \\ &= \sum_{r=1}^R \left\langle \otimes_{n=1}^{|I|} \mathbf{x}^{(n)}, \mathcal{V}^{(r)} \right\rangle \cdot \left\langle \otimes_{n=|I|+1}^N \mathbf{x}^{(n)}, \bar{\mathcal{V}}^{(r)} \right\rangle. \end{aligned}$$

By defining $g_r : \times_{n=1}^{|I|} \mathbb{R}^{D_n} \rightarrow \mathbb{R}$ and $\bar{g}_r : \times_{n=|I|+1}^N \mathbb{R}^{D_n} \rightarrow \mathbb{R}$, for $r \in [R]$, as:

$$g_r(\mathbf{x}^{(1)}, \dots, \mathbf{x}^{(|I|)}) = \left\langle \otimes_{n=1}^{|I|} \mathbf{x}^{(n)}, \mathcal{V}^{(r)} \right\rangle, \quad \bar{g}_r(\mathbf{x}^{(|I|+1)}, \dots, \mathbf{x}^{(N)}) = \left\langle \otimes_{n=|I|+1}^N \mathbf{x}^{(n)}, \bar{\mathcal{V}}^{(r)} \right\rangle,$$

we arrive at the following representation of f_{Θ} as a sum, where each summand is a product of two functions — one that operates over inputs indexed by I and another that operates over inputs indexed by $[N] \setminus I$:

$$f_{\Theta}(\mathbf{x}^{(1)}, \dots, \mathbf{x}^{(N)}) = \sum_{r=1}^R g_r(\mathbf{x}^{(1)}, \dots, \mathbf{x}^{(|I|)}) \cdot \bar{g}_r(\mathbf{x}^{(|I|+1)}, \dots, \mathbf{x}^{(N)}).$$

Since the separation rank of f_{Θ} is the minimal number of summands required to express it in such a manner, we conclude that $\text{rank}[\mathcal{W}_{\Theta}; I] = R \geq \text{sep}(f_{\Theta}; I)$.

Proof of upper bound ($\text{rank}[\mathcal{W}_{\Theta}; I] \leq \text{sep}(f_{\Theta}; I)$). Towards proving the upper bound, we establish the following lemma.

Lemma 50. *Given $f : \times_{n=1}^N \mathbb{R}^{D_n} \rightarrow \mathbb{R}$ and any $(\mathbf{x}^{(1, h_1)} \in \mathbb{R}^{D_1})_{h_1=1}^{H_1}, \dots, (\mathbf{x}^{(N, h_N)} \in \mathbb{R}^{D_N})_{h_N=1}^{H_N}$, let $\mathcal{W} \in \mathbb{R}^{H_1 \times \dots \times H_N}$ be the tensor defined by $\mathcal{W}_{h_1, \dots, h_N} := f(\mathbf{x}^{(1, h_1)}, \dots, \mathbf{x}^{(N, h_N)})$ for all $(h_1, \dots, h_N) \in [H_1] \times \dots \times [H_N]$. Then, for any $I \subset [N]$:*

$$\text{rank}[\mathcal{W}; I] \leq \text{sep}(f; I).$$

In words, for any tensor holding the outputs of f over a grid of inputs, the rank of its matricization according to I is upper bounded by the separation rank of f with respect to I .

Proof. If $\text{sep}(f; I)$ is ∞ or zero, i.e. f cannot be represented as a finite sum of separable functions (with respect to I) or is identically zero, then the claim is trivial. Otherwise, denote $R := \text{sep}(f; I)$, and assume without loss of generality that $I = [|I|]$. Let $g_1, \dots, g_R : \times_{n=1}^{|I|} \mathbb{R}^{D_n} \rightarrow \mathbb{R}$ and $\bar{g}_1, \dots, \bar{g}_R : \times_{n=|I|+1}^N \mathbb{R}^{D_n} \rightarrow \mathbb{R}$ such that:

$$f(\mathbf{x}^{(1)}, \dots, \mathbf{x}^{(N)}) = \sum_{r=1}^R g_r(\mathbf{x}^{(1)}, \dots, \mathbf{x}^{(|I|)}) \cdot \bar{g}_r(\mathbf{x}^{(|I|+1)}, \dots, \mathbf{x}^{(N)}). \quad (\text{C.31})$$

We define $(\mathcal{V}^{(r)} \in \mathbb{R}^{D_1 \times \dots \times D_{|I|}})_{r=1}^R$ to be the tensors holding the outputs of $(g_r)_{r=1}^R$ over the grid of inputs

$$(\mathbf{x}^{(1, h_1)})_{h_1=1}^{H_1}, \dots, (\mathbf{x}^{(|I|, h_{|I|})})_{h_{|I|}=1}^{H_{|I|}},$$

i.e. for all $h_1, \dots, h_{|I|} \in [H_1] \times \dots \times [H_{|I|}]$ and $r \in [R]$ it holds that $\mathcal{V}_{h_1, \dots, h_{|I|}}^{(r)} = g_r(\mathbf{x}^{(1, h_1)}, \dots, \mathbf{x}^{(|I|, h_{|I|})})$. Similarly, we let $(\bar{\mathcal{V}}^{(r)} \in \mathbb{R}^{D_{|I|+1} \times \dots \times D_N})_{r=1}^R$ be the tensors holding the outputs of $(\bar{g}_r)_{r=1}^R$ over their respective grid of inputs, i.e. for all $h_{|I|+1}, \dots, h_N \in [H_{|I|+1}] \times \dots \times [H_N]$ and $r \in [R]$ it holds that $\bar{\mathcal{V}}_{h_{|I|+1}, \dots, h_N}^{(r)} = \bar{g}_r(\mathbf{x}^{(|I|+1, h_{|I|+1})}, \dots, \mathbf{x}^{(N, h_N)})$.

By Equation (C.31) and the definitions of \mathcal{W} , $(\mathcal{V}^{(r)})_{r=1}^R$, and $(\bar{\mathcal{V}}^{(r)})_{r=1}^R$, we have that for any $h_1, \dots, h_N \in [H_1] \times \dots \times [H_N]$:

$$\begin{aligned} \mathcal{W}_{h_1, \dots, h_N} &= f(\mathbf{x}^{(1, h_1)}, \dots, \mathbf{x}^{(N, h_N)}) \\ &= \sum_{r=1}^R g_r(\mathbf{x}^{(1, h_1)}, \dots, \mathbf{x}^{(|I|, h_{|I|})}) \cdot \bar{g}_r(\mathbf{x}^{(|I|+1, h_{|I|+1})}, \dots, \mathbf{x}^{(N, h_N)}) \\ &= \sum_{r=1}^R \mathcal{V}_{h_1, \dots, h_{|I|}}^{(r)} \cdot \bar{\mathcal{V}}_{h_{|I|+1}, \dots, h_N}^{(r)}, \end{aligned}$$

which means that $\mathcal{W} = \sum_{r=1}^R \mathcal{V}^{(r)} \otimes \bar{\mathcal{V}}^{(r)}$. From the linearity of the matricization operator and Lemma 37 we then get that $\llbracket \mathcal{W}; I \rrbracket = \sum_{r=1}^R \llbracket \mathcal{V}^{(r)}; I \rrbracket \circ \llbracket \bar{\mathcal{V}}^{(r)}; \emptyset \rrbracket$. Since $\llbracket \mathcal{V}^{(r)}; I \rrbracket$ is a column vector and $\llbracket \bar{\mathcal{V}}^{(r)}; \emptyset \rrbracket$ is a row vector for all $r \in [R]$, we have arrived at a representation of $\llbracket \mathcal{W}; I \rrbracket$ as a sum of R tensor products between two vectors. A tensor product of two vectors is a rank one matrix, and so, due to the sub-additivity of rank we conclude: $\text{rank} \llbracket \mathcal{W}; I \rrbracket \leq R = \text{sep}(f; I)$. \square

Now, consider the grid of inputs defined by the standard bases of $\mathbb{R}^{D_1}, \dots, \mathbb{R}^{D_N}$, *i.e.* by:

$$(\mathbf{e}^{(1, d_1)} \in \mathbb{R}^{D_1})_{d_1=1}^{D_1}, \dots, (\mathbf{e}^{(N, d_N)} \in \mathbb{R}^{D_N})_{d_N=1}^{D_N},$$

where $\mathbf{e}^{(n, d_n)}$ is the vector holding one at its d_n 'th entry and zero elsewhere for $n \in [N]$ and $d_n \in [D_n]$. With Lemma 50 in hand, $\text{rank} \llbracket \mathcal{W}_H; I \rrbracket \leq \text{sep}(f_\Theta; I)$ follows by showing that \mathcal{W}_H is the tensor holding the outputs of f_Θ over this grid of inputs. Indeed, for all $d_1, \dots, d_N \in [D_1] \times \dots \times [D_N]$:

$$f_\Theta(\mathbf{e}^{(1, d_1)}, \dots, \mathbf{e}^{(N, d_N)}) = \langle \otimes_{n=1}^N \mathbf{e}^{(n, d_n)}, \mathcal{W}_H \rangle = (\mathcal{W}_H)_{d_1, \dots, d_N}.$$

\square

Appendix D

On the Ability of Graph Neural Networks to Model Interactions Between Vertices

D.1 Tightness of Upper Bounds for Separation Rank

Theorem 7 upper bounds the separation rank with respect to $\mathcal{I} \subseteq \mathcal{V}$ of a depth L GNN with product aggregation. According to it, under the setting of graph prediction, the separation rank is largely capped by the $(L - 1)$ -walk index of \mathcal{I} , *i.e.* the number of length $L - 1$ walks from $\mathcal{C}_{\mathcal{I}}$ — the set of vertices with an edge crossing the partition $(\mathcal{I}, \mathcal{I}^c)$. Similarly, for prediction over $t \in \mathcal{V}$, separation rank is largely capped by the $(L - 1, t)$ -walk index of \mathcal{I} , which takes into account only length $L - 1$ walks from $\mathcal{C}_{\mathcal{I}}$ ending at t . Theorem 8 provides matching lower bounds, up to logarithmic terms and to the number of walks from $\mathcal{C}_{\mathcal{I}}$ being replaced with the number of walks from any single admissible subset $\mathcal{C} \in \mathcal{S}(\mathcal{I})$ (Definition 13). Hence, the match between the upper and lower bounds is determined by the portion of $\mathcal{C}_{\mathcal{I}}$ that can be covered by an admissible subset.

In this appendix, to shed light on the tightness of the upper bounds, we present several concrete examples on which a significant portion of $\mathcal{C}_{\mathcal{I}}$ can be covered by an admissible subset.

Complete graph. Suppose that every two vertices are connected by an edge, *i.e.* $\mathcal{E} = \{\{i, j\} : i, j \in \mathcal{V}\}$. For any non-empty $\mathcal{I} \subsetneq \mathcal{V}$, clearly $\mathcal{C}_{\mathcal{I}} = \mathcal{N}(\mathcal{I}) \cap \mathcal{N}(\mathcal{I}^c) = \mathcal{V}$. In this case, $\mathcal{C}_{\mathcal{I}} = \mathcal{V} \in \mathcal{S}(\mathcal{I})$, meaning $\mathcal{C}_{\mathcal{I}}$ is an admissible subset of itself. To see it is so, notice that for any $i \in \mathcal{I}, j \in \mathcal{I}^c$, all vertices are neighbors of both $\mathcal{I}' := \{i\}$ and $\mathcal{J}' := \{j\}$, which trivially have no repeating shared neighbors (Definition 12). Thus, up to a logarithmic factor, the upper and lower bounds from Theorems 7 and 8 coincide.

Chain graph. Suppose that $\mathcal{E} = \{\{i, i + 1\} : i \in [|\mathcal{V}| - 1]\} \cup \{\{i, i\} : i \in \mathcal{V}\}$. For any non-empty $\mathcal{I} \subsetneq \mathcal{V}$, at least half of the vertices in $\mathcal{C}_{\mathcal{I}}$ can be covered by an admissible subset. That is, there exists $\mathcal{C} \in \mathcal{S}(\mathcal{I})$ satisfying $|\mathcal{C}| \geq 2^{-1} \cdot |\mathcal{C}_{\mathcal{I}}|$. For example, such \mathcal{C} can be constructed algorithmically as follows. Let $\mathcal{I}', \mathcal{J}' = \emptyset$. Starting from $k = 1$, if $\{k, k + 1\} \subseteq \mathcal{C}_{\mathcal{I}}$ and one of $\{k, k + 1\}$ is in \mathcal{I} while the other is in \mathcal{I}^c , then assign $\mathcal{I}' \leftarrow \mathcal{I}' \cup (\{k, k + 1\} \cap \mathcal{I})$, $\mathcal{J}' \leftarrow \mathcal{J}' \cup (\{k, k + 1\} \cap \mathcal{I}^c)$, and $k \leftarrow k + 3$. That is, add each of $\{k, k + 1\}$ to either \mathcal{I}' if it is in \mathcal{I} or \mathcal{J}' if it is in \mathcal{I}^c , and skip vertex $k + 2$. Otherwise, set $k \leftarrow k + 1$. The process terminates once $k > |\mathcal{V}| - 1$. By construction, $\mathcal{I}' \subseteq \mathcal{I}$ and $\mathcal{J}' \subseteq \mathcal{I}^c$, implying that $\mathcal{N}(\mathcal{I}') \cap \mathcal{N}(\mathcal{J}') \subseteq \mathcal{C}_{\mathcal{I}}$. Due

to the chain graph structure, $\mathcal{I}' \cup \mathcal{J}' \subseteq \mathcal{N}(\mathcal{I}') \cap \mathcal{N}(\mathcal{J}')$ and \mathcal{I}' and \mathcal{J}' have no repeating shared neighbors (Definition 12). Furthermore, for every pair of vertices from $\mathcal{C}_{\mathcal{I}}$ added to \mathcal{I}' and \mathcal{J}' , we can miss at most two other vertices from $\mathcal{C}_{\mathcal{I}}$. Thus, $\mathcal{C} := \mathcal{N}(\mathcal{I}') \cap \mathcal{N}(\mathcal{J}')$ is an admissible subset of $\mathcal{C}_{\mathcal{I}}$ satisfying $|\mathcal{C}| \geq 2^{-1} \cdot |\mathcal{C}_{\mathcal{I}}|$.

General graph. For an arbitrary graph and non-empty $\mathcal{I} \subsetneq \mathcal{V}$, an admissible subset of $\mathcal{C}_{\mathcal{I}}$ can be obtained by taking any sequence of pairs $(i_1, j_1), \dots, (i_M, j_M) \in \mathcal{I} \times \mathcal{I}^c$ with no shared neighbors, in the sense that $[\mathcal{N}(i_m) \cup \mathcal{N}(j_m)] \cap [\mathcal{N}(i_{m'}) \cup \mathcal{N}(j_{m'})] = \emptyset$ for all $m \neq m' \in [M]$. Defining $\mathcal{I}' := \{i_1, \dots, i_M\}$ and $\mathcal{J}' := \{j_1, \dots, j_M\}$, by construction they do not have repeating shared neighbors (Definition 12), and so $\mathcal{N}(\mathcal{I}') \cap \mathcal{N}(\mathcal{J}') \in \mathcal{S}(\mathcal{I})$. In particular, the shared neighbors of each pair are covered by $\mathcal{N}(\mathcal{I}') \cap \mathcal{N}(\mathcal{J}')$, i.e. $\cup_{m=1}^M \mathcal{N}(i_m) \cap \mathcal{N}(j_m) \subseteq \mathcal{N}(\mathcal{I}') \cap \mathcal{N}(\mathcal{J}')$.

D.2 Extension of Analysis to Directed Graphs With Multiple Edge Types

In this appendix, we generalize the separation rank bounds from Theorems 7 and 8 to directed graphs with multiple edge types.

Let $\mathcal{G} = (\mathcal{V}, \mathcal{E}, \tau)$ be a directed graph with vertices $\mathcal{V} = [|\mathcal{V}|]$, edges $\mathcal{E} \subseteq \{(i, j) : i, j \in \mathcal{V}\}$, and a map $\tau : \mathcal{E} \rightarrow [Q]$ from edges to one of $Q \in \mathbb{N}$ edge types. For $i \in \mathcal{V}$, let $\mathcal{N}_{in}(i) := \{j \in \mathcal{V} : (j, i) \in \mathcal{E}\}$ be its *incoming neighbors* and $\mathcal{N}_{out}(i) := \{j \in \mathcal{V} : (i, j) \in \mathcal{E}\}$ be its *outgoing neighbors*. For $\mathcal{I} \subseteq \mathcal{V}$, we denote $\mathcal{N}_{in}(\mathcal{I}) := \cup_{i \in \mathcal{I}} \mathcal{N}_{in}(i)$ and $\mathcal{N}_{out}(\mathcal{I}) := \cup_{i \in \mathcal{I}} \mathcal{N}_{out}(i)$. As customary in the context of GNNs, we assume the existence of all self-loops (cf. Section 5.2.1).

Message-passing GNNs (Section 5.3) operate identically over directed and undirected graphs, except that in directed graphs the hidden embedding of a vertex is updated only according to its incoming neighbors. For handling multiple edge types, common practice is to use different weight matrices per type in the GNN's update rule (cf. [88, 189]). Hence, we consider the following update rule for directed graphs with multiple edge types, replacing that from Equation (5.2):

$$\mathbf{h}^{(l,i)} = \text{AGGREGATE} \left(\left\{ \left\{ \mathbf{W}^{(l,\tau(j,i))} \mathbf{h}^{(l-1,j)} : j \in \mathcal{N}_{in}(i) \right\} \right\}, \right) \quad (\text{D.1})$$

where $(\mathbf{W}^{(1,q)} \in \mathbb{R}^{D_h \times D_x})_{q \in [Q]}$ and $(\mathbf{W}^{(l,q)} \in \mathbb{R}^{D_h \times D_h})_{l \in \{2, \dots, L\}, q \in [Q]}$ are learnable weight matrices.

In our analysis for undirected graphs (Section 5.4.2), a central concept is $\mathcal{C}_{\mathcal{I}}$ — the set of vertices with an edge crossing the partition induced by $\mathcal{I} \subseteq \mathcal{V}$. Due to the existence of self-loops it is equal to the shared neighbors of \mathcal{I} and \mathcal{I}^c , i.e. $\mathcal{C}_{\mathcal{I}} = \mathcal{N}(\mathcal{I}) \cap \mathcal{N}(\mathcal{I}^c)$. We generalize this concept to directed graphs, defining $\mathcal{C}_{\mathcal{I}}^{\rightarrow}$ to be the set of vertices with an incoming edge from the other side of the partition induced by \mathcal{I} , i.e. $\mathcal{C}_{\mathcal{I}}^{\rightarrow} := \{i \in \mathcal{I} : \mathcal{N}_{in}(i) \cap \mathcal{I}^c \neq \emptyset\} \cup \{j \in \mathcal{I}^c : \mathcal{N}_{in}(j) \cap \mathcal{I} \neq \emptyset\}$. Due to the existence of self-loops it is given by $\mathcal{C}_{\mathcal{I}}^{\rightarrow} = \mathcal{N}_{out}(\mathcal{I}) \cap \mathcal{N}_{out}(\mathcal{I}^c)$. Indeed, for undirected graphs $\mathcal{C}_{\mathcal{I}}^{\rightarrow} = \mathcal{C}_{\mathcal{I}}$.

With the definition of $\mathcal{C}_{\mathcal{I}}^{\rightarrow}$ in place, Theorem 10 upper bounds the separation ranks a GNN can achieve over directed graphs with multiple edge types. A technical subtlety is that the bounds depend on walks of lengths $l = L - 1, L - 2, \dots, 0$, while those in Theorem 7 for undirected graphs depend only on walks of length $L - 1$. As shown in the proof of Theorem 7, this dependence exists in undirected graphs as well.

Though, in undirected graphs with self-loops, the number of length $l \in \mathbb{N}$ walks from $\mathcal{C}_{\mathcal{I}}$ decays exponentially as l increases. One can therefore replace the sum over walk lengths with walks of length $L - 1$ (up to a multiplicative constant). By contrast, in directed graphs this is not true in general, e.g., when $\mathcal{C}_{\mathcal{I}}^{\rightarrow}$ contains only vertices with no outgoing edges (besides self-loops).

Theorem 10. *For a directed graph with multiple edge types \mathcal{G} and $t \in \mathcal{V}$, let $f^{(\theta, \mathcal{G})}$ and $f^{(\theta, \mathcal{G}, t)}$ be the functions realized by depth L graph and vertex prediction GNNs, respectively, with width D_h , learnable weights θ , and product aggregation (Equations (5.3) to (5.5) and (D.1)). Then, for any $\mathcal{I} \subseteq \mathcal{V}$ and assignment of weights θ it holds that:*

$$\text{(graph prediction)} \quad \log(\text{sep}(f^{(\theta, \mathcal{G})}; \mathcal{I})) \leq \log(D_h) \cdot \left(\sum_{l=1}^L \rho_{L-l}(\mathcal{C}_{\mathcal{I}}^{\rightarrow}, \mathcal{V}) + 1 \right), \quad (\text{D.2})$$

$$\text{(vertex prediction)} \quad \log(\text{sep}(f^{(\theta, \mathcal{G}, t)}; \mathcal{I})) \leq \log(D_h) \cdot \sum_{l=1}^L \rho_{L-l}(\mathcal{C}_{\mathcal{I}}^{\rightarrow}, \{t\}). \quad (\text{D.3})$$

Proof sketch (proof in Appendix D.7.4). The proof follows a line identical to that of Theorem 7, only requiring adjusting definitions from undirected graphs to directed graphs with multiple edge types. \square

Towards lower bounding separation ranks, we generalize the definitions of vertex subsets with no repeating shared neighbors (Definition 12) and admissible subsets of $\mathcal{C}_{\mathcal{I}}$ (Definition 13) to directed graphs.

Definition 16. We say that $\mathcal{I}, \mathcal{J} \subseteq \mathcal{V}$ have no outgoing repeating shared neighbors if every $k \in \mathcal{N}_{\text{out}}(\mathcal{I}) \cap \mathcal{N}_{\text{out}}(\mathcal{J})$ has only a single incoming neighbor in each of \mathcal{I} and \mathcal{J} , i.e. $|\mathcal{N}_{\text{in}}(k) \cap \mathcal{I}| = |\mathcal{N}_{\text{in}}(k) \cap \mathcal{J}| = 1$.

Definition 17. For $\mathcal{I} \subseteq \mathcal{V}$, we refer to $\mathcal{C} \subseteq \mathcal{C}_{\mathcal{I}}^{\rightarrow}$ as an *admissible subset* of $\mathcal{C}_{\mathcal{I}}^{\rightarrow}$ if there exist $\mathcal{I}' \subseteq \mathcal{I}, \mathcal{J}' \subseteq \mathcal{I}^c$ with no outgoing repeating shared neighbors such that $\mathcal{C} = \mathcal{N}_{\text{out}}(\mathcal{I}') \cap \mathcal{N}_{\text{out}}(\mathcal{J}')$. We use $\mathcal{S}^{\rightarrow}(\mathcal{I})$ to denote the set comprising all admissible subsets of $\mathcal{C}_{\mathcal{I}}^{\rightarrow}$:

$$\mathcal{S}^{\rightarrow}(\mathcal{I}) := \{ \mathcal{C} \subseteq \mathcal{C}_{\mathcal{I}}^{\rightarrow} : \mathcal{C} \text{ is an admissible subset of } \mathcal{C}_{\mathcal{I}}^{\rightarrow} \}.$$

Theorem 11 generalizes the lower bounds from Theorem 8 to directed graphs with multiple edge types.

Theorem 11. *Consider the setting and notation of Theorem 10. Given $\mathcal{I} \subseteq \mathcal{V}$, for almost all assignments of weights θ , i.e. for all but a set of Lebesgue measure zero, it holds that:*

$$\text{(graph prediction)} \quad \log(\text{sep}(f^{(\theta, \mathcal{G})}; \mathcal{I})) \geq \max_{\mathcal{C} \in \mathcal{S}^{\rightarrow}(\mathcal{I})} \log(\alpha_{\mathcal{C}}) \cdot \rho_{L-1}(\mathcal{C}, \mathcal{V}), \quad (\text{D.4})$$

$$\text{(vertex prediction)} \quad \log(\text{sep}(f^{(\theta, \mathcal{G}, t)}; \mathcal{I})) \geq \max_{\mathcal{C} \in \mathcal{S}^{\rightarrow}(\mathcal{I})} \log(\alpha_{\mathcal{C}, t}) \cdot \rho_{L-1}(\mathcal{C}, \{t\}), \quad (\text{D.5})$$

where:

$$\alpha_{\mathcal{C}} := \begin{cases} D^{1/\rho_0(\mathcal{C}, \mathcal{V})} & , \text{if } L = 1 \\ (D - 1) \cdot \rho_{L-1}(\mathcal{C}, \mathcal{V})^{-1} + 1 & , \text{if } L \geq 2 \end{cases}$$

$$\alpha_{\mathcal{C}, t} := \begin{cases} D & , \text{if } L = 1 \\ (D - 1) \cdot \rho_{L-1}(\mathcal{C}, \{t\})^{-1} + 1 & , \text{if } L \geq 2 \end{cases}$$

with $D := \min\{D_x, D_h\}$. If $\rho_{L-1}(\mathcal{C}, \mathcal{V}) = 0$ or $\rho_{L-1}(\mathcal{C}, \{t\}) = 0$, the respective lower bound (right hand side of Equation (D.4) or Equation (D.5)) is zero by convention.

Proof sketch (proof in Appendix D.7.5). The proof follows a line identical to that of Theorem 8, only requiring adjusting definitions from undirected graphs to directed graphs with multiple edge types. \square

D.3 Representing Graph Neural Networks With Product Aggregation as Tensor Networks

In this appendix, we prove that GNNs with product aggregation (Section 5.3) can be represented through tensor networks — a graphical language for expressing tensor contractions, widely used in quantum physics literature for modeling quantum states (cf. [210]). This representation facilitates upper bounding the separation ranks of a GNN with product aggregation (proofs for Theorem 7 and its extension in Appendix D.2), and is delivered in Appendix D.3.3. We note that analogous tensor network representations were shown for variants of recurrent and convolutional neural networks [132, 133]. For the convenience of the reader, we lay out basic concepts from the field of tensor analysis in Appendix D.3.1 and provide a self-contained introduction to tensor networks in Appendix D.3.2 (see [169] for a more in-depth treatment).

D.3.1 Primer on Tensor Analysis

For our purposes, a *tensor* is simply a multi-dimensional array. The *order* of a tensor is its number of axes, which are typically called *modes* (e.g. a vector is an order one tensor and a matrix is an order two tensor). The *dimension* of a mode refers to its length, i.e. the number of values it can be indexed with. For an order $N \in \mathbb{N}$ tensor $\mathcal{A} \in \mathbb{R}^{D_1 \times \dots \times D_N}$ with modes of dimensions $D_1, \dots, D_N \in \mathbb{N}$, we will denote by $\mathcal{A}_{d_1, \dots, d_N}$ its (d_1, \dots, d_N) 'th entry, where $(d_1, \dots, d_N) \in [D_1] \times \dots \times [D_N]$.

It is possible to rearrange tensors into matrices — a process known as *matricization*. The matricization of \mathcal{A} with respect to $\mathcal{I} \subseteq [N]$, denoted $\llbracket \mathcal{A}; \mathcal{I} \rrbracket \in \mathbb{R}^{\prod_{i \in \mathcal{I}} D_i \times \prod_{j \in \mathcal{I}^c} D_j}$ is its arrangement as a matrix where rows correspond to modes indexed by \mathcal{I} and columns correspond to the remaining modes. Specifically, denoting the elements in \mathcal{I} by $i_1 < \dots < i_{|\mathcal{I}|}$ and those in \mathcal{I}^c by $j_1 < \dots < j_{|\mathcal{I}^c|}$, the matricization $\llbracket \mathcal{A}; \mathcal{I} \rrbracket$ holds the entries of \mathcal{A} such that $\mathcal{A}_{d_1, \dots, d_N}$ is placed in row index $1 + \sum_{l=1}^{|\mathcal{I}|} (d_{i_l} - 1) \prod_{l'=l+1}^{|\mathcal{I}|} D_{i_{l'}}$ and column index $1 + \sum_{l=1}^{|\mathcal{I}^c|} (d_{j_l} - 1) \prod_{l'=l+1}^{|\mathcal{I}^c|} D_{j_{l'}}$.

Tensors with modes of the same dimension can be combined via *contraction* — a generalization of matrix multiplication. It will suffice to consider contractions where one of the modes being contracted is the last mode of its tensor.

Definition 18. Let $\mathcal{A} \in \mathbb{R}^{D_1 \times \dots \times D_N}$, $\mathcal{B} \in \mathbb{R}^{D'_1 \times \dots \times D'_{N'}}$ for orders $N, N' \in \mathbb{N}$ and mode dimensions $D_1, \dots, D_N, D'_1, \dots, D'_{N'} \in \mathbb{N}$ satisfying $D_n = D'_{N'}$ for some $n \in [N]$. The *mode- n contraction* of \mathcal{A} with \mathcal{B} , denoted $\mathcal{A} *_{n} \mathcal{B} \in \mathbb{R}^{D_1 \times \dots \times D_{n-1} \times D'_1 \times \dots \times D'_{N'-1} \times D_{n+1} \times \dots \times D_N}$, is given element-wise by:

$$(\mathcal{A} *_{n} \mathcal{B})_{d_1, \dots, d_{n-1}, d'_1, \dots, d'_{N'-1}, d_{n+1}, \dots, d_N} = \sum_{d_n=1}^{D_n} \mathcal{A}_{d_1, \dots, d_n} \cdot \mathcal{B}_{d'_1, \dots, d'_{N'-1}, d_n},$$

for all indices $d_1 \in [D_1], \dots, d_{n-1} \in [D_{n-1}], d'_1 \in [D'_1], \dots, d'_{N'-1} \in [D'_{N'-1}], d_{n+1} \in [D_{n+1}], \dots, d_N \in [D_N]$.

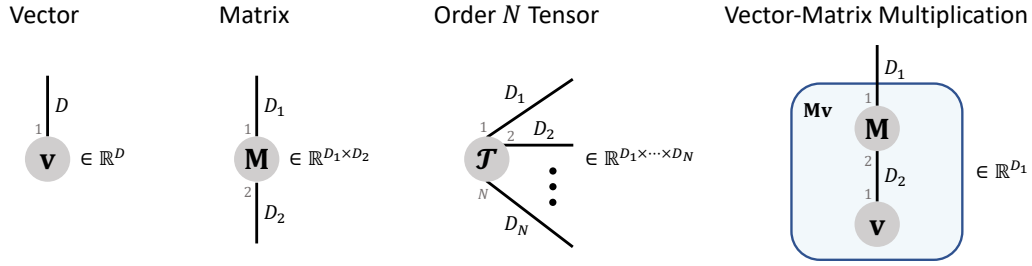


Figure D.1: Tensor network diagrams of (from left to right): a vector $\mathbf{v} \in \mathbb{R}^D$, matrix $\mathbf{M} \in \mathbb{R}^{D_1 \times D_2}$, order $N \in \mathbb{N}$ tensor $\mathcal{T} \in \mathbb{R}^{D_1 \times \dots \times D_N}$, and vector-matrix multiplication $\mathbf{M}\mathbf{v} \in \mathbb{R}^{D_1}$. The mode index associated with a leg's end point is specified in gray, and the weight of the leg, specified in black, determines the mode dimension.

For example, the mode-2 contraction of $\mathbf{A} \in \mathbb{R}^{D_1 \times D_2}$ with $\mathbf{B} \in \mathbb{R}^{D'_1 \times D_2}$ boils down to multiplying \mathbf{A} with \mathbf{B}^\top from the right, *i.e.* $\mathbf{A} *_2 \mathbf{B} = \mathbf{A}\mathbf{B}^\top$. It is oftentimes convenient to jointly contract multiple tensors. Given an order N tensor \mathcal{A} and $M \in \mathbb{N}_{\leq N}$ tensors $\mathcal{B}^{(1)}, \dots, \mathcal{B}^{(M)}$, we use $\mathcal{A} *_i \mathcal{B}^{(i)}$ to denote the contraction of \mathcal{A} with $\mathcal{B}^{(1)}, \dots, \mathcal{B}^{(M)}$ in modes $1, \dots, M$, respectively (assuming mode dimensions are such that the contractions are well-defined).

D.3.2 Tensor Networks

A *tensor network* is an undirected weighted graph $\mathcal{T} = (\mathcal{V}_{\mathcal{T}}, \mathcal{E}_{\mathcal{T}}, w_{\mathcal{T}})$ that describes a sequence of tensor contractions (Definition 18), with vertices $\mathcal{V}_{\mathcal{T}}$, edges $\mathcal{E}_{\mathcal{T}}$, and a function mapping edges to natural weights $w_{\mathcal{T}} : \mathcal{E}_{\mathcal{T}} \rightarrow \mathbb{N}$. We will only consider tensor networks that are connected. To avoid confusion with vertices and edges of a GNN's input graph, and in accordance with tensor network terminology, we refer by *nodes* and *legs* to the vertices and edges of a tensor network, respectively.

Every node in a tensor network is associated with a tensor, whose order is equal to the number of legs emanating from the node. Each end point of a leg is associated with a mode index, and the leg's weight determines the dimension of the corresponding tensor mode. That is, an end point of $e \in \mathcal{E}_{\mathcal{T}}$ is a pair $(\mathcal{A}, n) \in \mathcal{V}_{\mathcal{T}} \times \mathbb{N}$, with n ranging from one to the order of \mathcal{A} , and $w_{\mathcal{T}}(e)$ is the dimension of \mathcal{A} in mode n . A leg can either connect two nodes or be connected to a node on one end and be loose on the other end. If two nodes are connected by a leg, their associated tensors are contracted together in the modes specified by the leg. Legs with a loose end are called *open legs*. The number of open legs is exactly the order of the tensor produced by executing all contractions in the tensor network, *i.e.* by contracting the tensor network. Figure D.1 presents exemplar tensor network diagrams of a vector, matrix, order $N \in \mathbb{N}$ tensor, and vector-matrix multiplication.

D.3.3 Tensor Networks Corresponding to Graph Neural Networks With Product Aggregation

Fix some undirected graph \mathcal{G} and learnable weights $\theta = (\mathbf{W}^{(1)}, \dots, \mathbf{W}^{(L)}, \mathbf{W}^{(o)})$. Let $f^{(\theta, \mathcal{G})}$ and $f^{(\theta, \mathcal{G}, t)}$, for $t \in \mathcal{V}$, be the functions realized by depth L graph and vertex prediction GNNs, respectively, with width D_h and product aggregation (Equations (5.2) to (5.5)). For $\mathbf{X} = (\mathbf{x}^{(1)}, \dots, \mathbf{x}^{(|\mathcal{V}|)}) \in \mathbb{R}^{D_x \times |\mathcal{V}|}$, we construct tensor networks $\mathcal{T}(\mathbf{X})$ and

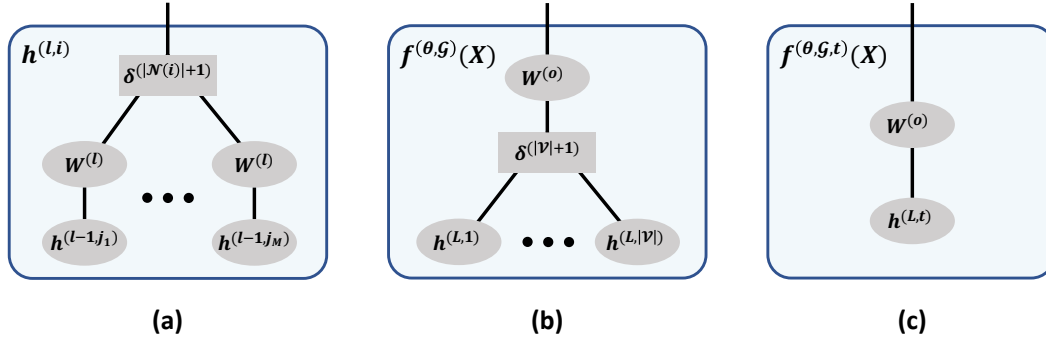


Figure D.2: Tensor network diagrams of the operations performed by GNNs with product aggregation (Section 5.3). **(a)** Hidden embedding update (cf. Equations (5.2) and (5.5)): $\mathbf{h}^{(l,i)} = (\mathbf{W}^{(l)} \mathbf{h}^{(l-1, j_1)}) \odot \dots \odot (\mathbf{W}^{(l)} \mathbf{h}^{(l-1, j_M)})$, where $\mathcal{N}(i) = \{j_1, \dots, j_M\}$, for $l \in [L], i \in \mathcal{V}$. **(b)** Output layer for graph prediction (cf. Equations (5.3) and (5.5)): $f^{(\theta, \mathcal{G})}(\mathbf{X}) = \mathbf{W}^{(o)}(\mathbf{h}^{(L, 1)} \odot \dots \odot \mathbf{h}^{(L, |\mathcal{V}|)})$. **(c)** Output layer for vertex prediction over $t \in \mathcal{V}$ (cf. Equation (5.4)): $f^{(\theta, \mathcal{G}, t)}(\mathbf{X}) = \mathbf{W}^{(o)} \mathbf{h}^{(L, t)}$. We draw nodes associated with δ -tensors as rectangles to signify their special (hyper-diagonal) structure, and omit leg weights to avoid clutter (legs connected to $\mathbf{h}^{(0,i)} = \mathbf{x}^{(i)}$, for $i \in \mathcal{V}$, have weight D_x while all other legs have weight D_h).

$\mathcal{T}^{(t)}(\mathbf{X})$ whose contraction yields $f^{(\theta, \mathcal{G})}(\mathbf{X})$ and $f^{(\theta, \mathcal{G}, t)}(\mathbf{X})$, respectively. Both $\mathcal{T}(\mathbf{X})$ and $\mathcal{T}^{(t)}(\mathbf{X})$ adhere to a tree structure, where each leaf node is associated with a vertex feature vector, *i.e.* one of $\mathbf{x}^{(1)}, \dots, \mathbf{x}^{(|\mathcal{V}|)}$, and each interior node is associated with a weight matrix from $\mathbf{W}^{(1)}, \dots, \mathbf{W}^{(L)}, \mathbf{W}^{(o)}$ or a δ -tensor with modes of dimension D_h , holding ones on its hyper-diagonal and zeros elsewhere. We denote an order $N \in \mathbb{N}$ tensor of the latter type by $\delta^{(N)} \in \mathbb{R}^{D_h \times \dots \times D_h}$, *i.e.* $\delta_{d_1, \dots, d_N}^{(N)} = 1$ if $d_1 = \dots = d_N$ and $\delta_{d_1, \dots, d_N}^{(N)} = 0$ otherwise for all $d_1, \dots, d_N \in [D_h]$.

Intuitively, $\mathcal{T}(\mathbf{X})$ and $\mathcal{T}^{(t)}(\mathbf{X})$ embody unrolled computation trees, describing the operations performed by the respective GNNs through tensor contractions. Let $\mathbf{h}^{(l,i)} = \odot_{j \in \mathcal{N}(i)} (\mathbf{W}^{(l)} \mathbf{h}^{(l-1, j)})$ be the hidden embedding of $i \in \mathcal{V}$ at layer $l \in [L]$ (recall $\mathbf{h}^{(0, j)} = \mathbf{x}^{(j)}$ for $j \in \mathcal{V}$), and denote $\mathcal{N}(i) = \{j_1, \dots, j_M\}$. We can describe $\mathbf{h}^{(l,i)}$ as the outcome of contracting each $\mathbf{h}^{(l-1, j_1)}, \dots, \mathbf{h}^{(l-1, j_M)}$ with $\mathbf{W}^{(l)}$, *i.e.* computing $\mathbf{W}^{(l)} \mathbf{h}^{(l-1, j_1)}, \dots, \mathbf{W}^{(l)} \mathbf{h}^{(l-1, j_M)}$, followed by contracting the resulting vectors with $\delta^{(|\mathcal{N}(i)|+1)}$, which induces product aggregation (see Figure D.2(a)). Furthermore, in graph prediction, the output layer producing $f^{(\theta, \mathcal{G})}(\mathbf{X}) = \mathbf{W}^{(o)}(\odot_{i \in \mathcal{V}} \mathbf{h}^{(L, i)})$ amounts to contracting $\mathbf{h}^{(L, 1)}, \dots, \mathbf{h}^{(L, |\mathcal{V}|)}$ with $\delta^{(|\mathcal{V}|+1)}$, and subsequently contracting the resulting vector with $\mathbf{W}^{(o)}$ (see Figure D.2(b)); while for vertex prediction, $f^{(\theta, \mathcal{G}, t)}(\mathbf{X}) = \mathbf{W}^{(o)} \mathbf{h}^{(L, t)}$ is a contraction of $\mathbf{h}^{(L, t)}$ with $\mathbf{W}^{(o)}$ (see Figure D.2(c)).

Overall, every layer in a GNN with product aggregation admits a tensor network formulation given the outputs of the previous layer. Thus, we can construct a tree tensor network for the whole GNN by starting from the output layer — Figure D.2(b) for graph prediction or Figure D.2(c) for vertex prediction — and recursively expanding nodes associated with $\mathbf{h}^{(l,i)}$ according to Figure D.2(a), for $l = L, \dots, 1$ and $i \in \mathcal{V}$. A technical subtlety is that each $\mathbf{h}^{(l,i)}$ can appear multiple times during this procedure. In the language of tensor networks this translates to duplication of nodes. Namely, there are multiple copies of the sub-tree representing $\mathbf{h}^{(l,i)}$ in the tensor network — one copy per appearance when unraveling the recursion. Figure D.3 displays examples for tensor network diagrams of $\mathcal{T}(\mathbf{X})$ and $\mathcal{T}^{(t)}(\mathbf{X})$.

We note that, due to the node duplication mentioned above, the explicit definitions of $\mathcal{T}(\mathbf{X})$ and $\mathcal{T}^{(t)}(\mathbf{X})$ entail cumbersome notation. Nevertheless, we provide them in

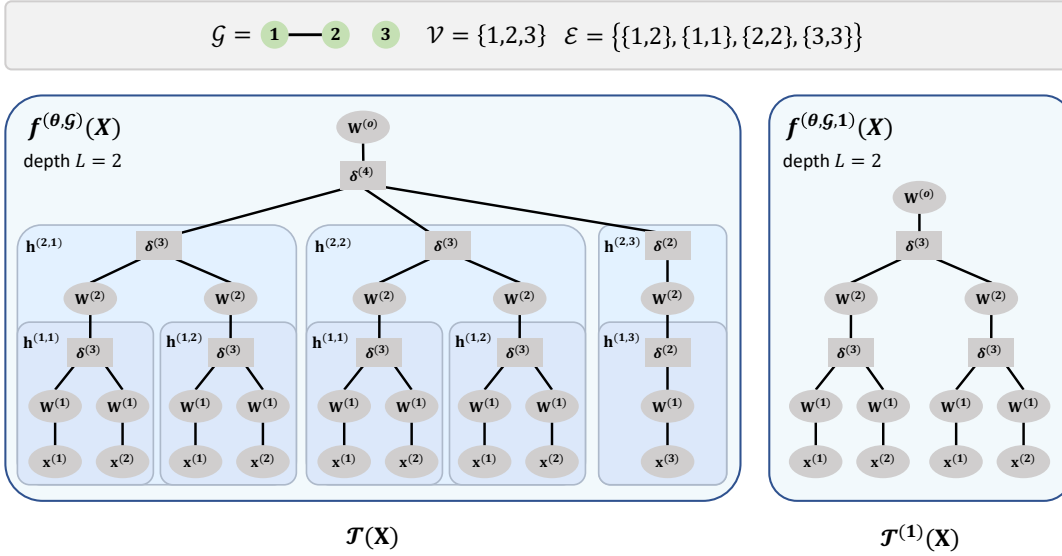


Figure D.3: Tensor network diagrams of $\mathcal{T}(\mathbf{X})$ (left) and $\mathcal{T}^{(t)}(\mathbf{X})$ (right) representing $f^{(\theta, \mathcal{G})}(\mathbf{X})$ and $f^{(\theta, \mathcal{G}, t)}(\mathbf{X})$, respectively, for $t = 1 \in \mathcal{V}$, vertex features $\mathbf{X} = (\mathbf{x}^{(1)}, \dots, \mathbf{x}^{(|\mathcal{V}|)})$, and depth $L = 2$ GNNs with product aggregation (Section 5.3). The underlying input graph \mathcal{G} , over which the GNNs operate, is depicted at the top. We draw nodes associated with δ -tensors as rectangles to signify their special (hyper-diagonal) structure, and omit leg weights to avoid clutter (legs connected to $\mathbf{x}^{(1)}, \mathbf{x}^{(2)}, \mathbf{x}^{(3)}$ have weight D_x while all other legs have weight D_h). See Appendix D.3.3 for further details on the construction of $\mathcal{T}(\mathbf{X})$ and $\mathcal{T}^{(t)}(\mathbf{X})$, and Appendix D.3.3.1 for explicit formulations.

Appendix D.3.3.1 for the interested reader.

D.3.3.1 Explicit Tensor Network Definitions

The tree tensor network representing $f^{(\theta, \mathcal{G})}(\mathbf{X})$ consists of an initial input level — the leaves of the tree — comprising $\rho_L(\{i\}, \mathcal{V})$ copies of $\mathbf{x}^{(i)}$ for each $i \in \mathcal{V}$. We will use $\mathbf{x}^{(i, \gamma)}$ to denote the copies of $\mathbf{x}^{(i)}$ for $i \in \mathcal{V}$ and $\gamma \in [\rho_L(\{i\}, \mathcal{V})]$. In accordance with the GNN inducing $f^{(\theta, \mathcal{G})}$, following the initial input level are $L + 1$ layers. Each layer $l \in [L]$ includes two levels: one comprising $\rho_{L-l+1}(\mathcal{V}, \mathcal{V})$ nodes standing for copies of $\mathbf{W}^{(l)}$, and another containing δ -tensors — $\rho_{L-l}(\{i\}, \mathcal{V})$ copies of $\delta^{(|\mathcal{N}^{(i)}|+1)}$ per $i \in \mathcal{V}$. We associate each node in these layers with its layer index and a vertex of the input graph $i \in \mathcal{V}$. Specifically, we will use $\mathbf{W}^{(l, i, \gamma)}$ to denote copies of $\mathbf{W}^{(l)}$ and $\delta^{(l, i, \gamma)}$ to denote copies of $\delta^{(|\mathcal{N}^{(i)}|+1)}$, for $l \in [L], i \in \mathcal{V}$, and $\gamma \in \mathbb{N}$. In terms of connectivity, every leaf $\mathbf{x}^{(i, \gamma)}$ has a leg to $\mathbf{W}^{(1, i, \gamma)}$. The rest of the connections between nodes are such that each sub-tree whose root is $\delta^{(l, i, \gamma)}$ represents $\mathbf{h}^{(l, i)}$, *i.e.* contracting the sub-tree results in the hidden embedding for $i \in \mathcal{V}$ at layer $l \in [L]$ of the GNN inducing $f^{(\theta, \mathcal{G})}$. Last, is an output layer consisting of two connected nodes: a $\delta^{(|\mathcal{V}|+1)}$ node, which has a leg to every δ -tensor from layer L , and a $\mathbf{W}^{(0)}$ node. See Figure D.4 (left) for an example of a tensor network diagram representing $f^{(\theta, \mathcal{G})}(\mathbf{X})$ with this notation.

The tensor network construction for $f^{(\theta, \mathcal{G}, t)}(\mathbf{X})$ is analogous to that for $f^{(\theta, \mathcal{G})}(\mathbf{X})$, comprising an initial input level followed by $L + 1$ layers. Its input level and first L layers are structured the same, up to differences in the number of copies for each node. Specifically, the number of copies of $\mathbf{x}^{(i)}$ is $\rho_L(\{i\}, \{t\})$ instead of $\rho_L(\{i\}, \mathcal{V})$, the number of copies of $\mathbf{W}^{(l)}$ is $\rho_{L-l+1}(\mathcal{V}, \{t\})$ instead of $\rho_{L-l+1}(\mathcal{V}, \mathcal{V})$, and the number

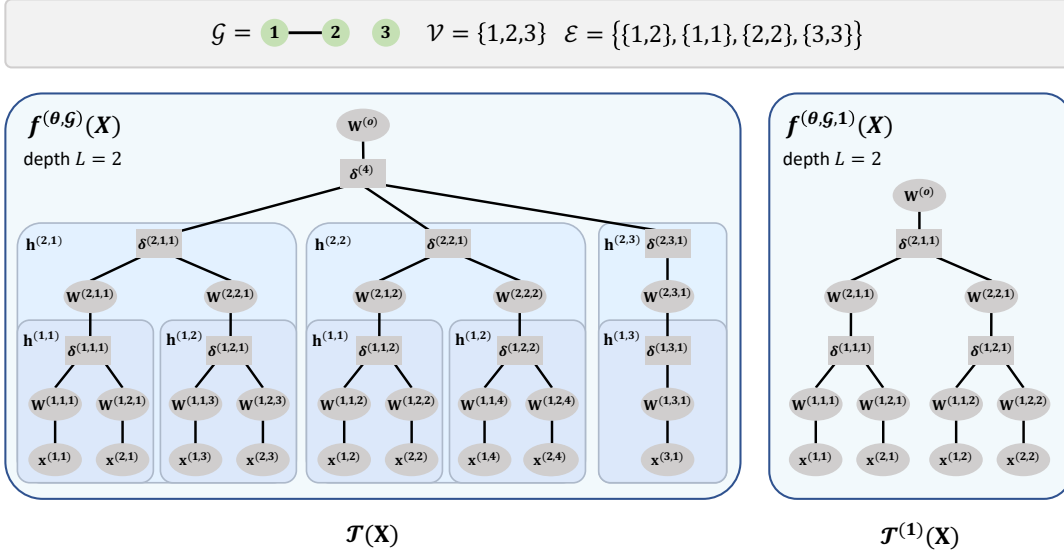


Figure D.4: Tensor network diagrams (with explicit node duplication notation) of $\mathcal{T}(\mathbf{X})$ (left) and $\mathcal{T}^{(t)}(\mathbf{X})$ (right) representing $f^{(\theta, \mathcal{G})}(\mathbf{X})$ and $f^{(\theta, \mathcal{G}, t)}(\mathbf{X})$, respectively, for $t = 1 \in \mathcal{V}$, vertex features $\mathbf{X} = (x^{(1)}, \dots, x^{(|\mathcal{V}|)})$, and depth $L = 2$ GNNs with product aggregation (Section 5.3). This figure is identical to Figure D.3, except that it uses the explicit notation for node duplication detailed in Appendix D.3.3.1. Specifically, each feature vector, weight matrix, and δ -tensor is attached with an index specifying which copy it is (rightmost index in the superscript). Additionally, weight matrices and δ -tensors are associated with a layer index and vertex in \mathcal{V} (except for the output layer δ -tensor in $\mathcal{T}(\mathbf{X})$ and $\mathbf{W}^{(o)}$). See Equations (D.6) and (D.7) for the explicit definitions of these tensor networks.

of copies of $\delta^{(|\mathcal{N}(i)|+1)}$ is $\rho_{L-l}(\{i\}, \{t\})$ instead of $\rho_{L-l}(\{i\}, \mathcal{V})$, for $i \in \mathcal{V}$ and $l \in [L]$. The output layer consists only of a $\mathbf{W}^{(o)}$ node, which is connected to the δ -tensor in layer L corresponding to vertex t . See Figure D.4 (right) for an example of a tensor network diagram representing $f^{(\theta, \mathcal{G}, t)}(\mathbf{X})$ with this notation.

Formally, the tensor network producing $f^{(\theta, \mathcal{G})}(\mathbf{X})$, denoted

$$\mathcal{T}(\mathbf{X}) = (\mathcal{V}_{\mathcal{T}(\mathbf{X})}, \mathcal{E}_{\mathcal{T}(\mathbf{X})}, w_{\mathcal{T}(\mathbf{X})}),$$

is defined by:

$$\begin{aligned} \mathcal{V}_{\mathcal{T}(\mathbf{X})} := & \left\{ \mathbf{x}^{(i, \gamma)} : i \in \mathcal{V}, \gamma \in [\rho_L(\{i\}, \mathcal{V})] \right\} \cup \\ & \left\{ \mathbf{W}^{(l, i, \gamma)} : l \in [L], i \in \mathcal{V}, \gamma \in [\rho_{L-l+1}(\{i\}, \mathcal{V})] \right\} \cup \\ & \left\{ \delta^{(l, i, \gamma)} : l \in [L], i \in \mathcal{V}, \gamma \in [\rho_{L-l}(\{i\}, \mathcal{V})] \right\} \cup \\ & \left\{ \delta^{(|\mathcal{V}|+1)}, \mathbf{W}^{(o)} \right\}, \\ \mathcal{E}_{\mathcal{T}(\mathbf{X})} := & \left\{ \{(\mathbf{x}^{(i, \gamma)}, 1), (\mathbf{W}^{(1, i, \gamma)}, 2)\} : i \in \mathcal{V}, \gamma \in [\rho_L(\{i\}, \mathcal{V})] \right\} \cup \\ & \left\{ \{(\delta^{(l, i, \gamma)}, j), (\mathbf{W}^{(l, \mathcal{N}(i), j, \phi_{l, i, j}(\gamma))}, 1)\} : l \in [L], i \in \mathcal{V}, j \in [|\mathcal{N}(i)|], \gamma \in [\rho_{L-l}(\{i\}, \mathcal{V})] \right\} \cup \\ & \left\{ \{(\delta^{(l, i, \gamma)}, |\mathcal{N}(i)| + 1), (\mathbf{W}^{(l+1, i, \gamma)}, 2)\} : l \in [L-1], i \in \mathcal{V}, \gamma \in [\rho_{L-l}(\{i\}, \mathcal{V})] \right\} \cup \\ & \left\{ \{(\delta^{(|\mathcal{V}|+1)}, i), (\delta^{(L, i, 1)}, |\mathcal{N}(i)| + 1)\} : i \in \mathcal{V} \right\} \cup \left\{ \{(\delta^{(|\mathcal{V}|+1)}, |\mathcal{V}| + 1), (\mathbf{W}^{(o)}, 2)\} \right\}, \end{aligned}$$

$$w_{\mathcal{T}(\mathbf{X})}(e) := \begin{cases} D_x & , \text{ if } (\mathbf{x}^{(i, \gamma)}, 1) \text{ is an endpoint of } e \in \mathcal{E}_{\mathcal{T}} \text{ for some } i \in \mathcal{V}, \gamma \in [\rho_L(\{i\}, \mathcal{V})] \\ D_h & , \text{ otherwise} \end{cases},$$

(D.6)

where $\phi_{l,i,j}(\gamma) := \gamma + \sum_{k < i \text{ s.t. } k \in \mathcal{N}(j)} \rho_{L-l}(\{k\}, \mathcal{V})$, for $l \in [L], i \in \mathcal{V}$, and $\gamma \in [\rho_{L-l}(\{i\}, \mathcal{V})]$, is used to map a δ -tensor copy corresponding to i in layer l to a $\mathbf{W}^{(l)}$ copy, and $\mathcal{N}(i)_j$, for $i \in \mathcal{V}$ and $j \in [|\mathcal{N}(i)|]$, denotes the j 'th neighbor of i according to an ascending order (recall vertices are represented by indices from 1 to $|\mathcal{V}|$).

Similarly, the tensor network producing $f^{(\theta, \mathcal{G}, t)}(\mathbf{X})$, denoted

$$\mathcal{T}^{(t)}(\mathbf{X}) = (\mathcal{V}_{\mathcal{T}^{(t)}(\mathbf{X})}, \mathcal{E}_{\mathcal{T}^{(t)}(\mathbf{X})}, w_{\mathcal{T}^{(t)}(\mathbf{X})}),$$

is defined by:

$$\begin{aligned} \mathcal{V}_{\mathcal{T}^{(t)}(\mathbf{X})} &:= \left\{ \mathbf{x}^{(i,\gamma)} : i \in \mathcal{V}, \gamma \in [\rho_L(\{i\}, \{t\})] \right\} \cup \\ &\quad \left\{ \mathbf{W}^{(l,i,\gamma)} : l \in [L], i \in \mathcal{V}, \gamma \in [\rho_{L-l+1}(\{i\}, \{t\})] \right\} \cup \\ &\quad \left\{ \delta^{(l,i,\gamma)} : l \in [L], i \in \mathcal{V}, \gamma \in [\rho_{L-l}(\{i\}, \{t\})] \right\} \cup \\ &\quad \left\{ \mathbf{W}^{(o)} \right\}, \\ \mathcal{E}_{\mathcal{T}^{(t)}(\mathbf{X})} &:= \left\{ \{(\mathbf{x}^{(i,\gamma)}, 1), (\mathbf{W}^{(1,i,\gamma)}, 2)\} : i \in \mathcal{V}, \gamma \in [\rho_L(\{i\}, \{t\})] \right\} \cup \\ &\quad \left\{ \{(\delta^{(l,i,\gamma)}, j), (\mathbf{W}^{(l, \mathcal{N}(i)_j, \phi_{l,i,j}^{(t)}(\gamma))}, 1)\} : l \in [L], i \in \mathcal{V}, j \in [|\mathcal{N}(i)|], \gamma \in [\rho_{L-l}(\{i\}, \{t\})] \right\} \cup \\ &\quad \left\{ \{(\delta^{(l,i,\gamma)}, |\mathcal{N}(i)| + 1), (\mathbf{W}^{(l+1,i,\gamma)}, 2)\} : l \in [L-1], i \in \mathcal{V}, \gamma \in [\rho_{L-l}(\{i\}, \{t\})] \right\} \cup \\ &\quad \left\{ \{(\delta^{(L,t,1)}, |\mathcal{N}(t)| + 1), (\mathbf{W}^{(o)}, 2)\} \right\}, \\ w_{\mathcal{T}^{(t)}(\mathbf{X})}(e) &:= \begin{cases} D_x & , \text{ if } (\mathbf{x}^{(i,\gamma)}, 1) \text{ is an endpoint of } e \in \mathcal{E}_{\mathcal{T}} \text{ for some } i \in \mathcal{V}, \gamma \in [\rho_L(\{i\}, \{t\})] \\ D_h & , \text{ otherwise} \end{cases}, \end{aligned} \tag{D.7}$$

where $\phi_{l,i,j}^{(t)}(\gamma) := \gamma + \sum_{k < i \text{ s.t. } k \in \mathcal{N}(j)} \rho_{L-l}(\{k\}, \{t\})$, for $l \in [L], i \in \mathcal{V}$, and $\gamma \in [\rho_{L-l}(\{i\}, \{t\})]$, is used to map a δ -tensor copy corresponding to i in layer l to a $\mathbf{W}^{(l)}$ copy.

Proposition 10 verifies that contracting $\mathcal{T}(\mathbf{X})$ and $\mathcal{T}^{(t)}(\mathbf{X})$ results in $f^{(\theta, \mathcal{G})}(\mathbf{X})$ and $f^{(\theta, \mathcal{G}, t)}(\mathbf{X})$, respectively.

Proposition 10. *For an undirected graph \mathcal{G} and $t \in \mathcal{V}$, let $f^{(\theta, \mathcal{G})}$ and $f^{(\theta, \mathcal{G}, t)}$ be the functions realized by depth L graph and vertex prediction GNNs, respectively, with width D_h , learnable weights θ , and product aggregation (Equations (5.2) to (5.5)). For vertex features $\mathbf{X} = (\mathbf{x}^{(1)}, \dots, \mathbf{x}^{(|\mathcal{V}|)}) \in \mathbb{R}^{D_x \times |\mathcal{V}|}$, let the tensor networks $\mathcal{T}(\mathbf{X}) = (\mathcal{V}_{\mathcal{T}(\mathbf{X})}, \mathcal{E}_{\mathcal{T}(\mathbf{X})}, w_{\mathcal{T}(\mathbf{X})})$ and $\mathcal{T}^{(t)}(\mathbf{X}) = (\mathcal{V}_{\mathcal{T}^{(t)}(\mathbf{X})}, \mathcal{E}_{\mathcal{T}^{(t)}(\mathbf{X})}, w_{\mathcal{T}^{(t)}(\mathbf{X})})$ be as defined in Equations (D.6) and (D.7), respectively. Then, performing the contractions described by $\mathcal{T}(\mathbf{X})$ produces $f^{(\theta, \mathcal{G})}(\mathbf{X})$, and performing the contractions described by $\mathcal{T}^{(t)}(\mathbf{X})$ produces $f^{(\theta, \mathcal{G}, t)}(\mathbf{X})$.*

Proof sketch (proof in Appendix D.7.6). For both $\mathcal{T}(\mathbf{X})$ and $\mathcal{T}^{(t)}(\mathbf{X})$, a straightforward induction over the layer $l \in [L]$ establishes that contracting the sub-tree whose root is $\delta^{(l,i,\gamma)}$ results in $\mathbf{h}^{(l,i)}$ for all $i \in \mathcal{V}$ and γ , where $\mathbf{h}^{(l,i)}$ is the hidden embedding for i at layer l of the GNNs inducing $f^{(\theta, \mathcal{G})}$ and $f^{(\theta, \mathcal{G}, t)}$, given vertex features $\mathbf{x}^{(1)}, \dots, \mathbf{x}^{(|\mathcal{V}|)}$. The proof concludes by showing that the contractions in the output layer of $\mathcal{T}(\mathbf{X})$ and $\mathcal{T}^{(t)}(\mathbf{X})$ reproduce the operations defining $f^{(\theta, \mathcal{G})}(\mathbf{X})$ and $f^{(\theta, \mathcal{G}, t)}(\mathbf{X})$ in Equations (5.3) and (5.4), respectively. \square

D.4 General Walk Index Sparsification

Our edge sparsification algorithm — Walk Index Sparsification (WIS) — was obtained as an instance of the General Walk Index Sparsification (GWIS) scheme described in Section 5.5. Algorithm 3 formally outlines this general scheme.

Algorithm 3 $(L - 1)$ -General Walk Index Sparsification (GWIS)

Input:

- \mathcal{G} — graph
- $L \in \mathbb{N}$ — GNN depth
- $N \in \mathbb{N}$ — number of edges to remove
- $\mathcal{I}_1, \dots, \mathcal{I}_M \subseteq \mathcal{V}$ — vertex subsets specifying walk indices to maintain for graph prediction
- $\mathcal{J}_1, \dots, \mathcal{J}_{M'} \subseteq \mathcal{V}$ and $t_1, \dots, t_{M'} \in \mathcal{V}$ — vertex subsets specifying walk indices to maintain with respect to target vertices, for vertex prediction
- ARGMAX — operator over tuples $(\mathbf{s}^{(e)} \in \mathbb{R}^{M+M'})_{e \in \mathcal{E}}$ that returns the edge whose tuple is maximal according to some order

Result: Sparsified graph obtained by removing N edges from \mathcal{G}

for $n = 1, \dots, N$ **do**

for every edge, compute walk indices of partitions after the edge's removal

for $e \in \mathcal{E}$ (excluding self-loops) **do**

initialize $\mathbf{s}^{(e)} = (0, \dots, 0) \in \mathbb{R}^{M+M'}$

remove e from \mathcal{G} (temporarily)

for every $m \in [M]$, set $\mathbf{s}_m^{(e)} = \text{WI}_{L-1}(\mathcal{I}_m) \# = \rho_{L-1}(\mathcal{C}_{\mathcal{I}_m}, \mathcal{V})$

for every $m \in [M']$, set $\mathbf{s}_{M+m}^{(e)} = \text{WI}_{L-1, t_m}(\mathcal{J}_m) \# = \rho_{L-1}(\mathcal{C}_{\mathcal{J}_m}, \{t_m\})$

add e back to \mathcal{G}

end for

prune edge whose removal harms walk indices the least according to the ARGMAX operator

let $e' \in \text{ARGMAX}_{e \in \mathcal{E}} \mathbf{s}^{(e)}$

remove e' from \mathcal{G} (permanently)

end for

D.5 Efficient Implementation of 1-Walk Index Sparsification

Algorithm 2 (Section 5.5) provides an efficient implementation for 1-WIS, *i.e.* Algorithm 1 with $L = 2$. In this appendix, we formalize the equivalence between the two algorithms, meaning, we establish that Algorithm 2 indeed implements 1-WIS.

Examining some iteration $n \in [N]$ of 1-WIS, let $\mathbf{s} \in \mathbb{R}^{|\mathcal{V}|}$ be the tuple defined by $\mathbf{s}_t = \text{WI}_{1,t}(\{t\}) = \rho_1(\mathcal{C}_{\{t\}}, \{t\})$ for $t \in \mathcal{V}$. Recall that $\mathcal{C}_{\{t\}}$ is the set of vertices with an edge crossing the partition induced by $\{t\}$. Thus, if t is not isolated, then $\mathcal{C}_{\{t\}} = \mathcal{N}(t)$ and $\mathbf{s}_t = \text{WI}_{1,t}(\{t\}) = |\mathcal{N}(t)|$. Otherwise, if t is isolated, then $\mathcal{C}_{\{t\}} = \emptyset$ and $\mathbf{s}_t = \text{WI}_{1,t}(\{t\}) = 0$. 1-WIS computes for each $e \in \mathcal{E}$ (excluding self-loops) a

tuple $\mathbf{s}^{(e)} \in \mathbb{R}^{|\mathcal{V}|}$ holding in its t 'th entry what the value of $\text{WI}_{1,t}(\{t\})$ would be if e is to be removed, for all $t \in \mathcal{V}$. Notice that $\mathbf{s}^{(e)}$ and \mathbf{s} agree on all entries except for $i, j \in e$, since removing e from the graph only affects the degrees of i and j . Specifically, for $i \in e$, either $\mathbf{s}_i^{(e)} = \mathbf{s}_i - 1 = |\mathcal{N}(i)| - 1$ if the removal of e did not isolate i , or $\mathbf{s}_i^{(e)} = \mathbf{s}_i - 2 = 0$ if it did (due to self-loops, if a vertex has a single edge to another then $|\mathcal{N}(i)| = 2$, so removing that edge changes $\text{WI}_{1,i}(\{i\})$ from two to zero). As a result, for any $e = \{i, j\}, e' = \{i', j'\} \in \mathcal{E}$, after sorting the entries of $\mathbf{s}^{(e)}$ and $\mathbf{s}^{(e')}$ in ascending order we have that $\mathbf{s}^{(e')}$ is greater in lexicographic order than $\mathbf{s}^{(e)}$ if and only if the pair $(\min\{|\mathcal{N}(i')|, |\mathcal{N}(j')|\}, \max\{|\mathcal{N}(i')|, |\mathcal{N}(j')|\})$ is greater in lexicographic order than $(\min\{|\mathcal{N}(i)|, |\mathcal{N}(j)|\}, \max\{|\mathcal{N}(i)|, |\mathcal{N}(j)|\})$. Therefore, at every iteration $n \in [N]$ Algorithm 2 and 1-WIS (Algorithm 1 with $L = 2$) remove the same edge.

D.6 Further Experiments and Implementation Details

D.6.1 Further Experiments

Figure D.5 supplements Figure 5.3 from Section 5.5.2 by including experiments with additional: (i) GNN architectures — GIN and ResGCN; and (ii) datasets — Chameleon, Squirrel, and Amazon Computers.

D.6.2 Further Implementation Details

We provide implementation details omitted from our experimental reports (Section 5.4.3, Section 5.5, and Appendix D.6.1). Source code for reproducing our results and figures, based on the PyTorch [172] and PyTorch Geometric [64] frameworks, can be found at https://github.com/noamrazin/gnn_interactions. All experiments were run either on a single Nvidia RTX 2080 Ti GPU or a single Nvidia RTX A6000 GPU.

D.6.2.1 Empirical Demonstration of Theoretical Analysis (Table 5.1)

Models. All models used, *i.e.* GCN, GAT, and GIN, had three layers of width 16 with ReLU non-linearity. To ease optimization, we added layer normalization [12] after each one. Mean aggregation and a linear output layer were applied over the last hidden embeddings for prediction. As in the synthetic experiments of [4], each GAT layer consisted of four attention heads. Each GIN layer had its ϵ parameter fixed to zero and contained a two-layer feed-forward network, whose layers comprised a linear layer, batch normalization [105], and ReLU non-linearity.

Data. The datasets consisted of 10000 train and 2000 test graphs. For every graph, we drew uniformly at random a label from $\{0, 1\}$ and an image from Fashion-MNIST. Then, depending on the chosen label, another image was sampled either from the same class (for label 1) or from all other classes (for label 0). We extracted patches of pixels from each image by flattening it into a vector and splitting the vector to 16 equally sized segments.

Optimization. The binary cross-entropy loss was minimized via the Adam optimizer [121] with default β_1, β_2 coefficients and full-batches (*i.e.* every batch contained the whole training set). Optimization proceeded until the train accuracy did not

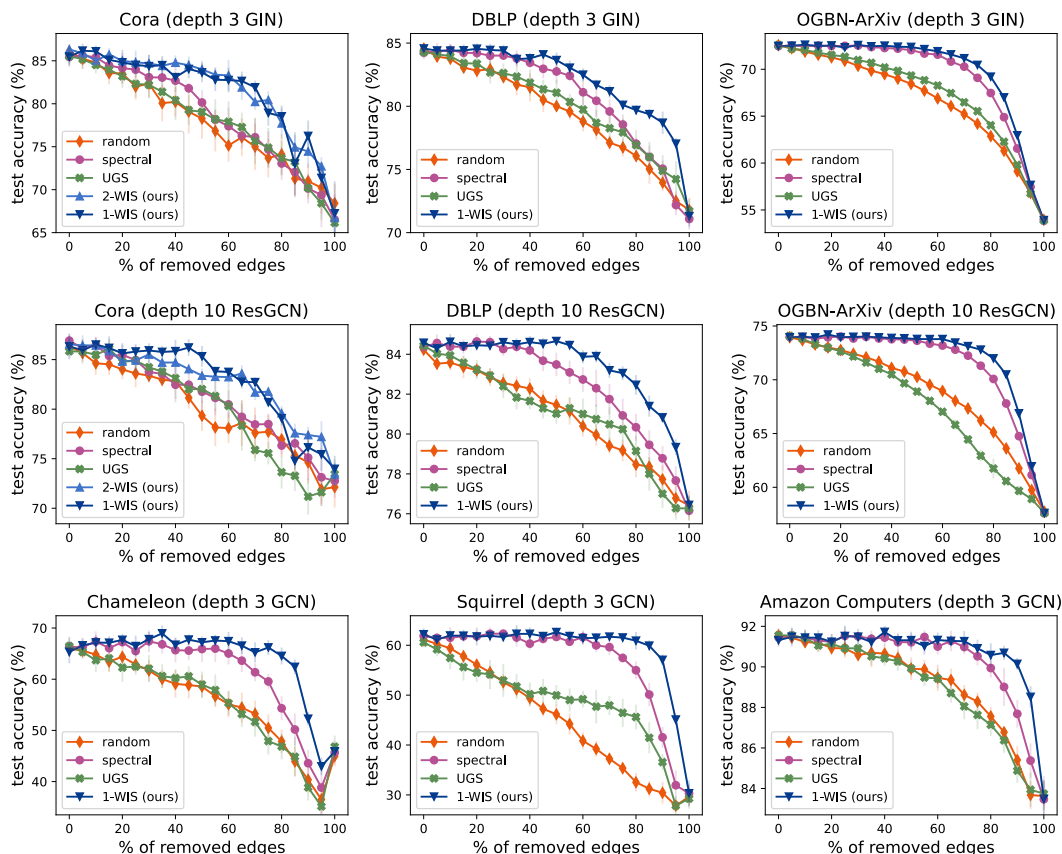


Figure D.5: Comparison of GNN accuracies following sparsification of input edges — WIS, the edge sparsification algorithm brought forth by our theory (Algorithm 1), markedly outperforms alternative methods. This figure supplements Figure 5.3 from Section 5.5.2 by including experiments with: (i) a depth $L = 3$ GIN over the Cora, DBLP, and OGBN-ArXiv datasets; (ii) a depth $L = 10$ ResGCN over the Cora, DBLP, and OGBN-ArXiv datasets; and (iii) a depth $L = 3$ GCN over the Chameleon, Squirrel, and Amazon Computers datasets. Markers and error bars report means and standard deviations, respectively, taken over ten runs per configuration for GCN and GIN, and over five runs per configuration for ResGCN (we use fewer runs due to the larger size of ResGCN). For further details see caption of Figure 5.3 as well as Appendix D.6.2.

improve by at least 0.01 over 1000 consecutive epochs or 10000 epochs elapsed. The learning rates used for GCN, GAT, and GIN were $5 \cdot 10^{-3}$, $5 \cdot 10^{-3}$, and 10^{-2} , respectively.

Hyperparameter tuning. For each model separately, to tune the learning rate we carried out five runs (differing in random seed) with every value in the range $\{10^{-1}, 5 \cdot 10^{-2}, 10^{-2}, 5 \cdot 10^{-3}, 10^{-3}\}$ over the dataset whose essential partition has low walk index. Since our interest resides in expressiveness, which manifests in ability to fit the training set, for every model we chose the learning rate that led to the highest mean train accuracy.

D.6.2.2 Edge Sparsification (Figures 5.3 and D.5)

Adaptations to UGS [39]. [39] proposed UGS as a framework for jointly pruning input graph edges and weights of a GNN. At a high-level, UGS trains two differentiable masks, m_g and m_θ , that are multiplied with the graph adjacency matrix and the GNN’s weights, respectively. Then, after a certain number of optimization steps, a

predefined percentage p_g of graph edges are removed according to the magnitudes of entries in m_g , and similarly, p_θ percent of the GNN’s weights are fixed to zero according to the magnitudes of entries in m_θ . This procedure continues in iterations, where each time the remaining GNN weights are rewinded to their initial values, until the desired sparsity levels are attained — see Algorithms 1 and 2 in [39]. To facilitate a fair comparison of our $(L - 1)$ -WIS edge sparsification algorithm with UGS, we make the following adaptations to UGS.

- We adapt UGS to only remove edges, which is equivalent to fixing the entries in the weight mask m_θ to one and setting $p_\theta = 0$ in Algorithm 1 of [39].
- For comparing performance across a wider range of sparsity levels, the number of edges removed at each iteration is changed from 5% of the current number of edges to 5% of the original number of edges.
- Since our evaluation focuses on undirected graphs, we enforce the adjacency matrix mask m_g to be symmetric.

Spectral sparsification [198]. For Cora and DBLP, we used a Python implementation of the spectral sparsification algorithm from [198], based on the PyGSP library implementation.¹ To enable more efficient experimentation over the larger scale OGBN-ArXiv dataset, we used a Julia implementation based on that from the Laplacians library.²

Models. The GCN and GIN models had three layers of width 64 with ReLU non-linearity. As in the experiments of Section 5.4.3, we added layer normalization [12] after each one. Every GIN layer had a trainable ϵ parameter and contained a two-layer feed-forward network, whose layers comprised a linear layer, batch normalization [105], and ReLU non-linearity. For ResGCN, we used the implementation from [39] with ten layers of width 64. In all models, a linear output layer was applied over the last hidden embeddings for prediction.

Data. All datasets in our evaluation are multi-class vertex prediction tasks, each consisting of a single graph. In Cora, DBLP, and OGBN-ArXiv, vertices represent scientific publications and edges stand for citation links. In Chameleon and Squirrel, vertices represent web pages on Wikipedia and edges stand for mutual links between pages. In Amazon Computers, vertices represent products and edges indicate that two products are frequently bought together. For simplicity, we treat all graphs as undirected. Table D.1 reports the number of vertices and undirected edges in each dataset. For all datasets, except OGBN-ArXiv, we randomly split the labels of vertices into train, validation, and test sets comprising 80%, 10%, and 10% of all labels, respectively. For OGBN-ArXiv, we used the default split from [99].

Table D.1: Graph size of each dataset used for comparing edge sparsification algorithms in Figures 5.3 and D.5.

	# of Vertices	# of Undirected Edges
Cora	2,708	5,278
DBLP	17,716	52,867
OGBN-ArXiv	169,343	1,157,799
Chameleon	2,277	31,396
Squirrel	5,201	198,423
Amazon Computers	13,381	245,861

¹See <https://github.com/epfl-lts2/pygsp/>.

²See <https://github.com/danspielman/Laplacians.jl>.

Table D.2: Optimization hyperparameters used in the experiments of Figures 5.3 and D.5 per model and dataset.

		Learning Rate	Weight Decay	Edge Mask ℓ_1 Regularization of UGS
GCN	Cora	$5 \cdot 10^{-4}$	10^{-3}	10^{-2}
	DBLP	10^{-3}	10^{-4}	10^{-2}
	OGBN-ArXiv	10^{-3}	0	10^{-2}
	Chameleon	10^{-3}	10^{-4}	10^{-2}
	Squirrel	$5 \cdot 10^{-4}$	0	10^{-4}
	Amazon Computers	10^{-3}	10^{-4}	10^{-2}
GIN	Cora	10^{-3}	10^{-3}	10^{-2}
	DBLP	10^{-3}	10^{-3}	10^{-2}
	OGBN-ArXiv	10^{-4}	0	10^{-2}
ResGCN	Cora	$5 \cdot 10^{-4}$	10^{-3}	10^{-4}
	DBLP	$5 \cdot 10^{-4}$	10^{-4}	10^{-4}
	OGBN-ArXiv	10^{-3}	0	10^{-2}

Optimization. The cross-entropy loss was minimized via the Adam optimizer [121] with default β_1, β_2 coefficients and full-batches (*i.e.* every batch contained the whole training set). Optimization proceeded until the validation accuracy did not improve by at least 0.01 over 1000 consecutive epochs or 10000 epochs elapsed. The test accuracies reported in Figure 5.3 are those achieved during the epochs with highest validation accuracies. Table D.2 specifies additional optimization hyperparameters.

Hyperparameter tuning. For each combination of model and dataset separately, we tuned the learning rate, weight decay coefficient, and edge mask ℓ_1 regularization coefficient for UGS, and applied the chosen values for evaluating all methods without further tuning (note that the edge mask ℓ_1 regularization coefficient is relevant only for UGS). In particular, we carried out a grid search over learning rates $\{10^{-3}, 5 \cdot 10^{-4}, 10^{-4}\}$, weight decay coefficients $\{10^{-3}, 10^{-4}, 0\}$, and edge mask ℓ_1 regularization coefficients $\{10^{-2}, 10^{-3}, 10^{-4}\}$. Per hyperparameter configuration, we ran ten repetitions of UGS (differing in random seed), each until all of the input graph’s edges were removed. At every edge sparsity level (0%, 5%, 10%, \dots , 100%), in accordance with [39], we trained a new model with identical hyperparameters, but a fixed edge mask, over each of the ten graphs. We chose the hyperparameters that led to the highest mean validation accuracy, taken over the sparsity levels and ten runs.

Due to the size of the ResGCN model, tuning its hyperparameters entails significant computational costs. Thus, over the Cora and DBLP datasets, per hyperparameter configuration we ran five repetitions of UGS with ResGCN instead of ten. For the large-scale OGBN-ArXiv dataset, we adopted the same hyperparameters used for GCN.

Other. To allow more efficient experimentation, we compute the edge removal order of 2-WIS (Algorithm 1) in batches of size 100. Specifically, at each iteration of 2-WIS, instead of removing the edge e' with maximal walk index tuple $s^{(e')}$, the 100 edges with largest walk index tuples are removed. For randomized edge sparsification algorithms — random pruning, the spectral sparsification method of [198], and the adaptation of UGS [39] — the evaluation runs for a given dataset and percentage of removed edges were carried over sparsified graphs obtained using different random seeds.

D.7 Deferred Proofs

D.7.1 Additional Notation

For vectors, matrices, or tensors, parenthesized superscripts denote elements in a collection, e.g. $(\mathbf{a}^{(i)} \in \mathbb{R}^D)_{i=1}^N$, while subscripts refer to entries, e.g. $\mathbf{A}_{d_1, d_2} \in \mathbb{R}$ is the (d_1, d_2) 'th entry of $\mathbf{A} \in \mathbb{R}^{D_1 \times D_2}$. A colon is used to indicate a range of entries, e.g. $\mathbf{a}_{:d}$ is the first d entries of $\mathbf{a} \in \mathbb{R}^D$. We use $*$ to denote tensor contractions (Definition 18), \circ to denote the Kronecker product, and \odot to denote the Hadamard product. For $P \in \mathbb{N}_{\geq 0}$, the P 'th Hadamard power operator is denoted by \odot^P , i.e. $[\odot^P \mathbf{A}]_{d_1, d_2} = \mathbf{A}_{d_1, d_2}^P$ for $\mathbf{A} \in \mathbb{R}^{D_1 \times D_2}$. Lastly, when enumerating over sets of indices an ascending order is assumed.

D.7.2 Proof of Theorem 7

We assume familiarity with the basic concepts from tensor analysis introduced in Appendix D.3.1, and rely on the tensor network representations established for GNNs with product aggregation in Appendix D.3. Specifically, we use the fact that for any $\mathbf{X} = (\mathbf{x}^{(1)}, \dots, \mathbf{x}^{(|\mathcal{V}|)}) \in \mathbb{R}^{D_x \times |\mathcal{V}|}$ there exist tree tensor networks $\mathcal{T}(\mathbf{X})$ and $\mathcal{T}^{(t)}(\mathbf{X})$ (described in Appendix D.3.3 and formally defined in Equations (D.6) and (D.7)) such that: (i) their contraction yields $f^{(\theta, \mathcal{G})}(\mathbf{X})$ and $f^{(\theta, \mathcal{G}, t)}(\mathbf{X})$, respectively (Proposition 10); and (ii) each of their leaves is associated with a vertex feature vector, i.e. one of $\mathbf{x}^{(1)}, \dots, \mathbf{x}^{(|\mathcal{V}|)}$, whereas all other aspects of the tensor networks do not depend on $\mathbf{x}^{(1)}, \dots, \mathbf{x}^{(|\mathcal{V}|)}$.

The proof proceeds as follows. In Appendix D.7.2.1, by importing machinery from tensor analysis literature (in particular, adapting Claim 7 from [133]), we show that the separation ranks of $f^{(\theta, \mathcal{G})}$ and $f^{(\theta, \mathcal{G}, t)}$ can be upper bounded via cuts in their corresponding tensor networks. Namely, $\text{sep}(f^{(\theta, \mathcal{G})}; \mathcal{I})$ is at most the minimal multiplicative cut weight in $\mathcal{T}(\mathbf{X})$, among cuts separating leaves associated with vertices of the input graph in \mathcal{I} from leaves associated with vertices of the input graph in \mathcal{I}^c , where multiplicative cut weight refers to the product of weights belonging to legs crossing the cut. Similarly, $\text{sep}(f^{(\theta, \mathcal{G}, t)}; \mathcal{I})$ is at most the minimal multiplicative cut weight in $\mathcal{T}^{(t)}(\mathbf{X})$, among cuts of the same form. We conclude in Appendices D.7.2.2 and D.7.2.3 by applying this technique for upper bounding $\text{sep}(f^{(\theta, \mathcal{G})}; \mathcal{I})$ and $\text{sep}(f^{(\theta, \mathcal{G}, t)}; \mathcal{I})$, respectively, i.e. by finding cuts in the respective tensor networks with sufficiently low multiplicative weights.

D.7.2.1 Upper Bounding Separation Rank via Multiplicative Cut Weight in Tensor Network

In a tensor network $\mathcal{T} = (\mathcal{V}_{\mathcal{T}}, \mathcal{E}_{\mathcal{T}}, w_{\mathcal{T}})$, every $\mathcal{J}_{\mathcal{T}} \subseteq \mathcal{V}_{\mathcal{T}}$ induces a cut $(\mathcal{J}_{\mathcal{T}}, \mathcal{J}_{\mathcal{T}}^c)$, i.e. a partition of the nodes into two sets. We denote by

$$\mathcal{E}_{\mathcal{T}}(\mathcal{J}_{\mathcal{T}}) := \{\{u, v\} \in \mathcal{E}_{\mathcal{T}} : u \in \mathcal{J}_{\mathcal{T}}, v \in \mathcal{J}_{\mathcal{T}}^c\}$$

the set of legs crossing the cut, and define the *multiplicative cut weight* of $\mathcal{J}_{\mathcal{T}}$ to be the product of weights belonging to legs in $\mathcal{E}_{\mathcal{T}}(\mathcal{J}_{\mathcal{T}})$, i.e.:

$$w_{\mathcal{T}}^{\prod}(\mathcal{J}_{\mathcal{T}}) := \prod_{e \in \mathcal{E}_{\mathcal{T}}(\mathcal{J}_{\mathcal{T}})} w_{\mathcal{T}}(e).$$

For $\mathbf{X} = (\mathbf{x}^{(1)}, \dots, \mathbf{x}^{(|\mathcal{V}|)}) \in \mathbb{R}^{D_x \times |\mathcal{V}|}$, let $\mathcal{T}(\mathbf{X})$ and $\mathcal{T}^{(t)}(\mathbf{X})$ be the tensor networks corresponding to $f^{(\theta, \mathcal{G})}(\mathbf{X})$ and $f^{(\theta, \mathcal{G}, t)}(\mathbf{X})$ (detailed in Appendix D.3.3), respectively. Both $\mathcal{T}(\mathbf{X})$ and $\mathcal{T}^{(t)}(\mathbf{X})$ adhere to a tree structure. Each leaf node is associated with a vertex feature vector (*i.e.* one of $\mathbf{x}^{(1)}, \dots, \mathbf{x}^{(|\mathcal{V}|)}$), while interior nodes are associated with weight matrices or δ -tensors. The latter are tensors with modes of equal dimension holding ones on their hyper-diagonal and zeros elsewhere. The restrictions imposed by δ -tensors induce a modified notion of multiplicative cut weight, where legs incident to the same δ -tensor only contribute once to the weight product (note that weights of legs connected to the same δ -tensor are equal since they stand for mode dimensions).

Definition 19. For a tensor network $\mathcal{T} = (\mathcal{V}_{\mathcal{T}}, \mathcal{E}_{\mathcal{T}}, w_{\mathcal{T}})$ and subset of nodes $\mathcal{J}_{\mathcal{T}} \subseteq \mathcal{V}_{\mathcal{T}}$, let $\mathcal{E}_{\mathcal{T}}(\mathcal{J}_{\mathcal{T}})$ be the set of edges crossing the cut $(\mathcal{J}_{\mathcal{T}}, \mathcal{J}_{\mathcal{T}}^c)$. Denote by $\tilde{\mathcal{E}}_{\mathcal{T}}(\mathcal{J}_{\mathcal{T}}) \subseteq \mathcal{E}_{\mathcal{T}}(\mathcal{J}_{\mathcal{T}})$ a subset of legs containing for each δ -tensor in $\mathcal{V}_{\mathcal{T}}$ only a single leg from $\mathcal{E}_{\mathcal{T}}(\mathcal{J}_{\mathcal{T}})$ incident to it, along with all legs in $\mathcal{E}_{\mathcal{T}}(\mathcal{J}_{\mathcal{T}})$ not connected to δ -tensors. Then, the *modified multiplicative cut weight* of $\mathcal{J}_{\mathcal{T}}$ is:

$$\tilde{w}_{\mathcal{T}}^{\Pi}(\mathcal{J}_{\mathcal{T}}) := \prod_{e \in \tilde{\mathcal{E}}_{\mathcal{T}}(\mathcal{J}_{\mathcal{T}})} w_{\mathcal{T}}(e).$$

Lemma 51 establishes that $\text{sep}(f^{(\theta, \mathcal{G})}; \mathcal{I})$ and $\text{sep}(f^{(\theta, \mathcal{G}, t)}; \mathcal{I})$ are upper bounded by the minimal modified multiplicative cut weights in $\mathcal{T}(\mathbf{X})$ and $\mathcal{T}^{(t)}(\mathbf{X})$, respectively, among cuts separating leaves associated with vertices in \mathcal{I} from leaves associated vertices in \mathcal{I}^c .

Lemma 51. For any $\mathbf{X} = (\mathbf{x}^{(1)}, \dots, \mathbf{x}^{(|\mathcal{V}|)}) \in \mathbb{R}^{D_x \times |\mathcal{V}|}$, let $\mathcal{T}(\mathbf{X}) = (\mathcal{V}_{\mathcal{T}(\mathbf{X})}, \mathcal{E}_{\mathcal{T}(\mathbf{X})}, w_{\mathcal{T}(\mathbf{X})})$ and $\mathcal{T}^{(t)}(\mathbf{X}) = (\mathcal{V}_{\mathcal{T}^{(t)}(\mathbf{X})}, \mathcal{E}_{\mathcal{T}^{(t)}(\mathbf{X})}, w_{\mathcal{T}^{(t)}(\mathbf{X})})$ be the tensor network representations of $f^{(\theta, \mathcal{G})}(\mathbf{X})$ and $f^{(\theta, \mathcal{G}, t)}(\mathbf{X})$ (described in Appendix D.3.3 and formally defined in Equations (D.6) and (D.7)), respectively. Denote by $\mathcal{V}_{\mathcal{T}(\mathbf{X})}[\mathcal{I}] \subseteq \mathcal{V}_{\mathcal{T}(\mathbf{X})}$ and $\mathcal{V}_{\mathcal{T}^{(t)}(\mathbf{X})}[\mathcal{I}] \subseteq \mathcal{V}_{\mathcal{T}^{(t)}(\mathbf{X})}$ the sets of leaf nodes in $\mathcal{T}(\mathbf{X})$ and $\mathcal{T}^{(t)}(\mathbf{X})$, respectively, associated with vertices in \mathcal{I} from the input graph \mathcal{G} . Formally:

$$\begin{aligned} \mathcal{V}_{\mathcal{T}(\mathbf{X})}[\mathcal{I}] &:= \{\mathbf{x}^{(i, \gamma)} \in \mathcal{V}_{\mathcal{T}(\mathbf{X})} : i \in \mathcal{I}, \gamma \in [\rho_L(\{i\}, \mathcal{V})]\}, \\ \mathcal{V}_{\mathcal{T}^{(t)}(\mathbf{X})}[\mathcal{I}] &:= \{\mathbf{x}^{(i, \gamma)} \in \mathcal{V}_{\mathcal{T}^{(t)}(\mathbf{X})} : i \in \mathcal{I}, \gamma \in [\rho_L(\{i\}, \{t\})]\}. \end{aligned}$$

Similarly, denote by $\mathcal{V}_{\mathcal{T}(\mathbf{X})}[\mathcal{I}^c] \subseteq \mathcal{V}_{\mathcal{T}(\mathbf{X})}$ and $\mathcal{V}_{\mathcal{T}^{(t)}(\mathbf{X})}[\mathcal{I}^c] \subseteq \mathcal{V}_{\mathcal{T}^{(t)}(\mathbf{X})}$ the sets of leaf nodes in $\mathcal{T}(\mathbf{X})$ and $\mathcal{T}^{(t)}(\mathbf{X})$, respectively, associated with vertices in \mathcal{I}^c . Then, the following hold:

$$\text{(graph prediction)} \quad \text{sep}(f^{(\theta, \mathcal{G})}; \mathcal{I}) \leq \min_{\substack{\mathcal{J}_{\mathcal{T}(\mathbf{X})} \subseteq \mathcal{V}_{\mathcal{T}(\mathbf{X})} \\ \text{s.t. } \mathcal{V}_{\mathcal{T}(\mathbf{X})}[\mathcal{I}] \subseteq \mathcal{J}_{\mathcal{T}(\mathbf{X})} \text{ and } \mathcal{V}_{\mathcal{T}(\mathbf{X})}[\mathcal{I}^c] \subseteq \mathcal{J}_{\mathcal{T}(\mathbf{X})}^c}} \tilde{w}_{\mathcal{T}(\mathbf{X})}^{\Pi}(\mathcal{J}_{\mathcal{T}(\mathbf{X})}), \quad (\text{D.8})$$

$$\text{(vertex prediction)} \quad \text{sep}(f^{(\theta, \mathcal{G}, t)}; \mathcal{I}) \leq \min_{\substack{\mathcal{J}_{\mathcal{T}^{(t)}(\mathbf{X})} \subseteq \mathcal{V}_{\mathcal{T}^{(t)}(\mathbf{X})} \\ \text{s.t. } \mathcal{V}_{\mathcal{T}^{(t)}(\mathbf{X})}[\mathcal{I}] \subseteq \mathcal{J}_{\mathcal{T}^{(t)}(\mathbf{X})} \text{ and } \mathcal{V}_{\mathcal{T}^{(t)}(\mathbf{X})}[\mathcal{I}^c] \subseteq \mathcal{J}_{\mathcal{T}^{(t)}(\mathbf{X})}^c}} \tilde{w}_{\mathcal{T}^{(t)}(\mathbf{X})}^{\Pi}(\mathcal{J}_{\mathcal{T}^{(t)}(\mathbf{X})}), \quad (\text{D.9})$$

where $\tilde{w}_{\mathcal{T}(\mathbf{X})}^{\Pi}(\mathcal{J}_{\mathcal{T}(\mathbf{X})})$ is the modified multiplicative cut weight of $\mathcal{J}_{\mathcal{T}(\mathbf{X})}$ in $\mathcal{T}(\mathbf{X})$ and $\tilde{w}_{\mathcal{T}^{(t)}(\mathbf{X})}^{\Pi}(\mathcal{J}_{\mathcal{T}^{(t)}(\mathbf{X})})$ is the modified multiplicative cut weight of $\mathcal{J}_{\mathcal{T}^{(t)}(\mathbf{X})}$ in $\mathcal{T}^{(t)}(\mathbf{X})$ (Definition 19).

Proof. We first prove Equation (D.8). Examining $\mathcal{T}(\mathbf{X})$, notice that: (i) by Proposition 10 its contraction yields $f^{(\theta, \mathcal{G})}(\mathbf{X})$; (ii) it has a tree structure; and (iii) each of its leaves is associated with a vertex feature vector, *i.e.* one of $\mathbf{x}^{(1)}, \dots, \mathbf{x}^{(|\mathcal{V}|)}$, whereas all other aspects of the tensor network do not depend on $\mathbf{x}^{(1)}, \dots, \mathbf{x}^{(|\mathcal{V}|)}$. Specifically, for any \mathbf{X} and \mathbf{X}' the nodes, legs, and leg weights of $\mathcal{T}(\mathbf{X})$ and $\mathcal{T}(\mathbf{X}')$ are identical, up to the assignment of features in the leaf nodes. Let $\mathcal{F} \in \mathbb{R}^{D_x \times \dots \times D_x}$ be the order $\rho_L(\mathcal{V}, \mathcal{V})$ tensor obtained by contracting all interior nodes in $\mathcal{T}(\mathbf{X})$. The above implies that we may write $f^{(\theta, \mathcal{G})}(\mathbf{X})$ as a contraction of \mathcal{F} with $\mathbf{x}^{(1)}, \dots, \mathbf{x}^{(|\mathcal{V}|)}$. Specifically, it holds that:

$$f^{(\theta, \mathcal{G})}(\mathbf{X}) = \mathcal{F} *_{n \in [\rho_L(\mathcal{V}, \mathcal{V})]} \mathbf{x}^{(\mu(n))}, \quad (\text{D.10})$$

for any $\mathbf{X} = (\mathbf{x}^{(1)}, \dots, \mathbf{x}^{(|\mathcal{V}|)}) \in \mathbb{R}^{D_x \times |\mathcal{V}|}$, where $\mu : [\rho_L(\mathcal{V}, \mathcal{V})] \rightarrow \mathcal{V}$ maps a mode index of \mathcal{F} to the appropriate vertex of \mathcal{G} according to $\mathcal{T}(\mathbf{X})$. Let $\mu^{-1}(\mathcal{I}) := \{n \in [\rho_L(\mathcal{V}, \mathcal{V})] : \mu(n) \in \mathcal{I}\}$ be the mode indices of \mathcal{F} corresponding to vertices in \mathcal{I} . Invoking Lemma 52 leads to the following matricized form of Equation (D.10):

$$f^{(\theta, \mathcal{G})}(\mathbf{X}) = (\circ_{n \in \mu^{-1}(\mathcal{I})} \mathbf{x}^{(\mu(n))})^\top \llbracket \mathcal{F}; \mu^{-1}(\mathcal{I}) \rrbracket (\circ_{n \in \mu^{-1}(\mathcal{I}^c)} \mathbf{x}^{(\mu(n))}),$$

where \circ denotes the Kronecker product.

We claim that $\text{sep}(f^{(\theta, \mathcal{G})}; \mathcal{I}) \leq \text{rank} \llbracket \mathcal{F}; \mu^{-1}(\mathcal{I}) \rrbracket$. To see it is so, denote

$$R := \text{rank} \llbracket \mathcal{F}; \mu^{-1}(\mathcal{I}) \rrbracket$$

and let $\mathbf{u}^{(1)}, \dots, \mathbf{u}^{(R)} \in \mathbb{R}^{D_x^{\rho_L(\mathcal{I}, \mathcal{V})}}$ and $\bar{\mathbf{u}}^{(1)}, \dots, \bar{\mathbf{u}}^{(R)} \in \mathbb{R}^{D_x^{\rho_L(\mathcal{I}^c, \mathcal{V})}}$ be such that

$$\llbracket \mathcal{F}; \mu^{-1}(\mathcal{I}) \rrbracket = \sum_{r=1}^R \mathbf{u}^{(r)} (\bar{\mathbf{u}}^{(r)})^\top.$$

Then, defining $g^{(r)} : (\mathbb{R}^{D_x})^{|\mathcal{I}|} \rightarrow \mathbb{R}$ and $\bar{g}^{(r)} : (\mathbb{R}^{D_x})^{|\mathcal{I}^c|} \rightarrow \mathbb{R}$, for $r \in [R]$, as:

$$g^{(r)}(\mathbf{X}_{\mathcal{I}}) := \left\langle \circ_{n \in \mu^{-1}(\mathcal{I})} \mathbf{x}^{(\mu(n))}, \mathbf{u}^{(r)} \right\rangle, \quad \bar{g}^{(r)}(\mathbf{X}_{\mathcal{I}^c}) := \left\langle \circ_{n \in \mu^{-1}(\mathcal{I}^c)} \mathbf{x}^{(\mu(n))}, \bar{\mathbf{u}}^{(r)} \right\rangle,$$

where $\mathbf{X}_{\mathcal{I}} := (\mathbf{x}^{(i)})_{i \in \mathcal{I}}$ and $\mathbf{X}_{\mathcal{I}^c} := (\mathbf{x}^{(j)})_{j \in \mathcal{I}^c}$, we have that:

$$\begin{aligned} f^{(\theta, \mathcal{G})}(\mathbf{X}) &= (\circ_{n \in \mu^{-1}(\mathcal{I})} \mathbf{x}^{(\mu(n))})^\top \left(\sum_{r=1}^R \mathbf{u}^{(r)} (\bar{\mathbf{u}}^{(r)})^\top \right) (\circ_{n \in \mu^{-1}(\mathcal{I}^c)} \mathbf{x}^{(\mu(n))}) \\ &= \sum_{r=1}^R \left\langle \circ_{n \in \mu^{-1}(\mathcal{I})} \mathbf{x}^{(\mu(n))}, \mathbf{u}^{(r)} \right\rangle \cdot \left\langle \circ_{n \in \mu^{-1}(\mathcal{I}^c)} \mathbf{x}^{(\mu(n))}, \bar{\mathbf{u}}^{(r)} \right\rangle \\ &= \sum_{r=1}^R g^{(r)}(\mathbf{X}_{\mathcal{I}}) \cdot \bar{g}^{(r)}(\mathbf{X}_{\mathcal{I}^c}). \end{aligned}$$

Since $\text{sep}(f^{(\theta, \mathcal{G})}; \mathcal{I})$ is the minimal number of summands in a representation of this form of $f^{(\theta, \mathcal{G})}$, indeed, $\text{sep}(f^{(\theta, \mathcal{G})}; \mathcal{I}) \leq R = \text{rank} \llbracket \mathcal{F}; \mu^{-1}(\mathcal{I}) \rrbracket$.

What remains is to apply Claim 7 from [133], which upper bounds the rank of a tensor's matricization with multiplicative cut weights in a tree tensor network. In particular, consider an order $N \in \mathbb{N}$ tensor \mathcal{A} produced by contracting a tree tensor network \mathcal{T} . Then, for any $\mathcal{K} \subseteq [N]$ we have that $\text{rank} \llbracket \mathcal{A}; \mathcal{K} \rrbracket$ is at most the minimal modified multiplicative cut weight in \mathcal{T} , among cuts separating leaves corresponding to modes \mathcal{K} from leaves corresponding to modes \mathcal{K}^c . Thus, invoking

Claim 7 from [133] establishes Equation (D.8):

$$\text{sep}(f^{(\theta, \mathcal{G})}; \mathcal{I}) \leq \text{rank} \left[\mathcal{F}; \mu^{-1}(\mathcal{I}) \right] \leq \min_{\substack{\mathcal{J}_{\mathcal{T}(\mathbf{X})} \subseteq \mathcal{V}_{\mathcal{T}(\mathbf{X})} \\ \text{s.t. } \mathcal{V}_{\mathcal{T}(\mathbf{X})}[\mathcal{I}] \subseteq \mathcal{J}_{\mathcal{T}(\mathbf{X})} \text{ and } \mathcal{V}_{\mathcal{T}(\mathbf{X})}[\mathcal{I}^c] \subseteq \mathcal{J}_{\mathcal{T}(\mathbf{X})}^c}} \tilde{w}_{\mathcal{T}(\mathbf{X})}^{\Pi}(\mathcal{J}_{\mathcal{T}(\mathbf{X})}).$$

Equation (D.9) readily follows by steps analogous to those used above for proving Equation (D.8). \square

D.7.2.2 Cut in Tensor Network for Graph Prediction (Proof of Equation (5.6))

For $\mathbf{X} = (\mathbf{x}^{(1)}, \dots, \mathbf{x}^{(|\mathcal{V}|)}) \in \mathbb{R}^{D_x \times |\mathcal{V}|}$, let $\mathcal{T}(\mathbf{X}) = (\mathcal{V}_{\mathcal{T}(\mathbf{X})}, \mathcal{E}_{\mathcal{T}(\mathbf{X})}, w_{\mathcal{T}(\mathbf{X})})$ be the tensor network corresponding to $f^{(\theta, \mathcal{G})}(\mathbf{X})$ (detailed in Appendix D.3.3 and formally defined in Equation (D.6)). By Lemma 51, to prove that

$$\text{sep}(f^{(\theta, \mathcal{G})}; \mathcal{I}) \leq D_h^{4\rho_{L-1}(\mathcal{C}_{\mathcal{I}}, \mathcal{V})+1},$$

it suffices to find $\mathcal{J}_{\mathcal{T}(\mathbf{X})} \subseteq \mathcal{V}_{\mathcal{T}(\mathbf{X})}$ satisfying: (i) leaves of $\mathcal{T}(\mathbf{X})$ associated with vertices in \mathcal{I} are in $\mathcal{J}_{\mathcal{T}(\mathbf{X})}$, whereas leaves associated with vertices in \mathcal{I}^c are not in $\mathcal{J}_{\mathcal{T}(\mathbf{X})}$; and (ii) $\tilde{w}_{\mathcal{T}(\mathbf{X})}^{\Pi}(\mathcal{J}_{\mathcal{T}(\mathbf{X})}) \leq D_h^{4\rho_{L-1}(\mathcal{C}_{\mathcal{I}}, \mathcal{V})+1}$, where $\tilde{w}_{\mathcal{T}(\mathbf{X})}^{\Pi}(\mathcal{J}_{\mathcal{T}(\mathbf{X})})$ is the modified multiplicative cut weight of $\mathcal{J}_{\mathcal{T}(\mathbf{X})}$ (Definition 19). To this end, define $\mathcal{J}_{\mathcal{T}(\mathbf{X})}$ to hold all nodes in $\mathcal{V}_{\mathcal{T}(\mathbf{X})}$ corresponding to vertices in \mathcal{I} . Formally:

$$\begin{aligned} \mathcal{J}_{\mathcal{T}(\mathbf{X})} := & \left\{ \mathbf{x}^{(i, \gamma)} : i \in \mathcal{I}, \gamma \in [\rho_L(\{i\}, \mathcal{V})] \right\} \cup \\ & \left\{ \mathbf{W}^{(l, i, \gamma)} : l \in [L], i \in \mathcal{I}, \gamma \in [\rho_{L-l+1}(\{i\}, \mathcal{V})] \right\} \cup \\ & \left\{ \delta^{(l, i, \gamma)} : l \in [L], i \in \mathcal{I}, \gamma \in [\rho_{L-l}(\{i\}, \mathcal{V})] \right\}. \end{aligned}$$

Clearly, $\mathcal{J}_{\mathcal{T}(\mathbf{X})}$ upholds (i).

As for (ii), there are two types of legs crossing the cut induced by $\mathcal{J}_{\mathcal{T}(\mathbf{X})}$ in $\mathcal{T}(\mathbf{X})$. First, are those connecting a δ -tensor with a weight matrix in the same layer, where one is associated with a vertex in \mathcal{I} and the other with a vertex in \mathcal{I}^c . That is, legs connecting $\delta^{(l, i, \gamma)}$ with $\mathbf{W}^{(l, \mathcal{N}(i)_j, \phi_{l, i, j}(\gamma))}$, where $i \in \mathcal{V}$ and $\mathcal{N}(i)_j \in \mathcal{V}$ are on different sides of the partition $(\mathcal{I}, \mathcal{I}^c)$ in the input graph, for $j \in [|\mathcal{N}(i)|]$, $l \in [L]$, $\gamma \in [\rho_{L-l}(\{i\}, \mathcal{V})]$. The δ -tensors participating in these legs are exactly those associated with some $i \in \mathcal{C}_{\mathcal{I}}$ (recall $\mathcal{C}_{\mathcal{I}}$ is the set of vertices with an edge crossing the partition $(\mathcal{I}, \mathcal{I}^c)$). So, for every $l \in [L]$ and $i \in \mathcal{C}_{\mathcal{I}}$ there are $\rho_{L-l}(\{i\}, \mathcal{V})$ such δ -tensors. Second, are legs from δ -tensors associated with $i \in \mathcal{I}$ in the L 'th layer to the δ -tensor in the output layer of $\mathcal{T}(\mathbf{X})$. That is, legs connecting $\delta^{(L, i, 1)}$ with $\delta^{(|\mathcal{V}|+1)}$, for $i \in \mathcal{I}$. Legs incident to the same δ -tensor only contribute once to $\tilde{w}_{\mathcal{T}(\mathbf{X})}^{\Pi}(\mathcal{J}_{\mathcal{T}(\mathbf{X})})$. Thus, since the weights of all legs connected to δ -tensors are equal to D_h , we have that:

$$\tilde{w}_{\mathcal{T}(\mathbf{X})}^{\Pi}(\mathcal{J}_{\mathcal{T}(\mathbf{X})}) \leq D_h^{1 + \sum_{l=1}^L \sum_{i \in \mathcal{C}_{\mathcal{I}}} \rho_{L-l}(\{i\}, \mathcal{V})} = D_h^{1 + \sum_{l=1}^L \rho_{L-l}(\mathcal{C}_{\mathcal{I}}, \mathcal{V})}.$$

Lastly, it remains to show $\sum_{l=1}^L \rho_{L-l}(\mathcal{C}_{\mathcal{I}}, \mathcal{V}) \leq 4\rho_{L-1}(\mathcal{C}_{\mathcal{I}}, \mathcal{V})$, since in that case Lemma 51 implies:

$$\text{sep}(f^{(\theta, \mathcal{G})}; \mathcal{I}) \leq \tilde{w}_{\mathcal{T}(\mathbf{X})}^{\Pi}(\mathcal{J}_{\mathcal{T}(\mathbf{X})}) \leq D_h^{4\rho_{L-1}(\mathcal{C}_{\mathcal{I}}, \mathcal{V})+1},$$

which yields Equation (5.6) by taking the log of both sides.

The main idea is that, in an undirected graph with self-loops, the number of length $l \in \mathbb{N}$ walks from vertices with at least one neighbor decays exponentially when l decreases. Observe that $\rho_l(\mathcal{C}_{\mathcal{I}}, \mathcal{V}) \leq \rho_{l+1}(\mathcal{C}_{\mathcal{I}}, \mathcal{V})$ for all $l \in \mathbb{N}$. Hence:

$$\sum_{l=1}^L \rho_{L-l}(\mathcal{C}_{\mathcal{I}}, \mathcal{V}) \leq 2 \sum_{l \in \{1,3,\dots,L-1\}} \rho_{L-l}(\mathcal{C}_{\mathcal{I}}, \mathcal{V}). \quad (\text{D.11})$$

Furthermore, any length $l \in \mathbb{N}_{\geq 0}$ walk $i_0, i_1, \dots, i_l \in \mathcal{V}$ from $\mathcal{C}_{\mathcal{I}}$ induces at least two walks of length $l+2$ from $\mathcal{C}_{\mathcal{I}}$, distinct from those induced by other length l walks — one which goes twice through the self-loop of i_0 and then proceeds according to the length l walk, *i.e.* $i_0, i_0, i_0, i_1, \dots, i_l$, and another that goes to a neighboring vertex (exists since $i_0 \in \mathcal{C}_{\mathcal{I}}$), returns to i_0 , and then proceeds according to the length l walk. This means that $\rho_{L-l}(\mathcal{C}_{\mathcal{I}}, \mathcal{V}) \leq 2^{-1} \cdot \rho_{L-l+2}(\mathcal{C}_{\mathcal{I}}, \mathcal{V}) \leq \dots \leq 2^{-\lfloor l/2 \rfloor} \cdot \rho_{L-l}(\mathcal{C}_{\mathcal{I}}, \mathcal{V})$ for all $l \in \{3, 5, \dots, L-1\}$. Going back to Equation (D.11), this leads to:

$$\begin{aligned} \sum_{l=1}^L \rho_{L-l}(\mathcal{C}_{\mathcal{I}}, \mathcal{V}) &\leq 2 \sum_{l \in \{1,3,\dots,L-1\}} 2^{\lfloor l/2 \rfloor} \cdot \rho_{L-l}(\mathcal{C}_{\mathcal{I}}, \mathcal{V}) \\ &\leq 2 \sum_{l=0}^{\infty} 2^{-l} \cdot \rho_{L-l}(\mathcal{C}_{\mathcal{I}}, \mathcal{V}) \\ &= 4\rho_{L-1}(\mathcal{C}_{\mathcal{I}}, \mathcal{V}), \end{aligned}$$

completing the proof of Equation (5.6).

D.7.2.3 Cut in Tensor Network for Vertex Prediction (Proof of Equation (5.7))

This part of the proof follows a line similar to that of Appendix D.7.2.2, with differences stemming from the distinction between the operation of a GNN over graph and vertex prediction tasks.

For $\mathbf{X} = (\mathbf{x}^{(1)}, \dots, \mathbf{x}^{(|\mathcal{V}|)}) \in \mathbb{R}^{D_x \times |\mathcal{V}|}$, let $\mathcal{T}^{(t)}(\mathbf{X}) = (\mathcal{V}_{\mathcal{T}^{(t)}(\mathbf{X})}, \mathcal{E}_{\mathcal{T}^{(t)}(\mathbf{X})}, w_{\mathcal{T}^{(t)}(\mathbf{X})})$ be the tensor network corresponding to $f^{(\theta, \mathcal{G}, t)}(\mathbf{X})$ (detailed in Appendix D.3.3 and formally defined in Equation (D.7)). By Lemma 51, to prove that

$$\text{sep}(f^{(\theta, \mathcal{G}, t)}; \mathcal{I}) \leq D_h^{4\rho_{L-1}(\mathcal{C}_{\mathcal{I}, \{t\}})},$$

it suffices to find $\mathcal{J}_{\mathcal{T}^{(t)}(\mathbf{X})} \subseteq \mathcal{V}_{\mathcal{T}^{(t)}(\mathbf{X})}$ satisfying: (i) leaves of $\mathcal{T}^{(t)}(\mathbf{X})$ associated with vertices in \mathcal{I} are in $\mathcal{J}_{\mathcal{T}^{(t)}(\mathbf{X})}$, whereas leaves associated with vertices in \mathcal{I}^c are not in $\mathcal{J}_{\mathcal{T}^{(t)}(\mathbf{X})}$; and (ii) $\tilde{w}_{\mathcal{T}^{(t)}(\mathbf{X})}^{\Pi}(\mathcal{J}_{\mathcal{T}^{(t)}(\mathbf{X})}) \leq D_h^{4\rho_{L-1}(\mathcal{C}_{\mathcal{I}, \{t\}})}$, where $\tilde{w}_{\mathcal{T}^{(t)}(\mathbf{X})}^{\Pi}(\mathcal{J}_{\mathcal{T}^{(t)}(\mathbf{X})})$ is the modified multiplicative cut weight of $\mathcal{J}_{\mathcal{T}^{(t)}(\mathbf{X})}$ (Definition 19). To this end, define $\mathcal{J}_{\mathcal{T}^{(t)}(\mathbf{X})}$ to hold all nodes in $\mathcal{V}_{\mathcal{T}^{(t)}(\mathbf{X})}$ corresponding to vertices in \mathcal{I} . Formally:

$$\begin{aligned} \mathcal{J}_{\mathcal{T}^{(t)}(\mathbf{X})} &:= \left\{ \mathbf{x}^{(i,\gamma)} : i \in \mathcal{I}, \gamma \in [\rho_L(\{i\}, \{t\})] \right\} \cup \\ &\quad \left\{ \mathbf{W}^{(l,i,\gamma)} : l \in [L], i \in \mathcal{I}, \gamma \in [\rho_{L-l+1}(\{i\}, \{t\})] \right\} \cup \\ &\quad \left\{ \delta^{(l,i,\gamma)} : l \in [L], i \in \mathcal{I}, \gamma \in [\rho_{L-l}(\{i\}, \{t\})] \right\} \cup \\ &\quad \mathcal{W}^{(o)}, \end{aligned}$$

where $\mathcal{W}^{(o)} := \{\mathbf{W}^{(o)}\}$ if $t \in \mathcal{I}$ and $\mathcal{W}^{(o)} := \emptyset$ otherwise. Clearly, $\mathcal{J}_{\mathcal{T}^{(t)}(\mathbf{X})}$ upholds (i).

As for (ii), the legs crossing the cut induced by $\mathcal{J}_{\mathcal{T}^{(t)}(\mathbf{X})}$ in $\mathcal{T}^{(t)}(\mathbf{X})$ are those connecting a δ -tensor with a weight matrix in the same layer, where one is associated with a vertex in \mathcal{I} and the other with a vertex in \mathcal{I}^c . That is, legs connecting $\delta^{(l,i,\gamma)}$ with $\mathbf{W}^{(l,\mathcal{N}(i)_j,\Phi_{l,i,j}^{(i)}(\gamma))}$, where $i \in \mathcal{V}$ and $\mathcal{N}(i)_j \in \mathcal{V}$ are on different sides of the partition $(\mathcal{I}, \mathcal{I}^c)$ in the input graph, for $j \in [|\mathcal{N}(i)|]$, $l \in [L]$, $\gamma \in [\rho_{L-l}(\{i\}, \{t\})]$. The δ -tensors participating in these legs are exactly those associated with some $i \in \mathcal{C}_{\mathcal{I}}$ (recall $\mathcal{C}_{\mathcal{I}}$ is the set of vertices with an edge crossing the partition $(\mathcal{I}, \mathcal{I}^c)$). Hence, for every $l \in [L]$ and $i \in \mathcal{C}_{\mathcal{I}}$ there are $\rho_{L-l}(\{i\}, \{t\})$ such δ -tensors. Legs connected to the same δ -tensor only contribute once to $\tilde{w}_{\mathcal{T}^{(t)}(\mathbf{X})}^{\Pi}(\mathcal{J}_{\mathcal{T}^{(t)}(\mathbf{X})})$. Thus, since the weights of all legs connected to δ -tensors are equal to D_h , we have that:

$$\tilde{w}_{\mathcal{T}^{(t)}(\mathbf{X})}^{\Pi}(\mathcal{J}_{\mathcal{T}^{(t)}(\mathbf{X})}) = D_h^{\sum_{l=1}^L \sum_{i \in \mathcal{C}_{\mathcal{I}}} \rho_{L-l}(\{i\}, \{t\})} = D_h^{\sum_{l=1}^L \rho_{L-l}(\mathcal{C}_{\mathcal{I}}, \{t\})}.$$

Lastly, it remains to show $\sum_{l=1}^L \rho_{L-l}(\mathcal{C}_{\mathcal{I}}, \{t\}) \leq 4\rho_{L-1}(\mathcal{C}_{\mathcal{I}}, \{t\})$, as in that case Lemma 51 implies:

$$\text{sep}(f^{(\theta, \mathcal{G}, t)}; \mathcal{I}) \leq \tilde{w}_{\mathcal{T}^{(t)}(\mathbf{X})}^{\Pi}(\mathcal{J}_{\mathcal{T}^{(t)}(\mathbf{X})}) \leq D_h^{4\rho_{L-1}(\mathcal{C}_{\mathcal{I}}, \{t\})},$$

which leads to Equation (5.7) by taking the log of both sides.

The main idea is that, in an undirected graph with self-loops, the number of length $l \in \mathbb{N}$ walks ending at t that originate from vertices with at least one neighbor decays exponentially when l decreases. First, clearly $\rho_l(\mathcal{C}_{\mathcal{I}}, \{t\}) \leq \rho_{l+1}(\mathcal{C}_{\mathcal{I}}, \{t\})$ for all $l \in \mathbb{N}$. Therefore:

$$\sum_{l=1}^L \rho_{L-l}(\mathcal{C}_{\mathcal{I}}, \{t\}) \leq 2 \sum_{l \in \{1, 3, \dots, L-1\}} \rho_{L-l}(\mathcal{C}_{\mathcal{I}}, \{t\}). \quad (\text{D.12})$$

Furthermore, any length $l \in \mathbb{N}_{\geq 0}$ walk $i_0, i_1, \dots, i_{l-1}, t \in \mathcal{V}$ from $\mathcal{C}_{\mathcal{I}}$ to t induces at least two walks of length $l+2$ from $\mathcal{C}_{\mathcal{I}}$ to t , distinct from those induced by other length l walks — one which goes twice through the self-loop of i_0 and then proceeds according to the length l walk, i.e. $i_0, i_0, i_0, i_1, \dots, i_{l-1}, t$, and another that goes to a neighboring vertex (exists since $i_0 \in \mathcal{C}_{\mathcal{I}}$), returns to i_0 , and then proceeds according to the length l walk. This means that $\rho_{L-l}(\mathcal{C}_{\mathcal{I}}, \{t\}) \leq 2^{-1} \cdot \rho_{L-l+2}(\mathcal{C}_{\mathcal{I}}, \{t\}) \leq \dots \leq 2^{-\lfloor l/2 \rfloor} \cdot \rho_{L-1}(\mathcal{C}_{\mathcal{I}}, \{t\})$ for all $l \in \{3, 5, \dots, L-1\}$. Going back to Equation (D.12), we have that:

$$\begin{aligned} \sum_{l=1}^L \rho_{L-l}(\mathcal{C}_{\mathcal{I}}, \{t\}) &\leq 2 \sum_{l \in \{1, 3, \dots, L-1\}} 2^{\lfloor l/2 \rfloor} \cdot \rho_{L-1}(\mathcal{C}_{\mathcal{I}}, \{t\}) \\ &\leq 2 \sum_{l=0}^{\infty} 2^{-l} \cdot \rho_{L-1}(\mathcal{C}_{\mathcal{I}}, \{t\}) \\ &= 4\rho_{L-1}(\mathcal{C}_{\mathcal{I}}, \{t\}), \end{aligned}$$

concluding the proof of Equation (5.7). \square

D.7.2.4 Technical Lemma

Lemma 52. For any order $N \in \mathbb{N}$ tensor $\mathcal{A} \in \mathbb{R}^{D \times \dots \times D}$, vectors $\mathbf{x}^{(1)}, \dots, \mathbf{x}^{(N)} \in \mathbb{R}^D$, and subset of mode indices $\mathcal{I} \subseteq [N]$, it holds that $\mathcal{A} *_{i \in [N]} \mathbf{x}^{(i)} = (\circ_{i \in \mathcal{I}} \mathbf{x}^{(i)})^{\top} \llbracket \mathcal{A}; \mathcal{I} \rrbracket (\circ_{j \in \mathcal{I}^c} \mathbf{x}^{(j)}) \in \mathbb{R}$.

Proof. The identity follows directly from the definitions of tensor contraction, matricization, and Kronecker product (Appendix D.7.1):

$$\mathcal{A} *_{i \in [N]} \mathbf{x}^{(i)} = \sum_{d_1, \dots, d_N=1}^D \mathcal{A}_{d_1, \dots, d_N} \cdot \prod_{i \in [N]} \mathbf{x}_{d_i}^{(i)} = (\circ_{i \in \mathcal{I}} \mathbf{x}^{(i)})^{\top} \llbracket \mathcal{A}; \mathcal{I} \rrbracket (\circ_{j \in \mathcal{I}^c} \mathbf{x}^{(j)}).$$

□

D.7.3 Proof of Theorem 8

We assume familiarity with the basic concepts from tensor analysis introduced in Appendix D.3.1.

We begin by establishing a general technique for lower bounding the separation rank of a function through *grid tensors*, also used in [135, 215, 136, 179]. For any $f : (\mathbb{R}^{D_x})^N \rightarrow \mathbb{R}$ and $M \in \mathbb{N}$ template vectors $\mathbf{v}^{(1)}, \dots, \mathbf{v}^{(M)} \in \mathbb{R}^{D_x}$, we can create a grid tensor of f , which is a form of function discretization, by evaluating it over each point in $\{(\mathbf{v}^{(d_1)}, \dots, \mathbf{v}^{(d_N)})\}_{d_1, \dots, d_N=1}^M$ and storing the outcomes in an order N tensor with modes of dimension M . That is, the grid tensor of f for templates $\mathbf{v}^{(1)}, \dots, \mathbf{v}^{(M)}$, denoted $\mathcal{B}(f) \in \mathbb{R}^{M \times \dots \times M}$, is defined by $\mathcal{B}(f)_{d_1, \dots, d_N} = f(\mathbf{v}^{(d_1)}, \dots, \mathbf{v}^{(d_N)})$ for all $d_1, \dots, d_N \in [M]$.³ Lemma 53 shows that $\text{sep}(f; \mathcal{I})$ is lower bounded by the rank of $\mathcal{B}(f)$'s matricization with respect to \mathcal{I} .

Lemma 53. For $f : (\mathbb{R}^{D_x})^N \rightarrow \mathbb{R}$ and $M \in \mathbb{N}$ template vectors $\mathbf{v}^{(1)}, \dots, \mathbf{v}^{(M)} \in \mathbb{R}^{D_x}$, let $\mathcal{B}(f) \in \mathbb{R}^{M \times \dots \times M}$ be the corresponding order N grid tensor of f . Then, for any $\mathcal{I} \subseteq [N]$:

$$\text{rank}[\mathcal{B}(f); \mathcal{I}] \leq \text{sep}(f; \mathcal{I}).$$

Proof. If $\text{sep}(f; \mathcal{I})$ is ∞ or zero, i.e. f cannot be represented as a finite sum of separable functions (with respect to \mathcal{I}) or is identically zero, then the claim is trivial. Otherwise, denote $R := \text{sep}(f; \mathcal{I})$, and let $g^{(1)}, \dots, g^{(R)} : (\mathbb{R}^{D_x})^{|\mathcal{I}|} \rightarrow \mathbb{R}$ and $\bar{g}^{(1)}, \dots, \bar{g}^{(R)} : (\mathbb{R}^{D_x})^{|\mathcal{I}^c|} \rightarrow \mathbb{R}$ such that:

$$f(\mathbf{X}) = \sum_{r=1}^R g^{(r)}(\mathbf{X}_{\mathcal{I}}) \cdot \bar{g}^{(r)}(\mathbf{X}_{\mathcal{I}^c}), \quad (\text{D.13})$$

where $\mathbf{X} := (\mathbf{x}^{(1)}, \dots, \mathbf{x}^{(N)})$, $\mathbf{X}_{\mathcal{I}} := (\mathbf{x}^{(i)})_{i \in \mathcal{I}}$, and $\mathbf{X}_{\mathcal{I}^c} := (\mathbf{x}^{(j)})_{j \in \mathcal{I}^c}$. For $r \in [R]$, let $\mathcal{B}(g^{(r)})$ and $\mathcal{B}(\bar{g}^{(r)})$ be the grid tensors of $g^{(r)}$ and $\bar{g}^{(r)}$ over templates $\mathbf{v}^{(1)}, \dots, \mathbf{v}^{(M)}$, respectively. That is, $\mathcal{B}(g^{(r)})_{d_i; i \in \mathcal{I}} = g^{(r)}((\mathbf{v}^{(d_i)})_{i \in \mathcal{I}})$ and $\mathcal{B}(\bar{g}^{(r)})_{d_j; j \in \mathcal{I}^c} = \bar{g}^{(r)}((\mathbf{v}^{(d_j)})_{j \in \mathcal{I}^c})$ for all $d_1, \dots, d_N \in [M]$. By Equation (D.13) we have that for any $d_1, \dots, d_N \in [M]$:

$$\begin{aligned} \mathcal{B}(f)_{d_1, \dots, d_N} &= f(\mathbf{v}^{(d_1)}, \dots, \mathbf{v}^{(d_N)}) \\ &= \sum_{r=1}^R g^{(r)}((\mathbf{v}^{(d_i)})_{i \in \mathcal{I}}) \cdot \bar{g}^{(r)}((\mathbf{v}^{(d_j)})_{j \in \mathcal{I}^c}) \\ &= \sum_{r=1}^R \mathcal{B}(g^{(r)})_{d_i; i \in \mathcal{I}} \cdot \mathcal{B}(\bar{g}^{(r)})_{d_j; j \in \mathcal{I}^c}. \end{aligned}$$

Denoting by $\mathbf{u}^{(r)} \in \mathbb{R}^{M^{|\mathcal{I}|}}$ and $\bar{\mathbf{u}}^{(r)} \in \mathbb{R}^{M^{|\mathcal{I}^c|}}$ the arrangements of $\mathcal{B}(g^{(r)})$ and $\mathcal{B}(\bar{g}^{(r)})$ as vectors, respectively for $r \in [R]$, this implies that the matricization of $\mathcal{B}(f)$ with respect to \mathcal{I} can be written as:

$$[\mathcal{B}(f); \mathcal{I}] = \sum_{r=1}^R \mathbf{u}^{(r)} (\bar{\mathbf{u}}^{(r)})^\top.$$

We have arrived at a representation of $[\mathcal{B}(f); \mathcal{I}]$ as a sum of R outer products between two vectors. An outer product of two vectors is a matrix of rank at most one. Consequently, by sub-additivity of rank we conclude: $\text{rank}[\mathcal{B}(f); \mathcal{I}] \leq R = \text{sep}(f; \mathcal{I})$. □

³The template vectors of a grid tensor $\mathcal{B}(f)$ will be clear from context, thus we omit them from the notation.

In the context of graph prediction, let $\mathcal{C}^* \in \operatorname{argmax}_{\mathcal{C} \in \mathcal{S}(\mathcal{I})} \log(\alpha_{\mathcal{C}}) \cdot \rho_{L-1}(\mathcal{C}, \mathcal{V})$. Then, by Lemma 53, to prove that Equation (5.8) holds for weights θ , it suffices to find template vectors for which $\log(\operatorname{rank} \llbracket \mathcal{B}(f^{(\theta, \mathcal{G})}); \mathcal{I} \rrbracket) \geq \log(\alpha_{\mathcal{C}^*}) \cdot \rho_{L-1}(\mathcal{C}^*, \mathcal{V})$. Notice that, since the outputs of $f^{(\theta, \mathcal{G})}$ vary polynomially with the weights θ , so do the entries of $\llbracket \mathcal{B}(f^{(\theta, \mathcal{G})}); \mathcal{I} \rrbracket$ for any choice of template vectors. Thus, according to Lemma 59, by constructing weights θ and template vectors satisfying $\log(\operatorname{rank} \llbracket \mathcal{B}(f^{(\theta, \mathcal{G})}); \mathcal{I} \rrbracket) \geq \log(\alpha_{\mathcal{C}^*}) \cdot \rho_{L-1}(\mathcal{C}^*, \mathcal{V})$, we may conclude that this is the case for almost all assignments of weights, meaning Equation (5.8) holds for almost all assignments of weights. In Appendix D.7.3.1 we construct such weights and template vectors.

In the context of vertex prediction, let $\mathcal{C}_t^* \in \operatorname{argmax}_{\mathcal{C} \in \mathcal{S}(\mathcal{I})} \log(\alpha_{\mathcal{C}, t}) \cdot \rho_{L-1}(\mathcal{C}, \{t\})$. Due to arguments analogous to those above, to prove that Equation (5.9) holds for almost all assignments of weights, we need only find weights θ and template vectors satisfying $\log(\operatorname{rank} \llbracket \mathcal{B}(f^{(\theta, \mathcal{G}, t)}); \mathcal{I} \rrbracket) \geq \log(\alpha_{\mathcal{C}_t^*}) \cdot \rho_{L-1}(\mathcal{C}_t^*, \{t\})$. In Appendix D.7.3.2 we do so.

Lastly, recalling that a finite union of measure zero sets has measure zero as well establishes that Equations (5.8) and (5.9) jointly hold for almost all assignments of weights. \square

D.7.3.1 Weights and Template Vectors Assignment for Graph Prediction (Proof of Equation (5.8))

We construct weights θ and template vectors satisfying $\log(\operatorname{rank} \llbracket \mathcal{B}(f^{(\theta, \mathcal{G})}); \mathcal{I} \rrbracket) \geq \log(\alpha_{\mathcal{C}^*}) \cdot \rho_{L-1}(\mathcal{C}^*, \mathcal{V})$, where $\mathcal{C}^* \in \operatorname{argmax}_{\mathcal{C} \in \mathcal{S}(\mathcal{I})} \log(\alpha_{\mathcal{C}}) \cdot \rho_{L-1}(\mathcal{C}, \mathcal{V})$.

If $\rho_{L-1}(\mathcal{C}^*, \mathcal{V}) = 0$, then the claim is trivial since there exist weights and template vectors for which $\llbracket \mathcal{B}(f^{(\theta, \mathcal{G})}); \mathcal{I} \rrbracket$ is not the zero matrix (e.g. taking all weight matrices to be zero-padded identity matrices and choosing a single template vector holding one in its first entry and zeros elsewhere).

Now, assuming that $\rho_{L-1}(\mathcal{C}^*, \mathcal{V}) > 0$, which in particular implies that $\mathcal{I} \neq \emptyset, \mathcal{I} \neq \mathcal{V}$, and $\mathcal{C}^* \neq \emptyset$, we begin with the case of GNN depth $L = 1$, after which we treat the more general $L \geq 2$ case.

Case of $L = 1$: Consider the weights $\theta = (\mathbf{W}^{(1)}, \mathbf{W}^{(o)})$ given by $\mathbf{W}^{(1)} := \mathbf{I} \in \mathbb{R}^{D_h \times D_x}$ and $\mathbf{W}^{(o)} := (1, \dots, 1) \in \mathbb{R}^{1 \times D_h}$, where \mathbf{I} is a zero padded identity matrix, i.e. it holds ones on its diagonal and zeros elsewhere. We choose template vectors $\mathbf{v}^{(1)}, \dots, \mathbf{v}^{(D)} \in \mathbb{R}^{D_x}$ such that $\mathbf{v}^{(m)}$ holds the m 'th standard basis vector of \mathbb{R}^D in its first D coordinates and zeros in the remaining entries, for $m \in [D]$ (recall $D := \min\{D_x, D_h\}$). Namely, denote by $\mathbf{e}^{(1)}, \dots, \mathbf{e}^{(D)} \in \mathbb{R}^D$ the standard basis vectors of \mathbb{R}^D , i.e. $\mathbf{e}_d^{(m)} = 1$ if $d = m$ and $\mathbf{e}_d^{(m)} = 0$ otherwise for all $m, d \in [D]$. We let $\mathbf{v}_{:D}^{(m)} := \mathbf{e}^{(m)}$ and $\mathbf{v}_{D+1:}^{(m)} := 0$ for all $m \in [D]$.

We prove that for this choice of weights and template vectors, for all $d_1, \dots, d_{|\mathcal{V}|} \in [D]$:

$$f^{(\theta, \mathcal{G})}(\mathbf{v}^{(d_1)}, \dots, \mathbf{v}^{(d_{|\mathcal{V}|})}) = \begin{cases} 1 & , \text{if } d_1 = \dots = d_{|\mathcal{V}|} \\ 0 & , \text{otherwise} \end{cases} . \quad (\text{D.14})$$

To see it is so, notice that:

$$f^{(\theta, \mathcal{G})}(\mathbf{v}^{(d_1)}, \dots, \mathbf{v}^{(d_{|\mathcal{V}|})}) = \mathbf{W}^{(o)}(\odot_{i \in \mathcal{V}} \mathbf{h}^{(1,i)}) = \sum_{d=1}^{D_h} \prod_{i \in \mathcal{V}} \mathbf{h}_d^{(1,i)},$$

with $\mathbf{h}^{(1,i)} = \odot_{j \in \mathcal{N}(i)} (\mathbf{W}^{(1)} \mathbf{v}^{(d_j)}) = \odot_{j \in \mathcal{N}(i)} (\mathbf{I} \mathbf{v}^{(d_j)})$ for all $i \in \mathcal{V}$. Since $\mathbf{v}_{:D}^{(d_j)} = \mathbf{e}^{(d_j)}$ for all $j \in \mathcal{N}(i)$ and \mathbf{I} is a zero-padded $D \times D$ identity matrix, it holds that:

$$f^{(\theta, \mathcal{G})}(\mathbf{v}^{(d_1)}, \dots, \mathbf{v}^{(d_{|\mathcal{V}|})}) = \sum_{d=1}^D \prod_{i \in \mathcal{V}, j \in \mathcal{N}(i)} \mathbf{e}_d^{(d_j)}.$$

Due to the existence of self-loops (i.e. $i \in \mathcal{N}(i)$ for all $i \in \mathcal{V}$), for every $d \in [D]$ the product $\prod_{i \in \mathcal{V}, j \in \mathcal{N}(i)} \mathbf{e}_d^{(d_j)}$ includes each of $\mathbf{e}_d^{(d_1)}, \dots, \mathbf{e}_d^{(d_{|\mathcal{V}|})}$ at least once. Consequently, $\prod_{i \in \mathcal{V}, j \in \mathcal{N}(i)} \mathbf{e}_d^{(d_j)} = 1$ if $d_1 = \dots = d_{|\mathcal{V}|} = d$ and $\prod_{i \in \mathcal{V}, j \in \mathcal{N}(i)} \mathbf{e}_d^{(d_j)} = 0$ otherwise. This implies that $f^{(\theta, \mathcal{G})}(\mathbf{v}^{(d_1)}, \dots, \mathbf{v}^{(d_{|\mathcal{V}|})}) = 1$ if $d_1 = \dots = d_{|\mathcal{V}|}$ and $f^{(\theta, \mathcal{G})}(\mathbf{v}^{(d_1)}, \dots, \mathbf{v}^{(d_{|\mathcal{V}|})}) = 0$ otherwise, for all $d_1, \dots, d_{|\mathcal{V}|} \in [D]$.

Equation (D.14) implies that $\llbracket \mathcal{B}(f^{(\theta, \mathcal{G})}); \mathcal{I} \rrbracket$ has exactly D non-zero entries, each in a different row and column. Thus, $\text{rank} \llbracket \mathcal{B}(f^{(\theta, \mathcal{G})}); \mathcal{I} \rrbracket = D$. Recalling that $\alpha_{\mathcal{C}^*} := D^{1/\rho_0(\mathcal{C}^*, \mathcal{V})}$ for $L = 1$, we conclude:

$$\log(\text{rank} \llbracket \mathcal{B}(f^{(\theta, \mathcal{G})}); \mathcal{I} \rrbracket) = \log(D) = \log(\alpha_{\mathcal{C}^*}) \cdot \rho_0(\mathcal{C}^*, \mathcal{V}).$$

Case of $L \geq 2$: Let $M := \binom{D}{\rho_{L-1}(\mathcal{C}^*, \mathcal{V})} = \binom{D + \rho_{L-1}(\mathcal{C}^*, \mathcal{V}) - 1}{\rho_{L-1}(\mathcal{C}^*, \mathcal{V})}$ be the multiset coefficient of D and $\rho_{L-1}(\mathcal{C}^*, \mathcal{V})$ (recall $D := \min\{D_x, D_h\}$). By Lemma 57, there exists $\mathbf{Z} \in \mathbb{R}_{>0}^{M \times D}$ for which

$$\text{rank}(\odot^{\rho_{L-1}(\mathcal{C}^*, \mathcal{V})}(\mathbf{Z}\mathbf{Z}^\top)) = \binom{D}{\rho_{L-1}(\mathcal{C}^*, \mathcal{V})},$$

with $\odot^{\rho_{L-1}(\mathcal{C}^*, \mathcal{V})}(\mathbf{Z}\mathbf{Z}^\top)$ standing for the $\rho_{L-1}(\mathcal{C}^*, \mathcal{V})$ 'th Hadamard power of $\mathbf{Z}\mathbf{Z}^\top$. For this \mathbf{Z} , by Lemma 54 below we know that there exist weights θ and template vectors such that $\llbracket \mathcal{B}(f^{(\theta, \mathcal{G})}); \mathcal{I} \rrbracket$ has an $M \times M$ sub-matrix of the form $\mathbf{S}(\odot^{\rho_{L-1}(\mathcal{C}^*, \mathcal{V})}(\mathbf{Z}\mathbf{Z}^\top))\mathbf{Q}$, where $\mathbf{S}, \mathbf{Q} \in \mathbb{R}^{M \times M}$ are full-rank diagonal matrices. Since the rank of a matrix is at least the rank of any of its sub-matrices:

$$\begin{aligned} \text{rank}(\llbracket \mathcal{B}(f^{(\theta, \mathcal{G})}); \mathcal{I} \rrbracket) &\geq \text{rank}(\mathbf{S}(\odot^{\rho_{L-1}(\mathcal{C}^*, \mathcal{V})}(\mathbf{Z}\mathbf{Z}^\top))\mathbf{Q}) \\ &= \text{rank}(\odot^{\rho_{L-1}(\mathcal{C}^*, \mathcal{V})}(\mathbf{Z}\mathbf{Z}^\top)) \\ &= \binom{D}{\rho_{L-1}(\mathcal{C}^*, \mathcal{V})}, \end{aligned}$$

where the second transition stems from \mathbf{S} and \mathbf{Q} being full-rank. Applying Lemma 58 to lower bound the multiset coefficient, we have that:

$$\text{rank}(\llbracket \mathcal{B}(f^{(\theta, \mathcal{G})}); \mathcal{I} \rrbracket) \geq \binom{D}{\rho_{L-1}(\mathcal{C}^*, \mathcal{V})} \geq \left(\frac{D-1}{\rho_{L-1}(\mathcal{C}^*, \mathcal{V})} + 1 \right)^{\rho_{L-1}(\mathcal{C}^*, \mathcal{V})}.$$

Taking the log of both sides while recalling that $\alpha_{\mathcal{C}^*} := (D - 1) \cdot \rho_{L-1}(\mathcal{C}^*, \mathcal{V})^{-1} + 1$, we conclude that:

$$\log(\text{rank} \left[\left[\mathcal{B} \left(f^{(\theta, \mathcal{G})} \right); \mathcal{I} \right] \right]) \geq \log(\alpha_{\mathcal{C}^*}) \cdot \rho_{L-1}(\mathcal{C}^*, \mathcal{V}).$$

Lemma 54. *Suppose that the GNN inducing $f^{(\theta, \mathcal{G})}$ is of depth $L \geq 2$ and that $\rho_{L-1}(\mathcal{C}^*, \mathcal{V}) > 0$. For any $M \in \mathbb{N}$ and matrix with positive entries $\mathbf{Z} \in \mathbb{R}_{>0}^{M \times D}$, there exist weights θ and $M + 1$ template vectors $\mathbf{v}^{(1)}, \dots, \mathbf{v}^{(M+1)} \in \mathbb{R}^{D_x}$ such that $\left[\left[\mathcal{B} \left(f^{(\theta, \mathcal{G})} \right); \mathcal{I} \right] \right]$ has an $M \times M$ sub-matrix $\mathbf{S}(\odot^{\rho_{L-1}(\mathcal{C}^*, \mathcal{V})}(\mathbf{Z}\mathbf{Z}^\top))\mathbf{Q}$, where $\mathbf{S}, \mathbf{Q} \in \mathbb{R}^{M \times M}$ are full-rank diagonal matrices and $\odot^{\rho_{L-1}(\mathcal{C}^*, \mathcal{V})}(\mathbf{Z}\mathbf{Z}^\top)$ is the $\rho_{L-1}(\mathcal{C}^*, \mathcal{V})$ 'th Hadamard power of $\mathbf{Z}\mathbf{Z}^\top$.*

Proof. Consider the weights $\theta = (\mathbf{W}^{(1)}, \dots, \mathbf{W}^{(L)}, \mathbf{W}^{(o)})$ given by:

$$\begin{aligned} \mathbf{W}^{(1)} &:= \mathbf{I} \in \mathbb{R}^{D_h \times D_x}, \\ \mathbf{W}^{(2)} &:= \begin{pmatrix} 1 & 1 & \dots & 1 \\ 0 & 0 & \dots & 0 \\ \vdots & \vdots & \dots & \vdots \\ 0 & 0 & \dots & 0 \end{pmatrix} \in \mathbb{R}^{D_h \times D_h}, \\ \forall l \in \{3, \dots, L\} : \mathbf{W}^{(l)} &:= \begin{pmatrix} 1 & 0 & \dots & 0 \\ 0 & 0 & \dots & 0 \\ \vdots & \vdots & \dots & \vdots \\ 0 & 0 & \dots & 0 \end{pmatrix} \in \mathbb{R}^{D_h \times D_h}, \\ \mathbf{W}^{(o)} &:= (1 \ 0 \ \dots \ 0) \in \mathbb{R}^{1 \times D_h}, \end{aligned}$$

where \mathbf{I} is a zero padded identity matrix, i.e. it holds ones on its diagonal and zeros elsewhere. We define the templates $\mathbf{v}^{(1)}, \dots, \mathbf{v}^{(M)} \in \mathbb{R}^{D_x}$ to be the vectors holding the respective rows of \mathbf{Z} in their first D coordinates and zeros in the remaining entries (recall $D := \min\{D_x, D_h\}$). That is, denoting the rows of \mathbf{Z} by $\mathbf{z}^{(1)}, \dots, \mathbf{z}^{(M)} \in \mathbb{R}_{>0}^D$, we let $\mathbf{v}_{:D}^{(m)} := \mathbf{z}^{(m)}$ and $\mathbf{v}_{D+1:}^{(m)} := 0$ for all $m \in [M]$. We set all entries of the last template vector to one, i.e. $\mathbf{v}^{(M+1)} := (1, \dots, 1) \in \mathbb{R}^{D_x}$.

Since $\mathcal{C}^* \in \mathcal{S}(\mathcal{I})$, i.e. it is an admissible subset of $\mathcal{C}_{\mathcal{I}}$ (Definition 13), there exist $\mathcal{I}' \subseteq \mathcal{I}, \mathcal{J}' \subseteq \mathcal{I}^c$ with no repeating shared neighbors (Definition 12) such that $\mathcal{C}^* = \mathcal{N}(\mathcal{I}') \cap \mathcal{N}(\mathcal{J}')$. Notice that \mathcal{I}' and \mathcal{J}' are non-empty as $\mathcal{C}^* \neq \emptyset$ (this is implied by $\rho_{L-1}(\mathcal{C}^*, \mathcal{V}) > 0$). We focus on the $M \times M$ sub-matrix of $\left[\left[\mathcal{B} \left(f^{(\theta, \mathcal{G})} \right); \mathcal{I} \right] \right]$ that includes only rows and columns corresponding to evaluations of $f^{(\theta, \mathcal{G})}$ where all variables indexed by \mathcal{I}' are assigned the same template vector from $\mathbf{v}^{(1)}, \dots, \mathbf{v}^{(M)}$, all variables indexed by \mathcal{J}' are assigned the same template vector from $\mathbf{v}^{(1)}, \dots, \mathbf{v}^{(M)}$, and all remaining variables are assigned the all-ones template vector $\mathbf{v}^{(M+1)}$. Denoting this sub-matrix by $\mathbf{U} \in \mathbb{R}^{M \times M}$, it therefore upholds:

$$\mathbf{U}_{m,n} = f^{(\theta, \mathcal{G})} \left((\mathbf{x}^{(i)} \leftarrow \mathbf{v}^{(m)})_{i \in \mathcal{I}'}, (\mathbf{x}^{(j)} \leftarrow \mathbf{v}^{(n)})_{j \in \mathcal{J}'}, (\mathbf{x}^{(k)} \leftarrow \mathbf{v}^{(M+1)})_{k \in \mathcal{V} \setminus (\mathcal{I}' \cup \mathcal{J}')} \right),$$

for all $m, n \in [M]$, where we use $(\mathbf{x}^{(i)} \leftarrow \mathbf{v}^{(m)})_{i \in \mathcal{I}'}$ to denote that input variables indexed by \mathcal{I}' are assigned the value $\mathbf{v}^{(m)}$. To show that \mathbf{U} obeys the form

$$\mathbf{S}(\odot^{\rho_{L-1}(\mathcal{C}^*, \mathcal{V})}(\mathbf{Z}\mathbf{Z}^\top))\mathbf{Q}$$

for full-rank diagonal $\mathbf{S}, \mathbf{Q} \in \mathbb{R}^{M \times M}$, we prove there exist $\phi, \psi : \mathbb{R}^{D_x} \rightarrow \mathbb{R}_{>0}$ such that $\mathbf{U}_{m,n} = \phi(\mathbf{v}^{(m)}) \langle \mathbf{z}^{(m)}, \mathbf{z}^{(n)} \rangle^{\rho_{L-1}(\mathcal{C}^*, \mathcal{V})} \psi(\mathbf{v}^{(n)})$ for all $m, n \in [M]$. Indeed, defining \mathbf{S} to hold $\phi(\mathbf{v}^{(1)}), \dots, \phi(\mathbf{v}^{(M)})$ on its diagonal and \mathbf{Q} to hold $\psi(\mathbf{v}^{(1)}), \dots, \psi(\mathbf{v}^{(M)})$ on its diagonal, we have that $\mathbf{U} = \mathbf{S}(\odot^{\rho_{L-1}(\mathcal{C}^*, \mathcal{V})}(\mathbf{Z}\mathbf{Z}^\top))\mathbf{Q}$. Since \mathbf{S} and \mathbf{Q} are clearly full-rank (diagonal matrices with non-zero entries on their diagonal), the proof concludes.

For $m, n \in [M]$, let $\mathbf{h}^{(l,i)} \in \mathbb{R}^{D_h}$ be the hidden embedding for $i \in \mathcal{V}$ at layer $l \in [L]$ of the GNN inducing $f^{(\theta, \mathcal{G})}$, over the following assignment to its input variables (*i.e.* vertex features):

$$(\mathbf{x}^{(i)} \leftarrow \mathbf{v}^{(m)})_{i \in \mathcal{I}'}, (\mathbf{x}^{(j)} \leftarrow \mathbf{v}^{(n)})_{j \in \mathcal{J}'}, (\mathbf{x}^{(k)} \leftarrow \mathbf{v}^{(M+1)})_{k \in \mathcal{V} \setminus (\mathcal{I}' \cup \mathcal{J}')}.$$

Invoking Lemma 60 with $\mathbf{v}^{(m)}, \mathbf{v}^{(n)}, \mathcal{I}'$, and \mathcal{J}' , for all $i \in \mathcal{V}$ it holds that:

$$\mathbf{h}_1^{(L,i)} = \phi^{(L,i)}(\mathbf{v}^{(m)}) \langle \mathbf{z}^{(m)}, \mathbf{z}^{(n)} \rangle^{\rho_{L-1}(\mathcal{C}^*, \{i\})} \psi^{(L,i)}(\mathbf{v}^{(n)}) \quad , \quad \forall d \in \{2, \dots, D_h\} : \mathbf{h}_d^{(L,i)} = 0,$$

for some $\phi^{(L,i)}, \psi^{(L,i)} : \mathbb{R}^{D_x} \rightarrow \mathbb{R}_{>0}$. Since

$$\begin{aligned} \mathbf{U}_{m,n} &= f^{(\theta, \mathcal{G})} \left((\mathbf{x}^{(i)} \leftarrow \mathbf{v}^{(m)})_{i \in \mathcal{I}'}, (\mathbf{x}^{(j)} \leftarrow \mathbf{v}^{(n)})_{j \in \mathcal{J}'}, (\mathbf{x}^{(k)} \leftarrow \mathbf{v}^{(M+1)})_{k \in \mathcal{V} \setminus (\mathcal{I}' \cup \mathcal{J}')} \right) \\ &= \mathbf{W}^{(o)} (\odot_{i \in \mathcal{V}} \mathbf{h}^{(L,i)}) \end{aligned}$$

and $\mathbf{W}^{(o)} = (1, 0, \dots, 0)$, this implies that:

$$\begin{aligned} \mathbf{U}_{m,n} &= \prod_{i \in \mathcal{V}} \mathbf{h}_1^{(L,i)} \\ &= \prod_{i \in \mathcal{V}} \phi^{(L,i)}(\mathbf{v}^{(m)}) \langle \mathbf{z}^{(m)}, \mathbf{z}^{(n)} \rangle^{\rho_{L-1}(\mathcal{C}^*, \{i\})} \psi^{(L,i)}(\mathbf{v}^{(n)}). \end{aligned}$$

Rearranging the last term leads to:

$$\mathbf{U}_{m,n} = \left(\prod_{i \in \mathcal{V}} \phi^{(L,i)}(\mathbf{v}^{(m)}) \right) \cdot \langle \mathbf{z}^{(m)}, \mathbf{z}^{(n)} \rangle^{\sum_{i \in \mathcal{V}} \rho_{L-1}(\mathcal{C}^*, \{i\})} \cdot \left(\prod_{i \in \mathcal{V}} \psi^{(L,i)}(\mathbf{v}^{(n)}) \right).$$

Let $\phi : \mathbf{v} \mapsto \prod_{i \in \mathcal{V}} \phi^{(L,i)}(\mathbf{v})$ and $\psi : \mathbf{v} \mapsto \prod_{i \in \mathcal{V}} \psi^{(L,i)}(\mathbf{v})$. Noticing that their range is indeed $\mathbb{R}_{>0}$ and that $\sum_{i \in \mathcal{V}} \rho_{L-1}(\mathcal{C}^*, \{i\}) = \rho_{L-1}(\mathcal{C}^*, \mathcal{V})$ yields the sought-after expression for $\mathbf{U}_{m,n}$:

$$\mathbf{U}_{m,n} = \phi(\mathbf{v}^{(m)}) \langle \mathbf{z}^{(m)}, \mathbf{z}^{(n)} \rangle^{\rho_{L-1}(\mathcal{C}^*, \mathcal{V})} \psi(\mathbf{v}^{(n)}).$$

□

D.7.3.2 Weights and Template Vectors Assignment for Vertex Prediction (Proof of Equation (5.9))

This part of the proof follows a line similar to that of Appendix D.7.3.1, with differences stemming from the distinction between the operation of a GNN over graph and vertex prediction. Namely, we construct weights θ and template vectors satisfying $\log(\text{rank} \left[\mathcal{B} \left(f^{(\theta, \mathcal{G}, t)} \right); \mathcal{I} \right]) \geq \log(\alpha_{\mathcal{C}_t^*}) \cdot \rho_{L-1}(\mathcal{C}_t^*, \{t\})$, where:

$$\mathcal{C}_t^* \in \text{argmax}_{\mathcal{C} \in \mathcal{S}(\mathcal{I})} \log(\alpha_{\mathcal{C}, t}) \cdot \rho_{L-1}(\mathcal{C}, \{t\}).$$

If $\rho_{L-1}(\mathcal{C}_t^*, \{t\}) = 0$, then the claim is trivial since there exist weights and template

vectors for which $\llbracket \mathcal{B}(f^{(\theta, \mathcal{G}, t)}); \mathcal{I} \rrbracket$ is not the zero matrix (e.g. taking all weight matrices to be zero-padded identity matrices and choosing a single template vector holding one in its first entry and zeros elsewhere).

Now, assuming that $\rho_{L-1}(\mathcal{C}_t^*, \{t\}) > 0$, which in particular implies that $\mathcal{I} \neq \emptyset, \mathcal{I} \neq \mathcal{V}$, and $\mathcal{C}_t^* \neq \emptyset$, we begin with the case of GNN depth $L = 1$, after which we treat the more general $L \geq 2$ case.

Case of $L = 1$: Consider the weights $\theta = (\mathbf{W}^{(1)}, \mathbf{W}^{(0)})$ given by $\mathbf{W}^{(1)} := \mathbf{I} \in \mathbb{R}^{D_h \times D_x}$ and $\mathbf{W}^{(0)} := (1, \dots, 1) \in \mathbb{R}^{1 \times D_h}$, where \mathbf{I} is a zero padded identity matrix, i.e. it holds ones on its diagonal and zeros elsewhere. We choose template vectors $\mathbf{v}^{(1)}, \dots, \mathbf{v}^{(D)} \in \mathbb{R}^{D_x}$ such that $\mathbf{v}^{(m)}$ holds the m 'th standard basis vector of \mathbb{R}^D in its first D coordinates and zeros in the remaining entries, for $m \in [D]$ (recall $D := \min\{D_x, D_h\}$). Namely, denote by $\mathbf{e}^{(1)}, \dots, \mathbf{e}^{(D)} \in \mathbb{R}^D$ the standard basis vectors of \mathbb{R}^D , i.e. $\mathbf{e}_d^{(m)} = 1$ if $d = m$ and $\mathbf{e}_d^{(m)} = 0$ otherwise for all $m, d \in [D]$. We let $\mathbf{v}_{:D}^{(m)} := \mathbf{e}^{(m)}$ and $\mathbf{v}_{D+1:}^{(m)} := 0$ for all $m \in [D]$.

We prove that for this choice of weights and template vectors, for all $d_1, \dots, d_{|\mathcal{V}|} \in [D]$:

$$f^{(\theta, \mathcal{G}, t)}(\mathbf{v}^{(d_1)}, \dots, \mathbf{v}^{(d_{|\mathcal{V}|})}) = \begin{cases} 1 & , \text{if } d_j = d_{j'} \text{ for all } j, j' \in \mathcal{N}(t) \\ 0 & , \text{otherwise} \end{cases}. \quad (\text{D.15})$$

To see it is so, notice that:

$$f^{(\theta, \mathcal{G}, t)}(\mathbf{v}^{(d_1)}, \dots, \mathbf{v}^{(d_{|\mathcal{V}|})}) = \mathbf{W}^{(0)} \mathbf{h}^{(1, t)} = \sum_{d=1}^{D_h} \mathbf{h}_d^{(1, t)},$$

with $\mathbf{h}^{(1, t)} = \odot_{j \in \mathcal{N}(t)} (\mathbf{W}^{(1)} \mathbf{v}^{(d_j)}) = \odot_{j \in \mathcal{N}(t)} (\mathbf{I} \mathbf{v}^{(d_j)})$. Since $\mathbf{v}_{:D}^{(d_j)} = \mathbf{e}^{(d_j)}$ for all $j \in \mathcal{N}(t)$ and \mathbf{I} is a zero-padded $D \times D$ identity matrix, it holds that:

$$f^{(\theta, \mathcal{G}, t)}(\mathbf{v}^{(d_1)}, \dots, \mathbf{v}^{(d_{|\mathcal{V}|})}) = \sum_{d=1}^D \prod_{j \in \mathcal{N}(t)} \mathbf{e}_d^{(d_j)}.$$

For every $d \in [D]$ we have that $\prod_{j \in \mathcal{N}(t)} \mathbf{e}_d^{(d_j)} = 1$ if $d_j = d$ for all $j \in \mathcal{N}(t)$ and $\prod_{j \in \mathcal{N}(t)} \mathbf{e}_d^{(d_j)} = 0$ otherwise. This implies that $f^{(\theta, \mathcal{G}, t)}(\mathbf{v}^{(d_1)}, \dots, \mathbf{v}^{(d_{|\mathcal{V}|})}) = 1$ if $d_j = d_{j'}$ for all $j, j' \in \mathcal{N}(t)$ and $f^{(\theta, \mathcal{G}, t)}(\mathbf{v}^{(d_1)}, \dots, \mathbf{v}^{(d_{|\mathcal{V}|})}) = 0$ otherwise, for all $d_1, \dots, d_{|\mathcal{V}|} \in [D]$.

Equation (D.15) implies that $\llbracket \mathcal{B}(f^{(\theta, \mathcal{G}, t)}); \mathcal{I} \rrbracket$ has a sub-matrix of rank D . Specifically, such a sub-matrix can be obtained by examining all rows and columns of $\llbracket \mathcal{B}(f^{(\theta, \mathcal{G}, t)}); \mathcal{I} \rrbracket$ corresponding to some fixed indices $(d_i \in [D])_{i \in \mathcal{V} \setminus \mathcal{N}(t)}$ for the vertices that are not neighbors of t . Thus, $\text{rank} \llbracket \mathcal{B}(f^{(\theta, \mathcal{G}, t)}); \mathcal{I} \rrbracket \geq D$. Notice that necessarily $\rho_0(\mathcal{C}_t^*, \{t\}) = 1$, as it is not zero and there can only be one length zero walk to t (the trivial walk that starts and ends at t). Recalling that $\alpha_{\mathcal{C}_t^*, t} := D$ for $L = 1$, we therefore conclude:

$$\log\left(\text{rank} \llbracket \mathcal{B}(f^{(\theta, \mathcal{G}, t)}); \mathcal{I} \rrbracket\right) \geq \log(D) = \log(\alpha_{\mathcal{C}_t^*, t}) \cdot \rho_0(\mathcal{C}_t^*, \{t\}).$$

Case of $L \geq 2$: Let $M := \left(\binom{D}{\rho_{L-1}(\mathcal{C}_t^*, \{t\})} \right) = \binom{D + \rho_{L-1}(\mathcal{C}_t^*, \{t\}) - 1}{\rho_{L-1}(\mathcal{C}_t^*, \{t\})}$ be the multiset coefficient of D and $\rho_{L-1}(\mathcal{C}_t^*, \{t\})$ (recall $D := \min\{D_x, D_h\}$). By Lemma 57, there exists $\mathbf{Z} \in$

$\mathbb{R}_{>0}^{M \times D}$ for which

$$\text{rank}\left(\odot^{\rho_{L-1}(\mathcal{C}_t^*, \{t\})}(\mathbf{Z}\mathbf{Z}^\top)\right) = \left(\binom{D}{\rho_{L-1}(\mathcal{C}_t^*, \{t\})}\right),$$

with $\odot^{\rho_{L-1}(\mathcal{C}_t^*, \{t\})}(\mathbf{Z}\mathbf{Z}^\top)$ standing for the $\rho_{L-1}(\mathcal{C}_t^*, \{t\})$ 'th Hadamard power of $\mathbf{Z}\mathbf{Z}^\top$. For this \mathbf{Z} , by Lemma 55 below we know that there exist weights θ and template vectors such that $\llbracket \mathcal{B}(f^{(\theta, \mathcal{G}, t)}); \mathcal{I} \rrbracket$ has an $M \times M$ sub-matrix of the form $\mathbf{S}(\odot^{\rho_{L-1}(\mathcal{C}_t^*, \{t\})}(\mathbf{Z}\mathbf{Z}^\top))\mathbf{Q}$, where $\mathbf{S}, \mathbf{Q} \in \mathbb{R}^{M \times M}$ are full-rank diagonal matrices. Since the rank of a matrix is at least the rank of any of its sub-matrices:

$$\begin{aligned} \text{rank}\left(\llbracket \mathcal{B}(f^{(\theta, \mathcal{G}, t)}); \mathcal{I} \rrbracket\right) &\geq \text{rank}\left(\mathbf{S}(\odot^{\rho_{L-1}(\mathcal{C}_t^*, \{t\})}(\mathbf{Z}\mathbf{Z}^\top))\mathbf{Q}\right) \\ &= \text{rank}\left(\odot^{\rho_{L-1}(\mathcal{C}_t^*, \{t\})}(\mathbf{Z}\mathbf{Z}^\top)\right) \\ &= \left(\binom{D}{\rho_{L-1}(\mathcal{C}_t^*, \{t\})}\right), \end{aligned}$$

where the second transition is due to \mathbf{S} and \mathbf{Q} being full-rank. Applying Lemma 58 to lower bound the multiset coefficient, we have that:

$$\text{rank}\left(\llbracket \mathcal{B}(f^{(\theta, \mathcal{G}, t)}); \mathcal{I} \rrbracket\right) \geq \left(\binom{D}{\rho_{L-1}(\mathcal{C}_t^*, \{t\})}\right) \geq \left(\frac{D-1}{\rho_{L-1}(\mathcal{C}_t^*, \{t\})} + 1\right)^{\rho_{L-1}(\mathcal{C}_t^*, \{t\})}.$$

Taking the log of both sides while recalling that $\alpha_{\mathcal{C}_t^*, t} := (D-1) \cdot \rho_{L-1}(\mathcal{C}_t^*, \{t\})^{-1} + 1$, we conclude that:

$$\log(\text{rank}\llbracket \mathcal{B}(f^{(\theta, \mathcal{G}, t)}); \mathcal{I} \rrbracket) \geq \log(\alpha_{\mathcal{C}_t^*, t}) \cdot \rho_{L-1}(\mathcal{C}_t^*, \{t\}).$$

Lemma 55. Suppose that the GNN inducing $f^{(\theta, \mathcal{G}, t)}$ is of depth $L \geq 2$ and $\rho_{L-1}(\mathcal{C}_t^*, \{t\}) > 0$. For any $M \in \mathbb{N}$ and matrix with positive entries $\mathbf{Z} \in \mathbb{R}_{>0}^{M \times D}$, there exist weights θ and $M+1$ template vectors $\mathbf{v}^{(1)}, \dots, \mathbf{v}^{(M+1)} \in \mathbb{R}^{D_x}$ such that $\llbracket \mathcal{B}(f^{(\theta, \mathcal{G}, t)}); \mathcal{I} \rrbracket$ has an $M \times M$ sub-matrix $\mathbf{S}(\odot^{\rho_{L-1}(\mathcal{C}_t^*, \{t\})}(\mathbf{Z}\mathbf{Z}^\top))\mathbf{Q}$, where $\mathbf{S}, \mathbf{Q} \in \mathbb{R}^{M \times M}$ are full-rank diagonal matrices and $\odot^{\rho_{L-1}(\mathcal{C}_t^*, \{t\})}(\mathbf{Z}\mathbf{Z}^\top)$ is the $\rho_{L-1}(\mathcal{C}_t^*, \{t\})$ 'th Hadamard power of $\mathbf{Z}\mathbf{Z}^\top$.

Proof. Consider the weights $\theta = (\mathbf{W}^{(1)}, \dots, \mathbf{W}^{(L)}, \mathbf{W}^{(0)})$ defined by:

$$\begin{aligned} \mathbf{W}^{(1)} &:= \mathbf{I} \in \mathbb{R}^{D_h \times D_x}, \\ \mathbf{W}^{(2)} &:= \begin{pmatrix} 1 & 1 & \cdots & 1 \\ 0 & 0 & \cdots & 0 \\ \vdots & \vdots & \cdots & \vdots \\ 0 & 0 & \cdots & 0 \end{pmatrix} \in \mathbb{R}^{D_h \times D_h}, \\ \forall l \in \{3, \dots, L\} : \mathbf{W}^{(l)} &:= \begin{pmatrix} 1 & 0 & \cdots & 0 \\ 0 & 0 & \cdots & 0 \\ \vdots & \vdots & \cdots & \vdots \\ 0 & 0 & \cdots & 0 \end{pmatrix} \in \mathbb{R}^{D_h \times D_h}, \\ \mathbf{W}^{(0)} &:= (1 \ 0 \ \cdots \ 0) \in \mathbb{R}^{1 \times D_h}, \end{aligned}$$

where \mathbf{I} is a zero padded identity matrix, i.e. it holds ones on its diagonal and zeros

elsewhere. We let the templates $\mathbf{v}^{(1)}, \dots, \mathbf{v}^{(M)} \in \mathbb{R}^{D_x}$ be the vectors holding the respective rows of \mathbf{Z} in their first D coordinates and zeros in the remaining entries (recall $D := \min\{D_x, D_h\}$). That is, denoting the rows of \mathbf{Z} by $\mathbf{z}^{(1)}, \dots, \mathbf{z}^{(M)} \in \mathbb{R}_{>0}^D$, we let $\mathbf{v}_{:D}^{(m)} := \mathbf{z}^{(m)}$ and $\mathbf{v}_{D+1:}^{(m)} := 0$ for all $m \in [M]$. We set all entries of the last template vector to one, i.e. $\mathbf{v}^{(M+1)} := (1, \dots, 1) \in \mathbb{R}^{D_x}$.

Since $\mathcal{C}_t^* \in \mathcal{S}(\mathcal{I})$, i.e. it is an admissible subset of $\mathcal{C}_{\mathcal{I}}$ (Definition 13), there exist $\mathcal{I}' \subseteq \mathcal{I}, \mathcal{J}' \subseteq \mathcal{I}^c$ with no repeating shared neighbors (Definition 12) such that $\mathcal{C}_t^* = \mathcal{N}(\mathcal{I}') \cap \mathcal{N}(\mathcal{J}')$. Notice that \mathcal{I}' and \mathcal{J}' are non-empty as $\mathcal{C}_t^* \neq \emptyset$ (this is implied by $\rho_{L-1}(\mathcal{C}_t^*, \{t\}) > 0$). We focus on the $M \times M$ sub-matrix of $\llbracket \mathcal{B}(f^{(\theta, \mathcal{G}, t)}); \mathcal{I} \rrbracket$ that includes only rows and columns corresponding to evaluations of $f^{(\theta, \mathcal{G}, t)}$ where all variables indexed by \mathcal{I}' are assigned the same template vector from $\mathbf{v}^{(1)}, \dots, \mathbf{v}^{(M)}$, all variables indexed by \mathcal{J}' are assigned the same template vector from $\mathbf{v}^{(1)}, \dots, \mathbf{v}^{(M)}$, and all remaining variables are assigned the all-ones template vector $\mathbf{v}^{(M+1)}$. Denoting this sub-matrix by $\mathbf{U} \in \mathbb{R}^{M \times M}$, it therefore upholds:

$$\mathbf{U}_{m,n} = f^{(\theta, \mathcal{G}, t)} \left((\mathbf{x}^{(i)} \leftarrow \mathbf{v}^{(m)})_{i \in \mathcal{I}'}, (\mathbf{x}^{(j)} \leftarrow \mathbf{v}^{(n)})_{j \in \mathcal{J}'}, (\mathbf{x}^{(k)} \leftarrow \mathbf{v}^{(M+1)})_{k \in \mathcal{V} \setminus (\mathcal{I}' \cup \mathcal{J}')} \right),$$

for all $m, n \in [M]$, where we use $(\mathbf{x}^{(i)} \leftarrow \mathbf{v}^{(m)})_{i \in \mathcal{I}'}$ to denote that input variables indexed by \mathcal{I}' are assigned the value $\mathbf{v}^{(m)}$. To show that \mathbf{U} obeys the form

$$\mathbf{S}(\odot^{\rho_{L-1}(\mathcal{C}_t^*, \{t\})}(\mathbf{Z}\mathbf{Z}^\top))\mathbf{Q}$$

for full-rank diagonal $\mathbf{S}, \mathbf{Q} \in \mathbb{R}^{M \times M}$, we prove there exist $\phi, \psi : \mathbb{R}^{D_x} \rightarrow \mathbb{R}_{>0}$ such that $\mathbf{U}_{m,n} = \phi(\mathbf{v}^{(m)}) \langle \mathbf{z}^{(m)}, \mathbf{z}^{(n)} \rangle^{\rho_{L-1}(\mathcal{C}_t^*, \{t\})} \psi(\mathbf{v}^{(n)})$ for all $m, n \in [M]$. Indeed, defining \mathbf{S} to hold $\phi(\mathbf{v}^{(1)}), \dots, \phi(\mathbf{v}^{(M)})$ on its diagonal and \mathbf{Q} to hold $\psi(\mathbf{v}^{(1)}), \dots, \psi(\mathbf{v}^{(M)})$ on its diagonal, we have that $\mathbf{U} = \mathbf{S}(\odot^{\rho_{L-1}(\mathcal{C}_t^*, \{t\})}(\mathbf{Z}\mathbf{Z}^\top))\mathbf{Q}$. Since \mathbf{S} and \mathbf{Q} are clearly full-rank (diagonal matrices with non-zero entries on their diagonal), the proof concludes.

For $m, n \in [M]$, let $\mathbf{h}^{(l,i)} \in \mathbb{R}^{D_h}$ be the hidden embedding for $i \in \mathcal{V}$ at layer $l \in [L]$ of the GNN inducing $f^{(\theta, \mathcal{G}, t)}$, over the following assignment to its input variables (i.e. vertex features):

$$(\mathbf{x}^{(i)} \leftarrow \mathbf{v}^{(m)})_{i \in \mathcal{I}'}, (\mathbf{x}^{(j)} \leftarrow \mathbf{v}^{(n)})_{j \in \mathcal{J}'}, (\mathbf{x}^{(k)} \leftarrow \mathbf{v}^{(M+1)})_{k \in \mathcal{V} \setminus (\mathcal{I}' \cup \mathcal{J}')}.$$

Invoking Lemma 60 with $\mathbf{v}^{(m)}, \mathbf{v}^{(n)}, \mathcal{I}'$, and \mathcal{J}' , it holds that:

$$\mathbf{h}_1^{(L,t)} = \phi^{(L,t)}(\mathbf{v}^{(m)}) \langle \mathbf{z}^{(m)}, \mathbf{z}^{(n)} \rangle^{\rho_{L-1}(\mathcal{C}_t^*, \{t\})} \psi^{(L,t)}(\mathbf{v}^{(n)}), \quad \forall d \in \{2, \dots, D_h\} : \mathbf{h}_d^{(L,t)} = 0,$$

for some $\phi^{(L,t)}, \psi^{(L,t)} : \mathbb{R}^{D_x} \rightarrow \mathbb{R}_{>0}$. Since

$$\begin{aligned} \mathbf{U}_{m,n} &= f^{(\theta, \mathcal{G}, t)} \left((\mathbf{x}^{(i)} \leftarrow \mathbf{v}^{(m)})_{i \in \mathcal{I}'}, (\mathbf{x}^{(j)} \leftarrow \mathbf{v}^{(n)})_{j \in \mathcal{J}'}, (\mathbf{x}^{(k)} \leftarrow \mathbf{v}^{(M+1)})_{k \in \mathcal{V} \setminus (\mathcal{I}' \cup \mathcal{J}')} \right) \\ &= \mathbf{W}^{(o)} \mathbf{h}^{(L,t)} \end{aligned}$$

and $\mathbf{W}^{(o)} = (1, 0, \dots, 0)$, this implies that:

$$\mathbf{U}_{m,n} = \mathbf{h}_1^{(L,t)} = \phi^{(L,t)}(\mathbf{v}^{(m)}) \langle \mathbf{z}^{(m)}, \mathbf{z}^{(n)} \rangle^{\rho_{L-1}(\mathcal{C}_t^*, \{t\})} \psi^{(L,t)}(\mathbf{v}^{(n)}).$$

Defining $\phi := \phi^{(L,t)}$ and $\psi := \psi^{(L,t)}$ leads to the sought-after expression for $\mathbf{U}_{m,n}$:

$$\mathbf{U}_{m,n} = \phi(\mathbf{v}^{(m)}) \langle \mathbf{z}^{(m)}, \mathbf{z}^{(n)} \rangle^{\rho_{L-1}(\mathcal{C}_{i,r,t}^*)} \psi(\mathbf{v}^{(n)}).$$

□

D.7.3.3 Technical Lemmas

For completeness, we include the *vector rearrangement inequality* from [132], which we employ for proving the subsequent Lemma 57.

Lemma 56 (Lemma 1 from [132]). *Let $\mathbf{a}^{(1)}, \dots, \mathbf{a}^{(M)} \in \mathbb{R}_{\geq 0}^D$ be $M \in \mathbb{N}$ different vectors with non-negative entries. Then, for any permutation $\sigma : [M] \rightarrow [M]$ besides the identity permutation it holds that:*

$$\sum_{m=1}^M \langle \mathbf{a}^{(m)}, \mathbf{a}^{(\sigma(m))} \rangle < \sum_{m=1}^M \|\mathbf{a}^{(m)}\|^2.$$

Taking the P 'th Hadamard power of a rank at most D matrix results in a matrix whose rank is at most the multiset coefficient $\binom{D}{P} := \binom{D+P-1}{P}$ (see, e.g., Theorem 1 in [5]). Lemma 57, adapted from Appendix B.2 in [135], guarantees that we can always find a $\binom{D}{P} \times D$ matrix \mathbf{Z} with positive entries such that $\text{rank}(\odot^P(\mathbf{Z}\mathbf{Z}^\top))$ is maximal, i.e. equal to $\binom{D}{P}$.

Lemma 57 (adapted from Appendix B.2 in [135]). *For any $D \in \mathbb{N}$ and $P \in \mathbb{N}_{\geq 0}$, there exists a matrix with positive entries $\mathbf{Z} \in \mathbb{R}_{>0}^{\binom{D}{P} \times D}$ for which:*

$$\text{rank}(\odot^P(\mathbf{Z}\mathbf{Z}^\top)) = \binom{D}{P},$$

where $\odot^P(\mathbf{Z}\mathbf{Z}^\top)$ is the P 'th Hadamard power of $\mathbf{Z}\mathbf{Z}^\top$.

Proof. We let $M := \binom{D}{P}$ for notational convenience. Denote by $\mathbf{z}^{(1)}, \dots, \mathbf{z}^{(M)} \in \mathbb{R}^D$ the row vectors of $\mathbf{Z} \in \mathbb{R}_{>0}^{M \times D}$. Observing the (m, n) 'th entry of $\odot^P(\mathbf{Z}\mathbf{Z}^\top)$:

$$\left[\odot^P(\mathbf{Z}\mathbf{Z}^\top) \right]_{m,n} = \langle \mathbf{z}^{(m)}, \mathbf{z}^{(n)} \rangle^P = \left(\sum_{d=1}^D \mathbf{z}_d^{(m)} \cdot \mathbf{z}_d^{(n)} \right)^P,$$

by expanding the power using the multinomial identity we have that:

$$\begin{aligned} \left[\odot^P(\mathbf{Z}\mathbf{Z}^\top) \right]_{m,n} &= \sum_{\substack{q_1, \dots, q_D \in \mathbb{N}_{\geq 0} \\ \text{s.t. } \sum_{d=1}^D q_d = P}} \binom{P}{q_1, \dots, q_D} \prod_{d=1}^D (\mathbf{z}_d^{(m)} \cdot \mathbf{z}_d^{(n)})^{q_d} \\ &= \sum_{\substack{q_1, \dots, q_D \in \mathbb{N}_{\geq 0} \\ \text{s.t. } \sum_{d=1}^D q_d = P}} \binom{P}{q_1, \dots, q_D} \left(\prod_{d=1}^D (\mathbf{z}_d^{(m)})^{q_d} \right) \cdot \left(\prod_{d=1}^D (\mathbf{z}_d^{(n)})^{q_d} \right), \end{aligned} \tag{D.16}$$

where in the last equality we separated terms depending on m from those depending on n .

Let $(\mathbf{a}^{(q_1, \dots, q_D)} \in \mathbb{R}^M)_{q_1, \dots, q_D \in \mathbb{N}_{\geq 0} \text{ s.t. } \sum_{d=1}^D q_d = P}$ be M vectors that, for all $q_1, \dots, q_D \in \mathbb{N}_{\geq 0}$ satisfying $\sum_{d=1}^D q_d = P$ and $m \in [M]$, are defined by $\mathbf{a}_m^{(q_1, \dots, q_D)} = \prod_{d=1}^D (\mathbf{z}_d^{(m)})^{q_d}$. As can be seen from Equation (D.16), we can write:

$$\odot^P(\mathbf{Z}\mathbf{Z}^\top) = \mathbf{A}\mathbf{S}\mathbf{A}^\top,$$

where $\mathbf{A} \in \mathbb{R}^{M \times M}$ is the matrix whose columns are $(\mathbf{a}^{(q_1, \dots, q_D)})_{q_1, \dots, q_D \in \mathbb{N}_{\geq 0} \text{ s.t. } \sum_{d=1}^D q_d = P}$ and $\mathbf{S} \in \mathbb{R}^{M \times M}$ is the diagonal matrix holding $\binom{P}{q_1, \dots, q_D}$ for every $q_1, \dots, q_D \in \mathbb{N}_{\geq 0}$ satisfying $\sum_{d=1}^D q_d = P$ on its diagonal. Since all entries on the diagonal of \mathbf{S} are positive, it is of full-rank, i.e. $\text{rank}(\mathbf{S}) = M$. Thus, to prove that there exists $\mathbf{Z} \in \mathbb{R}_{>0}^{M \times D}$ for which $\text{rank}(\odot^P(\mathbf{Z}\mathbf{Z}^\top)) = M$, it suffices to show that we can choose $\mathbf{z}^{(1)}, \dots, \mathbf{z}^{(M)}$ with positive entries inducing $\text{rank}(\mathbf{A}) = M$, for \mathbf{A} as defined above. Below, we complete the proof by constructing such $\mathbf{z}^{(1)}, \dots, \mathbf{z}^{(M)}$.

We associate each of $\mathbf{z}^{(1)}, \dots, \mathbf{z}^{(M)}$ with a different configuration from the set:

$$\left\{ \mathbf{q} = (q_1, \dots, q_D) : q_1, \dots, q_D \in \mathbb{N}_{\geq 0}, \sum_{d=1}^D q_d = P \right\},$$

where note that this set contains $M = \binom{D}{P}$ elements. For $m \in [M]$, denote by $\mathbf{q}^{(m)}$ the configuration associated with $\mathbf{z}^{(m)}$. For a variable $\gamma \in \mathbb{R}$, to be determined later on, and every $m \in [M]$ and $d \in [D]$, we set:

$$\mathbf{z}_d^{(m)} = \gamma^{\mathbf{q}_d^{(m)}}.$$

Given these $\mathbf{z}^{(1)}, \dots, \mathbf{z}^{(M)}$, the entries of \mathbf{A} have the following form:

$$\mathbf{A}_{m,n} = \prod_{d=1}^D (\mathbf{z}_d^{(m)})^{\mathbf{q}_d^{(n)}} = \prod_{d=1}^D (\gamma^{\mathbf{q}_d^{(m)}})^{\mathbf{q}_d^{(n)}} = \gamma^{\sum_{d=1}^D \mathbf{q}_d^{(m)} \cdot \mathbf{q}_d^{(n)}} = \gamma^{\langle \mathbf{q}^{(m)}, \mathbf{q}^{(n)} \rangle},$$

for all $m, n \in [M]$. Thus, $\det(\mathbf{A}) = \sum_{\text{permutation } \sigma: [M] \rightarrow [M]} \text{sign}(\sigma) \cdot \gamma^{\sum_{m=1}^M \langle \mathbf{q}^{(m)}, \mathbf{q}^{(\sigma(m))} \rangle}$ is polynomial in γ . By Lemma 56, $\sum_{m=1}^M \langle \mathbf{q}^{(m)}, \mathbf{q}^{(\sigma(m))} \rangle < \sum_{m=1}^M \|\mathbf{q}^{(m)}\|^2$ for all σ which is not the identity permutation. This implies that $\sum_{m=1}^M \|\mathbf{q}^{(m)}\|^2$ is the maximal degree of a monomial in $\det(\mathbf{A})$, and it is attained by a single element in $\sum_{\text{permutation } \sigma: [M] \rightarrow [M]} \text{sign}(\sigma) \cdot \gamma^{\sum_{m=1}^M \langle \mathbf{q}^{(m)}, \mathbf{q}^{(\sigma(m))} \rangle}$ — that corresponding to the identity permutation. Consequently, $\det(\mathbf{A})$ cannot be the zero polynomial with respect to γ , and so it vanishes only on a finite set of values for γ . In particular, there exists $\gamma > 0$ such that $\det(\mathbf{A}) \neq 0$, meaning $\text{rank}(\mathbf{A}) = M$. The proof concludes by noticing that for a positive γ the entries of the chosen $\mathbf{z}^{(1)}, \dots, \mathbf{z}^{(M)}$ are positive as well. \square

Additionally, we make use of the following lemmas.

Lemma 58. For any $D, P \in \mathbb{N}$, let $\binom{D}{P} := \binom{D+P-1}{P}$ be the multiset coefficient. Then:

$$\binom{D}{P} \geq \left(\frac{D-1}{P} + 1 \right)^P.$$

Proof. For any $N \geq K \in \mathbb{N}$, a known lower bound on the binomial coefficient is $\binom{N}{K} \geq \left(\frac{N}{K}\right)^K$. Hence:

$$\binom{\binom{D}{P}}{P} = \binom{D+P-1}{P} \geq \left(\frac{D+P-1}{P}\right)^P = \left(\frac{D-1}{P} + 1\right)^P.$$

□

Lemma 59. For $D_1, D_2, K \in \mathbb{N}$, consider a polynomial function mapping variables $\theta \in \mathbb{R}^K$ to matrices $\mathbf{A}(\theta) \in \mathbb{R}^{D_1 \times D_2}$, i.e. the entries of $\mathbf{A}(\theta)$ are polynomial in θ . If there exists a point $\theta^* \in \mathbb{R}^K$ such that $\text{rank}(\mathbf{A}(\theta^*)) \geq R$, for $R \in [\min\{D_1, D_2\}]$, then the set $\{\theta \in \mathbb{R}^K : \text{rank}(\mathbf{A}(\theta)) < R\}$ has Lebesgue measure zero.

Proof. A matrix is of rank at least R if and only if it has a $R \times R$ sub-matrix whose determinant is non-zero. The determinant of any sub-matrix of $\mathbf{A}(\theta)$ is polynomial in the entries of $\mathbf{A}(\theta)$, and so it is polynomial in θ as well. Since the zero set of a polynomial is either the entire space or a set of Lebesgue measure zero [35], the fact that $\text{rank}(\mathbf{A}(\theta^*)) \geq R$ implies that $\{\theta \in \mathbb{R}^K : \text{rank}(\mathbf{A}(\theta)) < R\}$ has Lebesgue measure zero. □

Lemma 60. Let $\mathbf{v}, \mathbf{v}' \in \mathbb{R}_{\geq 0}^{D_x}$ whose first $D := \min\{D_x, D_h\}$ entries are positive, and disjoint $\mathcal{I}', \mathcal{J}' \subseteq \mathcal{V}$ with no repeating shared neighbors (Definition 12). Denote by $\mathbf{h}^{(l,i)} \in \mathbb{R}^{D_h}$ the hidden embedding for $i \in \mathcal{V}$ at layer $l \in [L]$ of a GNN with depth $L \geq 2$ and product aggregation (Equations (5.2) and (5.5)), given the following assignment to its input variables (i.e. vertex features):

$$(\mathbf{x}^{(i)} \leftarrow \mathbf{v})_{i \in \mathcal{I}'}, (\mathbf{x}^{(j)} \leftarrow \mathbf{v}')_{j \in \mathcal{J}'}, (\mathbf{x}^{(k)} \leftarrow \mathbf{1})_{k \in \mathcal{V} \setminus (\mathcal{I}' \cup \mathcal{J}')},$$

where $\mathbf{1} \in \mathbb{R}^{D_x}$ is the vector holding one in all entries. Suppose that the weights $\mathbf{W}^{(1)}, \dots, \mathbf{W}^{(L)}$ of the GNN are given by:

$$\begin{aligned} \mathbf{W}^{(1)} &:= \mathbf{I} \in \mathbb{R}^{D_h \times D_x}, \\ \mathbf{W}^{(2)} &:= \begin{pmatrix} 1 & 1 & \cdots & 1 \\ 0 & 0 & \cdots & 0 \\ \vdots & \vdots & \cdots & \vdots \\ 0 & 0 & \cdots & 0 \end{pmatrix} \in \mathbb{R}^{D_h \times D_h}, \\ \forall l \in \{3, \dots, L\} : \mathbf{W}^{(l)} &:= \begin{pmatrix} 1 & 0 & \cdots & 0 \\ 0 & 0 & \cdots & 0 \\ \vdots & \vdots & \cdots & \vdots \\ 0 & 0 & \cdots & 0 \end{pmatrix} \in \mathbb{R}^{D_h \times D_h}, \end{aligned}$$

where \mathbf{I} is a zero padded identity matrix, i.e. it holds ones on its diagonal and zeros elsewhere. Then, for all $l \in \{2, \dots, L\}$ and $i \in \mathcal{V}$, there exist $\phi^{(l,i)}, \psi^{(l,i)} : \mathbb{R}^{D_x} \rightarrow \mathbb{R}_{>0}$ such that:

$$\mathbf{h}_1^{(l,i)} = \phi^{(l,i)}(\mathbf{v}) \langle \mathbf{v}_{:D}, \mathbf{v}'_{:D} \rangle^{\rho_{l-1}(\mathcal{C}, \{i\})} \psi^{(l,i)}(\mathbf{v}') \quad , \quad \forall d \in \{2, \dots, D_h\} : \mathbf{h}_d^{(l,i)} = 0,$$

where $\mathcal{C} := \mathcal{N}(\mathcal{I}') \cap \mathcal{N}(\mathcal{J}')$.

Proof. The proof is by induction over the layer $l \in \{2, \dots, L\}$. For $l = 2$, fix $i \in \mathcal{V}$. By the update rule of a GNN with product aggregation:

$$\mathbf{h}^{(2,i)} = \odot_{j \in \mathcal{N}(i)} (\mathbf{W}^{(2)} \mathbf{h}^{(1,j)}).$$

Plugging in the value of $\mathbf{W}^{(2)}$ we get:

$$\mathbf{h}_1^{(2,i)} = \prod_{j \in \mathcal{N}(i)} \left(\sum_{d=1}^{D_h} \mathbf{h}_d^{(1,j)} \right), \quad \forall d \in \{2, \dots, D_h\} : \mathbf{h}_d^{(2,i)} = 0. \quad (\text{D.17})$$

Let $\bar{\mathbf{v}}, \bar{\mathbf{v}}' \in \mathbb{R}^{D_h}$ be the vectors holding $\mathbf{v}_{:D}$ and $\mathbf{v}'_{:D}$ in their first D coordinates and zero in the remaining entries, respectively. Similarly, we use $\bar{\mathbf{1}} \in \mathbb{R}^{D_h}$ to denote the vector whose first D entries are one and the remaining are zero. Examining $\mathbf{h}^{(1,j)}$ for $j \in \mathcal{N}(i)$, by the assignment of input variables and the fact that $\mathbf{W}^{(1)}$ is a zero padded identity matrix we have that:

$$\begin{aligned} \mathbf{h}^{(1,j)} &= \odot_{k \in \mathcal{N}(j)} (\mathbf{W}^{(1)} \mathbf{x}^{(k)}) = (\odot^{|\mathcal{N}(j) \cap \mathcal{I}'|} \bar{\mathbf{v}}) \odot (\odot^{|\mathcal{N}(j) \cap \mathcal{J}'|} \bar{\mathbf{v}}') \odot (\odot^{|\mathcal{N}(j) \setminus (\mathcal{I}' \cup \mathcal{J}')|} \bar{\mathbf{1}}) \\ &= (\odot^{|\mathcal{N}(j) \cap \mathcal{I}'|} \bar{\mathbf{v}}) \odot (\odot^{|\mathcal{N}(j) \cap \mathcal{J}'|} \bar{\mathbf{v}}'). \end{aligned}$$

Since the first D entries of $\bar{\mathbf{v}}$ and $\bar{\mathbf{v}}'$ are positive while the rest are zero, the same holds for $\mathbf{h}^{(1,j)}$. Additionally, recall that \mathcal{I}' and \mathcal{J}' have no repeating shared neighbors. Thus, if $j \in \mathcal{N}(\mathcal{I}') \cap \mathcal{N}(\mathcal{J}') = \mathcal{C}$, then j has a single neighbor in \mathcal{I}' and a single neighbor in \mathcal{J}' , implying $\mathbf{h}^{(1,j)} = \bar{\mathbf{v}} \odot \bar{\mathbf{v}}'$. Otherwise, if $j \notin \mathcal{C}$, then $\mathcal{N}(j) \cap \mathcal{I}' = \emptyset$ or $\mathcal{N}(j) \cap \mathcal{J}' = \emptyset$ must hold. In the former $\mathbf{h}^{(1,j)}$ does not depend on \mathbf{v} , whereas in the latter $\mathbf{h}^{(1,j)}$ does not depend on \mathbf{v}' .

Going back to Equation (D.17), while noticing that $|\mathcal{N}(i) \cap \mathcal{C}| = \rho_1(\mathcal{C}, \{i\})$, we arrive at:

$$\begin{aligned} \mathbf{h}_1^{(2,i)} &= \prod_{j \in \mathcal{N}(i) \cap \mathcal{C}} \left(\sum_{d=1}^{D_h} \mathbf{h}_d^{(1,j)} \right) \cdot \prod_{j \in \mathcal{N}(i) \setminus \mathcal{C}} \left(\sum_{d=1}^{D_h} \mathbf{h}_d^{(1,j)} \right) \\ &= \prod_{j \in \mathcal{N}(i) \cap \mathcal{C}} \left(\sum_{d=1}^{D_h} [\bar{\mathbf{v}} \odot \bar{\mathbf{v}}']_d \right) \cdot \prod_{j \in \mathcal{N}(i) \setminus \mathcal{C}} \left(\sum_{d=1}^{D_h} \mathbf{h}_d^{(1,j)} \right) \\ &= \langle \mathbf{v}_{:D}, \mathbf{v}'_{:D} \rangle^{\rho_1(\mathcal{C}, \{i\})} \cdot \prod_{j \in \mathcal{N}(i) \setminus \mathcal{C}} \left(\sum_{d=1}^{D_h} \mathbf{h}_d^{(1,j)} \right). \end{aligned}$$

As discussed above, for each $j \in \mathcal{N}(i) \setminus \mathcal{C}$ the hidden embedding $\mathbf{h}^{(1,j)}$ does not depend on \mathbf{v} or it does not depend on \mathbf{v}' . Furthermore, $\sum_{d=1}^{D_h} \mathbf{h}_d^{(1,j)} > 0$ for all $j \in \mathcal{N}(i)$. Hence, there exist $\phi^{(2,i)}, \psi^{(2,i)} : \mathbb{R}^{D_x} \rightarrow \mathbb{R}_{>0}$ such that:

$$\mathbf{h}_1^{(2,i)} = \phi^{(2,i)}(\mathbf{v}) \langle \mathbf{v}_{:D}, \mathbf{v}'_{:D} \rangle^{\rho_1(\mathcal{C}, \{i\})} \psi^{(2,i)}(\mathbf{v}'),$$

completing the base case.

Now, assuming that the inductive claim holds for $l - 1 \geq 2$, we prove that it holds for l . Let $i \in \mathcal{V}$. By the update rule of a GNN with product aggregation $\mathbf{h}^{(l,i)} = \odot_{j \in \mathcal{N}(i)} (\mathbf{W}^{(l)} \mathbf{h}^{(l-1,j)})$. Plugging in the value of $\mathbf{W}^{(l)}$ we get:

$$\mathbf{h}_1^{(l,i)} = \prod_{j \in \mathcal{N}(i)} \mathbf{h}_1^{(l-1,j)}, \quad \forall d \in \{2, \dots, D_h\} : \mathbf{h}_d^{(l,i)} = 0.$$

By the inductive assumption $\mathbf{h}_1^{(l-1,j)} = \phi^{(l-1,j)}(\mathbf{v}) \langle \mathbf{v}_{:D}, \mathbf{v}'_{:D} \rangle^{\rho_{l-2}(\mathcal{C}, \{j\})} \psi^{(l-1,j)}(\mathbf{v}')$ for all $j \in \mathcal{N}(i)$, where $\phi^{(l-1,j)}, \psi^{(l-1,j)} : \mathbb{R}^{D_x} \rightarrow \mathbb{R}_{>0}$. Thus:

$$\begin{aligned} \mathbf{h}_1^{(l,i)} &= \prod_{j \in \mathcal{N}(i)} \mathbf{h}_1^{(l-1,j)} \\ &= \prod_{j \in \mathcal{N}(i)} \phi^{(l-1,j)}(\mathbf{v}) \langle \mathbf{v}_{:D}, \mathbf{v}'_{:D} \rangle^{\rho_{l-2}(\mathcal{C}, \{j\})} \psi^{(l-1,j)}(\mathbf{v}') \\ &= \left(\prod_{j \in \mathcal{N}(i)} \phi^{(l-1,j)}(\mathbf{v}) \right) \cdot \langle \mathbf{v}_{:D}, \mathbf{v}'_{:D} \rangle^{\sum_{j \in \mathcal{N}(i)} \rho_{l-2}(\mathcal{C}, \{j\})} \cdot \left(\prod_{j \in \mathcal{N}(i)} \psi^{(l-1,j)}(\mathbf{v}') \right). \end{aligned}$$

Define $\phi^{(l,i)} : \mathbf{v} \mapsto \prod_{j \in \mathcal{N}(i)} \phi^{(l-1,j)}(\mathbf{v})$ and $\psi^{(l,i)} : \mathbf{v}' \mapsto \prod_{j \in \mathcal{N}(i)} \psi^{(l-1,j)}(\mathbf{v}')$. Since the range of $\phi^{(l-1,j)}$ and $\psi^{(l-1,j)}$ is $\mathbb{R}_{>0}$ for all $j \in \mathcal{N}(i)$, so is the range of $\phi^{(l,i)}$ and $\psi^{(l,i)}$. The desired result thus readily follows by noticing that $\sum_{j \in \mathcal{N}(i)} \rho_{l-2}(\mathcal{C}, \{j\}) = \rho_{l-1}(\mathcal{C}, \{i\})$:

$$\mathbf{h}_1^{(l,i)} = \phi^{(l,i)}(\mathbf{v}) \langle \mathbf{v}_{:D}, \mathbf{v}'_{:D} \rangle^{\rho_{l-1}(\mathcal{C}, \{i\})} \psi^{(l,i)}(\mathbf{v}').$$

□

D.7.4 Proof of Theorem 10

The proof follows a line identical to that of Theorem 7 (Appendix D.7.2), requiring only slight adjustments. We outline the necessary changes.

Extending the tensor network representations of GNNs with product aggregation to directed graphs and multiple edge types is straightforward. Nodes, legs, and leg weights are as described in Appendix D.3 for undirected graphs with a single edge type, except that:

- Legs connecting δ -tensors with weight matrices in the same layer are adapted such that only incoming neighbors are considered. Formally, in Equations (D.6) and (D.7), $\mathcal{N}(i)$ is replaced by $\mathcal{N}_{in}(i)$ in the leg definitions, for $i \in \mathcal{V}$.
- Weight matrices $(\mathbf{W}^{(l,q)})_{l \in [L], q \in [Q]}$ are assigned to nodes in accordance with edge types. Namely, if at layer $l \in [L]$ a δ -tensor associated with $i \in \mathcal{V}$ is connected to a weight matrix associated with $j \in \mathcal{N}_{in}(i)$, then $\mathbf{W}^{(l, \tau(j,i))}$ is assigned to the weight matrix node, as opposed to $\mathbf{W}^{(l)}$ in the single edge type setting. Formally, let $\mathbf{W}^{(l,j,\gamma)}$ be a node at layer $l \in [L]$ connected to $\delta^{(l,i,\gamma')}$, for $i \in \mathcal{V}, j \in \mathcal{N}_{in}(i)$, and some $\gamma, \gamma' \in \mathbb{N}$. Then, $\mathbf{W}^{(l,j,\gamma)}$ stands for a copy of $\mathbf{W}^{(l, \tau(j,i))}$.

For $\mathbf{X} = (\mathbf{x}^{(1)}, \dots, \mathbf{x}^{(|\mathcal{V}|)}) \in \mathbb{R}^{D_x \times |\mathcal{V}|}$, let $\mathcal{T}(\mathbf{X})$ and $\mathcal{T}^{(t)}(\mathbf{X})$ be the tensor networks corresponding to $f^{(\theta, \mathcal{G})}(\mathbf{X})$ and $f^{(\theta, \mathcal{G}, t)}(\mathbf{X})$, respectively, whose construction is outlined above. Then, Lemma 51 (from Appendix D.7.2.1) and its proof apply as stated. Meaning, $\text{sep}(f^{(\theta, \mathcal{G})}; \mathcal{I})$ and $\text{sep}(f^{(\theta, \mathcal{G}, t)}; \mathcal{I})$ are upper bounded by the minimal modified multiplicative cut weights in $\mathcal{T}(\mathbf{X})$ and $\mathcal{T}^{(t)}(\mathbf{X})$, respectively, among cuts separating leaves associated with vertices of the input graph in \mathcal{I} from leaves associated with vertices of the input graph in \mathcal{I}^c . Therefore, to establish Equations (D.2) and (D.3), it suffices to find cuts in the respective tensor networks with sufficiently low modified multiplicative weights. As is the case for undirected graphs with a single edge type (see Appendices D.7.2.2 and D.7.2.3), the cuts separating nodes corresponding to vertices in \mathcal{I} from all other nodes yield the desired upper bounds. □

D.7.5 Proof of Theorem 11

The proof follows a line identical to that of Theorem 8 (Appendix D.7.3), requiring only slight adjustments. We outline the necessary changes.

In the context of graph prediction, let $\mathcal{C}^* \in \operatorname{argmax}_{\mathcal{C} \in \mathcal{S} \rightarrow (\mathcal{I})} \log(\alpha_{\mathcal{C}}) \cdot \rho_{L-1}(\mathcal{C}, \mathcal{V})$. By Lemma 53 (from Appendix D.7.3), to prove that Equation (D.4) holds for weights θ , it suffices to find template vectors for which $\log(\operatorname{rank} \left[\left[\mathcal{B} \left(f^{(\theta, \mathcal{G})} \right); \mathcal{I} \right] \right]) \geq \log(\alpha_{\mathcal{C}^*}) \cdot \rho_{L-1}(\mathcal{C}^*, \mathcal{V})$. Notice that, since the outputs of $f^{(\theta, \mathcal{G})}$ vary polynomially with θ , so do the entries of $\left[\left[\mathcal{B} \left(f^{(\theta, \mathcal{G})} \right); \mathcal{I} \right] \right]$ for any choice of template vectors. Thus, according to Lemma 59 (from Appendix D.7.3.3), by constructing weights θ and template vectors satisfying $\log(\operatorname{rank} \left[\left[\mathcal{B} \left(f^{(\theta, \mathcal{G})} \right); \mathcal{I} \right] \right]) \geq \log(\alpha_{\mathcal{C}^*}) \cdot \rho_{L-1}(\mathcal{C}^*, \mathcal{V})$, we may conclude that this is the case for almost all assignments of weights, meaning Equation (D.4) holds for almost all assignments of weights. For undirected graphs with a single edge type, Appendix D.7.3.1 provides such weights $\mathbf{W}^{(1)}, \dots, \mathbf{W}^{(L)}, \mathbf{W}^{(o)}$ and template vectors. The proof in the case of directed graphs with multiple edge types is analogous, requiring only a couple adaptations: (i) weight matrices of all edge types at layer $l \in [L]$ are set to the $\mathbf{W}^{(l)}$ chosen in Appendix D.7.3.1; and (ii) $\mathcal{C}_{\mathcal{I}}$ and $\mathcal{S}(\mathcal{I})$ are replaced with their directed counterparts $\mathcal{C}_{\mathcal{I}}^{\rightarrow}$ and $\mathcal{S}^{\rightarrow}(\mathcal{I})$, respectively.

In the context of vertex prediction, let $\mathcal{C}_t^* \in \operatorname{argmax}_{\mathcal{C} \in \mathcal{S} \rightarrow (\mathcal{I})} \log(\alpha_{\mathcal{C}, t}) \cdot \rho_{L-1}(\mathcal{C}, \{t\})$. Due to arguments similar to those above, to prove that Equation (D.5) holds for almost all assignments of weights, we need only find weights θ and template vectors satisfying $\log(\operatorname{rank} \left[\left[\mathcal{B} \left(f^{(\theta, \mathcal{G}, t)} \right); \mathcal{I} \right] \right]) \geq \log(\alpha_{\mathcal{C}_t^*}) \cdot \rho_{L-1}(\mathcal{C}_t^*, \{t\})$. For undirected graphs with a single edge type, Appendix D.7.3.2 provides such weights and template vectors. The adaptations necessary to extend Appendix D.7.3.2 to directed graphs with multiple edge types are identical to those specified above for extending Appendix D.7.3.1 in the context of graph prediction.

Lastly, recalling that a finite union of measure zero sets has measure zero as well establishes that Equations (D.4) and (D.5) jointly hold for almost all assignments of weights. \square

D.7.6 Proof of Proposition 10

We first prove that the contractions described by $\mathcal{T}(\mathbf{X})$ produce $f^{(\theta, \mathcal{G})}(\mathbf{X})$. Through an induction over the layer $l \in [L]$, for all $i \in \mathcal{V}$ and $\gamma \in [\rho_{L-l}(\{i\}, \mathcal{V})]$ we show that contracting the sub-tree whose root is $\delta^{(l, i, \gamma)}$ yields $\mathbf{h}^{(l, i)}$ — the hidden embedding for i at layer l of the GNN inducing $f^{(\theta, \mathcal{G})}$, given vertex features $\mathbf{x}^{(1)}, \dots, \mathbf{x}^{(|\mathcal{V}|)}$.

For $l = 1$, fix some $i \in \mathcal{V}$ and $\gamma \in [\rho_{L-1}(\{i\}, \mathcal{V})]$. The sub-tree whose root is $\delta^{(1, i, \gamma)}$ comprises $|\mathcal{N}(i)|$ copies of $\mathbf{W}^{(1)}$, each associated with some $j \in \mathcal{N}(i)$ and contracted in its second mode with a copy of $\mathbf{x}^{(j)}$. Additionally, $\delta^{(1, i, \gamma)}$, which is a copy of $\delta^{(|\mathcal{N}(i)|+1)}$, is contracted with the copies of $\mathbf{W}^{(1)}$ in their first mode. Overall, the execution of all contractions in the sub-tree can be written as $\delta^{(|\mathcal{N}(i)|+1)} *_{j \in [|\mathcal{N}(i)|]} (\mathbf{W}^{(1)} \mathbf{x}^{(\mathcal{N}(i)_j)})$, where $\mathcal{N}(i)_j$, for $j \in [|\mathcal{N}(i)|]$, denotes the j 'th neighbor of i according to an ascending order (recall vertices are represented by indices from 1 to $|\mathcal{V}|$). The base case concludes by Lemma 61:

$$\delta^{(|\mathcal{N}(i)|+1)} *_{j \in [|\mathcal{N}(i)|]} \left(\mathbf{W}^{(1)} \mathbf{x}^{(\mathcal{N}(i)_j)} \right) = \odot_{j \in [|\mathcal{N}(i)|]} \left(\mathbf{W}^{(1)} \mathbf{x}^{(\mathcal{N}(i)_j)} \right) = \mathbf{h}^{(1, i)}.$$

Assuming that the inductive claim holds for $l - 1 \geq 1$, we prove that it holds for l . Let $i \in \mathcal{V}$ and $\gamma \in [\rho_{L-l}(\{i\}, \mathcal{V})]$. The children of $\delta^{(l,i,\gamma)}$ in the tensor network are of the form $\mathbf{W}^{(l,\mathcal{N}(i),\phi_{l,i,j}(\gamma))}$, for $j \in [|\mathcal{N}(i)|]$, and each $\mathbf{W}^{(l,\mathcal{N}(i),\phi_{l,i,j}(\gamma))}$ is connected in its other mode to $\delta^{(l-1,\mathcal{N}(i),\phi_{l,i,j}(\gamma))}$. By the inductive assumption for $l - 1$, we know that performing all contractions in the sub-tree whose root is $\delta^{(l-1,\mathcal{N}(i),\phi_{l,i,j}(\gamma))}$ produces $\mathbf{h}^{(l-1,\mathcal{N}(i))}$, for all $j \in [|\mathcal{N}(i)|]$. Since $\delta^{(l,i,\gamma)}$ is a copy of $\delta^{(|\mathcal{N}(i)|+1)}$, and each $\mathbf{W}^{(l,\mathcal{N}(i),\phi_{l,i,j}(\gamma))}$ is a copy of $\mathbf{W}^{(l)}$, the remaining contractions in the sub-tree of $\delta^{(l,i,\gamma)}$ thus give:

$$\delta^{(|\mathcal{N}(i)|+1)} *_{j \in [|\mathcal{N}(i)|]} \left(\mathbf{W}^{(l)} \mathbf{h}^{(l-1,\mathcal{N}(i))} \right),$$

which according to Lemma 61 amounts to:

$$\delta^{(|\mathcal{N}(i)|+1)} *_{j \in [|\mathcal{N}(i)|]} \left(\mathbf{W}^{(l)} \mathbf{h}^{(l-1,\mathcal{N}(i))} \right) = \odot_{j \in [|\mathcal{N}(i)|]} \left(\mathbf{W}^{(l)} \mathbf{h}^{(l-1,\mathcal{N}(i))} \right) = \mathbf{h}^{(l,i)},$$

establishing the induction step.

With the inductive claim at hand, we show that contracting $\mathcal{T}(\mathbf{X})$ produces $f^{(\theta,\mathcal{G})}(\mathbf{X})$. Applying the inductive claim for $l = L$, we have that $\mathbf{h}^{(L,1)}, \dots, \mathbf{h}^{(L,|\mathcal{V}|)}$ are the vectors produced by executing all contractions in the sub-trees whose roots are $\delta^{(L,1,1)}, \dots, \delta^{(L,|\mathcal{V}|,1)}$, respectively. Performing the remaining contractions, defined by the legs of $\delta^{(|\mathcal{V}|+1)}$, therefore yields $\mathbf{W}^{(o)}(\delta^{(|\mathcal{V}|+1)} *_{i \in [|\mathcal{V}|]} \mathbf{h}^{(L,i)})$. By Lemma 61:

$$\delta^{(|\mathcal{V}|+1)} *_{i \in [|\mathcal{V}|]} \mathbf{h}^{(L,i)} = \odot_{i \in [|\mathcal{V}|]} \mathbf{h}^{(L,i)}.$$

Hence, $\mathbf{W}^{(o)}(\delta^{(|\mathcal{V}|+1)} *_{i \in [|\mathcal{V}|]} \mathbf{h}^{(L,i)}) = \mathbf{W}^{(o)}(\odot_{i \in [|\mathcal{V}|]} \mathbf{h}^{(L,i)}) = f^{(\theta,\mathcal{G})}(\mathbf{X})$, meaning contracting $\mathcal{T}(\mathbf{X})$ results in $f^{(\theta,\mathcal{G})}(\mathbf{X})$.

An analogous proof establishes that the contractions described by $\mathcal{T}^{(t)}(\mathbf{X})$ yield $f^{(\theta,\mathcal{G},t)}(\mathbf{X})$. Specifically, the inductive claim and its proof are the same, up to γ taking values in $[\rho_{L-l}(\{i\}, \{t\})]$ instead of $[\rho_{L-l}(\{i\}, \mathcal{V})]$, for $l \in [L]$. This implies that $\mathbf{h}^{(L,t)}$ is the vector produced by contracting the sub-tree whose root is $\delta^{(L,t,1)}$. Performing the only remaining contraction, defined by the leg connecting $\delta^{(L,t,1)}$ with $\mathbf{W}^{(o)}$, thus results in $\mathbf{W}^{(o)} \mathbf{h}^{(L,t)} = f^{(\theta,\mathcal{G},t)}(\mathbf{X})$. \square

D.7.6.1 Technical Lemma

Lemma 61. Let $\delta^{(N+1)} \in \mathbb{R}^{D \times \dots \times D}$ be an order $N + 1 \in \mathbb{N}$ tensor that has ones on its hyper-diagonal and zeros elsewhere, i.e. $\delta_{d_1, \dots, d_{N+1}}^{(N+1)} = 1$ if $d_1 = \dots = d_{N+1}$ and $\delta_{d_1, \dots, d_{N+1}}^{(N+1)} = 0$ otherwise, for all $d_1, \dots, d_{N+1} \in [D]$. Then, for any $\mathbf{x}^{(1)}, \dots, \mathbf{x}^{(N)} \in \mathbb{R}^D$ it holds that $\delta^{(N+1)} *_{i \in [N]} \mathbf{x}^{(i)} = \odot_{i \in [N]} \mathbf{x}^{(i)} \in \mathbb{R}^D$.

Proof. By the definition of tensor contraction (Definition 18), for all $d \in [D]$ we have that:

$$\left(\delta^{(N+1)} *_{i \in [N]} \mathbf{x}^{(i)} \right)_d = \sum_{d_1, \dots, d_N=1}^D \delta_{d_1, \dots, d_N, d}^{(N+1)} \cdot \prod_{i \in [N]} \mathbf{x}_{d_i}^{(i)} = \prod_{i \in [N]} \mathbf{x}_d^{(i)} = \left(\odot_{i \in [N]} \mathbf{x}^{(i)} \right)_d.$$

\square